Universidad de Las Palmas de Gran Canaria

Coleccion de Separatas

Año 2000

Facultad de Ciencias del Mar

Biblioteca de Ciencias Básicas "*Carlos Bas*"

Depósito Legal: GC-417-2001
ISBN 84-699-5328-1
Imprime: Servicio de Reprografía de la U.L.P.G.C.
http://www.ccbb.ulpgc.es/ccmar/biblioteca

INDICE

Eiguren Fernandez, A. ; Sosa Ferrera, Z. ; **Santana Rodríguez, J.J.** : Determination of polychlorinated dibenzofurans in blue mussels (*Mytilus edulis*) using microwave-assisted extraction prior to HPLC- fluorescence detection. **Luminiscence**, 2000, vol. 15, p. 94-95

Fuertes-Fuente, M. ; Martín-Izard, A. ; Boiron, M. C. ; **Mangas, J.** : Fluid evolution of rare-element and muscovite granitic pegmatites from central Galicia, NW Spain. **Mineralium Deposita**, 2000, vol. 35, p. 332-345

Fuertes Fuente, Mercedes ; Martín Izard, Agustín ; Boiron Marie Christine; **Mangas Viñuela, Jose** : P-T path and fluid evolution in the *franqueira granitic pegmatite*, Central Galicia, Northwestern Spain. **The Canadian Mineralogist**, 2000, vol. 38, p. 1163-1175

Garrido, M.J. ; **Haroun, R.J.** ; Lessios, H.A. : Annual reproductive peridiocity of the sea Urchin *Diadema Antillarum* Philippi in the Canary Islands. **Bulletin of Marine Science**, 2000, vol.67, nº 3, p. 989-996

Gimeno, D ; **Pérez Torrado, F.J.** ; Schneider, J.L. ; Wassmer, P. : Transformación de las coladas básicas alcalinas subaéreas en lavas almohadilladas en ambiente litoral: un ejemplo del Pioceno, Norte de la isla de Gran Canaria, **Geotemas**, vol. 1, nº 3, p. 325-328

Gómez Fernandez, F. ; Both, R.A. ; **Mangas, J.** ; Arribas, A. : Metallogenesis of Zn-Pb Carbonate-Hosted Mineralization in the Southeastern Region of the Picos de Europa (Central Northern Spain) Province: Geologic Fluid Inclusion, and Stable Isotope Studies. **Economic Geology**, 2000, vol. 95, p. 19-40

Gonzalez Dávila, Melchor ; Santana Casiano, J.Magdalena ; Laglera, Luis M. : Copper adsorption in diatom cultures. **Marine Chemistry**, 2000, vol. 70, p. 161-170

Hernandez García, Vicente ; Martín, Ana Y. ; **Castro José J.** : Evidence of external digestion of crustaceans in *Octopus vulgaris* paralarvae. **Journal of the Marine Biological Association of the United Kindom**, 2000, Vol. 80, p. 559-560

Hernández Guerra, Alonso ; Joyce, Terrence M. : Water Masses and Circulation in the Surface Layers of the Caribbean at 66° W. **Geophysical Research Letters**, 2000,vol. 27, nº 21, p. 3497-3500

Hernandez León, S. ; Almeida, C. ; Portillo Hahefeld, A. ; **Gómez, M.** ; Montero, I. : Biomass and potential feeding, respiration and growth of zooplankton in the Bransfield Strait (Antarctic Peninsula) during austral summer. **Polar Biol**, 2000, vol. 23, p. 679-690 213797

Herrero Bervera, E. ; **Mangas Viñuela, J.** ; Valet, J.P. : Paleomagnetic study of the ages of lavas on the island of Lanai'i, Hawai'i. **Journal of Volcanology and Geothermal Research**, 2000, vol. 104, p. 21-31 214402

Mahugo Santana C. ; Sosa Ferrera, Z. ; **Santana Rodriguez, J.J.** : Simultaneous optimization of surfactant concentration and organic modifier in micellar liquid chromatography. Application to the separation of phenolic compounds. **Analytical letters**, 2000, vol. 33, n° 8, p. 1691-1709 214405

Marián, Fernando D. ; García Jiménez, Pilar ; **Robaina, Rafael R.** : Polyamines in marine macroalgae: Levels of putrescine, spermidine and spermine in the thalli and changes in their concentration during glycerol-induced cell growth in vitro. **Phisiologia Plantarum**, 2000, vol. 110, p. 530-534 214471

Marián, Fernando D. ; García Jiménez, Pilar ; **Robaina Rafael R.** : Polyamine levels in the seagrass *Cymodocea nodosa*. **Aquatic Botany**, 2000, vol. 68, p. 179- 184 214286

Montero, D. ; Blazer, V.S.; Socorro, J. ; **Izquierdo, M.S.** ; Tort, L. : Dietary and culture influences on macrophage aggregate parameters in gilthead seabream (*Sparus aurata*) juveniles. **Aquaculture**, 1999, vol. 179, p. 523-534 213306

Pajuelo, José G.; **Lorenzo José M.** : Biology of the sand smelt, *Atherina presbyter* (Teleostei: Aatherinidae), off the Canary Islands (central-east Athlantic). **Enviromental Biology of Fishes**, 2000, vol. 59, p. 91-97 214538

Pajuelo, J.G. ; Lorenzo, J.M. : Reproduction, age, growth and mortality of axillary seabream, *Pagellus acarne* (Sparidae), from the Canarian archipielago. **J. Appl. Ichthyol**, 2000, vol. 16, p. 41-47 214539

Pérez Torrado, F.J.; Schneider, J.L.; Gimeno, D.; Wassmer, P.; Cabrera, M.C. : Mecanismos de transporte y emplazamiento de depósitos volcanoclásticos en el litoral NE de Gran Canaria (Islas Canarias). **Geotemas**, 2000, vol. 1, n° 3, p. 329-333 214796

Pavón Salas, N. ; Herrera, R.; **Hernandez Guerra, A.; Haroun, R.**: Distributional Pattern of Seagrasses in The Canary Islands (Central-East Atlantic Ocean). **Journal of Coastal Research**, 2000, vol. 16, nº 2, p. 329-335

Rodriguez, G.; Nistal, A.; Pérez, B.: Joint occurrence of high tide, surge and storm-waves on the northwest Spanish coast. **Boletín del Instituto Español de Oceanografía**, 1999, vol. 15, nº 1-4, p. 21-29

Santana Rodriguez, J.J.; Padrón Sanz, C.: Fluorescence techniques for the determination of polycyclic aromatic hidrocarbons in marine environment: an overview. **Analusis**, 2000, vol.28, nº 8, p. 710-717

Vergara Martín, José Manuel : Consideraciones socio-económicas sobre el momento actual de la acuicultura marina en España. **AquaTIC**, 2000, nº10, junio, 12 p.

JOURNAL OF GEOPHYSICAL RESEARCH, VOL. 105, NO. C7, PAGES 17,173–17,193, JULY 15, 2000

Lee region of Gran Canaria

Eric D. Barton,[1] Gotzon Basterretxea,[2] Pierre Flament,[3,4] E. Gay Mitchelson-Jacob,[5] Bethan Jones,[5] Javier Arístegui,[2] and Felix Herrera[6]

Abstract. The mountainous Canary Islands present obstacles to the trade winds and to the Canary Current flowing equatorward past them. In situ observations of hydrographic properties and surface winds south of Gran Canaria, together with advanced very high resolution radiometer and synthetic aperture radar images during 2 weeks in summer 1995 are analyzed. A cyclonic eddy shed from the west of the island drifted southwestward at 5 cm s^{-1}, while the southeast coast was approached by an upwelling filament originating off NW Africa. A wind lee region bounded by intense horizontal shear lines had a weak return islandward wind in its center. The lee formed a triangular, diurnally varying, warm water pool with two sea surface temperature maxima separated by lower temperatures below the return wind. Shallow temperature stratification occurred behind the island in contrast to the uniform surface mixed layer in exposed regions. Upwelling and downwelling of 10 - 20 m d^{-1} were indicated on the cyclonic and anticyclonic sides of the lee region. In the SAR images, lines of strong current shear along a temperature front between the cyclonic eddy and the upwelling filament were identifiable. However, the radar images were dominated by atmospheric phenomena, including mountain lee wave packets, windrows, and wind shear lines. Estimation of the wind field from the SAR backscatter intensity revealed complex structure and intensification on the edges of the warm lee.

1. Introduction

The Canary Island archipelago, which rises steeply from ocean depths of over 3000 m, forms an obstacle to the southwestward flows of both the Canary Current and the trade winds (Figure 1). The summit of Tenerife is at 3717 m, while that of Gran Canaria reaches 1949 m. The presence of lee regions behind the islands has long been recognized; becalming downwind of Gomera, Tenerife and Gran Canaria in August-September 1492 delayed Columbus' departure on the *Santa María* to discover the New World [*Columbus*, 1987].

The meteorology of the Canary Islands has been summarized by *Naya* [1984]. From March to September the trade winds are capped by an atmospheric temperature inversion between 400 and 1000 m. As the approaching air stream is forced up the slopes of the islands, a layer of stratocumulus is often formed at the base of the inversion. The stable inversion layer prevents the air from rising farther and diverts the flow around the island flanks. Some of the diverted flow is channeled back to the coasts down deep canyons to converge with the main flow, increasing wind speed and causing vertical motion and cloud production. Even at times of extensive stratocumulus the leeward coasts often remain clear because of subsidence down the lee slopes.

Warm oceanic "wakes" have been identified in satellite images as anomalously high surface temperature regions in the island lees [*Hernández-Guerra*, 1990; *Van Camp et al.*, 1991]. The extent of the wakes, which varied from island to island, was attributed to the differing heights of the islands. Wake orientation followed the prevailing winds. Wakes formed during the day by solar heating and weakened or disappeared in night time images. They were bounded by temperature fronts, presumably coincident with the boundary between the trade winds and the calm.

In this paper we report in situ observations of hydrographic structure and surface winds downstream of Gran Canaria and remote sensing advanced very high resolution radiometer (AVHRR) and synthetic aperture radar (SAR) imagery during 2 weeks of the strongest summer trade winds. Repeated sampling revealed the strong wind shear lines, the associated thermohaline structure, and the subsurface pycnocline distortion caused by Ekman pumping. The variability of the wake in relation to the larger-scale context and to features in the AVHRR and SAR images is discussed. Both atmospheric and oceanic phenomena have signatures in the radar images. The wind field inferred from the SAR backscatter intensity shows strong structure related to the extent of the warm lee.

2. Methods

Between July 24 and August 8 1995, conductivity-temperature-depth (CTD) sections spanning the lee region of Gran Canaria were made on eight occasions (Figure 1). Each consisted of 5 - 9 profiles to 200 m depth spaced at 4 km intervals from the lee into the open ocean trade winds. Six sections were made on the western (cyclonic) half, and two were made on the eastern (anticyclonic) half. The recently calibrated Seabird SBE 19 CTD and Sea Tech fluorometer

[1] School of Ocean Sciences, University of Wales, Bangor, UK.
[2] Facultad de Ciencias del Mar, Universidad de Las Palmas de Gran Canaria, Las Palmas de Gran Canaria, Spain.
[3] Department of Oceanography, University of Hawaii at Manoa, Honolulu.
[4] Also at Département d'Océanographie Spatiale, IFREMER, Brest, France
[5] Unit for Coastal and Estuarine Studies, University of Wales, Bangor, UK.
[6] Laboratorio de Comunicaciones y Teledetección, Universidad de La Laguna, Tenerife, Spain

Paper number 2000JC900010.
0148-0227/00/2000JC900010$09.00

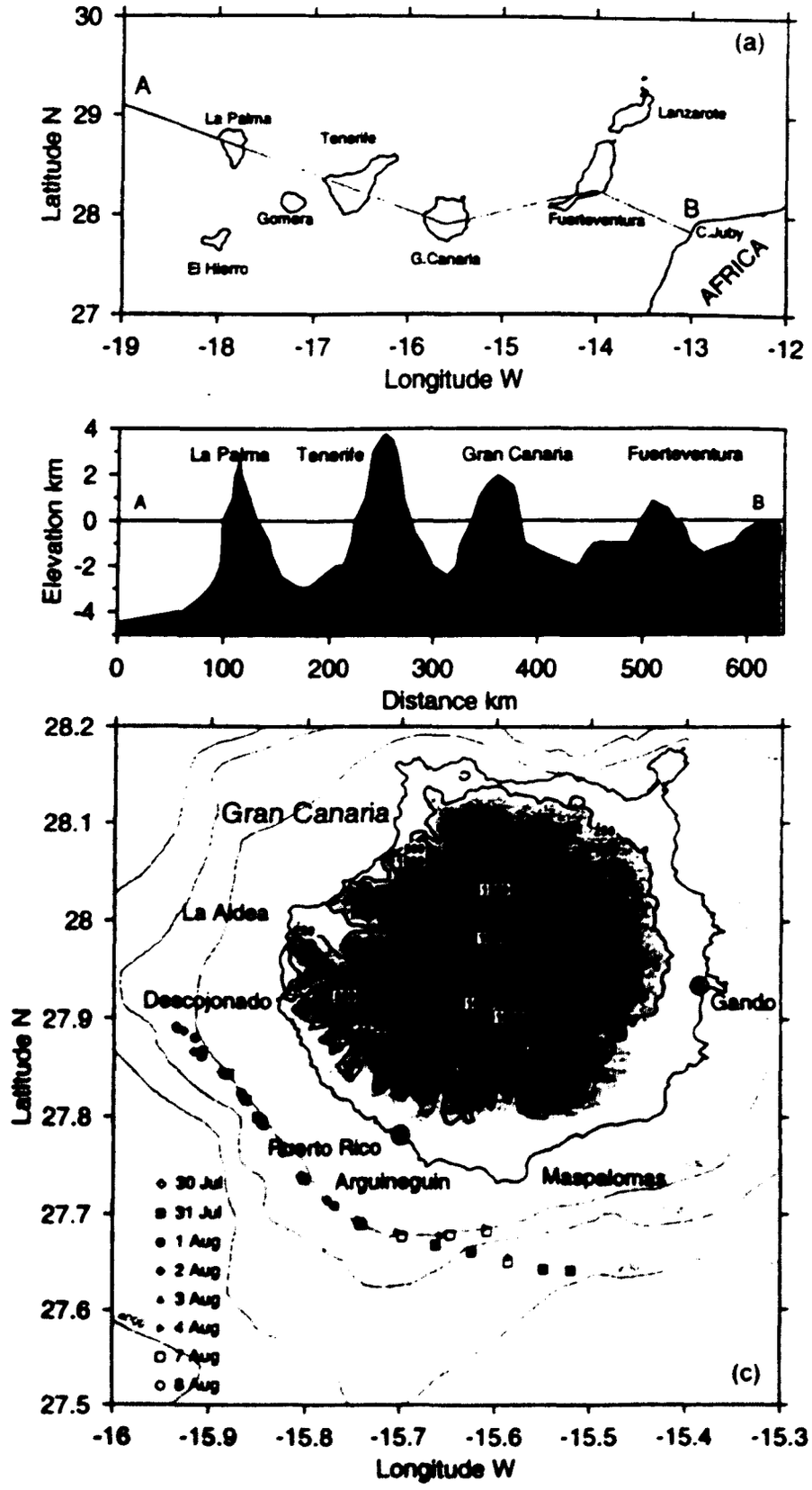

Figure 1. (a) The Canary Island archipelago lies < 100 km off the African coast. (b) Elevation profile along the line AB in Figure 1a. (c) Conductivity-temperature-depth station positions. The island and sea bed topography is shown in meters. Time series of wind were recorded at island sites marked by asterisks.

performed within specifications. The small research vessel could work only by day and only a few kilometers into the full strength of the trades.

On the vessel, relative wind velocity, air temperature, and atmospheric pressure were recorded at 1 min intervals ~ 10 m above sea level. The average speed, temperature, and pressure and the most frequent wind direction were recorded in each interval. The ship's latitude and longitude from a Magellan 1200 Global Positioning System navigator were logged every 2 s. The positions were edited following *Fleming and Hill*

[1982] to remove spurious values, reduce the noise level, and provide smoothed estimates every minute. The ship's velocity obtained by differencing subsequent positions yielded absolute wind velocity.

Wind velocities reported four times per day at 10 sites around the island were obtained for July and August. The Aeropuerto de Gran Canaria site at Gando on the low-lying east coast (Figure 1) is well exposed to the summer trade winds (Figure 2a), so is representative of the surrounding open ocean region. The airport wind record (Figure 2b) also indicates the timing of the CTD observations and the satellite images. The record from Puerto Rico (Figure 2c) represents conditions in the center of the lee coast, completely sheltered from the strong trades.

AVHRR images were captured four times daily at the Universidad de La Laguna high resolution picture transmission receiving station in Tenerife. The raw data were subsequently geolocated using the satellite orbit elements and adjusted using the island coastlines to reach a final ground location accuracy of ~ 2 km. Sea surface temperatures were then estimated from the five-channel records using the algorithm of *McClain et al.* [1985] to correct for atmospheric water vapor to an absolute precision better than 1°C. Clouds were detected and flagged using a combination of tests, including a textural test on the visible and infrared channels to detect small cumulus clouds and a differential test on the infrared channels to detect fog and low stratus clouds [*Saunders and Kriebel*, 1988]. The final cloud-masked SST images were remapped to a common Mercator grid, to eliminate geometric distortions due to earth rotation and curvature. The performance of the SST algorithm was checked over an area ~ 100 km x 200 km southwest of Tenerife, which remained cloud-free during the entire period, presumably as a result of air subsidence in the lee of the tallest island. The median temperatures computed for each image over this area indicated a bias of -0.35°C for NOAA 12 and -3°C for NOAA 9, using NOAA 14 as reference. The NOAA 12 and NOAA 9 images used here were corrected for these biases. The standard deviation of the corrected series of medians was 0.8°C.

SAR scenes were available for July 29 and 30 from ERS-1 and ERS-2, respectively. SAR intensities were converted to normalized radar backscatter cross section (NRSC) following procedures similar to *Lehner et al.*'s [1998]. The procedures differ slightly for the two satellites but involve correction for saturation in the analog to digital convertor of the satellite receiver in areas of relatively high backscatter [*Meadows and Wright*, 1994]. Correction is necessary because the prevalent wind speeds (>10 m s^{-1}) are high enough here to provoke saturation. Before application of the recalibration, intensities were smoothed to reduce "speckle" with an 8 x 8 convolution filter and then subsampled at every eighth pixel, increasing image pixel size to ~ (100 m)2. The smoothed intensities were calibrated using the method of Laur *et al.* [1997] to produce images of calibrated backscatter (in dB). From these, fields of estimated wind speed were determined by application of the empirical C band CMOD4 model developed originally for the ERS scatterometer by Stoffelen and Anderson [1997]. As discussed later, an assumed wind direction is a necessary input to the model as the SAR illuminates the targets in only one narrow range of directions as opposed to three widely separated ones for the ERS scatterometer.

3. Results

The synoptic situation on July 30 (Figure 2a) illustrates the Azores High and Saharan Low typical of boreal summer. The northeast-southwest trending isobars of the trade wind regime dominated the observation period. Winds at the Aeropuerto de Gran Canaria (Figure 2b) had a vector mean speed of 10.1 m s^{-1} during the months of July and August. The vector mean direction was 203°, coincident with the principal axis of variance of the wind fluctuations. A weak sea breeze regime had zonal and meridional amplitudes 2.1 and 1.6 m s^{-1}, respectively. The standard deviation of speed was ~ 3 m s^{-1}. Speed increased slightly to a maximum of 16.9 m s^{-1} on July 30, then decreased similarly through August.

Near Puerto Rico, on the southern lee coast, the July-August winds were weak and, on average, onshore (Figure 2c). The sea breeze regime there had zonal and meridional components of 0.5 and 1.7 m s^{-1}, respectively. The mean vector wind was 0.7 m s^{-1} toward 28°, with standard deviations in both eastward and northward components exceeding 2 m s^{-1}. The orientation of the principal axis was 315°. No trend in wind speed was evident.

3.1 Regional Context

The relative uniformity and strength of winds over the open ocean during the observation period are shown in Plate 1a, where ERS scatterometer winds are plotted for July 31. The overall direction was southwest, and wind speeds were stronger than 10 m s^{-1} in much of the area, exceeding 15 m s^{-1} southeast of Gran Canaria. The low spatial resolution and crude land masking does not permit examination of near-island effects. The overall current in the region is the slow southwestward drift of the Canary Current, but energetic mesoscale structure is indicated by the SST patterns and sea level anomalies (Plates 1b and 1c).

The sea level anomaly (SLA) field, from the combined TOPEX-Poseidon/ERS-1 observations [*Le Traon et al.*, 1995], was derived for the period July 25 to August 10 1995. Only the data from the ERS-1 half cycle corresponding most closely in time to the TOPEX-Poseidon data were used. This was to reduce the smearing of features owing to temporal changes over the 35 day cycle period, albeit at the cost of higher spatial resolution. Ground tracks, shown in Plate 1c as dotted lines, are irregularly distributed and data near land are rejected because of the possibility of signal saturation. The data were smoothed and interpolated to a regular grid using the Barnes algorithm [*Koch et al.*, 1983] before contouring and calculating the geostrophic velocity vectors. The original data are noisy, but the major features of the anomaly field correspond well to those of the SST image.

The SST image of early afternoon August 5 (Plate 1b) show a complex upwelling filament extending out from the African coast, several eddy-like structures, and warmer regions extending southwestward from most of the islands. The filament, arising from the coastal upwelling between Cape Bojador and Cape Juby, has been observed in different years [*Barton et al.*, 1998]. The cyclonic circulation associated with the filament and its extension southward and shoreward is evident in the SLA map (Plate 1c). A second filament apparent near latitude 26°N also coincides with offshore motion. Such filaments frequently carry cooler upwelled waters far offshore. In this case the Juby filament has two cool cores that almost reach Gran Canaria. There they turn southward and merge to approach the African coast again. Such double structure has been observed in Coastal Zone Color Scanner images by Hernández-Guerra *et al.* [1993]. The flow associated with a similar filament in August 1993 was >50 cm s^{-1} in the near-surface cold core [Navarro Pérez, 1996], somewhat faster than is indicated in the SLA map.

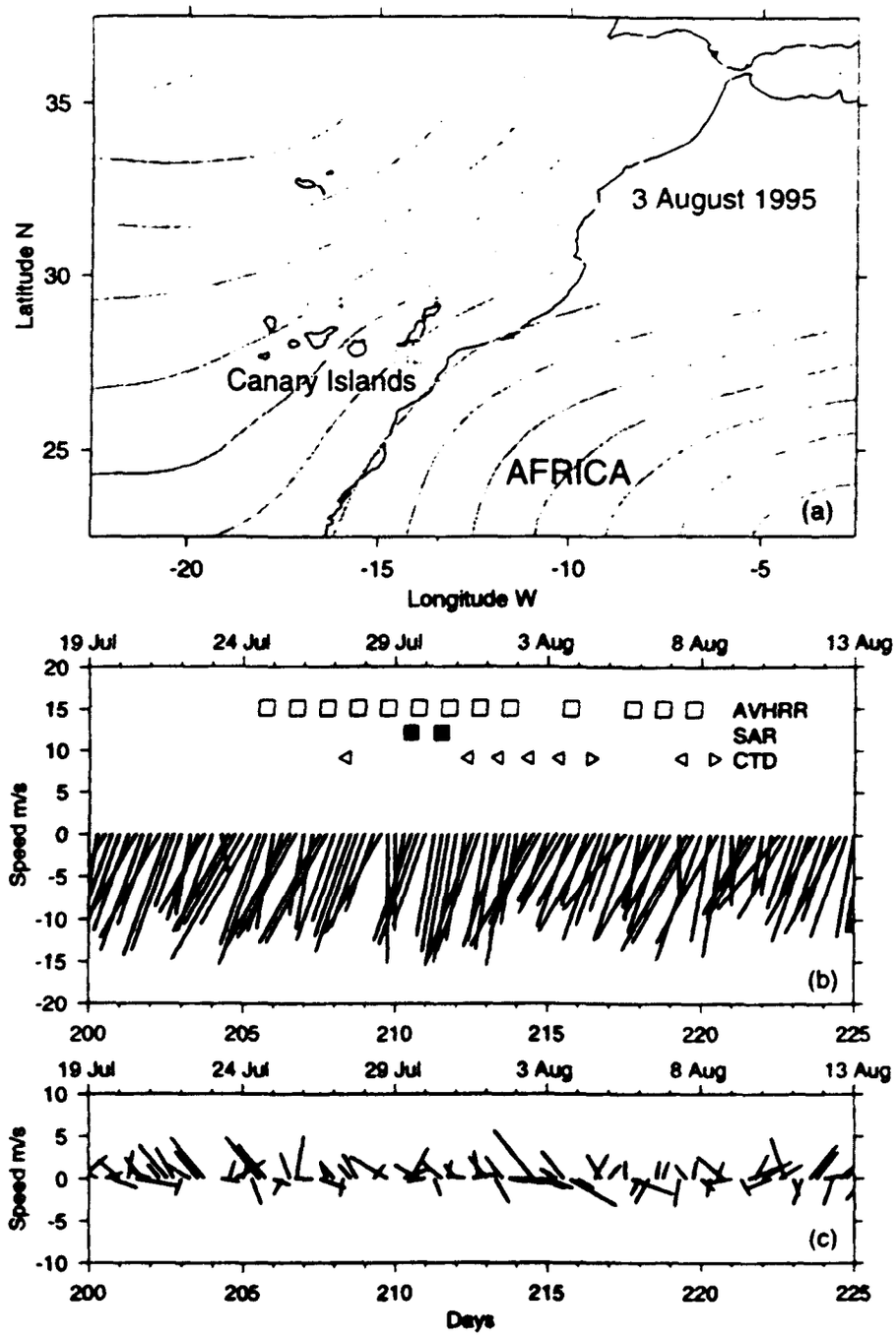

Figure 2. (a) Surface pressure map for July 30 1995. The strong gradient between the Azores High and Saharan Low is related to the trade wind regime. (b) Wind velocity time series from the airport at Gando on the east coast of Gran Canaria. Year day and date labels refer to the larger ticks. The positive y-direction indicates north. Days when advanced very high resolution radiometer (AVHRR) imagery was obtained are marked by open squares, days of synthetic aperture radar (SAR) images are marked by solid squares, and CTD samplings are marked by open triangles pointing left and right for western and eastern surveys, respectively. (c) Wind velocity time series from Puerto Rico on the south coast.

The eddy and warm lee features represent flow disturbance caused by the islands. The 100 km diameter anticyclone south of Tenerife (Plate 1b) has entrained streamers of warmer water from the lee of Gomera and cooler water from the channel south of Tenerife around its northern periphery. Cooler water is entrained generally around its southern edge. In the SLA map (Plate 1c), azimuthal geostrophic velocities up to 0.4 m s^{-1} occur around the anticyclone. The centripetal acceleration was not taken into account and could result in a supergeostrophic increase of ~ 20% given the radius of the feature. The good definition of this feature is partly caused by its persistence and fixed location. Similar anticyclones were observed in 1993 when a drifter traced its periphery with velocities close to 1 m s^{-1} [*Barton et al.*, 1998] and in 1996 by *Molina et al.* [1998].

Southeast of the anticyclone are traces of a cold-core cyclonic eddy shed from Gran Canaria. Younger, smaller cyclones are located west of Tenerife and La Palma. Similar structures, and their effect on primary production, are de-

scribed by *Arístegui et al.* [1997]. These cyclones and other details of the flow patterns suggested by the SST field, like the small instabilities on the southern boundary of the filament, are generally not apparent in the SLA field because they are small relative to the gap between ground tracks. Though the altimetry map is of anomalies with respect to a 3 year mean topography, the weak mean flow [*Navarro-Pérez and Barton*, 1998] allows detection of larger mesoscale structures seen in the SST map.

West coast waters off each island are cooler than east coast waters because of upwelling and downwelling caused by the trade wind-driven westward Ekman transport. Upwelling off western Fuerteventura was observed in situ by *Molina and Laatzen* [1989]. Behind Gran Canaria and other islands an almost triangular region of warmer surface water extends up to 100 km in the direction of the winds. The warm features result from the absence of wind mixing and the consequent production of a diurnal near-surface thermocline and associated elevated surface temperatures [*Flament et al.*, 1994]. Late night and early morning images do not show the feature as strongly, although it does not disappear completely.

3.2 Wind Structure in the Lee

The in situ winds across the lee of Gran Canaria (Figure 3) have been rotated into the principle axes of variance of the ship wind data set. A vector drawn vertically down the page is therefore directed toward 225°. The 20° difference between principal axes of the airport and ship winds reflects spatial variability of wind in the lee. An ill-defined reverse flow in the center of the lee on July 31 and August 7 suggests

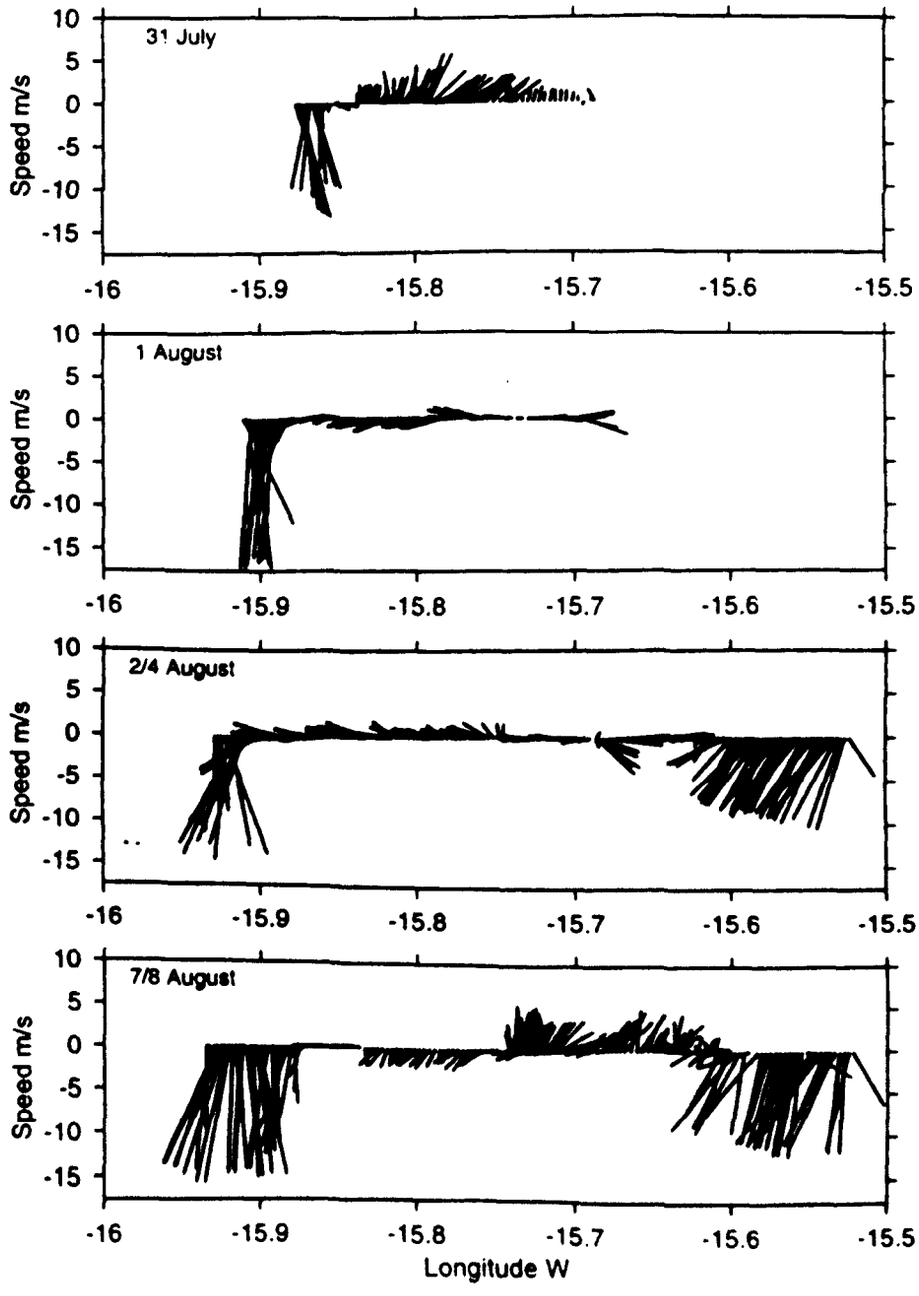

Figure 3. Profile of 10 m ship winds across the lee of Gran Canaria in August 1995. Strong shear zones bound the zone of weak recirculation in the lee. Flow is convergent towards both boundaries.

counterrotating eddies behind the island. In the strong shear zones on the lee boundaries, speed increases from 0 to 15 m s^{-1} in distances of ~2 km.

In most transects the cross-stream component of surface wind was convergent toward the shear boundary on both sides of the lee. The consequent upward motion of humid surface air characteristically forms narrow bands of cloud at the base of the inversion layer along the edges of the lee. Given the measured 10 m height values of relative humidity ~ 60%, atmospheric pressure around 1016 mbar, and air temperature of ~ 23°C, saturation would be reached at ~ 900 m, typical of the low level cloud strip. Midday radiosonde reports from Tenerife indicated inversion layer base heights between 850 and 1000 m. Such low-lying cloud features are seen in several satellite images, but they are often undetected because their width is less than the AVHRR resolution. In most transects the surface pressure dropped by 1 to 2 mbar on crossing the shear zone into the exposed region, consistent with convergence at the boundary.

3.3 Near-Surface Temperature Profiles

Sea surface CTD temperatures (Figure 4a) reveal the warm surface lee region and its strong boundaries. Contrast between the sheltered and exposed surface waters is slightly less than 1.5°C, although surface temperature in the lee is underestimated because the first CTD record was usually at several meters depth. Scatter in the distribution reflects differences in time of sampling and shifts in boundary position. A few stations were sampled in the early morning before insolation had time to warm the surface after night time heat loss and convective overturning. The position of the wind shear lines coincides with the strongest horizontal temperature gradients.

Temperature profiles (Figure 4b) from August 2 show subsurface differences between the trade wind and lee regions. In the exposed region, at the westernmost position, station 401, a well-mixed surface layer was bounded at 25 m depth by a strong thermocline. Just inside the wind boundary, station 403, a warmer, weakly stratified near-surface zone had developed above the mixed layer in response to diurnal heating and weaker wind. At 20-30 m depth, temperatures were similar to the previous station but the thermocline was twice as deep, at 65 m. In the center of the lee, station 405, the surface layer was considerably thicker with temperatures at all depths higher than elsewhere as a result of accumulated warming. The main thermocline was depressed to ~ 125 m, and there was evidence of nocturnal shallow overturning down to 20 m moderated by subsequent daytime surface warming. A similar progression was evident on the eastern anticyclonic boundary.

The pycnocline, estimated from the first maximum in Brunt-Vaisala frequency below the diurnal pycnocline (Figure 4c), showed a strong depression in the center of the island lee and shoaling to its sides, particularly to the west. Its depth ranged between 25 and 135 m over a distance of 15 km. Mean pycnocline depth in the undisturbed far field away from the islands is around 70 m in summer [*Aristegui et al.*, 1997], so anomalies associated with the lee were 50 - 60 m. Pycnocline depth was consistent throughout the sampling period except for an eastward shift of the structure in the last composite section August 7-8. *Lentz* [1992] observed that the surface mixed layer depth h in the NW African and other coastal upwelling regions was predicted remarkably well by the one-dimensional parameterization of *Pollard et al.* [1973]:

$$h = A\, u_* / (N f)^{1/2},$$

where the shear velocity $u_* = (\tau/\rho)^{1/2}$, τ is the wind stress, ρ is water density, N is the Brunt Vaisala frequency at the base of the mixed layer, f is the Coriolis parameter and A is a constant.

Taking observed values, in our case this formulation indicates a deeper mixed layer around 20 m in the exposed zones and a shallower layer about 5 m thick in the lee (Figure 4c). The predicted mixed layer depth was roughly as observed on the western end of the section, i.e., ~ 5 m less than the pycnocline depth, but was much shallower than pycnocline depth in the lee and at the eastern end. This is to be expected since the pycnocline is being upwelled in the west, where conditions similar to those of Lentz apply, and depressed in the east, where the surface mixed layer is independent of the main pycnocline.

3.4 Water Column Response

Sections for August 3-4 and August 7-8 (Figures 5 and 6, respectively) show the strong deepening of the thermocline and pycnocline behind the island in the center of the warm region. The earlier sections (not shown) across the western half of the lee region presented similar characteristics. Figure 5 shows the pycnocline to deepen from 40 m at the ends of the line to 95 m in the center. In the section of August 7-8 (Figure 6) the pycnocline shows a similar deepening in the western half of the section but remains near 80 m in the eastern half. The warm (>22.5°C), less dense (<25.3 kg m^{-3}) surface waters of the lee were clearly seen in all the sections.

In the earlier section (Figure 5) higher salinity was found to the east in the layers above 120 m but 3 days later was found to the west (Figure 6); this is especially clear in the salinity versus density plots. Over all the sections, salinity in the upper pycnocline near the 25.5 kg m^{-3} isopycnal ranged by 0.3 practical salinity units, indicating a variety of sources for water in the lee. Geostrophic velocities relative to the deepest available data at 200 dbar indicated a northward flow component in the western half of both sections and a southward one in the eastern half. The latter introduces low-salinity water from the upwelling filament, while the northward flow could bring in saline oceanic water.

A weak deep chlorophyll maximum (DCM) showed maximum values over 0.6 mg m^{-3} at the westernmost stations in the earlier sections. Chlorophyll at the sea surface was generally < 0.1 mg m^{-3} in the lee of the island and only marginally higher in the well-mixed exposed stations. The depths of the DCM and the pycnocline were not significantly correlated. The DCM in the lee of the island occurred above the pycnocline (density anomaly ~ 25.7 - 26.0 kg m^{-3}), whereas in the exposed regions it occurred below. This is possibly a phytoplankton response to the lower light levels associated with depression of the interface but more likely reflects different phytoplankton communities with different light and nutrient histories. The eastward shift of the deeper wake structure between August 3-4 and 7-8 is again evident.

3.5 Sea Surface Temperature Imagery Sequence

Corrected SSTs from early afternoon passes of the NOAA 14 satellite show the variation of cyclonic eddy, warm lee, and cool filament between July 24 and August 7 (Plate 2). Because the NOAA 14 pass of August 7 was cloud-contaminated, the evening pass of NOAA 9 is included. Midday

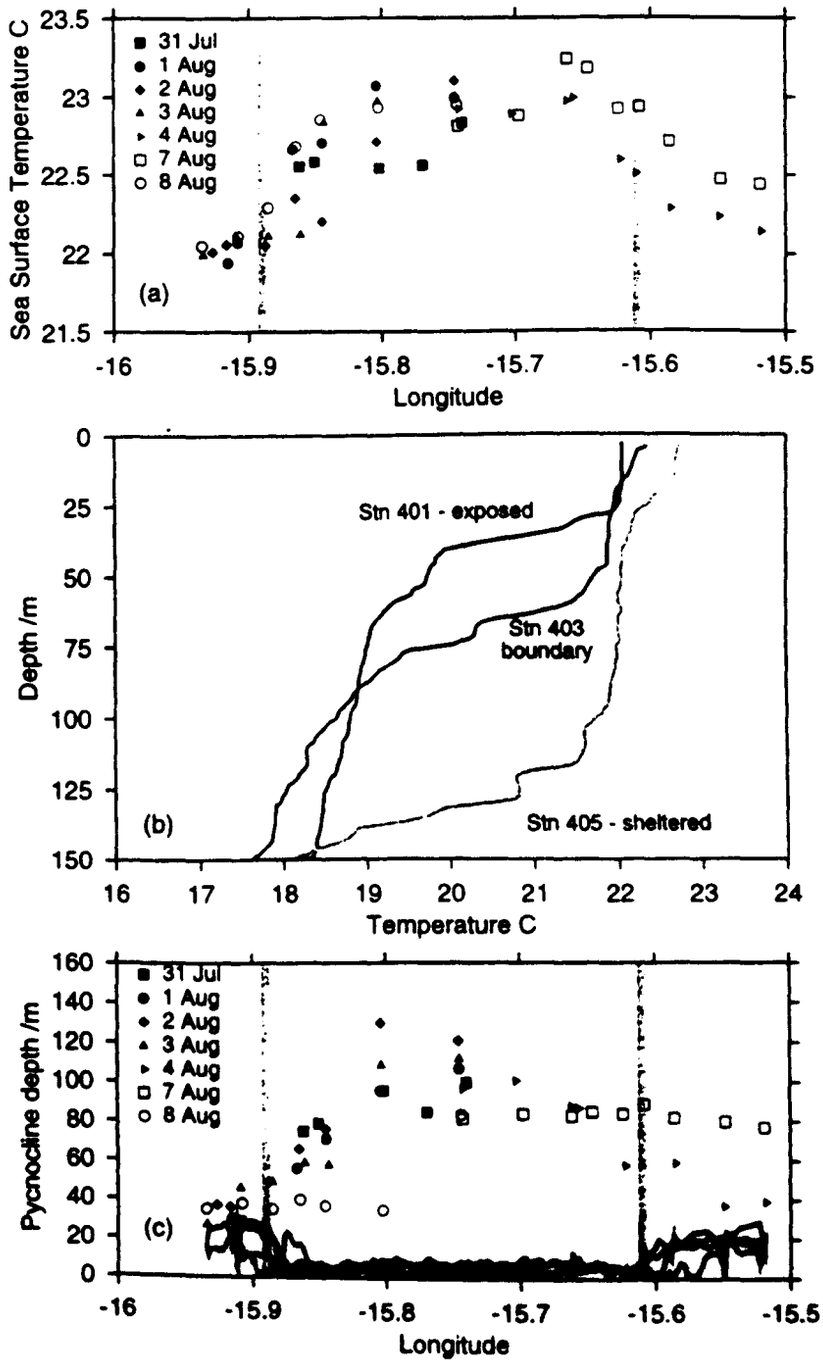

Figure 4. (a) Variation of CTD surface temperature across the lee region. The approximate position of the wind shear zone is indicated by wide vertical lines. (b) Vertical profiles of daytime temperature from the sheltered (station 405), boundary (station 403) and exposed (station 401) regions showing near-surface warming and thermocline depression in the lee. (c) Variation of pycnocline depth across the lee region. The position of the wind shear zone is indicated as in Figure 4a. The grey curves show mixed layer depth estimated from wind stress.

winds at island sites and subsampled ship winds (taken between 0800 and 1300 UT) are shown when available.

Winds at two sites in the northeast and northwest fluctuated widely in direction because of upwind topography, but most sites showed consistent speed and direction patterns. The strongest winds occurred around the end of July, when SSTs decreased noticeably. Temperatures were warmer on August 3 and 5 when winds weakened slightly. Cloud cover often obscured the northern coasts of the island, but the south coast remained cloud-free. The generally well defined warm lee was closely aligned with the predominant wind direction. Its length and overall shape were variable.

Close to the lee coast, an area of higher temperature occurred southwest of Arguineguin and a more persistent one occurred south of Punta Descojonado. On July 31, the western patch coincided with a region of null or weak shoreward winds. Slightly cooler temperatures in the center of the lee coincided with strongest shoreward winds. The eastern boundary of the lee was generally marked by a line of strong temperature contrast paralleling the east coast winds. All the

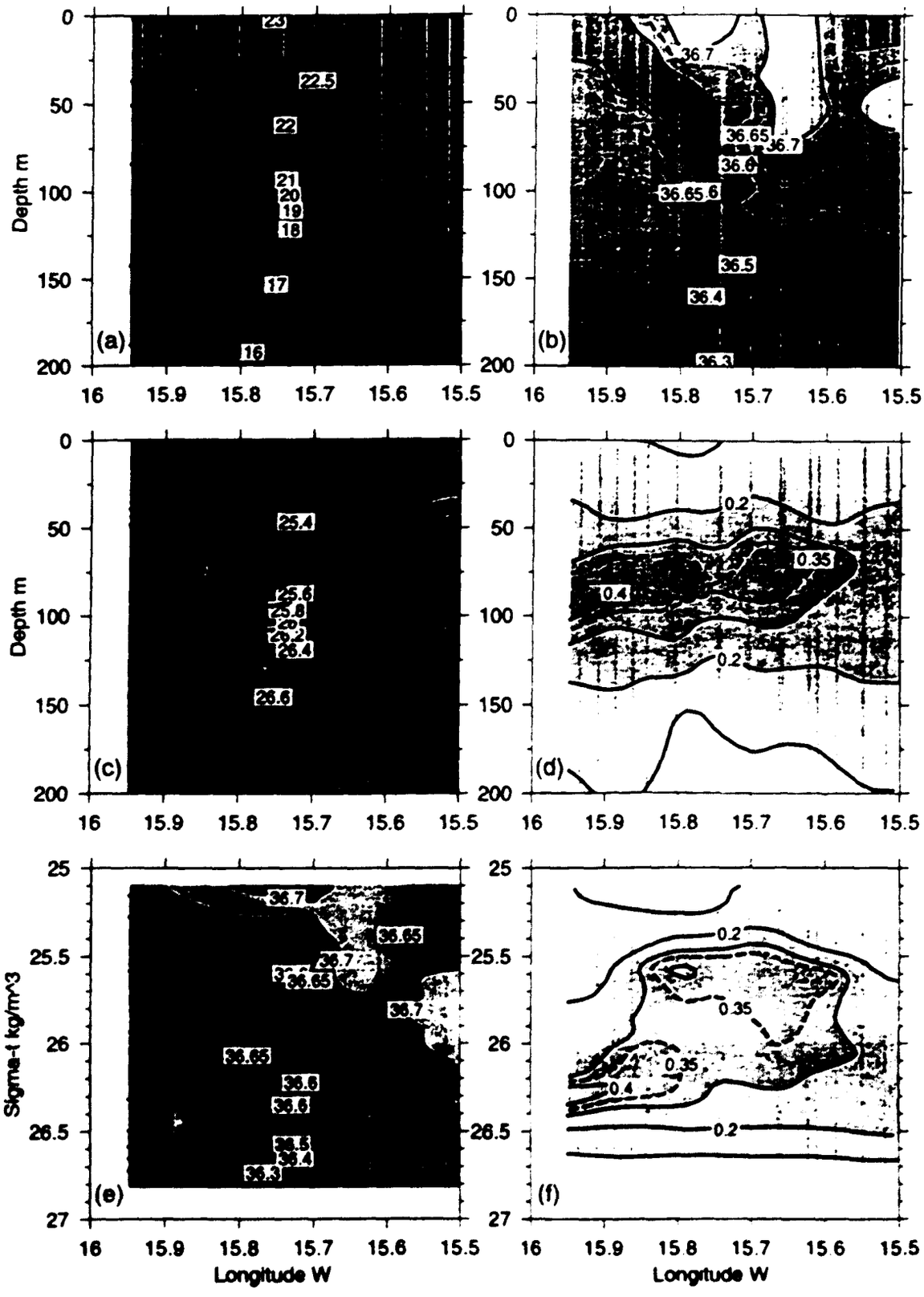

Figure 5. Depth sections of (a) temperature, (b) salinity, (c) density, and (d) chlorophyll and corresponding isopycnal sections of (e) salinity and (f) chlorophyll across the lee region made on August 3-4

images show surface waters cooler off the west of Gran Canaria than off the east, because surface Ekman transport provokes upwelling and downwelling, respectively.

The cyclonic eddy became less distinct as it moved southwestward at ~ 0.05 m s^{-1}. By August 7, when it reached the southern edge of the area shown, its surface temperature signal was virtually indistinguishable. Initially, the eddy and filament were separated by a narrow band of warmer waters from the lee and farther south, entrained around the north and east of the eddy. This band widened as the eddy moved away.

Throughout the period, two cores of cooler filament waters entered from the northwest and merged as they turned south. The southern core of cooler water was persistently stronger. Both showed variation in small-scale structure.

A sequence of images for July 25 and 26 shows the diurnal development of the surface temperature signature of the lee (Plate 3). The coolest temperatures were observed in the image just after sunrise (~0808 UT) when virtually no wake

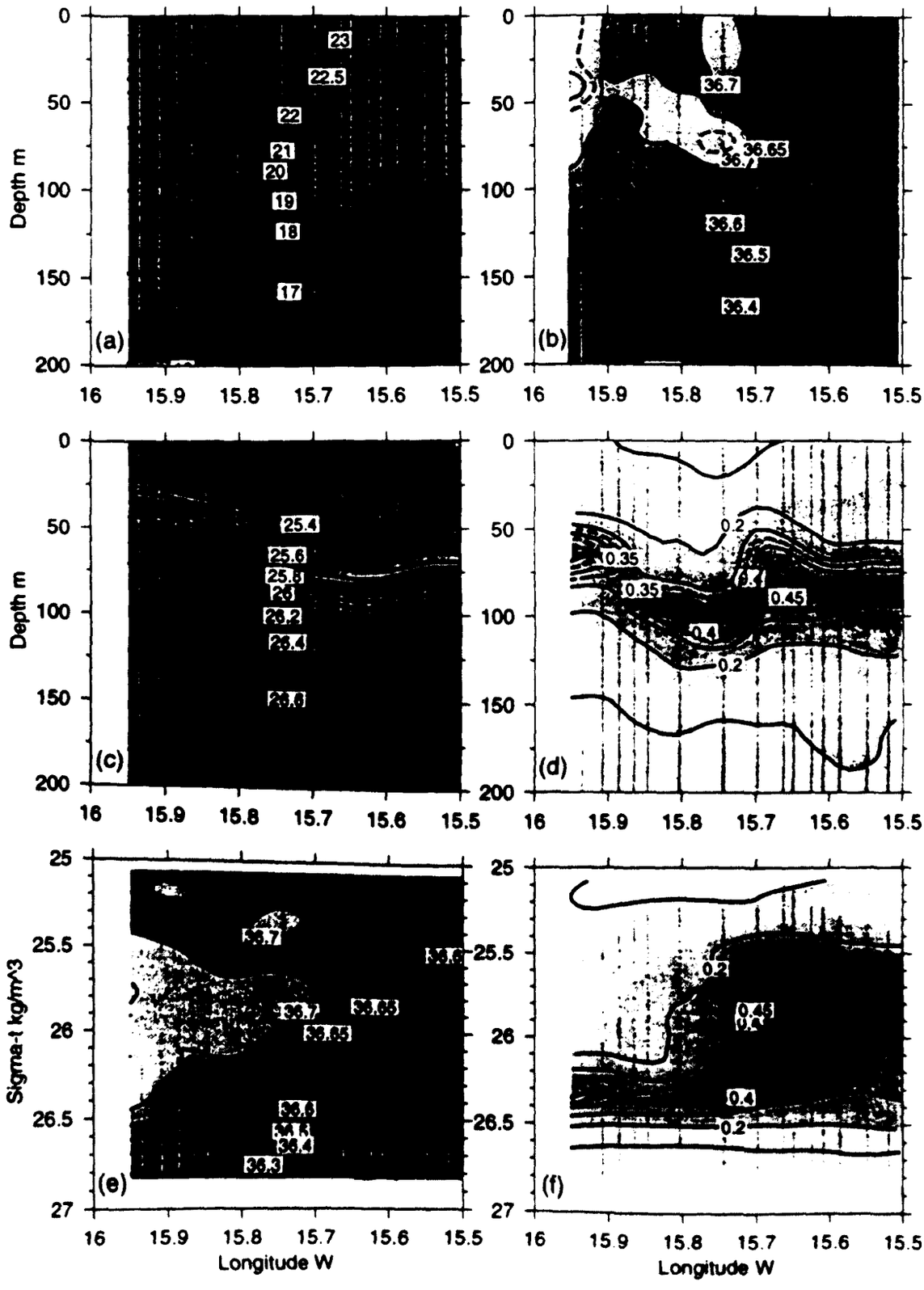

Figure 6. Depth sections of (a) temperature, (b) salinity, (c) density, and (d) chlorophyll and corresponding isopycnal sections of (e) salinity and (f) chlorophyll across the lee region made on August 7-8

anomaly was visible. By early afternoon (~1400 UT) a clearly defined wake region was established with sharp lateral boundaries. These had weakened by midevening (~2000 UT) to a diffuse anomaly that weakened gradually through the night, persisting until at least ~0300 UT on both days.

3.6 SAR and SST Features

The first pair of images (Figure 7a and 7b) depicts the SST on July 29 at 1050 UT and surface roughness 50 min later. Midday shore winds, superimposed, show the strong trades at east coast sites, weaker winds at inland elevations, and a reverse or zero flow on the lee coast. SSTs ranged between 19.5 and just over 22°C. The slightly warmer island wake extended some 60 km southwestward from Arguineguin as a narrow "tail" (TT' in Figure 7a) to intersect the tongue of warmer oceanic water entrained around the cold core eddy centered near 27.3°N, 16.3°W. Southeast of Gran Canaria, the offshore limit of the double-core upwelling filament met the warm tongue, forming a sharp temperature front and a line of strong shear (SS') between the southeastward flowing filament and the northwestward flow in the eddy. The eddy center was as cold as the filament of upwelled water.

In the corresponding SAR image (Figure 7b) structure in the surface roughness field extended several island diameters south of Gran Canaria. Unfortunately, no simultaneous in situ observations could be made to confirm identification of the offshore wind shear lines. A 3-4 km wide band of winds below the 3 m s^{-1} SAR threshold was evident near the southwest coast, where midday coastal winds registered 2-3 m s^{-1} onshore. Backscatter was strong along the anticyclonic wind shear line extending southwest from near Arguineguin (TTT'), farther west than is normally encountered. The western cyclonic shear boundary was evident as a weak contrast in the image.

In Figure 7b a series of alternating bright and dark bands, situated on the eastern side of TTT', have diffuse edges, suggesting atmospheric structures. Their eastern limit was ill defined, while the western limit was clearer in the north, where it coincided with the edge of the warm tail TT' (Figure 7a). It continued north in a curve along the eastern bound of the warmest wake waters to intersect the shore. The spacing of the banding, 2 - 5 km, was compatible with thermally forced horizontal roll vortices formed preferentially over the warm tail and extending at a small angle downwind [*LeMone*, 1973]. Given the reported inversion layer height of 800 m at Tenerife, the horizontal to vertical aspect ratio would be ~ 3:1 for such structures, as observed. However, the structures seem analogous to a shallow water ship wake, with a series of transverse waves decaying away from the disturbance point apparently near point T. Although the supporting information is meager, the structures appear to originate at the height of the inversion layer.

Another elongated bright line SS' represents a localized current shear along the temperature front between the southeastward flowing filament and the northwestward moving warm tongue entrained around the eddy. *Fu and Holt* [1983] reported similar structure in a Seasat SAR image in relation to an offshore intrusion of upwelled water off California. A similar, if weaker, bright line F could be identified near the eastern edge of the southern cold core in the filament near 27.3°N, 15.5°W, again presumably associated with localized current shear. The cyclonic eddy centered at 27.4°N, 16.3°W produced no signal in the SAR image.

In the northwest of the image (Figure 7b) a streaked appearance indicates wind rows, indicative of the predominant wind direction [*Johannessen et al.*, 1995]. This paralleled the wind direction at the exposed east coast stations and was consistent over a wide area, in agreement with surface pressure (Figure 2a) and scatterometer winds (Plate 1a). Wind rows were also seen in the southeast of the image but not in the lee, where wind direction is variable. Finally, a group of atmospheric gravity waves (GW) was identifiable near 27.7°N, 16.1°W. About eight waves of wavelength 2.5 km and crest length < 15 km were discernible in the group.

An estimate of wind speed is possible from the SAR backscatter intensity if a wind direction is known (or assumed) at each point in the image. An overall direction of 203° was taken on the basis of coastal winds, the wind row orientation, the scatterometer analysis, and daily meteorological charts. The structure of the wind field immediately downstream of the island is unknown, so these results do not strictly apply to the lee region. Estimating directions in small areas of the image from the orientation of wind rows [*Lehner et al.*, 1998], which are generally aligned with the wind, was impossible since in the lee region no defined windrows were visible. The calibrated backscatter values were averaged over 50 x 50 and subsampled at 25 pixel intervals, yielding wind speed estimates at 2.5 km resolution.

Estimated wind speed on July 29 (Figure 7c) reached 20 m s^{-1} on the eastern flank of the lee, suggesting significant enhancement. The higher values separated to either side of the wave-like features TTT', and a secondary maximum of speed occurred well downwind near 26.7°N. Minimum speeds close to 4 m s^{-1} occurred near the lee coast, with a trough of low speeds extending southwestward. Estimated speeds outside the disturbed region were ~ 14 m s^{-1}. Values were generally higher than expected but no *in situ* data at sea were available for comparison. Small local differences from the assumed wind direction do not affect the speed estimate greatly, and although values in the lee can be affected significantly by erroneous assumed direction, they would not be increased to values found outside.

Figure 7d shows the near-infrared AVHRR channel 2 (0.9 μm) from NOAA 9, taken 50 min before the ERS SAR image. This channel is sensitive to solar reflection and reveals a remarkable sun glint pattern that parallels exactly the pattern of waves seen in the SAR image (Figure 7b), confirming that they are caused by wind-induced variations of surface roughness.

The AVHRR image for the following day (Figure 8a) is from the pass at 0759 UT because of extensive cloud cover later in the day. Two hours after dawn, the warm lee was barely 1°C warmer than surrounding waters. The island winds were similar to the previous day, but the extended tail of warm water was not apparent. The strong temperature contrast between the cool upwelling filament and the warm water tongue entrained around the cyclonic eddy again formed an almost rectilinear feature (SS') oriented northwest-southeast. As before, surface waters off northwest Gran Canaria were cooler than off the east coast.

The SAR image for July 30 (Figure 8b) shows particularly clearly a wake-like feature that extends downwind almost 200 km. Dark areas close to the south coast of Gran Canaria indicate regions of wind below the threshold value of 3 m s^{-1} (confirmed by the adjacent coastal wind vectors). The calm zone was larger than on the previous day. The boundaries of the lee appear as linear features contrasting in brightness with

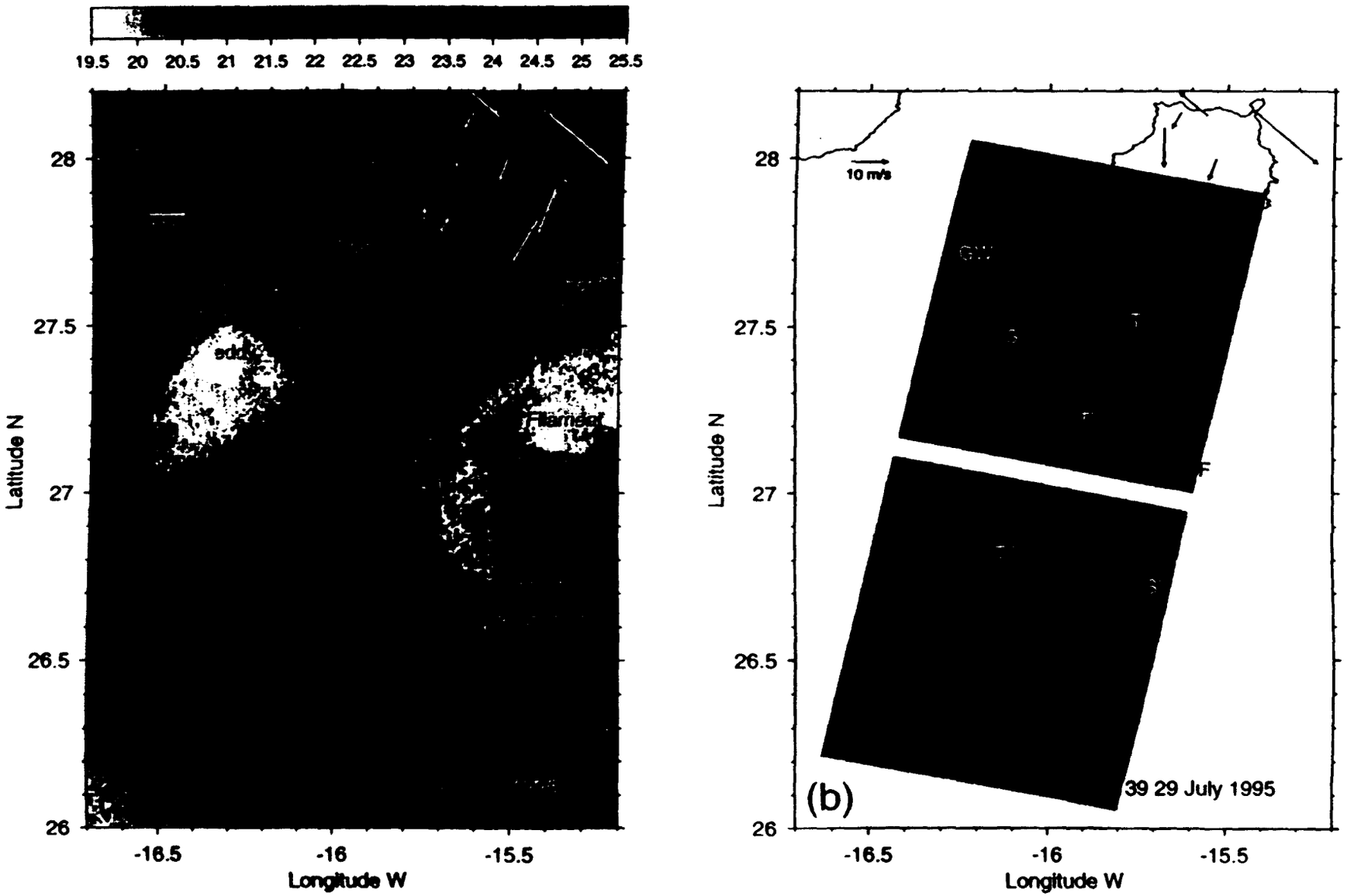

Figure 7. (a) AVHRR SST image for July 29. (b) SAR image of the same day. (c) Derived CMOD4 wind. (d) Near-infra red (channel 2) AVHRR in units of %albedo. Midday winds at shore sites are shown in Figures 7a - 7c. Labels are explained in the text.

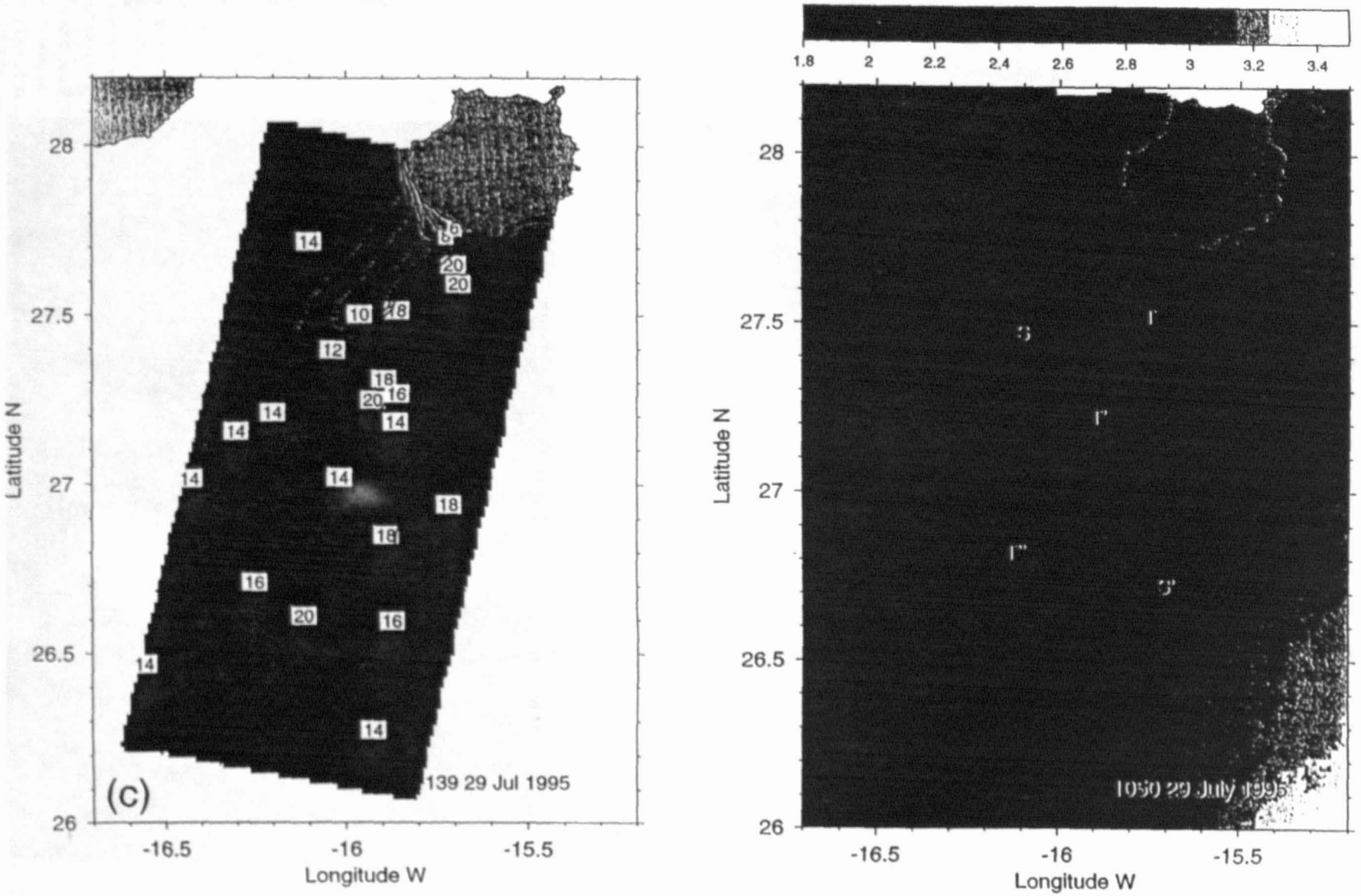

Figure 7. (continued)

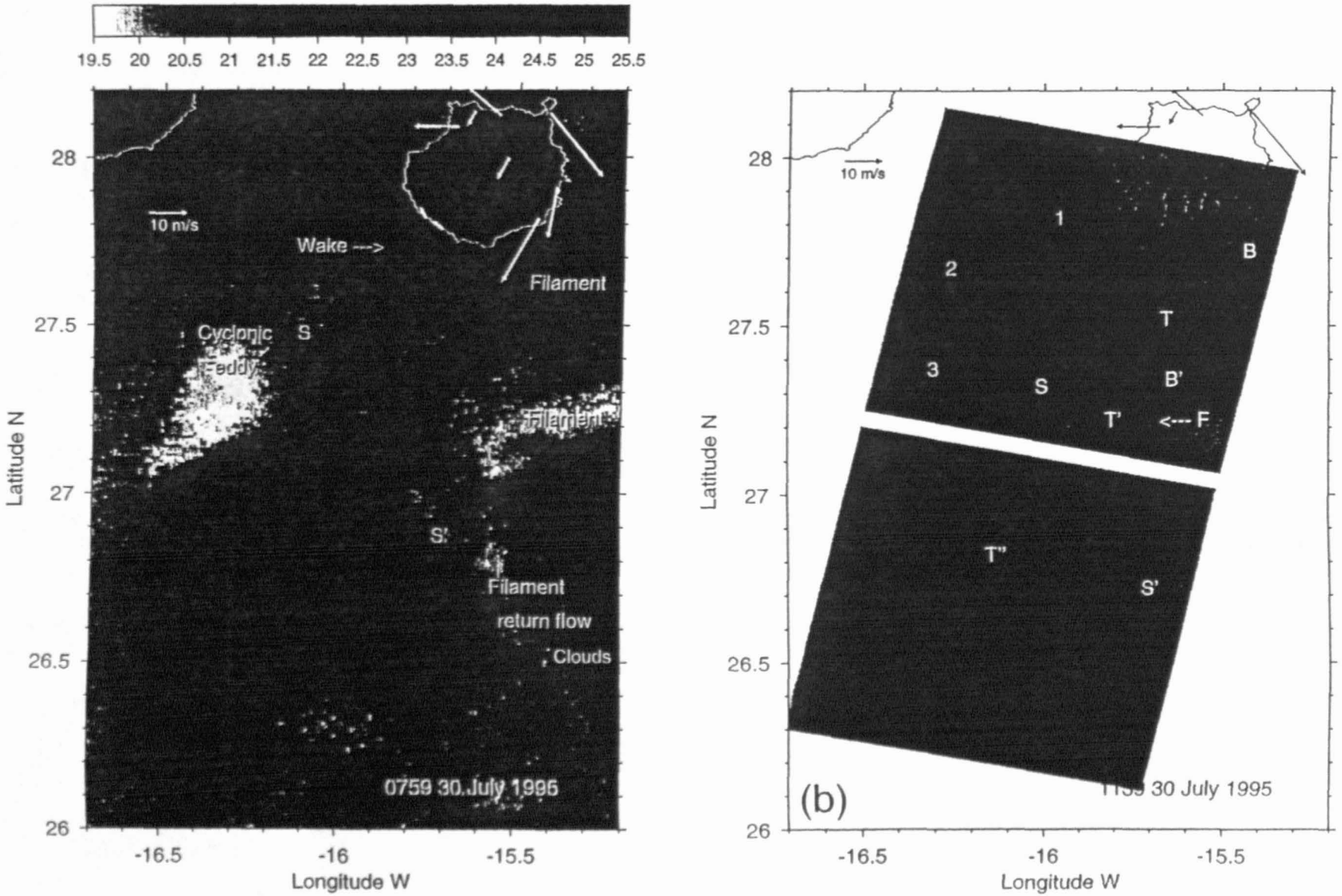

Figure 8. (a) AVHRR sea surface temperature images for July 30 .(b) SAR image same day. (c) Derived CMOD4 wind. (d) In situ wind vectors for 15 days in August 1993 from R/V *Hesperides* overlaid on speed contours from same data set. The midday winds at shore sites are shown in Figures 8a - 8c. Labels are explained in the text.

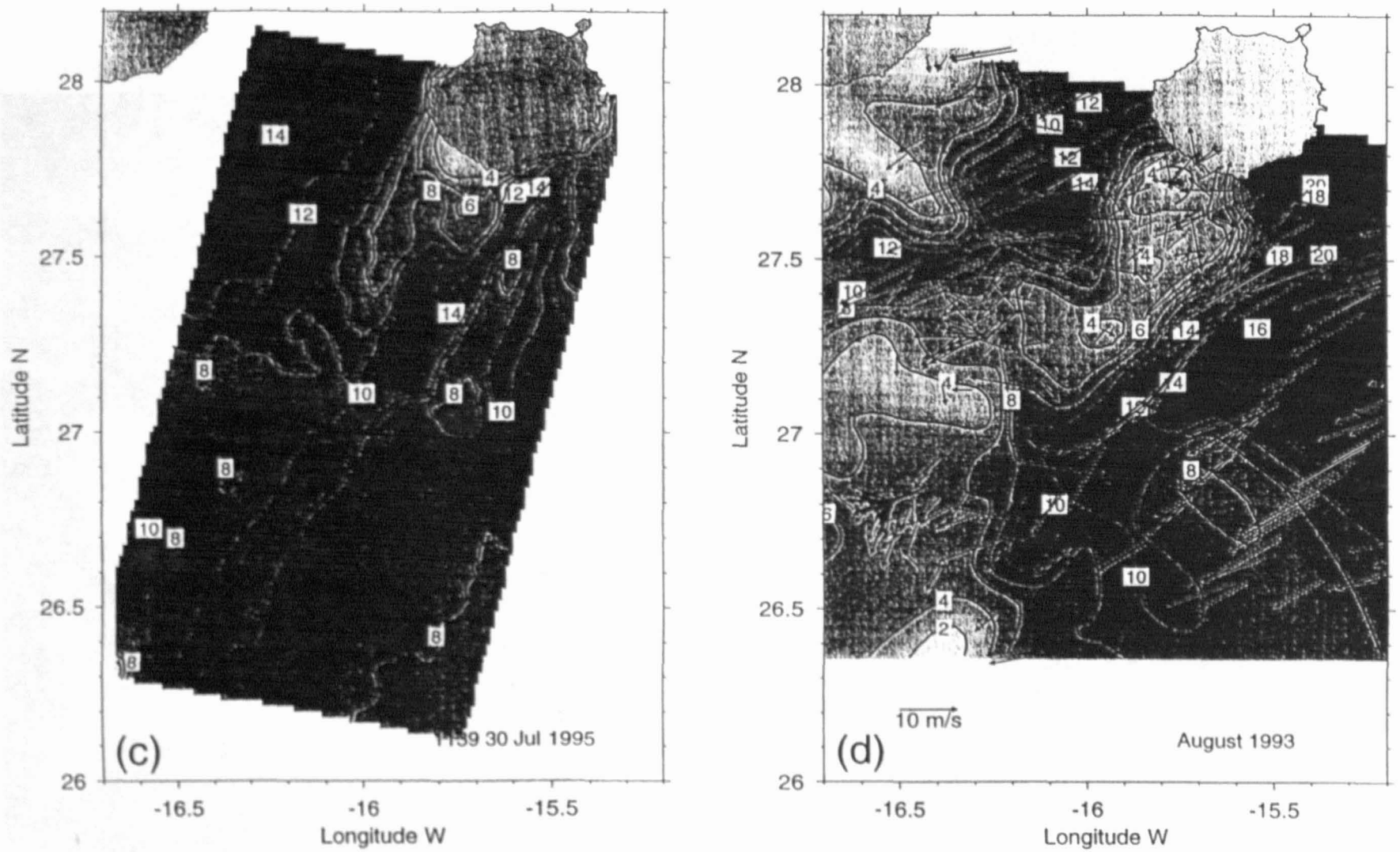

Figure 8. (continued)

surrounding areas. The eastern (anticyclonic) boundary TTT" is especially clear as a bright streak some 2 km wide and 180 km long parallel to the wind at the southeastern coast. The boundary had shifted 15-20 km eastward near the island.

The main bright boundary corresponds to the edge of the trade wind zone. About 100 km south of the island, where it intersected the current shear line SS', the orientation of the boundary changed, possibly as a result of changing atmospheric stability above the warm tongue. A weaker bright line BB', ~80 km long, diverged from the first on the southeast coast of Gran Canaria. Between the two, six darker bands parallel to the secondary front seem to be weakened examples of the wave-like structures of the previous day. BB' is likely therefore the diffuse eastern boundary. The current shear SS' had hardly moved from the previous day. A second bright line F (shown in zoom in Figure 9a) coincided with another temperature front on the western limit of the southern filament, again indicating strong horizontal shear.

The western (cyclonic) boundary, as a location of surface Ekman divergence, was less well defined but detectable as a broad, almost rectilinear feature of weak contrast. It extended southward from Punta Descojonado through S to converge with the eastern boundary near the break between SAR frames. The western half of the image shows many wind rows at separations of 2 - 4 km aligned along the predominant wind direction (close up in Figure 9b) as in the previous day's image.

Southwest of Gran Canaria, atmospheric internal wave packets (1, 2, and 3) emanate from near Punta Descojonado toward the southwest. The series is visible as several diffuse groups of lighter and darker bands oriented northwest-southeast with a crest length that is short (about 6 km) nearshore but increases with distance from the coast. The separation between the 6 - 10 diffuse crests in each group is ~ 3 km. The most offshore group is ~ 90 km southwest of the island. Group 2 is detailed in Figure 9c.

SAR wind speed estimates for July 30 (Figure 8c) were lower than the previous day, except in the northwest of the region. (The assumed direction was again 203°.) Enhanced wind speed extended some 150 km southwest along the boundary TTT", but the area of speeds near 20 m s^{-1} was small. Weaker enhancement occurred along the line BB'. The lee region was defined by winds < 10 m s^{-1} and immediately south west of the island, speeds < 3 m s^{-1} were indicated. There was some evidence of higher speeds in the lee center, reflecting the return flow seen in the in situ measurements on other days. The lee boundaries formed zones of strong wind shear despite uncertainty in wind direction within the lee.

Although there were no contemporaneous observations of ocean winds, a composite wind field measured over 15 days in August 1993 on R/V *Hesperides* (Figure 8d) shows the existence of an extended lee with weak flow counter to the trade winds. Maximum speeds measured reached the 20 m s^{-1} indicated on July 29 1995, in similar locations. Wind speeds in the northwest were also similar to the present estimates, ~ 14 m s^{-1}. Evidence of sheltering by the nearby island of Tenerife was also indicated. The 1993 wind field is not nearly, synoptic and the sparse observations limit interpretation, but the strong similarities with the SAR wind fields are encouraging.

4. Discussion

Biological enhancement around oceanic islands was established by *Doty and Ogury* [1956], but its physical causes are less well known. The role of oceanic islands in producing disturbances in the downstream current has been investigated in a number of cases. *Barkley* [1972] concluded that drifter tracks downstream of Johnson's Atoll in the Pacific North Equatorial Current were consistent with a von Karman vortex street. Other observations have indicated disturbance of the equatorial undercurrent east of the Galapagos [*White*, 1973] and production of eddies west of the Hawaiian Islands [*Patzert*, 1969; *Lumpkin*, 1998; *Flament et al.*, 1998]. *Heywood et al.* [1990] found an eddy trapped behind Aldabra Atoll in the Indian Ocean South Equatorial Current. Frequent production of, principally, cyclonic eddies south of Gran Canaria has been reported by *Arístegui et al.* [1994, 1997]. Theoretical and laboratory studies [e.g. *Boyer and Davis*, 1982; *Bearman*, 1984; *Sangrá*, 1995; *Heywood et al.*, 1996] show the Earth's rotation delays eddy shedding to higher Reynolds numbers and makes the vortex street asymmetrical by enhancing cyclonic eddies in the Northern Hemisphere. For islands like Aldabra Atoll, with low topographic relief, downstream flow effects clearly result from the direct disturbance of the current field by the island. This is less obvious for mountainous islands, where strong wind regimes may be perturbed to provide a second source of disturbance to the oceanic flow [*Patzert*, 1969].

In the present case, an extended and variable region sheltered from the trade winds is present behind Gran Canaria

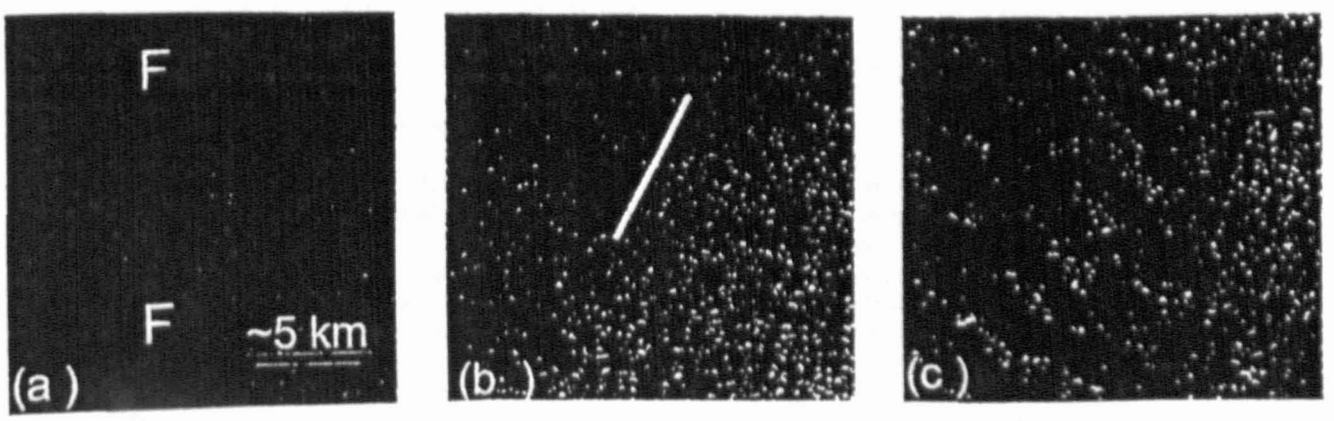

Figure 9. Enhanced close ups of SAR image of July 30 1995: (a) Shear front F, (b) wind rows in NW of image (the line is oriented at 205°) and (c) group 2 of the lee waves. The approximate distance scale is shown in Figure 9a.

(and the other Canary Islands). This lee was evident in AVHRR imagery as a warm surface temperature anomaly due to the dominance of surface heating over wind mixing. The extent of the temperature gradients that bound the lee suggests that the lines of intense wind shear persisted some 100 km or more downwind. The direct observations indicated that a weak return breeze cools the center of the lee, separating two temperature maxima beneath the areas of weakest wind. This is compatible with the presence of counterrotating wind eddies behind the island.

Chopra [1973], from mesoscale patterns in stratocumulus cloud, concluded that atmospheric vortices of 10-20 km radius were shed from alternate flanks of Gran Canaria at roughly 8 hour intervals, as in a von Karman vortex street. These structures formed a wake 60 km wide and 600 km long as they drifted downwind at some 70% of the ambient wind speed. Viscous forces made individual vortices expand, weaken, and disappear after about 30 hours. The observed shift in position of the eastern lee boundary between July 29 and 30 may result from atmospheric eddy shedding, although the wind direction could not be determined from the SAR images.

Atmospheric phenomena associated with the lee region, including mountain lee waves, convective rolls, and strong shears in the atmospheric boundary layer, are revealed by the SAR images. The atmospheric internal gravity (or mountain lee) waves arise near Punta La Aldea, the westernmost part of the island, where the winds strike shear cliffs rising hundreds of meters from the sea. Cap clouds frequently form as the wind passes over the 400 m high coastal peaks before descending to cross a 5 km wide valley and rising again over the 600 m high ridges between La Aldea and Descojonado (Figure 1). No similar wave-like features are seen on the east of the island, where a wide coastal plain slopes gradually into the island interior. Internal waves in the relatively low inversion layer are associated with fluctuations in wind velocity extending down to sea level [*Vachon et al.*, 1995]. Beneath troughs, increased wind velocity and sea surface roughness produces brighter bands in the SAR image, while under troughs, decreased velocity produces darker bands.

Zones of temperature contrast and current shear were also visible in the SAR images even though the radar intensity arises mainly from Bragg backscatter by the ~3 cm wind-driven capillary waves. When the 10 m wind is below a threshold value of ~ 3 m s^{-1}, there is no appreciable return signal [*Donelan and Pierson*, 1987], as observed in the nearshore lee. *Gower* [1994] reported that for winds between 2 and 5 m s^{-1}, surface slicks indicating patterns of current convergence may appear, but that at higher wind speeds, current-related features are obscured by the wind signal. *Beal et al.* [1997] identified Gulf Stream current features in SAR images when wind was < 10 m s^{-1}. In our case the shear line (SS' in Figs 7 and 8) was evident in winds up to 15 m s^{-1}, suggestive of unusually strong shear.

Current gradients across shear and convergence zones may interact with short surface gravity waves, produce refraction of long surface waves, cause wave breaking, and enhance surface roughness [*Robinson*, 1985]. The anticyclonic wind shear line was particularly evident in the SAR image of July 30 (Figure 8). This zone is visible at sea as a region of intense white capping and chop and a locus of convergence. The enhanced roughness may result in overestimation of the CMOD4 wind speed on the lee boundary. The air-sea temperature difference may reduce the accuracy of the speed estimates [*Apel*, 1994], especially in the lee where the sea surface temperature is higher. *Beal et al.* [1997] found consistent backscatter differences caused by spatial variability of the marine atmospheric boundary layer stability.

Close to the island, a warm surface wake in the wind lee persisted throughout the observation period, strengthening during the day and weakening at night. Outside the lee, surface heat input is distributed through a well-mixed surface layer, while inside, near-surface stratification develops. Nighttime convective overturning distributes the day time input over the shallower layers. The CTD sections showed upwelling of the pycnocline as expected close to the cyclonic wind shear line, but the greatest pycnocline depression was displaced toward the center of the lee in one section. This may be caused by an approach of the filament closer to the island. Since density surfaces in the upwelled filament waters are shallower than in oceanic waters, the filament would tend to counteract downwelling on the anticyclonic boundary of the lee. The position of maximum deepening therefore varies with the strength and position of the filament and with the wind. Variability of the filament has been reported by *Aristegui et al.* [1997] who have shown significant effects on the local biology. Salinity in the island lee results from the interplay between the upwelling filament and oceanic background flow. The salinity field seems to be separated into two halves across the wake, corresponding to waters from different sources, including the filament.

What is the relative importance of Ekman pumping and flow disturbance in producing the eddies? A well-defined wind lee is evident even in the several week composite wind field, so that mean Ekman forcing must be significant despite any short term variability caused by vortex shedding. On the lee boundaries, horizontal wind shear of 15 m s^{-1} per 2 km produces upwelling (or downwelling) as strong as that seen at the African coast; upwelling occurs on the exposed western coasts of the islands. The Ekman transport caused by 10 (15) m s^{-1} wind with a drag coefficient of 1.3×10^{-3} at 28°N is 1.9 (4.3) m^2 s^{-1}, which would cause upwelling (or downwelling) of 11 (24) m d^{-1}, assuming a constant rate over a Rossby radius of 15 km. Because of the lack of a solid boundary downstream, this upwelling or downwelling of the pycnocline will produce eddies on a length scale of the lee.

Even intermittent wind forcing, as in the Gulf of Tehuantepec, can produce energetic ocean eddies [*Barton et al.*, 1993; *Trasviña et al.*, 1995]. There, winds channelled through a mountain pass extend as a jet over the Pacific Ocean and spin up ocean eddies. Since there is no significant background current in the area, the Ekman pumping is the direct cause of the eddies. Even in the presence of currents, wind forcing has been reported to spin up eddies north of Hawaii [*Patzert*, 1969; *Lumpkin*, 1998]. *Chopra* [1973] stressed that vertical transfer of momentum to the ocean would weaken any vortices below the atmospheric inversion too quickly to form a vortex street. He interpreted *Patzert's* [1969] conclusion that the Hawaiian ocean eddies were wind driven as the explanation for the absence of an atmospheric vortex street, although subsequent observations show one to be present at times.

Here the existence of a cyclonic oceanic eddy downstream and a variable lee in the wind is clearly documented. The eddy, generated close to the island, moved southwestward at 5 km d^{-1} as its surface temperature signal weakened over the course of 12 days. Mutually exclusive ocean eddies and atmospheric vortices could, of course, exist at different times.

Wind downstream of Gran Canaria is persistent and strong so may be expected to produce or at least enhance oceanic eddies.

This area of filament-eddy exchanges provides an excellent laboratory: the repeatability and steadiness of the trade wind regime provides continuous forcing of coastal upwelling and filaments, while eddies reportedly spin off from Gran Canaria during most of the year. Both cyclonic and anticyclonic eddies have been observed south of the island; indeed, recent drifter observations have followed an anticyclone for 7 months as it drifted away from the island (P.Sangrá, *personal communication*, 1999). Interaction between eddies, filaments, and the island chain give rise to strong horizontal gradients and to lateral exchange of properties within a small geographical area. These can be of considerable significance for distribution of, say, larval distributions [*Rodríguez et al.*, 1999] or zooplankton [*Hernández-León*, 1988]. However, there have been no observations of eddy generation: details of their development, eventual fate, and how they interact with filaments remain poorly known.

Acknowledgments. The field work was carried out during the European Institute for Advanced Studies in Oceanography 1995 Summer School on Upwelling Systems held at the Universidad de Las Palmas de Gran Canaria funded by the Commission of the European Union and the United Nations Education and Science Organisation. The R/V *Bocaina* was made available courtesy of the Consejería de Agricultura y Pesca of the Canary Islands. We thank the crew and all those students who participated onboard. Shore winds were provided by the Spanish Instituto Nacional de Meteorología. ERS scatterometer data were kindly provided by Yves Quilfen (IFREMER). We thank Vincent Kerbaol (IFREMER) and Helen Dodds (UW) for assistance with the SAR wind speed calculations and Laurent Latché (UW) for processing the SLA data. E. G. Mitchelson-Jacob and E. D. Barton were Investigators in project AO2.UK131and P.Flament was Investigator in project AO2.USA198 of the European Space Agency, which provided the ERS-1 and 2 data.

References

Apel, J., An improved model of the ocean surface wave vector spectrum and its effects on radar backscatter, *J. Geophys. Res.*, *99*, 16,269-16,291, 1994.

Arístegui, J., P. Sangrá, S. Hernández-Leon, M. Cantón, A. Hernández-Guerra and J.L. Kerling, Island-induced eddies in the Canary Islands, *Deep Sea Res., Part I*, *41*, 1509-1525, 1994.

Arístegui, J., et al., The influence of island-generated eddies on chlorophyll distribution: A study of mesoscale variation around Gran Canaria, *Deep Sea Res., Part I*, *44*, 71-96, 1997.

Barkley, R.A., Johnston Atoll's wake, *J. Mar. Res.*, *30*, 201-216, 1972.

Barton, E.D., M.L. Argote, J. Brown, P.M. Kosro, M. Lavín, J.M. Robles, R.L. Smith, A. Trasviña, and H.S. Vélez, Supersquirt: Dynamics of the Gulf of Tehuantepec, Mexico, *Oceanography*, *6*, 23-30, 1993.

Barton E.D., et al., The transition zone of the Canary Current upwelling region, *Prog. Oceanogr.*, *41*, 455-504, 1998.

Beal, R.C., V.N. Kudryavtsev, D.R. Thompson, S.A. Grodsky, D.G. Tilley, V.A. Dulov, and H.C. Graber, The influence of the marine atmospheric boundary layer on ERS-1 synthetic aperture radar imagery of the Gulf Stream, *J. Geophys. Res.*, *102*, 5799-5814, 1997.

Bearman, P.W., Vortex shedding from oscillating bluff bodies, *Ann. Rev. Fluid Mech.*, *16*, 195-222, 1984.

Boyer, D.L., and P.A. Davis, Flow past a circular cylinder on a β-plane, *Philos. Trans. R. Soc. London, Ser. A*, *322*, 213-241, 1982.

Chopra K.P., Atmospheric and oceanic flow problems introduced by islands, *Adv. Geophys.*, *16*, 297-421, 1973.

Columbus, C., *The Log of Christopher Columbus*, translated from the Spanish by R.H. Fuson, 252 pp., Ashford, Southampton, England, U.K., 1987.

Donelan, M.A., and W.J. Pierson Jr., Radar scattering and equilibrium ranges in wind generated waves with application to scatterometry, *J. Geophys. Res.*, *92*, 4971-5029, 1987.

Doty, M.S., and M. Oguri, The island mass effect, *J. Cons. Perm. Int. Explor. Mer.*, *22*, 33-37, 1956.

Flament, P., J. Firing, M. Sawyer, and C. Trefois, Amplitude and horizontal structure of a large diurnal sea surface warming event during the coastal ocean dynamics experiment, *J. Phys. Oceanogr.*, *24*, 124-139, 1994.

Flament, P., S.C. Kennan, C.Lumpkin, and E.D. Stroup, The Atlas of Hawai'i, in *The Ocean*, edited by S. Juvik and J. Juvik, pp. 82-86, University of Hawai'i Press, Honolulu, 1998.

Fleming, H.E., and M.L. Hill, An objective procedure for detecting and correcting errors in geophysical data, 1., One-Dimensional applications, *J. Geophys. Res.*, *87*, 7312-7324, 1982.

Fu, L.-L., and B. Holt, Some examples of detection of oceanic mesoscale eddies by the Seasat Synthetic Aperture Radar, *J. Geophys. Res.*, *88*, 1844-1852, 1983.

Gower, J.F.R., Mapping coastal currents with SAR using naturally occurring surface slick patterns, Eur. Space Agency Spec. Publ., *ESA SP-361*, 415-418, 1994.

Hernández-Guerra, A., Estructuras oceanográficas observadas en las aguas que rodean las Islas Canarias mediante escenas de los sensores AVHRR y CZCS, Ph.D. thesis, 198 pp., Univ. de Las Palmas de Gran Canaria, Las Palmas de Gran Canaria, Spain, 1990.

Hernández-Guerra, A., J. Arístegui, M. Cantón, and L. Nykjaer, Phytoplankton pigment patterns in the Canary Islands as determined using Coastal Zone Color Scanner data, *Int. J. Remote Sens.*, *14*, 1431-1437, 1993.

Hernández-León, S., Gradients of mesozooplankton biomass and ETS activity in the wind-shear area as evidence of an island mass effect in the Canary Island waters, *J. Plankton Res.*, *10*, 1141-1154, 1988.

Heywood, K.J., E.D. Barton ,and J.H. Simpson, The effects of flow disturbance by an oceanic island, *J. Mar. Res.*, *18*, 55-73, 1990.

Heywood, K.J., D.P. Stevens, and G.R Bigg, Eddy formation behind the tropical island of Aldabra , *Deep-Sea Res., Part I*, *43*, 555-578,1996.

Johannessen, J.A., R.A. Shuchman, and O.M. Johannessen, Synthetic aperture radar on ERS-1, in *Oceanographic Applications of Remote Sensing*, edited by M. Ikeda and F.W. Dobson, pp. 27-44, CRC Press, Boca Raton, Fla., 1995.

Koch, S.E., M. DesJardins, and P.J. Kocin, An interactive Barnes objective map analysis scheme for use with satellite and conventional data, *J. Clim. Appl. Meteorol.*, *22*, 1487-1503, 1983.

Laur, H., P. Bally, P. Meadows, J. Sanchez, B. Schaettler, and E. Lopinto, Deviation of the Backscattering Coefficient σ_0 in ESA ERS PRI products, *ESA Doc. ES-TN-RS-PM-HL09, Vol. 2*, 4, pp.87, Eur. Space Agency, Paris, 1997.

Lehner, S., J. Horstmann, W. Koch, and W. Rosenthal, Mesoscale wind measurements using recalibrated ERS SAR images, *J. Geophys. Res.*, *103*, 7847-7856, 1998.

LeMone, M.A., The structure and dynamics of horizontal roll vortices in the planetary boundary layer, *J. Atmos. Sci.*, *30*, 1077-1091, 1973.

Lentz, S.J., The surface boundary layer in coastal upwelling regions, *J. Phys. Oceanogr.*, *22*, 1517-1539, 1992.

Le Traon, P.Y., P. Gaspar, F. Bouyssel, and H. Makhmara, Using

TOPEX/Poseidon data to enhance ERS-1 data. *J. Atmos. Oceanic Technol., 12*, 161-170, 1995.

Lumpkin, C.F., Eddies and currents of the Hawaiian Islands, Ph.D. thesis, 281 pp., Univ. of Hawaii at Manoa, Honolulu, 1998.

McClain, E.P., W. Pichel, and C. Walton, Comparative performance of AVHRR-based multichannel sea surface temperatures, *J. Geophys. Res., 90*, 11,587-11,601, 1985.

Meadows, P., and P.A. Wright, ERS-1 SAR analogue to digital converter saturation, Paper presented at CEOS SAR Calibration Workshop Comm. On Earth Obs. Sat., Ann Arbor, Michigan, Sept. 28-30,1994.

Molina, R., and F.L. Laatzen, Hidrografía en la región Canaria: Campaña Canarias I, *Bol. Inst. Esp. Oceanogr., 5*, 71-86, 1989.

Molina, R., J.M. Cabanas, and F.L. Laatzen, Corrientes e hidrografía en la región Canaria: Campaña Canaria 9205, *Bol. Inst. Esp. Oceanogr.*, 121, 43-52, 1998.

Navarro-Pérez, E., Physical oceanography of the Canary current: Short term, seasonal and interannual variability, Ph.D. thesis, Univ. of Wales, Bangor, 1996.

Navarro-Pérez, E., and E.D. Barton, The physical structure of an upwelling filament off the north-west African coast during August 1993, *S. Afr. J. Mar. Sci., 19*, 61-74, 1998.

Naya, A., *Meteorología Superior*, 546 pp., Espasa-Calpe, Madrid, 1984.

Patzert, W.C., Eddies in Hawaiian waters, *Rep. HIG-69-8*, 51 pp., Hawaii Inst. of Geophys., University of Hawaii at Manoa, Honolulu, 1969.

Pollard, R., P.B. Rhines, and R.O.R.Y. Thompson, The deepening of the wind-mixed layer, *Geophys. Fluid Dyn., 3*, 381-404, 1973.

Robinson, I.S., *Satellite Oceanography: An Introduction for Oceanographers and Remote-Sensing Scientists*, 455 pp., Ellis-Horwood, New York, 1985.

Rodríguez, J.M., S. Hernández-León, and E.D. Barton, Mesoscale distribution of fish larvae in relation to an upwelling filament off northwest Africa, *Deep Sea Res., Part I*, 46, 1969-1984, 1999.

Sangrá, P., Perturbación de un flujo geofísico por un obstáculo: aplicación a la isla de Gran Canaria, Ph.D. thesis, 200 pp., Univ. of Las Palmas de Gran Canaria, Las Palmas de Gran Canaria, Spain, 1995.

Saunders, R.W., and K.T. Kriebel, An improved method for detecting clear sky and cloudy radiances from AVHRR data, *Int. J. Remote Sensing*, 9, 123-150, 1988.

Stoffelen, A.D., and D.L.T. Anderson, Scatterometer data interpretation: Estimation and validation of the transfer function CMOD4, *J. Geophys. Res., 102*, 5767-5780, 1997.

Trasviña, A., E.D. Barton, J. Brown, H.S. Velez, P.M. Kosro, and R.L. Smith, Offshore wind forcing in the Gulf of Tehuantepec, Mexico: the asymmetric circulation, *J. Geophys. Res., 100*, 20,649-20,663, 1995.

Vachon, P.W., J.A. Johannessen and D.P. Browne, ERS-1 SAR Images of atmospheric gravity waves, *IEEE Trans. Geosci. Remote Sens., 33*, 1014-1025, 1995.

Van Camp, L., L. Nykjaer, E. Mittelstaedt, and P. Schlittenhardt, Upwelling and boundary circulation off northwest Africa as depicted by infrared and visible satellite observations, *Prog. Oceanogr., 26*, 357-402, 1991.

White, W.B., An oceanic wake in the undercurrent downstream from the Galapagos Archipelago, *J. Phys. Oceanogr., 3*, 156-161, 1973. 1992.

J. Aristegui and G. Basterretxea, Facultad de Ciencias del Mar, Universidad de Las Palmas de Gran Canaria, 35017, Las Palmas de Gran Canaria, Spain. (javier.aristegui@biologia.ulpgc.es; gotzon.basterretxea@songoku.uib.es)

E.D. Barton (corresponding author), School of Ocean Sciences, University of Wales, Bangor LL59 5 EY, Wales, U.K. (e.d.barton@sos.bangor.ac.uk)

P. Flament, Department of Oceanography, University of Hawaii at Manoa, Honolulu, HI 96822. (pierre@hawaii.edu)

F. Herrera, Laboratorio de Comunicaciones y TeledeteccíOn, Universidad de La Laguna, Tenerife, Spain (fherrera@ull.es terascan@ull.es)

B. Jones and E. G. Mitchelson-Jacob, Unit for Coastal and Estuarine Studies, University of Wales, Bangor LL59 5EY, Wales, U.K. (b.jones@bangor.ac.uk;e g.mitchelson-jacob@bangor.ac.uk)

(Received March 18, 1999; revised November 17, 1999; accepted December 22, 1999.)

MARINE ECOLOGY
PROGRESS SERIES

Reprint

Inter-Research
Nordbünte 23, D-21385 Oldendorf/Luhe, Germany
Tel: (+49) 4132 7127 Fax: (+49) 4132 8883
E-mail: ir@int-res.com Internet: www.int-res.com

Vol. 197: 27–40, 2000 | MARINE ECOLOGY PROGRESS SERIES
Mar Ecol Prog Ser | Published May 12

Mesoscale variability in phytoplankton biomass distribution and photosynthetic parameters in the Canary-NW African coastal transition zone

Gotzon Basterretxea*, Javier Arístegui

Facultad de Ciencias del Mar, Universidad de Las Palmas de Gran Canaria, 35017 Las Palmas de Gran Canaria, Spain

ABSTRACT: Pigment distribution and photosynthesis versus irradiance (P-E) responses in the mixed layer (ML) and in the chlorophyll maximum (CM) were examined in the coastal transition zone (CTZ) between the NW African coastal upwelling and the Canary Islands during August 1993. The sampling included 2 island-generated eddies in the lee of the archipelago and an upwelling filament from the African continental shelf, entrained around a cyclonic eddy about 100 km width. Chlorophyll *a* and P-E parameters (α, P_m) showed regional differences reflecting changes in the water column structure and phytoplankton species composition. The deep CM shoaled from ~100 to ~10 m as the African shelf was approached, and there was a clear offshore-onshore transition in the vertically integrated chlorophyll distribution and P-E responses related to the upwelling front. CM oceanic samples presented high α (0.020 to 0.042 mg C mg^{-1} chl h^{-1} [μmol m^{-2} s^{-1}]$^{-1}$) and photoinhibition, indicating adaptation to low irradiance. Differences between CM and ML in P-E responses decreased in the vicinity of the upwelling until they eventually became indistinguishable in a well-mixed station on the continental shelf. Island-generated eddies affected mainly the productivity and chlorophyll distributions at the deep CM. Nutrient input in the eddy center resulted in an increase of α in the CM to the level of the upwelling samples (~0.053 mg C mg^{-1} chl h^{-1} [μmol m^{-2} s^{-1}]$^{-1}$). On the basis of the mesoscale variability in the physical structure of the water column and the vertical distribution of chlorophyll, the CTZ was divided into 4 subregions with characteristic photosynthetic parameters. Average integrated production in these areas varied from ~100 mg C m^{-2} d^{-1} in the most oligotrophic subregion to more than 5000 mg C m^{-2} d^{-1} in the upwelling zone. The range of variation in the photosynthetic parameters in this CTZ was of the same magnitude as ranges observed in basin-scale studies of the Atlantic. Integrated production estimates are also in the lower and higher extremes of the observed values in the ocean. Our results highlight the importance of addressing the variability of the photosynthetic parameters in coastal upwelling-open ocean transition zones in order to model primary production at regional scales.

KEY WORDS: Phytoplankton · Chlorophyll · Primary production · Coastal transition zone · Filaments · Eddies

INTRODUCTION

Within the context of global climate change and the role of the ocean as a carbon dioxide sink, one of the main goals of biological oceanography has been the description and understanding of algal carbon fixation at regional and global scales. From the efforts of Koblents-Mishke (1983), based on ecosystem classifications and ship-based primary production measurements, to the present models based on biogeographical divisions and satellite-obtained ocean color data (e.g. Platt et al. 1988, Longhurst 1995, Sathyendranath et al. 1995), the technique for monitoring phytoplankton photosynthesis has significantly improved. Nevertheless, in global production models, 2 components have changed little: (1) the necessity for *in situ* observations and (2) the division of the ocean into compartments dependent on a variety of criteria

*E-mail: gotzon.basterretxea@biologia.ulpgc.es

Satellites provide information about sea-surface color fields from which near-surface chlorophyll fields are derived (Gordon et al. 1980). But most complex bio-optical models also require knowledge about depth-resolved optical properties of the water column, and some chlorophyll-specific parameters defining the photoadaptative response of phytoplankton: P_m, α, β (Platt et al. 1991, Sathyendranath et al. 1995), the absorption cross section (a^*) and quantum yield of phytoplankton (Kiefer & Mitchell 1983, Bidigare et al. 1987, 1992), or the optimal assimilation efficiency (P_{opt}) (Behrenfeld & Falkowski 1997a) for the biomass-to-production conversion.

An alternative approach is the use of relationships between sea surface temperature (SST) and nitrate concentration and the utilization of nitrate uptake to calculate the f-ratio (allochthonous nitrate-based production to total production ratio) as in Eppley & Peterson (1979) and Sathyendranath et al. (1991). However, this relationship is not useful for most warm oligotrophic water masses where surface concentrations of nitrate are undetectable (Balch & Byrne 1994).

The complexity of eco-physiological responses in marine systems renders difficult the computation of universally valid relationships between environmental and primary production changes. Consequently, the ocean has generally been divided into relatively homogeneous ecological domains (oceanic-coastal waters, polar-temperate-subtropical-tropical waters, etc.) where a general parameterization can be accomplished. Behrenfeld & Falkowski (1997b), in a review of primary production models, concluded that differences in estimates of global annual primary production are due to differences in biomass fields and in the selection of the photoadaptative variables but not to the model itself. Hence, a good estimation of primary production requires appropriate selection of the parameters for each region. Moreover, at smaller scales, the presence of different growth and loss characteristics in phytoplankton populations which are spatially heterogeneous means that the approach used at large scales can here lead to ambiguities (Marra 1980). Specific algorithms that account for local peculiarities (i.e. north-south, east-west gradients) or heterogeneities (recurrent or permanent mesoscale structures) should therefore be developed. Finally, links with contiguous regions to avoid excessively fragmented production maps would be desirable.

Coastal transition zones (CTZ) are boundary regions between subtropical gyres and coastal upwelling regions where intense mesoscale variability takes place (Kosro et al. 1991, Strub et al. 1991, Haynes et al. 1993, Barton et al. 1998). The productivity of these areas is uncertain since their intense variability has frequently not been considered. The development of satellite imagery in the last decades has provided evidence that the boundary between coastal upwelling and open ocean systems is highly irregular. Cold filaments have often been reported in the Canary Current (La Violette 1974, Van Camp et al. 1991, Hernández-Guerra et al. 1993) and other eastern boundary currents (Davis 1985, Flament et al. 1985, Kelly 1985, Shannon et al. 1985, Huyer & Kosro 1987, Strub et al. 1991, Swenson et al. 1992). These structures transport cold upwelled water from the shelf into the ocean, and their return flow introduces warm offshore waters to the nearshore zone (Mooers & Robinson 1984). Nutrient distributions and plankton biomass and production are also affected (Traganza et al. 1980, Abbott & Zion 1985, Abbott et al. 1990, Hood et al. 1991). Most observations have led to speculation that filaments act as vehicles to link rich shelf waters with open ocean oligotrophic waters (Mooers & Robinson 1984, Rienecker et al. 1985). Nevertheless, uncertainties remain about the origin of filaments and their contribution to seaward transport of coastal water.

Because filaments are relatively persistent and recurrent (e.g. Haynes et al. 1993), they may be especially important to the nutrient and carbon fluxes of coastal transition zones. The horizontal exchange of organic material and nutrients between filament and surrounding offshore waters could sustain high production rates outside the upwelling zone, or, alternatively, nutrient upwelling generated by the filament dynamics could significantly contribute to the offshore productivity (Jones et al. 1991).

In the present paper we examine the spatial and vertical distribution of phytoplankton biomass and photosynthesis versus irradiance (P-E) parameters, in a region including the Canary Islands and the nearby NW African Upwelling (NWAU). The transition from the rich coastal upwelling waters to the offshore oligotrophic system covers a region with distinct but closely linked physical and biological characteristics. Vertical stability promoted by thermal stratification, and consequently vertical transport of nutrients, varies from offshore to shelf waters but also varies in relation to mesoscale structures. Recent work has provided evidence of the importance of local mesoscale processes in phytoplankton biomass distribution and production in the Canary Islands (e.g. Arístegui et al. 1997). Knowledge of the effects of these mesoscale forcing functions on biomass accumulation and production is of critical importance when estimating regional and global carbon fixation rates.

METHODS

Field sampling. The observations reported in this paper were carried out during 4 to 27 August 1993 on

board BIO 'Hespérides'. The area under study covered the transition zone between the NWAU and offshore waters of the Canarian Archipelago. A transect across the islands to the African shelf was followed by a mesoscale survey of a coastal filament entrained around a cyclonic eddy and an adjacent island-generated eddy (Fig. 1). The eddy position was traced with lagrangian drifters (Barton et al. 1998) and sampled twice (C and D, Fig. 1) over an interval of 5 d. At the center of the eddy (Stn 174) a 24 h sampling was carried out.

CTD data were obtained at each station using a Sea Bird SBE-911 plus probe mounted on a 24 bottle rosette equipped with 12 l Niskin bottles. A Sea Tech fluorometer was attached to the system. Data from the CTD sensors were calibrated against reversible thermometer readings and salinity analyses (Autosal 2000) of discrete samples. The *in situ* fluorometer was calibrated with samples collected at 6 to 8 depths within the upper 100 m of the water column. For this, 500 ml samples were filtered through Whatman GF/F fiberglass filters and extracted overnight in 10 ml of 90% acetone at 4°C in the dark. For size fractionation, the same volume was filtered through 2 µm Millipore polycarbonate filters. Fluorescence before and after acidification was measured with a Turner Designs bench fluorometer (Holm-Hansen et al. 1965), calibrated with pure chlorophyll *a* (Sigma Chemical Corp.). Underwater scalar photosynthetically available radiation (PAR) profiles were measured using a QSP-200 sensor (Biospherical) and a QSR-240 sensor for on deck referencing.

Chlorophyll transport was calculated from ADCP records (see Barton et al. 1998) as in Jones et al. (1991). To calculate the transport J, the flux over an area centered on the grid point i,j, was integrated:

$$J = \sum_{i,j} J_{i,j}$$

$$J_{i,j} = \bar{v}_{i,j} C_{i,j} L_x L_z$$

where $\bar{v}_{i,j}$ = velocity perpendicular to a transect plane at the grid point; $C_{i,j}$ = concentration of chlorophyll at grid point i,j; L_x, L_z = length of the box around grid point i,j in the horizontal and vertical directions, respectively.

Primary production. Samples for primary production experiments were taken at 2 depths generally corresponding to the mixed layer (ML) and to the chlorophyll maximum (CM). All production stations were sampled around local noon to avoid diel variations of photosynthetic parameters (MacCaull & Platt 1977). P-E curves were performed in incubators containing 23 culture flasks (80 ml), where a light gradient up to ~1900 µmol m^{-2} s^{-1} was created using a halogen lamp as a light source. Neutral density filters were used to attenuate the light intensity in the incubator. Light in each bottle was measured with a quantum scalar irradiance meter QSL-100 (Biospherical Co.), and 7 to 14 µCi of ^{14}C-labeled sodium bicarbonate solution was added to each bottle. *In situ* temperatures were reproduced inside the incubator with a cooling bath to within ± 0.1°C. The added activity was estimated at the beginning of the incubation by counting 1 ml of solution in a vial with Protosol (NEN) and scintillation

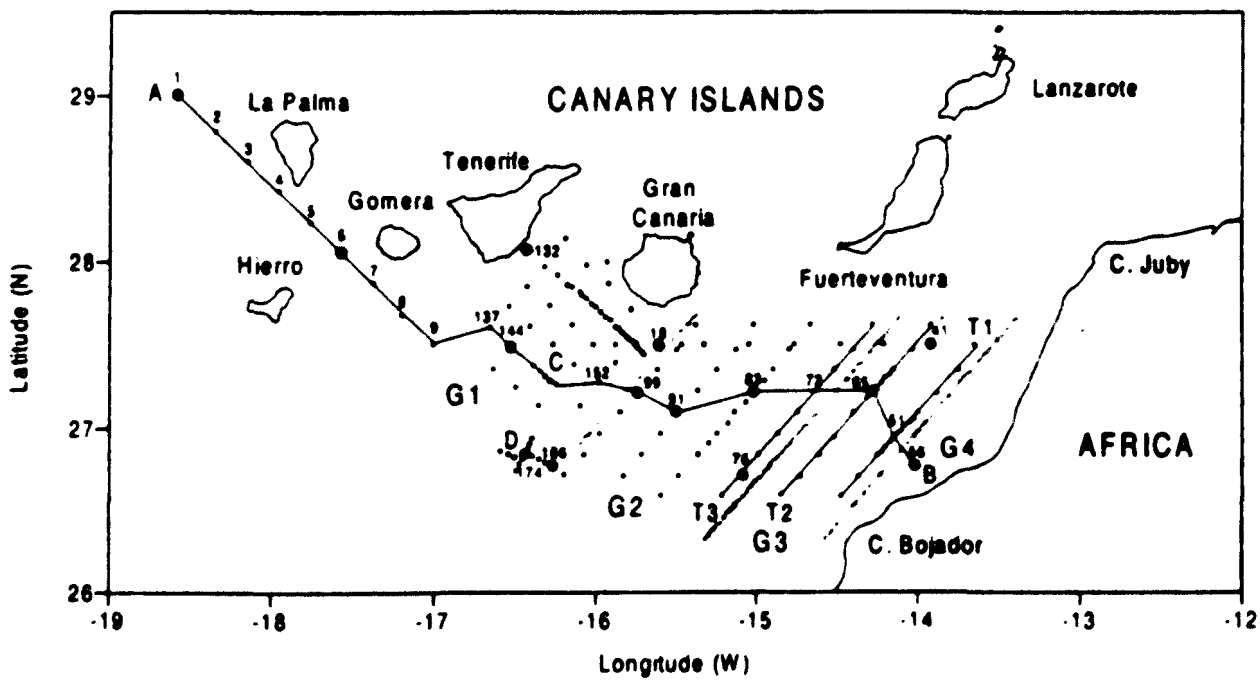

Fig. 1. Map of stations C and D mark the position of an island-generated eddy in 2 surveys A to B marks the position of the transect represented in Fig. 3 T1, T2 and T3 are the transects for which chlorophyll transport was calculated (Table 1) The region was divided into zones G1, G2, G3 and G4 for primary production estimations

cocktail. After 3 h of incubation, samples were filtered using low vacuum pressure (<0.3 bar) onto glass fiber filters (Whatman GF/F, 25 mm) and acidified with 1 ml of 2 N HCl for ~18 h to drive off inorganic carbon. Radioactivity was counted on board in a Beckman scintillation counter using Aquasol-II cocktail. An external standard was used for quench correction. Dark fixation was subtracted from illuminated bottle counts.

Chlorophyll-specific photosynthetic parameters α, P_m and β were fitted to standardized production values by non-linear regression fitting of the expression by Platt et al. (1980):

$$P(E) = P_s(1 - e^{(-\alpha E/P_s)})(e^{(\beta E/P_s)})$$

where $P(E)$ (mg C mg^{-1} chl h^{-1}) is the instantaneous production rate normalized to chlorophyll at irradiance E (µmol m^{-2} s^{-1}), α is the initial slope of the P-E curve at limiting light levels (mg C mg^{-1} chl h^{-1} [µmol m^{-2} s^{-1}]$^{-1}$), β is a parameter to characterize photoinhibition (mg C mg^{-1} chl h^{-1} [µmol m^{-2} s^{-1}]$^{-1}$), and P_s is the potentially maximum light-saturated rate of photosynthesis under conditions of no photoinhibition. In the absence of photoinhibition this expression can be reduced to the equation of Webb et al. (1974):

$$P(E) = P_m(1 - e^{(-\alpha E/P_m)})$$

where P_m and P_s can be related by the expression after Platt et al. (1980).

$$P_m = P_s(\alpha/\alpha + \beta)(\beta/\alpha+\beta)^{\beta/\alpha}$$

Integrated production calculations. Daily depth-integrated production rates (0 to 100 m) were estimated using measured light attenuation coefficients, surface P-E parameters and chlorophyll data for each station. Daily light variation was calculated assuming a sinusoidal variation of the measured midday surface irradiance. Production estimates based on 2 P-E curves (ML and CM) were performed assuming that the surface parameters were constant throughout the ML and decreased or increased linearly from the thermocline to the CM. No correction was made for diel variations of photosynthetic parameters since variations observed in the only diel study were unlikely to be representative of changes at every station.

As most chlorophyll profiles showed subsurface maxima, integrated production values were calculated assuming a non-uniform biomass profile. Hence the data were used to calculate a Gaussian curve from which parameters were derived for calculation of biomass at any depth (z):

$$B_z = B_0 + \frac{h}{\sigma\sqrt{2\pi}} \exp\left[-\frac{1}{2}\left(\frac{z - z_m}{\sigma}\right)^2\right]$$

where B_0 is the baseline pigment concentration (mg m^{-3}), z_m is the depth of the chlorophyll maximum (m), σ the width of the peak (m) and $h/(\sigma\sqrt{2\pi})$ is the height of the peak (h units are mg m^{-2}) measured from the baseline (Platt et al. 1991).

The light profile was calculated as follows: maximum photon flux at noon on the sea surface was obtained from averaged on deck records. Surface irradiance was assumed to vary as a sine function over the day. Losses of irradiance by reflectance at the sea surface were calculated from the values of Austin (1974) for 4 m s^{-1} winds. Light at depth z was obtained from $E_z = E_{z-1}\exp(-K\Delta z)$, where the average light attenuation coefficient K (m^{-1}) was computed from *in situ* measurements. Finally daily-integrated production values (P_{int}) were obtained by double integration over day-length and depth.

RESULTS

Hydrographic structure and distribution of phytoplankton biomass

The general hydrographic pattern during the cruise has been thoroughly described in Barton et al. (1998) and Navarro-Pérez & Barton (1998). An upwelling filament was situated between Cabo Juby and Cabo Bojador extending about 150 km seaward from the continental shelf, reaching the vicinity of Gran Canaria. At its offshore limit, the filament was entrained around a wide oval-shaped cyclonic eddy with its major axis aligned with the prevailing current. At depths below the mixed layer, the eddy presented a clear signal of low temperatures (Fig. 2).

Southwest of Gran Canaria, the signal of a smaller cold-core eddy was also evident. The eddy drifted southwestward at a speed of about 0.1 m s^{-1} (Barton 1994b) with a trajectory and position consistent with previous descriptions of island-generated eddies in the area (Arístegui et al. 1994).

Chlorophyll concentrations ranged from about 0.05 mg m^{-3} in the oceanic areas to more than 3 mg m^{-3} over the African shelf. A map of integrated (1 to 100 m) chlorophyll distribution (Fig. 2) reveals highest values over the continental shelf in the upwelling zone but rapidly decreasing in the offshore direction. Low chlorophyll values appear in the center of the filament eddy, while a localized maximum was observed on its southern flank (see 'Discussion').

With the aim of quantifying the importance of the filament as a mechanism of offshore transport of phytoplankton biomass, we calculated the chlorophyll transport based on ADCP records (Barton et al. 1998, Navarro-Perez & Barton 1998) across Transects T1, T2 and T3 (Fig. 1) as in Jones et al. (1991). Although the biomass signal along the jet rapidly disappeared, a net

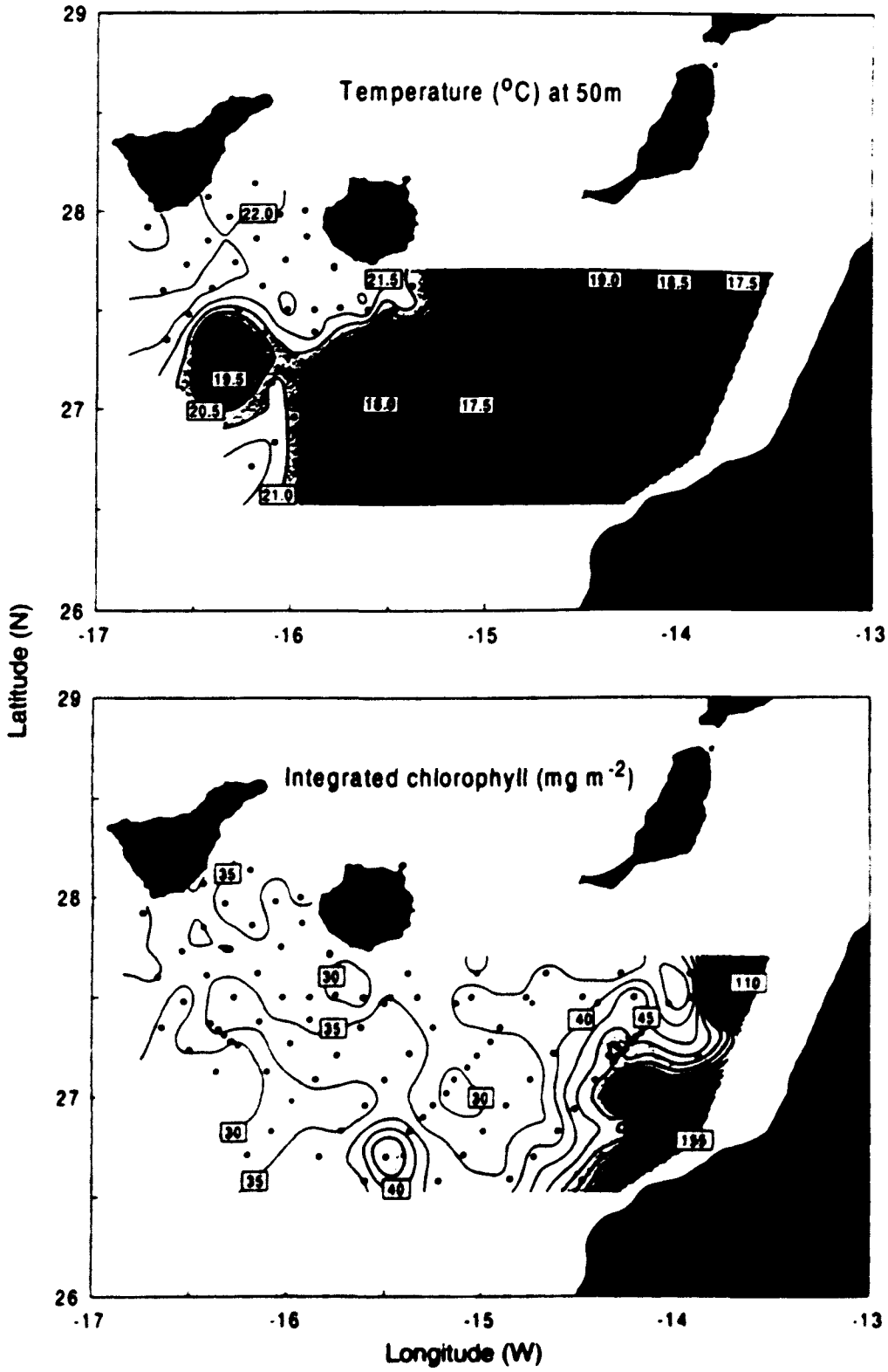

Fig. 2. Maps of temperature at 50 m depth (upper panel) and integrated chlorophyll (lower panel). Notice the presence of 2 cold-core eddies in the map of temperature. The larger one is associated with the upwelling filament and the smaller with Gran Canaria

seaward transport was expected in the section nearest to shore, where both current intensity and biomass are higher. Nevertheless, results show (Table 1) that even in the surface layer (0 to 50 m), where the signal of the filament is stronger, net transport is consistently shorewards.

A transect across and south of the islands (Fig. 3a) shows high variability downstream of the archipelago

Table 1. Chlorophyll transport (g s^{-1}) across Transects T1, T2 and T3

Transect	Depth range (m)	Seaward	Shoreward	Difference
T1	0–50	38	96	-57
	0–100	181	531	-350
T2	0–50	135	403	-268
	0–100	307	608	-301
T3	0–50	45	94	-49
	0–100	79	227	-148

Surface temperatures in the surface layer increase from 17.5°C on the African shelf to 22°C offshore. The upper part of the water column on the continental shelf is well mixed, while a sharp thermocline, progressively deeper, appears westwards. This trend is disrupted by the presence of mesoscale features leeward of the islands. Two temperature domes, presumably corresponding to 2 cold-core eddies, are observed southwest of the islands of La Gomera and Gran Canaria. The latter eddy is more intense (>50 m uplift) and exaggerated by the steep isothermal decline on its western side. This isoline deepening is caused by an adjacent anticyclonic structure observed in AVHRR images in the vicinity of Tenerife (Barton et al. 1998). West of La Palma (Stn 3) a third dome affecting the upper 80 m is also observed. The deep CM shoals in a west-east direction from 90 to 110 m at the westernmost stations to 10 m over the continental shelf. Intense doming due to eddies produces the elevation of the deep CM, as seen in the periphery of the eddy of Gran Canaria. This effect has been extensively discussed by Arístegui et al. (1997).

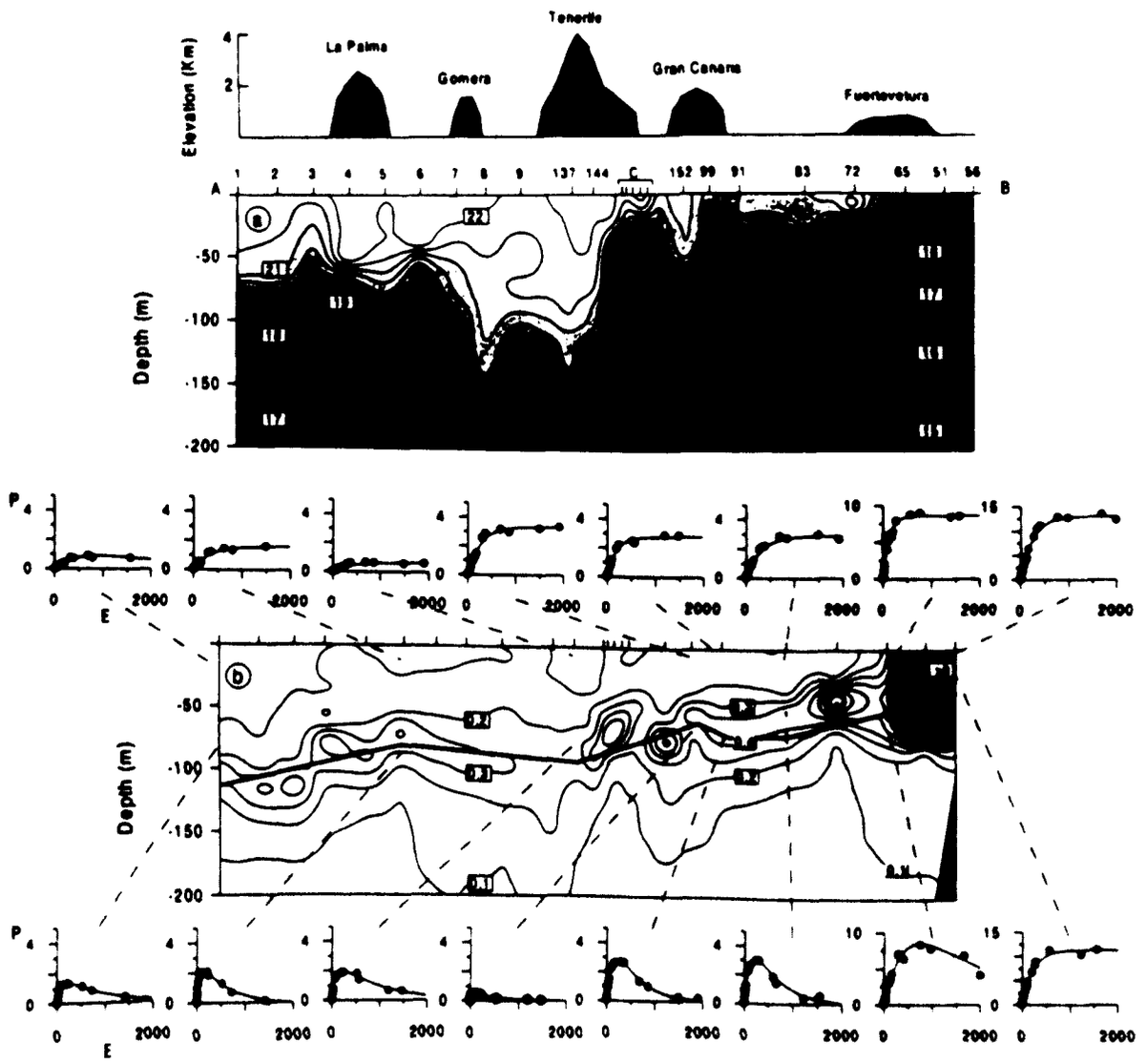

Fig. 3. Contour plots of temperature (°C, middle panel, a) and chlorophyll (mg m^{-3}; lower panels, b) along Transect A-B (dashed lines indicate the location and depth of P-E experiments; grey line marks the depth of 1% surface irradiance). Axes for P-E curves are P (mg C mg^{-1} chl a h^{-1}) and E (µmol m^{-2} s^{-1}). The position of the islands has been sketched as a reference (upper panel)

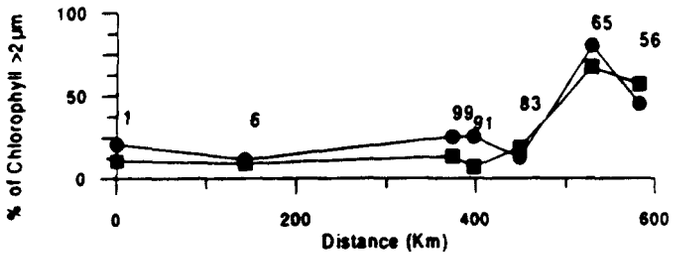

Fig. 4. Percentage of chlorophyll *a* >2 µm in a W-E transect in the mixed layer (●) and in the chlorophyll maximum (■)

Although the upwelling filament and its terminal eddy extend 100 km offshore to Stn 99, high surface chlorophyll values (>1 mg m^{-2}) are restricted to the stations in the upwelling area. Stn 65 is placed in the boundary between high-pigment-content upwelled waters and waters in the filament where values higher than those offshore are encountered only in the deep CM. A shift in the community structure also occurs at this point. Size fractionation of chlorophyll reveals picoplankton as the dominant size fraction outside the upwelling, accounting for 75 to 88% of the total biomass (Fig. 4). This percentage dramatically changes in upwelled waters and particularly in the front between both water masses (Stn 65) where large cells (>2 µm) dominate (80%). At this station a shallow thermocline (23 m depth) is already visible.

Primary production

P-E response curves along Transect A-B (Fig. 3b, Table 2) display a clear offshore-onshore transition. Two trends in the phytoplankton light response are particularly clear across the CTZ: (1) there is an increase in the magnitude of the P-E parameters as the nutrient-rich upwelling waters are approached and (2) the photosynthetic responses in the ML and CM become progressively alike as mixing increases towards the coastal upwelling. ML and CM parameters for the station on the continental shelf (Stn 56), where nutrient concentrations are high (almost 4 µM at 10 m), are similar and do not present significant photoinhibition. Both parameters are amongst the highest measured (average P_m and α, 12.11 ± 0.9 mg C mg^{-1} chl h^{-1} and 0.052 mg C mg^{-1} chl h^{-1} [µmol m^{-2} s^{-1}]$^{-1}$, respectively). By contrast, in open ocean waters differences between ML and CM parameters increase. Most CM samples exhibit higher α values and photoinhibition, indicating enhanced photosynthetic efficiency and adaptation to low irradiances in deep phytoplankton assemblages. The light adaptation parameter E_k (P_m/α) averages 267 ± 72 and 93 ± 49 µmol m^{-2} s^{-1} in the ML and CM, respectively. Of particular interest are the parameters at Stns 76 and 166 (Table 2). The former is located in the southern boundary of the filament. A high assimilation number (11.4 mg C mg^{-1} chl h^{-1}) was measured in the ML at this station, while at the deep CM, P_m is closer to the values observed in the rest of the filament structure. Conversely Stn 166, located in the island-generated eddy, shows anomalous high photosynthetic values in the CM sample (P_s = 6.94 mg C mg^{-1} chl h^{-1} and α = 0.52 mg C mg^{-1} chl h^{-1} [µmol m^{-2} s^{-1}]$^{-1}$). Similar α values in CM samples were measured only in the cyclonic eddy southwest of La Gomera (Stn 6) and over the African shelf (Stn 56). Nitrate concentrations at the subsurface sampling depth at these 3 stations were above detectable levels (>0.5 µM), an indication of nutrient-rich water upwelling or nutricline uplifting.

P-E parameters estimated for the ML at the 24 h station in the center of the eddy (Stn 174) displayed similar midday values (α = 0.008 mg C mg^{-1} chl h^{-1} [µmol m^{-2} s^{-1}]$^{-1}$ and P_m = 2.88 mg C mg^{-1} chl h^{-1}) to the nearby Stn 166, placed in a more marginal zone. There was a significant diurnal variation in light-saturated and light-limited photosynthesis (CV = 0.54 and 0.31), with maximum rates close to midday, but α presented

Table 2. P-E curve parameters α (mg C mg^{-1} chl h^{-1} [µmol m^{-2} s^{-1}]$^{-1}$), P_s (mg C mg^{-1} chl h^{-1}), β (mg C mg^{-1} chl h^{-1} [µmol m^{-2} s^{-1}]$^{-1}$), P_m (mg C mg^{-1} chl h^{-1}) and sampling depth (m)

Stn	Depth	α	P_s	β	P_m
1	20	0.003	2.61	0.0017	
6	15	0.005			1.62
18	15	0.008			1.75
41	10	0.015			4.16
56	3	0.053			13.02
65	20	0.075			9.08
76	10	0.012	11.42	0.0071	
83	10	0.011			3.05
91	10	0.016			2.89
99	10	0.014			3.53
132	10	0.009	5.30	0.0025	
144	10	0.003			0.68
166	10	0.007			2.81
1	80	0.023	1.93	0.0020	
6	80	0.055	3.11	0.0053	
18	80	0.020	2.27	0.0025	
41	30	0.027	5.81	0.0047	
56	20	0.052			11.21
65	40	0.035	8.72	0.0105	
76	40	0.034	5.51	0.0047	
83	50	0.042	5.87	0.0106	
91	70	0.035	5.87	0.0109	
99	70	0.020	0.60	0.0012	
132	60	0.023	3.85	0.0013	
144	75	0.032	2.82	0.0026	
166	60	0.052	6.94	0.0106	

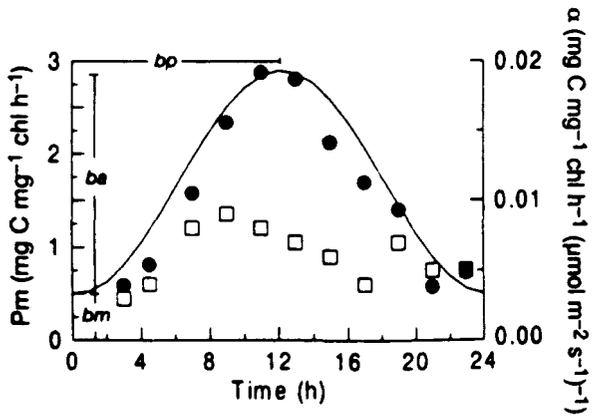

Fig. 5. Plots of P_m (●) and α (□) over time for a diel cycle at Stn 174. A sine curve

$$P_m(t) = b_m + b_a 2^{-n}[1 + \cos(2\pi/24)(t - b_p)]^n$$

(MacCaull & Platt 1977) for n = 1 has been overlaid as a reference

some random oscillations (Fig. 5). Nevertheless, these variations should be carefully interpreted since there is evidence that prolonged (>1 h) incubations may be biased by photoadaptative responses occurring on time scales of the same order or shorter than the incubation time that result in P-E variability (Lewis & Smith 1983).

With the aim of attaining general parameters to be used in a regional production model, we have grouped the stations where P-E experiments were carried out into 4 groups, according to the thermal structure of the water column and to the vertical distribution of phytoplankton biomass (Fig. 6). G1 includes the stations representative of offshore conditions with a deep CM around 100 m depth. This distribution is typical of warm offshore regions (Venrick et al. 1973, Herbland & Voituriez 1979, Cullen & Eppley 1981). Stations in the offshore extension of the filament or in the island-generated eddies (Stns 6 and 166) are included in G2. The latter present a thermocline structure similar to the waters of the filament although surface temperatures (>22°C) are in the range of offshore waters. G3 and G4 include stations in the upwelling front and on the continental shelf. Stn 76 shares characteristics with G2 and G3. Although it is far from the shelf, the structure of the water column, the vertical pigment distribution and the temperature-salinity characteristics at this location (Fig. 7) make it conform most to G3. Nevertheless, some other characteristics like the percentage of cells >2 μm (13% at Stn 76 and 49% at Stn 41) or the relation between the 1% light depth, deep CM

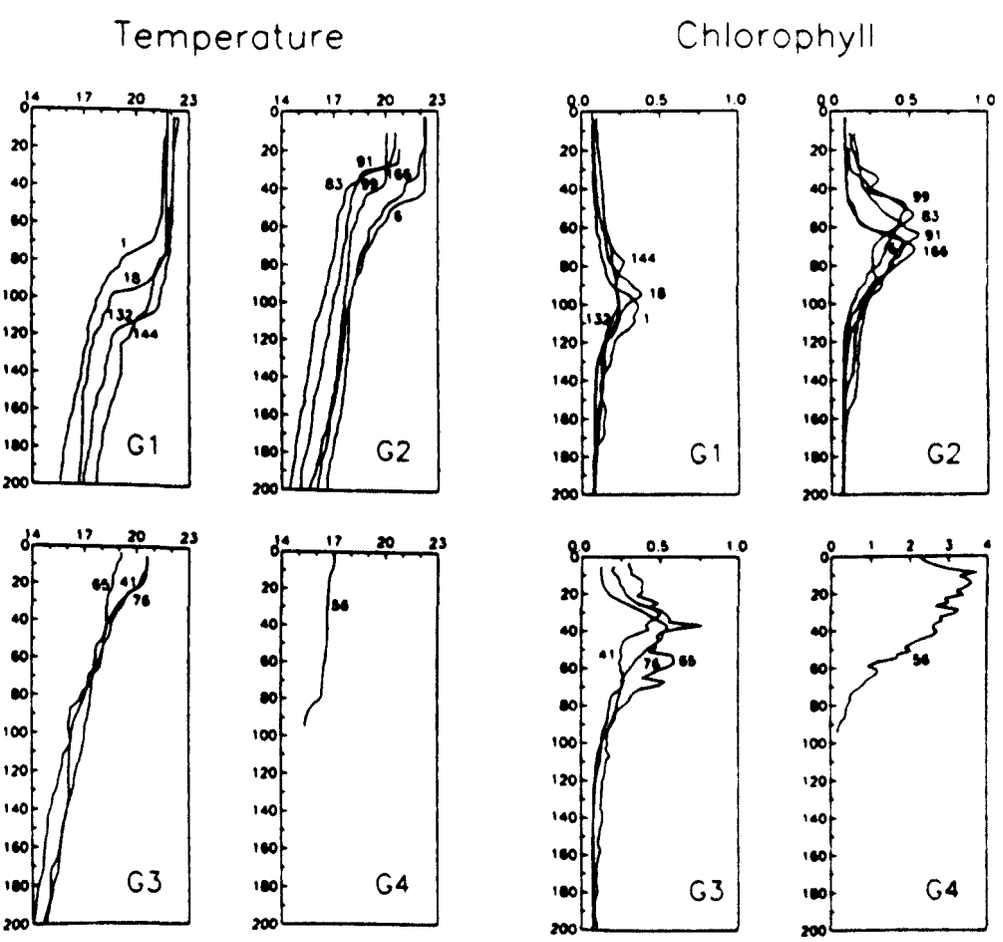

Fig. 6. Temperature (°C) and chlorophyll profiles (mg m^{-3}) for different groups of stations (see 'Results. Primary production' for group descriptions)

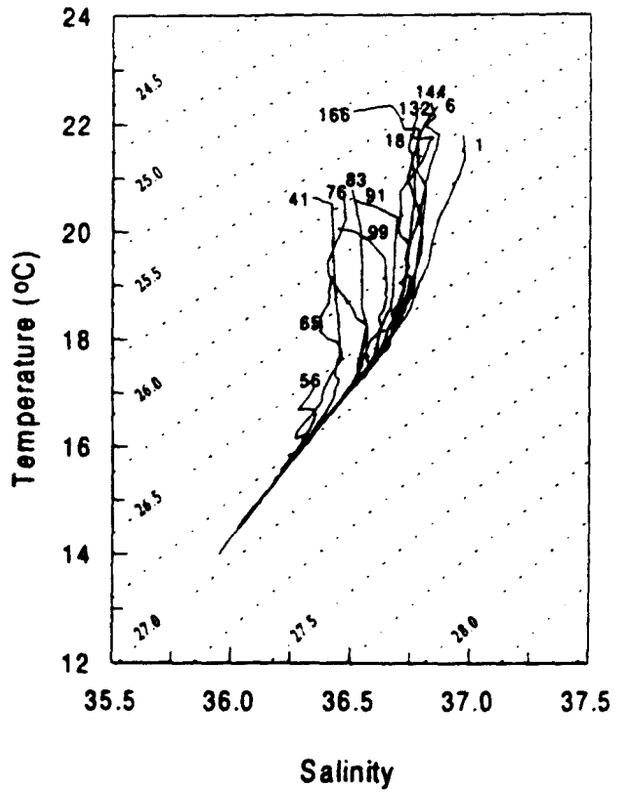

Fig. 7. Temperature-salinity characteristics (0 to 200 m) of P-E stations

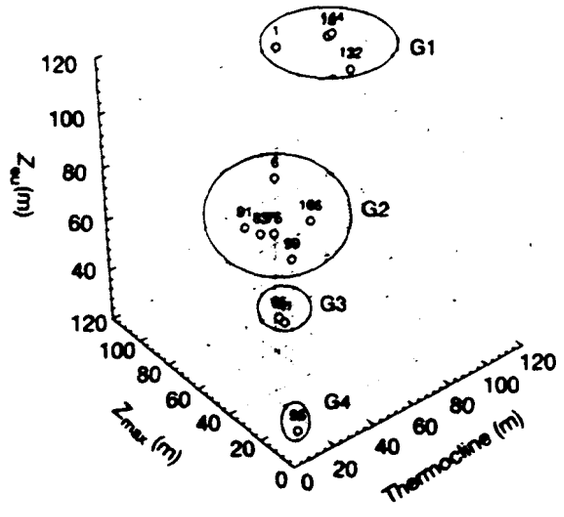

Fig. 8. Plot of grouped z_{max} (depth of the chlorophyll maximum), z_{eu} (depth of 1% PAR) and thermocline depth

and thermocline depths (Fig. 8) indicate similarities with the stations in the offshore filament.

Temperature-salinity plots (Fig. 7) reveal that along the CTZ gradient the upwelled water is mixed to varying degrees with offshore waters. The progressive transition in thermo-haline properties is disrupted by the gap between the stations placed farther offshore in the filament (Stns 91 and 99) and Stn 18 located only a few kilometers north. This gap separates upwelling-influenced waters from offshore and eddy waters.

Tables 3 & 4 synthesize some characteristics of each of the groups (Stn 76 has been excluded from averages). Chlorophyll profile parameters show clear differences between groups as result of the progressively sinking chlorophyll maximum depth (z_m) and the increase of the 1% light depth (z_{eu}) towards oceanic waters. In fact, there is a constant relation between these 2 parameters averaged by groups (Fig. 8). This is not the case with photosynthetic parameters. Stations affected by island-generated eddies do not fit well in G2 (Table 4) and have been treated as a separate group. Surface parameters in the eddies are in the range of G1, but values in the CM are clearly enhanced. The value of a is similar to that in the coastal upwelling and P_s is in the range of G3.

We calculated daily production rates per unit surface (P_{int}) for each of the areas indicated in Fig. 1 (G1, G2, G3 and G4) and for the cyclonic eddies based on ML parameters. Calculations were performed by 4 different methods: (1) averaging estimates of the stations in each region, (2) calculating an average P-E curve for each region and using the measured chlorophyll distribution for each station, (3) averaging the non-uniform biomass curve parameters for each region and applying the measured P-E curve for each station, and (4) using an average P-E curve and an average biomass profile for each region. Results from all 4 methods were very similar and maximum deviations (CV <

Table 3. Integrated chlorophyll (chl_{int}; mg m^{-2}), 1% light depth z_{eu} (m), and non-uniform biomass distribution curve fitting parameters z_{max} (m), σ (m), h (mg m^{-2}), B_0 (mg m^{-3}) for each zone (± SD)

	Chl_{int} (0–200 m)	z_{eu}	z_{max}	σ	h	B_0
G1 (n = 4)	28 ± 1	103 ± 8	96 ± 7	21 ± 9	9 ± 2	0.09 ± 0.01
G2 (n = 5)	33 ± 7	73 ± 8	68 ± 7	19 ± 7	16 ± 4	0.09 ± 0.01
G3 (n = 2)	41 ± 13	52 ± 1	41 ± 3	27 ± 0	25 ± 8	0.09 ± 0.01
G4 (n = 1)	179[a]	26	22	22	164	0.47

[a] 0 to 95 m

Table 4. Range of P-E parameters in mixed layer (ML) and chlorophyll maximum (CM) samples for each zone; α (mg C mg^{-1} chl h^{-1} [μmol m^{-2} s^{-1}]$^{-1}$), P_m (mg C mg^{-1} chl h^{-1}), P_s (mg C mg^{-1} chl h^{-1}) and β (mg C mg^{-1} chl h^{-1} [μmol m^{-2} s^{-1}]$^{-1}$)

	α (ML)	P_m (ML)	α (CM)	P_s (CM)	β (CM)
G1 (n = 4)	0.003–0.009	0.60–5.80	0.020–0.032	1.93–3.85	0.0013–0.0026
G2 (n = 3)	0.011–0.016	2.89–2.53	0.020–0.042	0.60–5.87	0.0012–0.0109
G3 (n = 2)	0.015–0.075	4.16–9.08	0.027–0.035	5.81–7.27	0.0047–0.0105
Eddies (n = 2)	0.005–0.007	1.62–2.81	0.052–0.055	3.11–6.94	0.0053–0.0106
G4 (n = 1)	0.053	13.02	0.052	11.21	0

17%) occurred in the offshore region (G1). Average estimates varied from 102 to 189 mg C m^{-2} d^{-1} for zones G1 and G2, 95 mg C m^{-2} d^{-1} in the eddies, 777 mg C m^{-2} d^{-1} for G3 and 5326 mg C m^{-2} d^{-1} for G4. However, when 2 P-E curves (ML and CM) were used in the calculations (1 for the ML and a linear interpolation below, see 'Methods') estimates for G1 and the eddies dramatically changed (72% increment in G1 and 131% in the eddies).

DISCUSSION

Phytoplankton distribution and transport

Physical and biological observations carried out during summer 1993 (the season of strongest trade winds in the area) reveal the presence of intense mesoscale variability in the CTZ off the NW African coast, affecting phytoplankton biomass distribution and primary production rates. Strong wind intensity enhances both coastal upwelling-related phenomena like filaments and island-generated eddy formation (Barton 1994a,b). Under these conditions eddy shedding is a common phenomenon that appears to be produced by the interaction of the islands with the southward flowing Canary Current (Arístegui et al. 1994).

Filaments enhance the exchange between upwelling and open ocean waters since their offshore transport can be significantly larger than Ekman transport (Kostianoy & Zatsepin 1996, Navarro-Perez & Barton 1998). In our study, the filament extended approximately 150 km offshore and then wrapped around a cyclonic eddy of 100 km diameter, to return shorewards. Chlorophyll distribution, although generally coherent with the temperature field, did not follow the entire path of the filament. Instead, waters with high chlorophyll levels dominated by large cells (>2 μm) were restricted to the shelf, and to a few stations in the filament jet. Sinking, lack of nutrients, grazing and losses by turbulent diffusion are possible explanations for phytoplankton decay. Relatively higher concentrations of chlorophyll, which could be indicative of cells sinking below the photic zone, were observed in slope waters and in the anticyclonic eddy south of Tenerife. The general trend of the CM presents a progressive deepening that parallels the enlargement of the euphotic layer.

Brink et al. (1991) suggest that sinking of near-surface water accounts for the rapid warming of surface waters with distance offshore in the filament. Our data show that there is a clear boundary marked by the presence of vertical isotherms indicating mixing. The real transition between the coastal upwelling and the filament takes place at Stn 65 (see temperature-salinity diagram, Fig. 7). Surface chlorophyll decreases by more than 1 mg m^{-3} in comparison to Stn 56, located 54 km shorewards, but the percentage of chlorophyll content in large cells is even higher than over the shelf. This effect has been corroborated by HPLC data on the same cruise (Van Lenning pers. comm.) that showed a higher contribution of diatoms to total chlorophyll at Stn 65 (max. 96%) than over the shelf (max. 87%), and could be attributed to species succession along the jet. Margalef (1982) suggests a theoretical succession that begins with small cells (flagellates and non-flagellates), continuing with medium-sized diatoms, and finally large-sized diatoms and dinoflagellates. This would explain the higher percentages of large cells observed in the upwelling front (Stn 65). This theory has been argued by Barber & Smith (1981), who stated that newly upwelled water communities are the midpoint of the ecological sequence, since 3-dimensional circulation along the upwelling determines what will be in the subsurface flow that is upstream of the vertical transport. In any case, this mechanism would only accelerate the community evolution from small to large cells. Surface assimilation numbers in the same distance decrease from 13.02 to 9.08, but the maximum α estimation corresponds to Stn 65. The assimilation number, a parameter related to algal metabolism, is likely to vary between early and late stages of an algal bloom as nutrient concentrations change (Wilkerson & Dugdale 1987, Dugdale & Wilkerson 1989), while light-limited photosynthesis rates are generally less affected by nutrient limitation (Geider & Osborne 1992).

Zooplankton grazing could also contribute to the chlorophyll decline. Barton et al. (1998) reported high zooplankton biomass in the center of the filament coinciding with a relative minimum in chlorophyll. This zooplankton maximum can be either the manifestation of transport of organisms along the filament or the result of *in situ* growth in waters of high phytoplankton content.

The decrease of phytoplankton biomass along the filament and the same magnitude of shoreward recirculation as offshore jet current velocities (Barton et al. 1998) result in a negative balance between offshore and onshore transport of chlorophyll. The magnitude of the along-jet imbalance is obviously dependent upon the area considered for transport calculations. Assuming the entire jet is covered, the larger the area of the return flux considered, the greater the imbalance obtained. In any case, apart from considerations on whether the net onshore transport value is real or not, the Cabo Bojador filament was clearly acting as a recirculation loop during our study. Seaward transport mainly occurred in the mixed layer while shoreward transportation presented maxima at deeper layers.

This situation clearly differs from studies based on ocean color images (Hernádez-Guerra et al. 1993) and field data (Arístegui et al. 1997) in the vicinity of Gran Canaria, an island 215 km off the upwelling, where high chlorophyll concentrations transported by filaments were observed. The nature of the filament and its genesis are critical for the biological consequences of the filament. The stage of development of the filament structure can also be important in terms of its biological consequences.

Variability in photosynthetic parameters

There is a considerable variability in the photosynthetic parameters in the Canaries region, due to the contrast between the oligotrophic surface waters of the eastern North Atlantic boundary current and the nutrient-rich upwelling waters. In the ML, extremely low α values were measured in the westernmost regions (G1 and G2), and the assimilation number varied by a factor of 19 (0.68 to 13.02 mg C mg^{-1} chl h^{-1}). This dramatic variation within a few hundred kilometers reflects the differences between 2 systems that occupy the lower and the higher extremes in the productivity range. The P_m values are similar to the range observed by Kyewalyanga et al. (1998) in a transect across the North Atlantic during spring 1993 and, similarly, low surface α values (<0.01) were observed by Marañon & Holligan (1999) in a meridional transect across the Atlantic at the same latitude of the Canary Islands. Hood et al. (1991), in a survey of the CTZ off northern California, observed significant differences in the phytoplankton P-E response curves; these were attributed to changes in the taxonomic composition, light history and physiological condition of cells. The contribution of each of these variables to photosynthetic changes in natural samples is, however, difficult to evaluate. Kennaway & Tett (1994) observed an onshore-offshore shift in phytoplankton species composition. Upwelling waters were dominated by diatoms and haptophytes, while in more stratified waters the surface community was mainly composed of *Synecococcus* and *Prochlorococcus* and haptophytes constituted the deep cm.

Differences in turbulence and species composition are also responsible for vertical variations in the photosynthetic responses. Over the shelf, similar responses between ML and CM samples were measured, and no photoinhibition was observed. The lack of photoinhibition in the CM sample at Stn 56 could be the result of enhanced turbulence near the coast caused by upwelling and mixing processes. Lewis et al. (1984) reported a relationship between ΔP_m, the differences in P_m at the surface and near the bottom of the mixed layer, and turbulent mixing rates. They argued that cells grown in turbulent waters present similar photosynthetic response due to a lack of photoadaptation. Conversely, when the rate of photoadaptation is high relative to turbulence-induced light fluctuation, differences in P_m appear. These differences are magnified at larger depth scales. Stratification beneath the pycnocline generates nutrient and light availability gradients where phytoplankton species composition and physiology vary. The rate of photoadaptation is likely to be high enough to overcome changes in light levels caused by vertical turbulent motions; therefore, phytoplankton cells should be well adapted. Moreover, if we consider that adaptation from high light to low light is faster than adaptation from low light to high light (Cullen & Lewis 1988), we could presume that slowly falling phytoplankton cells would easily adapt to progressively decreasing irradiance. However, sinking phytoplankton cells do not only experience changes in irradiance but also in light quality (primarily affecting α) and in nutrient availability. These factors generate different ecological niches throughout the water column which are occupied by distinct phytoplankton assemblages.

As an example, we can consider the effect of nitracline uplift in the center of the observed cyclonic eddies. The chlorophyll-specific rate of photosynthesis was clearly enhanced in these structures. There is evidence that nutrient limitation can modify photosynthesis parameters (Falkowski et al. 1985, Osborne & Geider 1986, Herzig & Falkowski 1989, Platt et al. 1992, Sathyendranath et al. 1996). However, Cullen et al. (1992b), in a

review focused on this issue, conclude that assimilation number is an unreliable diagnostic index of nutrient assimilation, and that only in laboratory cultures at controlled light and temperature conditions does low P_m imply nutritional deficiency. Therefore, increases in the photosynthetic parameters in the observed eddies may not necessarily correspond to a nutrient injection in the existing phytoplankton communities. Higher parameters in nutrient-rich waters could also be interpreted as the generation of a niche that is occupied by new communities with a different P-E performance. Falkowski et al. (1991), for an eddy in Hawaii, estimated a 67% increase in the chlorophyll-specific rate of photosynthesis and about a 20% increase in the integrated primary production compared to adjacent waters. For the same structure, Olaizola et al. (1993) reported an increase in the photosynthetic parameters in the DCM (α and P_m were 2.28 and 3.6 times higher, respectively, in the eddy than at other stations) and a change in the floristic composition. Several authors (Eppley et al. 1979, Balch et al. 1997, Marañon & Holligan 1999) have reported relationships between the depth of the nitracline and production rates. Balch et al. (1997) observed an exponential increase in production as the pycnocline shoaled in the Californian Upwelling, which they attributed to the photon flux increase at shallower depths. They also suggested that isopycnal and diapycnal mixing of nitrate-rich water was sufficient to sustain higher primary production levels when the pycnocline shoaled. This effect is also observed in the grouped photosynthetic parameters (Table 4), which show a progressive increase as the African shelf is approached. The phytoplankton photosynthetic response and therefore primary production in the G1 zone is, however, more variable and not related to isopycnal uplifting. This variability cannot be attributed to biomass changes (average integrated chlorophyll values are only slightly lower in G1 than in G2) but, instead, must be caused by the variability of the photosynthetic performance of algae (production at G2 is almost double that at G1). Marañon & Holligan (1999) have also addressed the importance of phytoplankton photosynthetic performance at larger scales.

Regional production estimates

Empirical relationships between chlorophyll and integrated primary production possibly offer the simplest approach to infer the productivity over vast oceanic areas (e.g. Eppley et al. 1985). With the aim of progressively attaining better estimations, these relations, the strength of which relies on their simplicity, have been implemented with more mechanistic approaches that require the introduction of physiological parameters. These algorithms have been fragmented into relations affecting to relatively biogeochemically homogeneous ocean compartments or 'provinces'. This has accounted for inter-regional differences; however, intra-regional variability is mainly reproduced in terms of biomass variations. From our results it is evident that other factors of variation should be included in order to achieve a more realistic representation of the intra-regional variability. In the most oligotrophic zone of the surveyed area (G1), spatial primary production increases are not accompanied by proportional increases in chlorophyll. We have observed variations in the ML of almost an order of magnitude for P_m values while, surface and integrated chlorophyll remained extremely constant. As Lewis (1992) states, the high variability of physiological parameters even over short time and restricted space is still limiting these methods. Uncoupling between production and chlorophyll could be explained if: (1) subtropical plankton assemblages present high and variable C:chl ratios or (2) if microzooplankton rapidly controls the produced biomass. Maximum C:chl ratios are typical from oceanic areas experiencing high irradiance. This effect is caused by the reduction of cell pigment content at high irradiance but also by restricted nutrient availability in stratified regions. Taylor et al. (1997), based on modeled results, report highest C:chl (>150) ratios in the surface layers between 25 and 35 degrees of latitude. An alternative, but not excluding, explanation is a zooplankton control over the newly produced biomass. A coupled phytoplankton-herbivore system in which grazing limits the standing crop has been suggested as an explanation for open ocean high-nutrient low-chlorophyll situations (Walsh 1976, Minas et al. 1986, Cullen et al. 1992a), but could also be applicable for most subtropical areas. In these regions mesoscale and smaller scale physical processes would control productivity.

In conclusion, our results show that transition zones between highly productive upwelling systems and oligotrophic open ocean waters present a large variability in photosynthetic parameters. Unless this variability is considered in productivity models, regional production estimations can be greatly biased.

Acknowledgements. We wish to thank Dr E. D. Barton for his helpful comments and corrections, and the crew and technical staff of the BIO 'Hespérides' for their invaluable help during the cruise. This work was supported by project FRENTES (CICYT, AMB 95-0731), and through MAST I Program 0031 and the CANIGO program of the European Commission.

LITERATURE CITED

Abbott MR, Zion PM (1985) Satellite observations of phytoplankton variability during an upwelling event. Contin Shelf Res 4:661–680

Abbott MR, Brink KH, Booth CR, Blasco D, Codispoti LA, Niiler PP, Ramp SR (1990) Observations of phytoplankton and nutrients from a Lagrangian drifter off northern California. J Geophys Res 95(C6):9393–9409

Arístegui J, Sangrá P, Hernández-León S, Cantón M, Hernández-Guerra A, Kerling JL (1994) Island-induced eddies in the Canary Islands. Deep-Sea Res 41:1509–1525

Arístegui J, Tett P, Hernández-Guerra A, Basterretxea G, Montero MF, Wild K, Sangrá P, Hernández-León S, Cantón M, García-Braun JA, Pacheco M, Barton ED (1997) The influence of island-generated eddies on chlorophyll distribution: a study of mesoscale variation around Gran Canaria. Deep-Sea Res 44(1):71–96

Austin RW (1974) The remote sensing of spectral radiance from below the ocean surface. In: Jerlov NG, Nielsen ES (eds) Optical aspects of oceanography. Academic Press, San Diego, CA, p 317–344

Balch WM, Byrne CF (1994) Factors affecting the estimate of primary production from space. J Geophys Res 99(C4): 7555–7570

Balch WM, Bowler BC, Byrne CF (1997) Sea surface temperature gradients, baroclinicity, and vegetation gradients in the sea. J Plankton Res 19(12):1829–1858

Barber RT, Smith RL (1981) Coastal upwelling ecosystems. In: Longhurst AR (ed) Analysis of marine ecosystems. Academic Press, London, p 31–68

Barton ED (1994a) Frontal structures downwind and downstream of Gran Canaria. Ann Geophysicae 12(II), C267

Barton ED (1994b) European Coastal Transition Zone: Islas Canarias. Final Report, MAST Project 0031, European Commission, Bangor

Barton ED, Arístegui J, Tett P, Cantón M, García-Braun J, Hernández-León S, Nykjaer L, Almeida C, Almunia J, Ballesteros S, Basterretxea G, Escánez J, García-Weill L, Hernández-Guerra A, López-Laatzen F, Molina R, Montero MF, Navarro-Pérez E, Rodríguez-Pérez JM, van Lenning K, Vélez H, Wild K (1998) The transition zone of the Canary Current upwelling region. Prog Oceanogr 41(4):455–504

Behrenfeld MJ, Falkowski PG (1997a) Photosynthetic rates derived from satellite-based chlorophyll concentration. Limnol Oceanogr 42(1):1–20

Behrenfeld MJ, Falkowski PG (1997b) A consumer's guide to phytoplankton primary productivity models. Limnol Oceanogr 42(7):1479–1491

Bidigare RR, Smith RC, Baker KS, Marra J (1987) Oceanic primary production estimates from measurements of spectral irradiance and pigment concentrations. Global Biogeochem Cycles 1:171–186

Bidigare RR, Prézelin BB, Smith RC (1992) Bio-optical models and the problems of scaling. In: Falkowski PG, Woodhead AD (eds) Primary productivity and biogeochemical cycles in the sea. Environmental Science Research, Vol 143 Plenum Press, New York, p 175–212

Brink KH, Beardsley RC, Niiler PP, Abott M, Huyer A, Ramp S, Stanton T, Stuart D (1991) Statistical properties of near-surface flow in the California coastal transition zone. J Geophys Res 96(C8):14693–14706

Cullen JJ, Eppley RW (1981) Chlorophyll maximum layers off the southern California bight and possible mechanisms of their formation and maintenance. Oceanol Acta 4:23–32

Cullen JJ, Lewis MR (1988) The kinetics of algal photoadaptation in the context of vertical mixing. J Plankton Res 10(5):1039–1063

Cullen JJ, Lewis MR, Davis CO, Barber RT (1992a) Photosynthetic characteristics and estimated growth rates indicate grazing is the proximate control of primary production in the Equatorial Pacific. J Geophys Res 97:639–654

Cullen JJ, Yang X, MacIntyre HL (1992b) Nutrient limitation of marine photosynthesis. In: Falkowski PG, Woodhead AD (eds) Primary productivity and biogeochemical cycles in the sea. Plenum Press, New York, p 69–88

Davis RE (1985) Drifter observations of coastal surface currents during CODE: the method and descriptive view. J Geophys Res 90:4741–4755

Dugdale RC, Wilkerson FP (1989) New production in the upwelling center of Point Conception, California: temporal and spatial patterns. Deep-Sea Res 36:985–1007

Eppley RW, Peterson BJ (1979) Particulate organic matter flux and the planktonic new production in the deep ocean. Nature 282:677–680

Eppley RW, Renger EH, Harrison WG (1979) Nitrate and phytoplankton production in southern California coastal waters. Limnol Oceanogr 24:291–301

Eppley RW, Stewart E, Abbott MR, Heyman U (1985) Estimated ocean primary production from satellite chlorophyll. Introduction to regional differences and statistics from Southern California Bight. J Plankton Res 7:57–70

Falkowski PG, Dubinsky Z, Wyman K (1985) Growth-irradiance relationships in phytoplankton. Limnol Oceanogr 30: 311–321

Falkowski PG, Ziemann D, Kolber Z, Bienfang PK (1991) Role of eddy pumping in enhancing primary production in the ocean. Nature 352:55–58

Flament P, Armi L, Washburn L (1985) The evolving structure of an upwelling filament. J Geophys Res 90:11765–11778

Geider RJ, Osborne BA (1992) Algal photosynthesis: the measurement of algal gas exchange. Chapman and Hall, New York

Gordon HR, Clark DK, Mueller JL, Hovis WA (1980) Phytoplankton pigments from the Nimbus-7 Coastal Zone Color Scanner: comparisons with surface measurements. Science 210:63–66

Haynes R, Barton ED, Pilling I (1993) Development, persistence, and variability of upwelling filaments off the Atlantic coast of the Iberian Peninsula. J Geophys Res 98(C12):22681–22692

Herbland A, Voituriez B (1979) Hydrological structure analysis for estimating the primary production in the Tropical Atlantic Ocean. J Mar Res 37:87–101

Hernández-Guerra A, Arístegui J, Cantón M, Nykjaer L (1993) Phytoplankton pigment patterns in the Canary Islands area as determined using Coastal Zone Colour Scanner data. Int J Remote Sensing 14(7):1431–1437

Herzig R, Falkowski PG (1989) Nitrogen limitation in *Isochrysis galbana* (Haptoficeae). I. Photosynthetic energy conversion and growth efficiencies. J Phycol 25:462–471

Holm-Hansen O, Lorenzen CJ, Holmes RW, Strickland JDH (1965) Fluorometric determination of chlorophyll. J Cons Int Explor Mer 30:3–15

Hood RR, Abbott MR, Huyer A (1991) Phytoplankton and photosynthetic light response in the coastal transition zone off northern California in June 1987. J Geophys Res 96(C8):14769–14780

Huyer A, Kosro PM (1987) Mesoscale surveys over the shelf and slope in the upwelling region near Point Arena, California. J Geophys Res 92:1655–1681

Jones BH, Mooers CNK, Rienecker MM, Stanton T, Washburn L (1991) Chemical and biological structure and transport of a cool filament associated with a jet-eddy system off northern California in July 1986 (OPTOMA21). J Geophys Res 96(C12):22207–22225

Kelly KA (1985) The influence of winds and topography on the sea surface temperature patterns over the northern California slope. J Geophys Res 90:11783–11798

Kennaway GM, Tett P (1994) A scanning electron microscope study of flagellate assemblies from the Hespérides Cruise 9308. Data Report 0031–17, School of Ocean Sciences, University of Wales, Bangor

Kiefer DA, Mitchell BG (1983) A simple steady state description of phytoplankton growth based on absorption cross section and quantum efficiency. Limnol Oceanogr 28: 770–776

Koblents-Mishke OI (1983) An attempt to classify the marine pelagic ecosystems on the basis of primary production and its spatial variability. Oceanology 23(2):233–239

Kosro PM, Huyer A, Rampt SR, Smith RL, Chavez FP, Cowles TJ, Abbott MR, Strub PT, Barber RT, Jessen P, Small LF (1991) The structure of the transition zone between coastal waters and the open ocean off northern California, winter and spring 1987. J Geophys Res 96(C8):14707–14730

Kostianoy AG, Zatsepin AG (1996) The West African coastal upwelling filaments and cross-frontal water exchange conditioned by them. In: Dejenidi S (ed) The coastal ocean in a global change perspective. J Mar Syst 7:349–359

Kyewalyanga MN, Platt T, Sathyendranath S, Lutz VA, Stuart V (1998) Seasonal variations in physiological parameters of phytoplankton across the North Atlantic. J Plankton Res 20(1):17–42

La Violette PE (1974) A satellite-aircraft thermal study of the upwelled waters off Spanish Sahara. J Phys Oceanogr 4(4):674–684

Lewis MR (1992) Satellite ocean color observations of global biogeochemical cycles. In: Falkowski PG, Woodhead AD (eds) Primary productivity and biogeochemical cycles in the sea. Plenum Press, New York, p 139–153

Lewis MR, Smith JC (1983) A small volume, short-incubation-time method for measurement of photosynthesis as a function of incident irradiance. Mar Ecol Prog Ser 13:99–102

Lewis MR, Horne EPW, Cullen JJ, Oakey NS, Platt T (1984) Turbulent motions may control phytoplankton photosynthesis in the upper ocean. Nature 311(5981):49–50

Longhurst A (1995) Seasonal cycles of pelagic production and consumption. Prog Oceanogr 36:77–167

MacCaull WA, Platt T (1977) Diel variations in the photosynthetic parameters of the coastal marine phytoplankton. Limnol Oceanogr 23:723–731

Marañon E, Holligan PM (1999) Photosynthetic parameters of phytoplankton from 50° N to 50° S in the Atlantic Ocean. Mar Ecol Prog Ser 176:205–214

Margalef R (1982) Ecología. Omega, Barcelona

Marra J (1980) Vertical mixing and primary production. In: Falkowski PG (ed) Primary productivity in the sea. Environmental Science Research, Vol 19. Plenum Press, New York, p 121–137

Minas HJ, Minas M, Packard TT (1986) Productivity in upwelling areas deduced from hydrographic and chemical fields. Limnol Oceanogr 31:1182–1206

Mooers CNK, Robinson AL (1984) Turbulent jets and eddies in the California Current and inferred cross-shore transports. Science 223:51–53

Navarro-Pérez E, Barton ED (1998) The physical structure of an upwelling filament off the north-west African coast during August 1993. In: Pillar SC, Moloney CL, Payne AIL, Shillington FA (eds) Benguela dynamics: impacts of variability on shelf-sea environments and their living resources. S Afr J Mar Sci 19:61–74

Olaizola M, Ziemann DA, Bienfang PK, Walsh WA, Conquest LD (1993) Eddy-induced oscillations of the pycnocline affect the floristic composition and depth distribution of phytoplankton in the subtropical Pacific. Mar Biol 116: 533–542

Osborne BA, Geider RJ (1986) Effects of nitrate limitation on photosynthesis in the diatom *Phaeodactilum tricornutum* Bohlin (Bacillariophyceae). Plant Cell Environ 9:617–625

Platt T, Gallegos CL, Harrison WG (1980) Photoinhibition of photosynthesis in natural assemblages of marine phytoplankton. J Mar Res 38:687–701

Platt T, Sathyendranath S, Caverhill C, Lewis MR (1988) Oceanic primary production and available light: Further algorithms for remote sensing. Deep-Sea Res 35:855–879

Platt T, Caverhill C, Sathyendranath S (1991) Basin-scale estimates of oceanic primary production by remote sensing: The North Atlantic. J Geophys Res 96:15147–15159

Platt T, Sathyendranath S, Ulloa O, Harrison WG, Hoepffner N, Goes J (1992) Nutrient control of phytoplankton photosynthesis in the Western North Atlantic. Nature 356: 229–231

Rienecker MM, Mooers CNK, Hagan DE, Robinson AL (1985) A cool anomaly off northern California: an investigation using IR imagery and *in situ* data. J Geophys Res 90: 4807–4818

Sathyendranath S, Platt T, Horne EPW, Harrison WG, Ulloa O, Outerbridge R, Hoepffner N (1991) Estimation of new production in the ocean by compound remote sensing. Nature 353:129–133

Sathyendranath S, Longhurst A, Caverhill CM, Platt T (1995) Regionally and seasonally differentiated primary production in the North Atlantic. Deep-Sea Res 42(10): 1773–1802

Sathyendranath S, Platt T, Stuart V, Irwin B, Veldhuis MJW, Kraay GW, Harrison WG (1996) Some bio-optical characteristics of phytoplankton in the NW Indian Ocean. Mar Ecol Prog Ser 132:299–311

Shannon LV, Walters NM, Mostert SA (1985) Satellite observations of surface temperature and near-surface chlorophyll in the southern Benguela region. In: Shannon LV (ed) South African Ocean Color and Upwelling Experiment. Sea Fisheries Research Institute, Cape Town, p 183–210

Strub PT, Kosro PM, Huyer A (1991) The nature of cold filaments in the California current system. J Geophys Res 96(C8):14743–14768

Swenson MS, Niiler PP, Brink KH, Abbott MR (1992) Drifter observations of a cold filament off Point Arena, California, in July 1988. J Geophys Res 97(C3):3593–3610

Taylor AH, Geider RJ, Gilbert FJH (1997) Seasonal and latitudinal dependencies of phytoplankton carbon-to-chlorophyll *a* ratios: results of a modelling study. Mar Ecol Prog Ser 152:51–66

Traganza ED, Nestor DA, McDonald AK (1980) Satellite observations of a nutrient upwelling off the coast of California. J Geophys Res 85:4104–4106

Van Camp L, Nykjaer L, Mittelstaedt E, Schlittenhardt P (1991) Upwelling and boundary circulation off Northwest Africa as depicted by infrared and visible satellite observations. Prog Oceanogr 26:357–402

Venrick EL, McGowan JA, Mantyla AW (1973) Deep maxima of photosynthetic chlorophyll in the Pacific Ocean. Fish Bull US 71:41–52

Walsh JJ (1976) Herbivory as a factor in patterns of nutrient utilization in the sea. Limnol Oceanogr 21:1–13

Webb WL, Newton M, Starr D (1974) Carbon dioxide exchange of *Alnus rubra*: a mathematical model. Oecologia 17:281–291

Wilkerson FP, Dugdale RC (1987) The use of large shipboard barrels and drifters to study the effects of coastal upwelling on phytoplankton dynamics. Limnol Oceanogr 32: 368–382

Editorial responsibility: Otto Kinne (Editor)

Submitted: May 17, 1999; Accepted: October 26, 1999

ELSEVIER

Aquaculture 179 (1999) 277–290

Aquaculture

Combined effect of lipid level and fish meal quality on liver histology of gilthead seabream (*Sparus aurata*)

M.J. Caballero [a,*], G. López-Calero [b], J. Socorro [b], F.J. Roo [b], M.S. Izquierdo [a], A.J. Fernandez [c]

[a] *Departamento de Biología, Universidad de las Palmas de Gran Canaria, Campus Universitario de Tafira, 35017 Las Palmas de Gran Canaria, Canary Islands, Spain*

[b] *Instituto Canario de Ciencias Marinas, Gobierno de Canarias, P.O. Box 56, 35200, Telde, Las Palmas de Gran Canaria, Canary Islands, Spain*

[c] *Departamento de Morfología, Universidad de las Palmas de Gran Canaria, Francisco Inglott Artiles, 12A, 35016 Las Palmas de Gran Canaria, Canary Islands, Spain*

Abstract

Effect of eight diets comparing three different lipid levels (15, 22 and 27%) and two fish meal qualities were studied on growth and liver histology. Fish meal quality was judged by the content of biogenic amines and temperature processing techniques. The experiment included a comparison of pelleted feed with extruded feed for the 22% lipid diet. A total of 1140 gilthead seabream of 70 g average initial body weight were randomly stocked in 500-l fiberglass tanks in duplicate groups of 60 fish. After 2 months of experiment, the fish were transferred to 1-m^3 tanks. Fish were fed twice a day to apparent satiation for 6 months until they reached about 400 g (commercial size). Fish fed diets containing high quality fish meal showed, in general, a higher growth than those fish fed with low quality fish meal. For diets containing high quality fish meal, the fish fed 22 and 27% dietary lipid had significantly higher growth than those fish fed 15% dietary lipid. On the contrary, in diets containing low quality fish meal, only fish fed 27% dietary lipid showed significantly the higher growth rate. Fish fed the pelletized diets showed a lower growth than those fish fed extruded diets. Livers from fish fed diets containing high quality fish meal and 27% lipid showed foci of swelling hepatocytes that were not found for low quality fish meal at the same dietary lipid content. Ultrastructurally, these foci were characterized to present irregular nuclei displaced to periphery of hepatocytes and large lipid droplets in the cytoplasm. Livers from fish fed high and low fish meal qualities with 22% lipid showed similar morphological characters of

* Corresponding author. Tel.: +34-928-132900; fax: +34-928-132904; E-mail: mjcaballero@iccm.rcanaria.es

0044-8486/99/$ - see front matter
PII S0044-8486(99)00165-9

hepatocytes to those that fed 15% lipid, but the difference was observed in the nuclei displacement.

Keywords: Gilthead seabream; Meal quality; Lipids; Growth; Histology; Liver

1. Introduction

In the last years there has been a trend in commercial fish feed formulations to increase dietary lipid levels to improve feed utilization for the optimization of production. The use of fish meal as a major source of dietary protein and lipid is also a common practice in commercial diets (Tacon, 1994), its quality being increasingly considered important for good growth performance. The combined effect of dietary lipid level and fish meal quality is of crucial importance to obtain optimal growth and reduce final production costs. However, the effect of both mentioned parameters on the quality of the produced fish must be also considered.

The use of the liver as an indicator organ of the nutritional and physiological status in fish is well-known (Hibiya, 1982; Storch and Juario, 1983; Segner and Juario, 1986). Several authors have described liver alterations produced by different nutritional factors. Godino et al. (1990) described hepatic disturbances in gilthead seabream fed diets stored at high temperature. Changes in hepatocytes of red drum fed diets containing menhaden oil and soybean oil were observed by Tucker et al. (1997). Other authors have described pathological conditions in livers as result of dietary lipid imbalances (Bautista and De la Cruz, 1988; Watanabe et al., 1989). Bell et al. (1995) observed a high degree of vacuolation due to lipid deposition in livers of turbot fed marine fish oil that was not observed in fish fed diets containing borage oil, suggesting the cause to be due to the higher level of unsaturate lipid in marine fish oil, which may present a greater risk from lipid peroxidation and be the cause of the mortalities observed. In *Clarias gariepinus* larvae, Verreth et al. (1994) showed that lipid volume in the liver of larvae fed high HUFA-enriched *Artemia* was higher than in livers of larvae fed low HUFA-enriched *Artemia*, probably due to different digestibilities. Also, these authors concluded that feeding level can result in an accumulation of lipid in the liver and be a more the most decisive parameter for larval growth and metabolic performance of the liver than feed type.

Histological studies concerning the effects of fish meal quality are scarce. Aksnes and Mundheim (1997) reported a high content of lipid in the hepatocytes with atrophic and pycnotic nuclei of halibut fed fish meal produced from spoiled raw material compared with fresh raw fish. Although, the effect of fish meal quality on growth has been studied by several authors. For salmonids, Pike et al. (1990) found an average of 15% increase in growth of fish fed diets containing high quality fish meal compared with fish fed diets containing fair so average quality fish meal. Aksnes and Mundheim (1997) reported a reduction in growth of Atlantic halibut fed fish meal containing high levels of biogenic amines.

Previous workers have shown that structural alterations of liver can provide information on diet quality, diet metabolism and the nutritional status of the fish (Storch et al.,

1983; Escaffre and Bergot, 1986; Segner and Braunbeck, 1988). Thus, the objective of this work was to study the combined effect of fish meal quality and lipid content on growth and liver histology in gilthead seabream feed these type of diets. This specie is one of the most important marine fish for Mediterranean aquaculture.

2. Materials and methods

2.1. Fish and diets experimental

A total of 1140 gilthead seabream (*Sparus aurata*) of 70 g average initial body weight provided by a local commercial farm (ADSA) were weighed and randomly stocked in 500-l fiberglass tanks in groups of 60 fish. Once the fish reached about 150 g, they were transferred to 1-m^3 tanks. The flow rate of the water in all tanks was increased from 4 to 10 l min^{-1} during the experimental period whereas temperature range from 20.7–24.4°C. Prior to starting the experiment, the fish were acclimated for 1 week with a commercial diet (Mistral 3 mm, Proaqua, Palencia, Spain). Fish were fed twice a day to apparent satiation, 6 days a week during 6 months of experimental period (April–October) until the fish reached a final body weight of about 400 g, which is a standard commercial size for the Mediterranean market. The diets were fed to duplicate groups of fish. The fish were individually weighed and measured once each month and at the end of experiment.

Eight experimental diets were prepared with different dietary lipid content (15, 22 and 27%) combined with two different fish meal qualities, "good" (71.6% protein, 8.0% lipid) and "poor" (71.5% protein, 10.0% lipid). Diet formulations and compositions are shown in Table 1. The high quality meal contained 0.5 g/kg cadaverine and 0.2 g/kg histamine and was processed at 60°C. The low quality meal contained 1.5 g/kg cadaverine and 0.24 g/kg histamine and was processed at 100°C. All diets were processed by extrusion. In addition, the 22% lipid diets were also pelletized for each of the fish meals assayed.

2.2. Histology sampling

At the end of the experimental period livers from 15 fish per tank were removed for different histological examinations.

2.2.1. Light microscopy

Livers from eight fish per tank were collected. Samples were fixed in 10% buffered formalin, dehydrated in a graded ethanol series and embedded in paraffin. Sections series of 4 μm were stained with hematoxylin and eosin (H&E).

2.2.2. Transmission electron microscopy

Livers from two fish per tank were fixed in 2.5% glutaraldehyde in 0.2 M phosphate buffer (pH 7.2). Fifty-nanometer sections of liver were stained with uranyl acetate and lead citrate and observed with a Philips CM-10 transmission electron microscopy. The diameter of lipid droplet was measured for morphometric analysis on the electron

Table 1
Ingredients and chemical composition of the experimental diets

	Diet number							
	Extruded						Pelletized	
	1	2	3	4	5	6	7	8
Ingredients (g / 100 g)								
FM "good"	44.6	0	48.6	0	52.6	0	48.6	0
FM "poor"	0	45.6	0	49.7	0	53.7	0	49.7
Fish oil	7.4	6.4	13.4	12.3	19.4	18.3	13.4	12.3
Soybean meal	22	22	17	17	12	12	17	17
Bread crumbles	22	22	17	17	12	12	17	17
Wheat meal	2.0	2.0	2.0	2.0	2.0	2.0	2.0	2.0
Soybean lecithin[a]	0.5	0.5	0.5	0.5	0.5	0.5	0.5	0.5
Inositol	0.03	0.03	0.03	0.03	0.03	0.03	0.03	0.03
Betafin	0.4	0.4	0.4	0.4	0.4	0.4	0.4	0.4
Vitamin mix[b]	1.0	1.0	1.0	1.0	1.0	1.0	1.0	1.0
Mineral mix[c]	0.5	0.5	0.5	0.5	0.5	0.5	0.5	0.5
Chemical composition (g / 100 g dry matter)								
Crude protein (Nx 6.25)	47.7	51.7	47.5	49.8	48.3	49.7	47.9	48.0
Lipid*	15.1	16.0	22.8	24.1	27.0	29.2	23.7	23.9
Ash	9	7.4	8.5	11.3	9.2	7.7	9	8.0
Carbohydrate[d]	28.2	24.9	21.2	14.8	12.1	13.4	19.4	20.1
Gross energy (MJ/kg)[e]	22	22	24	24	25	25	24	24
Cadaverine	0.50	1.50	0.50	1.50	0.50	1.50	0.50	1.50
Histamine	0.20	0.24	0.20	0.24	0.20	0.24	0.20	0.24

[a] Soybean lecitin obtained from Denota (Norway).
[b] Provides per kilogram feed: vitamin A 3000 IU (Rovimix A 500P); vitamin D_3 1600 IU (Rovimix D_3 500); vitamin E 160 mg (Rovimix E50SD); thiamin 12 mg (thiamin mononitrate); riboflavin 24 mg (Rovimix B280SD); pyridoxine 12 mg (pyrodoxin HCl); vitamin C 60 mg (Rovimix Stay-C25); pantothenic acid 48 mg (Rovimix Calpan); biotin 0.6 mg (Rovimix H2); folic acid 6.0 mg (Rovimix Folic 80SD); niacin 120 mg (Rovimix Niacin); vitamin B_{12} 0.024 mg (B12 1% FG); menadione Na-bisulfite 12 mg. The vitamins were obtained from Hoffman La Roche (Switzerland).
[c] Provides per kilogram feed: $MnSO_4 \cdot H_2O$ 10 mg; $MgHPO_4 \cdot 3H_2O$ 500 mg; $FeSO_4 \cdot 2H_2O$ 50 mg; $ZnSO_4 \cdot H_2O$ 80 mg; $CuSO_4 \cdot 5H_2O$ 5 mg; KH_2PO_4 400 mg; K_2CO_3 400 mg; K_2CO_3 400 mg; $CaCO_3$, 18.89 mg.
[d] Carbohydrate = NFE + fiber = 1000-protein-lipid-ash.
[e] GE = Calculated gross energy content.
* Proximate values (15, 22 or 27%) were used in all the text.

transmission microscopy plates using a video-equipped Hitachi VK-C150DE and Imago® Imagen software. Ten areas per liver were selected from fish fed the different dietary lipid levels. The mean diameter of the lipid droplets was calculated for samples from fish fed each diet.

2.2.3. *Lipid identification*

Livers from three fish per tank were fixed in liquid nitrogen for 5 min. Frozen sections of 5 μm were cut in cryostat (Reichert-Jung 2800 Frigocut N) and stained with Oil-Red O (70% ethanol).

2.3. Statistical analysis

All data were subjected to one-way analysis of variance (ANOVA) and differences among means were detected with Tukey's test at $P < 0.05$ level (Sokal and Rohlf, 1995).

3. Results

3.1. Growth

Growth results comparing dietary lipid levels for each quality of meal showed in general higher values for the highest dietary lipid content. Thus, for the high quality fish meal, 22 and 27% dietary lipid produced significantly ($P < 0.05$) higher growth rates than 15% dietary lipid (Fig. 1). For the low quality fish meal, 27% dietary lipid produced higher growth compared to 22 and 15% dietary lipid (Fig. 1).

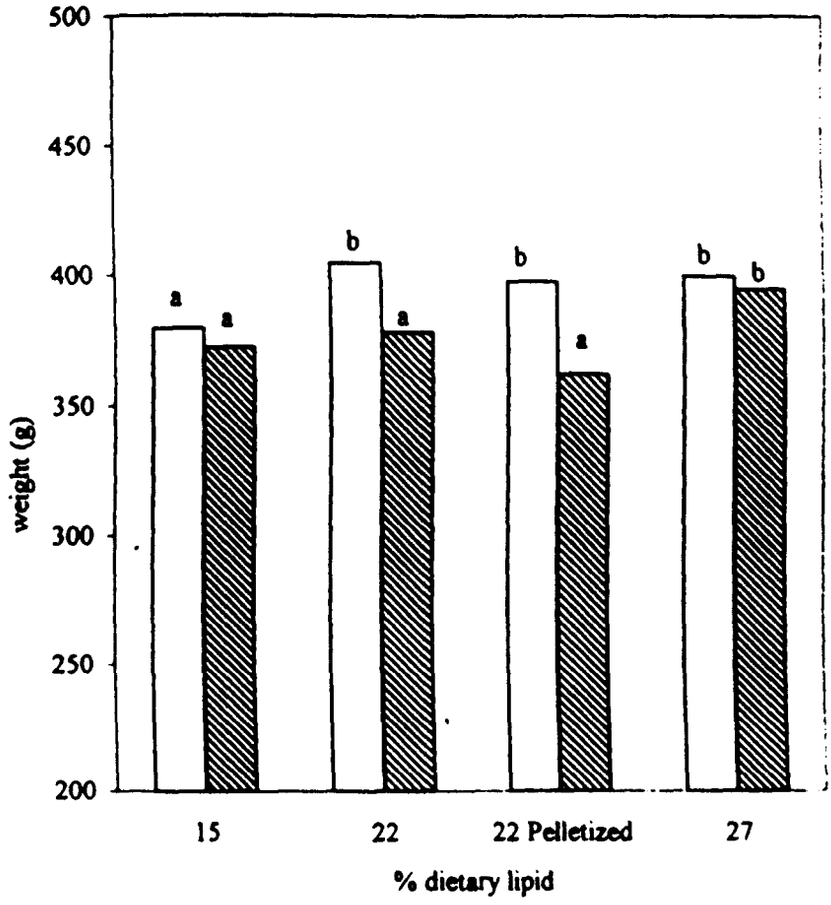

Fig. 1. Effect of dietary lipid content and fish meal quality (□ — high quality fish meal, box with diagonal lines — low quality fish meal) on growth rate of gilthead seabream. Different letters denote significant difference ($P < 0.05$)

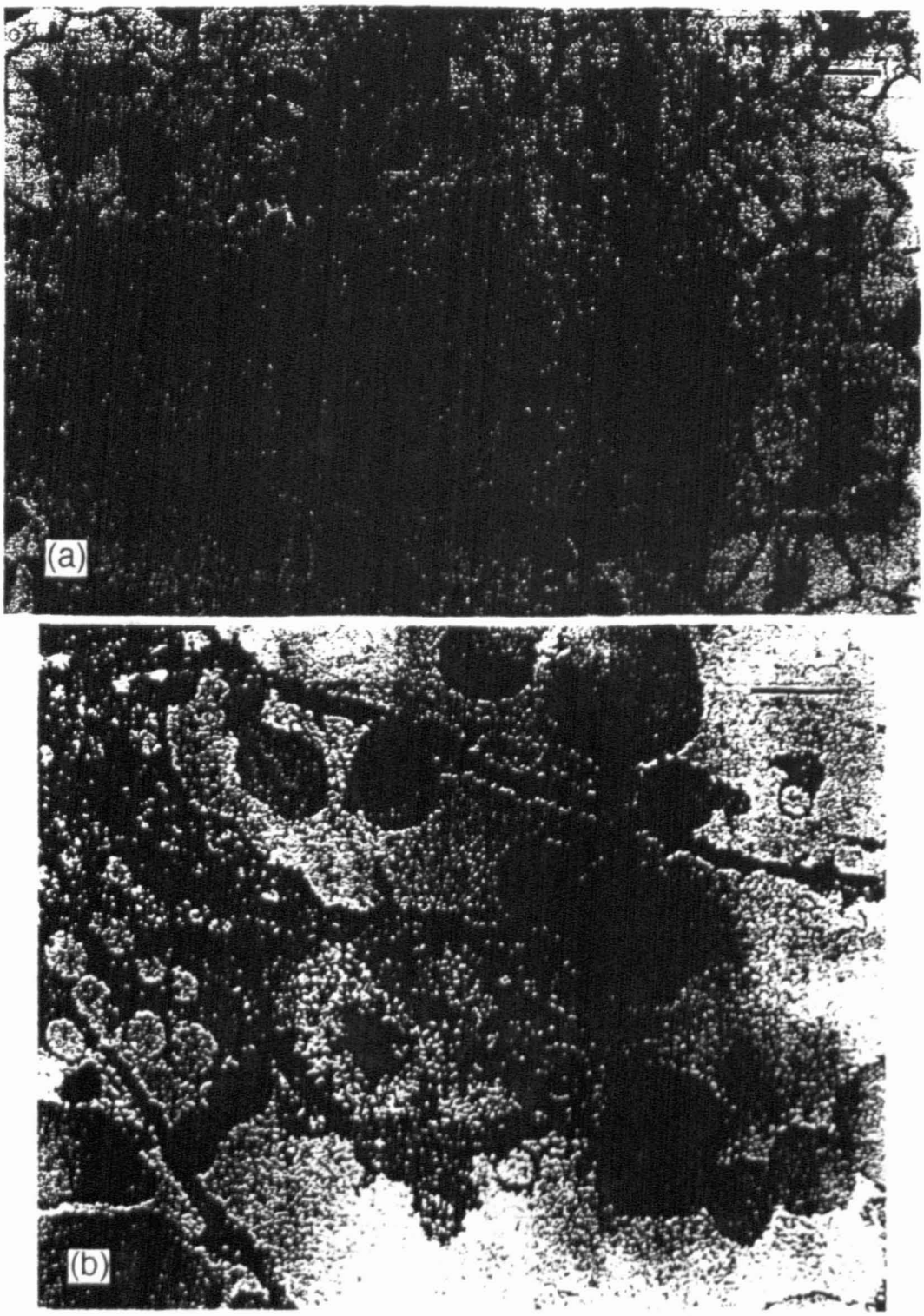

Fig. 2. Hepatocytes from fish fed experimental diets. Diet: 15% dietary lipid content. (a) Large and spherical nucleus centrally located (H&E). Bar = 10 μm. (b) Electron micrograph. Bar = 2.5 μm. N: nucleus; L: lipid droplet.

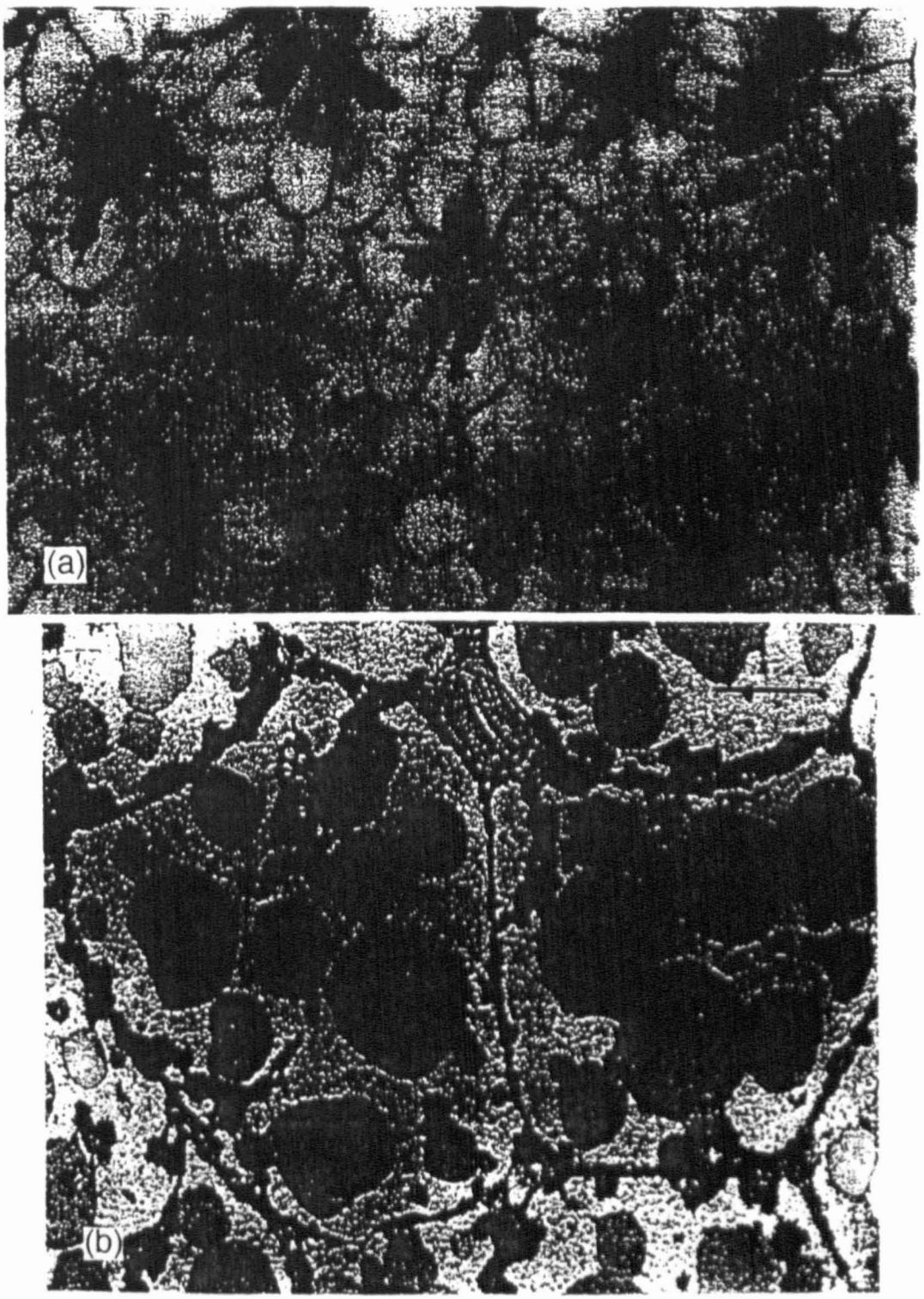

Fig. 3. Hepatocytes from fish fed experimental diets. Diet: 22% dietary lipid content. (a) Nucleus homogeneous with shape regular but displaced to hepatocyte peripheral (H&E). Bar = 10 μm. (b) Electron micrograph. Bar = 5 μm.

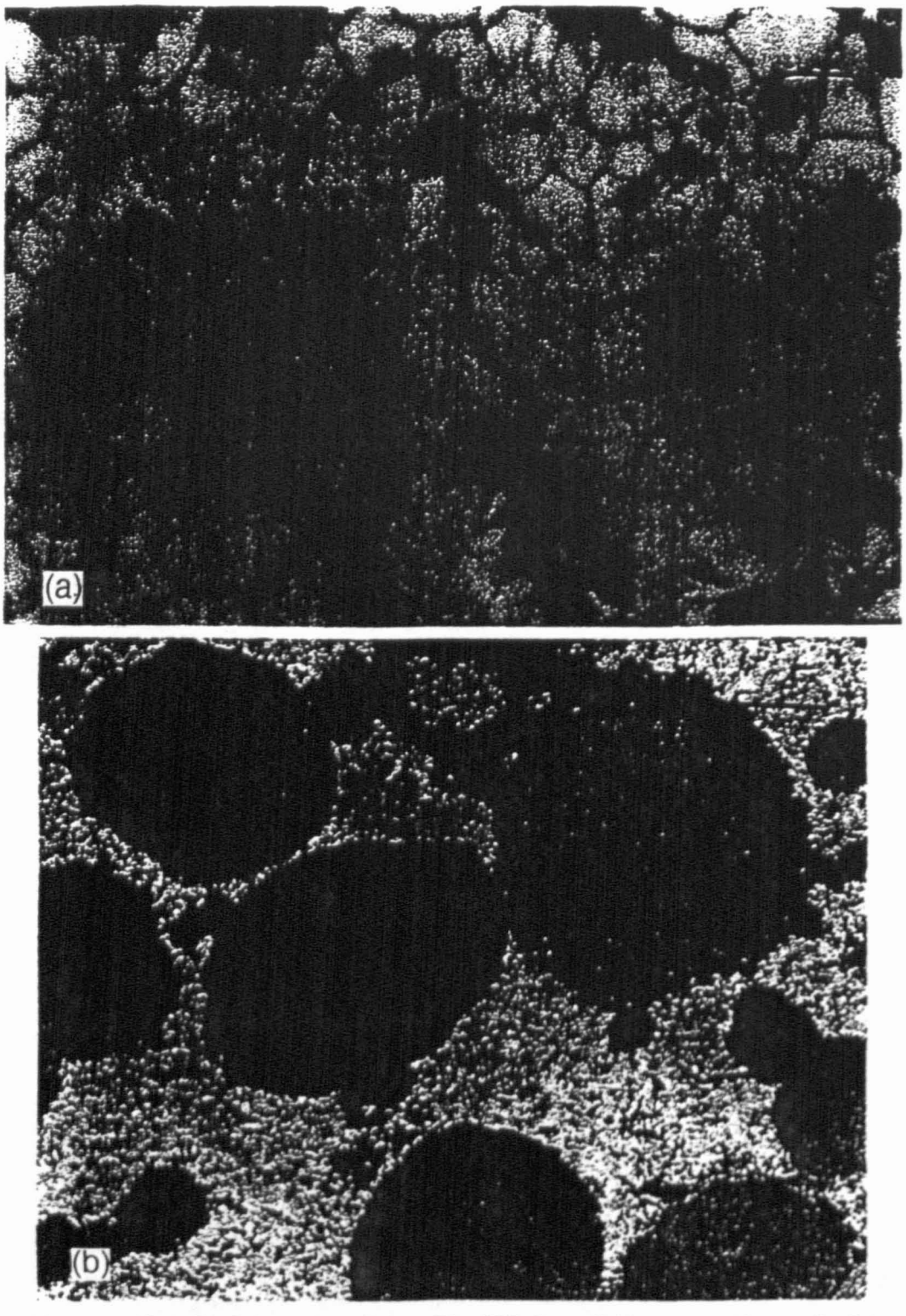

Fig. 4. Hepatocytes from fish fed experimental diets. Diet: 27% dietary lipid content and low quality fish meal. (a) Note hepatocyte with a morphology similar to livers from fish fed diets 22% dietary lipid (see Fig. 3a) (H&E). Bar = 10 μm. (b) Electron micrograph. Note the nucleus spherical. Bar = 2.5 μm.

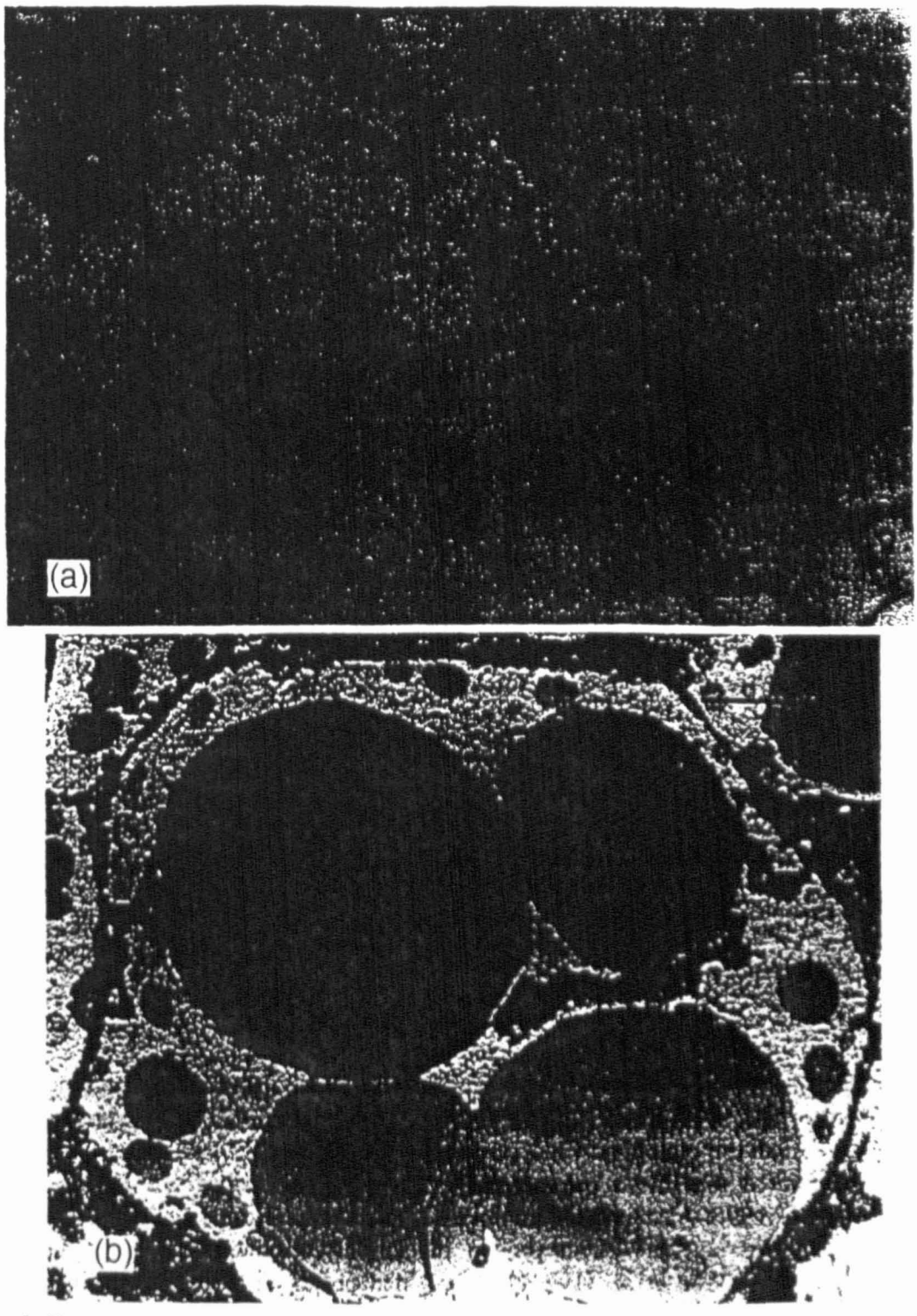

Fig. 5. Hepatocytes from fish fed experimental diets. Diet: 27% dietary lipid content and high quality fish meal. (a) Note swelling hepatocytes with enlarged irregular nucleus located at the periphery of the cell (H&E). Bar = 10 μm. (b) Electron micrograph. Note large lipid droplets. Bar = 5 μm.

Comparing growth results between the two fish meal qualities for each lipid level assayed, no differences in average final weight were found for fish fed diets with 15 and 27% dietary lipid (Fig. 1). On the contrary, for 22% dietary lipid fish fed with high quality fish meal, both pelletized and extruded, resulted in significantly ($P < 0.05$) better growth compared to fish fed diets containing the low quality fish meal (Fig. 1).

3.2. Histological examinations

Livers from fish fed 15% lipid had the same histological characteristics for both meal qualities assayed. Hepatocytes showed large and spherical nuclei centrally located with prominent nucleolus and a moderate eosinophilic cytoplasm (Fig. 2a).

There was no effect of fish meal quality on liver parenchymal morphology in fish fed the 22% lipid diet. Hepatocytes were similar to fish fed 15% lipid, the nuclei homogeneous in shape and chromatin density, but having migrated to the cell periphery (Fig. 3a).

Transmission electron microscopy studies agreed with this observation. Hepatocytes of fish fed the lowest dietary lipid levels showed a greater number of small lipid droplets (1.92 ± 1.83 μm diameter) and large nuclei with a high electron density nucleolus (Fig. 2b). On the contrary, hepatocytes from fish fed the 22% lipid diet showed a significantly ($P < 0.05$) higher lipid droplet diameter (4.35 ± 5.32 μm diameter) (Fig. 3b).

For the 27% dietary lipid level, fish fed the low quality meal showed similar characteristics as fish fed the 22% lipid diet containing the same fish meal (Fig. 4a and b).

On the contrary, fish fed the high quality meal and 27% lipid showed foci of swelling hepatocytes with enlarged irregular nuclei located at the periphery of the cell (Fig. 5a). Observation with transmission electron microscopy revealed large lipid droplets (4.47 ± 5.86 μm diameter) in a small number that coalesced among them, causing nuclei and cellular organella displacement to periphery of hepatocytes (Fig. 5b).

No differences were found in livers from fish fed the extruded and pelletized diets containing 22% dietary lipid.

4. Discussion

The quality of fish meal has been evaluated depending on the processing temperature and content of biogenic amines. Fish meal processing conditions such as temperature significantly affect the biological value of the product (Pike et al., 1990). Recent studies have demonstrated that these parameters influence fish growth (Pike et al., 1990; Moksness et al., 1995; Aksnes and Mundheim, 1997; Aksnes et al., 1997). In this way, temperature processing can affect protein digestibility, influencing in turn growth performance. Thus, Pike et al. (1990) reported that protein digestibility in mink was significantly reduced with increased processing temperature of fish meal. In addition, Aksnes and Mundheim (1997) described a reduction of 4% in protein digestibility for diets processed at high temperatures and, consequently, a reduction in growth for halibut

fed those diets. In the present study, fish growth showed a tendency to decrease when fish were fed diets prepared with low quality fish meal processed at 100°C compared to diets prepared with meals of high quality processed at 60°C. Differences in the processing temperature for the fish meals studied could be responsible for the different growth observed. In this respect, Danielssen et al. (1989) reported better growth rates in turbot fed a diet containing LT (low-temperature-processed) fish meal. Similar results have been observed for rainbow trout, Atlantic salmon (Mundheim and Opstvedt, 1989), and chinook salmon (McCallum and Higgs, 1989). Moksness et al. (1995) concluded that heat treatment may significantly alter the free amino acids in a diet, with negative effects on attractiveness and/or palatability, affecting juvenile wolffish growth.

In relation to dietary lipid level, lower growth rates were obtained in fish fed diets with 15% lipid content in both qualities of fish meal assayed. This could be related to an insufficient lipid level to meet energy needs, leading to a subsequent utilization of dietary protein for energy. This idea is in accordance with histological examinations of liver from fish fed these diets, where large and spherical nuclei centrally located in the hepatocytes and small lipid droplets were observed (Fig. 2a and b). This reflects the utilization of lipid by fish fed the lowest dietary lipid levels to obtain energy in agreement with the growth results. Thus, the low dietary lipid content of these diets may be responsible for the lack of effect of fish meal quality.

Growth of fish fed 22% dietary lipid increased in comparison with fish fed 15% dietary lipid regardless of or fish meal quality employed and indicates a protein sparing effect of dietary lipid. Protein retention is enhanced by the protein-sparing effect of dietary lipid (Kaushik and Cowey, 1991; Kaushik and Médale, 1994). Arzel et al. (1994) showed an increase in protein utilization by brown trout fed diets with high-lipid content. Van der Meer et al. (1997) reported an increase in protein deposition in *Colossoma macropomun* fed high dietary lipid levels. Vergara et al. (1996) reported a protein sparing effect of dietary lipid when increased from 9 to 15%, resulting in improved growth of *S. aurata*. In the present study, the effect of dietary lipid content was evident, but the sparing effect observed for 22% dietary lipid was more evident, for fish fed diets containing high quality fish meal that showed significantly higher growth.

The nuclear displacement to the hepatocyte periphery in livers from fish fed 22% dietary lipid and the larger lipid droplets showed in the ultrastructural study (Fig. 3a and b) may be only a reflection of liver adaptation to an increment of dietary lipid content. This could be in agreement with the results obtained by Mosconi-Bac (1987) who suggested that the presence of numerous and voluminous lipid droplets in hepatocytes may be a physiological response to lipid excess and therefore represents an energy storage but not a pathological situation. Segner and Witt (1990) also found that the increase of lipid in liver of turbot after the start of weaning may only be due to a change of feed and can be considered as an expression of a well-fed status rather than a pathological syndrome. Fontagné et al. (1998) reported that common carp larvae fed *Artemia* showed larger sized enterocytes and voluminous hepatocytes. These authors concluded that this is only a mechanical consequence of fat accumulation indicating a well-fed status and may not be related to nutritional disorders. In most marine fish, high lipid reserves in the liver appears to be an adaptive mechanism to periods of low trophic activities at low water temperatures (Kaushik, 1997).

Elevation of dietary lipid levels from 22 to 27% improved growth of fish fed low quality fish meal. However, the good growth obtained by feeding the fish 22% dietary lipid and high quality fish meal was not further improved when dietary lipid levels were increased up to 27%. This could be due to a possible sparing effect promoted by 27% dietary lipid when low quality fish meal was used, which was evident for high quality fish meal when dietary lipid levels increased from 15 to 22%.

Fish meal quality effects were observed on the hepatocytes' morphology. On the hand, for fish fed low quality fish meal similar hepatic morphology was observed when 27% (Fig. 4a and b) and 22% lipid levels (Fig. 3a) were fed. On the other hand, foci of swelling hepatocytes with enlarged irregular nuclei located at the periphery of the cell (Fig. 5a and b) were observed in fish fed the highest dietary lipid content and high quality fish meal. This observation agrees well with the fact that the increase in dietary lipid levels up to 27% was not able to further promote protein sparing in fish fed high fish meal quality, leading to an increased deposition of dietary fat in hepatocytes which was not observed when low quality fish meal was fed. Aksnes and Mundheim (1997) reported similar morphological characteristics on liver histology in Atlantic halibut fed diets with fish meal from spoiled raw materials and 16.7% lipid. These authors suggested a negative effect caused by the high biogenic amine content in that fish meal. In the present study, the biogenic amine content was lower that those reported by those authors, thus the dietary lipid level could affect liver histology more than the biogenic amine content in the diets.

The structural modifications of nuclei observed within hepatocytes could reflect a nutritional pathology. Several authors have reported that the hepatonuclear size can be used as an indicator of the nutritional condition of fish (Escaffre and Bergot, 1986; Segner and Braunbeck, 1988; Strüssmann and Takashima, 1990). Mosconi-Bac (1987) observed modifications of shape, nuclei chromatin density and the atypical deposition of lipid droplets in livers of European seabass fed artificial diets as an alteration in fatty acid metabolism, thus being signs of true nutritional pathology. Ghittino (1978) also considered this type of lipid deposition as a pathological process and has referred to it as fatty degeneration or steatosis, that can be used as an indicator of hepatic disturbances in the fat metabolism. Spisni et al. (1998) described steatosis as a liver alteration due to an excessive dietary intake of lipid which saturates the physiological capability of the liver leading to lipid droplet accumulation. Similar hepatic lipid deposition due to excessive caloric intake has been described for other vertebrates such as poultry, denoting a pathological situation (Stake et al., 1980).

In conclusion, the hepatic morphology observed in gilthead seabream fed diets containing 22% lipid and high or low quality meal reflects the storage of lipidic reserve without pathological consequences, whereas for diets with 27% lipid and high quality meal the steatosis observed could reflect the non-utilization of dietary lipid which was not observed for diets with low quality fish meal and same lipid level. Hence, these results show that the beneficial effects of dietary lipid level follow a curves and the location of the optimum point depends on the quality of the fish meal.

Finally, this work confirmed that the study of histological alterations due to nutritional imbalances provides an idea of the cell and tissue condition, complementing the information obtained with growth studies to evaluate the nutritional status of fish.

References

Aksnes, A., Mundheim, H., 1997. The impact of raw material freshness and processing temperature for fish meal on growth, feed efficiency and chemical composition of Atlantic halibut (*Hippoglossus hippoglossus*). Aquaculture 149, 87–106.

Aksnes, A., Izquierdo, M.S., Robaina, L., Vergara, J., Montero, D., 1997. Influence of fish meal quality and feed pellet on growth, feed efficiency and muscle composition in gilthead seabream (*Sparus aurata*). Aquaculture 153, 251–261.

Bautista, M.N., De la Cruz, M.C., 1988. Linoleic ($\omega 6$) and linolenic ($\omega 3$) acids in the diet of fingerling milkfish (*Chanos chanos* Forsskal). Aquaculture 71, 347–358.

Bell, J.G., Tocher, D.R., MacDonald, F.M., Sargent, J.R., 1995. Effects of dietary borage oil (enriched in γ-linoleic acid, 18:3($n-6$)) or marine fish oil (enriched in eicopentaenoic acid, 20:5($n-3$)) on growth, mortalities, liver histopathology and lipid composition of juvenile turbot (*Scophthalmus maximus*). Fish Physiol. Biochem. 14, 373–383.

Danielssen, D.S., Gulbrandsen, K.E., Hjertnes, T., 1989. Fish meal quality in dry feed for turbot (*Scophthalmus maximus* L.). Eur. Aquacult. Soc., Spec. Publ. 7, 83–84.

Escaffre, A.M., Bergot, P., 1986. Morphologie quantitative du foie des alevins de truite arcen-ciel (*Salmo gairdnerii*) issus de gros ou de petits oeufs: incidence de la date de premier repas. Arch. Hydrobiol. 107, 331–348.

Fontagné, S., Geurden, Y., Escaffre, A.M., Bergot, P., 1998. Histological changes induced by dietary phospholipids in intestine and liver of common carp (*Cyprinus carpio* L.) larvae. Aquaculture 161, 213–223.

Ghittino, P., 1978. L'ascite della cieca (*Anguilla anguilla*) d'allevamento da degenerazione lipoidea epatica. Riv. Ital. Piscic. Ittiop. A 13, 97–100.

Godino, C., Santiago, A., Santamaria, J., 1990. Estudio histopatológico de las alteraciones producidas en higado de doradas (*Sparus aurata*) alimentadas con piensos almacenados a diferentes temperaturas. III Congreso Nacional Acuicultura, 715–720.

Hibiya, T., 1982. An Atlas of Fish Histology: Normal Pathological and Features. Kodansha, Tokyo, Japan.

Kaushik, S.J. 1997. Nutritional and the improvement of the seabass and seabream production in the Mediterranean region. Recent Developments in the Nutrition and Feeding of Marine Finfish of Interest to the Mediterranean. ALIIA Trades Show, Thessaloniki, Greece, September 27th.

Kaushik, S.J., Cowey, C.B., 1991. Dietary factors affecting nitrogen excretion by fish. In: Cowey, C.B., Cho, C.Y. (Eds.), Nutritional Strategy and Aquaculture Waste. Proceedings of the First International Symposium on Nutritional Strategies in Management of Aquaculture Waste. University of Guelph, Guelph, Ontario, Canada, 3–19 pp.

Kaushik, S.J., Médale, F., 1994. Energy requirements, utilization and dietary supply to salmonids. Aquaculture 124, 81–97.

McCallum, I.M., Higgs, D.A., 1989. Aspects of protein utilization in juvenile chinook salmon (*Oncorhynchus tshawytscha*). Nutritive value of marine protein sources considering the effects of processing conditions. Aquaculture 77, 181–200.

Moksness, E., Rosenlund, G., Lie, O., 1995. Effect of fish meal quality on growth of juvenile wolffish, *Anarhichas lupus* L. Aquacult. Res. 26, 109–115.

Mosconi-Bac, N., 1987. Hepatic disturbances induced by artificial feed in the sea bass (*Dicentrarchus labrax*) during the first year of life. Aquaculture 153, 251–261.

Mundheim, H., Opstvedt, O., 1989. Effect of dietary level of protein and fiber on apparent protein digestibility in the rainbow trout (*Oncorhynchus mykiss*) and salmon (*Salmon salar*) and comparison of protein digestibility in mink (*Mustela vison*), rainbow trout and salmon. In: Takeda, M., Watanabe, T. (Eds.), The Current Status of Fish Nutrition in Aquaculture. Laboratory of Fish Nutrition, Tokyo, pp. 195–200.

Pike, I.H., Andorsdottir, G., Mundheim, H., 1990. The role of fish meal in diets for salmonids. Technical Bulletin No. 24. IAFMM, March.

Segner, H., Braunbeck, T., 1988. Hepatocellular adaptation to extreme nutritional conditions in ide, *Leuciscus idus melanotus* L. (Cyprinidae). A morphofunctional analysis. Fish Physiol. Biochem. 5, 79–97.

Segner, H., Juario, J.V., 1986. Histological observations on the rearing of milkfish, *Chanos chanos*, fry using different diets. J. Appl. Ichthyol. 4, 162–173.

Segner, H., Witt, U., 1990. Weaning experiments with turbot (*Scophthalmus maximus*): electron microscopic study of liver. Mar. Biol. 105, 353–361.

Sokal, R.R., Rohlf, F.J., 1995. Biometry. Freeman, New York.

Spisni, E., Tugnoli, M., Ponticelli, A., Mordenti, T., Tomasi, V., 1998. Hepatic steatosis in artificially fed marine teleosts. J. Fish Dis. 21, 177–184.

Stake, P.E., Fredrickson, T.N., Bourdeau, C.A., 1980. Induction of fatty liver-hemorrhagic syndrome in laying hens by exogenous β-estradiol. Avian Dis. 25, 410–422.

Storch, V., Juario, J.V., 1983. The effect of starvation and subsequent feeding on the hepatocytes of *Chanos chanos* (Forsskal) fingerlings and fry. J. Fish Biol. 23, 95–103.

Storch, V., Stählin, W., Juario, J.V., 1983. Effect of different diets on the ultrastructure of hepatocytes of *Chanos chanos* fry (Chanidae: Teleostei): an electron microscopic and morphometric analysis. Mar. Biol. 74, 101–104.

Strüssmann, C.A., Takashima, F., 1990. Hepatocyte nuclear size and nutritional condition of larval pejerrey, *Odontesthes bonariensis* (Cuvier et Valenciennes). J. Fish Biol. 36, 59–65.

Tacon, A., 1994. Feed ingredients for carnivorous fish species. Alternatives to fish meal and other fishery resources. Fish Circ. No. 881. FAO, Rome.

Tucker, J.W., Llellis, W.A., Vermeer, G.K., Roberts, D.E., Woodward, P.N., 1997. The effects of experimental started diets with different levels of soybean or menhaden oil on red drum (*Sciaenops ocellatus*). Aquaculture 149, 323–339.

Van der Meer, M.B., Zamora, J.E., Verdegem, M.C.J., 1997. Effect of dietary lipid level on protein utilization and the size and proximate composition of body compartments of *Colossoma macropomun* (Cuvier). Aquacult. Res. 28, 405–417.

Vergara, J.M., Robaina, L., Izquierdo, M.S., De la Higuera, M., 1996. Protein sparing effect of lipids in diets for fingerlings of gilthead seabream. Fish. Sci. 62, 624–628.

Verreth, J., Coppoolse, J., Segner, H., 1994. The effect of low HUFA- and high HUFA-enriched *Artemia*, fed at different feeding levels, on growth, survival, tissue fatty acids and liver histology of *Clarias gariepinus* larvae. Aquaculture 126, 137–150.

Watanabe, T., Thongrod, S., Takeuchi, T., Satoh, S., Kubota, S.S., Fujimaki, Y., Young-Cho, C., 1989. Effect of dietary $n-6$ and $n-3$ fatty acids on growth, fatty acid composition and histological changes of white fish *Coregonus lavaretus maraena*. Nippon Suisan Gakkaishi 55, 1977–1982.

Caracterización de las familias hidrogeoquímicas en el acuífero de La Aldea (Gran Canaria)

M.C. Cabrera[1], F. Delgado Mangas[2], J. Muñoz Sanz[1], F.J. Pérez Torrado[1] y E. La Moneda[3]

1 Departamento de Física-Geología. Facultad de Ciencias del Mar, ULPGC. Campus Universitario de Tafira. 35017- Las Palmas de Gran Canaria. España. ccabrera@cicei.ulpgc.es
2 Dpto. Ingeniería del Terreno/CIHS. ETSICCP. UPC. C/Gran Capitán s/n, Módulo D-2. Barcelona. España.
3 Instituto Tecnológico Geominero de España. C/Alonso Alvarado, 43, 2°-A. 35002-Las Palmas de G.C.

ABSTRACT

The hydrogeochemical study of groundwater at La Aldea aquifer (West Gran Canaria) has allowed to characterize different groundwater families, depending on the exploited materials and/or the existence of some modifying phenomena. Cl-Mg and Na-Mg waters are related with basalts exploitation; Cl-Na high saline waters come from Las Tabladas cliff, and are suffering a mixing with the alluvial groundwater. The mixing waters are Cl-Na-Ca, and can evolve to Cl-SO_4-Na and SO_4-Cl-Na when irrigation returns are present.

Key words: *volcanic aquifer, salinization, hydrogeochemical family, irrigation returns, Gran Canaria.*

INTRODUCCIÓN

El área de estudio se encuentra en el extremo más occidental de la isla de Gran Canaria, en el municipio de S. Nicolás de Tolentino, conocido tradicionalmente como "La Aldea" (Fig. 1). Se caracteriza por su relieve abrupto, con la existencia de grandes desniveles debidos a la intensa actividad erosiva que se ha desarrollado en la isla que ha llevado a la formación de profundos barrancos. En general, las costas son altas y escarpadas, ofreciendo abrigo únicamente la Playa de La Aldea, que está abierta hacia el oeste.

Como precedentes de estudios dedicados a la hidrogeología de las islas cabe destacar los proyectos Canarias SPA-15 (1974) y MAC-21 (1980). Durante ambos proyectos se visitaron varios pozos de la zona de estudio, destacándose en el SPA-15 el alto contenido en fluoruros en la zona. Sin embargo, no fue hasta 1992 cuando se llevó a cabo un inventario exhaustivo de todas las captaciones de la zona (Plan Hidrológico de Gran Canaria, 1993). Este inventario sirvió de base para el informe hidrogeológico de la zona que se elaboró dentro del proyecto "Development of analytical and sampling methods for priority pesticides and relevant transformation products in aquifers" (Muñoz, Cabrera *et al.*, 1996), dedicado al estudio de la contaminación por plaguicidas de las aguas subterráneas. En este estudio salió a la luz la existencia de aguas extremadamente salobres (con contenidos en cloruros que superan los 7.000 mg/l), cuyo origen está en estudio. La presente comunicación presenta la situación espacial de los tipos de agua presentes en la zona así como unas primeras interpretaciones sobre su caracterización hidrogeoquímica.

FUNCIONAMIENTO DEL SISTEMA ACUÍFERO

El modelo de flujo de la isla se puede esquematizar como un cuerpo único de agua aunque estratificado y heterogéneo en el que la recarga tiene lugar en las cumbres y la circulación hacia la costa, con salidas intermedias en manantiales (hoy secos y substituidos por las extracciones de los pozos) y al mar, y descarga artificial por pozos. El flujo se canaliza preferentemente por los materiales más permeables próximos a la superficie (SPA-15, 1974) (Custodio *et al.*, 1989).

El Valle de La Aldea se abre hacia el Oeste de la isla, rodeado por altas montañas. El Barranco, excavado en basaltos pertenecientes a la Fm. Basaltos Antiguos (14.5-14.1 Ma), presenta en su lecho una capa de conglomerados aluviales, con un espesor medio de 15-20 m. Al Norte de la zona (Las Tabladas) existe un escarpe rocoso en el que afloran una sucesión de materiales detríticos y volcánicos de los Ciclos I, II y III de formación de la isla. Entre ellos destacan unos depósitos ignimbríticos deslizados con intercalaciones de materiales alterados hidrotermalmente conocidos localmente como "azulejos".

Existen en la zona más de 370 pozos de gran diámetro (3-4 m), excavados a mano, con profundidades que oscilan entre los 10 y los 47 m, con una media de 22.5 m (Plan Hidrológico de Gran Canaria, 1992). Todos los pozos situa-

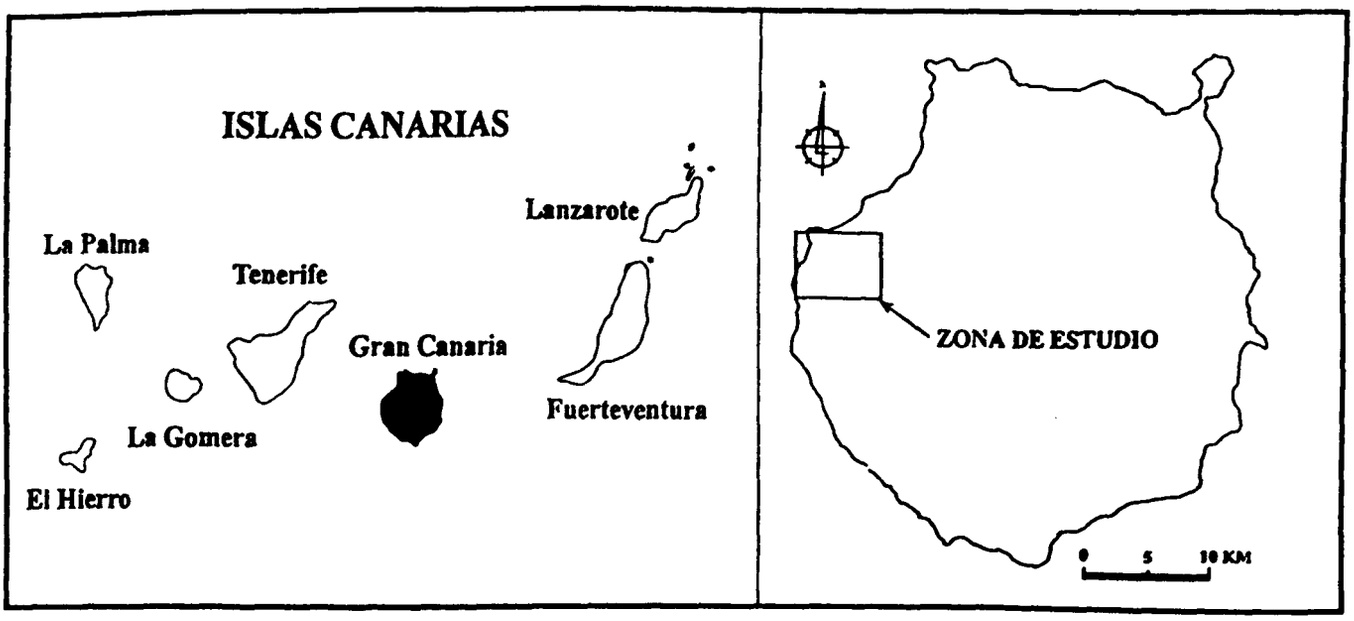

FIGURA 1: *Mapa de situación de la zona de estudio.*

dos en la parte central del acuífero explotan agua de los conglomerados aluviales, aunque algunos atraviesan también los basaltos situados debajo, sacando agua conjuntamente de ambos materiales. En el Barranco de Tocodomán, los pozos explotan exclusivamente los Basaltos Antiguos. El flujo se produce desde el Este al Oeste, siguiendo el Barranco, de manera que en los bordes del acuífero, los materiales basálticos ceden agua a los conglomerados. En la zona central del acuífero, se trataría de un medio de doble permeabilidad, en el que la Fm. Basaltos Antiguos funciona como un acuitardo frente a los conglomerados, que constituyen el acuífero principal (Muñoz *et al.*, 1996), mientras que en el Barranco de Tocodomán, el agua procede exclusivamente de los materiales basálticos.

DIFERENCIACIÓN DE LAS FAMILIAS HIDROGEOQUÍMICAS

El estudio hidrogeoquímico en la zona se ha basado en más de 160 análisis de agua, realizados en 1992 y 1997. El examen detallado de esta información ha incluido, entre otras cosas, la diferenciación de varias familias de agua, lo que ha permitido correlacionarlas con los materiales de que proceden y con los procesos modificadores que pueden haber sufrido. La distribución espacial de estas familias de refleja en la figura 2, que representa, mediante diagramas de Stiff modificados, los análisis realizados en 1997.

Las familias de agua que pueden diferenciarse son las siguientes:

- *Aguas cloruradas sódicas*: situadas a lo largo del escarpe de Las Tabladas, presentan un contenido en sales disueltas que oscila entre los 1.7 y los 13.26 g/l. Composicionalmente son muy semejantes al agua de mar, y en general presentan un incremento en el contenido en Ca^{++} y CO_3H^- atribuible a la disolución de CO_3Ca y de Mg^{++}, debido posiblemente a la entrada de agua de los basaltos antiguos. En algunos pozos hay un incremento notable en el sulfato respecto al agua de mar, que coincide con un alto contenido en NO_3^-.
- *Aguas cloruradas sódico cálcicas*: Con contenidos en sales disueltas entre 1.2 y 2.8 g/l, se sitúan bordeando a las anteriores hacia el centro del aluvial. En general, las aguas de este tipo son muy semejantes entre sí, pudiéndose observar variaciones del contenido en sulfatos y en los contenidos en Mg^{++} en algunos pozos.
- *Aguas cloruradas sulfatadas sódicas y sulfatadas cloruradas sódicas*: situadas en zonas con explotaciones de tomates, estas aguas son anómalas dentro de los rangos de composición química del acuífero, debido a los altos contenidos en sulfatos. Presentan un contenido en nitratos que puede alcanzar los 400 mg/l.
- *Aguas cloruradas magnésicas*: se encuentran al sur de la zona de estudio, en los pozos que explotan exclusivamente los materiales basálticos. Tienen una salinidad alta (TSD=3-4 g/l).
- *Aguas sulfatadas magnésicas*: situadas en el Barranco de Tocodomán, son similares a las anteriores, pero con un mayor contenido en sulfatos.
- *Agua bicarbonatada sódica:* se trata de un tipo de agua anómala, con un contenido en sales disueltas en torno a 0.8 g/l. Son similares al agua de presa con un ligero descenso en el Ca^{++}.

DISCUSIÓN Y CONCLUSIONES

La distribución de las aguas en la zona central del acuífero permite caracterizar la entrada de aguas con una alta salinidad procedentes de Las Tabladas (aguas cloruradas sodicas). Al llegar al Valle, este agua sufre un lavado con

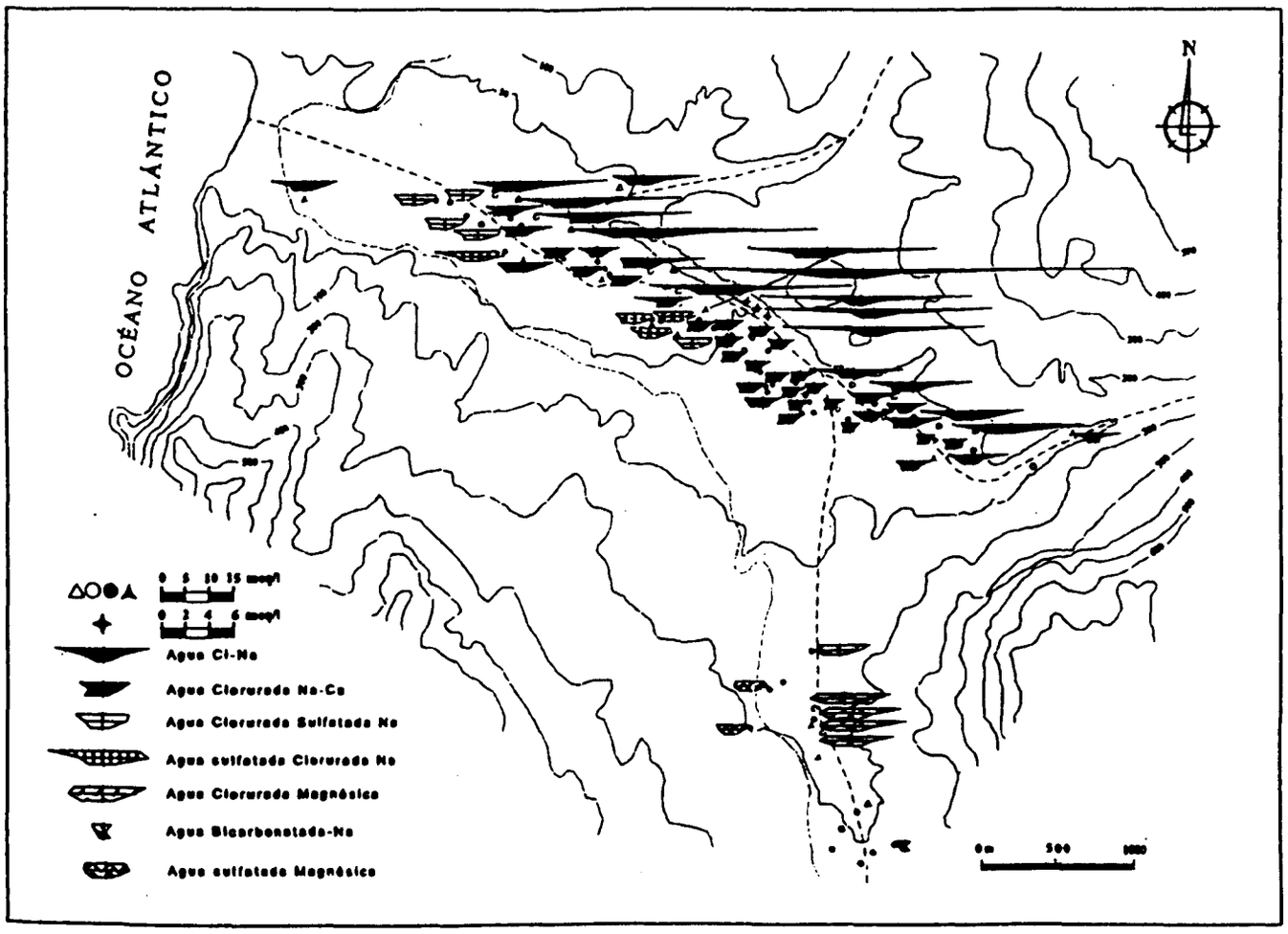

FIGURA 2: *Mapa hidrogeoquímico de la zona de estudio con diagramas de stiff modificados.*

las aguas que discurren por el aluvial dando lugar a las aguas cloruradas sódico cálcicas y posteriormente incorporan un porcentaje alto de retornos de riego, sufriendo un aumento en los contenidos en nitratos (aguas cloruradas sulfatadas sódicas y sulfatadas cloruradas sódicas). El origen de dicha salinidad está actualmente en estudio, aunque se puede adelantar que parece deberse a una mezcla de tres procesos: contaminación por retornos de riego, efecto climático que produciría una aridificación de la recarga y lavado de materiales con un alto contenido en sales (azulejos).

La situación de las aguas cloruradas magnésicas permite relacionarlas con la explotación de los Basaltos Antiguos, según una relación roca-agua ya indicada en el SPA-15 (Fernandopullé, 1975). Las aguas sulfatadas magnésicas proceden también de estos materiales, y presentan contenidos algo más altos en nitratos apuntando a la existencia de contaminación por retornos de riego. El agua bicarbonatada sódica, anómala dentro del acuífero, no tiene un origen claro, aunque se puede sospechar que el pozo puede estar experimentando algún aporte del agua procedente de las presas que discurre por un canal en la ladera de la montaña, a cotas algo superiores al pozo.

AGRADECIMIENTOS

El presente estudio ha sido financiado mediante un Convenio de colaboración entre el Consejo Insular de Aguas de Gran Canaria, la Fundación Universitaria de Las Palmas y la Universidad de Las Palmas de G.C. y por el Proyecto CICYT con fondos FEDER 1FD97-0525.

REFERENCIAS

Custodio, E., Jiménez, J., Núñez, J.A., Puga, L. y Braojos, J.J. (1989): Hydrogeology of the Canary Islands (Spain). Hidrogeología y Recursos Hidráulicos, vol. XIV. Asoc. Esp. Hidr. Subt. ITGE. Madrid: 205-227.

Fernandopullé, D. (1975): "Chemical clasification of groundwater and factors influencing hydrochemistry in Gran Canaria Island". Simp. Intern. Hidr. Terr. Volc.: 529-560.

MAC-21. (1980): Proyecto de Planificación y Explotación de los Recurso de agua en el Archipiélago Canario. Com. Interminist. Coord. Est. Mat. Aguas Canarias.

Muñoz, R., Cabrera, M.C., Hernández, F. y Socorro, A.R. (1996): Final Project Report. EU Contract EV5V-CT93-0322-Group 4, 87 p. + Appendix.

Plan Hidrológico de Gran Canaria (PHGC) (1992): Inventario de ptos. de agua, inédito.

SPA-15. (1975): Estudio científico de los recursos de agua en las Islas Canarias (SPA/69/515). Minist. Obras Públ, Dir. Gral. Obr. Hidr. UNESCO. Las Palmas de Gran Canaria, Madrid. 3 vol. + mapas.

"Beachrocks" de La Palma, Islas Canarias

F. Calvet[1], A. Aguilar[1], J.C. Carracedo[2], F.J. Pérez-Torrado[3], C. Recio[4] y A. Travé[1]

1 Departament de Geoquímica, Petrologia i Prospecció Geològica, Facultat de Geologia, Universitat de Barcelona, 08071- Barcelona
2 Estación Volcanológica de Canarias, CSIC, Avda. Astrofísico Francisco Sánchez, 3, 38080-La Laguna (Tenerife)
3 Departamento de Física-Geología, Facultad de Ciencias del Mar, Universidad de Las Palmas de Gran Canaria, 35017 - Las Palmas de Gran Canaria
4 Servicio General de Análisis de Isótopos Estables, Facultad de Ciencias, Universidad de Salamanca, 37008 - Salamanca

ABSTRACT

The "beachrocks" studied crop out in the southwestern part of the island of La Palma (Canary Islands), specifically in the Puerto Naos, Charco Verde, Las Zamoras, Chica and Echentive beaches. All these beaches are developed on the lavas of the Cumbre Vieja volcano, corresponding to different eruptions with ages from 20.000 to less than 30 years.

The beachrocks are up to 1.5 m in thickness, attain some tens of metres in width and consist of several decimetric-thick horizons, dipping 2-15º seaward. The beachrocks are rudstones and arenites, with volcanic clasts as main components. The porosity of the beachrocks is intergranular and locally intragranular, both partially occluded by cements, neomorphic texture and locally by internal sediment.

The beachrocks are cemented by different types of aragonite (fibrous, microfibrous and botroidal) and HMC (micritic and peloidal) cements. The HMC micritic cement constitutes the first cementation phase. The aragonitic cements, with a very high content of strontium (with a mean of 10.000 ppm) and a high content of sodium (with a mean of 2.000 ppm), constitute the second phase of cementation. The peloidal cement is the third phase of cementation. The oxygen isotopic composition of the aragonite cement ranges from -4.2 to -2.4 ‰ PDB and the carbon isotopic composition of the fibrous aragonite cement varies from +4.0 to +4.9 ‰ PDB.

***Key words**: beachrocks, marine cements, Holocene, La Palma (Canary Islands).*

INTRODUCCIÓN

Las arenas y los clastos de playa litificados mediante cementos carbonatados dan lugar a una roca que se denomina "beachrock" (Ginsburg, 1953). Las playas son un emplazamiento ideal para la precipitación de cementos marinos, ya que las condiciones de alta energía (debida a la acción del oleaje y de las mareas) y la presencia de un sedimento tamaño arena y/o rudita con una alta porosidad y permeabilidad original, aseguran volúmenes adecuados de agua sobresaturada capaz de circular a través del sedimento produciendo su cementación. En general, esta cementación ocurre en la zona intermareal (Neumeier, 1998), pero también puede ocurrir en la parte alta de la zona submareal (Alexandersson, 1972) y en la parte baja de la zona supramareal (Holail y Rashed, 1992). Los "beachrocks" se disponen generalmente paralelos, y a veces perpendiculares, a la línea de costa formando cuerpos continuos de hasta varias decenas de kilómetros, parches métricos discontinuos o nódulos decimétricos. En general, no exceden del metro de potencia, aunque se han citado depósitos de hasta 5 metros de potencia (Amieux *et al.*, 1989), y buzan suavemente (con un máximo de 15º) en dirección al mar siguiendo la disposición de la playa, desarrollándose en la parte alta del "shoreface".

El interés del estudio de los "beachrocks" actuales o subactuales recae en su potencial como protectores eficaces contra la erosión litoral gracias a su morfología en horizontes inclinados hacia el mar y a su gran resistencia a la erosión. Además, como los "beachrocks" se originan en la zona intermareal, su localización permite determinar las variaciones del nivel del mar en el registro fósil.

Los principales objetivos de este trabajo son: i) Caracterizar desde un punto de vista geométrico, textural y petrográfico los "beachrocks" de la isla de La Palma (Islas Canarias); ii) Presentar las características microtexturales, mineralógicas y geoquímicas (geoquímica elemental e isótopos estables) de los distintos tipos de cementos y texturas neomórficas; iii) Interpretar el origen de los "beachrocks".

CARACTERÍSTICAS GEOLÓGICAS DE LA PALMA

La isla de La Palma está situada en el extremo occidental del Archipiélago Canario. En ella afloran tanto materiales de las fases de crecimiento submarino como subaéreo

(Fig. 1). La formación submarina, de edad Pliocena, ha sido levantada y basculada por las intrusiones magmáticas posteriores, por lo que las formaciones subaéreas, Cuaternarias, descansan sobre una discordancia angular y erosiva.

La construcción subaérea de La Palma se caracteriza por la formación de varios edificios volcánicos superpuestos y yuxtapuestos, con una tendencia general de migración del volcanismo en dirección Norte-Sur (Carracedo *et al.*, 1997). La etapa final de construcción de La Palma (los últimos 150.000 años) se caracteriza por la concentración de la actividad eruptiva en un rift de dirección N-S (el edificio Volcánico Cumbre Vieja), localizado en le mitad meridional de la isla (Fig. 1). La actividad eruptiva en el edificio Cumbre Vieja continúa en la actualidad, con al menos una docena de erupciones durante el Holoceno, de las cuales aproximadamente la mitad corresponden a los últimos 500 años (periodo histórico), siendo la del volcán Teneguía en 1971 la última erupción volcánica ocurrida en Canarias. Esta actividad se produce asimismo en el extremo submarino del rift, lo que permite suponer que tanto el rift como la isla seguirán creciendo en esta misma dirección.

DISPOSICIÓN DE LOS "BEACHROCKS" DE LA PALMA

Los "beachrocks" estudiados se localizan a lo largo de la costa suroccidental de la Palma, entre el pueblo de Punta Naos y el faro de Fuencaliente. Más concretamente, los "beachrocks" afloran en las playas de Punta Naos, Charco Verde, Las Zamoras, Chica y Echentive, todas ellas desarrolladas sobre lavas que conforman la costa occidental del edificio volcánico de Cumbre Vieja (Fig. 1).

"Beachrock" de la playa de Punta Naos. La playa de Punta Naos se desarrolla sobre las lavas volcánicas de la erupción del año 1585 (Carracedo *et al.*, 1997). En estos "beachrocks" se aprecia una abundante presencia (sobre un 40%) de cantos derivados de los materiales volcánicos submarinos pliocenos, mientras que en la playa actual más del 90% de los cantos son basálticos derivados de las lavas de Cumbre Vieja. La existencia de un "delta lávico" al norte de Punta Naos, formado por lavas de la erupción de 1949 (Carracedo *et al.*, 1997), pudo provocar un corte en el suministro litoral de cantos de la formación submarina desde el lugar de aporte (desembocadura del Barranco de Las Angustias) hasta Punta Naos. De esta forma, estos "beachrocks" deben haberse formado con posterioridad a la erupción de 1585 y con anterioridad a la de 1949.

Geométricamente se presentan con una potencia aproximada de 1.5 m, anchura de unos 20 m, se extienden unos 200 m a lo largo de la playa y buzan entre 5 y 10° hacia el mar. Texturalmente, el "beachrock" está constituido por ruditas y arenitas.

"Beachrock" de la playa de Charco Verde. Se desarrollan sobre lavas tipo "plataformas" que presentan edades inferiores a los 20.000 años (Carracedo *et al.*, 1997), siendo parcialmente cubiertos por lavas de la erupción de 1585. El "beachrock" tiene aproximadamente unos 50 cm de potencia, unos 10 m de ancho y se extiende unos 200 m a lo largo de la playa y directamente sobre las lavas "plataformas". Presenta un solo horizonte bien cementado constituido por ruditas, generalmente en la parte superior, y arenitas, con buzamientos entre 2 y 4° hacia el mar.

"Beachrock" de la playa de Las Zamoras. Esta playa se localiza sobre lavas volcánicas del tipo "plataforma" de edades inferiores a 20.000 años (Carracedo *et al.*, 1997). El "beachrock", destruido parcialmente durante el temporal del 6 de enero de 1999, tenía aproximadamente 1 m de potencia, unos 15 m de ancho, se extendía unos 50 m a lo largo de la playa, buzando unos 10° hacia el mar, y estaba constituido por microconglomerados y arenitas bien cementadas. El horizonte superior, poco cementado, estaba formado por ruditas, microconglomerados y arenitas. La superficie superior de este horizonte presentaba depresiones de 5 a 20 cm de profundidad y de algunos decímetros de diámetro interpretadas como estructuras de disolución (karst intermareal) del tipo "kamenitza".

"Beachrock" de la playa Chica Esta playa, prolongación meridional de la anterior, se desarrolla también sobre lavas tipo "plataforma". El "beachrock" tiene unos 30 cm de potencia, unos 10 m de ancho, y forma parches métricos en distintos puntos de la playa. Presenta buzamientos entre 10 a 15° hacia el mar y está constituido por ruditas y arenitas bien cementadas.

"Beachrock" de la playa de Echentive La playa y lagos de Echentive se desarrollan sobre lavas de la erupción de 1677, y están parcialmente cubiertos por lavas de la erupción del Teneguía en 1971 (Carracedo *et al.*, 1997). Los lagos se sitúan en la zona más interna de la playa, a unos 200 m de la línea de costa y presentan diámetros de unos 30 m y profundidades de hasta 4 m. El "beachrock" aflora en los márgenes, en concreto en la zona intermareal, de los lagos, tiene 1 m de potencia y está constituido por brechas de cantos angulosos a subangulosos de lavas volcánicas.

CEMENTOS DE LOS "BEACHROCKS"

El principal rasgo diagenético de los "beachrocks" es la cementación mediante cementos de aragonito y de HMC. Los cementos de aragonito son el cemento fibroso, el cemento microfibroso y el cemento botroidal, y los cementos de HMC son el micrítico y el peloidal.

El cemento micrítico de HMC es relativamente abundante, ocupa la porosidad intergranular, presenta localmen-

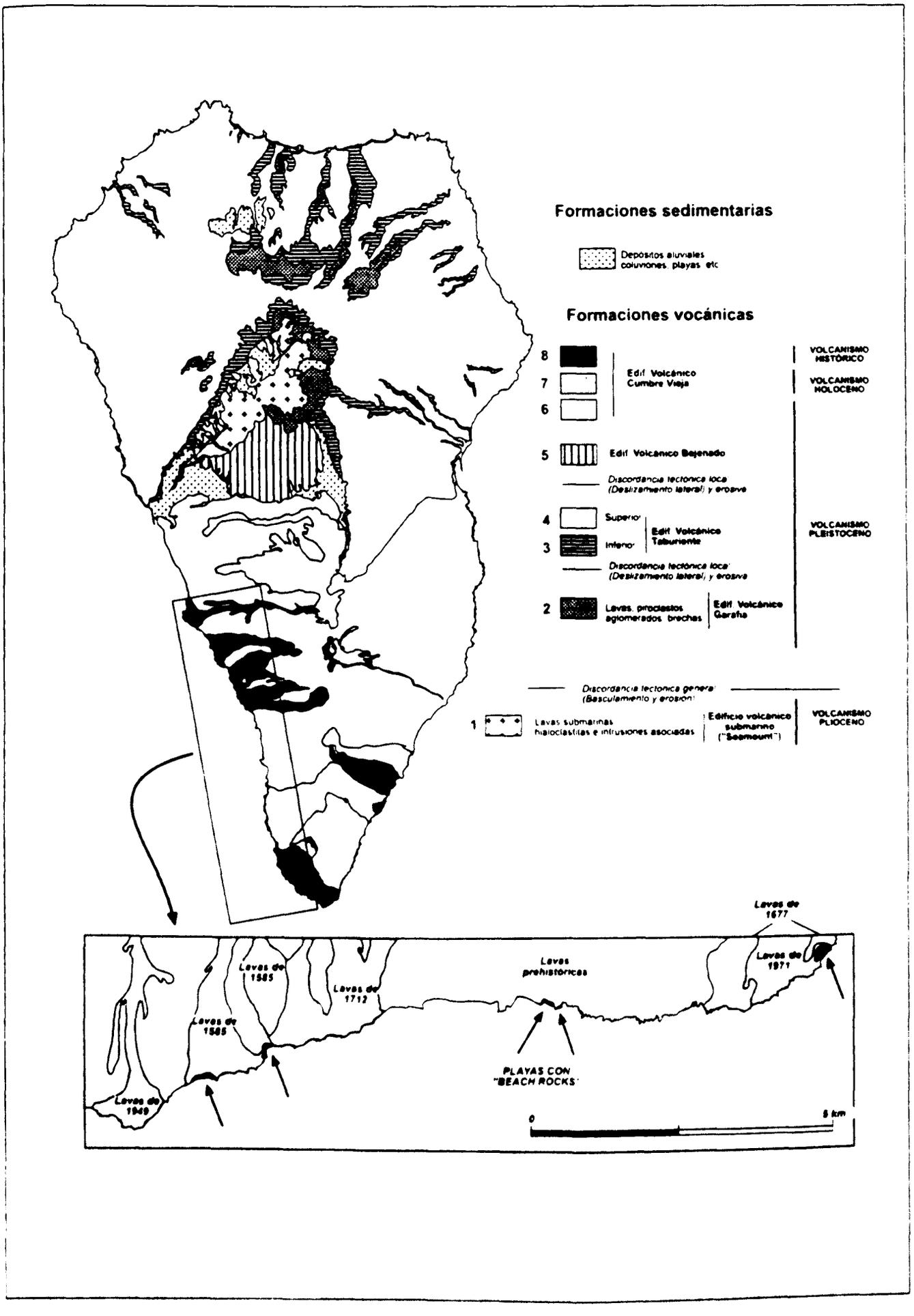

FIGURA 1. *Esquema geológico de La Palma y situación de los "beachrocks" estudiados*

te características de "microbialites" y constituye la primera etapa de cementación de los "beachrocks". Texturas similares al cemento micrítico de HMC han sido descritas en numerosos "beachrocks" por Alexandersson (1972), Bernier *et al.*, (1990), Holail y Rashed (1992), Font y Calvet (1997), Neumeier (1998), entre otros.

El cemento fibroso de aragonito ocupa gran parte de la porosidad intergranular, localmente también la porosidad intragranular, y está constituido por cristales fibrosos de 50 µm a 1.4 mm de largo y entre 7 y 100 µm de ancho. Cementos similares han sido reconocidos en "beachrocks" por Ginsburg (1953), Beier (1985), Bernier *et al.*, (1990), Font y Calvet (1997) y Neumeier (1998). Los valores del estroncio de este cemento varían entre 5.900 y 12.850 ppm, con una media de 9.210 ppm (que equivale a un aragonito con casi un 1% de CO_3Sr). El contenido en sodio oscila entre 1.290 y 2.530 ppm, con una media de 1.810 ppm. El cemento fibroso de aragonito constituye la segunda etapa de cementación de los "beachrocks" cuando está presente el cemento micrítico.

El cemento peletoidal de HMC ocupa la porosidad intrapartícula y constituye la última etapa de cementación de los "beachrocks". Los peloides, de 20 a 50 µm de diámetro, estan constituidos por cristales de HMC de 1 a 4 µm. Cementos similares han sido descritos en "beachrocks" por Amieux *et al.*, (1989), Font y Calvet (1997), Neumeier (1998), entre otros.

ISÓTOPOS ESTABLES DE LOS CEMENTOS

Los valores de la composición isotópica del oxígeno del cemento fibroso de aragonito varían entre –4.2 ‰ PDB y –2.4 ‰ PDB. Los cementos aragoníticos del "beachrock" de Charco Verde (con una media de –4.0 ‰ PDB) presentan valores más ligeros que los "beachrocks" de playa Chica (con una media de –3.0 ‰ PDB).

Los valores de $\delta^{18}O$ de los cementos aragoníticos de la isla de La Palma son similares a algunos de los descritos por Neumeier (1998) en "beachrocks" de la Polinesia (Océano Pacífico). Pero en general son algo más ligeros que los cementos aragoníticos citados por Magaritz *et al.*, (1979) y Beier (1985), y bastante más ligeros que los cementos de aragonito y/o de HMC de "beachrocks" del Mediterráneo y del Mar Rojo (Holail y Rashed, 1992).

Los principales factores que podrían explicar los valores relativamente ligeros en los "beachrocks" analizados son: i) la menor salinidad del agua marina en Canarias; ii) la temperatura del agua marina, y iii) la influencia de agua meteórica.

i) La salinidad del agua marina en Canarias varía entre 36.2 y 37.2‰. La salinidad del Mediterráneo varía entre 38.8 y 39.5‰ en Creta (Neumeier, 1998) y entre 37.5 y 38.0‰ en Córcega (Bernier *et al.*, 1990), mientras que la salinidad en el Mar Rojo oscila entre 39.8 y 40.8‰ (Neumeier, 1998). En la Polinesia francesa la salinidad varía entre 35 y 36‰. Así, los cementos de aragonito de los "beachrocks" tienden a presentar valores más ligeros cuando la salinidad es baja (Canarias y Polinesia) y valores más pesados cuando la salinidad del agua marina es alta (Mediterráneo, Mar Rojo).

ii) La temperatura del agua marina en Canarias varía entre un 17 y 25°C. La temperatura en Creta oscila entre 15 y 25°C (Neumeier, 1998), en Córcega entre 13 y 23°C (Bernier *et al.*, 1990), en el mar Rojo entre 21 y 29°C (Neumeier, 1998), y en la Polinesia francesa entre 27 y 29,5°C (Neumeier, 1998). Los cementos aragoníticos de la Polinesia francesa son los que presentan una composición similar a los de La Palma, pero han precipitado en aguas mucho más calientes, lo que parece indicar que la temperatura del agua marina no es el factor determinante en el control de la composición isotópica del oxígeno de los cementos aragoníticos de los "beachrocks".

iii) Los valores relativamente ligeros de la composición isotópica del oxígeno de los cementos de aragonito de los "beachrocks" de la isla de La Palma sugieren que precipitaron en un medio marino con cierta influencia de aguas meteóricas. Valores similares a los descritos en la isla de La Palma han sido interpretados en otros ejemplos de "beachrocks" de forma similar (Magaritz *et al.*, 1979; Neumeier, 1998).

Los valores de la composición isotópica del carbono del cemento fibroso de aragonito de los "beachrocks" de la isla de La Palma varían entre +4.0 y +4.9 ‰ PDB. Los valores de $\delta^{13}C$ de los cementos estudiados son muy similares a los de los cementos aragoníticos de los "beachrocks" de las Bahamas (Beier, 1985) y relativamente similares a los de los cementos aragoníticos de los "beachrocks" del Mediterráneo en Israel (Magaritz *et al.*, 1979) y de la Polinesia francesa (Neumeier, 1998). Los valores de la composición isotópica de los cementos aragoníticos de los "beachrocks" estudiados indican que se formaron en equilibrio con el agua marina a partir de la cual precipitaron.

DESARROLLO Y EVOLUCIÓN DE LOS "BEACHROCKS"

La evolución de los depósitos de playa, y en concreto de la formación y posterior exhumación de los "beachrocks" en la isla de La Palma, durante los últimos 20.000 años, se explica a partir de las siguientes etapas: i) Desarrollo de las playas, las cuales constituyen la "roca encajante" de los "beachrocks"; ii) Formación de los "beachrocks"; y iii) Retrogradación y erosión de la playas.

i) El desarrollo de las playas implica un aporte disponible de clastos-granos y un fondo submarino más o menos llano. El sedimento de las playas es exclusivamente de origen terrígeno (clastos-granos procedentes de lavas volcánicas), ya que no hay material procedente de la plataforma marina (componentes esqueléticos). Los posibles aportes de material terrígeno son la erosión litoral (marina) de

las lavas volcánicas y el aporte debido al drenaje de los barrancos (caso del barranco de Las Angustias en el ejemplo de Punta Naos). Además, para el desarrollo de un perfil de playa en esta isla se necesita la formación de un fondo submarino más o menos llano y no excesivamente profundo que podría estar relacionado con la entrada de las lavas subaéreas en el fondo submarino.

ii) Los "beachrocks" se localizan en la zona intermareal y posiblemente en la parte más interna del perfil de la playa. El ejemplo de Echentive podría ser la clave para comprender la formación de los "beachrocks" en el contexto de playas de gravas volcánicas. En la actualidad, sólo en la parte más interna de la playa (lagos) de Echentive se produce la cementación (cemento fibroso de aragonito) de los depósitos de playa. La precipitación de este cemento seguramente continua en la zona intermareal en dirección a la línea de costa y está cubierta por los depósitos supramareales. A partir de la composición isotópica del oxígeno de los cementos estudiados se ha deducido que estos cementos se formaron en aguas marinas con una cierta influencia de agua meteórica, lo cual es congruente con las observaciones actuales en la playa de Echentive.

iii) La retrogradación y erosión de las antiguas playas ha exhumado los "beachrocks" los cuales en la actualidad se localizan en el "foreshore" de las playas recientes.

AGRADECIMIENTOS

Este trabajo ha sido subvencionado por el Proyecto nº 68/98 de la Fundación Universitaria de Las Palmas y parte de los análisis por el proyecto CICYT PB97-0883.

REFERENCIAS

Alexandersson, T. (1972): Mediterranean Beachrock Cementation: Marine Precipitation of Mg-Calcite. En: D.J. Stanley (ed.) The Mediterranean Sea. Dowden, Hutchinson y Ross, Inc., Stroudsburg: 203-223.

Amieux, P., Bernier, P., Dalongeville, R. y Medwecki de, V. (1989): Cathodoluminiscence of carbonate-cemented Holocene beachrock from the Togo coastline (West Africa): an approach to early diageneis. Sedimentary Geology, 65: 261-272.

Beier, J.A. (1985): Diagenesis of Quaternary Bahamian Beachrock: Petrographic and Isotopic Evidence. Jour. Sed. Petrol., 55: 755-761.

Bernier, P., Bonvallot, J., Dalongeville, R. y Prieur, A. (1990): Le beach-rock de Temae (Ile de Moorea-Polynésie française). Signification géomorphologique et processus diagénétiques. Z. Geomorph. N.F., 34: 435-450.

Carracedo, J.C., Day, S.J., Guillou, H. y Gravestock, P.J. (1997): Geological map of Cumre Vieja Volcano (La Palma, Canary Island). International Workshop on Volcanism and Volcanic Hazards in Immature Intraplate Oceanic Islands, La Palma.

Font, Y. y Calvet, F. (1997): "Beachrocks" Holocenos de la Isla de la Reunión, Océano Índico. Cuadernos de Geología Ibérica, 22: 87-102.

Ginsburg, R.N. (1953): Beachrock in South Florida. Jour. Sed. Petrol., 23: 85-92.

Holail, H. y Rasched, M. (1992): Stable isotopic composition of carbonate-cemented recent beachrock along the Mediterranean and the Red Sea coasts of Egypt. Marine Geology, 106: 141-148.

Magaritz, M., Gavish, E., Backler, N. y Kafri, U. (1979): Carbon and oxygen isotope composition-indicators of cementation environment in Recent, Holocene, and Pleistocene sediments along the Coast of Israel. Jour. Sed. Petrol., 49: 401-412.

Neumeier, U. (1998): Le rôle de l'activité microbienne dans la cimentation précoce des beachrocks (sédiments intertidaux). Terre & Environnement, 12: 1-183.

Mediterranean Storms

Edited by

P. Claps
Department of Environmental Engineering and Physics (DIFA)
University of Basilicata - Potenza (Italy)

F. Siccardi
Center for Environmental Monitoring (CIMA)
University of Genova, Savona, Italy

Proceedings of the EGS Plinius Conference
held at Maratea, Italy, 14 - 16 October 1999

EDITORIALE BIOS

ISBN 88-7740-296-2

Via Sicilia, 5 - C.P. 528 - 87100 Cosenza
Tel. e Fax +39 984 396300
Web site: www.edibios.it

Mediterranean Storms
(Proceedings of the EGS Plinius Conference held at Maratea, Italy, October 1999)

Mesoscale convective systems during 1990-94: characteristics and synoptic environment

L. CANA[a], E. HERNÁNDEZ[b], R. GARCÍA[b] & D. GRISOLÍA-SANTOS[a]

[a] *Departamento de Física. Campus de Tafira. Universidad de Las Palmas de Gran Canaria. 35017 – Las Palmas de G. C. Spain*
e-mail: lcana@física.ulpgc.es
[b] *Departmento de Ciencias Atmosféricas. Fac. de CC. Físicas. Universidad Complutense de Madrid. 28040 – Madrid. Spain*

ABSTRACT

Mesoscale Convective Systems (MCSs) data registers from June to December during 1990-94 were obtained from the Spanish National Meteorological Institute (INM). Sixty seven Mesoscale Convective Systems (MCSs) and fifteen Mesoscale Convective Complexes (MCCs) were identified through this database. Most of the MCCs and MCSs developed during the last week of September. The dominant synoptic patterns related to the mesoscale systems were cold fronts at the surface with warm and moist low-level cores, and cut-off low or deep trough throughout the middle and upper levels. These synoptic patterns were found in all the cases studied.

The hourly centroid location of the MCC was used to trace their tracks, which followed a general direction towards the E or NE in almost all cases. These trajectories are clearly related to the synoptic patterns found. Finally, a Skew T- Log p thermodinamic diagram from the nearest sounding station to a developing MCC is shown.

1 INTRODUCTION

In the first days of Autumn, intense precipitation over the Mediterranean area of the Iberian Peninsula and the Balearic Islands are frequently registered without an exact periodicity.

These intense storms originate flash floods that cause important damages to property and loss of human lives.

These mesoscale systems are not only characteristic of the western Mediterranean area.

Their origin is clearly convective, having features in common with the Mesoscale Convective Systems (MCS) and Mesoscale Convective Complexes (MCC) described by Maddox (1980). Summaries of MCS and MCC characteristics have been published (Maddox et al. 1982; Rodgers et al. 1983, 1985; Augustine and Howard 1988, 1991). These papers are centered mainly on the MCCs observed in America and some locations in China, even though Augustine and Howard (1991) mentioned these special convective structures in Hungary, Austria and Yugoslavia.

This work provides a climatological information of the MCSs and MCCs occurred during 1990-94 over the Iberian Peninsula and western Mediterranean area.

The synoptic patterns related to their genesis and development are identified. The track of each MCC has been computed. Finally, some information about the physical phenomena involved in their evolution is presented.

2 METHODOLOGY

The analysis has been centered on the MCS and MCC observed over the western Mediterranean area from June to December during 1990-94. According to the INM historical data, the intense precipitations caused by the convective systems are observed mainly from June to November, and specially during the months of September and October. METEOSAT and NOAA infrared (IR) images were obtained at the INM.

The reports of the convective systems characteristics published by Canalejo *et al.* (1993, 1994), Carretero *et al.* (1993), Martin *et al.* (1994) and Elvira *et al.* (1996) will be used to characterize the evolution of the convective systems. Both, images and reports, will be used used to identify and extract information on MCSs and MCCs.

The MCS and MCC criteria and key definition (Augustine and Howard, 1991) used in this work are given in Table 1. As pointed out by Augustine and Howard (1988) and McAnelly and Cotton (1989), the area within the single colder threshold proposed by Maddox (1980) adequately defines the life cycle, while the use of the second criterion (the use of the -32° C threshold) is redundant and introduces ambiguity.

Criteria:	Mesoscale Convective Systems (MCS)	Mesoscale Convective Complexes (MCC)
Minimum size	CCCS (IR temperature $\leq$ -52° C) must have an area $\geq$ 10 000 km^2	CCCS (IR temperature $\leq$ -52° C) must have an area $\geq$ 50 000 km^2
Duration	Minimum size must be exceeded for a period $\geq$ 3h	Minimum size must be exceeded for a period $\geq$ 6h
Shape	Minor axis/major axis is $\geq$ 0.7 at time of maximum areal extent of the -52° C continuous cloud shield (Only for MCC)	
Initiation	Time when minimum size is first satisfied.	
Maximum extent	Time when the CCCS (IR temperature $\leq$ -52° C) is at its maximum size.	
Termination	Time when minimum size is no longer satisfied.	

Table 1. Definitions of MCSs and MCCs based on enhanced IR satelite Imagery (Augustine and Howard, 1991). CCCS: Continuous Cold Cloud Shield

Once the convective systems have been identified, the synoptic patterns related to their life cycle will be determined from the surface, 850, 700, 500 and 300 hPa levels published in the INM daily meteorological bulletins. The hourly geographical coordinates of the -52° C centroid area will also be plotted on maps to set the tracks of each one of the MCCs identified. The trajectories will allow us to determine several characteristics, as the direction followed by the systems or the physical processes involved in their life cycle. Finally, a skew T-Log p thermodynamic diagram of the nearest sounding station will be plotted for a MCC. Thus, the thermodynamic structure of storm environment will be analyzed following a methodology simmilar to that used by Keenan *et al.* (1994), Bringi *et al.* (1996) or Alberoni *et al.* (1996).

3 RESULTS

Satellite images and related data from June to December from 1990 to 1994 were used in the present analysis. Applying the characteristics of Table 1 to the IR images of 82 mesoscale convective systems detected during 1990-94, 67 of them would be classified as MCSs and only 15 could be classified as MCCs (Cana, 1997).

The time distribution of these phenomena (Fig. 1) shows that most of the MCCs were developed between September and October. The last ten days of September registered 60% of the MCC (Fig. 2). The annual time distribution shows an asymmetric distribution for the analyzed period, with a non uniform

interannual variability. In order to explain these remarkable variations, the synoptic patterns related to each MCC have been analyzed. For all the identified MCSs and MCCs during 1990-94, two synoptic patterns have been detected.

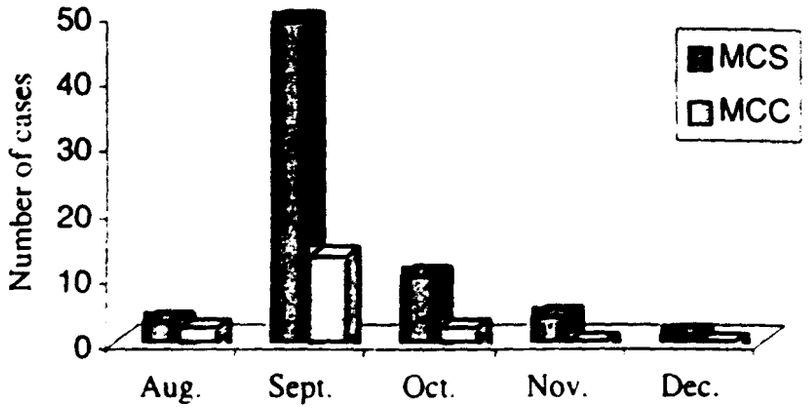

Figure 1: Time distribution of MCSs and MCCs during 1990-94

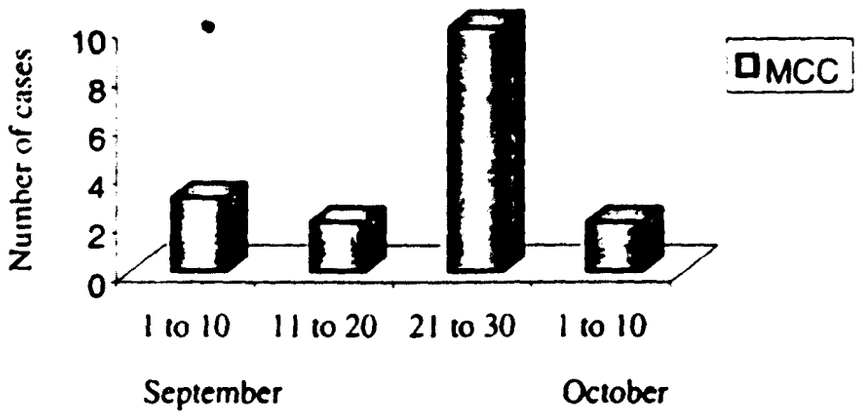

Figure 2. MCC distribution during 1990-94

The first one (Class 1) can be characterized by a 500 hPa and 300 hPa standard level trough, and a cold front related to a low at the West or over the Peninsula at the surface level (Fig. 3a, 3b) . Usually a 300 hPa jet is also present on the life cycle of the MCC. This situation originates prefrontal MCCs. The trough is the most significant element of this pattern, with a N-S or NE-SW axis. A thermal wave reaching frequently -24° C at 500 hPa can be identified together with the trough. A similar pattern has been reported over the United States, where both the trough at 500 hPa level and the presence of a cold front at the surface, have been mentioned (Loherer and Johnson, 1995).

The second meteorological pattern (Class 2) can be characterized by a cut-off low at 500 hPa and 300 hPa levels. At surface, the North Africa low (usually over Algeria) is accompanied by a high pressure area at the West of the

Peninsula and a second one over Central Europe or South of the U. Kingdom (Fig. 4a, 4b). The main characteristic related to this pattern is the genesis of high pressure and low pressure areas isolated from the general circulation. The cut-off low usually presents a cold core (between -16° and -24° C).

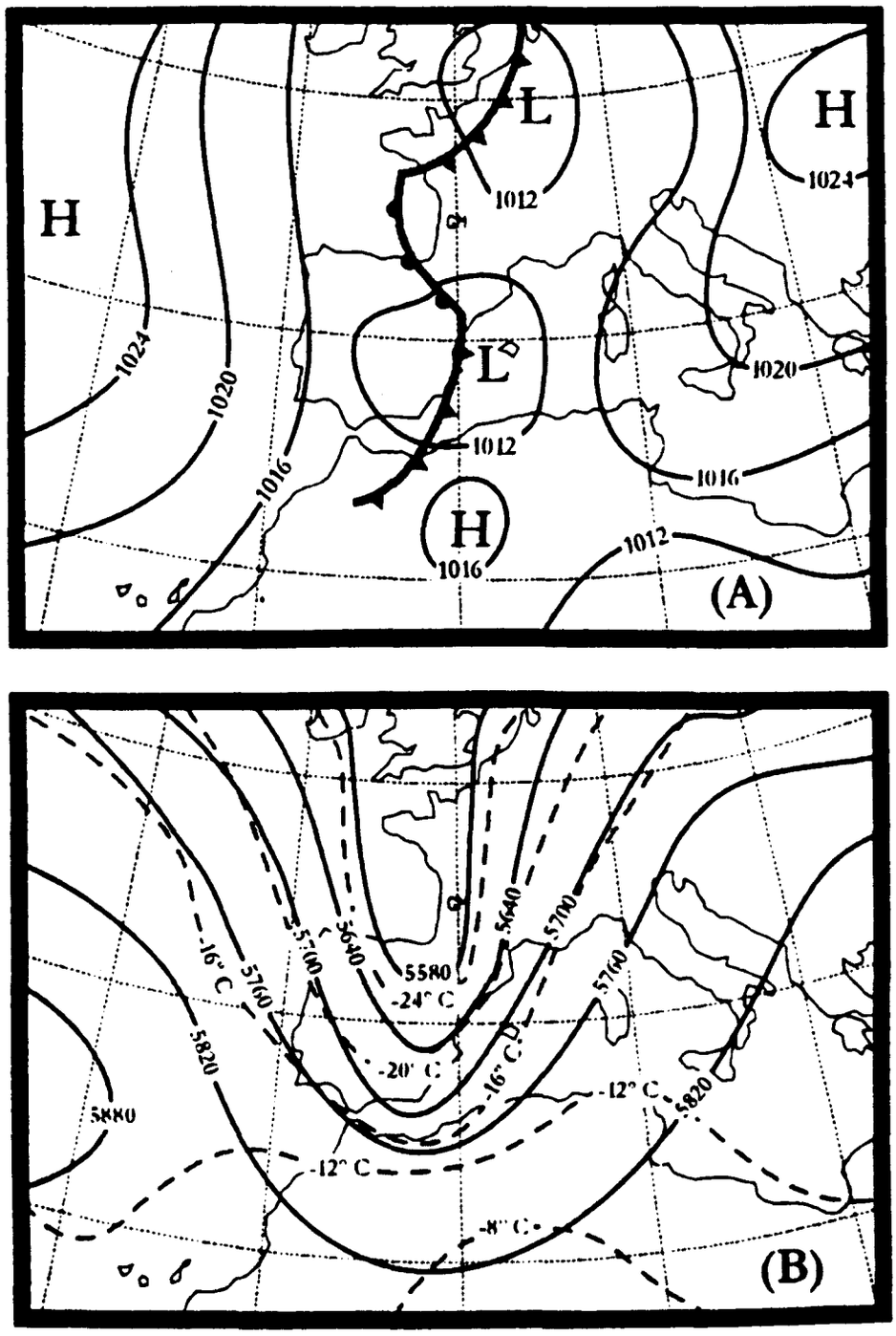

Figure 3. Schematic represention of the two categories found. Synoptic pattern scheme for Class 1. A) Surface level, B) 500 hPa level

The existence of a jet in the proximity of a developing MCC has been verified in 70% of the registered MCC cases over the Iberian Peninsula during 1990-94 (Cana, 1997). The relation between convective systems and jets has

been discussed for several cases in the U. S. Great Plains, which has been described by Keyser and Johnson (1984) and Ucellini (1986). The study of the synoptic patterns for the analyzed period shows that the presence of the above described patterns, is a necessary condition, but not enough, for MCC development.

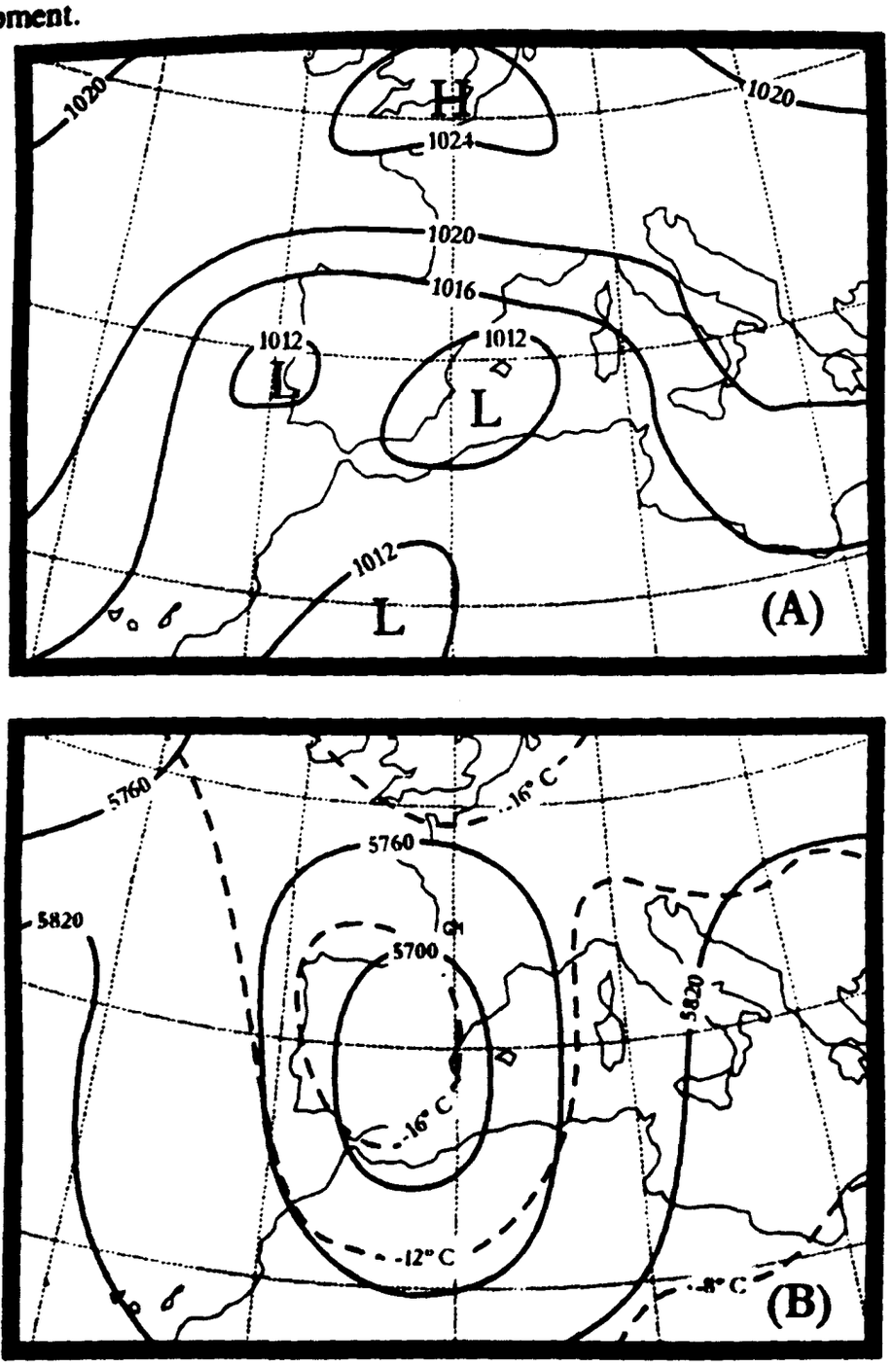

Figure 4. Same as Fig. 3 except for Class 2.

The tracks of each one of the MCCs define two different groups related to the genesis and evolution of the MCCs (not shown). The first one generates and develops near the coast or over the Mediterranean sea, following a eastward or

northeastward path. The second group forms over the interior of the Iberian Peninsula, evolving to the interior of the continent and following similar directions. Both groups follow geostrophic trajectories moving to the right of the 500 hPa flow level, a conclusion in agreement with Miller and Fritsch (1991). The analysis suggests at least two different physical processes involved into their development: the instability of overheated air masses from Africa crossing over the Mediterranean sea (Hernández *et al.*, 1987), and the orographic forcing that implies an air-mass ascent (Cana, 1997). In order to show this feature, the skewT - Log p plot for the 26/9/92 MCC is shown.

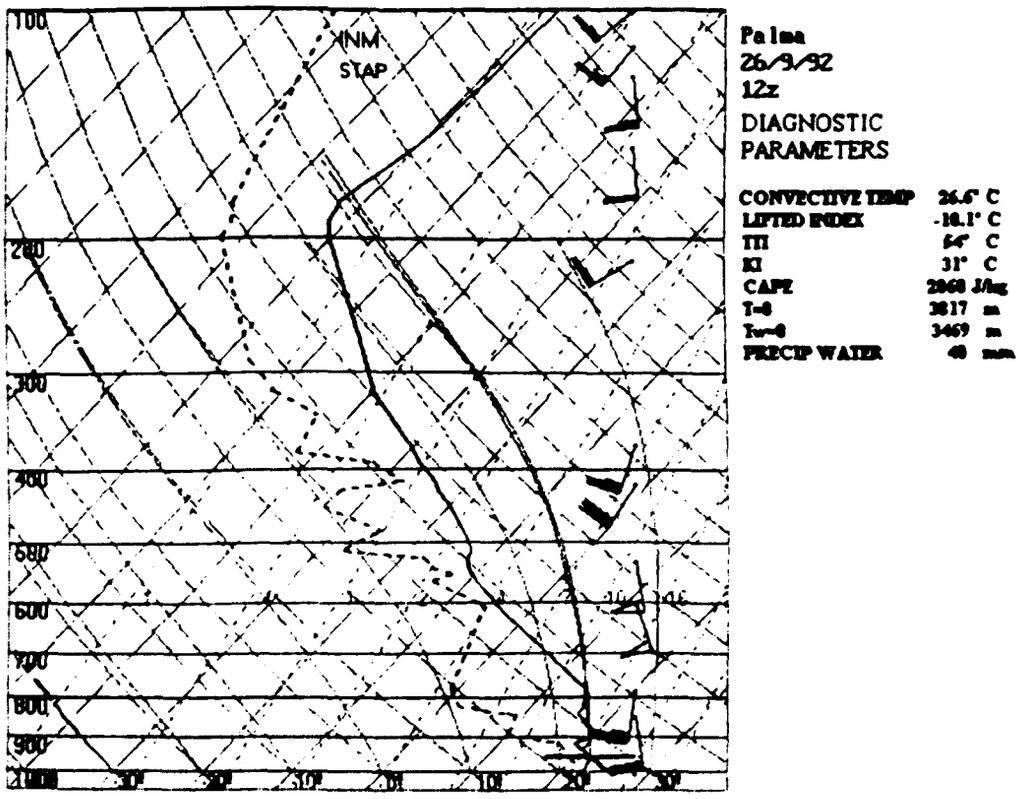

Figure 5. Skew *T* - Log *p* plot of the sounding taken from Palma de Mallorca station on 1200 UTC, 26 September 1992. Full barb is 5 m s^{-1}.

Unfortunately, there are no sounding stations close to the affected area, so the sounding from Palma de Mallorca sounding station (Balearic Islands) at 1200 UTC has been used. It shows a SE flow on the low level layers of the atmosphere (Fig. 5), bringing the necessary humidity to the MCC genesis (17.5 g kg^{-1} mixing ratio and 26.2° C on surface, 8.6 g kg^{-1} and 16.0° C at 1500 m height). From this level, there is a 13-18 m s^{-1} southerly flow. A remarkable characteristic of the Palma de Mallorca sounding is the evolution of T and Td from the surface to the 300 hPa standard level, which presents a low temperature (-42.3° C). The convective indexes reflect favorable conditions for the convection (TTI, 54° C; KI, 31° C; LI -10.1° C). The Convective Available Potential Energy (CAPE) at 1200 UTC was moderately high (2060 m^2s^{-2}), with a total precipitable water content in the sounding of 40 mm.

REFERENCES

Alberoni P.P., S. Nanni, M. Crespi & M. Monai. 1996. The Supercell Thunderstorm on 8 June 1990: Mesoscale Analysis and Radar Observations. *Meteor. Atmos. Phys.*, **58**, 123-128.

Augustine, J. & K. W. Howard, 1988. Mesoscale convective complexes over the United States during 1985. *Mon. Wea. Rev.*, **116**, 685-701.

Augustine, J. & K. W. Howard, 1991. Mesoscale convective complexes over the United States during 1986 and 1987. *Mon. Wea. Rev.*, **119**, 1575-1589.

Bringi V.N., L. Liu, P.C. Kenedy, V. Chandrasekar & S. Rutledge. 1996. Dual Multiparameter Radar Observations of Intense Convective Storms: the 24 June 1992 Case study. *Meteorol. Atmos. Phys.* **59**, 3-31.

Cana, L.C. 1997. Desarrollo de la actividad frontogenetica en diferentes situaciones de precipitacion intensa. Ph.D. Thesis, Department of Atmospheric Sciences, Universidad Complutense, Madrid, 197 pp.

Canalejo, M.; O. Carretero & R. Riosalido. 1993. Sistemas Convectivos de Mesoescala. Tech. Note - 9. I.N.M., 136 pp.

Canalejo, M.; O. Carretero & R. Riosalido. 1994. Sistemas Convectivos de Mesoescala. Tech. Note - 14. I.N.M., 54 pp.

Carretero, O.; M. Canalejo & R. Riosalido. 1993. Sistemas Convectivos de Mesoescala. Tech. Note - 12. I.N.M., 122 pp.

Elvira, B.; O. Carretero & R. Riosalido. 1996. Sistemas Convectivos de Mesoescala. Tech. Note - 24. I.N.M., 146 pp.

Hernández E, J. Díaz, L.C. Cana & A. García. 1995. Analysis of the atmosphere behavior in the proximities of an orographic obstacle. *Nonlinear Processes in Geophysics*, 2, 30 - 48.

Keenan T.D., B. Ferrier & J. Simpson. 1994. Development and Structure of a Maritime Continent Thunderstorm. *Meteorol. Atmos. Phys.* **53**, 185-222.

Keyser, D & D.R. Johnson. 1984. Effects of diabatic heating on the ageostrophic circulation of an upper tropospheric jet streak. *Mon. Wea. Rev.*, **112**, 1709-1724.

Loehrer, S. & R. H. Johnson. 1995. Surface pressure and precipitation life cycle characteristics of PRE-STORM Mesoscale Convective Systems. *Mon. Wea. Rev.*, **123**, 600-621.

Maddox, R.A. 1980. Mesoscale convective complexes. *Bull. Amer. Meteor. Soc.*, **61**, 1374-1387.

Maddox, R. A. , D.M. Rodgers & K.W. Howard, 1982. Mesoscale Convective Complexes over the United States during 1981-annual summary. *Mon. Wea. Rev.*, **110**, 1501-1514.

Martin, F.; F. Elizaga, O. Carretero & R. Riosalido. 1994. Sistemas Convectivos de Mesoescala. Tech. Note - 15. I.N.M., 136 pp.

McAnelly, R. L. & W. R. Cotton, 1989. The precipitation life cycle of mesoscale convective complexes over the central United States. *Mon. Wea. Rev.*, **117**, 784-808.

Miller D. & J. M. Fritsch, 1991. Mesoscale Convective Complexes in the Western Pacific Region. *Mon. Wea. Rev.*, **119**, 2978-2992.

Rodgers, D.M., K. W. Howard & E.C. Johnston, 1983. Mesoscale Convective Complexes over the United States during 1982-annual summary. *Mon. Wea. Rev.*, **111**, 2363-2369.

Rodgers, D.M., M.J. Magnano & J.H. Arns, 1985. Mesoscale Convective Complexes over the United States during 1983. *Mon. Wea. Rev.*, **113**, 888-901.

Ucellini, L.W. 1986. The possible influence of upstream upper-level baroclinic processes on the development of the QEII storm. *Mon. Wea. Rev*, **114**, 1019-1027.

SCI. MAR., 63 (3-4): 343-354 SCIENTIA MARINA 1999

BIOLOGY AND FISHERY OF DOLPHINFISH AND RELATED SPECIES. E. MASSUTÍ and B. MORALES-NIN (eds.)

Parasitism of dolphinfishes, *Coryphaena hippurus* and *Coryphaena equiselis*, in the western Mediterranean (Balearic Islands) and central-eastern Atlantic (Canary Islands)*

ENRIQUE CARBONELL[1], ENRIC MASSUTÍ[2], JOSÉ JUAN CASTRO[3] and ROSA MARÍA GARCÍA[1]

[1]Departamento de Biología, Universidad de Valencia, Dr. Moliner, 59, 46100 Burjassot, Valencia (Spain)
[2]I.E.O.- Centre Oceanogràfic de les Balears, Moll de Ponent s/n, P.O.Box 291, 07080 Palma de Mallorca (Spain)
[3]Departamento de Biología, Universidad de Las Palmas de Gran Canarias, P.O. Box 550, 35117 Las Palmas de Gran Canarias (Spain)

SUMMARY: A total of 648 dolphinfishes were examined for internal and external parasites in western Mediterranean (Balearic Islands) and central-eastern Atlantic (Canary Islands) waters in order to make a comparative study between the two areas. The specimens studied from the Mediterranean Sea was *Coryphaena hippurus*, with 62 large individuals captured from May to September and 497 juveniles captured from August to December. The specimens studied from the central-eastern Atlantic were 39 adult *C. hippurus* and 49 adult *Coryphaena equiselis*. Parasites were found in 70% of the fish examined, and represented a total of nine endoparasitic taxa: six digeneans (Class Trematoda, Subclass Digenea, *Dinurus tornatus*, *Dinurus breviductus*, *Dinurus longisinus*, *Lecithocladium excisum*, *Bathycotyle branchialis* and *Hirudinella* sp.), two nematodes (Class Nematoda, Order Spirurida, *Philometroides* sp. and *Metabronema magna*) and one acanthocephalan (Phyllum Acanthocephala, *Rhadinorhynchus pristis*). Seven crustacean copepod ectoparasites were identified: *Caligus quadratus*, *Caligus productus*, *Caligus bonito*, *Caligus coryphaenae* (Family Caligidae) and *Euryphorus nymphae* (Family Euriphoridae) were found in gill mucus masses or on the inner surface of the operculum, the lernaeopodid *Neobrachiella coryphaenae* (Family Lernaeopodidae) was attached to gill filaments and the pennellid *Pennella filosa* (Family Pennellidae) was anchored to fins and rays or, deeply, to muscular tissue and abdominal cavity. The relationships between feeding habits, parasite recruitment and parasite transmission were analysed, some ecological aspects of all the parasitic species are discussed, and some comments are made on parasite-host relationships.

Key words: *Coryphaena hippurus*, *Coryphaena equiselis*, parasitism, western Mediterranean, central-eastern Atlantic.

INTRODUCTION

The dolphinfishes (Pisces: Coryphaenidae), common dolphinfish (*Coryphaena hippurus* L.) and pompano dolphin (*Coryphaena equiselis* L.), are epipelagic species distributed world-wide in tropical and subtropical waters where surface water temperatures exceed 20°C (Gibbs and Collette, 1959). In the Atlantic, they are natural inhabitants and their spawning is probably year round, although it is most intense during the months with higher water surface temperatures (Shcherbachev, 1973). In the Mediterranean Sea, *C. hippurus* appear seasonally and undergo a reproductive cycle during the summer months, following the appearance of adult specimens every year in May-

*Received June 15, 1998. Accepted May 8, 1999

June, when the water surface temperature reaches >18°C (Massutí and Morales-Nin, 1995). Juveniles are captured from late August to early December and then, when water temperatures fall to 18°C, they possibly migrate to the warmer waters of the Atlantic Ocean.

Dolphinfishes are top-level predators, but they are not very selective and feed on a wide range of pelagic organisms. In addition, they are very agile and capable of taking fast-moving prey (Palko *et al.*, 1982). *C. hippurus* grows rapidly throughout its life and has a maximum life span of about 4 years, reaching lengths and weights in excess of one metre and 10 kg respectively (Beardsley, 1967; Rose and Hassler, 1968). *C. equiselis* is a relatively little known species which does not reach such a large size as *C. hippurus*, and its maximum known length is 74 cm (Herald, 1961). *C. equiselis* is more pelagic and oceanic, and consequently is rarely caught in coastal waters. Its distribution range is more tropical and according to Mather and Day (1954) it is not generally found in waters with surface water temperatures lower than 24°C. *C. equiselis* does not extend as far beyond the tropics as *C. hippurus*. There are few reports of *C. equiselis* in the Mediterranean Sea, and hence its presence in these waters is not well known.

Although several authors have reported parasites of dolphinfishes in every ocean, and an exhaustive list can be found in Palko *et al.* (1982), only a few focus on the study of the parasite community of these species by considering the ecology of the parasites. Burnett-Herkes (1974) analysed the ectoparasites on the gills and in the buccal cavity of *C. hippurus*, whereas Manooch *et al.* (1984) studied its gastrointestinal parasites. Both studies were carried out along the South-Eastern and Gulf coasts of the United States in the Western Atlantic.

Therefore the objective of this study was to carry out, for the first time, a complete analysis of the parasitic community of dolphinfishes in the eastern Atlantic and the Mediterranean, and to study the relationships between diet and parasite recruitment in order to identify possible pathways of parasitic infection and life cycle. Special reference is made to the parasites which *C. hippurus* probably brings from the Atlantic to the Mediterranean Sea and those which this species acquires in the Mediterranean and carries to Atlantic waters. Our aim is to provide basic information that will allow parasites to be used as potential biological tags for *C. hippurus* in the study of its migratory routes between these two areas.

MATERIALS AND METHODS

The fishes were collected from two areas, the Balearic Islands (western Mediterranean) and the Canary Islands (central-eastern Atlantic). In the laboratory, the fish were measured to the nearest centimetre fork length (FL), weighed and sexed. Integument, fins, natural openings and gills of every fish were examined. The gills were dissected in order to survey all the gill arches for parasites. In all cases, the parasites were collected and, in addition to their number, size, shape and location, any pathological alterations were also recorded. Once any parasites were found, they were fixed in buffered gluteraldehyde (10%) for later identification, directly or after being cleared with lactophenol.

TABLE I - Number of specimens of *C. hippurus* and *C. equiselis* captured in Mediterranean and Atlantic waters, by fork length intervals. Year and month of capture and the surface water temperature are also given

	BALEARIC ISLANDS *Coryphaena hippurus*					
Fork length, cm	60-124	<20	20-29	30-39	40-49	50-59
1990	20	7	57	35	35	18
1991	18	4	27	38	28	17
1995	24	—	12	44	140	35
Month of capture	May-June	August	August	Sep-Oct	Oct-Nov	Nov-Dec
Temperature °C	16-18	27-28	27-28	25-26	24-22	20-16

	CANARY ISLANDS		
	Coryphaena hippurus		*Coryphaena equiselis*
Fork length, cm	69-102	38-53	32-52
1994-95	25	14	49
Month of capture	June	October	June
Temperature °C	21	23	21

From the Mediterranean area, a total of 62 adult *C. hippurus*, ranging from 60 to 124 cm FL, were sampled during May-September in 1990, 1991 and 1995. In the same years, 497 juveniles (14-58 cm FL) were obtained from August to early December. From the Atlantic area, 25 adult (69-102 cm FL) and 24 juvenile (38-53 cm FL) specimens of *C. hippurus* were sampled during June and October in 1994 and 1995 respectively. In this area, 49 *C. equiselis* between 36 and 52 cm FL were also sampled during June in 1995.

To establish differences in parasitism as a function of size, the fish examined were differentiated into six size intervals in order to obtain a sufficient number of specimens per group. Size intervals, number of fish analysed per size group, year and month of capture and the surface water temperature range are summarised in Table 1. For each parasite, the infection level by size group was analysed according to standard methods (Margolis *et al.*, 1982).

RESULTS

Endoparasites

Endoparasites were found in 390 of the specimens examined (70%). A total of eleven parasitic taxa could be identified (seven digeneans, one cestode, two nematodes and one acanthocephalan), of which nine were to species level. The change in prevalence, intensity and abundance of the main species in relation to the size of the hosts is presented in Table 2 and 3.

Class TREMATODA
Subclass Digenea
Family Hemiuridae
Dinurus spp.

The most frequent and most numerous endoparasites were four species of the genus *Dinurus* Looss, 1907. These were *D. tornatus* (Rud, 1819) Looss, 1917, *D. barbatus* (Cohn, 1902) Looss, 1907, *D. breviductus* Looss, 1907 and *D. longisinus* Looss, 1907. *D. tornatus* was the dominant species. These parasites were found in the stomach of specimens of *C. hippurus* and *C. equiselis* captured in both areas. For the prevalence and other ecological parameters there were marked differences depending on the annual cycles, but in general adult fish were the most infected in both areas.

Lecithocladium excisum (Rudolphi, 1819) Looss, 1907

This other gastric hemiurid was only found in the Mediterranean, from juvenile fish <50 cm FL in the

TABLE 2. – Infection parameters of the helminth species (*Dinurus* spp., *Lecithocladium excisum*, *Floriceps saccatus*, *Rhadinorhynchus pristis* and *Metabronema magna*) of *Coryphaena hippurus* captured in Mediterranean waters (FL: fork length in cm; first row: prevalence, second row: mean intensity ± SD; third row: mean abundance ± SD; fourth row: range)

FL	*Dinurus* spp 1990	*Dinurus* spp 1991	*Dinurus* spp 1995	*L. excisum* 1991	*F. saccatus* 1990	*F. saccatus* 1991	*F. saccatus* 1995	*R. pristis* 1995	*M. magna* 1995
>60	10 12±11.3 1.2±4.5 4-20	100 25.6±7.9 25.6±7.9 6-30	56.5 16.5±8.5 9.3±10.4 5-30		60 3±1.5 1.8±1.9 1-5	33.3 1.5±0.5 0.5±0.8 1-2	21.7 3.2±3.3 0.7±1.9 1-9	25 2.3±1.2 0.6±1.2 1-4	60.8 2.1±0.8 1.3±1.2 1-3
20-29				7.4 6±1.4 0.4±1.6 5-7					16.6 1 0.2±0.4 0-1
30-39				10.3 10.2±5.7 1.1±3.5 2-15					40.9 1.9±0.8 0.8±1.1 1-2
40-49		17.8 8.2±5.5 1.5±3.8 1-16		3.6 3 0.1±0.6 0-3	2.8 2 0.06±0.3 0-2	3.6 1 0.03±0.2 0-1			64.3 1.3±0.6 0.8±1 1-3
50-59	5.5 2 0.1±0.5 0-2	47 18.7±11.3 7.2±11 3-40			27.7 1.6±0.9 0.4±0.8 1-2				47.3 1.3±0.6 0.6±0.8 1-3

TABLE 3. - Infection parameters of the helminth species (*Dinurus* spp. and *Rhadinorhynchus pristis*) of *Coryphaena hippurus* and *Coryphaena equiselis* captured in Atlantic waters. (FL: fork length in cm; first row: prevalence; second row: mean intensity ± SD; third row: mean abundance ± SD; fourth row: range).

	Coryphaena hippurus		*Coryphaena equiselis*	
FL	*Dinurus* spp. 1994	*R. pristis* 1994	*Dinurus* spp. 1995	*R. pristis* 1995
>60	24 18.8±14.2 4.5±10.4 1-30	12 3±1 0.35±1 1-5		
30-39				10 2.3±0.6 0.15±0.6 1-4
40-49			4 7.5±2.1 0.3±1.5 6-9	

1991 cycle. Its prevalence, intensity and abundance were low.

Family Bathycotylidae
Bathycotyle branchialis Darr, 1902

Collected from gills of three large specimens of *C. hippurus* captured in Mediterranean waters.

Family Hirudinellidae
Hirudinella sp.

Collected from the stomach of two large specimens of *C. hippurus* captured in the Mediterranean

Class CESTODA
Order Trypanorhyncha
Family Lacystorhynchidae
Floriceps saccatus Cuvier, 1817

Plerocerci were found in specimens of *C. hippurus* larger than 30 cm FL captured in both areas. A total of 91 cysts containing a single plerocercoid were collected from the abdominal cavity and the surface serosa of the viscera. Cyst size was variable and ranged from 20 to 50 mm. The shape of the cysts also showed a great variety of forms, but they always had a terminal globular region, where the larva occurred, and a tail-like structure. The smallest cysts (4-7 mm in length) showed an enlarged or hood-like scolex with two rounded extensions. The medium sized larvae measured 10-12 mm and had tentacles and two leaflike bothridia. The largest plerocercoids (15-25 mm in length) showed two deeply indented bothridia, which superficially looked like four bothridia. Most cysts were attached to the parietal peritoneum and mesenteries (80%), whereas 10% were fixed to the gonadal parenchyma, 7% to the hepatic serosa and 3% to the pancreas surface.

The parasitism of this cestode from both areas has been studied in detail by Carbonell *et al.* (1998).

Class NEMATODA
Order Spirurida
Family Cystidicolidae
Metabronema (Cystidicoloides) magna
(Taylor, 1925)

Some cysts were collected from the walls of the pyloric caeca and in the pancreatic tissue of *C. hippurus* specimens captured in the Mediterranean. They contained several adult nematodes belonging to this species. The cysts measured 30-50 mm in length and 20-30 mm in width, and they were poorly defined, solid, opaque and included in the tissues. Most of the cysts were calcified. The infection appeared in small fish, and the prevalence increased rapidly, remaining high at all fish sizes, although it was only possible to follow the changes of the infection during the 1995 cycle. In the youngest fish, the cysts constituted a solid mass of conjunctive tissue which contained a male and various females encrusted irregularly in the mass. In the larger fish, the calcification was constant and complete, with most of the nematodes being broken and fragmented.

Family Dracunculidae
Philometroides sp.

Three large females (between 15 and 20 cm in length) were collected in the abdominal cavity of two medium-sized *C. hippurus* captured in the Mediterranean

Phyllum ACANTHOCEPHALA
Polymorphida
Family Rhadinorhynchidae
Rhadinorhynchus pristis (Rudolphi, 1802)
Luhe, 1911

This was collected in adult *C. hippurus* captured both in Mediterranean and Atlantic waters but its prevalence was low. Most specimens were found free in the stomach and some others were introduced into the pyloric caecal wall, with the spiny proboscis

TABLE 4. – Infection parameters of the copepod species (*Caligus* spp., *Pennella filosa* and *Neobrachiella coryphaenidae*) of *Coryphaena hippurus* captured in Mediterranean waters (FL: fork length in cm; first row: prevalence; second row: mean intensity ± SD; third row: mean abundance ± SD; fourth row: range).

FL	*Caligus* spp 1990	*Caligus* spp 1991	*Caligus* spp 1995	*P. filosa* 1990	*P. filosa* 1991	*P. filosa* 1995	*N. coryphaenidae* 1995
>60	10	50	37.5	80	44.5	31.3	12.5
	3±1.4	11.4±11	6.7±11.5	7.2±8.3	5±4.7	3.6±4.7	5.5±2.1
	0.3±0.9	5.7±9.6	2.5±7.4	5.7±8	2.2±4	1.1±3	0.7±2
	2-4	1-32	1-30	1-33	1-12	1-12	4-7
20-29	24.5	59.2	83.3				16.7
	2.6±2.1	2.4±2	2.5±3.5				3.5±0.7
	0.6±1.5	1.4±1.9	2.1±3.3				0.6±1.4
	1-3	1-8	1-12				3-4
30-39	71.4	57.9	77.3				18.2
	4.1±3.2	4±3.7	2.4±1.8				2.4±1.2
	2.9±3.2	2.3±3.4	1.9±1.9				0.4±1
	1-15	1-16	1-6				1-5
40-49	82.8	92.8	45				35.7
	7.3±7.6	5.7±5.4	4.1±3				3.3±4.3
	6±7.4	5.7±5.4	1.8±2.9				1.1±3
	1-30	1-20	1-18				1-6
50-59	83.3	76.5	34.3				45.7
	6.4±4.3	5.1±3.9	6.7±4.1				2.5±1.3
	5.3±4.6	3.9±4	2.3±4				1.3±1.6
	1-15	2-16	2-14				1-6

encapsulated in the caecal walls or deeply in pancreatic tissue. This species was also found in *C. equiselis* specimens smaller than 40 cm FL.

Ectoparasites

Seven species were found, all of which were crustacean copepods. Their infection parameters are given in Table 4 and 5.

Class COPEPODA
Order Shiponostomatoida.
Family Caligidae
Caligus spp.

Collected in the gills of *C. hippurus* captured in the Mediterranean and throughout all the size intervals considered. *Caligus quadratus* Shiino, 1957 was the dominant species. Other species of this genus, such as *C. coryphaenae* Steenstrup and Lütken, 1861, *C. bonito* Wilson, 1905 and *C. productus* Müller, 1785 were also found. They were located in large masses of mucus surrounding the gills (60%) and on the inner surface of the operculum (40%). *C. hippurus* and *C. equiselis* from the Atlantic area were not infected by these copepods. The prevalence in juvenile fish was higher than in adults. It was also higher during the months with higher water surface temperature. Parasite females were more abundant than males, with the sex-ratio being 7:1.

Table 5. – Infestation paraeters of the copepod species*uryphorus nymph*of *Coryphaena hippurus* and *Coryphaena equiselis* captured in Atlantic waters (FL: fork length in cm; first row: prevalence; second row: mean intensity ± SD; third row: mean abundance ± SD; fourth row: range)

FL	*Coryphaena hippurus* 1994	*Coryphaena equiselis* 1995
>60	80	
	13.5±11.4	
	10.8±11.5	
	2-30	
40-49	78.6	18.4
	11.4±8.7	7.9±2
	8.9±9	1.4±3.2
	2-30	6-11

Family Euryphoridae
Euryphorus nymphae Steenstrup and Lütken, 1861

Collected from both species in specimens bigger than 40 cm FL captured in Atlantic waters. The proportion between parasite females and males was 2:1. This species, as well as *Caligus* spp., produced an abundant mucus hypersecretion in the gills, and the parasites were found in this mucus mass. They were

also present on the inner surface of the operculum. Though the examined fish were dead, the parasites were still highly active and they could be found in the oral cavity, skin on the head and other skin locations.

Family Lernaeopodidae
Neobrachiella coryphaenidae Pearse, 1952

Collected from *C. hippurus* juvenile and adult specimens captured in the Mediterranean. The infection took place in juvenile fish during the months with high water temperatures, and in every case parasites were attached to the gill filaments by their appendages. Only a few parasites carried dwarf males. Mucus hypersecretion or any other anatomical alteration were not observed.

Family Pennellidae
Pennella filosa Linnaeus, 1758

Collected only from large specimens of *C. hippurus* captured in Mediterranean waters during May-September in 1990, 1991 and 1995. Young fish caught in this sea, and the ones from the Canary Islands, were not infected by this parasite. Although the ecological parameters were different during the three years studied, in every case they showed an increasing tendency as the fish became older. The parasites were mainly attached to the dorsal and anal fins (50%), to dorsolateral muscular tissue (25%) and to the abdominal cavity (22%). Mixed parasite locations were frequent in fish larger than 100 cm FL (40%). The depth at which the cephalothorax or radicular apparatus was anchored varied according to parasite location. Thus, it was deeper in the abdominal cavity and musculature than in fin rays or subcutaneous tissue. Some parasites were hyperparasitized by the cirriped *Conchoderma auritum*. Skin and muscular necrosis were always present, and the head and horns of the parasite were immersed in a bloody and inflammatory exudate mass. The cephalothorax was surrounded by a fibrous conjunctive tissue capsule and the adjacent tissues showed different rates of inflammatory alterations with fistulizations.

30% of the material found corresponded to premetamorphic forms that lacked cephalic horns and showed simple branchial filaments, without ramifications or at most with primary branches that always arose from the main branch. They were premetamorphic females with a fragile, whitish body of small size (45±14 mm in length; range 22-64 mm). The rest were composed of pregravid and gravid females with three well-developed horns, an intensely keratinized body and a dark brown colour. The size was 41-135 mm (59±19 mm). The gills consisted of the main filament from which primary, secondary and even tertiary branches arose, but they were always without anastomosis.

DISCUSSION

The results obtained allowed the little existing information concerning the parasite fauna of dolphinfishes in the Mediterranean and Central-Eastern Atlantic to be extended. None of the species found in the Mediterranean had been reported in this area until now. The Mediterranean records were limited to Dollfus (1927), who reported a metacercaria of the hemiurid trematode *Dinurus notatus*, Lozano-Cabo (1961) who found the isopod *Anilocra physodes*, and Delamare-Deboutteville and Nunes-Ruivo (1958) who reported the two parasitic gill copepods *Brachiella coryphaenae* and *Caligus belone*. By contrast, all the species found in the Canary Islands had been reported in Atlantic waters, although most of these records correspond to the western coast (e.g. Cable and Linderoth, 1963; Ho, 1963). The only available information from the central-western Atlantic were studies on trematodes from fishes off Ghana and Senegal (Fischthal, 1972; Fischthal and Thomas, 1972b).

Endoparasitism

The presence of gastric hemiurid digenean parasites in juvenile and adult specimens of *C. hippurus* suggests that infection takes place in Mediterranean as well as in Atlantic waters. The life cycle of these endoparasites is relatively complex, typical of many helminth parasites, with several intermediate hosts. It may follow the typical model described by Koie (1979, 1990b, 1990c), who reported benthic gastropods as first intermediate hosts where the cercariae develop, whereas metacercariae occur in the haemocoel of copepods and chaetognaths. This author also showed that some decapod larvae may be infected by eating the cercariae and that the definitive hosts were clupeids, scombrids and other plankton-feeding fishes. As all these organisms are present in the Mediterranean and Atlantic waters, it appears that *C. hippurus* could acquire the parasites

either through the ingestion of copepods and other crustaceans with metacercariae or through eating small infected fish, which act as second intermediate hosts (Gibson and Bray, 1986). These authors seem to conclude that non clupeid fish could acquire the hemiurids by feeding upon clupeids or other plankton-feeders. The infection of metacercariae hemiurid digeneans from clupeid fish and crustaceans has been recorded in *C. hippurus* by several authors (Dollfuss, 1927; Yamaguti, 1971; Manooch *et al.*, 1984).

Similarly to other areas of the Pacific and Atlantic, fish, crustaceans and cephalopods have been reported as main components of the diet of *C. hippurus* in the Mediterranean (Massutí *et al.*, 1998). Nevertheless, an important change takes place during the ontogenic development of the species. Whereas amphipod and crustacean larvae make up more than 50% of the diet of juvenile specimens smaller than 30 cm, cephalopods and mainly fish are the most important preys for bigger fish. Taking into account that the *Dinurus* species appeared in juveniles (>40 cm FL) and adult specimens (>60 cm FL), the transmission mechanism from invertebrates does not seem probable and their infection is likely to be produced from ingestion of clupeid or other plankton-feeder fishes such as carangids, which are an important component of the *C. hippurus* diet.

The only data that we possess on the biological cycle of the species of *Dinurus* are due to Dollfus (1927) and Szidat (1950). The first author suggests that certain metacercariae found in the body cavity of the crustacean decapod *Cerataspis monstrosa* belong to *Dinurus notatus*, a stomach parasite of *C. hippurus*, for which two forms of transmission are quoted as being possible: through invertebrates (copepods, decapods and chaetognaths) or through vertical migratory fish (clupeids, carangids and scombrids). Szidat (1950), on the other hand, considers that the clupeids are intermediate hosts for *Dinurus breviductus*, whose metacercariae encyst or encapsulate in the skin of *Sardina pilchardus* and *Sardinella aurita*, where the parasite produces a type of "black spot disease".

On the other hand, the other gastric hemiurid *Lecithocladium excisum* was only found in juveniles. This species is reported for the first time in *C. hippurus*. Its cycle is known through the experimental studies of Koie (1991). As in *Dinurus*, its first intermediate hosts are gastropod molluscs and the cercariae are found in the haemocoel of calanoid copepod crustaceans. Metacercariae have also been described in jellyfish, in the ctenophores *Pleurobrachia*, in diverse species of *Sagitta* and in the coelom of the polychaete *Tomopteris*. These non-crustacean invertebrates are certainly infected when eating copepods with metacercariae, and should therefore be considered as paratenic hosts. In our case, the infection by this trematode is early, which suggests that it took place when *C. hippurus* juveniles preyed on pelagic crustaceans, although the possible infection route by paratenic hosts such as *Sagitta* and other invertebrate components of the pelagic system cannot be ruled out.

The other two digeneans *Bathycotyle branchialis* and *Hirudinella* sp. only appeared in a few cases in Mediterranean waters, and can be considered rare as secondary parasitic species. *B. branchialis* had been previously reported in the gills of large *C. hippurus* specimens from the Straits of Florida (Burnett-Herkes, 1974), although it is not proved whether this parasite infects the gills or is vomited from the stomach, as we have found in *Dinurus* spp. Two species of *Bathycotyle* have been described, *B. branchialis* in scombrids and *B. coryphaenae* in *C. hippurus*. The only data to differentiate them is the presence of an external opening of the Laurer's canal in the first species (Gibson and Bray, 1979). Although it is not clear whether the Laurer's canal has an external opening or not, we have seen a dorsal opening in our specimens and in consequence we have considered them as *B. branchialis*. The life history of this species is not known. The genus *Hirudinella* is a typical stomach parasite of marine teleosts (mainly scombrids and tunas), although coryphaenids are habitual hosts (Yamaguti, 1971). Due to their great morphological variability, many studies have described up to fourteen different species of this genus, although Yamaguti (1971) stated that a wide-ranging revision is required. The life cycle of this endoparasite is also unknown.

Floriceps saccatus plerocerci have been recorded in teleosts, whereas adult cestodes are gut parasites of several elasmobranchs from the Atlantic and Pacific Oceans (Campbell and Beveridge, 1994). The only reference for these plerocercoids in coryphaenids was reported by Dollfus (1946) from specimens caught in French Atlantic waters. Its presence in *C. hippurus* coming from the Atlantic Ocean as well as in the juvenile fish born in the Mediterranean Sea indicated that the recruitment of this parasite is possible in both areas. The absence of parasitism in *C. equiselis* may be due to the small

size of these specimens in the sample, which included individuals in the 30-52 cm fork length range. In the same way, the diet composition may possibly play a role in the recruitment of the parasites. The high prevalence observed in adult fish (Carbonell *et al.*, 1998) could suggest that the development of the cysts in *C. hippurus* is slow or that they get the infection late. Unfortunately, the time needed by the ingested procercoid larvae to develop into plerocercoid larvae, and the time needed for the defence mechanisms of *C. hippurus* to produce the large cysts of conjunctive tissue are both unknown. In any case, the above mentioned authors have postulated a four host cycle for this species, with crustaceans and plankton-feeder fishes as intermediate hosts for procercoid larvae, *C. hippurus* as a paratenic host for plerocercoid larvae and sharks as final hosts where the stage matures. This agrees with the experimental observations of Nakajima and Egusa (1972g), who demonstrated that copepod and teleost fish are necessary for procercoid maturation and other teleosts for plerocercoid development.

Metabronema magna is a nematode common in the stomachs of salmonids (Anderson, 1992). In marine fish, it had only been described in *Caranx* sp. and *Sparus* sp. (Skrjabin, 1991). This spirurid requires the participation of an intermediate host such as the crustacean amphipods, decapods and mysidacean larvae (Black and Lankester, 1980), in which the third larval stage can develop. Although they have been found in fish of all sizes and ages, it must be supposed that early infection takes place when *C. hippurus* feed on amphipods and decapods. The fact that the cysts generated by these nematodes are made of conjunctive tissue in fish with sizes smaller than 50-60 cm FL and are completely calcified in larger sized fish seems to suggest that the infection has been early. Given the rapid growth of *C. hippurus* (Beardsley, 1967; Rose and Hassler, 1968) however, it is not unexpected that conjunctive cysts have been observed in fish from 20 to 60 cm FL.

The other spirurid nematode *Philometroides* sp. is also reported for the first time in *C. hippurus*. However, in contrast, it only appeared in a few specimens from Mediterranean waters. The only species of this genus known to date is *Philometroides seriolae*, which was detected in marine fishes from Japanese waters (Skrjabin, 1991). Our specimens have the typical cuticular plates of this species, but we are not sure if they belong to it.

The acanthocephalan *Rhadinorhynchus pristis* appeared in fish from both areas, but with low prevalence. This species was reported for the first time in dolphinfishes from Caribbean waters (Cable and Linderoth, 1963), although it is widely distributed in a great number of epipelagic fishes (Yamaguti, 1963; Petrochenko, 1971). The fact that this endoparasite has been found in *C. equiselis* specimens between 30 and 40 cm FL, and that in *C. hippurus* it only appeared in adult fish, suggests that the infection of this species could occur in Atlantic waters, before the seasonal migration of these specimens to the Mediterranean. It is known that the paratenic hosts have great importance in the biological cycles of the acanthocephalans. Thus, infection could occur when both species eat paratenic teleosts.

Ectoparasitism

Caligus quadratus and the other *Caligus* species have been recorded in all oceans as ectoparasites of coryphaenids. They have been found in the skin as well as in the oral cavity, operculum, gill cavity and gill filaments (Palko *et al.*, 1982). They are monoxenous copepods whose copepodite infective forms have flat bodies with a circular dorsal carapace, and they swim freely in the water within the pelagic ecosystem. As the entire life cycle of *C. hippurus* takes place in the same habitat, it is not unusual that this species can be strongly parasitised during juvenile as well as adult stages. The infection starts in the early growth period, reaches its maximum in intermediate aged fish and decreases in adults. This could suggest an immunogenic condition in large specimens, which acquire resistance as they become older due to the repeated contacts between parasites and host. Nevertheless, it is difficult to reach any definitive conclusions about the infection data since the caligids have the ability to leave their host and infect other hosts (Kabata, 1979). Also, we must take into account the relationship between coryphaenids and floating objects, which have been postulated as cleaning stations where pelagic fishes go to have their parasites removed by other fish (Gooding and Magnuson, 1967).

Eurysphorus nymphae is also a world-wide species that has been recorded as an ectoparasite of coryphaenids. This copepod parasitizes the same habitat as *Caligus* spp. and it seems that although it was a prevalent species in central-western Atlantic waters, it was not found in specimens captured in the Mediterranean, where *Caligus* spp. were predominant. These differences could be related to water

surface temperatures, since they ranged between 16 and 27°C in the Mediterranean Sea, whereas in the Atlantic the temperatures were less variable, ranging from 20 to 23°C. We cannot either explain the fact that the other ectoparasite copepod *Neobrachiella coryphaenae* was only found during 1995 in the Mediterranean and was absent in 1990 and 1991 and in Atlantic waters. The life history of this species is direct and the postembryonic stages belong to the planktonic community, which rises every night to surface waters (Kabata, 1981).

Pennella filosa is a mesoparasitic copepod which has been reported in *Xiphias gladius*, *Mola mola*, in some tuna species and in marine mammals (Kabata, 1992). Recently, *P. filosa* has been found embedded in the flesh of *Lepidocybium flavobrunneum* captured in the northwestern Atlantic (Benz and Hogans, 1993). Only *Pennella pustulosa* and *Pennella varians* had been reported in *C. hippurus* from Australian and Atlantic waters respectively (Yamaguti, 1963). Nevertheless, it is probable that both species could be synonymous with *P. filosa*, due to the great morphological variability of this pennellid copepod (Kabata, 1979; Hogans, 1987; Raibaut, 1991). This anatomic plasticity has also been observed by us, and although it is related to parasite age, it is mainly related to its location. In effect, there are important morphological differences if the parasite is attached to hard surfaces (fin rays) or if it is deeply anchored in muscular tissue or in the abdominal cavity.

P. filosa has an incompletely known life cycle, due to the lack of data on its chalimus larval phases and the metamorphosis of the infective preadults. However, it is probably similar to other pennellid species, which are the only copepod parasites that show a two-host life cycle. Some teleost fish (sometimes the same final host) and cephalopods have been reported as intermediate hosts of pennellids (Kabata, 1981). Rose and Hamon (1953) have also reported chalimus stages and free males of *P. filosa* in the gills of the cephalopods *Sepia* and *Loligo*. This parasite is characteristic of large specimens, which have a diet composed of almost 20% cephalopods and 60% teleost fish (Massutí *et al.*, 1998). Thus, its infection as the fish became older could be related to a higher catch and predation activity on squids (*Illex coindetii* and *Todarodes sagittatus*) and other cephalopods (*Histioteuthis* spp.). The predatory contacts might allow the invasion of infective forms from the gills and mantle of squids to the skin of *C. hippurus*.

P. filosa has not been found parasitising *C. hippurus* in any sea or ocean of the world. The only references to this parasite refer to the previously mentioned fish where the presence of *P. filosa* has always been occasional, with the collection of only a few parasites which very often appear to be incomplete due to the lack of the head. In our case, we obtained a total of 160 parasites, all them exclusively parasitising the large breeding fish that every year visit the Mediterranean Sea. The presence of 30% premetamorphic parasites, as well as young females, makes us suspect that infection takes place in the Mediterranean Sea after the breeding fish cross the Strait of Gibraltar and subsequently disperse through the whole sea. On the other hand, Pascual (pers. com.), studying cephalopods captured in the Alborán Sea and other areas of the southwestern Mediterranean, has proved that all the cuttlefishes and squids captured in these areas were parasitised (100%) in the mantle and gills by larval chalimus phases, possibly belonging to copepod pennellids. Consequently, it is very probable that *C. hippurus* is infected when predating on these cephalopods during its passage through the southwestern Mediterranean.

CONCLUSIONS

The study of the relationships between diet and parasite recruitment allows some comments to be made on the life cycles of some of the parasites found. Regarding the endoparasites (Fig. 1), a cycle of three hosts can be proposed for *Dinurus* spp., in which the benthic gastropod molluscs and planktophage fish, mainly clupeids, would take part as intermediate hosts, with *Coryphaena hippurus* and *C. equiselis* being the definitive or final hosts. A similar cycle could be applied to the other gastric hemiurid *Lecithocladium excisum* but in this case the secondary hosts would be larvae of copepods and pelagic decapods. The nematode *Metabronema magna* and the acanthocephalan *Rhadinorhynchus pristis* would have a cycle of two hosts, the first being pelagic amphipods and the second being larvae of diverse crustaceans in whose haemocoel the stage III infective larvae and the cystacanths would develop respectively. Finally, a cycle of four hosts is suggested for the cestode *Floriceps saccatus*, with crustacean larvae as primary hosts, planktophage fish as secondary hosts, *C. hippurus* as the tertiary host and various sharks as final hosts.

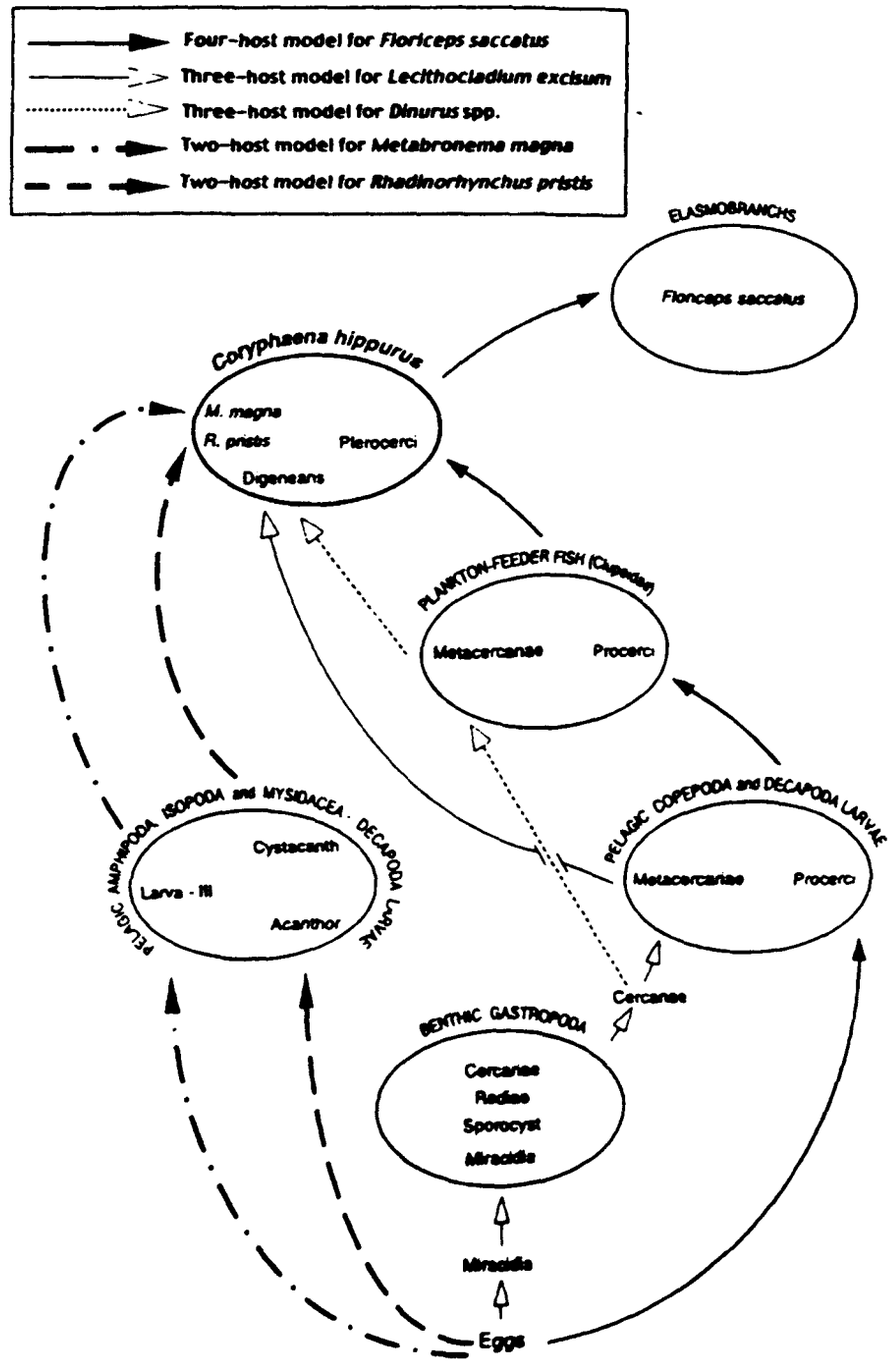

FIG 1 - Proposed life cycles for the endoparasites *Floriceps saccatus*, *Lecithocladium excisum*, *Dinurus* spp., *Metabrachema magna* and *Rhadinorhynchus pristis*

Regarding the ectoparasites (Fig. 2), *Pennella filosa* is a copepod that needs two hosts, a fish or a cetacean as a definitive host and cephalopod molluscs as intermediate hosts. These last ones are infected by copepodite larvae that develop four chalimus stages in the mollusc, the last of which are differentiated sexually and are fertilised. The males then disappear and the fertilised females infect *C hippurus* where they undergo extensive metamorphosis. This explains the great importance of the physical contacts between definitive and intermediate hosts. The remaining copepod parasites have copepodite and pelagic chalimus phases which form part of the planktonic community, where the fourth chalimus stage differentiates into preadult males and females that are the infective forms for the gills of the coryphaenids.

The present study shows that the life cycle and behaviour of *C hippurus* and *C equiselis* are of great importance in the recruitment, development, and transmission of parasites in the Atlantic Ocean and in the Mediterranean Sea. In both species, the

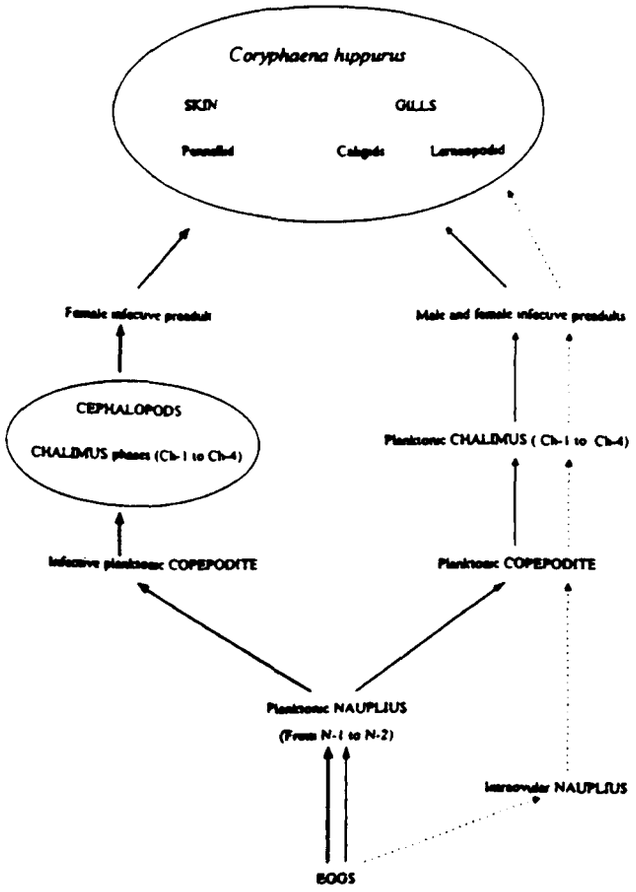

FIG. 2. – Proposed life cycles for the ectoparasites. Left: Cycle for *Pennella filosa*. Right: Caligid cycle for *Caligus* spp and *Eurypho-rus nymphae*. Lernaeopodid cycle for *Neobrachiella coryphaenae*.

recruitment of parasites is qualitatively similar to that of the large fish whose diet is based almost exclusively on teleost fish. Therefore, the feeding habits, surface water temperature, and length and body weight of fishes are related to parasite recruitments (Fig. 3).

This study shows that there are several parasites of *C. hippurus* that are potentially useful as biological tags for studying its migratory movements and stock differentiation within the Mediterranean, and between this area and adjacent Atlantic waters. Within the endoparasites, the trypanorhynch species *F. saccatus*, widely recognised as a long-lived parasite, and the acanthocephalan *R. pristis*, despite its low prevalence, probably have the greatest potential as biological tags. These species have a sufficient life span and remain in an identifiable form in *C. hippurus* long enough to cover the time scale of the investigation. For the same reason, the usually short life spans (<1 year) of adult digeneans in the alimentary tract of fish, tends to limit the use of these species as biological tags. Of the ectoparasite copepods found, *P. filosa* has a particular advantage as a tag because it is a large, very easily seen ectoparasite that leaves a prominent scar after its death, thereby extending its usefulness as a tag beyond its actual life span.

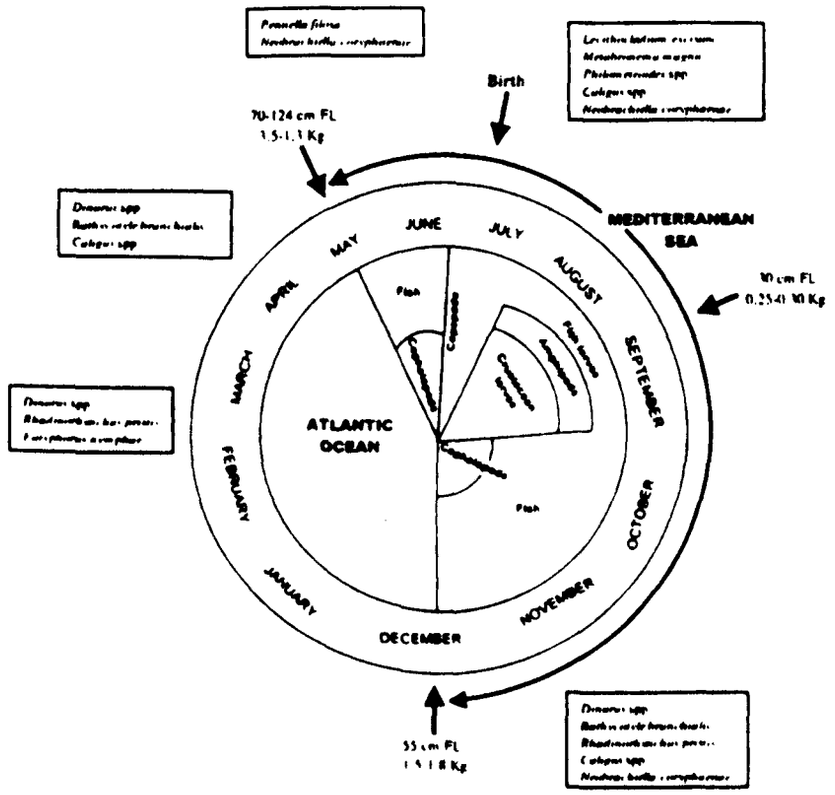

FIG 3 – Reproductive cycle of *Coryphaena hippurus* from the Atlantic Ocean to the Mediterranean Sea. Length and weight of captured fishes, diet and parasite recruitments. FL: fork length (cm).

REFERENCES

Anderson, R.C. – 1992. *Nematode Parasites of Vertebrates*. Farnham Royal Bucks CAB International, Wallingford. 578 pp.

Beardsley, G.L. – 1967. Age, growth and reproduction of the dolphin *Coryphaena hippurus* from the straits of Florida. *Copelia*, 2: 441-451.

Benz, G.W and W.E. Hogans. – 1993. *Penella filosa* (L. 1758) (Copepoda: Siphonostomatoida) from the escolar *Lepidocybium flavobrunneum* (Smith, 1849) in the north-west Atlantic. *Syst. Parasit.*, 26 (2): 127-131.

Black, G.A. and N.W. Lankester. – 1980. Migration and development of swim bladder nematode *Cystidicola* sp. (Metabronematidae) in their definitive host. *Can. J. Zoo.*, 58: 1997-2005.

Burnett-Herkes, J. – 1974. Parasites of the gills and buccal cavity of the dolphin, *Coryphaena hippurus*, from the Straits of Florida. *Trans. Am. Fish. Soc.*, 103: 101-106.

Cable, R.M. and J. Linderoth. – 1963. Taxonomy of some Acanthocephala from marine fishes with reference to species Curaçao and Jamaica. *J. Parasi.*, 49: 706-716.

Campbell, R.A. and I. Beverdge. – 1994. Order Trypanorhyncha Diesing, 1863. In: L.F. Khalil, A. Jones and R.A. Bray (eds.): *Keys to the Cestode Parasites of Vertebrates*, pp. 51-148. CAB International, Wallingford, UK.

Carbonell, E., J.J. Castro and E. Massuti. – 1998. *Floriceps saccatus* plerocerci (Trypanorhyncha, Lacistorhynchidae) as parasite of dolphin fish (*Coryphaena hippurus* L.) and pompano dolphin (*Coryphaena equiselis* L.) in Western Mediterranean and Eastern Atlantic waters. Ecological and biological aspects. *J. Parasit.*, 84(5): 1035-1039.

Delamare-Deboutville, C. and L. Nunes-Ruivo. – 1958. Copépodes parasites des Poissons méditerranéens. *Vie et Milieu*, IV (2): 201-218.

Dollfus, R.P. 1927. Sur une métacercaire progénétique d'Hemiuridae. *Bulletin Biologique de la France et de la Belgique*, 61: 49-58.

Dollfus, R.P. 1946. Notes diverses sur des tetrarhynchides. *Mem. Mus. Hist. Nat.*, 22(5): 179-220.

Fischthal, J.H. – 1972. Zoogeography of digenetic trematodes from West African marine fishes. *Soc. Wash.*, 39: 192-203.

Fischthal, J.H. and J.D.Thomas. – 1972b. Digenetic trematodes of marine fishes from Senegal. *Bul. Inst. Fond. Afr. Noire*, Serie A, 34: 292-322.

Gibbs, Jr., R.H. and B.B. Collette. – 1959. On the identification, distribution and biology of the dolphins, *Coryphaena hippurus* and *C. equiselis*. *Sci.Gulf Carib.*, 9: 117-152.

Gibson, D.I. and R.A. Bray. – 1979. *The Hemiuroidea terminology, systematics and evolution*. *Bull. Brit. Mus. (N.H.) Zool. Ser.*, 36 (2): 35-146.

Gibson, D.I. and R.A. Bray. – 1986. *The Hemiuridae (Digenea) of fishes from the north-east Atlantic*. *Bull. Brit. Mus. (N.H.) Zool. Ser.*, 51: 1-125.

Gooding, R.M. and J.J. Magnusson. – 1967. Ecological significance of a drifting object to pelagic fishes. *Pacific Sci.*, 21: 486-497.

Herald, E.S. – 1961. *Living fishes of the world*. Doubleday and Co. Inc. Garden City, NY. pp. 304.

Hogans, W.E. – 1987. Morphological variation in *Penella balaenopterae* and *P. filosa* (Copepoda: Penellidae) with a review of the genus *Penella* Oken, 1816, parasitic on cetacea. *Bull. Mar. Sci.*, 40: 442-453.

Ho, J.S. – 1963. Of five species of Formosan parasitic copepods belonging to the Suborder Caligoida. *Crustaceana*, 5: 81-98.

Kabata, Z. – 1979. *Parasitic copepoda of British fishes*. Ray Society, London. 468 pp.

Kabata, Z. – 1981. Copepoda (Crustacea) parasitic of fishes: problems and perspectives. *Adv. Parasit.*, 19: 1-17.

Kabata, Z. – 1992. *Copepods parasitic on fishes*. Synopsis of British fauna, 47. Linnean Society, London.

Koie, M. – 1979. On the morphology and life-history of *Derogenes varicus* (Muller, 1784) Looss, 1901 (Trematoda: Hemiuridae). *Zeitschrift für Parasitenkunde*, 59: 67-68.

Koie, M. – 1990b. Redescription of the cercaria of *Lecithochirium rufoviride* (Rudolphi, 1819) Luhe, 1901 (Digenea, Hemiuridae). *Ophelia*, 31: 85-95.

Koie, M. – 1990c. On the morphology and life-history of *Hemiurus luehei* Odhner, 1905 (Digenea: Hemiuridae). *J. Helmint.*, 64: 193-202.

Koie, M. – 1991. Aspects of the morphology and life cycle of *Lecithocladium excisum* (Digenea: Hemiuridae), a parasite of *Scomber* spp. *Int. J. Parasit.*, 21(5): 592-602.

Lozano-Cabo, F. – 1961. Biometria, biologia y pesca de la lampuga (*Coryphaena hippurus*) de las Islas Baleares. *Academia de Ciencias Exactas, Fisicas y Naturales de Madrid. Series de* Ciencias Naturales, 21: 1-93.

Manooch, I.I.I, C.S., D.L. Mason and R.S. Nelson. R.S. -1984. Food and gastrointestinal parasites of dolphin *Coryphaena hippurus* collected along the southeastern and Gulf coast of the United States. *Bull. Japan Soc. Sci. Fish.*, 50: 1511-1525.

Margolis, L., G.W. Esch, J.C. Holmes, A.M. Kuris and G.A. Schad – 1982. The use of ecological terms in parasitology (Report of an *ad hoc* Committee of the American Society of Parasitologists). *J. Parasit.*, 68: 131-133.

Massuti, E. and B. Morales-Nin. – 1995. Seasonality and reproduction of dolphin fish (*Coryphaena hippurus*) in the western Mediterranean. *Sci. Mar.*, 59: 357-364.

Massuti, E., S. Deudero, P. Sánchez and B. Morales-Nin. – 1998. Diet and feeding of dolphin (*Coryphaena hippurus* L.) in western Mediterranean waters. *Bull. Mar. Sci.*, 63 (2): 329-341.

Mather, F.J. and C.G. Day. – 1954. Observations of pelagic fishes of the tropical Atlantic. *Copeia*, 1954: 179-188.

Nakajima, K. and S. Egusa. – 1972g. *Cysticercus* parasitizing cultived yellow-tail. Life cycle. *Fish pathology*, 7: 6-14.

Palko, B.J., G.L. Beardsley and W.J. Richards. – 1982. Synopsis of the biological data on dolphinfishes, *Coryphaena hippurus* Linnaeus and *Coryphaena equiselis* Linnaeus. *FAO Fish. Syn.*, 130: 1-28.

Petrochenko, V.I. – 1971. *Acanthocephala of Domestic and Wild Animals*. Israel Program for Scientific Translations, Jerusalem, pp. 439.

Raibaut, A. – 1991. A propos des Pennelles (Copepodes) parasites de Cetaces. *Actes des Premieres Rencontres de Cétologie Méditerrnée*, Port-La-Nouvelle, 8-9 Juin 1991: 43-49.

Rose, M. and M. Hamon. – 1953. A propos de *Penella varians* Steenstrup and Lutken, 1861, parasites des branchies de Cephalopodes. *Bulletin Soc. Hist. Nat. Afr. Nord*, 44(5-6): 172-183.

Rose, C.D. and W.W. Hassler. – 1968a. Age and growth of the dolphin *Coryphaena hippurus* in North Carolina waters. *Trans. Am. Fish. Soc.*, 97: 271-276.

Shcherbachev, Yu. N. 1973. – The biology and distribution of the dolphins (Pisces, Coryphaenidae). *J. Ichth.*, 13: 182-191.

Szidat, L. – 1950. Los parásitos del róbalo. *Congreso Nacional de Pesquerias, Buenos Aires*, 2: 235-270.

Skrjabin, K.I. – 1991. *Key to Parasitic Nematodes*. 4 vol. E.J. Brill, NY. 1097 pp.

Yamaguti, S. – 1963. *Systema Helminthum. Vol. V. Acanthocephala*. Interscience Publish. N. 423 pp.

Yamaguti, S. – 1963. *Parasitic copepoda and branchiura of fishes*. John and Sons Inc. USA. 1104 pp.

Yamaguti, S. – 1971. *Synopsis of Digenetic Trematodes of Vertebrates*. Vol. 2. Tokyo: Keigaku Publishing Co. 337 pp.

SCI. MAR., 64 (1) 115-116 SCIENTIA MARINA 2000

NOTE

First record of *Holocentrus ascensionis* (Osbeck, 1765) (Osteichthyes: Holocentridae) in the Canary Islands (Central-east Atlantic)*

JOSÉ J. CASTRO-HERNÁNDEZ and ANA Y. MARTÍN-GUTIÉRREZ

Departamento de Biología, Universidad de Las Palmas de Gran Canaria, Apdo. 550, Canary Islands, Spain.

SUMMARY: The capture of a specimen of *Holocentrus ascensionis* (Osbeck, 1765), a species previously unrecorded in the Eastern Atlantic north of Gabon, is reported from Gran Canaria Island (Canary Islands, Central-East Atlantic).

Key words: *Holocentrus ascensionis*; Central-East Atlantic, Canary Islands.

In February 1999 a specimen of *Holocentrus ascensionis* was fished off the south-east coast of Gran Canaria Island (Canary Islands). The fish was caught using a trap (Hernández-García *et al.*, 1998) located over the sea bottom at 35 m depth. The squirrelfish was housed in a 100-l glass aquarium for nine days in order to check its taxonomical status and to observe its behaviour in the tank. In the Eastern Atlantic, the presence of this species has been previously reported in St. Helena and Ascension Islands and from Angola and Gabon (Greenfield, 1981; Ben-Tuvia, 1990). This is the first time that it has been recorded north of the equator, and as a member of the ichthyofauna of the Canary Islands (28°N).

The fish was 205.0 mm of total length (Table 1). The distinctive characters agreed with those given by Greenfield (1981). The body moderately compressed (the standard length/height ratio was 3.06), relatively slender and oblong. The caudal peduncle was slender and long. Edges of membrane bones of head were serrate and spiny. Three conspicuous strong spines on the side of the head (2 opercular spines and a preopercular one). The upper opercular spine twice size of the lower opercular one. These two opercular spines clearly shorter than the preopercular one. Upper jaw was long, extending beyond posterior margin of pupil. Anterior portion of the dorsal fin had 11 spines and the posterior portion of this fin had 16 soft rays. A posterior soft dorsal fin 1.75 times higher than the anterior portion of the dorsal fin (this aspect is not well drawn in Greenfield, 1981). The anal fin with 4 spines (the first very small and almost inlaid in the body) was followed by 10 soft rays (Fig. 1). Fifty one scales in the lateral-line.

During housing in the aquarium, the color of the back and upper sides was reddish (or orange) with golden reflections (Fig. 1). It showed two dark greenish stripes following scales intersections on upper sides, fading posteriorly. The nine stripes below these were less distinct, pink to white near the

*Received April 14, 1999 Accepted June 29, 1999

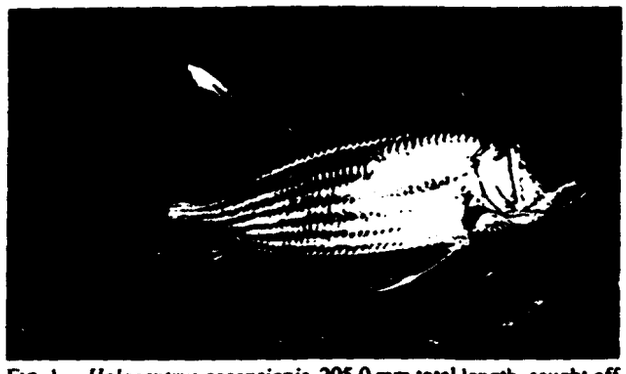

FIG. 1. – *Holocentrus ascensionis*, 205.0 mm total length, caught off Gran Canaria Island.

belly, when the fish was calm. When the fish was excited or frightened, the nine lower stripes became white, and three white-pink vertical bands appeared from the pectoral fin region to the anal fin region. The last band was wider than the other two, beginning at the anal fin and continuing to the end of the caudal peduncle. The lower sides, belly and breast were shine-white. The snout and top of the head were dark red, with the upper portion of the maxilla and the vertical branch of the preopercular bone white. It showed a white streak diagonally across the cheek, from the upper jaw to the preopercular spine. The lower jaw was white but the lower lip was red. The iris was bright red near the pupil, the distal margin blackish. The dorsal fin spines were yellowish or yellowish-green, but the interspinal membranes were white after the spine, and yellowish-green just before the next spine. The soft dorsal fin rays were pink with the membrane showing an intermediate dark vertical line between rays. The outer caudal fin rays were white (the rest pink). The first three anal spines were white and the fourth spine and soft rays were pink. The pectoral fins were pink, but the upper edge of the first rays were darker red. Pelvic fin spine and anterior margin of first ray were white, while the other pelvic fin rays were pink.

When caugth the squirrelfish produced sounds, a behavior that was also reported by Moulton (1958) in the Bimini area (Central-west Atlantic). During housing, the fish was fed with pelletized food used for feeding fish in aquaculture.

This record supports the comments made by Greenfield (1981) who indicated that possibly the geographical distribution of this species was more wide-spread along the African coast. In the Western Atlantic, this species occurs from North Carolina (USA) to Santos (Brazil) (Greenfield, 1981; Ben-Tuvia, 1990), and probably in the Eastern Atlantic it has a similar latitudinal distribution (from Angola to Canary Islands, at least). Possibly, its populations are scarce north of the equator or it is confused with *Adioryx hastatus* or *Myripristis jacobus* and catch is reported as red squirrelfish, as suggested by Robins *et al.* (1986) in the West Atlantic, where it is included in market shipments of red snapper.

TABLE 1. – Morphometric (in mm) and meristic data of the specimen of *Holocentrus ascensionis* caught in Gran Canaria Island.

Total length	205.0
Fork length	170.3
Standard length	162.0
Head length	47.9
Eye diameter	14.9
Base of the anterior portion of the dorsal fin	68.6
Base of the posterior portion of the dorsal fin	26.4
Base of anal fin	24.8
Predorsal distance (anterior portion)	21.5
Predorsal distance (posterior portion)	116.5
Prepectoral distance	52.9
Preanal distance	119.0
Prepelvic distance	56.2
Pectoral length	32.2
Pelvic length	37.2
Body depth	52.9
Fin rays	
Dorsal	XI+16
Pectoral	13
Anal	IV+10
Scales in the lateral-line	51

ACKNOWLEDGEMENTS

Our thanks to the Fishermen's Association of Castillo del Romeral (Gran Canaria) for making possible this new record of the ichthyofauna of the Canary Islands. Thanks are also given to Dr. Teresa Moreno for her assistance with the photographic material.

REFERENCES

Ben-Tuvia, A. – 1990 Holocentridae. In Quéro, J.C., J.C. Hureau, C. Karrer, A. Post and L. Saldanha *Check-list of Fishes of the Eastern Tropical Atlantic*. Vol. II. pp:627-628. Junta Nacional de Investigação Científica e Tecnológica. Lisbon

Greenfield, D.W. – 1981 Holocentridae. In Fischer, W.G. G. Bianchi and W.B. Scott *FAO Species Identification Sheets for Fishery Purposes. Eastern Central Atlantic (fishing Areas 34, 47 (in part)* Canada Funds-in-Trust. Ottawa, Department of Fisheries and Oceans Canada, by arrangement with the Food and Agriculture Organization of the United Nations. Vol. II

Hernández-García, V., J.L. Hernández-López and J.J. Castro – 1998. The octopus (*Octopus vulgaris*) in the small-scale trap fishery off the Canary Islands (Central-East Atlantic). *Fish. Res.*, 35: 183-189

Moulton, J.M. – 1958 The acoustical behavior of some fishes in the Bimini area. *Biol. Bull.* 114: 357-374

Robins, C.R., G.C. Ray, J. Douglass and R. Freund – 1986 *A field guide to Atlantic coast fishes of North America*. The Peterson Field Guide Series. Houghton Mifflin Company. Boston

Scient. ed. M. Harmelin-Vivien

for the design of new fluorophores based on the D–A–D configuration.

REFERENCES

1. Anstead GM Katzenellenbogen JA. J. Phys. Chem. 1990; 94:1328.
2. Fery-Forgues S Le Bris MT Mialocq JC Pouget J Rettig W Valeur B. J. Phys. Chem. 1992; 96:701–716.
3. Marcotte N Fery-Forgues S Lavabre D Marguet S Pivovarenko VG. J. Phys. Chem. 1999; 103:3163–3170, and references cited.
4. Barnabas MV Liu A Trifunac AD Krongauz VV Chang CT. J. Phys. Chem. 1992; 96:212–217.
5. Marcotte N Fery-Forgues S. J. Photochem. Photobiol. (in press).
6. Kawski A. Acta. Phys. Pol. 1966; 29:507.

Determination of polychlorinated dibenzofurans in blue mussels (*Mytilus edulis*) using microwave-assisted extraction prior to HPLC-fluorescence detection

A. Eiguren Fernández, Z. Sosa Ferrera and J. J. Santana Rodríguez

Department of Chemistry, Faculty of Marine Sciences, University of Las Palmas de G.C., 35017 Las Palmas de G.C., Spain

In the last few years, increasing attention has been paid to the toxical effects of polychlorinated dibenzofurans (PCDFs) and their impact on marine and terrestial biota. Blue mussels often serve as indicator organisms because of their capability of accumulating lopophilic pollutants and their relatively small enzymatic degradation potential, in order to assess the water quality of marine ecosystems (1).

In this work, the microwave-assisted extraction (MAE) technique, using a non-ionic surfactant, polyoxyethylene 10 lauryl ether (POLE), is optimized as prior step to the analysis of PCDFs by high-performance liquid chromatography (HPLC) with fluorescence detection in blue mussels. MAE methodology allows a simple and rapid analysis of different kind of compounds present in diverse media (2, 3) and the use of surfactants reduces the cost and toxicological effects of the process.

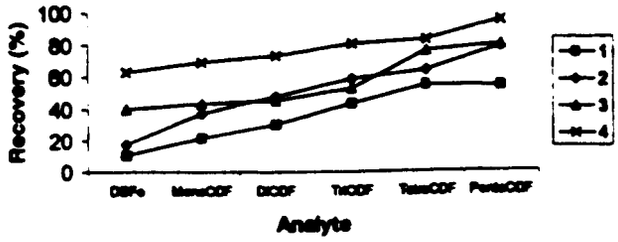

Figure 1. Recovery percentages for each analyte when the extraction time varies. (1, □) 15–15–15 min; (2, ◆) 15–10–10 min; (3, □) 10–10–10 min; (4,X) 10–10–10–10 min.

RESULTS AND DISCUSSION

Extraction process

To optimize the MAE process, different parameters have to be studied. Factors such as pH, volume and concentration of the extractant have been studied previuosly (Eiguren Fernandéz *et al.*, unpublished data, and results show that these factors have no influence on the extraction process. The effect of the extraction time, power and number of washing steps is shown in this work.

The mussels (*Mytilus edulis*) were homogenized and liophilized. Samples of 2 g were spiked with an appropriate amount of each analyte and were allowed to equilibrate for 24 h in a rotatory system. The samples were then transferred to the extraction vessels.

For the initial conditions, a extraction power of 80% and three washing steps were established (Eiguren Fernández *et al.*, unpublished data). The effect of extraction time of each step was studied using three different intervals: (a) 15–15–15 min; (b) 15–10–10 min; and (c) 10–10–10 min. The results obtained for these conditions show low recovery percentages (Table 1). Fig. 1 shows that the recovery percentage increases with the number of chlorine atoms in the molecule, and also increases when the extraction time decreases for each analyte. In order to obtain higher recoveries, a new extraction step was added, (d) 10–10–10–10 min. Under

Table 1. Effect of the extraction time on the recovery percentages

Analyte	Abbreviation	15–15–15*	15–10–10*	10–10–10*	10–10–10–10*
Dibenzofuran	DBFo	10	17	40	63
4-Chlordibenzofuran	MonoCDF	21	37	43	69
2,8-Dichlorodibenzofuran	DiCDF	30	48	45	73
2,4,8-Trichlorodibenzofuran	TriCDF	43	59	53	81
2,3,7,8-Tetrachlodibenzofuran	TetraCDF	55	64	86	83
1,2,3,4,8-Pentachlorodibenzofuran	PentaCDF	54	79	80	95

* Time (min).

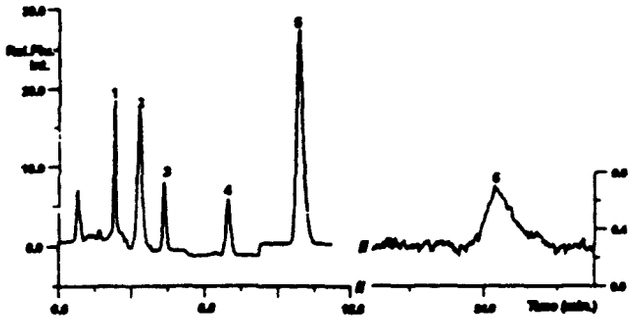

Figure 2. Elution of six PCDFs after MAE extraction process. (1) DBFo; (2) MonoCDF; (3) DiCDF; (4) TriCDF; (5) TetraCDF; (6) PentaCDF.

this condition, satisfactory recovery percentages were obtained (Table 1, Fig. 1).

Chromatographic analysis

The extracts were analysed using a HPLC system with fluorescence detection. 20 μL of the extracted solution were directly injected in the chromatographic system to obtain the separation of the PCDFs. Chromatographic conditions were established in an isocratic methanol:-water (85:15, v/v) mobile phase and 1 mL/min flow rate (Fig. 2). Determination of the different analytes was carried out by monitoring the relative fluorescence intensity at the maximum λ_{ex} and λ_{em} for each analyte (4).

REFERENCES

1. Stronkhorst J. Mar. Poll. Bull. 1992;24:250–258.
2. Letellier M, Budzinski H, Garrigues P. LC-GC International 1999; April: 222–225.
3. Ackley KL, B'Hymer H, Sutton KL, Caruso JA. J. Anal. At. Spectrom. 1999;14:845–850.
4. Eiguren Fernández A, Sosa Ferrera Z, Santana Rodríguez JJ. Analyst 1999;124:487–491.

Luminescence analysis in transparency range of tissue at linear and non-linear absorption

Asatur Lalayan,
Yerevan State University, Physics Department, A. Manoogian 1, Yerevan, 375025, Armenia

In recent years, a number of research works in oncology have led to the development of new modalities for the diagnosis of malignant tissue by the luminescence method. Currently, photosensitizers of the 'second generation' have been becoming more attractive for researchers in the field of cancer phototherapy (1–3). These drugs have strong absorption in the red–near-infrared spectral region and this peculiarity allows provision of more effective photoaction because of the high penetration depths of the photons into the tissue volume. The molecules of sensitizers, which may be excited in red and near-infrared spectra, simultaneously possess luminescence, shifted to longer wavelength. When both excitation and luminescence wavelengths are located in the 'transparency window' of tissue (about 600–1100 nm), this peculiarity makes them very suitable for fluorescence diagnosis in the optical depth of tissue. The other pathway of red fluorescence excitation is two-photon absorption using infrared high-intensity laser irradiation. However, the strong scattering of light in turbid organic media is a serious limitation factor for non-linear optical effects. Besides two-photon luminescence, which strongly depended on intensity, can be detected at such high intensity values, when tissue photodamage also appears.

In the present work, the fluorescence spectra of both one-photon and two-photon excitation schemes have been studied using Nd:YAG laser with nanosecond/picosecond operation mode. Fluorescence spectra from the optically deep located chlorin e_6 and Zn-phthalocyanine molecules at 660 nm wavelength of nanosecond laser excitation were registered. In this case the fluorescence peak was located near to the laser excitation peak and was registered using a glass filter (KS-19), with transmission coefficients of 10^{-4}% and 90% for 660 and 700 nm, respectively. After spectral cutting, the fluorescence peak was located at 715 nm and 695 nm, respectively for chlorin e_6 and Zn- phthalocyanine, and differed from laser irradiation. The recognizing depth of tissue at red excitation of both sensitizers increase up to 10 mm, as distinct from the 2–4 mm depth at short (355 and 532 nm) excitation wavelengths.

Non-linear excited fluorescence spectra of tissues, sensitized by chlorin e_6 and haematoporphyrin derivatives under picosecond pulses of train irradiation (λ = 1064nm, intensity 100 MW/cm^2, pulse duration 33 ps) were obtained. The localization of the fluorescence peaks of the dyes coincides with that in case of one-photon nanosecond excitation at 355 nm. However, in case of two-photon excitation, the background fluorescence is practically absent and high fluorescence signal contrast (≈1000) is achieved. It can be explained that more effective two-photon absorption of injected dyes, in comparison with endogenous fluorescent agents, is taking place. Using nanosecond radiation of the same wavelength and pulse energy density, the fluorescence spectra were prevented from registering because the cross-section of two-photon absorption was low in several orders.

To summarize, we have shown the possibilities of

Mineralium Deposita (2000) 35: 332–345

ARTICLE

M. Fuertes-Fuente · A. Martin-Izard
M. C. Boiron · J. Mangas

Fluid evolution of rare-element and muscovite granitic pegmatites from central Galicia, NW Spain

Received: 14 October 1999 / Accepted: 5 October 1999

Abstract Fluid inclusions have been studied in three pegmatite fields in Galicia, NW Iberian Peninsula. Based on microthermometry and Raman spectroscopy, eight fluid systems have been recognized. The first fluid may be considered to be a pegmatitic fluid which is represented by daughter mineral (silicates)-rich aqueous inclusions. These inclusions are primary and formed above 500 °C (dissolution of daughter minerals). During pegmatite crystallization, this fluid evolved to a low-density, volatile-rich aqueous fluid with low salinity (93% H_2O; 5% CO_2; 0.5% CH_4; 0.2% N_2; 1.3% NaCl) at minimum *P–T* conditions around 3 ± 0.5 kbar and 420 °C. This fluid is related to rare-metal mineralization. The volatile enrichment may be due to mixing of magmatic fluids and fluids equilibrated with the host rock. A drop in pressure from 3 ± 0.5 to 1 kbar at a temperature above 420 °C, which may be due to the transition from predominantly lithostatic to hydrostatic pressure, is recorded by two-phase, water-rich inclusions with a low-density vapour phase (CO_2, CH_4 and N_2). Another inclusion type is represented by two-phase, vapour-rich inclusions with a low-density vapour phase (CO_2, CH_4 and N_2), indicating a last stage of decreasing temperature (360 °C) and pressure (around 0.5 kbar), probably due to progressive exhumation. Finally, volatile (CO_2)-rich aqueous inclusions, aqueous inclusions (H_2O-NaCl) and mixed-salt aqueous inclusions with low *Th*, are secondary in character and represent independent episodes of hydrothermal fluid circulation below 310 °C and 0.5 kbar.

Editorial handling: B. Lehmann

M. Fuertes-Fuente (✉) · A. Martin-Izard
Departamento de Geologia,
Universidad de Oviedo, Arias de Velasco s/n,
33005 Oviedo, Spain
e-mail: mercedf@asturias.geol.uniovi.es

M. C. Boiron
CREGU-UMR G2R,
Faculté des Sciences, Université H. Poincaré,
Nancy I BP 2354501 – Vandoeuvre-lès-Nancy Cedex, France

J. Mangas
Departamento de Física,
Universidad de Las Palmas de G.C.,
Apdo.550, 35080 Las Palmas, Spain

Introduction

Most previous research on fluid inclusions in pegmatites has been focused on the fluid evolution related to some of the internal evolution stages of pegmatites (e.g. Mangas and Arribas 1987; Thomas and Spooner 1988; Doria et al. 1989; Charoy et al. 1992; Nwe and Morteani 1993; Martin-Izard et al. 1995) or to establish the fluid evolution associated with different stages of pegmatite crystallization (e.g. London 1986; Whitworth and Rankin 1989; Chakoumakos and Lumpkin 1990; Linnen and Williams-Jones 1994; Fuertes-Fuente and Martin-Izard 1998); all of these studies have been carried out in bodies that only belong to some of the pegmatite classes or to a type or subtype of the rare-element class. A great many of these studies have concentrated on fluid inclusions in different units of highly fractionated pegmatites (e.g. London 1986; Chakoumakos and Lumpkin 1990). Consequently, fluid inclusion studies on different classes of granitic pegmatites which focused on relating the fluid evolution to the stages of pegmatite crystallization and, moreover, on comparing fluid regimes between different pegmatites classes are rarer. An examination of a spectrum of different classes and types of pegmatites is required to broaden the fluid inclusion research in pegmatites (Cerny 1994).

In the central part of Galicia, in the northwest of the Iberian Peninsula, there are several occurrences of granitic pegmatites, which are referred to as pegmatites from Area Esquistosa de Galicia Central (AEGC). Some of these pegmatites are barren while others contain minerals of rare elements such as Nb, Ta, Sn, Be and Li and may be of economic interest because of their enrichment in these elements. A group of spodumene-bearing pegmatites was cited by Parga Pondal and

Martinez Cardoso (1948). In a summary of tin metalliferous ores in Galicia Occidental, Ypma (1966) described "pegmatite-aplites" as being of possible economic interest. Hensen (1967) described the mineralogy and petrography of some pegmatites being mined at that time for cassiterite and beryl. Knorring and Vidal Romani (1981) dealt with the mineralogy of a spodumene-bearing pegmatite also mined in the past. Fuertes-Fuente and Martin-Izard (1998) documented in more detail a zoned field of rare-element pegmatites in the AEGC known as Forcarei Sur. These authors proposed five pegmatite groups, each group being made up of pegmatites belonging to different types and subtypes of the rare-element class. The degree of differentiation and rare-metal mineralization of these groups increases with the distance to the parental granite according to Cerny's (1989) model. Two other pegmatite fields, which were formed from two different parental granites, have been established in the AEGC (Fuertes-Fuente 1996) known as Lalín and Forcarei Norte. The former consists of pegmatites belonging to two types of the rare-element class and the latter is formed by barren pegmatites of the muscovite class. Systematic studies of the fluid inclusions associated with these pegmatites have only been made in two rare-element pegmatites of the Forcarei Sur field (Fuertes-Fuente and Martin-Izard 1998). Microthermometric studies and Raman analysis of fluid inclusions have been done in order to determine the *P-V-T-X* conditions of the multistage fluid circulation in the pegmatites of the three different pegmatite fields (Forcarei Sur, Forcarei Norte and Lalín) from AEGC. The current work makes use of these data to propose a general model of fluid evolution in relation to the different stages of pegmatite crystallization in the AEGC pegmatites and to compare fluid systems in the different classes of AEGC pegmatites.

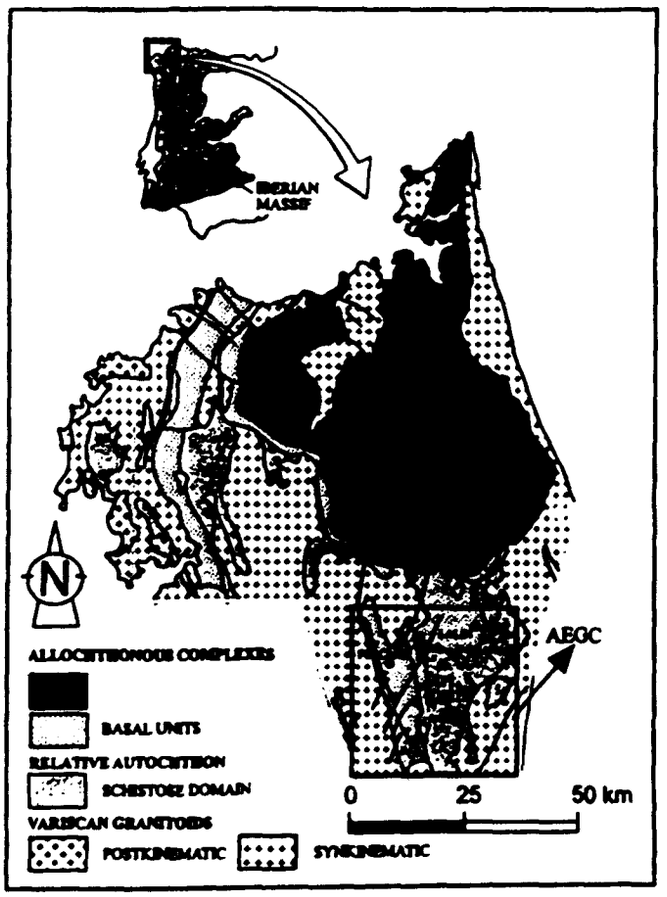

Fig. 1 Geological map of the NW Iberian Massif showing where the studied area (AEGC) is located in the Galician-Tras-Os-Montes Zone. (Modified from Martinez Catalán et al. 1996)

Geological setting

The AEGC pegmatites are located in the Galicia-Tras-Os-Montes Zone defined by Farias et al. (1987) in the Variscan Belt of the Iberian Massif. This Zone consists of a metasedimentary unit (the Schistose Domain) and a pile of units which form allochthonous complexes thrusting over the Schistose Domain (Gil Ibarguchi and Arenas 1990; Fig. 1).

The area studied consists of the basal unit of one of these allochthonous complexes and the relative autochthon of the Schistose Domain, separated by the Lalín-Forcarei Thrust (LFT) (Martinez Catalán et al. 1996; Fig. 1). The allochthonous basal unit is made up of schists, paragneisses, felsic orthogneisses and amphibolites (Marquinez 1984; Farias et al. 1987) and has been dated as middle-upper Ordovician and older (Priem et al. 1970; Van Calsteren et al. 1979; Garcia Garzón et al. 1981). The relative autochthon, Ordovician or older to lower Devonian in age, is formed by schists, some of them graphite-rich, and subordinate quartzites (Marquinez 1984; Farias et al. 1987).

The tectonic style of the Galicia-Tras-Os-Montes Zone is dominated by the thrust regime related to nappe emplacement during the Variscan Orogeny. There are two Variscan deformation events associated with nappe emplacement: D1, recumbent folds with axial plane cleavage (S1); and D2, also consisting of recumbent folds with axial plane crenulation cleavage or schistosity (S2). After nappe emplacement the tectonic evolution becomes predominantly a wrench regime during a last deformation event (D3) which is characterized by folds with subvertical axial planes and shear zones. At the same time, large volumes of synkinematic and late synkinematic granitoids are emplaced (Ribeiro et al. 1990). As regards the metamorphism, the allochthonous basal unit has undergone an early high pressure (HP) metamorphism which characterizes the allochthonous complexes but is not observed in the relative autochthon. The end of this HP metamorphism was dated by Van Calsteren et al. (1979) and Santos Zalduegui et al. (1995) at 374 Ma. At the end of the emplacement of the allochthonous complexes into its present position, both allochthon and relative autochthon underwent a metamorphic event under greenschist-facies conditions (Gil Ibarguchi and Arenas 1990). Arenas (1985) suggested that this episode corresponds to a medium-pressure gradient with an average T of 375–425 °C and P of 2.5–3.5 kbar. The study of deformation-recrystallization relationships during Variscan events shows that the peak of this metamorphism was reached during D2 (Ribeiro 1970). Summarized data from the literature give ages for the main deformation events and metamorphism between 360–320 Ma (Dallmeyer et al. 1997) and the late deformation has been dated at about 315 ± 10 Ma (Capdevila and Vialette 1970).

In the area where AEGC pegmatites outcrop, this medium-pressure metamorphism varies from the chlorite to sillimanite-orthoclase isograde (Martinez Catalán et al. 1996) and is coeval with the development of a highly evolved schistosity (S2) which is affected by D3. During D3, NNW-SSE trending folds with vertical axial planes, such as the Forcarei and Lalín Synforms (Figs 1 and 2) folded the previous structure which is a major recumbent fold whose vergence is to the east. Its lower limb is affected by the

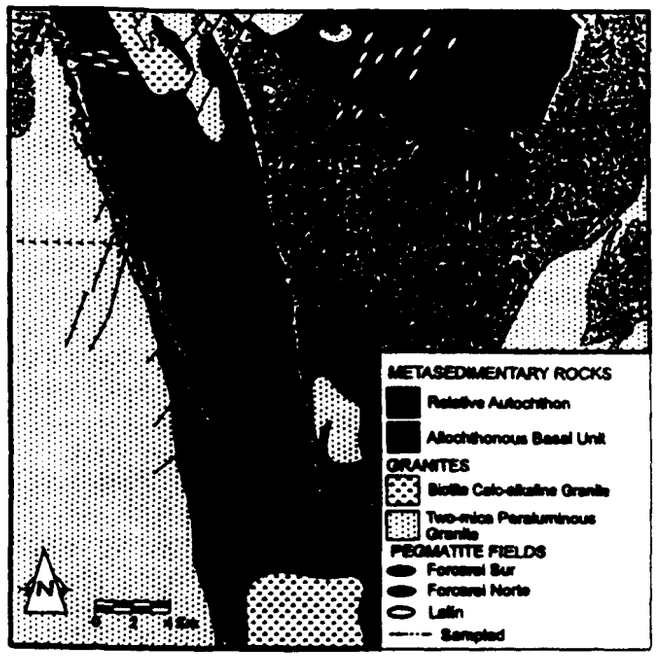

Fig. 2 Geological setting and schematic map of the three pegmatitic fields from the Area Esquistosa de Galicia Central (AEGC), Forcarei Sur, Forcarei Norte and Lalin. (Adapted from Barrera et al. 1989)

Lalin-Forcarei Thrust (LFT). Moreover, during D3, a ductile shear zone affected the western limb of the Forcarey Synform (Barrera et al. 1989). Late Variscan NE-SW to W-E faults, affecting the NNW-SSE trending folds and granitoids, are widespread in the area. In the investigated area, synkinematic (D3) granitoids are widely exposed and have been subdivided into two groups on the basis of petrology and geochemistry (Barrera et al. 1989): (1) calc-alkaline biotite granites and (2) peraluminous two-mica or muscovite granites. The AEGC pegmatites are related to these leucocratic granites (Fuertes-Fuente 1996; Fuertes-Fuente and Martin-Izard 1998). The emplacement of the peraluminous granites produced a contact metamorphism which developed andalusite and biotite. In this area, these granites have not been dated. However, ages of similar synkinematic (D3) leucocratic granites have been obtained in the range of 330–310 Ma (Capdevila and Vialette 1982).

The AEGC pegmatites

These are grouped into three pegmatite fields: Forcarei Norte, Forcarei Sur and Lalin (Fuertes-Fuente 1996; Fuertes-Fuente and Martin-Izard 1998; Fig. 2). Each field is an area populated by pegmatite groups which have a cogenetic relationship and have been generated by the same granite. These facts are mainly manifested by the whole-rock geochemistry and mineral chemistry of the pegmatites (Fuertes-Fuente 1996; Fuertes-Fuente and Martin-Izard 1998). Moreover, in each field the bodies have a common structural setting. The Forcarei Sur pegmatite field is located at the southern end of the Forcarei Synform western limb within the autochthon. The host-rock is affected by schistosity (S2) which controls the emplacement of the pegmatite bodies. The Forcarei Norte field is also controlled by S2 schistosity. This field is located at the northern end of the Forcarei Synform western limb within both the allochthon and the autochthon. The Lalin field consists of pegmatites in the Lalin Synform and at the northern end of the Forcarei Synform western limb. These bodies are hosted by both the autochthon and the allochthon, and occur aligned along NE-SW and E-W faults.

The geochemical characteristics, such as moderate to high concentrations of Li, Nb, Ta, Sn and P, along with the mineralogy and internal structure of these pegmatites allow us to classify (based on Cerny's 1994 classification) Forcarei Sur and Lalin bodies as rare-element pegmatites (Fuertes-Fuente 1996; Fuertes-Fuente and Martin-Izard 1998). On the other hand, the whole-rock geochemistry of the Forcarei Norte pegmatites shows very low concentrations of rare elements (Fuertes-Fuente 1996). Moreover, the mineral chemistry of muscovite, K-feldspar and garnet classifies these pegmatites as intermediate between the rare-element and muscovite classes (Fuertes-Fuente 1996).

In Forcarei Sur and Lalin several pegmatite groups are distinguished, each one being made up of pegmatite bodies of a particular type or subtype. Fuertes-Fuente (1996) and Fuertes-Fuente and Martin-Izard (1998) point out that these groups form a spatial sequence of pegmatite types/subtypes with an increasing degree of fractionation outward from the parental granite, in agreement with the zonation model of Cerny (1994). At Forcarei Sur, from the parental granite outward, the type/subtype sequence is: (a) barren pegmatites; (b) beryl type; (c) beryl-columbite-phosphate subtype; (d) albite-spodumene type and (e) albite type; at Lalin only albite-spodumene and albite types are exposed. The highly fractionated pegmatites of Forcarei Sur and Lalin (albite-spodumene and albite types) have a more or less well-developed internal zoning with zones of primary crystallization and metasomatic replacement units. The latter partially replace the primary crystallization zones and mainly consist of saccharoidal albite and minor quantities of quartz. The replacement units are widespread in the albite-type pegmatites of both fields.

The evolved pegmatites (spodumene-albite and albite types) of Forcarei Sur and Lalin are enriched in Be, Li, Nb, Ta, Sn and P which are concentrated as beryl, columbite-tantalite, tantaliferous cassiterite, apatite, spodumene and montebrasite (the last two in the albite-spodumene type). Apart from spodumene which only occurs in the primary crystallization zones, these rare-element bearing minerals appear in the replacement units. Montebrasite and apatite are also present as primary minerals in the primary crystallization zones. Frequently, Mn-rich apatite and eosphorite-childrenite replace the earlier metasomatic minerals of the replacement units. The primary crystallization zones and the replacement units have cavities which are filled by hydroxyl-herderite, bertrandite, adularia and quartz. These minerals also fill millimetre-sized veins which cross-cut the primary crystallization zones and the replacement units.

The barren muscovite pegmatites of the Forcarei Norte field present an internal zoning with zones of

primary crystallization and, sometimes small patches with mineralogical and textural characteristics of the replacement units but lacking rare-metal mineralization. Most of these patches are made up of albite and quartz; when primary crystals of beryl occur within or close to these patches, this earlier beryl is partially replaced by later beryl which often forms rims around the former.

The fluid inclusion study was carried out on minerals from the most fractionated rare-element pegmatites (albite type) of Lalín and Forcarei Sur and from the barren muscovite pegmatites of Forcarei Norte. The selected samples together with the inclusion types occurring in each one are summarized in Table 1.

Analytical techniques

Microthermometric studies of fluid inclusions were performed on 150–300 μm thick plates using a microscope equipped with a UMK50 Leitz objective and a Chaixmeca cooling and heating stage (Poty et al. 1976) in the Laboratory of Fluid Inclusions of Oviedo University (Spain) and Laboratory of Geology of the University of Las Palmas (Spain). The stage was calibrated with melting-point standards at $T > 25$ °C and natural and synthetic fluid inclusions at $T < 0$ °C. The vertical gradient is less than 0.1 °C at low temperatures within 40 μm of the wafer's surface (Dubois 1992). Measurements of phase changes at or below 31 °C are accurate to within ±0.1 °C and high temperature measurements to within ±2.0 °C. All the inclusions were cooled to −180 °C. The volumetric fraction of the aqueous liquid (*flw*) and the volumetric fraction of the volatile-rich liquid in the volatile-rich phase (*flc*) have been estimated by reference to the volumetric chart of Roedder (1984). Salinity is expressed in wt% equivalent NaCl (Bodnar 1993) and fluid density of volatile-free inclusions was determined by microthermometry (Potter and Brown 1977; Zhang and Frantz 1987).

The composition of the non-aqueous portion of individual inclusions was measured using a Dilor X-Y multichannel modular Raman spectrometer (at CREGU, Nancy, France). Bulk composition and density were computed from the *P-V-T-X* properties of individual inclusions in the C-O-H-(N-S) system (Dubessy 1984; Dubessy et al. 1989, 1992; Thiery et al. 1994; Bakker et al. 1996). All data were calculated from the microthermometric measurements and the Raman gas analyses, using a clathrate stability model in the H_2O-CH_4-N_2-NaCl-KCl $CaCl_2$ fluid system, between 253–293 K and 0–200 MPa (Bakker et al. 1996; Bakker 1995, 1997) and the computer program of Bakker (1997).

The *P-V-T-X* properties of aqueous carbonic inclusions were modelled for the H_2O-CO_2-CH_4 system using the equations of state of Kerrick and Jacobs (1981), Jacobs and Kerrick (1981) and the computer code of Dubessy (1984). For aqueous inclusions, the isochores have been drawn in the H_2O-NaCl system using the data from Zhang and Frantz (1987) and the computer program Macflincor 0.92 (Brown and Hagemann 1995).

The nomenclature of fluid inclusions is modified from Cathelineau et al. (1993) and is based on both microthermometric and Raman data. The type of total homogenization *Th* is indicated by *V* (to vapour phase), *L* (to liquid phase) and *C* (to critical state). The presence of C-H-O-(N) species is indicated by subscript *c* (only C-O-H-N volatile species are detected and H_2O is absent), *c-w* (both water and C-O-H-N volatile species are present), *w-c* (water is largely dominant; in general >80% and CO_2 has a low density), *w-(c)* (CO_2 is only detected by clathrate melting or by Raman spectrometry), and *w* (no C-H-O-N volatile species are detected by any methods). The presence of daughter minerals is shown by subscript *s*.

Electron images and energy-dispersive analyses of included crystalline solids were obtained on a JEOL JSM-6100 Autoscan electron microscope (SEM) and a LINK EXL-1000 energy-dispersive spectroscopy analyser (EDS) at Oviedo University.

Microthermometry and Raman spectrometry results

Taking into account the microthermometry and Raman spectrometry results, together with microscope observations on the number of phases present at room temperature, gas/liquid ratios and their origin (primary and secondary), the studied inclusions in the three AEGC pegmatite fields can be separated into eight types. Four of them are aqueous-carbonic inclusions with specific volume ratio, number of phases at room temperature

Table 1 Sample material and fluid inclusion types found

Pegmatite field	Sampled pegmatite		Sampled pegmatite zone and mineral studied (inclusion types)	
	Class	Type	Primary crystallization zone	Reemplacement unit
Forcarei Norte	Muscovite	Barren pegmatites	Coeval garnet and beryl (L_s-$_w$)	Late beryl overgrowths and quartz
Lalín	Rare-element	Albite pegmatites (P and rare-element rich: Nb, Ta, Be, Sn)[a]		Quartz (L_w-$_{(c)}$, L_w-$_c$, V_w-$_c$, V_c, L_w1, L_w2)
Forcarei Sur	Rare-element	Albite pegmatites (P and rare-element rich: Sn, Be, Nb, Ta)[a]		Coeval quartz and beryl (L_w-$_{(c)}$, V_w-$_c$, V_c-$_w$)
				Later Mn-rich apatite ($L_{w_{ap}}$)

[a] Minerals with fluid inclusions suitable for study were not found

and origin, the other four are aqueous inclusions with different salinities and dissolved salts, and one of them has daughter minerals. In aqueous-carbonic fluid inclusions with low molality of volatiles, the presence of a volatile phase was identified by the melting of clathrates or by Raman spectrometry. Clathrate was detected in the inclusions by the presence of a double freezing event during cooling (clathrate and ice; Collins 1979). In order to determine the melting temperature of the clathrate as accurately as possible, a freeze/refreeze technique was used (Roedder 1984; Shepherd et al. 1985). The microthermometric and Raman spectrometry results are summarized in Tables 2 and 3, respectively.

Aqueous-carbonic fluid inclusions

Lw-(c) and Lw-c types

These inclusion types are most frequent in samples of the replacement units from pegmatites of the three fields. They are observed in quartz and in beryl as small clusters or, sometimes, isolated. Fuertes-Fuente and Martin-Izard (1998) also described the presence of these inclusions in samples from an albite pegmatite of Forcarei Sur; in this case, the *Lw-(c)* type inclusions outline band sets which abruptly end a few millimetres from the crystal border (Fig. 3). These band sets lie in either one (quartz) or two directions (beryl), which are related to the *c*-axis of the two minerals. According to Roedder's criteria (1984), we consider *Lw-(c)* and *Lw-c* as primary. However, some *Lw-(c)* inclusions displaying irregular shape are aligned along small intragranular fractures, and are considered as pseudosecondary (Fig. 3).

The sizes vary from 5 to 40 μm. These inclusions contain two phases at room temperature (21 °C) and show a volumetric fraction of the aqueous phase (*flw*) between 60 and 80%; these described pseudosecondary *Lw-(c)* inclusions on small intragranular fractures have higher *flw* (90 and 95%).

Tm ice ranges from −7.8 to −3.5 °C at Lalín, −4.5 to −2 °C at Forcarei Norte, and −3.8 to −0.8 °C at Forcarei Sur. *Te* is observed around −20.8 °C. The melting temperatures of the clathrates (*Tm cl*) are between 6.4 and 11.2 °C at Lalín, and always above 10 °C at Forcarei Sur (10.8 to 16 °C) and Forcarei Norte (10.7 to 13.5 °C). In a few cases, the melting temperature of CO_2 (*Tm* CO_2) is detectable (*Lw-c* type) at around −58 °C, and the homogenization temperature of CO_2 (*Th* CO_2) to the vapour phase is around 22 °C. *Th* has two maxima, at 265 and 310 °C. The lower temperatures are observed for the *Lw-(c)* pseoudosecondary inclusions along intragranular fractures while the higher temperatures are recorded for the *Lw-(c)* and *Lw-c* primary inclusions.

Selected *Lw-(c)* and *Lw-c* fluid inclusions together with the mentioned pseudosecondary *Lw-(c)* inclusions located along small intragranular fractures (Fs-3, Fs-4 and Fn-9) from pegmatites of the three fields were analyzed by Raman spectrometry. The results are shown for each field in Table 3.

Vw-c type

Vw-c inclusions occur in quartz and beryl from the replacement units of pegmatites of the three fields. They appear as small clusters in crystals, isolated, and also related to small intragranular fractures (Fig. 3). These inclusions always occur in the same samples as type *Lw-(c)*, but the two types never occur together in the same cluster. The average size is 3 μm at Forcarei Sur, around 10 μm at Lalín and between 10 and 20 μm at Forcarei Norte. They show two phases at room temperature and the volumetric fraction of the aqueous phase is between 10 and 50%. Based on the criteria by Roedder (1984), they are primary and pseudosecondary inclusions.

Tm CO_2 has been measured between −57.5 and −63.5 °C. *Tm ice* ranges between −5.3 and −4.8 °C at Lalín, between −4 to −2 °C at Forcarei Sur and between −5.8 and −2.3 °C at Forcarei Norte. *Tm cl* ranges from 6.5 to 9.3 °C at Lalín, from 9.7 to 11.3 °C at Forcarei Norte and from 10.8 to 14.5 °C at Forcarei Sur. *Th* is between 300 and 400 °C to the vapour phase and, more rarely, to the critical phase or to the liquid phase.

Selected *Vw-c* fluid inclusions from pegmatites of the three fields were analyzed by Raman spectrometry. Bulk composition and density were calculated and the results are shown for each field in Table 3.

Vc-w type

Vc-w inclusions were previously studied by Fuertes-Fuente and Martin-Izard (1998). These inclusions have only been found in quartz and beryl of the replacement unit of an albite pegmatite (Forcarei Sur). Most of these inclusions occur along well-healed fracture planes which cross-cut several grains. Moreover these fracture planes cross-cut the mentioned band sets with *Lw-(c)* inclusions of the quartz and beryl crystals (Fig. 3). They are secondary in character (according to Roedder 1984). The inclusion morphology is rounded, elongate or irregular, and the size is around 9 μm. They have two phases at room temperature and *flw* is between 5 and 20%.

Tm CO_2 is observed between −60 and −62 °C. *Th* CO_2 varies from 6 to 7 °C to the vapour phase. *Tm cl* varies between 11.9 and 12.8 °C and occurs after CO_2 homogenization. *Tm ice* is around −3 °C. *Th* ranges between 340 and 360 °C to the vapour phase.

Selected *Vc-w* fluid inclusions of albite pegmatites from Forcarei Sur were analyzed by Raman spectrometry. Bulk composition and density are shown in Table 3.

V type: Vc and Vc-(w) subtypes

This type only appears in replacement unit samples of albite pegmatites from the Lalín field. The *V* type has been

Table 2 Summary of microthermometric data for the different types of fluid inclusions in the AEGC pegmatites[a]

Inclusion types	Ocurrences (host-mineral)	*Flw*	*Vs/Vt*	*Flc*	*Tm*CO_2	*Th*CO_2		Tmcl	*Tmice*	*Th*	
Type *Ls-w*	Forcarei Norte (garnet and beryl)	[90, 95] 90 *60*	[50, 90] 80 *60*	–	–	–	–	–	[−0.2, −1.7] −0.8 *60*	[290, 310] 295 *48*	*L*
Types *Lw-(c)*, *Lw-c*[b]	Lalin (quartz)	[60, 95] 80 95 *87*	–	–	[−58.3, −58][b] −58.3[b] *10*[b]	[21.8, 22][b] 22[b] *10*[b]	 G G	[6.4, 11.2] 9.3 *63*	[−3.5, −7.8] −6 −5 *70*	[190, 335] 260 310 *87*	*L*
	Forcarei Norte (quartz and beryl)	[50, 95] 70 90 *66*	–	–	–	–	–	[10.7, 13.5] 12.7 *64*	[−2,−4.5] −3 *61*	[190, 335] 265 310 *61*	*L*
	Forcarei Sur (quartz and beryl)	[50, 95] 80 90 *80*	–	–	–	–	–	[10.8, 16] 12.2 13.8 *61*	[−0.8, −3.8] −2 *56*	[193, 345] 275 310 *78*	*L*
Type *Vw-c*	Lalin (quartz)	[10, 50] 30 *39*	–	–	[−57.4,−60.9] −60.2 *27*	–	–	[6.5, 9.3] 7.6 *36*	[−4.8,−5.3] −4.8 −5.3 *6*	[296, 380] 370 *39*	*G* L(18)
	Forcarei Norte (quartz and beryl)	[10, 50] 30 *51*	–	–	[−57,−63.6] −58 *27*	–	–	[9.7, 11.3] 11.2 *40*	[−2.3, −5.8] −3 *43*	[300, 390] 350 380 *48*	*G*
	Forcarei Sur (quartz and beryl)	[10, 40] 25 *30*	–	–	[−58.2, −62] −60.4 *15*	–	–	[10.8, 14.5] 13.8 *25*	[−1.9, −3.8] −1.8 *15*	[340, 400] 368 *21*	*G* *C*(4) *L*(3)
Type *Vc-w*	Forcarei Sur (quartz and beryl)	[5, 20] 10 *11*	–	–	[−60, −62] −62 *11*	[6, 7] 6.8 *11*	*G*	[11.9, 12.8] 12 12.8 *11*	[−3, −3.2] −3 *11*	[340, 360] 360 *11*	*G*
Type *Lw*$_{ap}$	Forcarei Sur (apatite)	[60, 95] 80 90 *30*	–	–	–	–	–	–	[−2.2, −3.9] −3 −3.9 *30*	[220, 310] 235 385 *32*	*L*
Type *V* Subtype *Vc*	Lalin (quartz)	–	–	[10, 40] 25 *25*	[−56.8, −58.2] −57.4 −58.2 *25*	[27.8, 29.3] 28 29.3 *25*	*G*	–	–	–	–
Subtype *Vc-(w)*		[5, 30] 10 *36*	–	[10, 40] 25 30 *37*	[−56.9, −58.4] −57.4 −58.4 *37*	[27.7, 29.3] 28 29.3 *37*	*G*	[7.3, 8.8] 8.2 *28*	[−6, −7] −6.5 *12*	[240, 310] 310 *27*	*G*
Type *Lw1*	Lalin (quartz)	[90, 98] 90 *27*	–	–	–	–	–	–	[−1.4, −2.5] −2 *24*	[140, 203] 200 *27*	*L*
	Forcarei Norte (quartz and beryl)	[95, 99] 98 *31*	–	–	–	–	–	–	[−0.7, −4] −1.3 *18*	[105, 175] 175 *31*	*L*
Type *Lw2*	Lalin (quartz)	[95, 99] 99 *60*		–	–	–	–	–	[−15.6, −24.4] −15.6 *33*	[100, 212] 100 145 *60*	*L*

[a] *Flw* volumetric fraction of the aqueous phase; *Flc* volumetric fraction of the carbon-rich liquid in the carbon-rich phase; *Vs/Vt* volumetric fraction of the solid phases; *Tm*CO_2: melting temperature of CO_2; *Th*CO_2 homogenization temperature of CO_2, gaseous state (*G*), liquid state (*L*) and critical state (*C*); *Tmcl*: melting temperature of clathrate; *Tmice*: melting temperature of ice; *Th* total homogenization temperature, gaseous state (*G*), liquid state (*L*) and critical state (*C*). All temperatures °C. Range (first line), mode (second line) and number of measurements (third line, *italics*) are given for each type of fluid in each occurrence

[b] Type *Lw-c* only found in some samples from the Lalin pegmatites

Table 3 Microthermometric and Raman data, and interpreted bulk composition of the selected fluid inclusions from the studied AEGC pegmatites[a]

Fields	Types	No	Microthermometry						Raman data				Bulk composition					
			Flw (Flc)	*Tm*CO_2	*Th*CO_2	*Tmcl*	*Tmice*	*Th*	CO_2	CH_4	N_2	*dv*	X H_2O	X CO_2	X CH_4	X N_2	X NaCl	*D*
Lalin	*Lw-(c)*	L2-19	80	–	–	6.4	−7.8	318 *L*	82.5	17.4	0	0.1	94	3.2	0.2	0	2.5	0.8
	Lw-c	L2-8	80	−61.4	–	8.8	−6.5	310 *L*	82.9	7.8	9.2	0.2	93.6	4.5	0.2	0.2	1.5	0.8
		L1-14	70	−58.3	22 *G*	10.2	−6.3	335 *L*	93.2	6.7	0	0.2	92.3	7	0.3	0	0.4	0.8
	Vw-c	L3-25	10	−56.6	–	8.7	−4.8	370 *G*	100	0	0	0.1	90.3	9.5	0	0	0.1	0.5
		L2-14	30	−60.9	–	7.6	−5.3	378 *G*	91.2	3.6	5.1	0.1	89.7	9.3	0.3	0.4	0.3	0.4
	V																	
	Vc (Subtype)	L1-9	(25)	−56.6	29.1 *G*	–	–	–	100	0	0	0.3	0	100	0	0	0	0.3
		L1-1	(40)	−57.4	29.3 *G*	–	–	–	91.8	2.9	5.3	0.3	0	91.7	2.9	5.3	0	0.3
		L3-20	(30)	−58.2	27.8 *G*	–	–	–	93.7	6.0	0.3	0.3	0	93.7	6.0	0.3	0	0.3
	Vc-(w) (Subtype)	L3-1	10	−58.4	28 *G*	8.5	−7	250 *G*	92.7	2.8	4.4	0.1	61.0	35.5	1.0	1.6	0.9	0.6
Forcarei Sur	*Lw-(c)*	Fs-2	70	–	–	12.8	−2.8	360 *L*	44.4	49.4	6.1	0.2	87.4	4.4	4.9	0.6	2.7	0.7
		Fs-3	80	–	–	13.7	−3	256 *L*	72.8	17.8	9.3	0.5	78.2	15.7	3.9	1.9	0.3	0.9
		Fs-4	90	–	–	11.3	−2.5	260 *L*	56.7	24.3	18.8	0.3	89.9	5.5	2.3	1.8	0.4	0.9
	Vw-c	Fs1-1	40	−62	–	12	−2	400 *G*	53.2	40.2	6.6	0.2	91.4	5.0	2.8	0.8	0.6	0.5
		Fs1-2	40	−62	–	12	−2	340 *G*	58.12	33	8.8	0.1	92.0	4.2	3.3	0.4	0.6	0.5
	Vc-w	Fs9-1	5	−62.1	6.8 *G*	12.8	−3	360 *G*	53.48	41.48	5.04	0.1	31.2	36.8	27.3	4.5	0.1	0.3
Forcarei Norte	*Lw-(c)*	Fn-2	70	–	–	12.7	−2	315 *L*	73.8	19.2	6.6	0.3	91.1	7.2	1.3	0.4	0.5	0.8
		Fn1-1	80	–	–	10.7	−3.8	328 *L*	79.4	14.5	6.0	0.2	95.5	4.0	0.3	0.1	0.2	0.8
		Fn-9	90	–	–	11.3	−3	265 *L*	77.1	11.6	11.1	0.4	95.0	4.0	0.3	0.2	0.06	0.9
	Vw-c	Fn1-2	40	–	–	11.2	−4.3	320 *L*	89.0	10.9	0	0.1	89.3	9.8	0.9	0	0.01	0.5
		Fn-15	20	–	–	9.5	−3	350 *C*	100	0	0	0.1	79.8	20.1	0	0	0.05	0.3
		Fn1-7	30	−63.6	–	11.4	−3.8	360 *L*	70.9	17.9	11.0	0.1	75.7	17.2	4.0	2.4	0.8	0.5

[a] Composition in mol%. All other abbreviations as in Table 2 and text apart from: *dv*: density of volatile-rich phase. *D*: bulk density of the inclusion. All temperatures in °C

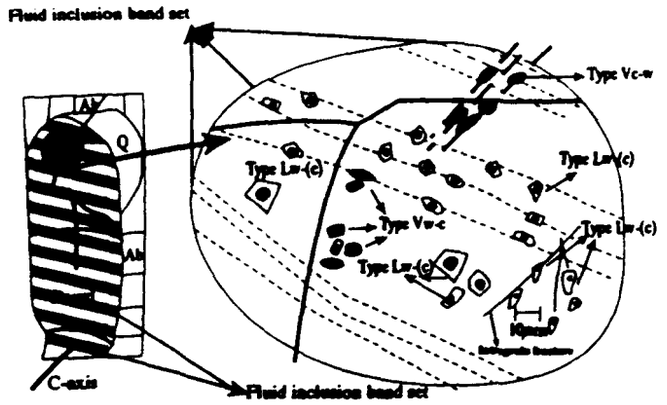

Fig. 3 Schematic distribution of fluid inclusions in a banded beryl from the Forcarei Sur field. (Modified from Fuertes-Fuente and Martin-Izard 1998)

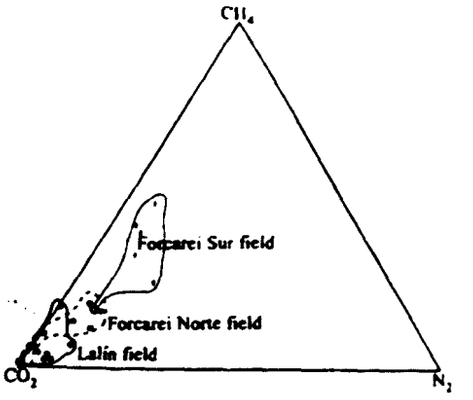

Fig. 4 CO_2-CH_4-N_2 ternary plot of the volatile-rich phase in fluid inclusions from the three pegmatite fields studied

subdivided into two subtypes, referred to as *Vc* and *Vc-(w)*, on the basis of the number of phases present at room temperature. *Vc* subtype inclusions have two phases at room temperature and they are made up of $CO_2(L)$ and CO_2 (V). *Vc-(w)* subtype inclusions are three-phase inclusions at room temperature and they are composed of $CO_2(L)$, $CO_2(V)$ and aqueous phase; the volumetric fraction of the aqueous phase is between 5 and 30%.

Both *Vc* and *Vc-(w)* subtypes occur together and outline fracture planes which cross-cut several grains. These fracture planes lie in two directions at right angles. In each fracture plane the microthermometric measurements are similar. Taking into account Roedder's criteria, these inclusions are secondary.

Vc inclusions: *Tm* CO_2 varies between −56.8 and −58.2 °C. *Th* CO_2 is between 27.8 and 29.3 °C to the vapour phase.

Vc-(w) inclusions: *Tm* CO_2 is between −56.9 and −58.4 °C, *Th* CO_2 is between 27.7 and 29.3 °C to the vapour phase. *Tm ice* is around −7 °C. *Tm cl* is between 7.3 and 8.8 °C. *Th* occurs between 240 and 310 °C to the vapour phase.

Selected *Vc* and *Vc-(w)* fluid inclusions of Lalín pegmatites were analyzed by Raman spectrometry. Bulk composition and density are shown in Table 3.

As far as the gas phase of the described aqueous-carbonic fluid inclusions is concerned, the following facts are noteworthy:

1. In the Lalín and Forcarei Norte pegmatite fields, CO_2 is the main component of the gas phase and is mixed with minor CH_4 and N_2, the last of which appears in a very low concentration in the Forcarei Norte field. In the Forcarei Sur field the gas phase is constituted by CO_2 and CH_4 with minor quantities of N_2.

Gas phase compositions of the aqueous-carbonic fluid of the three pegmatite fields are plotted in the CO_2-CH_4-N_2 ternary plot (Fig. 4). This shows that the CH_4 content of the aqueous-carbonic fluids increases from Lalín to Forcarei Sur, with Forcarei Norte in an intermediate position.

2. The gas phase of the aqueous-carbonic fluid inclusions displays low density. *Lw-(c)* inclusions have scattering gas densities due to the higher gas phase density *(dv)* of the *Lw-(c)* inclusions Fn-9, Fs-3 and Fs-4 (Table 3). Taking into account that these inclusions represent those associated with small intragranular fractures, a loss of some components during fracture development may have occurred.

Aqueous fluid inclusions

Ls-w type

These fluid inclusions appear in garnet and beryl samples taken from primary crystallization zones of Forcarei Norte pegmatites. In garnet, *Ls-w* inclusions are composed of a liquid water-rich phase, a water vapour bubble and daughter minerals. These inclusions display the following distribution: (1) aligned in two oblique directions and, from microscope observation, it is not possible to establish whether these directions are growth bands. Inclusion morphology is prismatic or elongate. The vapour phase occupies between 10 and 20% of the total volume of the inclusion; the solid phases, which occupy between 60 and 80% of the cavity, are made up of anhedral quartz identified using an optical microscope, and two or more other crystals (Fig. 5).(2) These are isolated inclusions with quartz and other daughter crystals, besides a liquid and a vapour phase. Both occurrences allow us to classify the *Ls-w* inclusions as primary according to Roedder's criteria.

Apart from quartz, the mineral identification of *Ls-w* inclusions under an optical microscope was difficult because of the small size. One daughter mineral, indicated as *s1*, was optically characterized by its high birefringence. SEM-EDS investigations showed that one of the included solids was albite, and the others were probably silicates. Traces of K, C, Na, Cl and S were occasionally detected as films on the walls of opened inclusions. The *s1* solid could not be identified from SEM-EDS.

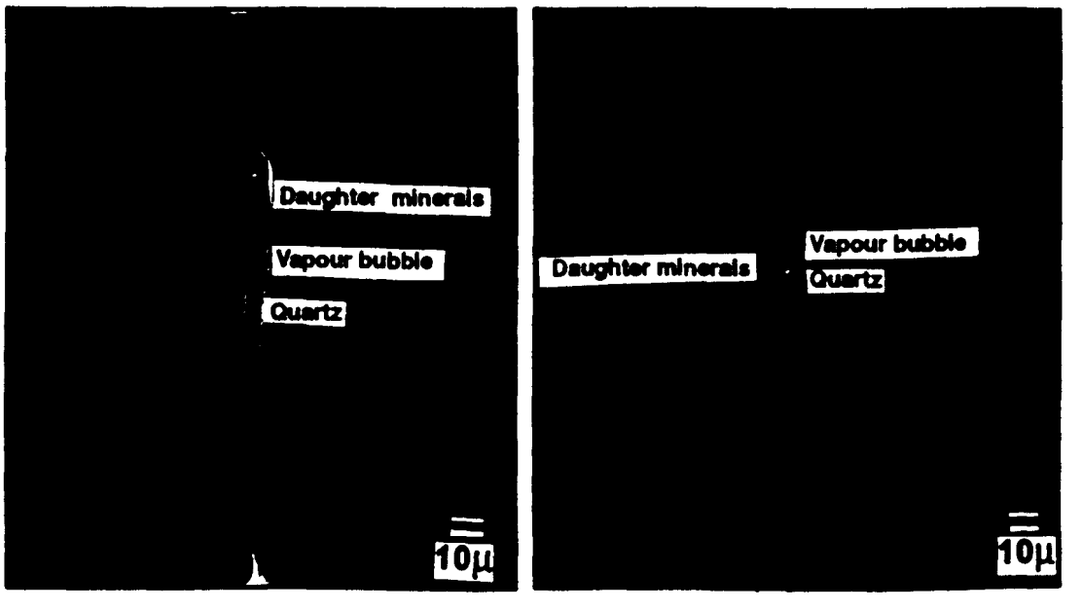

Fig. 5 Photomicrographs of two *Ls-w* type inclusions in garnet from the Forcarei Norte pegmatite. These inclusions contain a vapour phase, a liquid phase, and solid phases comprising quartz and several non-identified crystals

The first melting of ice (*Te*) is around −35 °C, and final ice melting temperatures (*Tm ice*) range from −0.2 to −1.7 °C. Homogenization temperatures (*Th*) are between 290 and 310 °C into the liquid phase. Above *Th*, solid *sl* begins to dissolve around 340 °C, and continues to dissolve up to 440 °C. Partial dissolution of the other minerals is also observed. Above 500 °C, all *Ls-w* inclusions decrepitate.

In the majority of the *Ls-w* inclusions, most of the enclosed solids are true daughter minerals, and constitute a mineral assemblage that is remarkably consistent throughout all *Ls-w* inclusions.

As was previously described, in Forcarei Norte pegmatites the beryl crystals of the primary crystallization zones affected by metasomatic replacement show two stages of growth. These are manifested by the presence of two zones with different clarity and abundance of inclusions (Fig. 6): (I) the first is cloudy with primary *Ls-w* inclusions of prismatic morphology lying in two directions: one parallel and the other at right angles to the *c*-axis. These *Ls-w* inclusions display the same microthermometric behaviour as in garnet. (II) The second zone is frequently located at the border of beryl crystals or forms irregular bands replacing the cloudy zone. The beryl is more transparent and has scarce inclusions belonging to *Lw-(c)*, *Lw-c* and *Vw-c* types (Fig. 6).

Lw_{ap} type

This inclusion type only appears in the later metasomatic Mn-rich apatite of the replacement units of the albite pegmatites, and was described by Fuertes-Fuente and Martin-Izard (1998) in apatite of an albite pegmatite from the Forcarei Sur field. The inclusions occur in two ways: isolated with rectangular or square morphology, and aligned in two oblique directions with prismatic morphology. They have two phases at room temperature. The volumetric fraction of the aqueous phase occupies between 60 to 80%, and the size ranges from 5 to 20 µm. Taking into account Roedder's criteria (1984), these inclusions are considered as primary ones.

Te varies between −48 and −50 °C. These temperatures are close to the eutectic temperatures of the H_2O-$CaCl_2$ system (*Te* = −49.8 °C, Crawford 1981). *Tm ice* ranges between −2 and −4 °C. *Th* ranges between 220 and 310 °C to the liquid phase. The salinity is low, ranging between 4 and 7 wt% equivalent NaCl.

Type Lw1

This type was found in quartz and beryl samples from the Lalin and Forcarei Norte fields. The inclusions are observed as fluid inclusion planes which cross-cut sev-

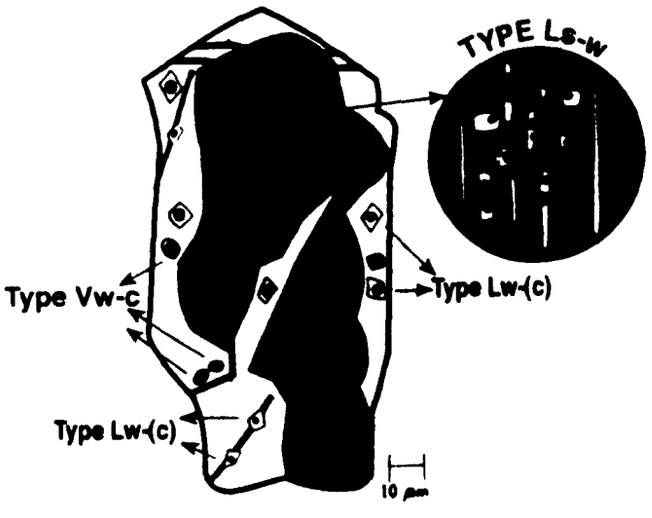

Fig. 6 Schematic distribution of fluid inclusions in a beryl from the Forcarei Norte field. The *dark zone* is the "old beryl" and the *clear zone* is the "new beryl"

eral grains and have different orientation and length. They are secondary inclusions on the basis of Roedder (1984). Inclusion morphology is irregular and size ranges from 1 to 10 μm. These inclusions are two phases with volumetric fractions of the aqueous phase ranging from 90 to 98%.

Tm ice varies between −1.4 and 2.5 °C (2.4 to 4.5 wt% equivalent NaCl) at Lalin, and from −1 to −4 °C (1 to 6 wt% equivalent NaCl) at Forcarei Norte. *Th* lies between 140 and 203 °C at Lalin and ranges from 105 to 175 °C in the liquid state at Forcarei Norte.

Type Lw2

This type appears in pegmatite samples from the Lalin field. *Lw2* inclusions are observed as fluid inclusion planes cross-cutting several grains and the *V* and *Lw1* inclusion planes. They are secondary in character. *Lw2* inclusions have two phases at room temperature, and the volumetric fraction of the aqueous phase is around 95%. They are irregular in morphology and variable in size, from 1 to 10 μm. *Te* is below −50 °C, thus *Lw2* inclusions probably contain cations such as Ca, Mg, K and Na in solution (Crawford 1981). *Tm ice* ranges between −16 and −25 °C (19 to 25 wt% equivalent NaCl), and *Th* ranges from 100 to 212 °C to the liquid phase.

Chronological relationship between the inclusion types

The *Ls-w* type occurs as primary inclusions in the garnet and in the earlier beryl cores (Fig. 6). Both minerals were taken from primary crystallization zones of the pegmatites. By contrast, *Lw-(c)*, *Lw-c* and *Vw-c* types appear as primary inclusions in beryl and quartz taken from replacement units (Fig. 3) or as primary inclusions in later mineral overgrowths such as the later beryl rims around the earlier beryl cores with *Ls-w* inclusions (Fig. 6). From microscope examination it is not easy to establish a chronological relationship between *Vw-c*, *Lw-(c)* and *Lw-c* types. However, the fact that *Vw-c* also occurs as pseudosecondary inclusions with the same microthermometric characteristics as *Vw-c* primary inclusions has allowed us to consider the *Vw-c* inclusion trapping as later than that of the *Lw-(c)* and *Lw-c* inclusions but very close in time. Lw_{ap} inclusions occur as primary inclusions in later metasomatic Mn-rich apatite which in the replacement units replaces some of the mentioned metasomatic minerals such as the *Lw-(c)*, *Lw-c* and *Vw-c* inclusion-bearing quartz.

Vc-w, *V*, *Lw1* and *Lw2* appear as secondary fluid inclusions in the cited primary and metasomatic minerals. From microscope examination it is not possible to establish a chronological relationship between these secondary inclusion types.

General *P–T* and bulk chemical evolution

On the basis of the chronological relationship between the established fluid inclusion types, several stages characterized by different fluid composition, pressure and temperature conditions can be established during the formation of these pegmatites. The calculated isochores for each inclusion type are shown in Fig. 7.

Stage E0: primary crystallization

The first stage of fluid trapping (E0) may be represented by the *Ls-w* type occurring as primary inclusions in minerals from the primary crystallization zones. There are not enough data to obtain the *Ls-w* isochores because the true composition of this fluid is not known. However, on the basis of some microthermometric data, such as the partial dissolution of daughter minerals and the temperature of inclusion decrepitation, it is possible to infer a trapping temperature of these inclusions above 500 °C. Three later stages can be distinguished in the three pegmatite fields (Fig. 7).

Stage E1: metasomatic replacement

This stage (E1) is represented by fluid inclusions belonging to types *Lw-(c)*, *Lw-c* and *Vw-c* appearing as primary inclusions in minerals of the replacement units. The minimum trapping conditions are given by *Th* (total homogenization temperature) and *Ph* (homogenization pressure), i.e. 310–335 °C and 1.4–1.8 kbar for the *Lw-(c)* (*Lw-c*) isochores from Lalin. In Forcarei Sur, the minimum trapping conditions (*Th*, *Ph*) are 360 °C and 2.25 kbar. In the case of Forcarei Norte pegmatites, the *Th* of *Lw-(c)* inclusions is 315 and 328 °C, and minimum trapping pressures are 1.9 and 2.25 kbar respectively.

The *P–T* conditions of trapping may be constrained by the mineral assemblage. The metasediments in which these pegmatite fields are emplaced have been affected

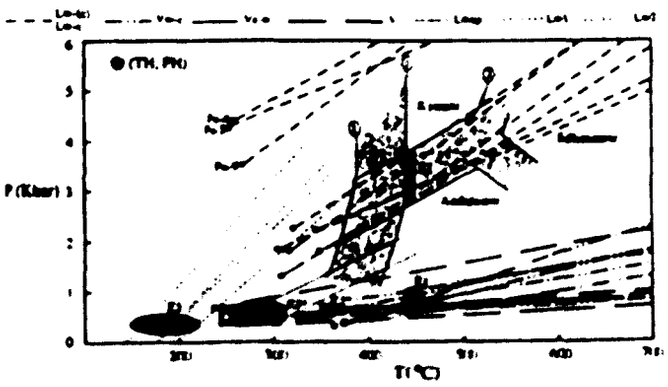

Fig. 7 *P–T* reconstruction diagram with the isochores of the different fluid inclusion types of the three pegmatite fields from the AEGC. The stability boundary of biotite (*1*) (Yardley 1989) and the aluminosilicate stability fields (*2*) (Robie and Hemingway 1984) are shown. The *dark zones* are the minimum *P–T* conditions for the different stages (E1, E2 and E3) of trapping for type *Lw-(c)* and *Lw-c*, *Vw-c*, *Vc-w*, *Lw1* and *Lw2* inclusions. The *E2** and *E3** *dark zones* represent the stages of trapping of *Vc-w* and Lw_{ap} inclusion types which were only found in the albite pegmatites from Forcarei Sur field

by contact metamorphism due to the parental granites and their associated pegmatites. The thermal metamorphism is characterized by andalusite and biotite. Taking into account the broad limits of the biotite stability field, the minimum temperatures lie between 380 and 420 °C (Yardley 1989; Fig. 7). Using the maximum stability conditions and the *Lw-(c)* and *Lw-c* isochores, approximate minimum pressures and temperatures for the fluid inclusion trapping can be estimated between 2 and 2.5 kbar at 380 °C and between 2.5 and 3.5 kbar at 420 °C for the Lalin and Forcarei Sur fields. In Forcarei Norte, *P–T* estimates are around 2.5 and 3 kbar at 380 °C and around 3.5 kbar at 420 °C. These *P–T* conditions agree with the presence of andalusite in the metasediments (Fig. 7). However, pressures above the andalusite stability limit (around 4 ± 0.5 kbar, Robie and Hemmingway 1984) are obtained for isochores that represent the *Lw-(c)* inclusions spatially associated with small intragranular fractures (Fs-3, Fs-4 and Fn-9). This anomalous pressure of trapping agrees with the previously mentioned fact that these inclusions have leaked after trapping.

On the other hand, *Vw-c* inclusions were trapped under lower pressures. The *Ph-Th* is around 0.3 kbar and 370–380 °C at Lalin, between 0.25–0.5 kbar and 340–400 °C at Forcarei Sur, and 0.5–0.75 kbar and 320–360 °C at Forcarei Norte.

As already mentioned, we consider the trapping of *Lw-(c)* and *Lw-c* type inclusions to have been before the *Vw-c* type, but close in time. In this way, the temperature regime during the *Vw-c* fluid inclusion trapping was probably similar to that of the *Lw-(c)* and *Lw-c*, thus the biotite stability criterion can also be used, i.e. temperature between 380 and 420 °C. Taking into account the homogenization temperatures of type *Vw-c* fluid inclusions (*Th* close to 400 °C), we consider a situation close to the upper biotite stability limit of around 420 °C. Therefore, in all three pegmatite fields, the estimate of the *P–T* pair for the *Vw-c* inclusion trapping is around 1 kbar (0.5–0.75 kbar at Lalin; around 0.8 kbar at Forcarei Sur, and 0.75–1 kbar at Forcarei Norte) at up to 420 °C (Fig. 7). We can extend the consideration to the previously described *Lw-(c)* and *Lw-c* trapping and assume a temperature close to the upper biotite stability limit. In this way, pressures of 3 ± 0.5 kbar at temperatures up to 420 °C are estimated for the *Lw-(c)* and *Lw-c* fluid inclusion trapping.

The drop in pressure during E1 from 3 ± 0.5 to 1 kbar at temperatures above 420 °C may be due to the transition from a predominantly lithostatic to a hydrostatic pressure regime, related to the development of the ductile shear zone which affected the Forcarei Sur and Norte pegmatite fields during the D3. The intragranular fractures, which in several cases host fluid inclusions with divergent composition and density (e.g. Fs-3, Fs-4 and Fn-9), may be related to mineral deformation during shear. In the Lalin field, the pegmatite bodies have intruded through faults developed in the last episode of the Variscan deformation. The progressive fracturing of the pegmatite bodies may reflect the change from predominantly lithostatic to hydrostatic pressure, beginning with small intragranular fractures. Larger fractures, which cross-cut several crystals and are related to type *V* inclusions, were developed later.

Stages E2 and E3: late hydrothermal processes

Stage E2 is characterized by secondary complex carbonic and aqueous-carbonic fluid inclusions.

In Forcarei Sur field pegmatites, stage E2 (Fig. 7) is represented by the *Vc-w* inclusions which are characterized by low density. The isochores give a minimum trapping pressure close to the true pressure of 0.5–0.75 kbar. Minimal trapping conditions are around 0.6 kbar and 360 °C.

In Lalin field pegmatites, stage E2 is represented by *V* type inclusions. These display low density and show a minimum trapping pressure close to the true pressure (Fig. 7). The presence of an aqueous phase in the *Vc-(w)* subtype allows us to apply the total homogenization temperature to the representative isochore of *Vc-(w)* subtype inclusions, and the obtained *Th-Ph* pair is 250 °C and 0.5 kbar. Thus the thermobarometric conditions for this stage E2 in Lalin pegmatites are around 0.5 kbar and 240–310 °C (from the value range of *Vc-(w)* subtype homogenization temperatures).

Stage E3 is characterized by saline-aqueous (Lw_{ap}, *Lw1* and *Lw2*) fluids. At Forcarei Sur, Lw_{ap} inclusion isochores indicate that the *Ph-Th* lies between 285 and 310 °C and between 0.3 and 0.6 kbar (Fig. 7). At Forcarei Norte and Lalin stage E3 is characterized by lower minimum temperature and pressure of trapping, between 100 and 200 °C and below 0.1 kbar respectively. Taking the steep slope of these isochores into account, a slight temperature increase produces a high pressure increase, but there are no data from mineral geothermometers. These inclusions may have been trapped when the pegmatite bodies were located at lower depth.

Discussion and conclusions

The composition of the different inclusion types for each pegmatite field enable us to propose a general model of fluid composition evolution.

The first fluid (*Ls-w*), which may be referred to as pegmatitic, is a silicate-rich aqueous fluid. The silicates present within it are quartz, albite and other unidentified silicates. It may have evolved through crystallization and cooling of the pegmatite bodies to comparatively solute-poor aqueous fluid. This aqueous-rich fluid progressively evolved to a low density volatile-rich aqueous fluid with low salinity which was trapped by *Lw-(c)* and *Lw-c* inclusions. It is distributed widely in all studied pegmatites and its average composition is 93 mol% H_2O–5 mol% CO_2–0.5 mol% CH_4–0.2 mol% N_2 and 1.3 mol% NaCl. It is trapped by minerals from the

replacement units. Therefore, it is related to the pegmatite stage when the rare-element mineralization occurred. The volatile enrichment may have been due to a mixture of magmatic fluids and fluids from the host rock, so the pegmatite was an open system which may have permitted the mixture of magmatic and host-rock derived fluids. The fluid described, with a pressure drop at relatively constant temperature, increases its volatile content (mainly CO_2) and decreases its salinity and H_2O content. The average composition of this fluid, which is trapped by *Vw-c* inclusions, is 86.8 mol% H_2O, 11 mol% CO_2, 1.5 mol% CH_4, 0.5 mol% N_2 and 0.36 mol% NaCl. The last stage of evolution of this fluid can be inferred from the *Vc-w* inclusion type of albite pegmatites from Forcarei Sur. These inclusions indicate the existence of a later aqueous-carbonic fluid circulation with a slight decrease in temperature and pressure, probably due to progressive exhumation of these bodies. In these albite pegmatites, with a decrease in temperature at constant pressure, there was a subsequent circulation of a hydrothermal aqueous fluid which altered the pegmatite bodies. From this fluid, later Mn-rich apatite was formed. In the Lalin field a later stage of carbonic-aqueous (type *V*) fluid circulation must be the result of heterogeneous trapping of a relatively high-density volatile phase-rich aqueous hydrothermal fluid introduced into the pegmatite through later fractures. Taking a general evolution of these bodies into account, a progressive transition from a magmatic (pegmatitic) stage to hydrothermal stage must have occurred.

Finally, there was a circulation of cool hydrothermal fluids (*Lw*1 and *Lw*2) which altered the pegmatite bodies through later fractures when the bodies were close to the surface. The low temperature alterations may have formed low temperature minerals such as hydroxyl-herderite, adularia and bertrandite.

In AEGC pegmatite fields, the CH_4 content of the aqueous-carbonic fluids increases from Lalin through Forcarei Norte to Forcarei Sur. This decrease in oxygen fugacity does not seem to be related to temperature variations because similar ranges of temperature for the aqueous-carbonic fluid trapping are recorded in the three pegmatite fields. Moreover, there is no correlation between fO_2 and mineralogy or the degree of pegmatite fractionation since the studied albite pegmatites of Forcarei Sur and Lalin have similar mineralogy and degree of fractionation, however, Forcarei Sur has a lower fO_2 and Lalin a higher one. As a possible explanation we are putting forward a very important interaction between the fluids and the host rock. As mentioned earlier, the host rock of the studied Forcarei Norte and Forcarei Sur pegmatites are graphite-rich schist (the autochthonous sequence), whereas the Lalin pegmatites studied are hosted by rocks which do not have this composition (the allochthonous sequence). Therefore, the fluid chemistry may have been controlled by graphite-fluid equilibration, implying a source of fluids external to the pegmatites (surrounding metamorphic series). The aqueous-carbonic fluids of the Forcarei Sur field are the CH_4-richest. In these pegmatites the replacement units are often located at the border zone of the bodies, and the samples for this study were taken from those areas adjacent to the contact with the host rock. This agrees with graphite-rich host-rock as a methane source.

The current study has shown that fluid inclusion data are useful for establishing the composition and evolution of pegmatitic fluids together with the *P–T* path model affecting the pegmatite bodies. This study has revealed the following major points:

1. The magmatic ("pegmatitic") fluid in AEGC pegmatites is preserved in primary fluid inclusions hosted by garnet. This fluid is aqueous and silicate-rich, having many of the characteristics of solution-melt inclusions which were described in Tanco pegmatite by London (1986). Similar fluid inclusions have also been found in other fluid inclusion studies in pegmatites (Doria et al. 1989; Linnen and Williams-Jones 1994).
2. This mentioned magmatic fluid evolved through crystallization and cooling of the pegmatite bodies to aqueous-carbonic fluids. The salinity of these fluids is similar to that of the low-salinity aqueous or aqueous-carbonic fluids observed in cassiterite-bearing pegmatites, e.g. La Fregeneda (Mangas and Arribas 1987), the Nong Sua aplite-pegmatite complex (Linnen and Williams-Jones 1994) and other tin-bearing pegmatites, e.g. Tanco (London 1986; Thomas and Spooner 1988).
3. The volatile enrichment may be due to a mixture of magmatic fluids and fluids from the host-rock. Thus, these pegmatites are an open-system.
4. The *P–T* path model shows an important drop in pressure (around 2 kbar) at constant temperature. We attribute it to the change from lithostatic to hydrostatic pressure, which is itself due to the development of a ductile shear zone and fracture system, both of which affected these bodies. This isothermal decompression is indicated in other pegmatite bodies, e.g. the Nong Sua aplite-pegmatite complex (Linnen and Williams-Jones 1994).
5. The dominant controls of rare-element mineralization in the replacement units of these pegmatites seem to be isothermal decompression and mixing with external carbonic fluids.

Acknowledgments This work has been financed by the CICYT project GEO 91-1077 (Educational Science Ministry of Spain) and supported by FPI via an MEC fellowship to the first author. We thank the reviewers for their encouraging suggestions which have improved significantly the content and clarity of the paper.

References

Arenas R (1985) Evolucion petrologica y geoquimica de la unidad aloctona inferior del complejo metamorfico basico-ultrabasico de Cabo Ortegal (Unidad de Moeche) y del silurico

parautoctono. Cadena Hercinica Iberica (NW de España). Ph D Thesis, Complutense de Madrid Univ, Madrid, Spain, 543 pp

Bakker RJ (1995) The application of a computerised and optimised clathrate stability model to fluid inclusion studies. ECROFI XIII Bol Soc Esp Mineral 18(1): 15–17

Bakker RJ (1997) Clathrates: computer programs to calculate fluid inclusions V-X properties using clathrate melting temperatures. Comput Geosci 23: 1–8

Bakker RJ, Dubessy J, Cathelineau M (1996) Improvements in clathrate modelling I: the H_2O system with various salts. Geochim Cosmochim Acta 60: 1657–1681

Barrera JL, Farias P, González F, Marquinez J, Martin LM, Martinez JR, Del Olmo A, De Pablo JG (1989) Mapa Geológico 1: 200,000 de Ourense/Verin. Memoria explicativa, Publicación del Instituto Tecnológico Geominero de España, Madrid

Bodnar RJ (1993) Revised equation and table for determining the freezing point depression of H_2O-NaCl solutions. Geochim Cosmochim Acta 57: 683–684

Brown PE, Hagemann SG (1995) Fluid inclusion data reduction and interpretation using Macflincor on the Macintosh. XIII ECROFI. Bol Soc Esp Mineral 18(1): 32–33

Capdevila R, Vialette (1970) Estimation radiométrique de l'age de la deuxième phase tectonique hercynienne en Galice moyenne (Nord-Ouest de l'Espagne. CR Acad Sci Ser D 270: 2527–2530

Cathelineau M, Boiron MC, Essarraj S, Dubessy J, Lespinasse M, Poty B (1993) Fluid pressure variations in relation to multistage deformation and uplift: a fluid inclusion study of Au quartz veins. Eur J Mineral 5: 107–121

Cerny P (1989) Exploration strategy and methods for pegmatite deposits of tantalum. In: Möller P, Cerny P, Saupé F (eds) Lanthanides, tantalum and niobium. Springer, Berlin Heidelberg New York, pp 274–302

Cerny P (1994) Rare-element granitic pegmatites. Part I: Anatomy and internal evolution of pegmatite deposits. Ore Deposits Models 2: 29–47

Chakoumakos BC, Lumpkin GR (1990) Pressure-temperature constraints on the crystallization of the Harding pegmatite, Taos County, New Mexico. Can Mineral 28: 287–298

Charoy B, Lhote F, Dusausoy Y, Noronha F (1992) The crystal chemistry of spodumene in some granitic aplite-pegmatite bodies of northern Portugal: a comparative review. Can Mineral 30: 639–651

Collins PLF (1979) Gas-hydrates in CO_2 bearing fluid inclusions and the use of freezing data for estimation of salinity. Econ Geol 74: 1435–1444

Crawford ML (1981) Phase equilibria in aqueous fluid inclusions. Mineralogical Association of Canada, Short Course Handbook 6, pp 75–100

Dallmeyer RD, Martinez Catalán JR, Arenas R, Gil Ibarguchi JI, Gutierrez-Alonso G, Farias P, Aller J, Bastida F (1997) Diachronous Variscan tectonothermal activity in the NW Iberian Massif: evidence from $^{40}Ar/^{39}Ar$ dating of regional fabrics. Tectonophysics 277(4): 307–337

Doria A, Charoy B, Noronha F (1989) Fluid inclusion studies in spodumene-bearing aplite-pegmatite dykes of Covas de Barroso, northern Portugal. ECROFI X Abstr, London, p25

Dubessy J (1984) Simulation des équilibres chimiques dans le système C-O-H: Consequences méthodologiques pour les inclusions fluides. Bull Mineral 107: 157–168

Dubessy J, Poty B, Ramboz C (1989) Advances in the C-O-H-N-S fluid geochemistry based on micro-Raman spectroscopic analysis of fluid inclusions. Eur J Mineral 1: 517–534

Dubessy J, Thiery R, Canals M (1992) Modelling of phase equilibria involving mixed gas clathrates. Application to the determination of molar volume of the vapour phase and of the salinity of the aqueous solution in fluid inclusions. Eur J Mineral 4: 873–884

Dubois M (1992) Fluides crustaux: approche experimentale et analytique. PhD Thesis, INPL, Nancy, France

Farias P, Gallastegui G, González Lodeiro F, Marquinez J, Martin Parra LM, De Pablo Macia JG, Rodriguez Fernández LR (1987) Aportaciones al conocimiento de la litoestratigrafía y estructura de Galicia Central. Mem Fac Cienc Univ Porto 1: 411–431

Fuertes-Fuente M (1996) Las pegmatitas del área de Lalin-Forcarei (Galicia) y las mineralizaciones de elementos escasos asociadas. PhD Thesis, Oviedo University, Oviedo, Spain, pp 283

Fuertes-Fuente M, Martin-Izard A (1998) The Forcarei Sur rare-element granitic pegmatite field and associated mineralization, Galicia, Spain. Can Mineral 36: 303–325

Garcia Garzón J, De Pablo Maciá JG, LLamas Borrajo JF (1981) Edades absolutas obtenidas mediante el método Rb-Sr en dos cuerpos de ortoneisses en Galicia Occidental. Bol Geol Mineral Esp 92: 463–466

Gil Ibarguchi JI, Arenas R (1990) Metamorphic evolution of the allochthonous complexes from the northwest of Iberian Peninsula. In: Dallmeyer RD, Martinez Garcia E (eds) Pre-Mesozoic geology of Iberia. Springer, Berlin Heidelberg New York, pp 237–246

Hesen BJ (1967) Mineralogy and petrography of some tin-lithium and beryllium bearing albite pegmatites near Doade, Galicia (Orense). Leidse Geol Medred 36: 249–259

Jacobs GK, Kerrick DM (1981) Methane: an equation of state with application to the ternary H_2O-CO_2-CH_4 system. Geochim Cosmochim Acta 45: 607–614

Kerrick DM, Jacobs GK (1981) A remodified Redlich-Kwong equation for H_2O-CO_2 and H_2O-CO_2-NaCl mixtures at elevated pressures and temperatures. Am J Sci 281: 735–767

Knorring VD, Vidal Romani JR (1981) On the mineralogy of the O Casteliño spodumene pegmatite near Lalin, Galicia, Spain. Cuad Lab Xeol Laxe 2: 259–262

Linnen RL, Williams-Jones AE (1994) The evolution of pegmatite-hosted Sn-W mineralization at Nong Sua, Thailand: evidence from fluid inclusions and stable isotopes. Geochim Cosmochim Acta 58(2): 735–747

London D (1986) Magmatic-hydrothermal transition in the Tanco rare-element pegmatite: evidence from fluid inclusions and phase-equilibrium experiments. Am Mineral 71: 376–395

Mangas J, Arribas A (1987) Fluid inclusion study in different types of tin deposits associated with the Hercynian granites of western Spain. Chem Geol 61: 193–208

Marquinez J (1984) La geologia del Area Esquistosa de Galicia Central (Cordillera Herciniana, NW de España). Mem IGME 100: 1–213

Martin-Izard A, Paniagua A, Moreiras D, Acevedo RD, Marcos-Pascual C (1995) Metasomatism at a granitic pegmatite-dunite contact in Galicia: the Franqueira occurrence of chrysoberyl (alexandrite), emerald and phenakite. Can Mineral 33: 775–792

Martinez Catalán JR, Arenas R, Diaz Garcia F, Rubio Pascual FJ, Abati J, Marquinez J (1996) Variscan exhumation of a subducted Paleozoic continental margin: the basal units of the Ordenes Complex, Galicia, NW Spain. Tectonics 15(1): 106–121

Nwe YY, Morteani G (1993) Fluid evolution in the H_2O-CH_4-NaCl-CO_2 system during emerald mineralization at Gravelotte Murchinson Greenstone Belt, northeast Transvaal, South Africa. Geochim Cosmochim Acta 57: 89–103

Parga Pondal I, Martinez Cardoso G (1948) Die Lithium-pegmatite von Lalin, Prov. Pontevedra, Galizien. Schweiz Mineral Petrol Mitt 28: 324–334

Potter RW, Brown DL (1977) The volumetric properties of aqueous sodium chloride solution from 0 °C to 500 °C at pressures up to 2000 bars based on a regression of available data in the literature. US Geol Surv Bull 1421-C: C1–C36

Poty B, Leroy J, Jachimowicz L (1976) Un nouvel appareil pour la mesure des températures sous le microscope: l'installation de microthermometrie Chaixmeca. Bull Soc Fr Minéral Cristallogr 99: 182–186

Priem HNA, Boelrijk NAIM, Verschure RH, Hebeda EH, Verdurmen EATh (1970) Dating event of acid plutonism

through the Paleozoic of the western Iberian Peninsula. Eclogae Geol Helv 63: 255-274

Ribeiro A (1970) Contribution a l'étude tectonique de Trás-Os-Montes Oriental. Mem Serv Geol Port 24: 179

Ribeiro A, Pereira E, Dias R (1990) Central-Iberian Zone. Allochthonous sequences. Structure in the geology of Iberia. In: Dallmeyer RD, Martínez García E (eds) Pre-Mesozoic geology of Iberia. Springer, Berlin Heidelberg New York, pp 237-246

Robie RA, Hemingway BS (1984) Entropies of kyanite, andalusite and sillimanite: additional constraints on the pressure and temperature of the Al_2SiO_5 triple point. Am Mineral 69: 298-306

Roedder E (1984) Fluid inclusions. Reviews in Mineralogy 12. Mineral Society of America, Washington, DC

Santos Zalduegui JF, Schärer U, Gil Ibarguchi JI (1995) Isotope constraints on the age and origin of magmatism and metamorphism in the Malpica-Tuy allochton, Galicia, NW-Spain. Chem Geol 121: 91-103

Shepherd TJ, Rankin AH, Alderton DHM (1985) A practical guide to fluid inclusion studies. Blackie, London, pp 1-235

Thiery R, Vidal J, Dubessy J (1994) Phase equilibria modelling applied to fluid inclusions: liquid-vapor equilibria and calculations of the molar volume in the CO_2-CH_4-N_2 system. Geochim Cosmochim Acta 58: 1073-1082

Thomas AV, Spooner ETC (1988) Fluid inclusions in the system H_2O-CH_4-NaCl-CO_2 from metasomatic tourmaline within the border unit of the Tanco zoned granitic pegmatite, S E Manitoba. Geochim Cosmochim Acta 52: 1065-1075

Van Calsteren PWC, Boelrijk NAIM, Hebeda EH, Priem HNA, Den Tex E, Verdurmen EATH, Verschure RH (1979) Isotopic dating of older elements (including the Cabo Ortegal mafic-ultramafic complex) in the Hercynian Orogen of NW Spain: manifestations of a presumed Early-Paleozoic mantle-plume. Chem Geol 24: 35-36

Whitworth MP, Rankin AH (1989) Evolution of fluid phases associated with lithium pegmatites from S-E Ireland. Mineral Mag 53: 271-284

Yardley BWD (1989) An introduction to metamorphic petrology. Longman Scientific and Technical, Essex, UK

Ypma PJM (1966) Structural petrology of an area near Santiago de Compostela (NW Spain). Leidse Geol Medred 45: 1-71

Zhang YG, Frantz JD (1987) Determination of the homogenization temperatures and densities of supercritical fluids in the system NaCl-KCl-$CaCl_2$-H_2O using synthetic fluid inclusions. Chem Geol 64: 335-350

The Canadian Mineralogist
Vol. 38, pp. 1163-1175 (2000)

P–T PATH AND FLUID EVOLUTION IN THE FRANQUEIRA GRANITIC PEGMATITE, CENTRAL GALICIA, NORTHWESTERN SPAIN

MERCEDES FUERTES-FUENTE[1] AND AGUSTIN MARTIN-IZARD

Departamento de Geología, Universidad de Oviedo, Arias de Velasco s/n, E-33005 Oviedo, Spain

MARIE CHRISTINE BOIRON

CREGU–UMR G2R, BP 23, F-54501 Vandoeuvre-lès-Nancy Cedex, France

JOSE MANGAS VIÑUELA

Departamento de Geología, Universidad de Las Palmas de G.C., Apdo. 550, E-35080 Las Palmas, Spain

Abstract

In Galicia, in the northwestern part of the Iberian Peninsula, there are several occurrences of granitic pegmatites. One of them, known as Franqueira, is a metasomatic deposit of gem-quality chrysoberyl, emerald and phenakite. The pegmatite is associated with a two-mica peraluminous Hercynian granite, and intrudes dunites of the Schistose domain in the Galician Trás-Os-Montes Zone. The composition of fluid inclusions in emerald and phenakite has been determined using a Raman microprobe to ascertain the paleofluid chemistry and the P–T conditions of fluid migration in the pegmatite. Three types of fluid inclusions have been identified in emerald and phenakite; three episodes of fluid circulation are distinguished. The first episode is represented by low-salinity aqueous-carbonic primary fluid inclusions in phenakite; these were trapped at 2.5 kbar and 400°C. An isothermal drop in pressure produced a second stage of fluid trapping under conditions of 400°C and 1 kbar. Fluid inclusions trapped in emerald indicate that during this second stage, it formed from phenakite and chrysoberyl in the presence of a CO_2- and CH_4-rich fluid. A third episode of fluid circulation suggests an independent stage of fluid circulation during late tectonic events, with temperatures ranging from 160° to 265°C and pressure below 0.5 kbar.

Keywords: granitic pegmatite, fluid inclusion, microthermometry, Raman microprobe, P–T path, fluid evolution, Franqueira, Galicia, Spain.

Sommaire

En Galice, dans le secteur nord-ouest de la Péninsule Ibérique, on trouve plusieurs massifs de pegmatites granitiques. Un de ceux-ci, Franqueira, est le site d'un gisement métasomatique de chrysobéryl, émeraude et phénakite gemmes. La pegmatite est associée à un massif hercynien de granite hyperalumineux à deux micas, mis en place dans des dunites du domaine de schistes de la zone Trás-Os-Montes. La composition des inclusions fluides dans l'émeraude et la phénakite a été établie au moyen d'une microsonde Raman afin de déterminer la composition du paléofluide et des conditions de pression et de température au cours de sa migration dans la pegmatite. Nous avons identifié trois types d'inclusions fluides dans l'émeraude et la phénakite, qui témoignent de trois épisodes de circulation d'une phase fluide. Le premier a donné des inclusions primaires aqueuses et primaires dans la phénakite, piégées à 2.5 kbar et 400°C. Une chute isotherme de la pression a produit un second stade de piégeage, à 400°C et 1 kbar. Les inclusions associées à ce deuxième épisode piégées dans l'émeraude indiquent un mode de sa formation par remplacement aux dépens de la phénakite et du chrysobéryl par une phase fluide riche en gaz carbonique et en méthane. Un troisième épisode de circulation serait indépendant des deux premiers, développé au cours d'une déformation tardive à une température allant de 160° à 265°C et une pression inférieure à 0.5 kbar.

(Traduit par la Rédaction)

Mots-clés: pegmatite granitique, inclusions fluides, microthermométrie, microsonde Raman, tracé de pression et de température, évolution de la phase fluide, Franqueira, Galice, Espagne.

[1] *E-mail address*: mercedf@asturias.geol.uniovi.es

Introduction

There are several occurrences of rare-element-enriched granitic pegmatite in the central part of Galicia, in the northwestern region of the Iberian Peninsula. One of these, Franqueira, is a well-documented example of a deposit of gem-quality chrysoberyl, emerald and phenakite in western Europe (Martin-Izard *et al.* 1995). The geological conditions of formation of the Franqueira deposit have led Martin-Izard *et al.* (1995) to include it in the suture-zone group (Snee & Kazmi 1989) or in the type-I deposit, the Ural Mountains type, in the classification of Giuliani *et al.* (1997), on the basis of exometasomatic phenomena (Fersman 1929, Sinkankas 1989, Giuliani *et al.* 1997). The deposit showing the closest similarity to Franqueira in its mineralogical association, geological environment and age of formation (Paleozoic), is Tokovaja, in the Ural Mountains, Russia (Sinkankas 1989, Laznicka 1985, Giuliani *et al.* 1997).

The purpose of this paper is to present the results of a combined Raman microprobe and fluid-inclusion study carried out on emerald and phenakite from the Franqueira deposit, located in the central part of Galicia, in the northwestern Iberian Peninsula. Results of these studies allow us to determine the evolution of fluids and the P–T–V–X conditions of the multistage circulation of fluids in the metasomatic zone around the pegmatite and also to establish the conditions of formation of the beryllium-bearing gems.

The origins of the fluids involved and the possible interaction between the pegmatite-derived fluids and those derived from the host rock also are discussed. From these results, a fluid immiscibility in the system H_2O–CH_4–CO_2–NaCl likely contributed to the evolution of the fluid in the case of Be-rich pegmatites that metasomatized adjacent ultramafic rocks.

The Franqueira Deposit

The Franqueira pegmatite is located in the northwestern part of the Iberian Peninsula, in the Galician Tras-Os-Montes Zone (Matte 1968, Farias *et al.* 1987, Martínez Catalán *et al.* 1996) (Fig. 1). The Tras-Os-Montes Zone consists of two domains: (1) schistose rocks, including mafic–ultramafic overthrusted complexes (Cambrian to Silurian in age), and (2) granitic rocks, including two-mica peraluminous synkinematic granitic rocks (330–310 Ma, Priem & Den Tex 1984, Serrano Pinto *et al.* 1987, Van Calsteren *et al.* 1979). The former is composed of metamorphic rocks and the Lalín–Forcarei Unit, the southern end of the large Ordenes Complex (Barrera *et al.* 1989, Monterrubio 1991). The Ordenes Complex, as well as the Lalín–Forcarei Unit, which overthrusts the other groups of the schist domain during D1 and D2 Hercynian deformation events (360–330 Ma, Dallmeyer *et al.* 1997), consists of gabbro, amphibolite, orthogneiss, dunite and other ultramafic rocks (Monterrubio 1991). The regional

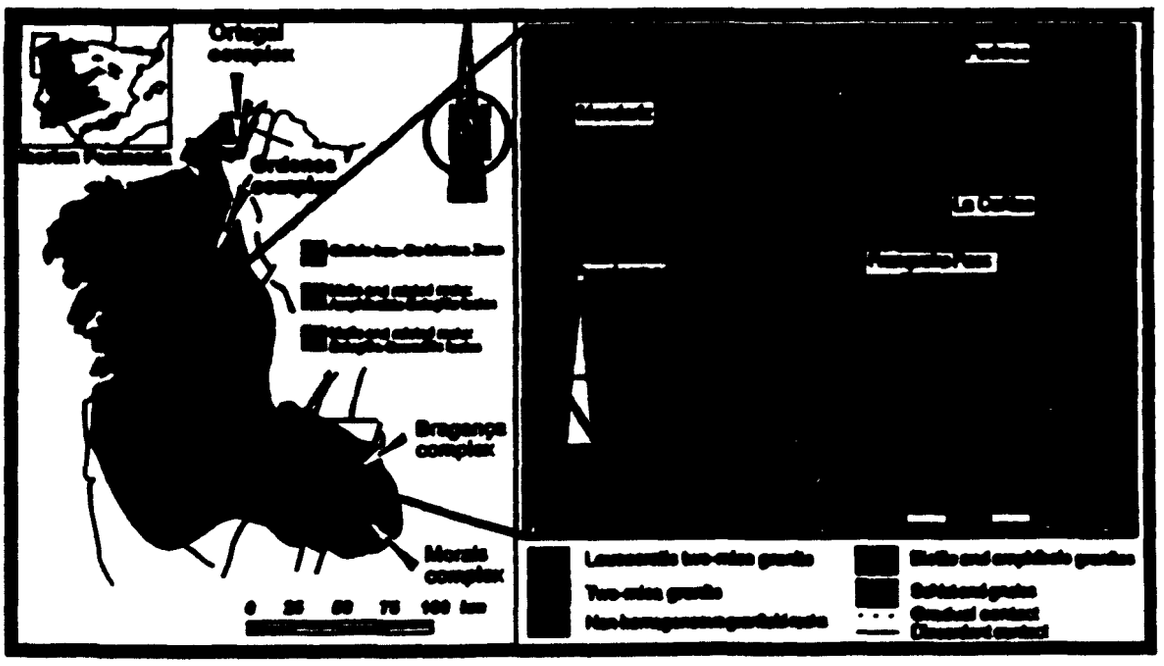

FIG. 1. Setting and schematic geological map of the Franqueira deposit, adapted from Barrera *et al.* (1989).

geological setting of the Franqueira pegmatite was outlined by Martin-Izard *et al.* (1995, 1996).

The Franqueira deposit occurs between ophiolite complexes of Galicia (Ordenes Complex) and Portugal (Bragança and Morais complexes). These complexes represent fragments of oceanic crust that were thrust over the schist of the schistose domain during the first and second phase of the Hercynian Orogeny. Heterogeneous two-mica granite (Barrera *et al.* 1989) were emplaced during the third tectonic phase (315 ± 10 Ma: Capdevila & Vialette 1970). At Franqueira, the pegmatite bodies, related to the heterogeneous two-mica granites, cross-cut an ultramafic rock of dunitic character and associated gabbroic rocks.

Martin-Izard *et al.* (1995) suggested that the dunite and hornblende gabbro considered here belong to a remnant of peridotitic and gabbroic rocks from the overthrusted complexes. This suggestion is supported by the fact that the geochemical and mineralogical characteristics of Franqueira dunite and gabbro are similar to those of the the Ordenes, Bragança and Morais complexes.

Later, during the intrusion of the Hercynian granites, the dunite and hornblende gabbro could have remained in the roof zone of the peraluminous heterogeneous two-mica granites, which normally have a suite of associated pegmatite bodies. The Franqueira pegmatite, which is enriched in Be, B and P, caused metasomatic alteration of the adjacent dunite, with formation of phlogopitite near the pegmatite, and tremolitite bodies and an anthophyllite rim close to the dunite. The Mg and Cr of these rocks were provided by the dunite. The addition of boron and phosphorus resulted in the formation of tourmaline and abundant apatite in the metasomatic facies, along with phlogopite. In the zones closest to the pegmatite, the Be spread out in the system and first developed chrysoberyl ("alexandrite") and phenakite porphyroblasts, isolated or intergrown in the phlogopitite.

The bodies of granitic pegmatites form a network of narrow, anastomosing subvertical dikes that trend approximately east–west. The dike system (Fig. 2) is exposed for 15–20 meters. Dike thickness ranges from 3 to 40 cm. Relics of dunite totally transformed to phlogopite are commonly found within the pegmatite.

The pegmatite bodies show a simple zonation with an aplitic border. Essential minerals are quartz, albite, muscovite and scarce K-feldspar, with apatite, tourmaline and zircon as accessory minerals. In the main zone of the pegmatite, albite is the most abundant mineral, with quartz in lesser proportion and some muscovite. Within the pegmatitic bodies of greater thickness, a banding can be observed in the central zone, in which a coarse-grained rock alternates with another of saccharoidal appearance. In the coarse-grained facies, there are crystals of coarse bladed albite with subhedral albite, interstitial euhedral quartz, and muscovite plates. In the saccharoidal facies, garnet and tourmaline abound.

The host rocks have a clearly defined contact with the pegmatites and are of a micaceous nature. The mica is phlogopite, and is the most abundant mineral (over 75%, up to 90%) in this facies (Fig. 2). The visible thickness of this rock is up to three meters, and it crops out for at least five meters. The accessory minerals are chrysoberyl ("alexandrite"), phenakite, beryl ("emerald"), tourmaline, garnet (mainly almandine), apatite (fluorapatite, 3.5 wt.% F) and zircon.

Chrysoberyl [Fig. 3A(C)] appears as subhedral porphyroblasts isolated in the phlogopite or as skeletal intergrowths within emerald, phenakite and apatite. Phenakite [Figs. 3A(P), 3B] appears as subhedral and colorless prismatic crystals up to 3 cm in size. Phenakite commonly has associated apatite crystals [Fig. 3A(A)]. Beryl appears as euhedral prismatic crystals with sizes

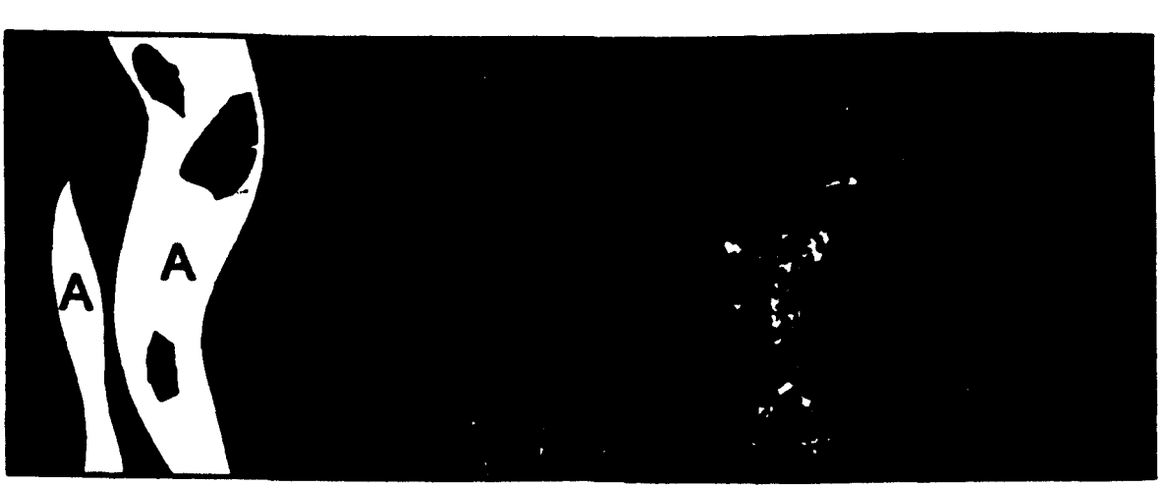

FIG. 2. View of the pegmatite dikes, which are lenticular (A). The pegmatite is hosted by phlogopitite (B) and tremolitite (C).

of up to 30 cm [Figs. 3A(B), 3B]; an intense green color and Cr content (up to 0.2 wt.%) give it its emerald-like character. It is the latest Be mineral and replaces the chrysoberyl and phenakite (Fig. 3A). Tourmaline (dravite) is developed at the contact between phlogopitite and the pegmatite.

Beryl porphyroblasts developed and partially replaced the other two Be minerals owing to the increasing activity of H_4SiO_4 (at constant temperature) in accordance with the reaction:

$$\text{chrysoberyl} + \text{phenakite} + 5H_4SiO_4 = \text{beryl} + 10H_2O \quad (1)$$

proposed by Barton (1986). Invariably, where chrysoberyl and phenakite are together, they are replaced by beryl (emerald) and appear as a skeletal intergrown within the emerald.

The phlogopitite grades into a tremolitite in which pockets of phlogopite are ubiquitous (Fig. 2). The visible thickness of this rock is up to six meters. In the tremolitite, the rock is essentially composed of tremolite, but some phlogopite is always present and locally, along dunite contacts, the tremolitite is rimmed by anthophyllite and titanite. Accessory minerals include zircon, apatite and ilmenite. Over a short distance (5 cm), the tremolitite grades into an anthophyllite zone and then into dunite.

The dunite outcrops only as relics of about one meter thick inside the tremolite rock. It is dark in color, granoblastic and of very compact texture, and the olivine is partially altered to tremolite and phlogopite. Olivine ($Fo_{86.6}$) forms a hypidiomorphic, partially serpentinized and chloritized aggregate. Chromian spinel is found as an accessory mineral, usually disseminated, although occasionally forming small aggregates.

Analytical Techniques

Microthermometric studies of fluid inclusions were performed on sections 100 to 300 μm thick using a microscope equipped with a UMK50 Leitz objective and a Chaixmeca cooling and heating stage (Poty *et al.* 1976) in the Laboratory of Geology of the University of

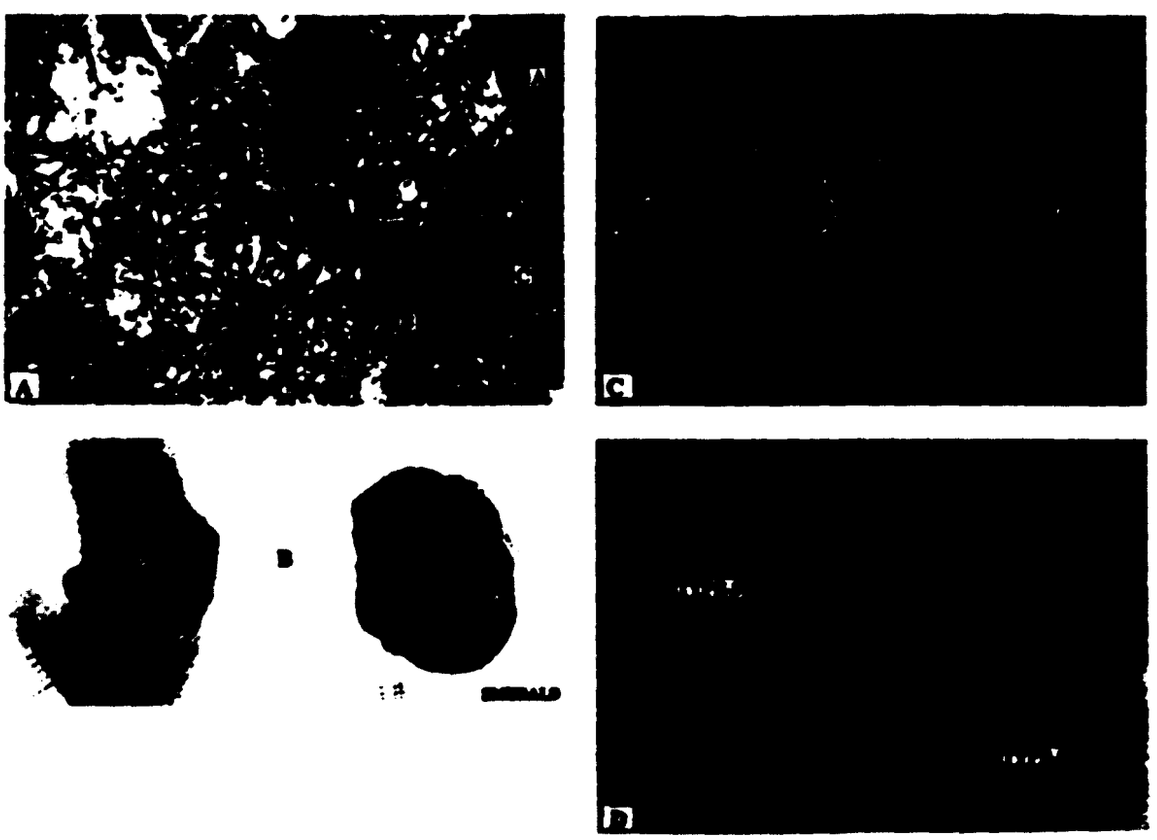

FIG. 3. A. Microscopic view of chrysoberyl (C), phenakite (P), beryl (B), and apatite (A). Phenakite and skeletal corroded crystals of chrysoberyl are included in emerald. XPL, 10×. B. Emerald and phenakite crystals used for the study of fluid inclusions. C. Primary complex CH_4 aqueous inclusions (type-1) in emerald crystals. XPL, 45×. D. Primary complex CO_2 aqueous inclusions (type-2) and secondary saline aqueous inclusions (type-3) in emerald crystals. XPL, 45×.

Las Palmas (Spain). The stage was calibrated according to the procedures outlined by Poty *et al.* (1976). The detailed analytical techniques of the microthermometric study are described in Martin-Izard *et al.* (1995).

The composition of the non-aqueous portion of individual inclusions was measured using a Dilor X–Y multichannel modular Raman spectrometer (at CRBGU). Bulk composition and density were computed from the P–V–T–X properties of individual inclusions in the C–O–H–(N–S) system (Dubessy 1984, Dubessy *et al.* 1989, 1992, Thiery *et al.* 1994, Bakker 1995). All data were calculated from the microthermometric measurements and the Raman analyses of the gas, using a clathrate stability model in the system H_2O–CH_4–N_2–NaCl–KCl–$CaCl_2$, between 253 and 293 K and between 0 and 200 MPa (Bakker 1995, Bakker *et al.* 1996) and the computer program of Bakker (1997).

The P–V–T–X properties of aqueous carbonic inclusions were modeled in terms of the system H_2O–CO_2–CH_4 using the state equations of Kerrick & Jacobs (1981) and Jacobs & Kerrick (1981) and the computer code of Dubessy (1984). Only in one case (type-1 inclusions in phenakite) did we use the equation of state of Bowers & Helgeson (1983). For aqueous inclusions, the isochores have been drawn in the H_2O–NaCl system using the data from Zhang & Frantz (1987) and the computer program Macflincor 0.92 (Brown & Hagemann 1995).

Selecting Samples, Inclusion Types and Microthermometric Results

In the Franqueira deposit, samples of emerald and phenakite (Fig. 3B) have been taken from the metasomatic phlogopite-rich zone (Martin-Izard *et al.* 1995). Both minerals have the potential to provide information on the conditions of metasomatism around the pegmatite. Fluids inclusions in chrysoberyl are scarce and are too small (less than 1 μm) for study.

Observations show that emerald and phenakite have a significant number of inclusions, isolated or in groups; these are interpreted as primary (Figs. 3C, D). Other inclusions related to fractures are classified as pseudosecondary or secondary on the basis of the criteria of Roedder (1984) (Fig. 3D). Inclusion morphology is equally variable, being roundish, elongate, tubular, subhedral negative crystal or irregular. The size of the inclusions studied ranges from 5 to 60 μm in size (Figs. 3C, D).

One hundred and twenty-five fluid inclusions were selected and studied by microthermometry in the two minerals. In all emerald and phenakite crystals studied (more than 10), fluid inclusions have the same morphological characteristics and volumetric ratios.

The fluid-inclusion studies of the Franqueira deposit reported by Martin-Izard *et al.* (1995) indicate the presence of three types of inclusions. Type 1 consists of complex CH_4-bearing aqueous inclusions (Fig. 3C). These show two phases at room temperature. The vapor phase occupies between 20 and 50% of the total volume of the inclusions. We consider these inclusions to be primary or pseudosecondary, and they are the most representative of emerald and phenakite.

After cooling and subsequent heating, the CH_4 liquid and vapor phases homogenized to either the vapor (V) or liquid (L) state or critical (C) stage. This occurs at temperatures ranging from –83 to –106°C into V and from –82 to –90°C into L phases in the emerald, and from –86 to –106°C into V, –88.5 to –110.5°C into L, and –86.5 and –89°C into C phases in the phenakite.

The temperature of initial ice melting, where measurable, was found to be mostly around the stable eutectic for the NaCl–H_2O system, –20.8°C (Potter & Brown 1977). Although the use of wt.% equivalent NaCl in such inclusions seems inappropriate, the overestimated salinity based on the final temperature of ice melting, with reference to the H_2O–NaCl system (Potter *et al.* 1978), ranges between 5 and 8 wt.% equivalent NaCl.

Total homogenization temperatures range between 318° and 369°C in the liquid state and between 354° and 373°C in the vapor state. Some of the measured inclusions decrepitated before total homogenization was achieved.

Type-2 inclusions are complex CO_2-bearing aqueous inclusions (Fig. 3D). These inclusions contain two phases at room temperature and show volumetric proportions Vg/Vt (vapor volume/total volume) below 50%. The inclusions appear only in the core of emerald crystals and have the same distribution as the type-1 inclusions, but are less abundant. Martin-Izard *et al.* (1995) considered these inclusions as primary or pseudosecondary and contemporaneous with type-1 inclusions. During cooling, the two-phase inclusions in some cases transform into three-phase inclusions (H_2O L + CO_2 V + CO_2 L). The melting of solid CO_2 has been measured at between –60.8° and –62.1°C. Salinities were overestimated approximately from the final melting of ice values and the formulae proposed by Potter *et al.* (1978) for the system H_2O–NaCl, and ranged from 5 to 10.5 wt.% equivalent NaCl.

Most of the total homogenization in the liquid state occurs between 320° and 378°C; only two inclusions homogenized into the gas and critical state at 381°C. This degree of variability in pattern of homogenization can be explained by small differences in the bulk composition of the fluid.

Type-3 inclusions are mixed-salt aqueous inclusions. These show two phases at room temperature in which the vapor bubble occupies less than 10% (Fig. 3D). These inclusions occur in both emerald and phenakite and are relatively scarce. The inclusions are secondary in character. Temperatures of first melting of ice vary between –45° and –55°C; these temperatures are lower than the eutectic temperature of the H_2O–NaCl system (Potter & Brown 1977). The temperature of final melt-

ing of ice ranges between –2.1 and –23°C. Taking into account these temperatures and the experimental data of Potter *et al.* (1978) for the system H_2O–NaCl, the salinity ranges between 3.5 and 24.7 wt.% equivalent NaCl. Homogenization temperatures range between 160° and 265°C in the liquid state.

The microthermometric measurements of Martin-Izard *et al.* (1995) are summarized in Table 1.

Clearly, from the above microthermometric data, no great differences exist between the fluid inclusion populations of emerald and phenakite; two discontinuous hydrothermal stages can be distinguished. The first hydrothermal stage was characterized by the circulation and trapping of aqueous fluid with some volatiles of type-1 and -2 inclusions (complex CH_4–CO_2 aqueous inclusions), with salinities below 10 wt.% equivalent NaCl, and a low density of bubbles. This fluid circulated at minimum temperatures of between 318° and 381°C, and the lithostatic or hydrostatic pressure was high enough to prevent boiling.

The characteristics of type-3 inclusions, showing a secondary character, lower temperatures of homogenization, lacking CH_4, CO_2 and other volatiles, having a variable salinity, and with solutions containing several cations, suggest an independent episode of hydrothermal fluid circulation during the later tectonic events. Thus, the second hydrothermal stage corresponds to the circulation and trapping of aqueous solutions of salinity below 24.7 wt.% equivalent NaCl, containing cations such as Ca, Mg, K and Na, among others, with densities ranging 0.9 to 1.15 g/cm^3, at minimum trapping temperatures ranging 160 and 265°C.

Raman Data

Raman microprobe analyses were carried out on type-1 (in phenakite and in emerald) and type-2 inclusions from Franqueira. From Raman analyses and microthermometric data, the density and composition of the volatile-rich phase together with the bulk density and composition were calculated. In order to obtain these data, the above-mentioned clathrate stability model was applied, but in the case of type-1 phenakite inclusion, results could not be obtained because the clathrate melting temperature (>20°C) is above the limits of stability of the model (between 253 and 293 K) and, moreover, there is a large difference between ice and clathrate melting temperatures. Nevertheless, it was possible to obtain a solution if we assumed that there was no salt in the system. This hypothesis is probably a reasonable estimate because the measured final ice melting temperature in these inclusions is low (–4°C), thus salinity is close to 6 wt.% equivalent NaCl. This value is low and, in any case, overestimated owing to the fact that the clathrate is present when the ice melts. On the basis of these facts, we assumed that there is no salt in the fluid trapped by phenakite.

All data are shown in Table 2. Raman microprobe analyses show that type-1 inclusions in emerald have a different density and composition of the volatile-rich phase than type-1 inclusions in phenakite.

H_2O is the main component of the fluid phase in type-1 inclusions trapped in emerald and phenakite. The volatile-rich phase of inclusions in both minerals is dominated by CH_4. In the case of type-1 inclusions trapped in phenakite, N_2 is present in higher quantities than in type-1 inclusions trapped in emerald; moreover, the type-1 fluid in emerald also contains CO_2. The composition of the volatile phase of type-1 inclusions in phenakite is 80.5 to 85.2 mole % CH_4 and 14.8 to 19.5 mole % N_2. The composition of the volatile phase in type-1 inclusions in emerald is 78.9 to 80 mole % CH_4, 2.5 to 15.7 mole % CO_2 and 5.4 to 7.5 mole % N_2.

Type-2 inclusions have also an aqueous composition and their volatile-rich phase is dominated by CO_2 and minor quantities of CH_4 and N_2. The volatile phase composition of type-2 inclusions is 52 to 68 mole % CO_2, 19.5 to 41.2 mole % CH_4 and 6.7 to 12.5 mole % N_2.

TABLE 1. SUMMARY OF THE MICROTHERMOMETRIC DATA FOR THE DIFFERENT TYPES OF FLUID INCLUSIONS IN THE FRANQUEIRA DEPOSIT

Type	host-mineral	N°	Tm_{CO_2}	Th_{CO_2}	Th_{CH_4}	Tm_{cl}	Tm_{ice}	Th
Type-1	emerald	39	-	-	-82 to -90 L -83 to -106 G	11.5 to 19	-3.5 to -5.2	318 to 369 L 354 G 320 to 378 L
Type-2	emerald	31	-60.8 to -62.1	-11.2 to 10 G	-	11.9 to 22	-3 to -7	381 G 381 C
Type-3	emerald	7	-	-	-	-	-1.3 to -23	160 to 265 L
Type-1	phenakite	40	-	-	-82.6 to -109 L -95 to -106 G -96.7 to -99 C	14.8 to 18.3	-3.5 to -5.2	322 to 350 L 363 to 373 G
Type-3	phenakite	8	-	-	-	-	-2.1 to -11	193 to 265 L

$TmCO_2$: melting temperature of CO_2; $ThCO_2$: homogenization temperature of CO_2, gaseous state (G), liquid state (L) and critical state (C); Tm_{cl}: melting temperature of clathrate; Tm_{ice}: melting temperature of ice; Th: total homogenization temperature, gaseous state (G), liquid state (L) and critical state (C). All temperatures are given in °C. N°: number of measurements. The data are summarized from Martin-Izard *et al.* (1995).

TABLE 2. RAMAN DATA AND BULK COMPOSITION OF THE FLUID INCLUSIONS SELECTED FROM THE FRANQUEIRA DEPOSIT, AND CORRESPONDING MICROTHERMOMETRIC DATA

			MICROTHERMOMETRY						RAMAN DATA				BULK COMPOSITION				
TYPES	host mineral	N°	Vg/ Vt	Tm_{CO2}	Th_{CO2}	Th_{CO2}	Tm_{cl}	Tm_{ice}	Th	CO_2	CH_4	N_2	δv	X_{H2O}	X_{CO2}	X_{CH4}	X_{N2}	X_{NaCl}
Type-1	phenakite	Fe-1	60	-	-	110.4 G	24	-4	371 G	-	80.5	19.5	0.28	70.2	-	24	5.8	-
		Fe-2	60	-	-	99.5 G	21.7	-4	370 G	-	85.2	14.8	0.23	73.8	-	22.4	3.8	-
Type-1	emerald	Eb6-2	50	-	-	-91 L	14	-5	369 L	15.7	78.9	5.4	0.13	88.5	2.3	8	0.5	0.7
		Eb6-1	50	-	-	-91 G	14	-	354 G	2.5	90	7.5	0.12	88.3	0.4	9.5	0.8	1
Type-2	emerald	Eb3-3	50	-59.4	10.2 G	-	13.4	-6.5	381 G	68	19.5	12.5	0.18	87	7.5	1.6	1	2.9
		Eb3-1	50	-62	8 G	-	13.4	-7	371 G	52.1	41.2	6.7	0.21	84.5	7.5	2.9	0.7	3

Raman data from the Franqueira deposit. Composition are given in mole %. Vg/Vt: volumetric ratio; Tm_{CO2}: melting temperature of CO_2; Th_{CO2}: homogenization temperature of CO_2, gaseous state (G), liquid state (L) and critical state (C); Tm_{cl}: melting temperature of clathrate; Tm_{ice}: melting temperature of ice; Th: total homogenization temperature, gaseous state (G), liquid state (L) and critical state (C). All temperatures are given in °C. δv: density of the volatile-rich phase.

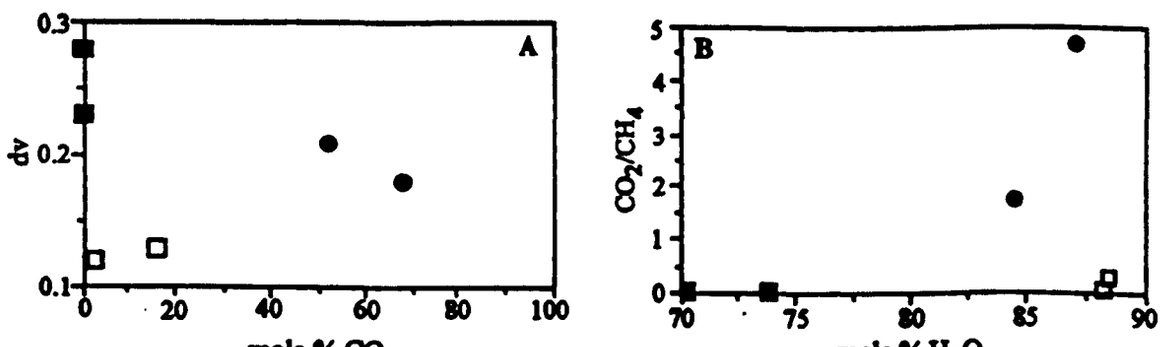

FIG. 4. A. Volatile density (δv) *versus* CO_2 mole %. B. CO_2:CH_4 ratio *versus* H_2O mole %. Determined from Raman analysis of individual fluid inclusions from the Franqueira deposit.

Figure 4A shows density *versus* CO_2 content of the volatile-rich phase for each inclusion type. It can be observed that type-1 inclusions may be divided into two groups, depending on whether they appear in phenakite or emerald. In the first case, the volatile-rich phase has a higher density, and no CO_2 is detected. But in the second case, there is CO_2, and the volatile-rich phase has a lower density. The type-2 inclusions, which only appear in the core of the emerald, reveal an increase in density and CO_2 content of the volatile-rich phase in relation to type-1 inclusions of the same mineral.

Taking into account the bulk composition of both types of inclusion, the CO_2/CH_4 ratio *versus* H_2O content (Fig. 4B) also shows two different groups in type-1 inclusions, depending on whether they appear in emerald or phenakite. Thus from type-1 fluid trapped in phenakite to type-1 fluid trapped in emerald, there is an increase in H_2O at a similar CO_2:CH_4 ratio. The fluid trapped in the emerald core (type 2) has a H_2O content similar to type-1 fluid in emerald but a higher CO_2:CH_4 ratio.

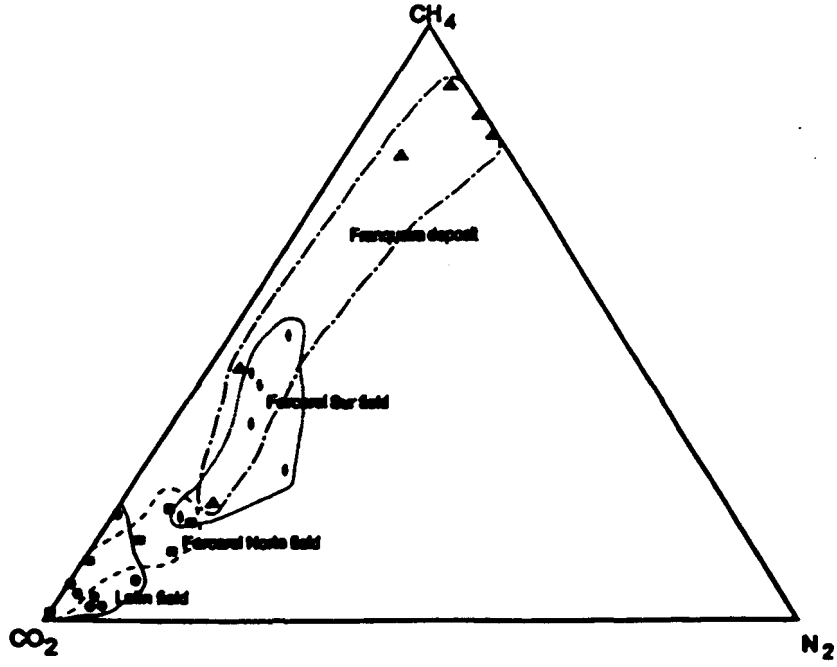

FIG. 5. CO_2–CH_4–N_2 ternary plot of the volatile-rich phase in the inclusions studied from the Franqueira deposit and each pegmatitic field from AEGC (Fuertes-Fuente *et al.* 2000). The plot shows selected results of Raman analyses of the aqueous–carbonic fluid of the Franqueira deposit and the three pegmatite fields from the AEGC.

The aqueous–carbonic fluids found in Franqueira can be compared with fluids from other granitic pegmatites of central Galicia (Fuertes-Fuente & Martin-Izard 1998, Fuertes-Fuente *et al.* 2000). These are known as AEGC pegmatites; they outcrop in three different pegmatite fields: Forcarei Sur (Fuertes-Fuente *et al.* 1995, Fuertes-Fuente & Martin-Izard 1998), Forcarei Norte and Lalín (Fuertes-Fuente 1996). The metasomatic fluids found (Fuertes-Fuente *et al.* 2000) have a composition, mainly that of their volatile phase, different for each AEGC pegmatite field, as demonstrated in the CO_2–CH_4–N_2 ternary plot (Fig. 5). Franqueira is the richest in CH_4 and, in the AEGC pegmatites, the CH_4 content of the aqueous–carbonic fluids increases from Lalín to Forcarei Sur, with an intermediate value in Forcarei Norte. The Franqueira samples were extracted from metasomatic wallrock, and this fact may explain why they are richer in CH_4 than the Forcarei Sur minerals in the pegmatite samples, which were extracted from minerals close to the pegmatite border (Fuertes-Fuente & Martin-Izard 1998). The minerals of the pegmatites from Forcarei Norte and Lalín were not extracted from the border of these bodies. This fact suggests a minor CH_4 content. The fact that Forcarei Norte is enriched in CH_4 compared to Lalín may be due to the fact that the metasediments in which Forcarei Norte pegmatites are enclosed have graphite horizons; these are absent in the metasedimentary units in which the Lalín pegmatites were emplaced (Fuertes-Fuente *et al.* 1995, 2000).

P–T Reconstruction

The calculated isochores of inclusions in emerald and phenakite from the Franqueira deposit are shown in Figure 6. The P–T evolution of the metasomatic fluids at Franqueira are discussed with reference to this figure. From these isochores, two stages of fluid circulation have been established during the metasomatic event.

The first stage is represented by trapping of type-1 fluid in phenakite at relatively high P–T conditions. The minimum conditions of trapping are those given by the Th–Ph pair, which is 370–371°C and 2–2.5 kbar. Martin-Izard *et al.* (1995) proposed temperatures between 380 and 420°C; we consider an average temperature of 400°C as the temperature closest to conditions of formation (Fig. 6). In this way, the fluid inclusions and Raman data in phenakite allow us to calculate a pressure for the first stage between 2.2 and 2.7 kbar, in agreement with the maximum of 4 kbar and, the most probable value, 2 kbar, proposed by Martin-Izard *et al.* (1995) on the basis of the thermodynamic equilibrium model in the system BeO–Al_2O_3–SiO_2–H_2O developed by Barton (1986) (Fig. 7).

Fluid-inclusion data give us temperatures of formation much lower than those corresponding to the chrysoberyl + quartz stability field (Fig. 6), close to the

euclase = beryl + phenakite + chrysoberyl (2)

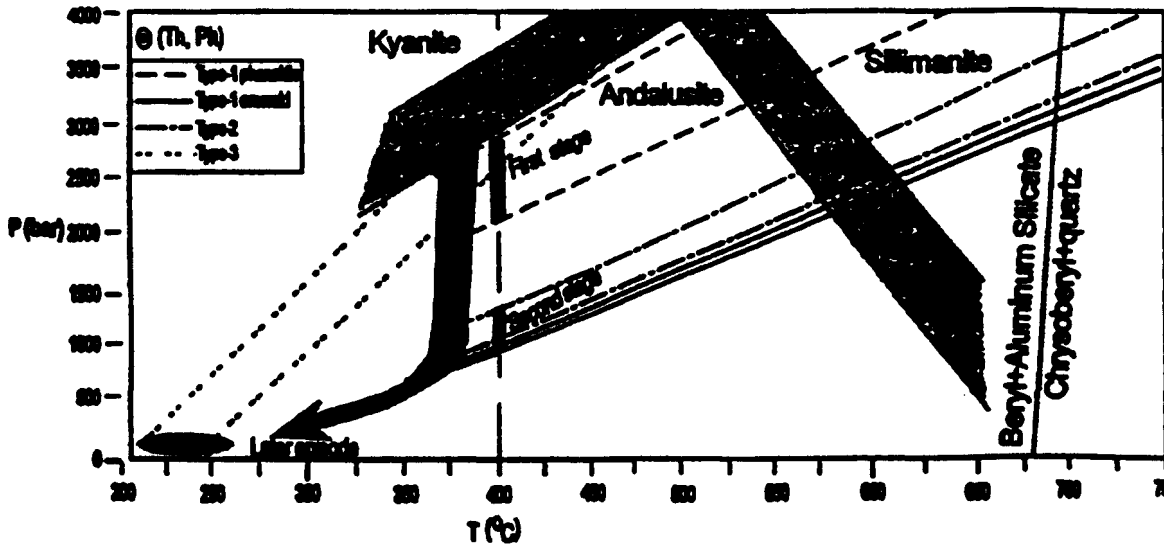

FIG. 6. P–T reconstruction, with the isochores representative of the different types of fluid inclusion in the Franqueira deposit. The dark zones are the minimum P–T conditions for the different stages of trapping of type-1 fluid inclusions in phenakite and emerald, type-2 and type-3 inclusions. The open circles on isochores represent the homogenization temperature and pressure. The vertical dashed line represents an average temperature (400°C) from the temperature range proposed by Martin-Izard *et al.* (1995) taking into account that the mineralization is formed by a contact metamorphic–metasomatic process.

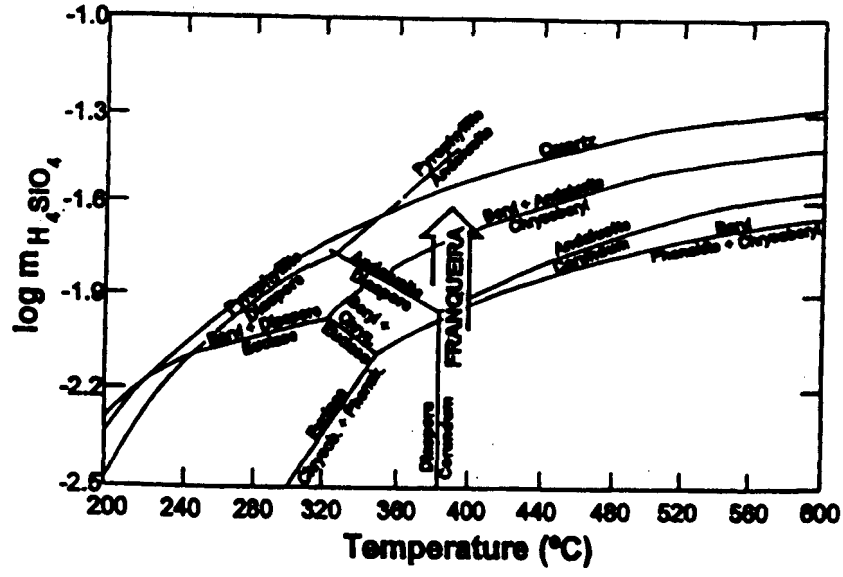

FIG. 7. Log mH_4SiO_4 – temperature projection at P = 1 kbar and activity of beryl = 0.1, showing a path consistent with the evolution of Be-assemblages at Franqueira (from Martin-Izard *et al.* 1995).

join. The absence of euclase indicates a minimum range of temperatures and pressures, *i.e.*, a P of 4 kbar and a T ranging from 350°C (for P = 1 bar) to about 450°C (for P = 4 kbar), in the stability field of andalusite.

The type-1 and type-2 fluids trapped in emerald display a lower density than type-1 fluid trapped in phenakite, yielding lower minimum pressures (Ph), in the 0.75–1 kbar range and a minimum temperatures (Th) in

the 354–381°C range. Taking into account the evolution of Be-bearing assemblages at Pranqueira (Martin-Izard *et al.* 1995), we consider that the temperature did not change with respect to the first stage, around 400°C (Fig. 6). If so, the pressure of this second stage is around 1 kbar. These data are also in agreement with the proposal by Martin-Izard *et al.* (1995).

During the first hydrothermal stage, the most probable pressure of trapping of type-1 fluid in phenakite is around 2 kbar and a temperature around 400°C. This pressure probably represents a lithostatic pressure indicative of a relatively deep structural level (7–8 km). The type-1 and type-2 inclusions in emerald display lower densities, thus these inclusions were trapped in the range of 1 kbar. Such variation could be explained by a pressure drop from lithostatic to partially hydrostatic conditions during decompression.

The characteristics and isochores of type-3 fluid inclusions (Martin-Izard *et al.* 1995) suggest a later unrelated episode of hydrothermal fluid circulation at minimum trapping temperatures ranging from 160°C to 265°C and pressures below 0.5 kbar.

Discussion

The evolution of the fluid associated with the metasomatic process is as follows. Under pressures between 2 and 2.5 kbar and a temperature close to 400°C, a first stage is developed in which an aqueous–carbonic fluid, dominated by H_2O and of very low salinity, is trapped. The fluid is composed of a volatile phase made up of methane and minor quantities of nitrogen, with an average composition of 72 mole % H_2O, 23.2 mole % CH_4 and 4.8 mole % N_2. A pressure drop produced a second stage of fluid trapping at 400°C and 1 kbar. During this latter stage, emerald formed from phenakite and chrysoberyl (reaction 1 and Fig. 6), thus indicating an increase in silica activity (Barton 1986). At that moment, two different fluids were simultaneously trapped by emerald: (1) an aqueous low-salinity fluid with a CH_4-rich volatile phase (type-1 inclusions), and (2) a CO_2-rich fluid with higher salinity (type-2 inclusions).

Two possible explanations are presented for discussion:

1) At the beginning of emerald crystallization, probably due to a drop in pressure during the second stage and an increase in SiO_2 activity, the initial metasomatic fluid trapped in phenakite evolved into two different aqueous fluids, CO_2-rich and CH_4-rich, in accordance with the reaction of CH_4 with H_2O to form CO_2 and H_2, the latest of which may diffuse away. Both fluids (CO_2-rich and CH_4-rich) have different densities, with the CO_2-rich fluid having the higher density (Fig. 4A). This fact could explain why the volatile phase with higher density and H_2O salinity was concentrated in the fluid trapped by the emerald core (type-2, CO_2-rich), whereas the volatile phase with the lower density and H_2O salinity (type-1, CH_4-rich) kept on getting trapped during the remainder of the emerald growth. In this way, two immiscible fluids are trapped in the emerald core. This agrees with a growth of emerald during a stage of heterogeneous trapping in the system H_2O–NaCl–CH_4–CO_2–N_2, as was proposed by Martin-Izard *et al.* (1995).

2) At the beginning of emerald crystallization, a fluid (type-2) from the pegmatite body circulated through the host rock and mixed with type-1 fluid found in phenakite, from which phenakite and, probably, chrysoberyl were formed. Note that several authors have observed that fluids in pegmatitic systems are generally dominated by CO_2 and H_2O: London (1986), Thomas & Spooner (1988), Konnerup-Madsen & Rose-Hansen (1982), and Fuertes-Fuente *et al.* (2000) So, the methane becomes more diluted with CO_2, and there is an enrichment in H_2O, the result of this mixture being the type-1 fluid, found in emerald. The aqueous–carbonic fluids from metasomatic tourmaline of the Tanco (Manitoba) pegmatite host-rock (Thomas & Spooner 1988) have an average composition of 91 mole % H_2O, 6 mole % CH_4, 1 mole % CO_2, and 2 mole % NaCl, which is comparable with that of type-1 fluid in emerald from Pranqueira. These authors suggested that the unusual chemistry of these fluids result from mixing of a wallrock-derived CH_4–H_2O fluid, possibly of metamorphic origin, with a fluid released from the pegmatite. At the Gravelotte mine (Nwe & Morteani 1993), phenakite and emerald, which replaces the former mineral, occur on the flanks of a highly metasomatized albitite pegmatite body and in the biotite schist at and near its contact. Nwe & Morteani (1993) described an earliest type-1 inclusion, found in phenakite and emerald, with low salinity (<6 wt% NaCl in phenakite and <7 wt% NaCl in emerald) and up to 18 mole % CH_4 and small amounts of CO_2, Th between 250 and 400°C (Th phenakite > Th emerald), a type-2 fluid inclusion found in emerald, which is variable in both CH_4–CO_2 contents and salinity (6 to 20 wt% NaCl), Th between 170 and 400°C, and later type-3 and type-4 inclusions with up to 38 wt% NaCl, CH_4–CO_2-free. They indicated that the earliest fluids in type-1 inclusions in the phenakite become slightly more saline in the early emerald, rimming the phenakite, with a reduction of the CH_4 content. With progressive crystallization of more emerald and formation of type-2 inclusions, salinities increase and become more variable within individual crystals. Moreover, CH_4 decreases, whereas CO_2 increases. These authors explained these facts as the result of a mixture between type-1 fluids with a dense, high-salinity NaCl brine during this stage, causing a continuous trend from type-1 to type-3 inclusions.

The fluid inclusions found in Pranqueira are rather similar to those at Gravelotte; nevertheless, there are some important differences, which indicate a somewhat different evolution of the fluid. We consider that type-1 fluid, found in phenakite at Gravelotte and Pranqueira,

are quite similar, but at Franqueira they have no CO_2. However, the emerald from Franqueira has two types of fluid inclusion, type-1 (emerald) and type-2 (only found in the emerald core). Neither type of fluid inclusion shows a variable range of salinity, and their homogenization temperatures lie within a narrow interval. In some cases, the type-2 Th is higher than type-1 Th and, in other cases, both Th ranges overlap each other (Table 1). Thus, at Franqueira, the main difference between the two types of fluid inclusion in emerald is the variable CO_2 and CH_4 contents. We thus consider that a mixture with a high-salinity NaCl brine, as at the Gravelotte deposit, is unlikely to have taken place at Franqueira. However, a mixture between a CH_4–H_2O fluid, which was perhaps derived from the wallrock, with a fluid released from the pegmatite, as at Tanco, seems to be more likely.

Nevertheless, the presence of the H_2O–CO_2 ($\pm$ CH_4) inclusions in the emerald crystal core only and the H_2O–CH_4–($\pm$ CO_2) inclusions in the whole of the emerald crystal, along with the fact that both inclusion types homogenize to vapor, liquid and in some cases the critical state, indicate that the immiscibility process is the more likely. If a CO_2-rich fluid is added during emerald growth, CO_2-rich inclusions should be found within the whole of the emerald crystal and should only homogenize in one way (liquid or vapor). On the other hand, in the case of an immiscibility due to the reaction proposed above, the CO_2-rich inclusions should be formed when the oxidation process occurs, in other words, during the crystallization of the emerald core. Moreover, the salt content is very constant and low in all type-1 and type-2 inclusions, but it is a little high in type-2 inclusions. Mixing of fluids probably generates fluids with different salinity and CO_2:CH_4 ratios, as is the case at Gravelotte (Nwe & Morteani 1993). In Franqueira, the very constant salinity and CO_2:CH_4 ratios agree with an immiscibility model more than with a mixing of fluids.

Concerning the origin of type-1 (phenakite) CH_4-rich fluid, Thomas & Spooner (1988) postulated that the wallrock-derived CH_4–H_2O fluid formed as a result of metamorphic reactions involving graphitic sediment. The CH_4 content of fluid inclusions from the AEGC pegmatite fields (Fig. 5) is clearly correlated with the abundance of graphitic horizons in the host rocks and the closeness of the pegmatite samples selected to the host rock, this attesting the role of the host rocks in the geochemical signature of the fluids (Fuertes-Fuente *et al.* 2000). The Franqueira samples were extracted from metasomatic wallrock, whereas the samples of AEGC pegmatites were extracted from zones within the pegmatite bodies. This fact may have an influence on the richness in CH_4 of the fluid inclusions at Franqueira (Fig. 5). However, graphite has not been reported from the pegmatite's host-rock at Franqueira nor at Gravelotte (Nwe & Morteani 1993). Moreover, we discard the possibility of a purely metamorphic origin for type-1 (phenakite) fluid; some components of this fluid must have been derived from the pegmatite, since Be, Al and Si are necessary for the formation of phenakite and chrysoberyl. These minerals could not have come from the host rock because beyond the metasomatic zone; it contains no phenakite. Thus we leave open the dicussion about the source of type-1 (phenakite) CH_4-rich fluid.

Acknowledgements

This work has been financed by the CICYT, project GEO 91/1077, PB 96/0555. Supported by FPI of MEC fellowship to Fuertes. We thank to the reviewers for their encouraging suggestions, which have improved significantly the content and clarity of the paper.

References

Bakker, R.J. (1995): The application of a computerised and optimised clathrate stability model to fluid inclusion studies. *ECROFI, Bol. Soc. Esp. Mineral.* **18**(1), 15-17.

_____ (1997): Clathrates: computer programs to calculate fluid inclusion V–X properties using clathrate melting temperatures. *Comput. Geosci.* **23**, 1-18.

_____, Dubessy, J. & Cathelineau, M. (1996): Improvements in clathrate modelling. I. The H_2O–CO_2 system with various salts. *Geochim. Cosmochim. Acta* **60**, 1657-1681.

Barrera, J.L., Farias, P., Gonzalez, F., Marquinez, J., Martin, L.M., Martinez, J.R., Del Olmo, A. & De Pablo, J.G. (1989): Mapa Geológico 1:200.000 de Ourense/Verin. Memoria explicativa. *Publicación Instituto Technologico Geominero de España, Madrid, Spain.*

Barton, M.D. (1986): Phase equilibria and thermodynamic properties of minerals in the BeO–Al_2O_3–SiO_2–H_2O (BASH) system, with petrologic applications. *Am. Mineral.* **71**, 277-300.

Bowers, T.S. & Helgeson, H.C. (1983): Calculation of the thermodynamic and geochemical consequences of nonideal mixing in the system H_2O–CO_2–NaCl on phase relations in geologic systems: equation of state for H_2O–CO_2–NaCl fluids at high pressures and temperatures. *Geochim. Cosmochim. Acta* **47**, 1247-1275.

Brown, P.E. & Hagemann, S.G. (1995): Fluid inclusion data reduction and interpretation using MacFlincor on the Macintosh. *ECROFI, Bol. Soc. Esp. Mineral.* **18**(1), 32-33.

Capdevila, R. & Vialette, P. (1970): Estimation radiométrique de l'âge de la deuxième phase tectonique hercynienne en Galice moyenne (Nord-Ouest de l'Espagne). *C.R. Acad. Sci. Paris* **270**, *Sér.* D, 2527-2530.

Dallmeyer, R.D., Martínez Catalán, J.R., Arenas, R., Gil Ibarguchi, J.I., Gutiérrez- Alonso, G., Farias, P., Bastida, F. & Aller, J.(1997) Diachronous Variscan tectonothermal activity in the NW Iberian Massif: evidence from $^{40}Ar/^{39}Ar$ dating of regional fabrics. *Tectonophys.* **277**, 307-337.

DUBESSY, J. (1984): Simulation des équilibres chimiques dans le système C–O–H. Conséquences méthodologiques pour les inclusions fluides. *Bull. Minéral.* 107, 155-168.

_____, POTY, B. & RAMBOZ, C. (1989): Advances in the C–O–H–N–S fluid geochemistry based on micro-Raman spectroscopic analysis of fluid inclusions. *Eur. J. Mineral.* 1, 517-534.

_____, THIERY, R. & CANALS, M. (1992): Modelling of phase equilibria involving mixed gas clathrates; application to the determination of molar volume of the vapor phase and salinity of the aqueous solution in fluid inclusions. *Eur. J. Mineral.* 4, 873-884.

FARIAS, P., GALLASTEGUI, G., GONZÁLEZ LODEIRO, F., MARQUÍNEZ, J., MARTÍN PARRA, L.M., MARTÍNEZ-CATALÁN, J.R., DE PABLO MACÍA, J.G. & RODRÍGUEZ FERNÁNDEZ, L.R. (1987) Aportaciones al conocimiento de la litoestratigrafía y estructura de Galicia Central. *Mem. Fac. Cienc. Univ. Porto* 1, 411-431.

FERSMAN, A.E. (1929): Geochemische Migration der Elemente. III. Smaragdgruben im Uralgebirge. *Abh. z. praktischen Geologie u. Bergwirtschaft* 1, 74-116.

FUERTES-FUENTE, M. (1996): *Las pegmatitas del área de Lalín-Forcarei (Galicia) y las mineralizaciones de elementos escasos asociadas.* Ph.D. thesis, Univ. of Oviedo, Oviedo, Spain.

_____ & MARTÍN-IZARD, A. (1998): The Forcarei Sur rare element (Sn, Ta, Nb, Li, Be, Rb and P) pegmatite field and its associated mineralization, Galicia, Spain. *Can. Mineral.* 36, 303-325.

_____, _____, BOIRON, M.A. & MANGAS, J. (2000): Fluid evolution of rare-element and muscovite granitic pegmatites from central Galicia, NW Spain. *Mineral. Deposita* 35, 332-345.

_____, _____ & MOREIRAS, D. (1995): The Forcarei Sur zoned pegmatitic field, Galicia, northwestern Spain. *In* Mineral Deposit (J. Paleva, B. Kribek & K. Žák, eds.). Balkema, Rotterdam, The Netherlands (439-442).

GIULIANI, G., CHEILLETZ, A., ZIMMERMANN, J.L., RIBEIRO-ALTHOFF, A.M., FRANCO-LANCHO, C. & PIRAUD, G. (1997): Les gisements d'émeraude du Brésil: genèse et typologie. *Chron. Recherche Géol. Minière* 526, 17-61.

JACOBS, G.K. & KERRICK, D.M. (1981): Methane: an equation of state with application to the ternary system H_2O–CO_2–CH_4. *Geochim. Cosmochim. Acta* 45, 607-614.

KERRICK, D.M. & JACOBS, G.K. (1981): A modified Redlich–Kwong equation for H_2O, CO_2 and H_2O–CO_2 mixtures at elevated pressures and temperatures. *Am. J. Sci.* 281, 735-767.

KOKFELT-MADSEN, J. & ROSE-HANSEN, J. (1982): Volatiles associated with alkaline igneous rift activity: fluid inclusions in the Ilimaussaq intrusion and the Gardar granitic complexes (south Greenland). *Chem. Geol.* 37, 79-93.

LAZNICKA, P. (1985): *Empirical Metallogeny: Depositional Environments, Lithological Associations and Local Metallic Ores. 1. Phanerozoic Environments, Associations and Deposits.* Elsevier, Amsterdam, The Netherlands.

LONDON, D. (1986): Magmatic-hydrothermal transition in the Tanco rare element pegmatite: evidence from fluid inclusions and phase-equilibrium experiments. *Am. Mineral.* 71, 376-395.

MARTÍN-IZARD, A., PANIAGUA, A., MOREIRAS, D., ACEVEDO, R.D. & MARCOS-PASCUAL, C. (1995): Metasomatism at a granitic pegmatite – dunite contact in Galicia: the Franqueira occurrence of chrysoberyl (alexandrite), emerald, and phenakite. *Can. Mineral.* 33, 775-792.

_____, _____, _____, _____ & _____ (1996): Metasomatism at a granitic pegmatite – dunite contact in Galicia: the Franqueira occurrence of chrysoberyl (alexandrite), emerald, and phenakite: reply. *Can. Mineral.* 34, 1332-1336.

MARTÍNEZ CATALÁN, J.R., ARENAS, R., DÍAZ GARCÍA, F., RUBIO PASCUAL, F.J., ABATI, J. & MARQUÍNEZ, J. (1996): Variscan exhumation of a subducted Paleozoic continental margin: the basal units of the Ordenes Complex, Galicia, NW Spain. *Tectonics* 15, 106-121.

MATTE, P.H. (1968): La structure de la virgation hercynienne de Galicia (Espagne). *Géol. Alpine* 44, 157-280.

MONTERRUBIO, S. (1991): *Mineralizaciones asociadas a rocas ultrabásicas en el hercínico español.* Ph.D. thesis, Univ. Complutense de Madrid, Madrid, Spain.

NWE, Y.Y. & MORTEANI, G. (1993): Fluid evolution in the H_2O–CH_4–CO_2–NaCl system during emerald mineralization at Gravelotte, Murchison Greenstone Belt, northeast Transvaal, South Africa. *Geochim. Cosmochim. Acta* 57, 89-103.

POTTER, R.W., II & BROWN, D.L. (1977): The volumetric properties of aqueous sodium chloride solutions from 0° to 500°C at pressures up to 2000 bars based on a regression of available data in the literature. *U.S. Geol. Surv., Bull.* 1421-C, 1-36.

_____, CLYNNE, M.A. & BROWN, D.L. (1978): Freezing point depression of aqueous sodium chloride solutions. *Econ. Geol.* 73, 284-285.

POTY, B., LEROY, J. & JACHIMOWICZ, L. (1976): Un nouvel appareil pour la mesure des températures sous le microscope; l'installation de microthermométrie Chaixmeca. *Bull. Soc. Fr. Minéral. Cristallogr.* 99, 182-186.

PRICHARD, H.M.A. & DEN TEX, E. (1984) Tracing crustal evolution in the NW Iberian Peninsula through the Pb–Sr and U–Pb systematics of Paleozoic granitoids: a review. *Phys. Earth Planet. Int.* 35, 121-130.

ROEDDER, E. (1984): Fluid inclusions. *Rev. Mineral.* 12.

SERRANO PINTO, M., CASQUET, C., IBARROLA, E., CORRETGE, L.G. & PORTUGAL FERREIRA, M. (1987): Síntese geocronológica dos granitoides do Maciço Hesperico. *In* Geología de los granitoides y rocas asociadas del Macizo Hesperico (F. Bea, A. Carnicero, M. Lopez-Plaza & M.D. Rodriguez Alonso, eds.). Rueda, Madrid, Spain (69-86).

SINKANKAS, J. (1989): *Emerald and Other Beryls*. Geoscience Press, Prescott, Arizona.

SNEE, L.W. & KAZMI, A.H. (1989): Origin and classification of Pakistani and world emerald deposits. *In* Emeralds of Pakistan: Geology, Gemology and Genesis (A.H. Kazmi & L.W. Snee, eds.). Van Nostrand Reinhold Co., New York, N.Y. (229-230).

THIERY, R., VIDAL, J. & DUBESSY, J. (1994): Phase equilibria modelling applied to fluid inclusions: liquid–vapor equilibria and calculations of the molar volume in the CO_2–CH_4–N_2 system. *Geochim. Cosmochim. Acta* **58**, 1073-1082.

THOMAS, A.V. & SPOONER, E.T.C. (1988): Fluid inclusions in the system H_2O–CH_4–NaCl–CO_2 from metasomatic tourmaline within the border unit of the Tanco zoned granitic pegmatite, S.E. Manitoba. *Geochim. Cosmochim. Acta* **52**, 1065-1075.

VAN CAELTEREN, P.W.C., BOELRIJK, N.A.I.M., HEBEDA, E.H., PRIEM, H.N.A., DEN TEX, E., VERDURMEN, E.A.T. & VERSCHURE, R.H. (1979): Isotopic dating of older elements (including the Cabo Ortegal mafic-ultramafic complex) in the Hercynian Orogen of NW Spain: manifestations of a presumed Early-Paleozoic mantle-plume. *Chem. Geol.* **24**, 35-56.

ZHANG, YI-GANG & FRANTZ, J.D. (1987): Determination of the homogenization temperatures and densities of supercritical fluids in the system NaCl–KCl–$CaCl_2$–H_2O using synthetic fluid inclusions. *Chem. Geol.* **64**, 335-350.

Received March 27, 1998, revised manuscript accepted September 21, 2000.

BULLETIN OF MARINE SCIENCE, 67(3): 989–996, 2000

ANNUAL REPRODUCTIVE PERIODICITY OF THE SEA URCHIN *DIADEMA ANTILLARUM* PHILIPPI IN THE CANARY ISLANDS

M. J. Garrido, R. J. Haroun and H. A. Lessios

ABSTRACT

The tropical sea urchin *Diadema antillarum* is found on both coasts of the Atlantic Ocean. Several studies exist of the reproductive cycles of western Atlantic populations, but despite the extreme abundance of the species in the Canary Islands, nothing is known about its reproduction in this region. We present data on annual reproductive periodicity of eastern Atlantic populations. We determined gonadal indices at two locations in the island of Gran Canaria, Canary Islands. Though water in the southern location is warmer, reproductive cycles are similar. Gonadal content increases between October and April (or May), then declines (presumably due to spawning) until September (or October). The spawning season coincides with the period of most rapid temperature rise, but the new reproductive cycle is initiated as temperature continues to increase. In addition to temperature, reproductive cycles may be related to seasonal increases of benthic algal productivity.

Intraspecific comparisons of reproductive cycles of marine invertebrates can aid in isolating environmental factors that promote synchrony between individuals and influence the timing of spawning of each population. Studies of conspecific populations of tropical echinoids have revealed wide variation in annual reproductive periodicity (Pearse and Cameron, 1991). In the Indo-West Pacific, *Diadema setosum* spawns from June to September in both Japan (Yoshida, 1952) and the Red Sea (Pearse, 1970), and also spawns in the austral summer months in the Great Barrier Reef (Stephenson, 1934), but it reproduces continuously throughout the year in the Philippines (Tuason and Gomez, 1979) and Singapore (Hori et al., 1987). *Tripneustes gratilla* reproduces from November to April in the Red Sea (Pearse, 1974, 1983), from September to November in Taiwan (Chen and Chang, 1981), from June to November in the Philippines (Tuason and Gomez, 1979) and from April to June in New South Wales, Australia (O'Connor et al., 1978). In the Caribbean, *Lytechinus variegatus* breeds between April and June in Bermuda (Moore et al., 1963), continuously with no discernible peaks in Panama (Lessios, 1985) throughout the year but with peaks between May and August in Florida (Moore et al., 1963; Moore and Lopez, 1972), between October and December in Puerto Rico (Cameron, 1986), and between June and September in Jamaica (Greenway, 1976). *Tripneustes ventricosus* breeds continuously in Florida (McPherson, 1965) and in Panama (Lessios, 1985), but it concentrates its reproduction to mid-winter and mid-summer in Puerto Rico (Cameron, 1986), or just the summer in Barbados (Lewis, 1958). *Echinometra lucunter* in Barbados spawns once a year in wave-swept areas, but twice a year in protected habitats (Lewis and Storey, 1984). The same species has well-defined reproductive periods in Florida (McPherson, 1969) and Puerto Rico (Cameron, 1986), but no discernible peaks in Panama (Lessios, 1981, 1985). *Diadema antillarum* is no exception to this variation in annual reproductive pattern among different populations. It spawns throughout the year in the Virgin Islands (Randall et al., 1964) and in Panama (Lessios, 1981), from January to April at Barbados (Lewis, 1966), from October to December in the Florida Keys (Bauer, 1976), and from April to October at Bermuda (Iliffe and Pearse, 1982). We were interested in determining whether populations on the other side of the Atlantic reproduce periodically, and if so, the nature of the cycles.

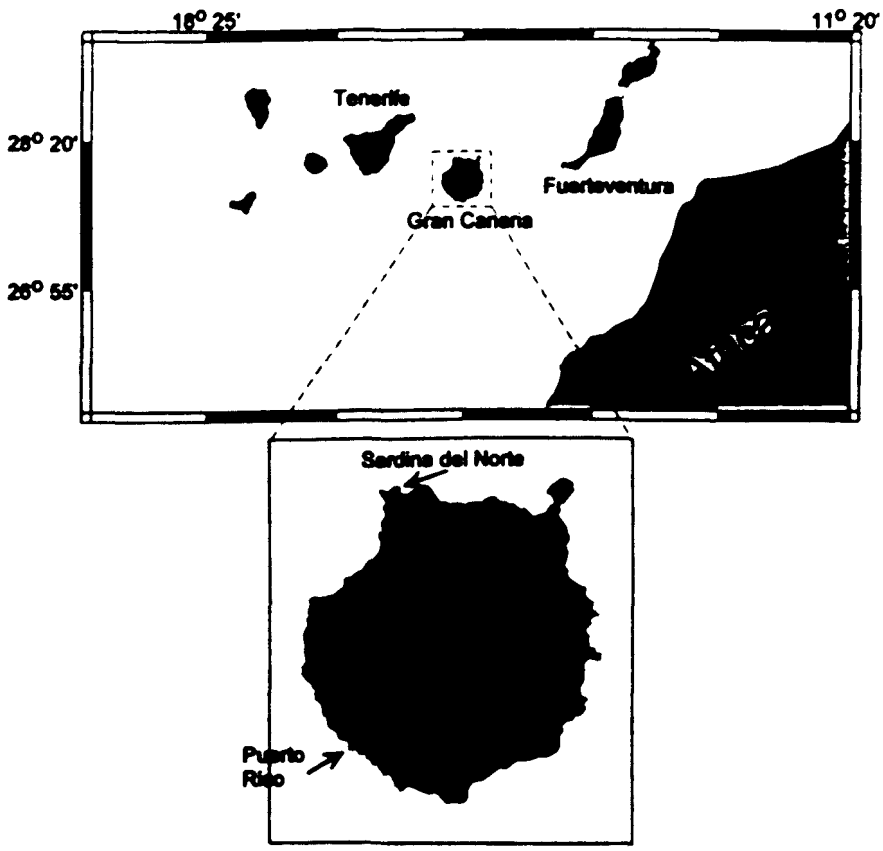

Figure 1. Localities in Gran Canaria Island (eastern Atlantic Ocean) where sea urchins were collected.

Materials and Methods

The island of Gran Canaria is located in the Canarian Archipelago, between Tenerife and Fuerteventura (Fig. 1). The prevailing trade winds blow from the northeast; they drive the sea surface waters southwards, forming the Canary Current. Coastal water temperatures in Gran Canaria from 1981 to 1985 fluctuated between 18° and 25°C (Llinas, 1988). The northern coast is subjected to higher turbulence and more mixing of the thermocline; during the winter months it becomes colder than the southern coast. Average temperatures in February are 1°C colder in the North than in the South. These environmental differences between North and South coasts of each island are a common feature of the entire Canary Archipelago (Aristegui et al., 1989).

We established two collecting stations, Sardina del Norte on the north coast of Gran Canaria, and Puerto Rico on the south coast (Fig. 1). 22 to 25 individuals of *D. antillarum* larger than 3 cm in horizontal diameter were sampled at depths of 4–6 m in monthly intervals from January 1997 to March 1998 . Collections were made each month at the same phase of the moon, to avoid complications arising from the lunar spawning cycle, which in *D. antillarum* is superimposed on the annual cycle (Iliffe and Pearse,1982; Lessios, 1984, 1988a, 1991). During each collection, sea surface temperature was measured with a hand thermometer.

Two dimensions were measured in each sea urchin to the nearest 0.1 mm: (1) the horizontal diameter of the test at the ambitus, and (2) the oral-aboral axis, as the distance between the apex of the periproct and the plane defined by the three lowest points of the test at the oral side. Then the sea urchins were dissected, and the total volume of the gonads was measured to the nearest 0.1 ml by displacement in sea water. The tests with the spines attached, along with the removed oral piece and the lantern, were labeled and dried for 24 h at 110°C. Then they were weighed to the nearest 0.01 g.

Gonad content was normalized through the calculation of gonadal indices. We defined gonadal index in two ways: (1) as the ratio of gonad volume to dry body weight, multiplied by 100 and (2)

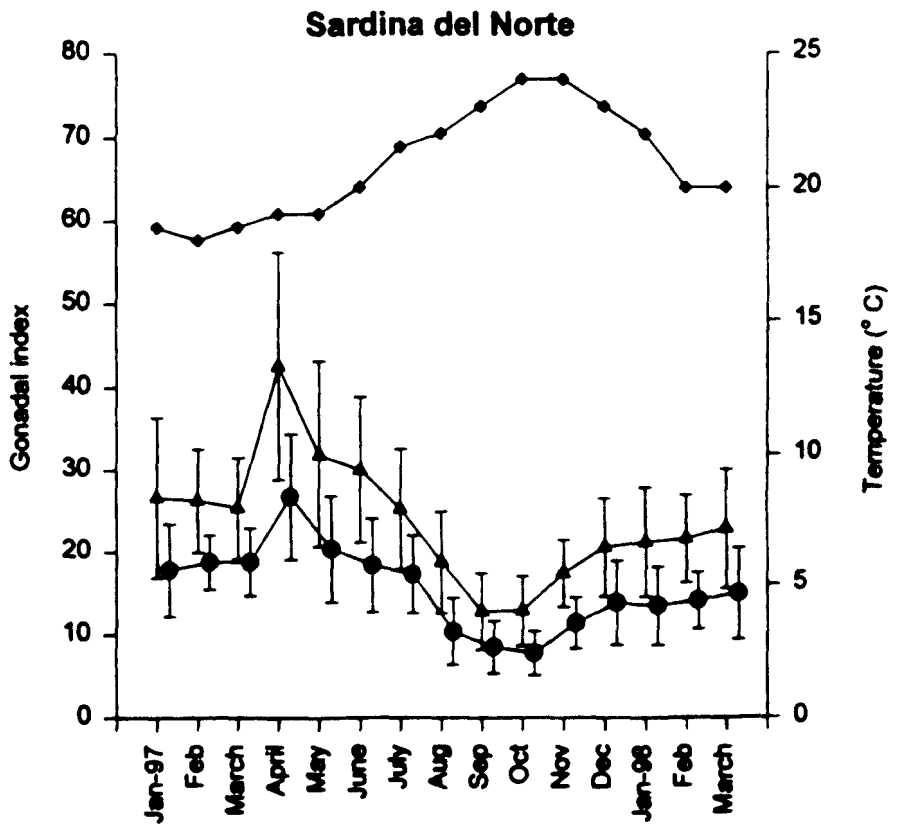

Figure 2. Mean and 1 SD of gonadal index of *Diadema antillarum* over time at Sardina del Norte. Gonadal index is calculated as ml of gonad per gram somatic dry weight, multiplied by 100 (triangles), or as ml of gonad per ml of test volume, multiplied by 100 (circles). Temperature (squares) is plotted on the right y axis.

as the ratio of gonad volume to test volume, multiplied by 100. Test volume was calculated as that of a solid created by an ellipse rotated around its shortest axis, i.e., $V = (4/3)\,\pi\,a^2\,b$, where a is the radius of the ambitus and b is 0.5 of the oral-aboral axis.

Results

As might be expected, there was a tight relationship between test volume and test weight [Volume (in ml) = −5.65 + 2.32 weight (in g), $r^2 = 0.76$, $P < 0.00001$]. Thus, fluctuations in gonadal content through time can be represented without altering conclusions as either volume of gonad per volume of test, or as volume of gonad per weight of somatic tissue. Both in Sardina del Norte (Fig. 2) and at Puerto Rico (Fig. 3) the trends deduced by either method are equivalent. Gonadal content increases between October and February as sea water temperatures decline. It continues to increase between February and April (in Sardina del Norte) or May (in Puerto Rico) as the temperature rises, then declines until September or October as the temperature continues to rise. The lowest gonadal content of the year does not coincide with the warmest month, because after October the sea urchins appear to start a new cycle of building up their gonads, even though the temperature continues to increase until November. The three months (January to March) sampled in both 1997 and 1998 have similar values of gonadal index between years, suggesting that the fluctuations are, indeed, periodic.

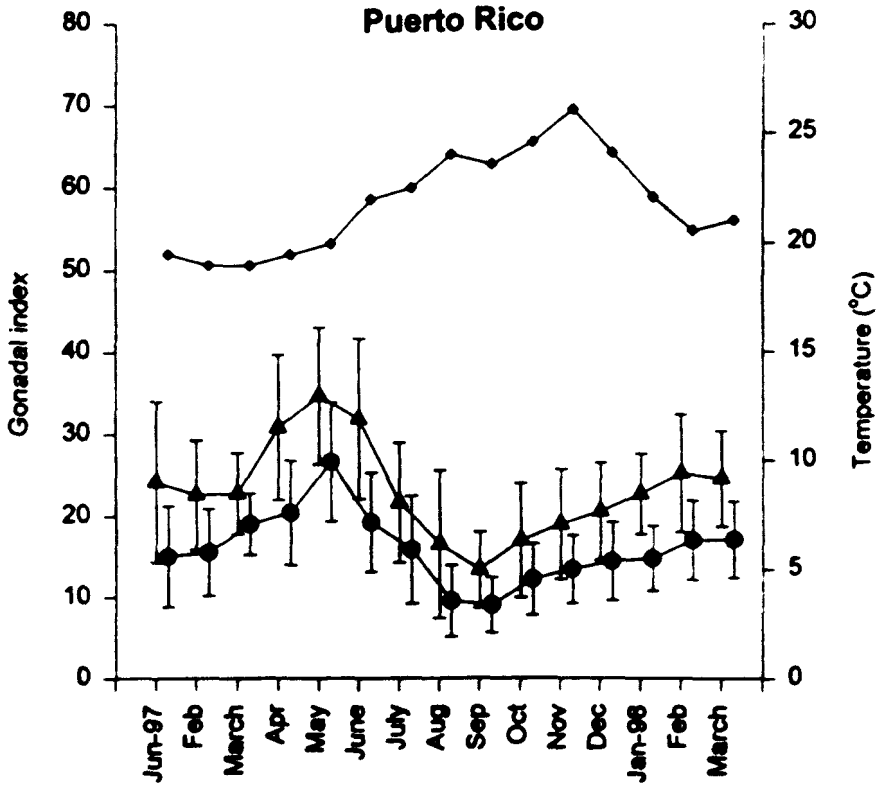

Figure 3. Mean and 1 SD of gonadal index of *Diadema antillarum* over time at Puerto Rico. Gonadal index is calculated as in Fig. 2. Note change of scale (relative to Figure 2) of the temperature axis on the right.

Discussion

Though the Canary Archipelago is south of Bermuda, it (along with Madeira) is the least tropical environment in which *D. antillarum* is found, because of water temperature regimes imposed by currents. The differences in water temperature between these areas are reflected in faunal composition. Unlike Bermuda, the Canaries lack hermatypic corals. *Diadema* is the only genus of tropical sea urchin extant in the Archipelago (Sanchez and Batet, 1991). The environment is seasonal not just in temperature, but also in primary productivity and zooplankton concentration (Braun et al., 1985; Arístegui et al., 1989; Fernández de Puelles and García-Braun, 1989). Thus, it is not surprising that populations in both localities we sampled showed well-defined, synchronized reproductive cycles. The question is which environmental variable (or combination of variables) controls reproductive cycles as a proximate or ultimate factor.

Evidence regarding the effects of temperature on gametogenic cycles of echinoids is often uncertain and sometimes conflicting (review in Pearse and Cameron, 1991). However, correlations between the reproductive cycles of natural populations and seasonal temperature fluctuations tend to support the possible existence of a link between the two. This tentative relation between temperature fluctuations and annual reproductive cycles is seen in previous studies of *D. antillarum*. On the Atlantic coast of Panama, where temperature fluctuations are minimal, this species shows little synchronization of the reproductive cycles of individuals comprising each population (Lessios, 1981). Limited data support a similar lack of a population-wide cycle in the Virgin Islands (Randall et al.,

1964). In Florida, where temperature fluctuates seasonally, there is clear accumulation of gonadal material between July and November, with a sharp decrease between November and December, correlated with decreasing sea water temperatures (Bauer, 1976). In Barbados, despite annual temperature fluctuations <1.5° C, *Diadema* has pronounced reproductive cycles, repeated from one year to the next, with spawning concentrated during the coldest months of April and May (Lewis, 1966). In Bermuda, another seasonal environment, gonads are being built up as temperature increases, but there are two apparent spawning periods, one in early summer, the other in late fall, thus complicating any direct correlation between temperature and reproduction (Iliffe and Pearse, 1982).

Our data indicate that in the Canaries there is a relation between water temperature and *D. antillarum* reproduction, but do not clarify whether the reproductive cycles respond to temperature per se. The animals appear to begin spawning in April at Sardina del Norte when the temperature reaches 19°C and in May at Puerto Rico, when the temperature has reached 20°C. In both locations the period of gonadal decline, which presumably signifies active spawning, coincides with the period of rapid temperature rise. Gonadal content reaches its minimum in September, when it is 23°C in Sardina del Norte and 23.5°C in Puerto Rico. In both localities, the spawning period coincides with the times of most rapid temperature increase, up to the point that the gonads reach their minimum relative size. However they stop declining in September–October, even though the temperature continues to rise. Iliffe and Pearse (1982) have attributed a similar quiescence of gonadal growth in *D. antillarum* at Bermuda to direct inhibition by high temperatures. This may well be true, but it also possible that this is an indirect result of repeated spawning. If the decline in gonadal index is the result of the inability of each animal to build up nutrients faster than they are depleted by the release of gametes, and if reproduction is triggered by increasing temperatures, a point will be reached at which gonads are at their minimum size, even as temperature continues to increase. Only when spawning stops, possibly as the result of a drop in temperature, will gonadal size begin to increase once again.

Of course, it is also quite possible that there is no direct link between temperature and reproduction, and that correlation between the two is the unavoidable coincidence of two independent variables each cycling with an annual period. Other seasonally fluctuating variables that may regulate reproduction in *D. antillarum* are photoperiod, phytoplankton blooms, and food availability. Pearse et al. (1986) have shown experimentally that gametogenesis in *Strongylocentrotus purpuratus* is under photoperiodic control. McClintock and Watts (1990) found a similar effect of photoperiod on the annual reproduction of the tropical species *Eucidaris tribuloides*. However, if photoperiod affects the reproductive cycles of *D. antillarum*, it must do so in different ways on the two sides of the Atlantic. Even though the latitude of Florida Keys and the Canaries only differs by 3°C, the cycles of *Diadema* populations from the two locations are 2 mo out of phase. Phytoplankton blooms have been shown to trigger spawning in *S. droebachiensis* (Starr et al., 1990, 1993). However, the seasonal peak in phytoplankton in the Canaries is reached in February, 2–3 mo before *D. antillarum* initiates its spawning (Braun et al., 1985; Arístegui et al., 1989; Fernández de Puelles and García-Braun, 1989). Thus, *Diadema* does not appear to time its reproduction in a manner that would maximize food for its larvae.

Though photoperiod and plankton blooms seem unlikely proximate or ultimate factors of *D. antillarum* annual reproductive cycles, food availability for the adults may not be entirely unrelated to reproduction. Though the species suffered severe mass mortality in the entire western Atlantic during 1983–4 (Lessios et al., 1984; Lessios, 1988b), its popu-

lations in the Canaries continue to be extremely dense. Subtidal hard substrata where *Diadema* is found are bare of macroalgae, even though shallower areas are thickly covered by *Cystoseira* and other erect algae (Johnston, 1969; Carillo Pérez and Cruz Simó, 1992). It is, therefore, possible that *Diadema* in the Canaries is food limited. No data exist on seasonal changes in benthic primary productivity. It is, however, known that where *Diadema* is absent, biomass of *C. albies-marina* increases rapidly between March and June (Medina and Haroun, 1993). This is likely to be due to the Spring disruption of the thermocline by turbulence that also causes an increase of nutrients and phytoplankton blooms. In areas where *Diadema* is present, these algae may be quickly consumed, so that there is no visible increase in standing crop; yet, they would represent a seasonal pulse of nutrition for *Diadema* . Such a pulse may be a contributing factor to the gonadal buildup we have seen between March and April. Increased benthic primary productivity due to turbulence may also account for the earlier initiation of reproduction (despite lower temperatures) in the northern locality, which is more exposed to the trade winds. Of course, fluctuations in food availability would be a factor in reproduction only to the extent that reproduction is negatively affected by inadequate food supply during part of the year. It remains to be determined whether such a limitation exists. Experimental studies are needed to determine the relative contributions of temperature and food in the control of gemetogenesis of *Diadema*.

Acknowledgments

We thank Á. Santana for statistical advice, and J. Suárez and the students of Marine Science Faculty, L. Alou, A. Torres, J. García, J. M. Alsina and J. C. Suárez for their help in the field and in the laboratory.

Literature Cited

Arístegui, J., S. Hernández-León, M. Gómez, L. Medina, A. Ojeda and S Torres. 1989. Influence of the north trade winds on the biomass and production of neritic plankton around Gran Canaria island. Topics Mar. Biol. 53: 223–229.

Bauer, J. C. 1976. Growth, aggregation and maturation in the echinoid, *Diadema antillarum* Philippi. Bull. Mar. Sci. 26: 273–277.

Braun, J. G., I. Orzaiz, J. D. Armas and F. Real 1985. Productividad y biomasa del ultraplancton, nanoplacton y fitoplancton de red en aguas de las Islas Canarias. Bol. Inst. Esp. Oceanogr. 2: 192–204.

Cameron, R. A. 1986. Reproduction, larval occurrence and recruitment in Caribbean sea-urchins. Bull. Mar. Sci. 39: 332–346.

Carillo Pérez, M., and T. Cruz Simó. 1992. Estudio de las comunidades vegetales marinas y poblaciones faunisticas del litoral de Timanfaya, Sevicio de Publicaciones de la Caja General de Ahorros de Canarias, Santa Cruz de Tenerife. 223 p.

Chen, C. P. and K.-H. Chang. 1981. Reproductive periodicity of the sea urchin *Tripneustes gratilla* (L.) in Taiwan compared with other regions. Int'l. J. Inv. Reprod. 3: 309–319.

Fernández de Puelles, M. and J. A. García-Braun. 1989. Dinámica de las comunidades planctónicas en una zona del Atlántico Subtropical (Isla de Tenerife). Bol. Inst. Esp. Oceanogr. 5: 87–100.

Greenway, M. 1976. The grazing of *Thalassia testudinum* in Kingston Harbour, Jamaica. Aquat. Bot. 2: 117–126.

Hori, R., V. P. E. Phang and T. J. Lam 1987. Preliminary study on the pattern of gonadal development of the sea urchin, *Diadema setosum*, off the coast of Singapore. Zool. Sci. 4: 665–673.

Iliffe, T. M. and J. S. Pearse 1982. Annual and lunar reproductive rhythms of the sea urchin, *Diadema antillarum* (Philippi) [sic] in Bermuda. Int'l. J. Inv. Reprod. 5: 139–148.

Johnston, C.S. 1969. Studies on the ecology and primary production of Canary Islands marine algae. Pages 213–222 *in* R. Margalef, ed. Proc. 6th Int'l. Seaweed Symp, vol. 6, Subsecretaría de la Marina Mercante, Madrid.

Lessios, H. A. 1981. Reproductive periodicity of the echinoids *Diadema* and *Echinometra* on the two coasts of Panama. J. Exp. Mar. Biol. Ecol. 50: 47-61.

_____. 1984. Possible prezygotic reproductive isolation in sea urchins separated by the Isthmus of Panama. Evolution 38: 1144–1148.

_____. 1985. Annual reproductive periodicity in eight echinoid species on the Caribbean coast of Panama. Pages 303–311 *in* B. F. Keegan and B. D. O'Connor, eds. Echinodermata. Proc. 5th Int'l. Echinoderm Conf., Galway, A.A. Balkema, Rotterdam.

_____. 1988a. Population dynamics of *Diadema antillarum* (Echinodermata: Echinoidea) following mass mortality in Panamá. Mar. Biol. 99: 515–526.

_____. 1988b. Mass mortality of *Diadema antillarum* in the Caribbean: what have we learned? A. Rev. Ecol. Syst. 19: 371–393.

_____. 1991. Presence and absence of monthly reproductive rhythms among eight Caribbean echinoids off the coast of Panama. J. Exp. Mar. Biol. Ecol. 153: 27–47.

_____, D. R. Robertson and J. D. Cubit. 1984. Spread of *Diadema* mass mortality through the Caribbean. Science 226: 335–337.

Lewis, J. B. 1958. The biology of the tropical sea urchin *Tripneustes esculentus* Leske in Barbados, British West Indies. Can. J. Zool: 36: 607–621.

_____. 1966. Growth and breeding in the tropical echinoid *Diadema antillarum* Philippi. Bull. Mar. Sci. 16: 151–158.

_____ and G. S. Storey. 1984. Differences in morphology and life history traits of the echinoid *Echinometra lucunter* from different habitats. Mar. Ecol. Prog. Ser. 15: 207–211.

Llinas, O. 1988. Análisis de la distribución de nutrientes en la masa de agua Noratlántica en las Islas Canarias. Ph.D. Thesis . Univ. La Laguna, Tenerife.

McClintock, J. B. and S. A. Watts. 1990. The effects of photoperiod on gametogenesis in the tropical sea urchin *Eucidaris tribuloides* (Lamarck) (Echinodermata, Echinoidea). J. Exp. Mar. Biol. Ecol. 139: 175–184.

McPherson, B. F., 1965. Contributions to the biology of the sea urchin *Tripneustes ventricosus*. Bull. Mar. Sci. 15: 228–244.

_____. 1969. Studies on the biology of the tropical sea urchins, *Echinometra lucunter* and *E. viridis*. Bull. Mar. Sci. 19: 194–213.

Medina, M. and R. Haroun. 1993. Preliminary study on the dynamics of *Cystoseira abies-marina* populations in Tenerife (Canary Islands). Courier Forsch.-Inst. Senckenberg. 159: 109–112.

Moore, H. B., T. Jutare, J. C. Bauer and J. A. Jones. 1963. The biology of *Lytechinus variegatus*. Bull. Mar. Sci. Gulf Carib. 13: 23–53.

_____ and N. N. Lopez. 1972. Factors controlling variation in the seasonal spawning pattern of *Lytechinus variegatus*. Mar. Biol. 14: 275–280.

O'Connor, C., G. Riley, S. Lefebre and D. Bloom. 1978. Environmental influences on histological changes in the reproductive cycle of four New South Wales sea urchins. Aquaculture 15: 1–17.

Pearse, J. S. 1970. Reproductive periodicities of Indo-Pacific invertebrates in the Gulf of Suez. III. The echinoid *Diadema setosum* (Leske). Bull. Mar. Sci. 20: 697–720.

_____. 1974. Reproductive patterns of tropical reef animals: three species of sea urchins. Proc. 2nd Int'l. Coral Reef Symp. 1: 235–240.

_____. 1983. The Gulf of Suez: signs of stress on a tropical biota. Pages 148–159 *in* M. F. Thompson, A. F. Latif and A. R. Bayoumi, eds. Proc. Int'l. Conf. Mar. Sci. Red Sea, Bull. Inst. Oceanogr. Fish (Egypt).

_____ and R. A. Cameron. 1991. Echinodermata: Echinoidea. Pages 513–662 *in* A. C. Giese, J. S. Pearse and V. B. Pearse, eds. Reproduction of marine invertebrates, vol. 6. Echinoderms and Lophophorates, Boxwood Press, Pacific Grove, California.

_____, V. B. Pearse and K. K. Davis. 1986. Photeperiodic regulation of gametogenesis and growth in the sea urchin *Strongylocentrotus purpuratus*. J. Exp. Zool. 237: 107–118.

Randall, J. E., R. E. Schroeder and W. A. Starck. 1964. Notes on the biology of the echinoid *Diadema antillarum*. Carib. J. Sci. 4: 421–433.

Sánchez, J. M. P. and E. M. Batet. 1991. Invertebrados marinos de Canarias, Ediciones del Cabildo Insular de Gran Canaria, Las Palmas de Gran Canaria. 335 p.

Starr, M., J. H. Himmelman and J. C. Therriault. 1990. Direct coupling of marine invertebrate spawning with phytoplankton blooms. Science 247: 1071–1074.

_____, _____, and _____. 1993. Environmental control of green sea urchin, *Strongylocentrotus droebachiensis*, spawning in the St. Lawrence Estuary. Can. J. Fish.. Aquat. Sci. 50: 894–901.

Stephenson, A. 1934. The breeding of reef animals. II. Invertebrates other than corals. Great Barrier Reef Exped. 1928–1929. Sci. Rep. 3: 247–272.

Tuason, A. Y. and E. D. Gomez. 1979. The reproductive biology of *Tripneustes gratilla* (Echinoidea: Echinodermata) with some notes on *Diadema setosum* Leske. Proc. Int'l. Symp. Mar. Biogeogr. Evol. Southern Hemisphere, Auckland, New Zealand. 17–20 July 1978 2: 707–716.

Yoshida, M., 1952. Some observations on the maturation of the sea urchin, *Diadema setosum*. Annotnes Zool. Jap. 25: 265–271.

DATE SUBMITTED: November 1, 1999. DATE ACCEPTED: May 19, 2000.

ADDRESSES: (M.J.G., R.J.H.) *Departamento de Biología, Facultad de Ciencias del Mar, Universidad de Las Palmas de Gran Canaria, 35017 Las Palmas de Gran Canaria, Spain.* CORRESPONDING AUTHOR: (H.A.L.) *Smithsonian Tropical Research Institute, Apartado 2072, Balboa, Panama. Tel. (507) 212-8708, Fax (507) 212-8790, E-mail: <lessiosh@naos.si.edu>.*

Transformación de coladas básicas alcalinas subaéreas en lavas almohadilladas en ambiente litoral: un ejemplo del Plioceno, Norte de la isla de Gran Canaria

D. Gimeno[1], F.J. Pérez Torrado[2], J.L. Schneider[3] y P. Wassmer[4]

1 Dpto. de Petrología, Geoquímica y Prospección Geológica. Facultad de Ciencias Geológicas. Universidad de Barcelona. Zona Universitaria de Pedralbes. 08071-Barcelona

2 Dpto. Física-Geología. Facultad de Ciencias del Mar. Universidad de Las Palmas de Gran Canaria. Campus Universitario de Tafira. 35017-Las Palmas de Gran Canaria

3 Département des Sciences de la Terre. Université de Lille. Bât. SN5. 59655 Villeneuve d'Ascq Cedex (Francia)

4 CEREG. Université de Strasbourg (Francia).

ABSTRACT

This note descrites the transition of a basic lava flow (4.3-4.15 m.y.) belonging to initial events of Roque Nublo volcanic group to submarine pillow lava flows in the northeastern shoreline of Gran Canaria island. The host littoral environment is characterized by a flat shallow shelf covered by a decimeter to meter thick level of white even laminated marine sediments. The lava rivers flowed some 20 km from the center of Gran Canaria island towards the sea, and 3 km inside of the shallow shelf. The bottom of the pillows level crops out in the range of 75-140 m above present sea level, and is constituted by a 20 m thick level of dominant pillow lava flows, and minor pillow breccia and hyaloclastite. It is characteristic the absence of hyaloclastite delta, and the pillow tubes are intrusive in the underlying white marine sediments. A number of lithofacies (peperitization, in situ hyaloclastite formation, fluidification of sediment, erosion and bulldozing of sediment) are characteristic of this lower section of pillow pile. The pillow shows evidence of shallow water column (multiple rind structure), fast flow (hollow pillows) and moderate degasification of the magma (segregation of phenocrystals towards the glassy rinds). The upper transition of the pillow pile to pahoehoe flows shows a characteristic lithofacies constituted by metric feeder tubes filled with hyaloclastites generated in situ.

Key words: *pillow lava, subaerial to submarine transition, feeder tubes filled with hyaloclastites in situ, Gran Canaria.*

INTRODUCCIÓN

La llegada de coladas lávicas a un medio subacuático es un fenómeno conocido desde antiguo, en especial en el caso de islas oceánicas (véase p.e. Jones y Nelson, 1970); es característica la formación de nubes de vapor en la zona de interacción agua-magma, la generación de hialoclastitas en las zonas de playa y, frecuentemente, un notable incremento areal en la zona emergida como se observó en la erupción del Teneguía en la isla de la Palma en el año 1971 (Afonso *et al.* 1974). Por el contrario, la transformación de coladas subaéreas en lavas almohadilladas en ambiente litoral es mucho menos conocida, debido esencialmente a que por motivos obvios se necesita estudiar afloramientos de difícil acceso. Los afloramientos de lavas almohadilladas y su significado general (entrada de flujos lávicos subaéreos canalizados por la red fluvial en una extensa plataforma marina de baja profundidad) que nos ocupan en esta nota son conocidos desde hace tiempo (Vuagnat 1960; Afonso *et al.* 1969; Lietz y Schmincke, 1975; Schmincke y Staudigel, 1976; ITGE, 1992) y aunque incluso han sido empleados por su excelencia para ilustrar este tipo de litofacies subacuáticas en obras de amplia difusión (Araña y Carracedo, 1978, McPhie *et al.* 1993) nunca han sido objeto de estudio específico.

CONTEXTO GEOLÓGICO

El crecimiento subaéreo de Gran Canaria se realizó durante 3 ciclos magmáticos conocidos como Ciclo I (Mioceno), Ciclo II o Roque Nublo (Plioceno) y Ciclo III (Plio-Cuaternario). Entre los Ciclos I y II (entre 8.5 y 5.3 m.a., aproximadamente) existe un periodo de inactividad volcánica (o atendiendo a datos recientes, habría que denominarlo como periodo de actividad volcánica muy residual —ver Pérez Torrado *et al.*, este volumen—) en el que tiene

lugar un fuerte desmantelamiento erosivo de la isla. Coincidiendo con este periodo y prolongándose durante el Ciclo II, se forman los depósitos volcano-sedimentarios de la Formación Detrítica de Las Palmas —FDLP— (Gabaldón *et al.*, 1989; ITGE, 1992) (Fig. 1), la cual se divide en tres miembros: a) Miembro Inferior formado durante este hiato volcánico y que comprende una serie de depósitos conglomeráticos (con cantos de naturaleza fonolítica del Ciclo I) de carácter aluvial; b) Miembro Medio, que comprende depósitos marinos de características litorales formados al final del hiato volcánico (entre los 5 a 4 m.a., aproximadamente), fruto de un periodo transgresivo en el que se encontraba inmersa Gran Canaria, a los que se asocian los depósitos de lavas almohadilladas descritos en esta nota, y c) Miembro Superior que incluye una sucesión de depósitos aluviales, laháricos y piroclásticos, con ocasionales lavas intercaladas, formados contemporáneamente al Ciclo II.

La actividad volcánica del Ciclo II se caracteriza por el desarrollo de un estratovolcán en el centro de la isla y en cuya evolución se suceden mecanismos eruptivos y materiales muy diferentes (Pérez Torrado *et al.*, 1995). Así, durante los primeros signos de actividad volcánica de este edificio, tiene lugar una serie de emisiones de lavas básicas (basaltos alcalinos a basanitas) que, canalizadas a través de una red de paleobarrancos y formando flujos tipo pahoehoe, logran alcanzar los sectores costeros del N y NE de la isla, ganando al mar una superficie de unos 40 km^2 (Pérez Torrado *et al.*, 1995) y formando una secuencia de estructuras de transformación que son el objeto de este estudio. Estas lavas han sido datadas en unos 4.15-4.3 m.a. (Lietz y Schmincke 1975, ITGE 1992) y sus principales afloramientos, reflejados en la cartografía oficial (ITGE, 1992), están ubicados en los barrancos de Tamaraceite y Quintanilla, barrios de Schaman, Escaleritas y Salto el Negro en Las Palmas de Gran Canaria, y frente costero entre Las Palmas de Gran Canaria y Punta de Arucas (Fig. 1).

CARACTERÍSTICAS DE LAS LAVAS ALMOHADILLADAS Y LITOFACIES MÁS SIGNIFICATIVAS

Las lavas almohadilladas reposan, bien sobre un nivel guía marino blanco (e.g., Barranco de Tamaraceite), bien sobre los conglomerados de clastos fonolíticos del Miembro Inferior de la FDLP (e.g., barrancos de Quintanilla y Tamaraceite) o bien directamente sobre materiales volcánicos fonolíticos del Ciclo I (e.g., barrio de Salto del Negro en Las Palmas). Donde los afloramientos presentan un perfil vertical completo, por encima del sustrato volcánico, los conglomerados y/o el nivel marino blanco aparecen los pillows y sobre ellos, sin aparente solución de continuidad en el panorama, las lavas pahoehoe correspondientes al apilamiento sucesivo y rápido de diferentes coladas métricas. En sí misma esta sucesión indica, tal como acertadamente han señalado los trabajos precedentemente citados, tanto el carácter y origen de estos depósitos subacuáticos a partir de flujos subaéreos como la profundidad del fondo marino en la plataforma en el momento de su llegada, de orden de unos 20 metros, que es el espesor promedio que muestran las coladas de pillows y las hialoclastitas que localmente aparecen asociadas. Hacia el interior de la isla esta potencia decrece gradualmente, al tiempo que crece l de las coladas pahoehoe que va de unos 10 metros en l costa actual hasta más de 30 metros en el interior. La cot actual de afloramiento del nivel basal de las coladas d pillows oscila desde unos 75 metros en los afloramiento de la costa hasta unos 140 metros en el Barrio d Tamaraceite.

Por lo que se refiere a las características de litofacies principales de los depósitos, hay que destacar la amplísima predominancia de las coladas de lavas almohadilladas sobre las hialoclastitas, así como la inexistencia de un delta de hialoclastitas s.str. Este tipo de deltas caracterizan e tramo inferior de muchos de los depósitos de pillow lava asociados a la llegada de coladas subaéreas al mar en isla oceánicas, llegando a presentar una potencia varias veces superior a la de las mismas lavas almohadilladas (véase Jones y Nelson, 1970, y referencias en dicho trabajo). Su ausencia confirma plenamente que la llegada de las colada lávicas se produjo sobre una amplia plataforma erosiva d carácter planar extensamente desarrollada posiblemente, ta como sugiere la edad de los pillows, en concomitancia co un proceso transgresivo de carácter eustático de orden ma yor (Lietz y Schmincke, 1975; Pérez Torrado *et al.*, 1995). Las evidencias cartográficas y de campo sugieren que l alimentación de los flujos de pillows se produjo a través d varios barrancos procedentes de sectores centrales de l isla, tras recorridos del orden de 20 o más kilómetros, d modo que lo que hoy aparece como un depósito continuo de coladas de pillow lavas, posiblemente corresponde a l coalescencia de diferentes aportes. Los aportes a partir d un barranco se debieron expandir radialmente a partir de punto de convergencia del barranco con la playa. Las dis tancias perpendiculares a la línea de costa trazadas por lo flujos de pillows son del orden de tres kilómetros, y e algunos de los afloramientos más septentrionales (p.e., ver tientes este y, especialmente, oeste, del barranco d Tamaraceite) se observa que el frente preservado se carac teriza por presentar un marcado predominio de la hialoclastitas, con un grosero desarrollo de estratificació en foresets dispuestos en abanico hacia la costa actual. eventual inyección de pillows (o presencia de brechas d pillows aislados en la hialoclastita) que interpretamos cons tituye el afloramiento distal del depósito.

Son varias las consecuencias que pueden deducirse d todos estos datos macroscópicos. La primera, el carácte erosivo del frente de las coladas de pillows y su capacida de arrastre de la lámina superficial de materiale inconsolidados subyacentes. En segundo lugar, la elevad tasa de aporte de flujos subaéreos, que permitió la llegada

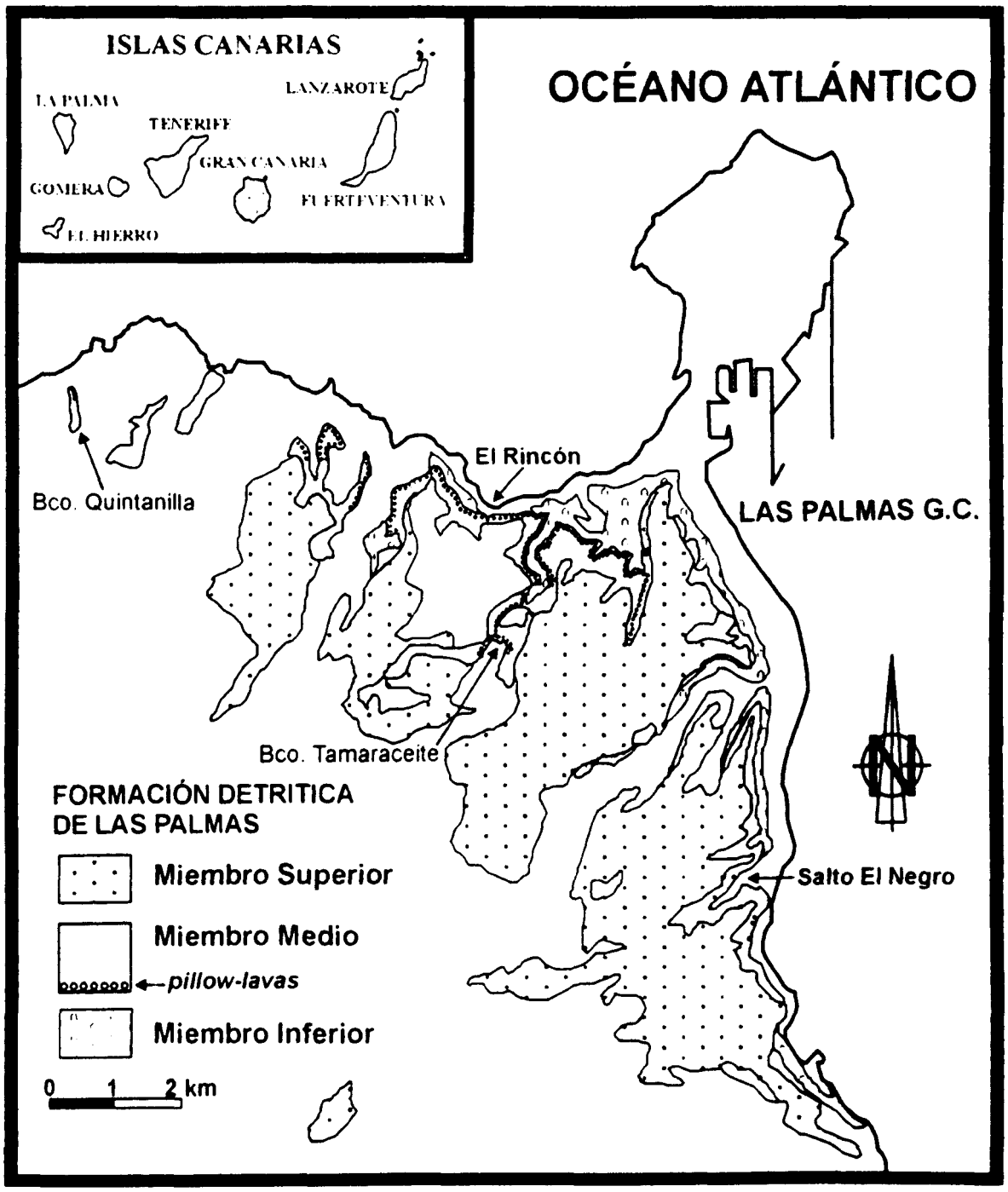

FIGURA 1: *Esquema geológico (modificado de ITGE, 1992) de la Formación Detrítica de Las Palmas y localización de los principales afloramientos de pillow lavas.*

rápida expansión de éstos en la plataforma marina sin que aparentemente se obturaran los focos de alimentación y dieran lugar a masas notables de hialoclastitas y, asociada a esta elevada tasa de aporte de lava a partir de cauces relativamente estrechos, la elevada velocidad de expansión de los flujos de lavas en la plataforma marina. Algunas erupciones recientes en islas oceánicas (p.e., algunas del archipiélago de Hawaii; o la del Teneguía, Afonso *et al.*, 1974) han demostrado que depósitos comparables pueden formarse en el curso de erupciones que duran tan sólo días o semanas.

Por lo que se refiere a las estructuras internas y externas de los pillows (y los lentejones de brechas de pillows asociados) presentes en el cuerpo principal del depósito, sólo cabe decir que su riqueza excede con creces los límites y objetivos de esta nota. Los afloramientos longitudinales y transversales presentes en muchos de los barrancos (p.e., el de Tamaraceite), permiten disponer de secciones tridimensionales completas de los cuerpos tubulares entrelazados de pillows, de dimensiones métricas y secciones transversales pluricentimétricas. Entre las estructuras diagnósticas queremos resaltar la abundancia de pillows implosionados con múltiples anillos vítreos, propios de medios muy poco profundos, la presencia abundante de pillows huecos y semihuecos con cúpulas estalagtíticas y bases estalagmíticas de lava, más abundantes en los secto-

res proximales respecto a los focos de alimentación a la salida de los barrancos, que hay que interpretar en el contexto de alta velocidad de los flujos de pillows, y la presencia de evidencias claras (segregación de fenocristales hacia el borde vítreo) de que las coladas no llegaron excesivamente desgasificadas al mar.

Finalmente, queremos resaltar la presencia de dos conjuntos de litofacies particularmente significativas en la base y el techo del paquete de pillows. En la base hay que destacar el carácter intrusivo, respecto al substrato sedimentario, de las coladas de pillows, es decir, la introducción de digitaciones tubulares (buzando en dirección al mar) en el nivel guía marino blanco, con la consiguiente peperitización e hialoclastización de los bordes vítreos de los pillows y la fluidificación del encajante sedimentario. En el techo de la colada hemos podido localizar unas estructuras macroscópicas que marcan el tránsito subaéreo-subacuático: consisten en tubos métricos de sección elíptica (eje mayor dispuesto verticalmente, con relación de ejes horizontal:vertical 1:3 a 1:2), consistentes en un anillo vítreo externo pluricentimétrico y un relleno hialoclastizado *in situ, densamente empaquetado, con fragmentos* centimétricos o menores. Proponemos denominar en lo sucesivo esta estructura tubos alimentadores con anillo vítreo y rellenos de hialoclastitas formadas in situ (feeder tubes filled with hyaloclastites in situ).

AGRADECIMIENTOS

Este trabajo se ha realizado en el marco de los proyectos de la CICYT PB96-0243 y MAR97-1925-E, y gozó en su día de financiación complementaria por parte del proyecto de la Comisión Europea BRE2-CT93-0559. Los autores desean agradecer especialmente a la Comandancia de Marina de Las Palmas de Gran Canaria por la hospitalidad en el cuartel de la Marina "Manuel Lois", así como al SEPRONA de la Guardia Civil por las facilidades dadas para la realización del trabajo en una zona protegida.

REFERENCIAS

Afonso, A., Aparicio, A., Hernández-Pacheco, A. y Rodríguez-Badiola, E. (1974): Morphology evolution of Teneguía volcano area. Estudios Geológicos, vol. Teneguía: 7-13.

Araña, V. y Carracedo, J.C. (1978): Los volcanes de las Islas Canarias. III Gran Canaria. Ed. Rueda, Madrid, 175 p.

Gabaldón, V., Cabrera, M.C. y Cueto, L.A. (1989): Formación detrítica de Las Palmas. Sus facies y evolución sedimentológica. ESF Meeting on Canarian Volcanism, Lanzarote: 210-215.

ITGE (1992): Memoria y mapa geológico a escala 1:100.000: Gran Canaria (21-21/21-22).

Jones, J.G. y Nelson, P.H.H. (1970): The flow of basalt lava from air into water, its structural expression and stratigraphic significance. Geol. Mag., 107 (1): 13-19.

Lietz, J. y Schmincke, H.U. (1975): Miocene-Pliocene sea level changes and volcanic episodes on Gran Canaria (Canary Islands) in the light of new K-Ar ages. Palaeogeography Palaeoclimatology Palaeoecology, 18: 213-239.

McPhie, J.; Doyle, M. y Allen, R. (1993): Volcanic textures. A guide to the interpretation of textures in volcanic rocks. Centre for Ore Deposit and Exploration Studies, University of Tasmania, Hobart, Tasmania, 198 p.

Navarro, J.M., Apancio, A. y García Cacho, L. (1969): Estudio de los depósitos sedimentarios de Tafira a Las Palmas. Estudios Geológicos, 25: 235-248.

Pérez Torrado, F.J., Carracedo, J.C. y Mangas, J. (1995): Geochronology and stratigraphy of the Roque Nublo Cycle, Gran Canaria, Canary Islands. J. Geol. Soc. London, 152: 807-818.

Vuagnat, M. (1960): Sur les laves en coussin des environs de Las Palmas, Grande Canarie (Note préliminaire). Archives des Sciences, Physiques et Natureles, Genève, 13: 153-157.

Economic Geology
Vol. 95, 2000, pp. 19–40

Metallogenesis of Zn-Pb Carbonate-Hosted Mineralization in the Southeastern Region of the Picos de Europa (Central Northern Spain) Province: Geologic, Fluid Inclusion, and Stable Isotope Studies

F. GÓMEZ-FERNÁNDEZ,[1]

Departamento de Ingeniería Minera, Escuela Universitaria de Ingeniería Técnica Minera, C/ Jesús Rubio 2, 24004 León, Spain

R. A. BOTH,

Department of Geology and Geophysics, University of Adelaide, South Australia 5005, Australia

J. MANGAS,

Departamento de Física-Geología, Universidad de Las Palmas de G.C., Aptdo. 550, 35080 Las Palmas de Gran Canaria, Spain

AND A. ARRIBAS

Departamento de Ingeniería Geológica, Escuela Técnica Superior de Ingenieros de Minas, C/ Ríos Rosas 21, 28003 Madrid, Spain

Abstract

The Zn-Pb deposits of the southeastern area of the Picos de Europa province display an epigenetic hydrothermal mineralization of moderate temperature hosted by intensely dolomitized limestones of Carboniferous age. They are structurally and lithologically controlled since the three phenomena of fracturing, dolomitization, and mineralization are interrelated. Two types of mineralization have been found: type I, granular dark brown-colored sphalerite, galena, and dolomite, and type II, toffee-colored sphalerite, galena, and calcite. Type II mineralization is later than type I.

The Aliva and Andara deposits are the two largest in the Picos de Europa area, and both contain type I and type II styles of mineralization. Fluid inclusion studies indicate that the mineralizing solutions for both stages were similar and had trapping temperatures between 170° and 200°C and salinities around 15 wt percent NaCl equiv. However, microthermometric data from sphalerite (I and II), dolomite I, calcite II, and fluorite samples show various stages of circulation and trapping of brines with spatial and temporal variations in salinity and temperature.

Calcite and dolomite from the mineralization have $\delta^{13}C_{PDB}$ values between 1 and 2.9 per mil ($\delta^{13}C_{\Sigma CO_2}$ = –0.8–1.1‰), and $\delta^{18}O_{SMOW}$ values between 11.5 and 16.2 per mil ($\delta^{18}O_{H_2O}$ varied from 0.7–1.9‰). Sulfides show $\delta^{34}S$ values between 12.9 and –16.8 per mil ($\delta^{34}S_{Aliva}$ for the Aliva deposit ranged between 13.4 and –2.5‰). The combined stable isotope data indicate evolved marine waters. Isotope evidence suggests that the mineralizing fluids were probably formation waters of the Palentine zone and the Picos de Europa province sediments. During the Permian, possibly during extensional tectonic phases, these brines moved toward and through the Picos de Europa province along late Hercynian fractures giving rise to the Zn-Pb mineralization.

Introduction

THE PICOS de Europa base metal mining district is located in the southeastern part of the Picos de Europa structural province, in northern Spain. Within this district, numerous deposits were mined for Zn and Pb between the late 1800s and 1989. The deposits are generally small, but the Aliva mine produced a total of 600,000 metric tons of ore at an average grade of 13 percent Zn and 2 percent Pb. The Aliva mine was also the source of exceptionally large and beautiful yellow sphalerite crystals ("blenda acaramelada"), the type II sphalerite in this paper, which were found in vugs and open fractures and served as a reflectivity standard for many years (Cissarz, 1932).

Previous geologic investigations of these deposits were carried out by Calderón (1900) who studied the geology of the area and the distribution of the main mineral occurrences, Adhelard (1968) who made a preliminary study of the sulfur isotopes, Arribas (1981) who studied the distribution of trace elements, Loredo and García Iglesias (1984) who analyzed fluid inclusions in yellow sphalerite, and Velasco and Pesquera (1979) who made a study of the optical properties of this mineral.

The present study of the Picos de Europa Zn-Pb deposits was commenced prior to the closure of the Aliva mine, in order to obtain geologic, mineralogical, and geochemical data on this and other deposits and, hence, improve our understanding of the genesis of this group of deposits.

Geologic Setting

The Cantabrian zone within the Hercynian Massif (also known in this part of Spain as the Asturian Massif) of the Iberian Peninsula was defined by Lotze (1945), and subsequently subdivided by Julivert (1971) into the following five structural provinces: (1) fold and nappe, (2) central coal basin, (3) Ponga nappe, (4) Picos de Europa, and (5) Pisuerga-Carrión. Later, Martínez-García (1981) proposed that the

[1] Corresponding author: email, dimfgf@unileon.es

Pisuerga-Carrión province be renamed the Palentine zone, because its distinctive geologic characteristics distinguish it from the Cantabrian zone. The mineral deposits dealt with in this study are located in the southeastern area of the Picos de Europa province, close to the overthrust boundary with the Palentine zone (Figs. 1 and 2).

The rocks in the southeastern sector of the Picos de Europa are of sedimentary origin, no igneous rocks are present. The stratigraphic sequence is largely comprised of Carboniferous-age sediments (Fig. 3), with both a preorogenic and a synorogenic sequence. The former is made up of the following carbonate formations: Portillas (15 m of bioclastic packestone-grainstone) and Genicera (22 m of nodular mudstone-wackestone that commonly forms the overthrust surface of reverse faults) of Tournaisian-Visean age; Barcaliente (290 m of laminated and sandy limestones and intraformational breccias) and Valdeteja (270 m of wackestone-grainstone) of Serpukhovian to Vereyan age, both forming the so-called "Caliza de Montaña"; and Picos de Europa (360 m of interbedded limestones and shales at the base overlain by bioclastic massive limestones) of Moscovian age. An angular unconformity separates the preorogenic Carboniferous carbonate rocks from the overlying synorogenic sequence comprised of the Lebeña Formation. The latter consists of over 440 m of turbidites, represented by black shales, conglomerates, sandstones, and calcarenites, with some calcirudites, of Kasimovian age. Discordant over Carboniferous rocks are Quaternary sediments, essentially piedmont breccias and glacial sediments.

The most noteworthy tectonic feature in the southeastern area of the Picos de Europa province is the existence of east-west to east-southeast–west-northwest–oriented imbricate thrust sheets verging to the south (Fig. 2). These were developed during the upper Carboniferous (lower Stephanian B stage), coinciding with the peak of the Hercynian orogeny in the region. According to Marquínez (1978) three structural units are present in this province: (1) Frontal, (2) Tesorero-Agero, and (3) Lechugales (Figs. 2 and 4). A further

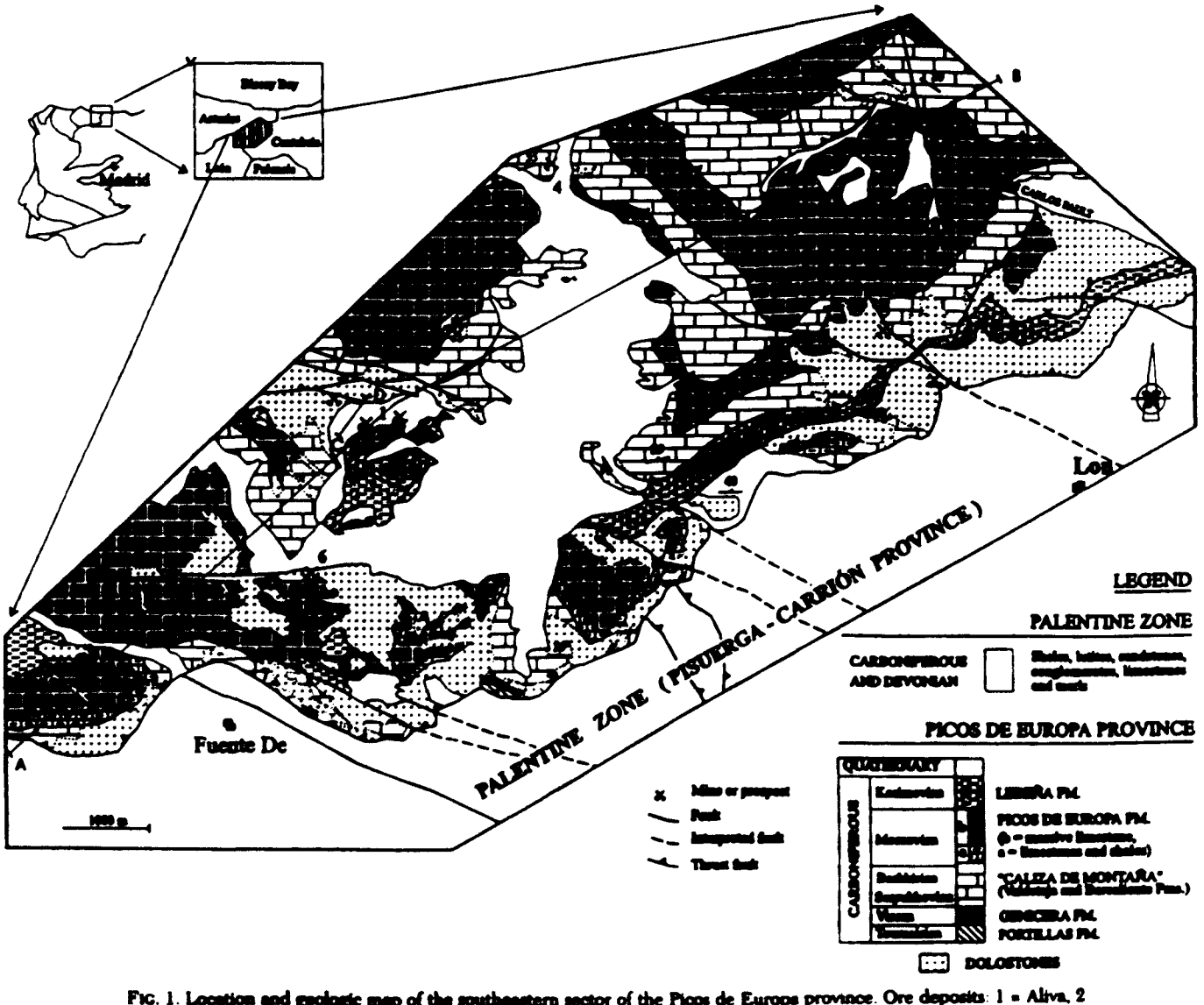

FIG. 1. Location and geologic map of the southeastern sector of the Picos de Europa province. Ore deposits: 1 = Aliva, 2 = Andara, 3 = Liordes, 4 = Vegas de Sotres, 5 = Las Caramas, 6 = La Colladina, 7 = Fuente De.

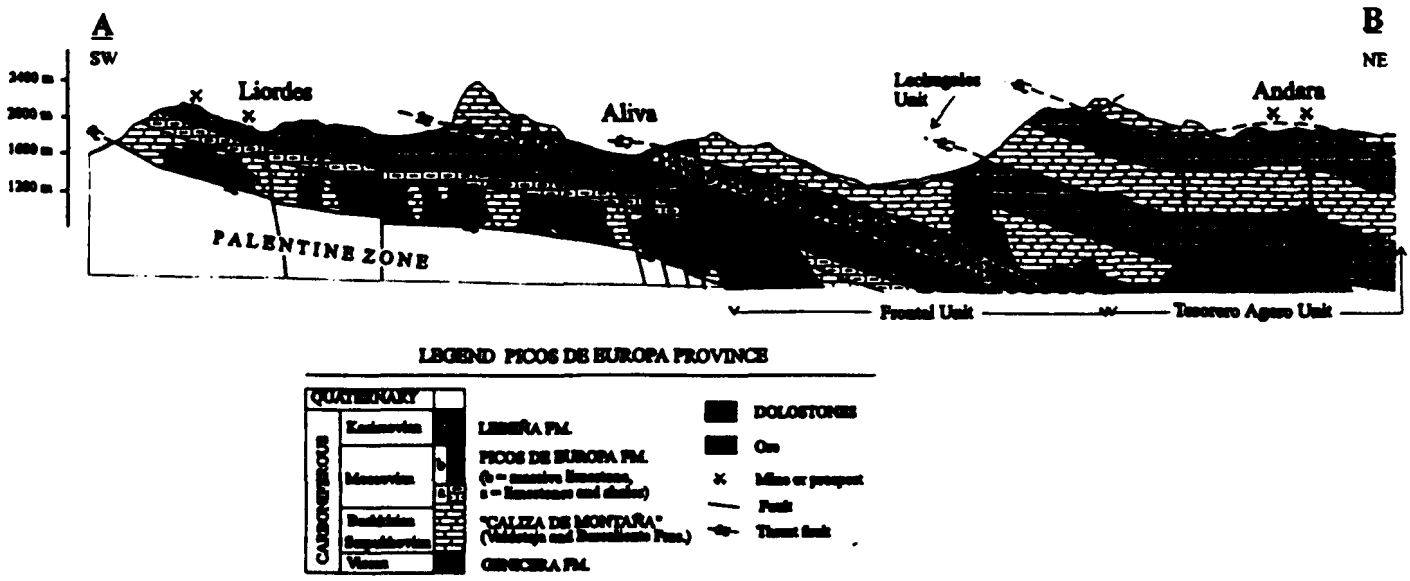

FIG. 2. Geologic cross section through the southeastern region of the Picos de Europa (see line AB in Fig. 1).

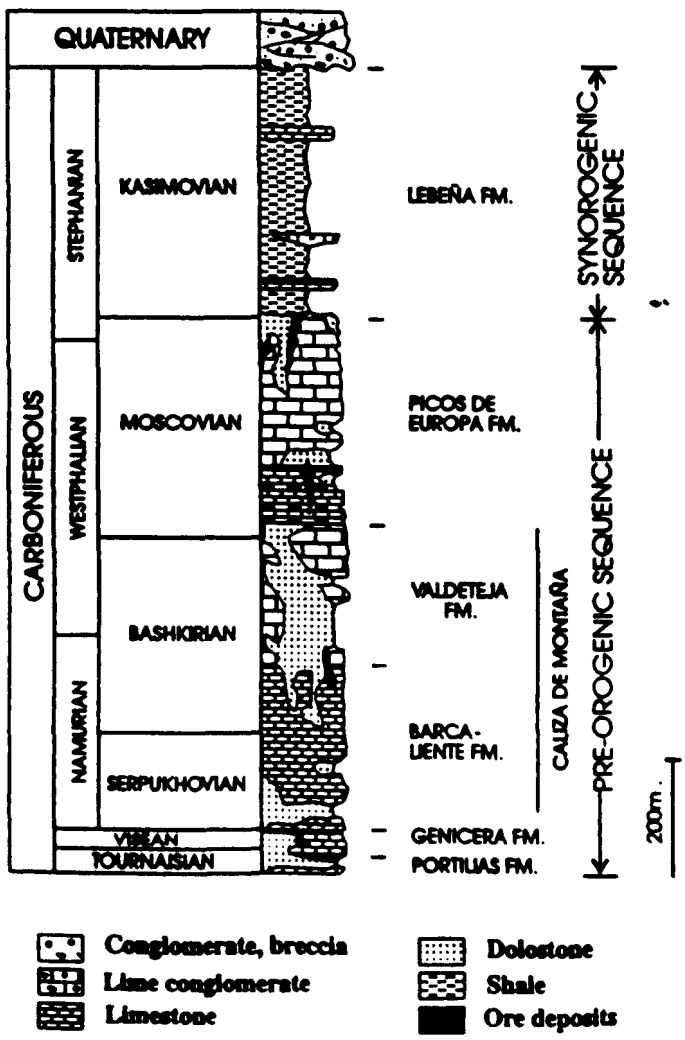

FIG. 3. Stratigraphy of the southeastern sector of Picos de Europa. Pb-Zn deposits in the Picos de Europa Formation are Aliva, Andara, Liordes, Las Caranas, La Colladina, and Fuente De. Las Vegas de Sotres is in the Caliza de Montaña (Barcaliente Formation; cf. Fig. 1).

important structural feature is a late Hercynian subvertical fault system which strikes N 105° to 120° E. These are strike-slip faults that cut the thrusts, and many cross the boundary between the Cantabrian and Palentine zones. Folds constitute a secondary structural feature in the Picos de Europa province, ranging from large-scale folds with a large radius of curvature, rendering them almost imperceptible, to smaller-scale folds with an irregular geometry associated with the thrust surfaces. The metamorphic grade associated with the Hercynian orogeny in the province is very low, never exceeding the lowest level of greenschist facies.

The geologic characteristics of the Palentine zone are quite different from those of the Cantabrian zone. The preorogenic stratigraphic sequence in the Palentine zone consists of 1,500 m of Silurian shales and sandstones and Devonian-Visean limestones, marls, shales, and sandstones. The first evidence of tectonic activity in this province is in the lowermost Namurian (Heredia et al., 1990). Subsequently, the province behaved as a synorogenic basin (Rodríguez-Fernández and Heredia, 1990), with deposition of sediments during diachronous emplacement of the four great thrust sheets (Palentinos-Valsurvio, Esla, Ponga, and Picos de Europa) present in this part of the Cantabrian zone. Prior to emplacement of the Picos de Europa thrust sheet, in the Stephanian B, more than 6,000 m of sediment (lutites, shales, sandstones, and some conglomerates and limestones), commonly turbiditic and with highly variable thicknesses, were deposited in the basin.

Permian sediments, discordant over the Carboniferous, crop out sporadically in the northern part of the Picos de Europa. In this region, the depositional environment at the base of the Permian sequence was litoral to marine, changing to continental toward the top.

Tectonic evolution of the region

An understanding of the tectonic evolution of the region is essential to the development of a model for the genesis of ore deposits within the Picos de Europa province. The sequence of events has been interpreted from studies of the Cantabrian

and Palentine zones and of the Permian-Mesozoic cover in neighboring areas, and is summarized below.

Hercynian compression: Emplacement of the thrust sheets occurred during the lower Stephanian B, with thrusting of the Picos de Europa province over the Palentine zone (Rodríguez-Fernández and Heredia, 1990). The thrusts have an east-west orientation, with northerly dips that are much more pronounced in the north than in the south of the Picos de Europa province.

Late and post-Hercynian extension: Extension in the late Carboniferous-Permian began along subvertical faults striking N 105° to 120° E, and in the north of the Picos de Europa province, along some of the east-west subvertical thrust planes. The Permian extension was of particular significance, resulting in marked changes in thickness of sediments, volcanism in various areas, and in the Palentine zone, intrusion of granodiorites. These effects have been related by Martínez-García and Tejerina (1979) and Martínez-García (1981) to the development of a Permian rift in the north of the Iberian plate.

Extension continued in several phases during the Triassic, Jurassic, and Cretaceous (García-Espina, 1991), with the Picos de Europa province remaining below the Basque-Cantabrian basin Mesozoic sediments (Alonso and Pulgar, 1995; Alonso et al., 1996).

Alpine compression: Onset of Alpine compression began in the Priabonian (late Eocene; Hines, 1985) with the peak of Alpine compression occurring in the Oligocene. The Alpine orogeny produced uplift and emergence of the Paleozoic Asturian Massif and overlying Mesozoic sediments. The erosion of the most superficial sediments allowed the Hercynian basement to crop out in the Cantabrian and Palentine zones.

Alpine shortening was achieved by means of some of the Hercynian east-west thrusts that dip steeply to the north, and by rejuvenation of some of the late Hercynian N 105° to 120° E faults that acted as reverse faults (Heredia and Rodríguez-Fernández, 1994). The fact that very few of these late Hercynian faults can be shown to have been involved in the Alpine shortening, suggests that the majority remained inactive at this time. Even the San Carlos fault (Fig. 2) associated with the formation of the Andara deposits, clearly does not cut the overlying Late Triassic sediments.

Dolomitization

Dolostones are common in all carbonate formations of the preorogenic sequence of the Picos de Europa province but are rare in the carbonate beds of the Lebeña Formation, where dolostones are found only in fault zones. The dolostones consist of pale brown to orange or gray crystals of dolomite, in some cases accompanied by white dolomite crystals occurring as patches or partially or completely filling cavities. The size of the dolomite crystals varies from 0.02 to 1.8 mm, with a mean of 1.35 mm, and the white crystals are the largest in all samples. The contacts between the two types are irregular and some coincide with stylolites. The dolomite crystals are generally free of impurities, but intergranular spaces may be occupied by idiomorphic pyrite and/or dark "dust," interpreted as the residue of leaching during dolomitization. The form of the crystals varies from subidiotopic to xenotopic. According to the terminology of Sibley and Gregg (1987) the textures of these rocks may be classified as unimodal or polymodal nonplanar, although some planar-s dolostones are present. The dolomitization process resulted in an increase in porosity with respect to the replaced limestone.

All dolostones of the preorogenic sequence have similar chemical compositions, with mean values of 19.31 percent MgO, 32.73 percent CaO, 45.88 percent CO_2, 0.53 percent FeO + Fe_2O_3, and 24 ppm Sr, compared to mean values of the limestones of 0.59 percent MgO, 55.06 percent CaO, 42.31 percent CO_2, 0.19 percent FeO + Fe_2O_3, and 332 ppm Sr (Gómez-Fernandez et al., 1993a). The data demonstrate the Fe-poor character of the dolostones, but show an enrichment by a factor of three compared to the limestones.

The limestone-dolostone contacts are sharp and discordant to the stratification (Fig. 2), with rhomboids of dolomite commonly present as simultaneous deposits on both allochemical and orthochemical elements of the limestone. The morphology of the dolostone bodies is generally irregular, with remnants of limestone enclosed by dolostone. Beneath shale beds dolomitization is commonly very extensive laterally, whereas elsewhere the dolostones form subvertical veinlike bodies around the N 105° to 120° E faults. Dolomitization affected large volumes of rock (36% of the carbonate rocks) in the lower (Frontal) structural unit beneath the impermeable shales of the Lebeña Formation, and smaller volumes in the upper structural units (5.5% in the Tesorero-Agero unit and 1.5% in the Lechugales unit) of the Picos de Europa province (Gómez-Fernández, 1992).

Criteria that provide evidence of the epigenetic nature of the dolomitization processes include the morphology of the dolostones (irregular and subvertical bodies associated with faults), sharp limestone-dolostone contacts discordant to the stratification, the dominant textures with moderately large crystals of dolomite, and the low Sr content of the dolostone in comparison with the limestones from which they originated (Veizer and Demovic, 1974; Jacobson and Usdowsky, 1976; Gómez-Fernández et al., 1993a). Since the dolostones are, in part, associated with the N 105° to 120° E faults, and since these faults cut the thrusts (Rodríguez-Fernández and Heredia, 1990), it follows that dolomitization in the Picos de Europa province took place after emplacement of the thrust sheets.

With respect to the source of the dolomitizing solutions, the shales of the Lebeña Formation do not represent a sufficient source of Mg for dolomitization on the scale observed in the Frontal unit of the Picos de Europa province. Furthermore, the greater abundance of dolostones in this unit, compared to the upper structural units, suggests an ascending component to the flow of the dolomitizing fluids, although this cannot be unequivocally demonstrated. The irregular morphology of the dolostone bodies probably reflects the nature of fluid circulation, with fluid advance achieved by means of replacement of limestone. The shales of the Lebeña Formation and at the base of the Picos de Europa Formation would have impeded fluid ascent, favoring dolomitization of carbonate beds within the Frontal unit. Only in highly fractured zones would the fluids have been able to reach the higher structural units.

Mineral Deposits

In the southeastern part of the Picos de Europa province there is a large number of ore deposits and occurrences of Zn-Pb (Fe, Cu, Hg, F, As, and Sb). The most important mines are those of Aliva (Fig. 4A, B) and Andara, followed by those of Liordes and Las Garamas, and smaller deposits such as Vegas de Sotres, Fuente De, and La Colladina (Fig. 1). These deposits are located in the Frontal, Tesorero-Agero, or Lechugales structural units and in the Barcaliente, Valdeteja, or Picos de Europa Formations (Figs. 1–3). The deposits are generally relatively small, the most noteworthy being the Aliva mine. From the late nineteenth century to the early part of the twentieth, zinc production came from oxidized minerals of the supergene zone in the Andara and Aliva mines, and from other minor deposits. From the 1950s to 1989, when the Aliva mine closed, primary sphalerite and galena were extracted (Gómez-Fernández and Arribas, 1994).

The mineral deposits are structurally and lithologically controlled since the three phenomena of fracturing, dolomitization, and mineralization are interrelated. The deposits are located close to the principal late Hercynian faults, which strike N 105° to 120° E, with lengths ranging from hundreds to thousands of meters and displacements of several hundred meters. Most of the orebodies are located on the southern sides of the faults (e.g., Andara, Liordes, etc.) and are associated with carbonates, particularly dolostones (e.g., Aliva). The fault zones are commonly found to be irregularly dolomitized, and since the mineralization is controlled by the presence of both dolostones and fractures, its geometry is largely vein type (e.g., Andara, Liordes, etc.). The mineralization is present as bulges or irregular bodies parallel to the fractures, although it is not found as continuous planar bodies. The Andara deposit consists of several subvertical veins striking 120° E, with widths of less than 20 m, lengths up to 200 m, and depths greater than 100 m. In the Aliva mine two major bodies of limestone, unaffected by dolomitization, are separated by a dolomitized zone associated with a zone of fracturing (Fig. 5), and the ore is generally situated at the limestone-dolostone contact. In the upper, eastern extremity of the mine, however, where limestone is in direct contact with the Lebeña Formation, the main ore is found at the contact of the limestone and shales of that formation.

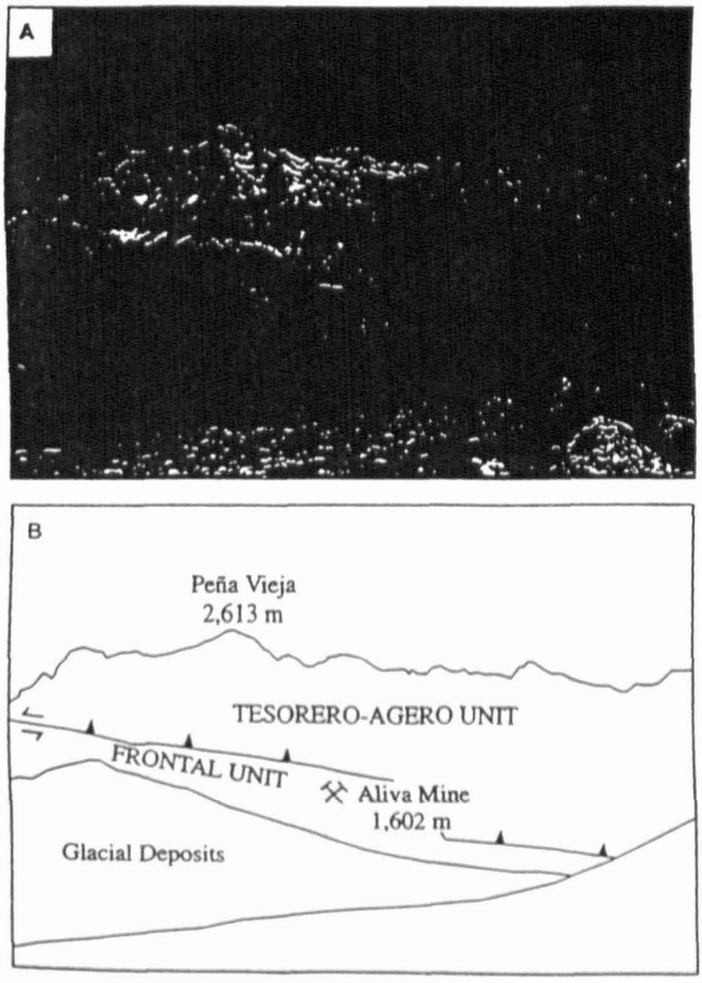

FIG. 4. A. General view of the Aliva mine area. B. Explanatory sketch.

The main ore zone in the Aliva mine extends from 1,640 m above sea level, at the surface, to 1,467 m, with plan dimensions of 200 × 410 m and a maximum thickness of 20 m. The ore follows a curved dolomitization front, which has the shape of an antiform plunging 26° in a west-northwest direction (Gómez-Fernández, 1992). The northeast limb is the better developed and dips 70° north-northeast, whereas on the southwest limb the orebody dips subhorizontally. Mineralized zones display gradational contacts with surrounding dolostone and are normally characterized by dispersed mineralization isolated from the main mineralized bodies, whereas contacts with limestone are sharper. The geometry of the mineralized bodies suggests that mineralization occurred by carbonate host-rock replacement.

Two types of mineralization (Fig. 6) have been distinguished in most of the deposits on the basis of appearance, texture, paragenesis, and geochemical characteristics (Fig. 7A–F) (Gómez-Fernández et al., 1993b). Type I mineralization (first phase) consists dominantly of dark brown sphalerite, galena, and dolomite. On a macroscopic scale, this type shows granular, laminated, and botryoidal textures, with alternating layers of brown and yellow sphalerite (Figs. 7C, 8C, and 8E). It is also present as cavity fillings, as replacement patches, and in hydrothermal dolomitic breccias located close to the dolostone-limestone contacts (Fig. 7A and B). All these minerals were deposited in several pulses.

Under the microscope, granular sphalerite occurs as zoned aggregates containing anhedral grains of chalcopyrite, tetrahedrite (Table 1), pyrite and dolomite (Fig. 8D), and calcite that are occasionally distributed in microfractures. Electron microprobe analyses confirm that the dark bands of type I sphalerite are Fe enriched with respect to the pale bands (Fig. 8F), which are Cu and Sb enriched (Gómez-Fernández, 1992). Galena is present as anhedral grains of various sizes, also containing inclusions of chalcopyrite and tetrahedrite (Fig. 8A, B), preferentially distributed in layers that occasionally cross the sphalerite bands. Pyrite can also be found as euhedral-subhedral crystals, either isolated or in groups.

Type II mineralization (second phase) is the more abundant in these deposits and is characterized by large crystals (up to 20 cm across) of the dominant minerals deposited during this period of mineralization, i.e., sphalerite, galena, and calcite (Fig. 6). Type II mineralization is found cementing

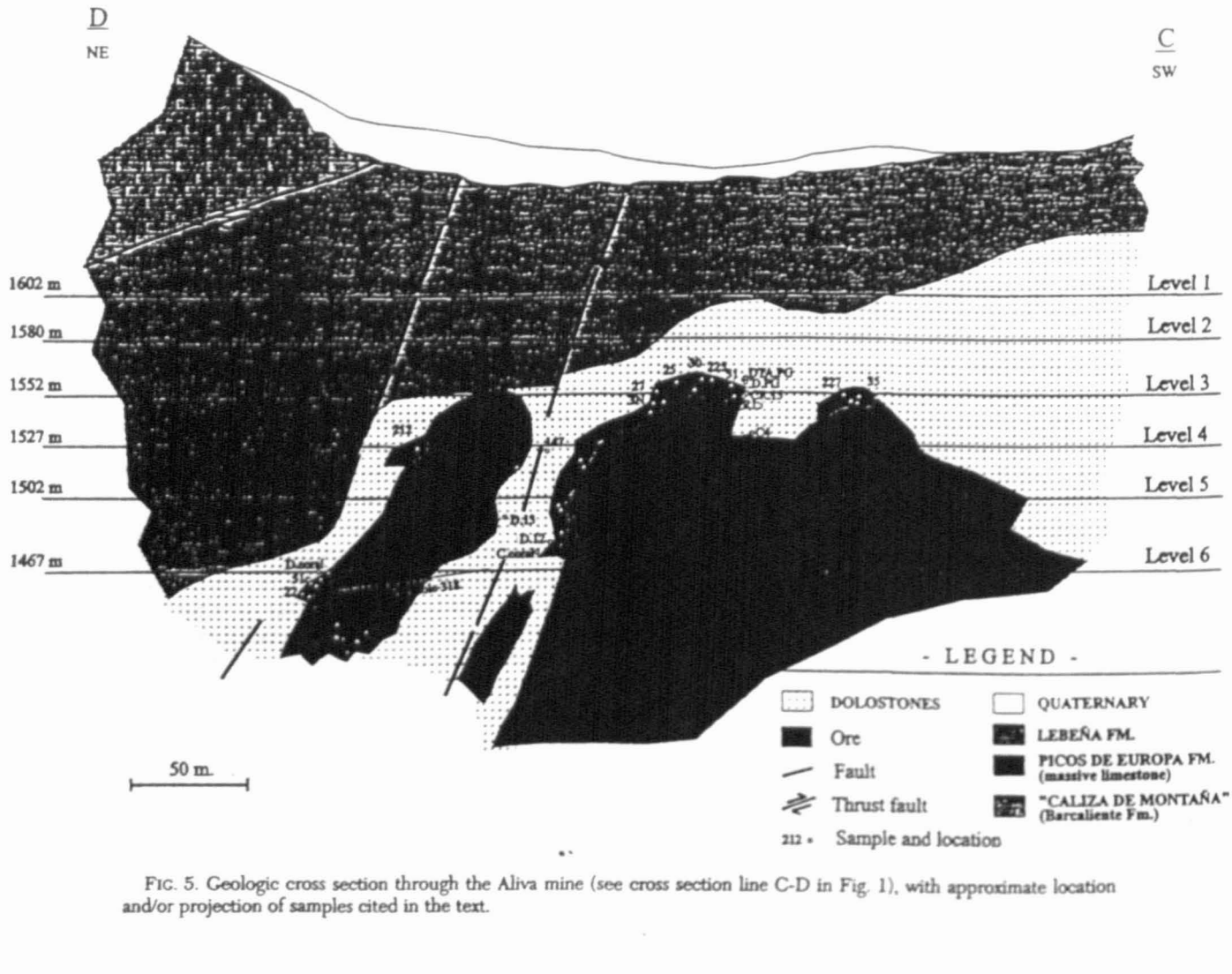

FIG. 5. Geologic cross section through the Aliva mine (see cross section line C-D in Fig. 1), with approximate location and/or projection of samples cited in the text.

breccias, filling fractures and fissures (Figs. 7D, 7E, and 9E), and replacing the host rock (Fig. 7F), with corrosion textures common in the wall rock. In about 60 percent of the ore, cementing breccias fill small to large (from less than 0.5 m to several meters across) cavities of hydrothermal origin.

Sphalerite occurs as transparent or translucent red, green, or yellow crystals (Fig. 9B). Electron microprobe, XRF, AAS, and ICP analyses (Table 2) have demonstrated that the reddish sphalerite has high contents of Hg, Cu, and Cd, the yellowish has high Bi, and the green is Cu deficient. Comparison of the electron microprobe and XRF analyses of sphalerites of types I and II shows that those of type I have higher Fe and Ge contents, and lower Hg contents than those of type II (Gómez-Fernández, 1992). The sphalerite is intergrown with galena and calcite, and to a lesser degree, dolomite. Small amounts of contemporaneous anhedral pyrite, as well as microscopic inclusions of chalcopyrite and tennantite (Table 1) are also present within the sphalerite (Fig. 9A). Quartz replaced by sphalerite has been occasionally observed under the microscope.

Milk-white calcite (Fig. 9D) is found in abundance, forming masses up to several meters across. The majority of the calcite is contemporaneous with, or later than, the sulfide minerals. Purplish-white or green fluorite occurs as individual crystals or in masses cutting the sphalerite or calcite.

Mapping shows no difference in the spatial distribution of type I and II mineralizations and there is no evidence of metal zoning within either of the two types. Both types are accompanied by graphitic matter, sericite, and microcrystalline quartz that form irregular layers and patches; these are also found well away from mineralized zones and were originally contained in the hydrothermally altered host carbonate rocks. There is evidence of tectonic deformation following the main phases of mineralization, with the presence of fractured sphalerite and curved cleavage planes in galena. Type I and II mineralizations coexist in most of the deposits and are found in similar geologic settings. Type II is later than type I (Figs. 7A, 7B, and 9F) and represents the greater part of the production of Zn and Pb in the region.

Although widespread dolomitization (Fig. 6) of the limestones preceded the main phases of mineralization in the entire region, other less significant dolomitization took place contemporaneously with, or later than, mineralization (Fig. 9C). Late-stage minerals include pyrite (either euhedral or anhedral), galena, rhombohedral dolomite, calcite, and fluorite, infilling fissures or dispersed within type II mineralization. The supergene phase of alteration of earlier minerals is represented by hydrozincite, smithsonite, cinnabar, malachite, azurite, aurichalcite, chalcocite, and Fe oxides.

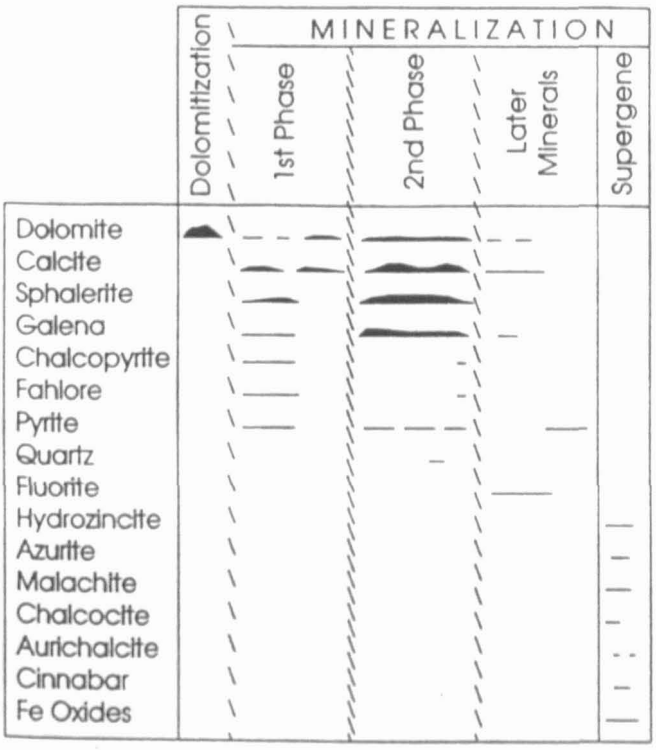

FIG. 6. Generalized paragenetic sequence in the Picos de Europa mining district.

Other Zn-Pb deposits in central northern Spain

In other areas of central northern Spain some deposits of Zn-Pb, and other minor metals, are hosted by both Paleozoic and Lower Cretaceous (Urgonian Complex) carbonate rocks. Because of their significance to an ore genesis interpretation of the southeastern Picos de Europa deposits, a brief summary is presented below.

Paleozoic-hosted ore deposits: Within the Picos de Europa province, to the north and east of the region studied in the present contribution, some small deposits of Pb-Zn-(Ba-Hg), with minor amounts of Cu-Fe sulfides, are also hosted by Carboniferous carbonate rocks, and to a lesser extent, the overlying Permian sediments. These are vein type deposits located in fractures that cut Carboniferous and Permian, but not Triassic, sediments (Martínez-García et al., 1991).

In the easternmost areas, where the Picos de Europa province is partly covered by postorogenic sediments, mineralization hosted also by Carboniferous rocks, but belonging to higher structural units than those hosting the Aliva and Andara deposits, was partly eroded and redeposited as detrital material during the Permian (Saulas, 1985; Barbanson, 1987). These authors interpret the age of this mineralization as Permian and related to the Permian rifting (Martínez-García, 1983).

Cretaceous-hosted ore deposits: In the Basque-Cantabrian basin, ankeritic dolostones and limestones of Aptian or Albian age (Lower Cretaceous) host very important Zn-Pb deposits. These deposits have been interpreted as being sedimentary exhalative (e.g., the Troya mine; Fernández-Martínez and Velasco, 1996), and sedimentary-exhalative or Mississippi Valley type (e.g., the Reocín mine; Seebold et al., 1989). Pb isotope studies of both types indicate a crustal source, most probably the thick sequence of Lower Cretaceous clastic sediments (Velasco et al., 1996). The origin of these deposits has also been interpreted as related to tectonic extension associated with the formation of the Basque-Cantabrian basin during the opening of the Bay of Biscay (Yusta and Velasco, 1996).

Geochemistry of Mineralization

In order to characterize the ore-forming environment better, a number of geochemical studies were undertaken. Fluid inclusion studies were performed on sphalerite, dolomite, calcite, and fluorite samples from the Aliva and Andara mines. Sulfur isotope analyses of sulfides and carbon and oxygen isotope analyses of carbonates from Aliva and other deposits were made in order to determine the physico-chemical characteristics of the mineralizing fluids. To define the contents and distribution of the rare earth elements (REE), XRF, ICP-MS, and INAA analyses were made of carbonates from both the mineralization and the host rocks of the Aliva mine.

Fluid inclusions

The fluid inclusion study was performed on minerals from the Aliva (sphalerite I, Fig. 10A; dolomite I ; sphalerite II, Fig. 10B; calcite II, Fig. 10C; late-stage fluorite, Fig. 10D) and Andara (sphalerite II) deposits. Methods employed were microthermometry, using a Chaixmeca cooling and heating stage, and cryogenic scanning electron microscopy, with a Jeol-Link CRYO-SEM-EDS system. The Aliva samples were selected from different mine levels: samples 36, 37, and 227 from level 1 (1,602 m); sample 200 from level 3 (1,552 m); samples 222 and 20 from level 4 (1,527 m), and sample 51a and 51c from level 6 (1,467 m).

The fluid inclusions are primary, pseudosecondary, or secondary in character and generally two phase (H_2O L + V) at

TABLE 1. Chemical Analyses of Falhore Associated with Type I and II Mineralizations

Sample no.	Mineralization type	Fe (wt %)	Ag (wt %)	Ni (wt %)	Bi (wt %)	Sn (wt %)	Cu (wt %)	S (wt %)	Zn (wt %)	Hg (wt %)	Sb (wt %)	As (wt %)
31	I	0.54	0.69	0.10		0.11	39.82	26.58	9.95	0.33	19.13	6.88
31	I	1.08	0.79	0.12		0.09	39.83	26.54	6.52	0.11	18.64	7.13
31	I	0.83	1.08		0.21	0.12	37.73	25.83	6.55	0.19	23.73	3.70
71A	II	2.39	0.03			0.05	43.69	28.08	5.66	0.28	6.19	15.83
71A	II	2.41	0.01	0.06	0.13	0.02	44.02	28.39	5.37	0.13	6.45	15.41
71A	II	3.16	0.12		0.19	0.03	45.52	28.35	5.14		4.93	16.68

Analytical method: Electron microprobe

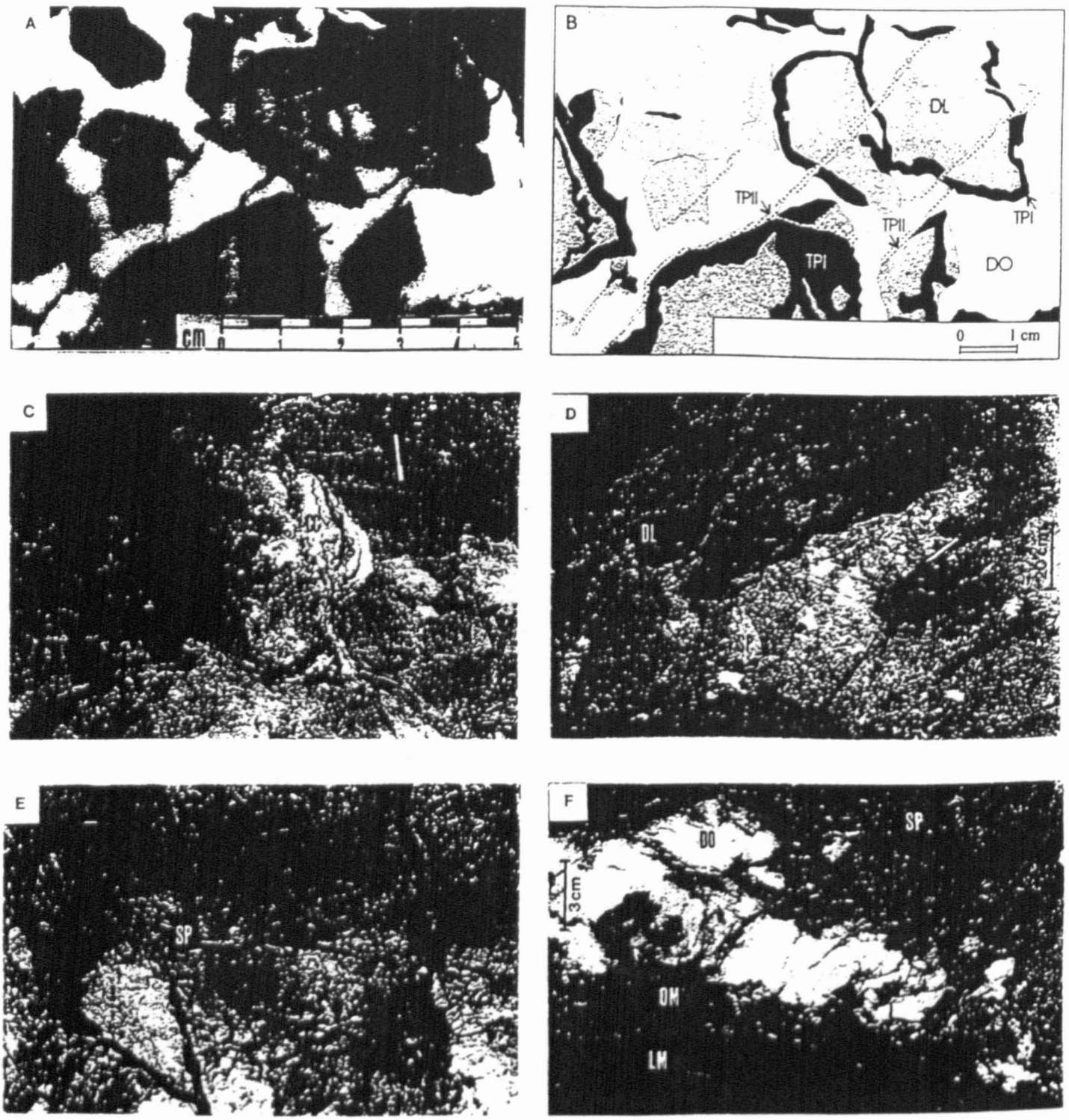

FIG. 7. A. Fissures filled with type II mineralization (sphalerite) cutting clasts and cements of a breccia partially cemented by type I mineralization. Note the presence of clasts completely or partially surrounded by a coating of type I sphalerite. Aliva mine (level 4). B. Explanatory sketch of A. C. Type I mineralization with calcite gangue in an outcrop of the Barcaliente Formation. Note the orientation of the sphalerite-calcite bands cutting the stratification represented by laminations of the algal limestone. Vegas de Sotres mine. D. Type II sphalerite cement in dolomitic breccia. Aliva mine (level 4). E. Fissures in whitish dolostone filled with type II sphalerite. Aliva mine (level 6). F. Mechanical contact between the Picos de Europa limestone and dolomite, sphalerite, and dolostone. The contact is marked by fine-grained carbonate and organic matter. Aliva mine (level 5). Abbreviations: DL = dolostone, DO = dolomite, LM = limestone, OM = carbonate and organic matter, SP = sphalerite, TPI = type I mineralization, TPII = type II mineralization.

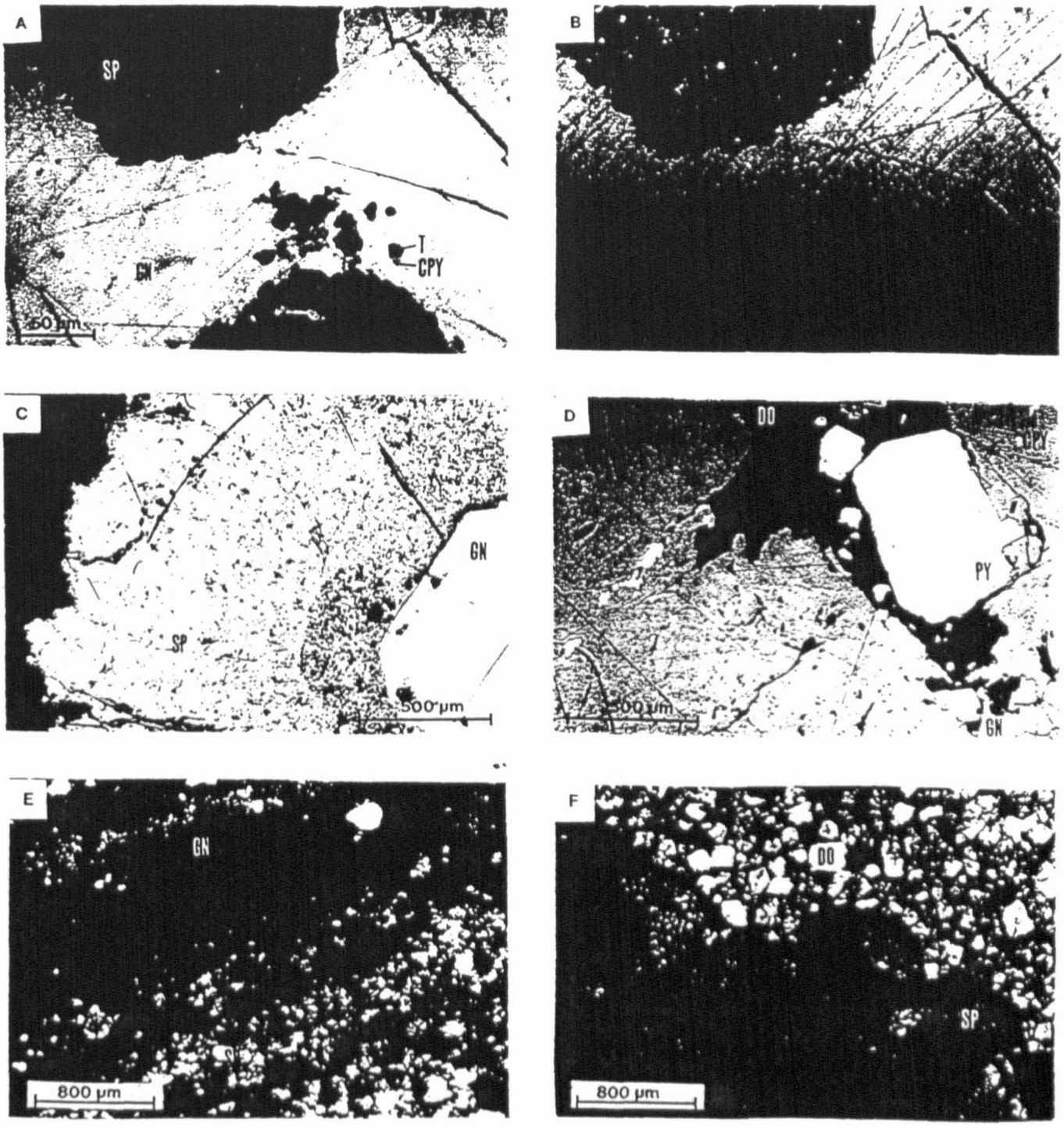

FIG. 8. A. Plane-polarized reflected light (oil immersion). Type I mineralization: two grains of sphalerite in galena, with inclusions of tetrahedrite and chalcopyrite in the galena. B. Same field of view as A (cross-polarized reflected light). Under crossed polars the chalcopyrite inclusions can be clearly seen in the dark-brown type I mineralization, dark brown sphalerite. C. Plane-polarized reflected light. Botryoidal banded brown sphalerite with euhedral galena and dolomite in type I mineralization. D. Plane-polarized reflected light. The main components of type I mineralization are euhedral pyrite with galena, sphalerite with chalcopyrite inclusions, and dolomite. E. Plane-polarized transmitted light. Alternating layers of brown sphalerite and galena in banded texture of type I mineralization. F. Plane-polarized transmitted light. Type I sphalerite surrounded by euhedral fine-grained dolomite. Abbreviations: CPY = chalcopyrite, DO = dolomite, GN = galena, PY = pyrite, SP = sphalerite, T = tetrahedrite.

TABLE 2. Chemical Analyses of Representative Sphalerites from the Picos de Europa Province

Sample no.	Mineral type	Orebody	Color	Hg	Cd	Ga	Ge	Cu	Bi	Fe	Zn (wt %)	S (wt %)	$\delta^{34}S$ (‰)	$\log f_{O_2}$
R15	Sp I	Aliva	Br.	415	1,062	<13	47			3,900	59.56	30.44	10.2	–47.0
R15	Sp I	Aliva	Br.	415	1,062	<13	47						10.3	
3N	Sp I	Aliva	Br.	350	944	<13	53			2,500	63.03	30,79	12.5	–46.6
31	Sp I	Aliva	Br.	500	904	<13	37			3,700	62.81	31.71		
31	Sp I	Aliva	Br.							1,100	67.55	33.63		
31	Sp I	Aliva	Br.					300		800	68.26	33.95		
31	Sp I	Aliva	P. Br.					800	1,800	5,500	65.60	32.36		
31	Sp I	Aliva	P. Br.					2,300		4,400	66.86	33.50		
31	Sp I	Aliva	P. Br.					200	2,300	1,000	68.25	33.29		
31	Sp I	Aliva	Br.					300	2,000	2,800	67.21	33.76		
31	Sp I	Aliva	D. Br.					1,400		8,600	65.27	32.08		
31	Sp I	Aliva	D. Br.					4,100		10,600	65.48	33.17		
31	Sp I	Aliva	Br.					5,200	2,100	2,700	66.11	33.11		
31	Sp I	Aliva	Br.					1,900		1,000	65.33	33.14		
31	Sp I	Aliva	Br.					3,200	3,500	2,000	67.33	33.32		
147	Sp I	Aliva	Br.	550	1,146	<13	46			5,600	63.85	31.21		
202	Sp I	Aliva	Br.	650	913	<13	36			6,800	62.07	28.56		
214	Sp I	Aliva	Br.	547	860	<13	55			3,200	61.64	29.84	11.9	–46.9
225	Sp I	Aliva	Br.	450	1,028	25	45			4,100	60.76	30.60		
12	Sp I	Garamas	Br.	280	1,070	<13	45			3,500	64.89	31.16	–3.8	–46.9
71A	Sp I	Liordes	Br.	320	850	<13	94			3,100	65.56	34.17		
828I	Sp I	Liordes	Br.	330	805	<13	83			3,000	64.37	32.06	8.6	–46.8
92	Sp I	Andara	Br.	1,200	1,536	<13	46			2,200	64.91	35.77	1.1	–46.4
710	Sp I	V.Sotres	Br.		800	<13	40			4,500	63.30	29.28	12.9	–47.1
V1	Sp II	Aliva	Gr.	800	860	<13	9	10		1,400	67.29	32.84		
V2	Sp II	Aliva	Gr.	800	779	<13	5	< 3		2,100	67.50	33.11		
C4	Sp II	Aliva	Red	2,000	936	<13	<4	61		500	67.40	33.47		
20	Sp II	Aliva	Or.	1,800	946	<13	9	154		800	67.44	32.97		
22	Sp II	Aliva	Or.	750	1,025	<13	6	111		1,300	67.60	33.14		
25	Sp II	Aliva	Y.	825	885	<13	6	55		1,200	67.51	33.02		
27	Sp II	Aliva	Or.	808	975	<13	23	191		1,600	67.42	32.64	–2.0	–46.2
30	Sp II	Aliva	Red	1,900	908	<13	<4	84		800	67.45	32.98		
34	Sp II	Aliva	Y.	1,110	951	<13	<4	82		2,400	67.12	32.24		
35	Sp II	Aliva	Y.	700	808	<13	10	35		1,100	67.58	33.11		
44	Sp II	Aliva	Y.	600	902	<13	8	30		2,400	67.61	33.23		
50	Sp II	Aliva	Y.	850	947	<13	10	79		1,200	67.11	32.72	–0.8	–45.9
54	Sp II	Aliva	Y.	1,000	743	<13	9	20		1,200	67.28	32.81	1.1	–45.9
139	Sp II	Aliva	Y.	1,500	822	<13	<4	58		800	67.50	32.62		
200	Sp II	Aliva	Or.	1,650	904	<13	12	80		1,600	67.18	33.60		
203	Sp II	Aliva	Or.	1,250	839	<13	<4	75		1,000	67.78	33.13		
209	Sp II	Aliva	Red	2,119	1,026	<13	9	136		1,600	67.12	33.88		
212	Sp II	Aliva	Or.	1,871	999	<13	22	268		600	67.20	32.75		
YS	Sp II	Fte.De	Y.	100	824	<13	9	866		4,900	65.55	32.80	–6.8	–47.2
828II	Sp II	Liordes	Y.	520	1,046	<13	11	140		1,900	65.95	34.74	4.2	–46.3
74	Sp II	Liordes	Y.	480	851	<13	<4	649		4,200	65.75	34.67		
71A	Sp II	Liordes	Y.							200	67.61	33.61		
71A	Sp II	Liordes	Y.					1,100	4,300	200	68.14	33.54		
71A	Sp II	Liordes	Y.						3,800	2,000	67.29	33.81		
71A	Sp II	Liordes	Red					3,100	500	8,00	66.93	33.62		
71A	Sp II	Liordes	Red					2,300	1,600	1,700	67.16	33.43		
78A	Sp II	Andara	Y.	935	1,143	<13	<4	288		1,800	66.66	37.13		
79	Sp II	Andara	Y.	1,200	1,192	<13	<4	102		900	66.23	37.04		
80A	Sp II	Andara	Y.	960	1,176	<13	<4	456		2,100	66.61	36.26		
84A	Sp II	Andara	Y.	850	1,118	<13	4	115		1,800	65.46	34.37	–0 4	–46.3
85A	Sp II	Andara	Y.	1,000	1,049	<13	<4	1,335		1,200	67.10	37.41		
99	Sp II	Andara	Y.	1,150	1,743	<13	<4	3,913		4,500	62.93	30.67		

Except where otherwise indicated, concentrations are in ppm
Analytical methods: Cd, Ga, and Ge (XRF), Bi and Cu (electron microprobe), Fe (XRF and electron microprobe), Zn, Hg, and S (AA)
Mineral abbreviations: Sp = sphalerite, I = type I mineralization, II = type II mineralization
Color abbreviations: Y. = yellow, Br. = brown, P. Br. = pale brown, D. Br. = dark brown, Or. = orange, Gr. = green

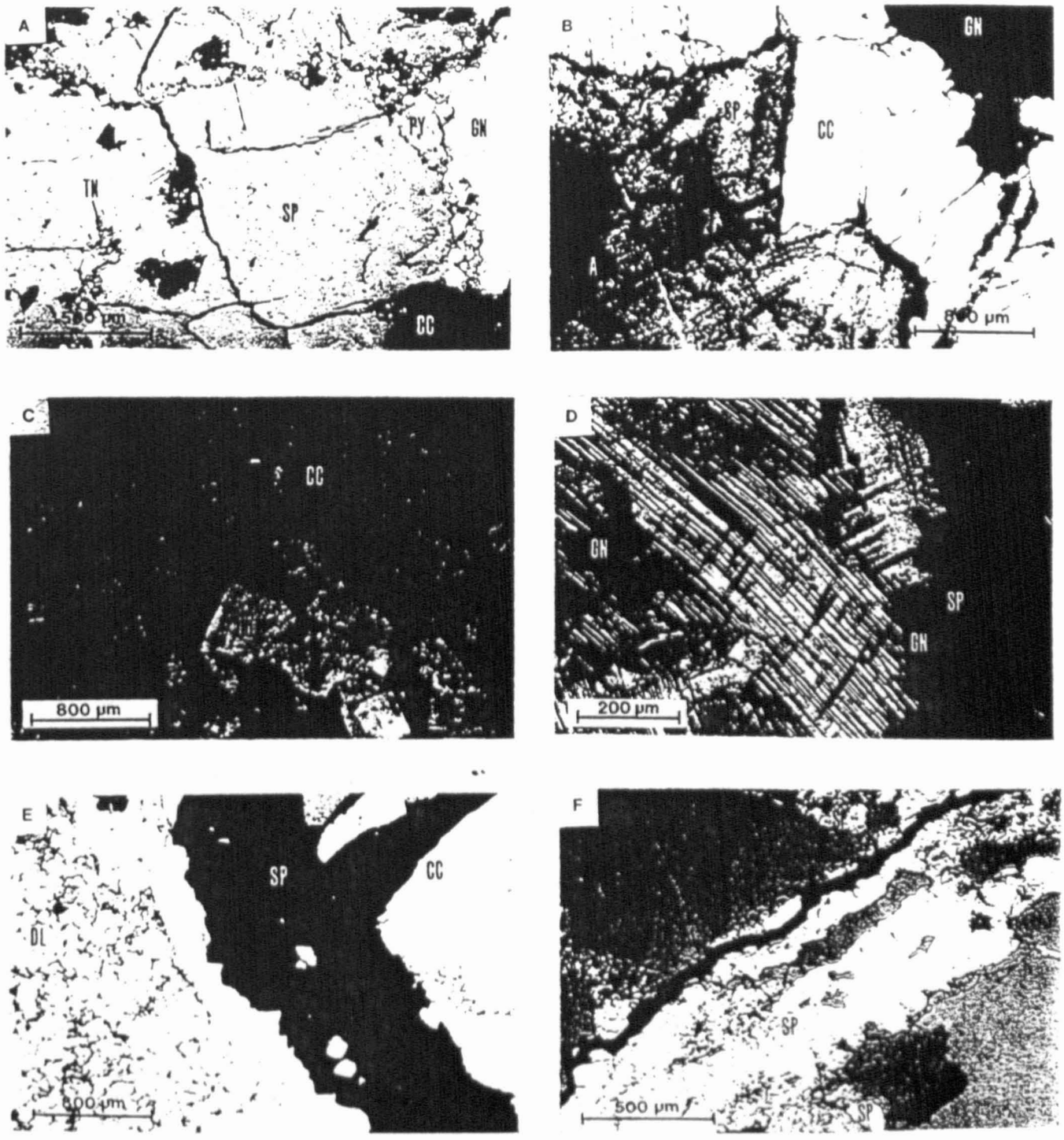

FIG. 9. A. Plane-polarized reflected light. In type II mineralization the yellow sphalerite contains numerous pyrite and some tennantite inclusions and has been partly replaced by galena and calcite. B. Plane-polarized transmitted light. Euhedral crystals of the typical Picos de Europa zoned, yellow sphalerite, surrounded by calcite and galena. C. Plane-polarized transmitted light. Euhedral dolomite crystals replacing fine-grained carbon-rich calcite of the host rock. This restricted dolomitization is related to the deposition of the type II sulfide mineralization. D. Plane-polarized transmitted light. Polysynthetic twinning in calcite of type II mineralization containing galena inclusions. The calcite has partly replaced sphalerite and galena. E. Plane-polarized transmitted light. Type II yellow sphalerite and calcite veinlets crossing dolomitized host carbonates. F. Plane-polarized reflected light. Type II yellow sphalerite veinlet cutting two layers of alternating type I brown sphalerite and dolomite. Abbreviations: CC = calcite, DL = dolostone, DO = dolomite, GN = galena, PY = pyrite, SP = sphalerite, TN = tennantite.

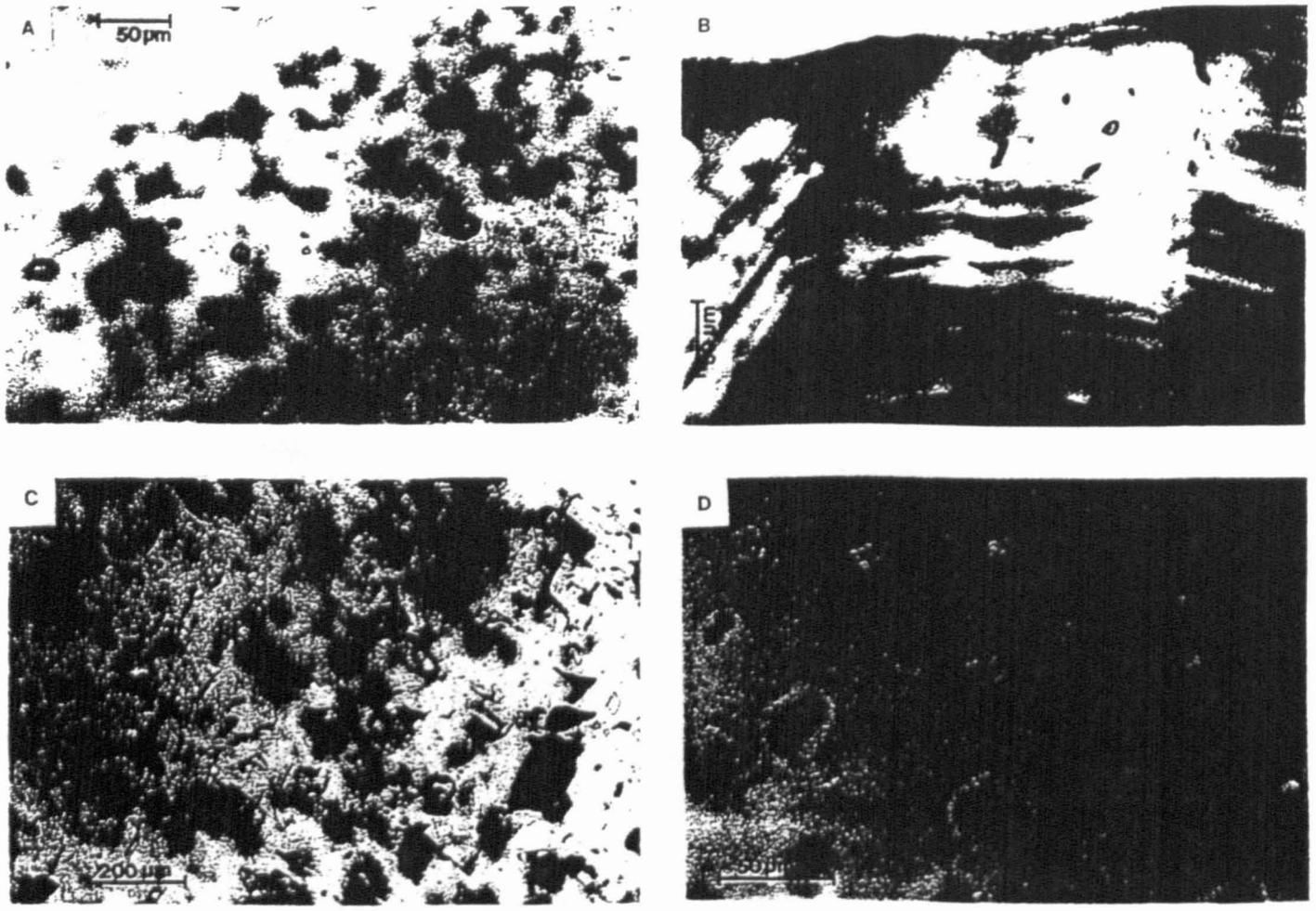

FIG. 10. Morphology, distribution, and types of fluid inclusions in Aliva minerals. A. Alignment of pseudosecondary fluid inclusions in type I sphalerite from the Aliva mine. B. Growth bands in type II sphalerite and distribution of primary and pseudosecondary fluid inclusions in clusters and lines. C. Primary and secondary fluid inclusions in calcite. Note that some of the inclusions are totally decrepitated. D. Pseudosecondary fluid inclusions in a healed fracture in fluorite.

room temperature, with the vapor bubble less than 20 percent of the total inclusion volume (Fig. 10A–D). In addition, a smaller number of fluid inclusions contain one (H_2O L), two (H_2O L + mechanically trapped solids), or three (H_2O L + V + mechanically trapped solids) phases. In order to avoid erroneous interpretations, fluid inclusions in fluorite, calcite, and dolomite which showed variable degrees of fill at room temperature, due to leakage or necking down as a consequence of postcrystallization deformation or partial decrepitation during the microthermometric processes, were not studied. Fluid inclusion morphology in the samples studied varies from polyhedral to round, or completely irregular, and sizes are generally below 30 μm. The fluid inclusions are, in general, abundant in fluorite and calcite, and scarce in sphalerite and dolomite.

More than 450 fluid inclusions have been studied and the microthermometric results are summarized in the Table 3 and Figure 11. Eutectic temperatures measured in the fluid inclusions varied between –45° and –55°C (cf. T_e = –54.4°C for the pure system H_2O-NaCl-$CaCl_2$). These temperatures indicate the presence of not only Na^+ and Ca^{2+} in the aqueous solutions but also, possibly, minor amounts of other cations such as Mg, Fe, K, etc. Such composition may be expected in view of the lithological context of the deposits. The absence of daughter minerals at room temperature and hydrates in the cooling experiments indicates that the mineralizing fluids were undersaturated in the H_2O-NaCl system with other cations. Final ice-melting temperatures ranged from –4° to –21.3°C, indicating salinities in terms of the system NaCl-H_2O (Potter et al., 1978) between 6.4 and 23.6 wt percent NaCl equiv and 1.2 and 5.7 molal, respectively. Homogenization temperatures ranged from 80° to 174°C, and since all fluid inclusions investigated were found to homogenize into the liquid phase, there is no evidence that the fluids boiled. The trapping temperatures of monophase liquid inclusions in fluorite were below 80°C. The CO_2 content of the mineralizing solutions must have been low, since no CO_2 (as "double bubbles") has been detected in the fluid inclusions.

X-ray microanalyses of fluid inclusions, following the method of Ayora and Fontarnau (1990), have been made of fluid inclusions in sphalerite I (sample 37) and confirm that the major constituents of the trapped solutions are H_2O and NaCl (the technique is capable of detecting 0.01 *m* Ca and K, and 0.35 *m* Mg). The mechanically trapped crystals in these

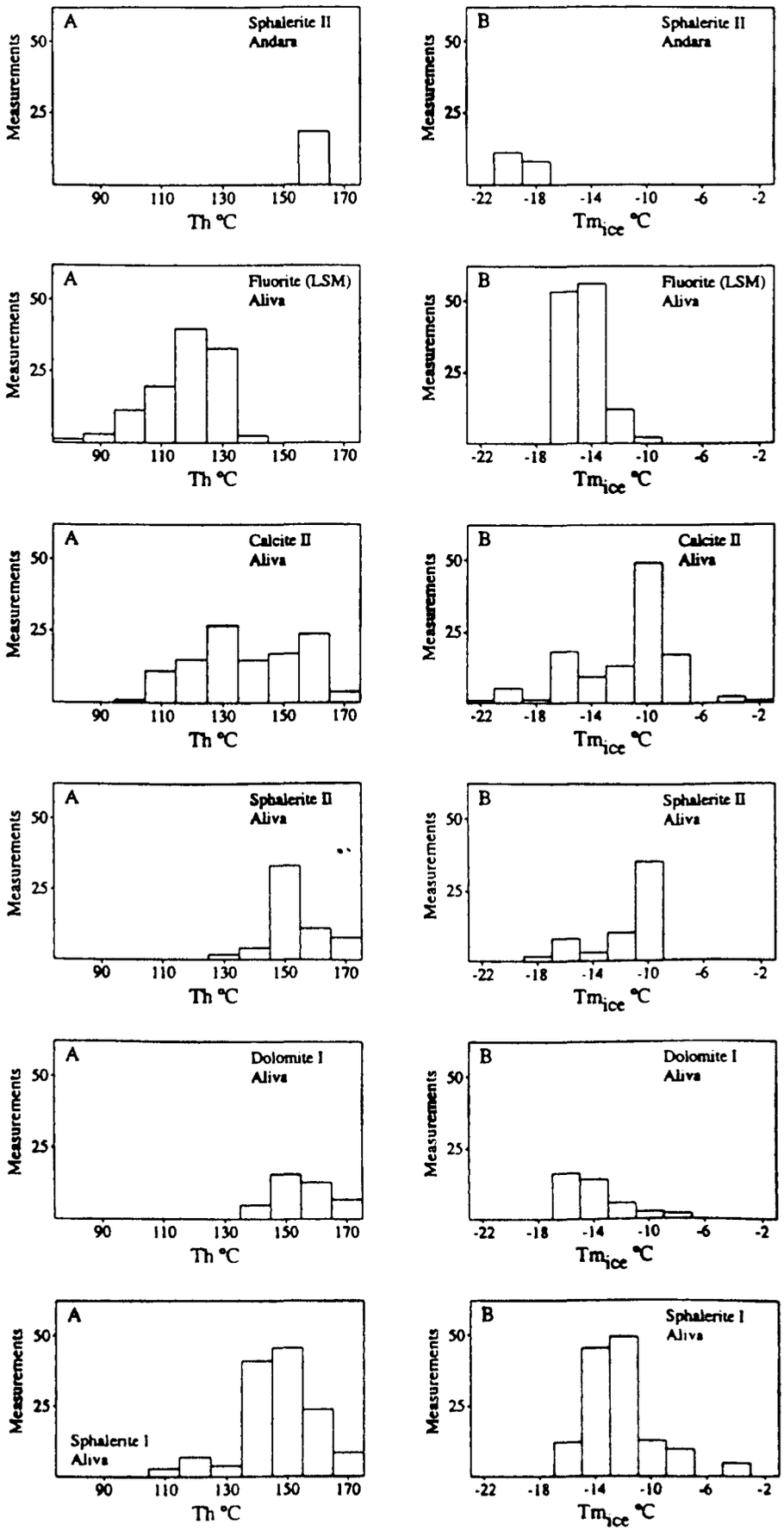

FIG. 11. T_h (A) and Tm_{ice} (B) of fluid inclusions from the Aliva and Andara deposits. Abbreviations: I = type I mineralization, II = type II mineralization, LSM = late-stage minerals.

TABLE 4. δ^{34} S, δ^{13}C, and δ^{18}O values (‰) of Various Minerals from Ore Deposits in the Southeastern Sector of Picos De Europa, Plus Isotope Characterization of the Mineralizing Fluids

Sample no.	Mineral	Orebody	δ^{34}S (mineral)	δ^{13}C (mineral)	δ^{18}O (mineral)	δ^{34}S[1] (H_2S)	δ^{13}C[2] (CO_2)	δ^{18}O[3] (H_2O)
R15 (1)	Sp I	Aliva	10.2			9.7		
R15 (2)	Sp I	Aliva	10.3			9.8		
R15	Gn I	Aliva	9.6			12.8		
3N	Sp I	Aliva	12.5			12.0		
3N	Gn I	Aliva	8.7			11.9		
214	Sp I	Aliva	11.9			11.4		
214	Gn I	Aliva	10.2			13.4		
36	Do I	Aliva		2.5	15.9		0.7	1.6
DTA.PG	Do I	Aliva		1.0	15.0		-0.8	0.7
DTA.23	Do[4]	Aliva		2.9	16.2		1.1	1.9
27	Sp II	Aliva	-2.0			-2.5		
27	Gn II	Aliva	-4.8			-1.6		
50	Sp II	Aliva	-0.8			-1.3		
50	Gn II	Aliva	-3.1			0.1		
54	Sp II	Aliva	1.1			0.6		
54	Gn II	Aliva	-1.8			1.4		
CTA.21	Cc II	Aliva		1.0	11.5		0.3	0.7
12	Sp I	Caramas	-3.8			-4.3		
12	Gn I	Caramas	-9.3			-6.1		
YS	Sp II	Fuente Dé	-6.8			-7.3		
YS	Gn II	Fuente Dé	-16.8			-13.6		
8281	Sp I	Liordes	8.6			8.1		
828II	Sp II	Liordes	4.2			3.7		
92	Sp I	Andara	1.1			0.6		
84A	Sp II	Andara	-0.4			-0.9		
710	Sp I	V.Sotres	12.9			12.4		

Abbreviations: Cc = calcite, Do = dolomite, Gn = galena, Sp = sphalerite, I = type I mineralization, II = type II mineralization

[1] δ^{34}S (H_2S) values in equilibrium with sphalerite and galena at 170°C, calculated from Ohmoto an Rye (1979); fluid inclusion data are not available for Liordes, Las Caramas, and Vegas de Sotres, hence values showed here are tentative

[2] $\delta^{13}C(CO_2)$ values in the mineralizing fluids, calculated from Ohmoto (1972, 1986)

[3] δ^{18}O values of the mineralizing fluids calculated from O'Neil et al. (1969) and Northrop and Clayton (1966) for 170°C

[4] Dolomite DTA.23 cannot be classified with certainty as either type I or II but is clearly earlier than calcite CTA.21 (type II)

interpreted according to data of Hall and Friedman (1969), Anderson (1973), Sverjensky (1986), and Taylor (1987) to be the result of hydrothermal alteration. As shown in Figure 13, the host limestones have a narrow range of δ^{13}C values (approx 4–5.5‰), which were very weakly modified during early dolomitization to slightly lower δ^{13}C values. These rocks were then progressively modified to lower δ^{13}C values through interaction with a hydrothermal fluid.

Sulfides: The δ^{34}S values of the sulfides show an overall range from 12.9 to –16.8 per mil (Table 4), the type II sulfides being lighter than the type I sulfides in every deposit (Fig. 14).

The near-neutral pH nature of the fluid is demonstrated by the dissolution and precipitation of carbonates, which indicates fluctuations in pH with time. As pyrite is found coexisting with sphalerite in both type I and II mineralization, fo_2 conditions may be calculated from the FeS content of the sphalerite according to Helgeson (1969), Craig and Scott (1974), and Barton and Skinner (1979). fo_2 at the site of mineral deposition appears to have been approximately the same in each mineralizing event ($\log fo_2 \approx -46$ to -47, Table 2).

Calculated $\delta^{34}S_{H_2S}$ values, using fractionation data of Ohmoto and Rye (1979), for the fluid from which the Aliva type I mineralization precipitated vary between 9.7 and 13.4 per mil, with an average of 11.6 per mil (Table 4). Corresponding values for Aliva type II range from –2.5 to 1.4 per mil, with an average of –0.6 per mil. Under the T-fo_2 -pH conditions described above, $\delta^{34}S_{fluid} = \delta^{34}S_{H_2S}$ for both type I and type II. Under these conditions, the difference in isotopic composition of sulfide minerals between the two types of mineralization cannot be explained on the basis of a constant $\delta^{34}S_{fluid}$ with changes in fluid conditions. On the contrary, it is evident that the δ^{34}S of the fluid was very different during the two mineralization phases, whereas the oxidation state was relatively constant.

Rare earth elements in carbonates

Analyses have been made of the REE distribution in nine representative samples of host limestone and dolostone located close to the Aliva mineralization (Table 6), and of the gangue calcite and dolomite. The results are shown in the distribution patterns, normalized to chondrite values (Fig. 15). A common feature of the carbonates is the existence of negative anomalies in Ce (variable Ce/Ce* between 0.65 and 0.9), being slightly higher in limestones and calcite cement than in dolostone and dolomite cements (Gómez-Fernández and Arribas, 1993). Ce deficiencies are a legacy of the generation of the mineralizing solutions (Evensen et al., 1978; Möller, 1983; Möller and Morteani, 1983).

Although the populations are too small to justify firm conclusions, all of the carbonates analyzed for REE have Yb/La-Yb/Ca ratios that plot within or near the field for

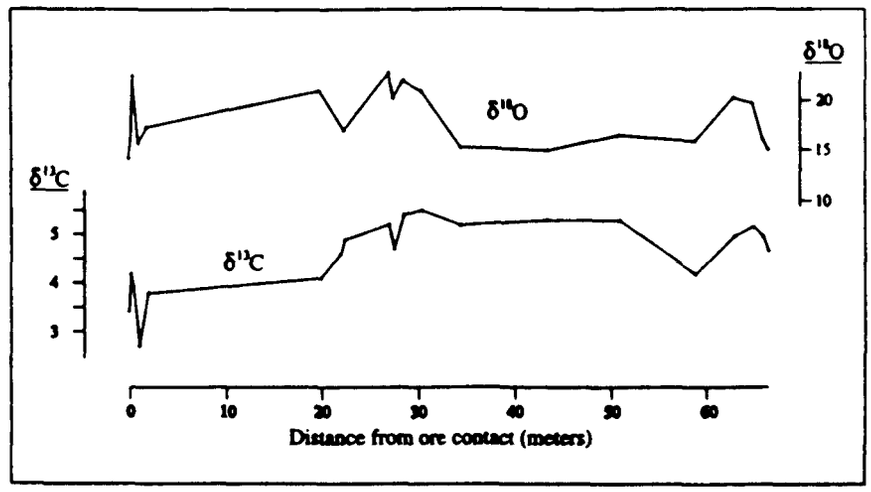

FIG. 12. Distribution of $\delta^{13}C$ and $\delta^{18}O$ values in Aliva carbonate host rocks and the distance from ore contact.

hydrothermal carbonates in the diagram of Parek and Möller (1977; Gómez-Fernández and Arribas, 1993; Fig. 16). This is to be expected for the calcite and dolomite of the mineralization, but the data for the limestones and dolostones also indicate that significant hydrothermal alteration has taken place, partially modifying the original distribution of REE. Thus, the limited REE data support the isotopic evidence for interaction between the mineralizing fluids and carbonate host rocks.

Metallogenetic Interpretation and Discussion

The $\delta^{34}S_{fluid}$ values > 10 per mil exclude a magmatic origin for the sulfur in type I mineralization, so that the relatively distant igneous activity in the Palentine zone during the Permian bears no relationship with the mineralization. The sulfur was most likely derived from sulfate reduction of marine water, this term being used in the broad sense to include evolved marine waters such as formation waters, basinal brines, etc. The field and stable isotope data point to a crustal origin of the mineralizing fluids, and possible sources include marine water contained in detrital sediments of exclusively Carboniferous age ($\delta^{34}S_{sulfate}$ = 15‰, Claypool et al., 1980) or isotopically heavier water resulting from a combination of Carboniferous, Devonian, and/or Silurian waters. On the basis of the isotopic data alone, another possible source of the mineralizing fluids is Permian marine water ($\delta^{34}S_{sulfate}$ = 10‰, Claypool et al., 1980), since marine sedimentation took place in the northern Picos de Europa during the Permian. However, as discussed below, geologic considerations do not support this alternative source.

TABLE 5. ^{13}C and ^{18}O Values (‰) of Aliva Carbonate Host Rocks and Distance from Ore Contact

Sample no.	Rock	Orebody	Distance from ore (m)	$\delta^{13}C_{PDB}$	$\delta^{18}O_{SMOW}$
C.R15	Limestone	Aliva	0	3.4	13.9
D.12	Dolostone	Aliva	0.3	4.2	16.2
D.PC	Dolostone	Aliva	0.5	3.9	22.2
C. coral	Limestone	Aliva	1.0	2.7	15.4
D.coral	Dolostone	Aliva	2.0	3.8	17.1
D.13	Dolostone	Aliva	20.0	4.1	20.7
DH.318–77.9	Limestone	Aliva	22.1	4.6	17.4
DH.318–77.5	Limestone	Aliva	22.5	4.9	16.8
DH.318–73.0	Limestone	Aliva	27.0	5.2	22.6
DH.318–72.5	Limestone	Aliva	27.5	4.7	20.0
DH.318–71.5	Limestone	Aliva	28.5	5.4	21.9
DH.318–69.5	Limestone	Aliva	30.5	5.5	20.7
DH.318–65.5	Limestone	Aliva	34.5	5.2	15.1
DH.318–56.5	Limestone	Aliva	43.5	5.3	14.8
DH.318–49.0	Limestone	Aliva	51.0	5.3	16.4
DH.318–41.0	Limestone	Aliva	59.0	4.2	15.8
DH.318–37.0	Limestone	Aliva	63.0	5.0	20.2
DH.318–35.0	Limestone	Aliva	65.0	5.2	19.7
DH.318–34.0	Limestone	Aliva	66.0	5.0	16.1
DH.318–33.5	Limestone	Aliva	66.5	4.7	15.1

Involvement of an isotopically lighter sulfur source is clearly required to explain the calculated $\delta^{34}S_{fluid}$ values for type II mineralization. The foetid nature of much of the limestone in the area suggests the existence of a high content of organic matter, rich in isotopically light carbon and sulfur. It is likely that, as a result of reaction with the host rocks, the mineralizing solutions became enriched in isotopically light sulfur derived from organic matter and diagenetic pyrite in the limestone. The difference in $\delta^{34}S$ values between sulfides of the two types of mineralization is, therefore, interpreted as the result of a greater interaction between the type II mineralizating fluid and the host rocks. The mineral textures provide supporting evidence for this interpretation in that they indicate rapid deposition of the type I mineralization (laminated sphalerites with very small inclusions of other sulfide crystals) and slower deposition of the type II mineralization with development of large crystals.

From the fluid inclusion study it can be concluded that chloride complexes were responsible for metal transportation. The experimental data of Barrett and Anderson (1988) show that Zn and Pb are soluble in aqueous solutions in the form of chloride complexes and that their solubility increases with increasing salinity and temperature. The marine waters would have been the source of chloride and some cations, and their heating during tectonic processes would have resulted in alteration of the surrounding rocks, releasing more cations and metals into the aqueous phase. On the other hand, pH

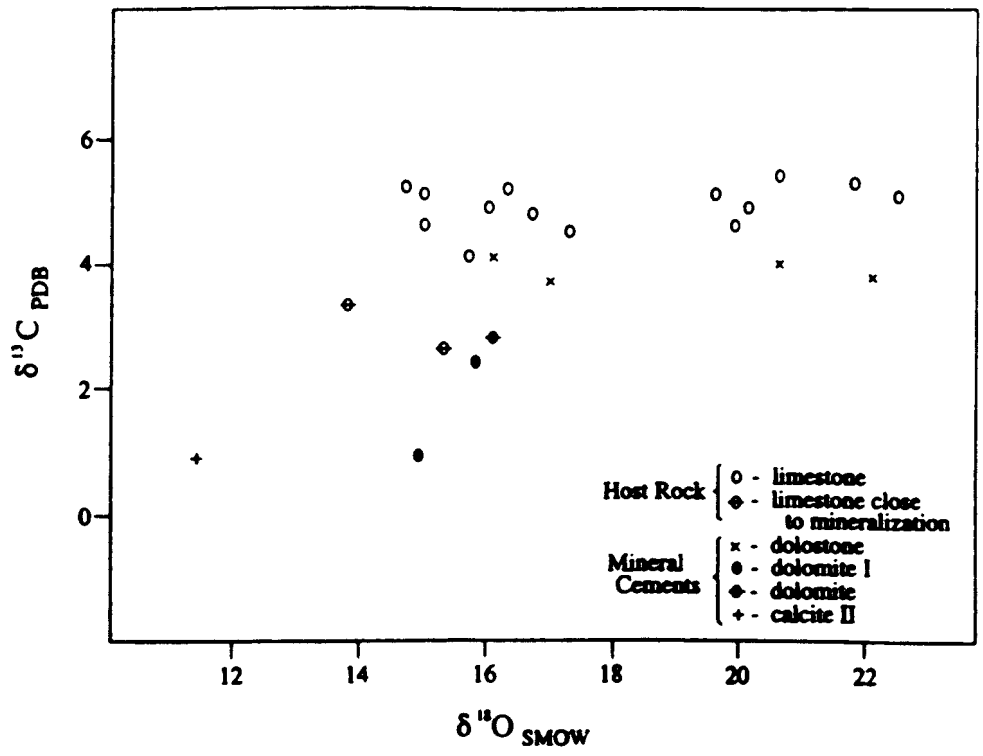

FIG. 13. Isotopic composition of carbonates from the Aliva mine.

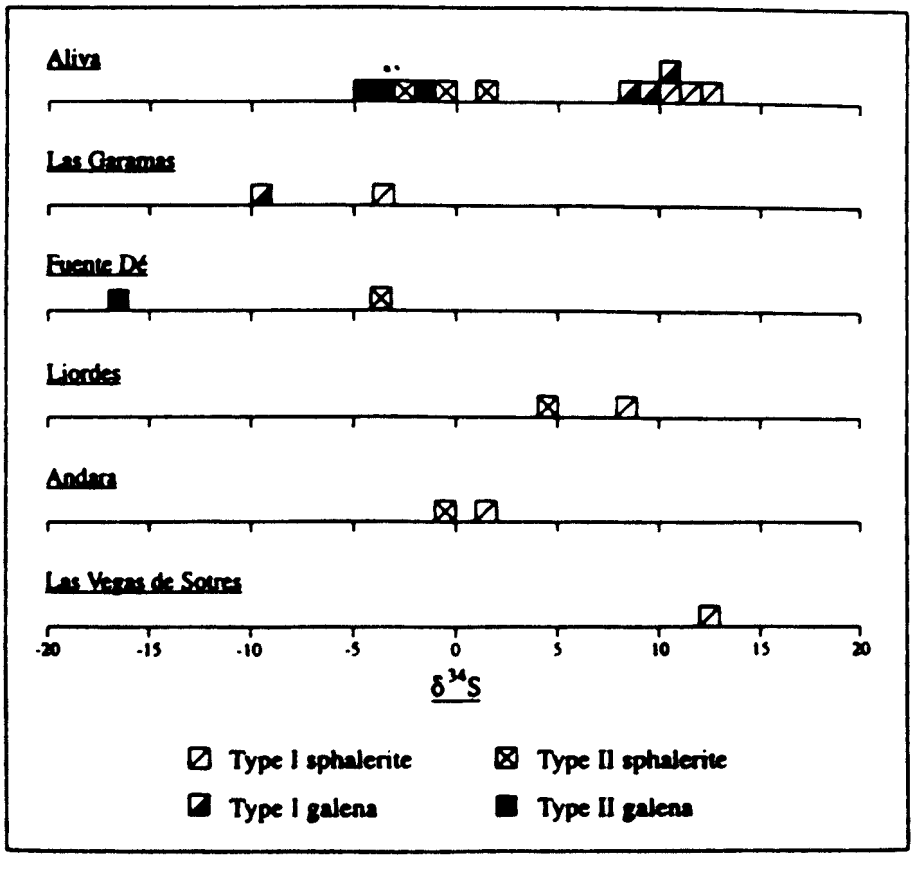

FIG. 14. Distribution of $\delta^{34}S$ values in sphalerite and galena from the southeastern sector of the Picos de Europa mining district.

TABLE 6. Distribution of Major and REE of Carbonate Gangue Minerals and Host Rocks in the Aliva Ore Deposit

Sample	1	2	3	4	5	6	7	8	9
SiO_2 (wt %)	2.01	0.42	0.07	0.05	0.2	0.13	0.04	0.19	0.08
Al_2O_3 (wt %)	0.06	0.16	0.01	0.01	0.05	0.05	0.01	0.15	0.01
Fe_2O_3 (wt %)	0.21	0.16	0.05	0.03	0.57	0.77	0.37	0.75	0.49
SO_3 (wt %)	0.2	0.17	0.05	0.05	0.05	0.13	0.02	0.02	0.02
CO_2 (wt %)	40.77	43.26	43.56	42	43.85	45.29	46.21	45.29	44.47
MgO (wt %)	0.67	0.78	0.54	0.57	19.76	19.31	19.5	18.97	19.48
CaO (wt %)	54.39	55.4	57.57	57.65	31.98	32.71	33.95	32.32	32.85
Ca (wt %)	38.88	39.60	41.15	41.21	22.86	23.38	22.27	23.10	23.48
Sr (ppm)	407	236	140	214	23	27	46	43	20
La (ppm)	15.00	2.20	57.20	25.70	1.00	1.00	3.20	1.50	2.20
Ce (ppm)	23.00	4.00	80.00	35.00	2.00	2.00	7.00	4.00	5.00
Pr (ppm)	3.70	1.00	14.00	5.90	0.40	0.40	1.10	0.90	1.20
Nd (ppm)	11.00	<3.00	45.00	18.00	<3.00	<3.00	4.00	<3.00	3.00
Sm (ppm)	1.80	0.40	8.00	2.90	0.20	0.20	0.80	0.70	1.00
Eu (ppm)	0.53	0.15	2.28	1.18	0.10	0.12	0.35	0.24	0.39
Gd (ppm)	2.10	0.60	8.60	3.20	0.20	0.40	1.20	1.00	1.50
Tb (ppm)	0.20	0.10	0.90	0.40	<0.10	<0.10	0.20	0.20	0.30
Dy (ppm)	1.80	0.60	5.50	2.50	0.40	0.40	1.30	1.10	1.90
Ho (ppm)	0.43	0.16	1.11	0.54	0.10	0.13	0.30	0.25	0.49
Er (ppm)	1.20	0.50	2.60	1.20	0.20	0.10	0.80	0.60	1.20
Tm (ppm)	0.10	<0.10	0.30	0.20	<0.10	<0.10	0.10	<0.10	0.10
Yb (ppm)	0.86	0.28	1.46	0.75	0.17	0.14	0.56	0.50	0.73
Lu (ppm)	0.13	0.04	0.19	0.10	0.02	0.02	0.08	0.07	0.10
Y (ppm)	16.00	6.00	37.00	18.00	4.00	3.00	10.00	7.00	16.00
Eu/Eu*	0.83	0.94	0.84	1.18	1.51	1.27	1.09	0.86	0.97
ΣREE	61.85	10.03	227.14	97.57	4.79	4.91	20.99	11.06	19.11
ΣREE + Y	77.85	16.03	264.14	115.57	8.79	7.91	30.99	18.06	35.11

Notes: 1, 2 = limestone; 3, 4 = gangue calcite; 5, 6 = dolostone; 7, 8, 9 = gangue dolomite

Analytical methods: INAA: La, Ce, Nd, Sm, Eu, Tb, Yb, and Lu; ICP/MS: Pr, Gd, Dy, Ho, Er, and Tm; XRF and ICP/MS: Y. ICP: SiO_2, Al_2O_3, Fe_2O_3, CO_2, SO_3, MgO, CaO, and Sr

increase in acidic solutions reacting with carbonate rocks leads to deposition of sphalerite and galena (Anderson, 1973; Sverjensky, 1986). It is likely, then, that an increase in pH was the major cause of the formation of the Picos de Europa deposits, but contributing factors may have been decreasing temperature, pressure, and salinity of the mineralizing fluids as they reacted with the host rocks.

Absolute dating of the age of mineralization has not been undertaken. However, timing of the ore-forming process can be partly constrained by comparison of the data and observations obtained during this study with the tectonic evolution of the region. Dolomitization was epigenetic, being geometrically related to the N 105° to 120° E directional faults, and therefore of late Carboniferous-Permian age or later. The mineralization commonly replaced dolostones, and thus, occurred later than dolomitization but before the last compressive events, because it is deformed. In view of the above, and on the basis of structural and morphological criteria, the possible age of the mineralization spans from the Carboniferous-Permian boundary to the end of the compressive events in the region, which probably took place during the Miocene (Hines, 1985).

It has also not been possible to establish with certainty the mechanism responsible for flow of the mineralizing fluids toward the sites of ore deposition. In a study of numerous Mississippi Valley-type ore districts, Leach and Sangster (1993) discussed the three mechanisms of fluid flow that have been proposed for this type of deposit: sediment diagenesis and compaction, tectonic drive during compressional events, and convecting cells in extensional structural settings. The following discussion considers these mechanisms in relation to possible ages of the mineralization in the southeastern part of the Picos de Europa province.

Permian age: During the Permian postorogenic extension, the Picos de Europa structural province consisted of a Carboniferous imbricate complex more than 2,800 m thick. Therefore neither tectonic drive, related to compression, nor compaction and diagenesis of the overlying Permian sediments could have given rise to deposition of Zn-Pb ores in the deep-seated Carboniferous thrust sheets (Frontal, Tesorero-Agero, and Lechugales tectonic units) which formed the basement below.

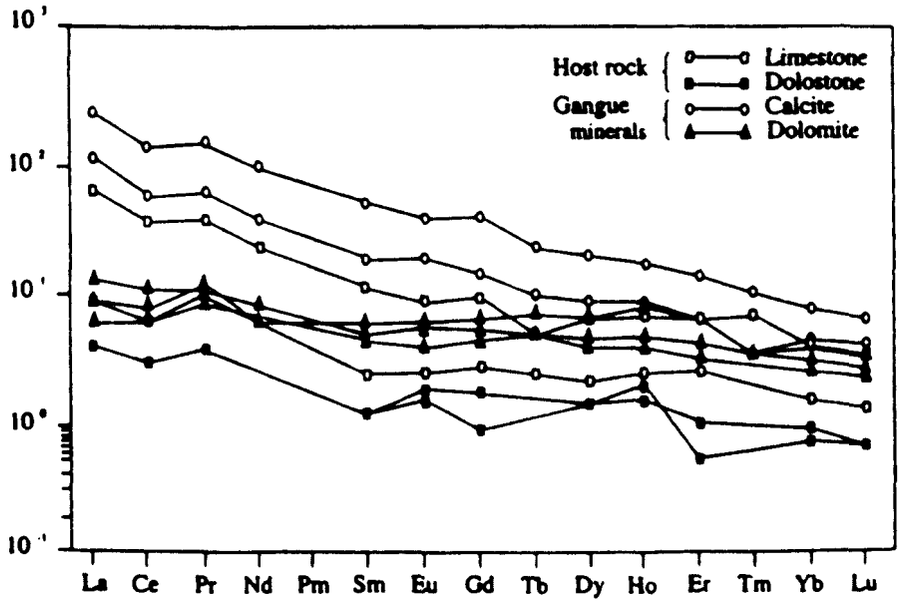

FIG. 15. Abundances of REE in Aliva carbonate gangue minerals and host rocks normalized to chondrite values

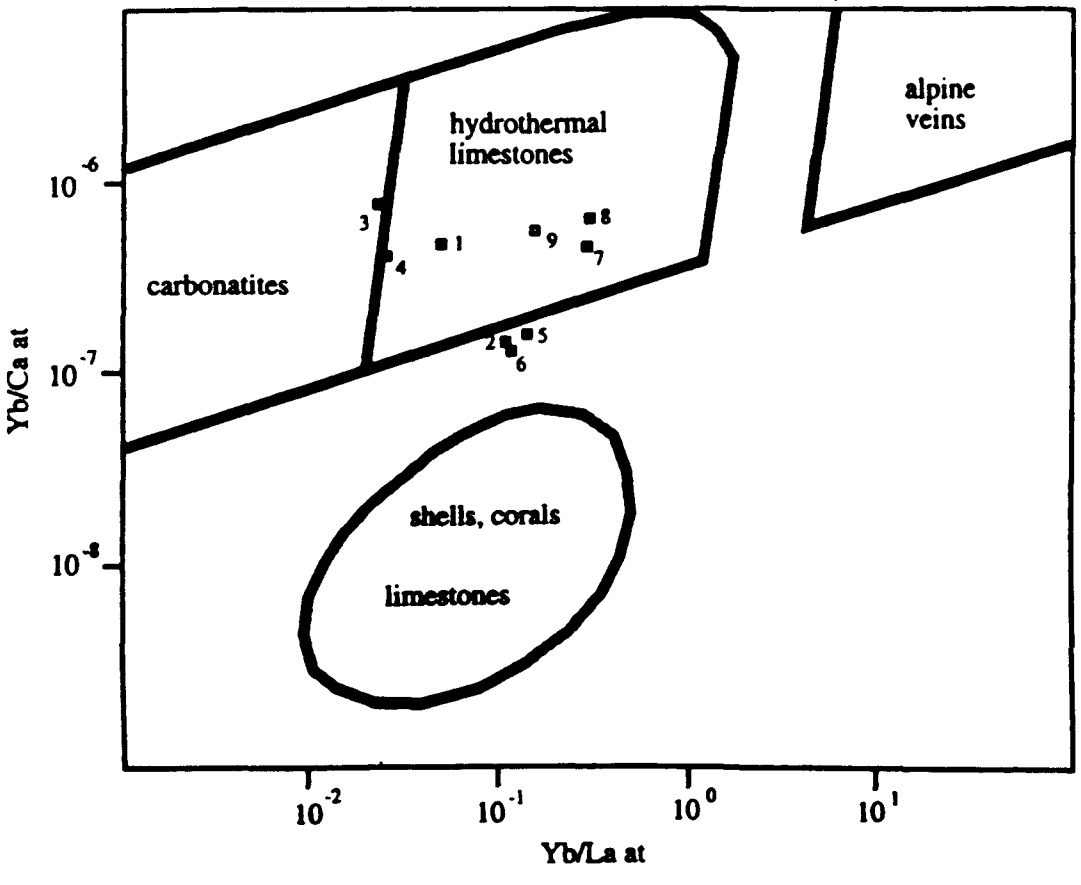

FIG. 16. Variation diagram of Yb/Ca vs. Yb/La for Aliva mine carbonates and fields for carbonates of various origins (after Parekh and Möller, 1977); at = atomic ratio. Numbered squares: 1, 2 = limestone; 3, 4 = gangue calcite; 5,6 = dolostone; 7, 8, 9 = gangue dolomite.

On the other hand, crustal thinning and increased geothermal gradient during the Permian extensional regime could have resulted in the generation of hydrothermal fluids and ore deposition during the first post-Carboniferous phase of extension. According to this model, hot brines charged with metals migrated toward and through the Picos de Europa structural province by means of convective circulation. The fluid source would probably have been mainly marine waters of Carboniferous age contained in detrital sediments of the Palentine zone and the Picos de Europa province, although, as discussed above, fluid may also have been contributed from other sources.

The numerous layers of metal-rich black shales of the Palentine zone represent the most probable source of metals. Other sources could be the sediments of the Lebeña Formation (Fig. 3) and/or the Precambrian basement underlying the Palentine zone, but the small volume of the former, and the deep-seated situation and high metamorphic grade of the latter, do not favor either as the source of metals.

Mesozoic age: During the Mesozoic the Picos de Europa province was covered by sediments being deposited in the Basque-Cantabrian basin. The classic concept of expulsion of fluids by diagenesis and compaction of sediments would suggest that ore deposition should have taken place mainly in the Mesozoic carbonates, rather than below. Likewise, the concept of tectonic drive related to compression must be rejected because, at that time, the Picos de Europa province was subjected to an extensional tectonic regime.

On the other hand, the possible existence during the Mesozoic of convecting cells related to extension, with deposition of metals in the Picos de Europa province, would require an explanation as to why such a process did not also operate in the first (i.e., Permian) phase of extension.

Tertiary age: Tectonic drive is the only possible fluid flow mechanism consistent with the compresive tectonic regime acting on the Picos de Europa province from the Priarbonian to the Miocene. However, Mesozoic waters from the Basque-Cantabrian basin and Tertiary waters could not have been involved in the mineralizing process during Tertiary compression, since at that time fluid flow would have been in the opposite direction, i.e., from the uplifted Picos de Europa structural province toward the surrounding Mesozoic and Tertiary sedimentary basins.

According to the above discussion, the most probable age of the Zn-Pb deposits of the southeastern part of the Picos de Europa is Permian. This reasoning is supported by the observations carried out in the northern part of the Picos de Europa structural province by Martínez-García (1983), who described Aliva-type Zn-Pb mineralization hosted in fractures which had ceased to be active by the Triassic, and those in the easternmost part of the Picos de Europa province by Saulas (1985) and Barbanson (1987), who described detrital

fragments of Zn-Pb mineralization in Permian rocks. This conclusion also implies that the regional dolomitization, which preceded Zn-Pn mineralization, also took place during the Permian.

Conclusions

The metallogenic characteristics of the Zn-Pb deposits located in the southeastern sector of the Picos de Europa structural province indicate that these deposits can be classified as Mississippi Valley type (Sangster, 1990, 1993; Leach and Sangster, 1993). The principal features that support such a classification are as follows: (1) the deposits are epigenetic Zn-Pb mineralization, hosted by platform carbonates, and controlled by faults and dolostone-limestone transitions; (2) the deposits show no mineral zoning; (3) mineral deposition was accompanied by alteration processes, including brecciation and dissolution of host rocks, (4) trapping temperatures of the mineralizing fluids were between 170° and 200°C and salinities were around 15 wt percent NaCl equiv, and (5) isotopic data suggest that the sulfur was derived from sulfate reduction of marine water.

In the Picos de Europa province, the platform carbonate rocks hosting the deposits underwent thrusting prior to the onset of the mineralizing process, and consequently, the southeastern Picos de Europa deposits were formed under an imbricate complex more than 1,000 m in thickness, without any apparent relation to the topographic surface.

Although questions remain concerning the age of the mineralization and the origin and mechanism of flow of the fluids, it is considered most likely that mineralization took place during the Permian, with expulsion of the metal-bearing brines related to extensional processes taking place at the end of the Hercynian orogeny.

Acknowledgments

The authors are grateful for M. Hitzman, G.D. Sevastopulo, and D. Rhodes for constructive reviews. We would also like to thank C. Ayora for assistance with X-ray microanalysis of frozen fluid inclusions, E. Cardellach for AAS analysis, Marisa F. Rojo for assistance with preparation of the manuscript, and Asturiana de Zinc, S.A., particularly José A. Alonso, José L. Díaz, and Paloma Marquínez, for having made this study possible. A special tribute is also offered in memory of the late Miguel A. Escayo for his support and advice to F.G.-F. during his doctoral study that forms the basis of the present publication.

January 29, 1998; June 16, 1999

REFERENCES

Adhelard, W., 1968, Untersuchungen blei-zinkgerstätten bei Santander (nord-Spanien): Inaugural dissertation zur Erlangung der Doktorwürde der Naturwissenschaftlichen, Munchen, Fakultät der Ludwig-Maximilians Universität, 49 p.

Alonso, J.L., and Pulgar, J.A., 1995, La estructura de la Zona Cantábrica, *in* Alamburu, C., and Bastida, F., eds., Geología de Asturias: Gijón, Spain, Editorial TREA, p. 103–112.

Alonso, J.L., Pulgar, J.A., García-Ramos, J.C., and Barba, P., 1996, Tertiary basins and Alpine tectonics in the Cantabrian Mountains (NW Spain), *in* Friend, D.F. and Dabrio, C.J., eds., Tertiary basins of Spain: The stratigraphic record of crustal kinematics: Cambridge, Cambridge University Press, p. 214–227.

Anderson, G.M., 1973, The hydrothermal transport and deposition of galena and sphalerite near 100°C: Economic Geology, v. 68, p. 480–492.

Arribas, A., 1981, Distribución geoquímica de los elementos en trazas en los yacimientos españoles del tipo BPGC: Fundación Juan March, Serie Universitaria, v. 146, 54 p.

Ayora, C., and Fontarnau, R., 1990, X-ray microanalysis of frozen inclusions at –140°C: Chemical Geology, v. 89, p. 135–148.

Barbanson, L., 1987, Les mineralisations Zn, Pb, Ba, Hg, Cu du socle et couverture carbonatés de la Province de Santander (Nord de l'Espagne): Unpublished Thèse pour Docteur d'Etat, Orléans, France, Université d'Orléans, 292 p.

Barrett, T.J., and Anderson, G.M., 1988, The solubility of sphalerite and galena in 1–5 *m* NaCl solutions to 300°C: Geochimica et Cosmochimica Acta, v. 52, p. 813–820.

Barton, P.B., and Skinner, B.J., 1979, Sulfide mineral stabilities, *in* Barnes, H.L., ed., Geochemistry of hydrothermal ore deposits: New York, John Wiley and Sons, p. 278–403.

Berh, H.J., Horn, E.E., Frentzel-Beyme, K., and Reutel, C., 1987, Fluid inclusion characteristics of the Variscan and post-Variscan mineralizing fluids in the Federal Republic of Germany: Chemical Geology, v. 61, p. 273–285.

Calderón, S., 1900, La blenda de los Picos de Europa: Real Sociedad Española de Historia Natural Actas, v. 29, p. 153–161.

Cardellach, E., Johnson, C.A., Tritlla, J., and Hanan, B., 1993, Las mineralizaciones de Pb-Zn de Cierco (Pirineo Central, Lérida): Datos de inclusiones fluidas y de isótopos estables de C, O, S, Sr: Sociedad Española de Mineralogía Boletín, v. 16, p. 73–74.

Cissarz, A., 1932, Reflexion messungen an absorbierenden kristallen: Zeitschrift für Kristallographie, v. 82, p. 438–450.

Claypool, G.E., Holser, W.T., Kaplan, I.R., Sakai, H., and Zak, Y., 1980, The age curves of sulfur and oxygen isotopes in marine sulfate and their mutual interpretation: Chemical Geology, v. 28, p. 199–260.

Craig, J.R., and Scott, S.D., 1974, Sulfide phase equilibria: Reviews in Mineralogy, v. 1, p. CS1–110.

Evensen, N.M., Hamilton, P.J., and O'Nions, R.K., 1978, Rare earth abundances in chondritic meteorites: Geochimica et Cosmochimica Acta, v. 42, p 1199–1212.

Fernández-Martínez, J., and Velasco, F., 1996, The Troya Zn-Pb carbonate-hosted SEDEX deposit, northern Spain: Society of Economic Geologists Special Publication 4, p. 364–377.

García-Espina, R., 1991, La estructura del borde occidental de la cuenca Vasco-Cantábrica en el área de Campoo (Cantabria-Palencia): Unpublished Tesis de Licenciatura, Oviedo, Spain, Oviedo University, 38 p.

Gómez-Fernández, F., 1992, Metalogenia de los yacimientos de Pb-Zn del sector Sudeste de Picos de Europa: Unpublished Ph.D. thesis, Salamanca, Spain, Salamanca University, 241 p.

Gómez-Fernández, F., and Arribas, A., 1993, Nota preliminar sobre la distribución de tierras raras en carbonatos y fluorita de la mina de Aliva (Cantabria, España): Sociedad Española de Mineralogía Boletín, v. 16, p. 115–120.

Gómez-Fernández, F., and Arribas, A., 1994, Descripción de las mineralizaciones de Pb-Zn del sector sudeste de Picos de Europa (Norte de España). Implicaciones metalogenéticas: Boletín Geológico y Minero, v. 105-3, p. 249–262.

Gómez-Fernández, F., Escayo, M.A., Alonso, J.A., and Seebold, I., 1993a, Caracterización y origen de las dolomías del sector sudeste de Picos de Europa (Norte de España): Estudios Geológicos, v. 49, p. 343–350.

Gómez-Fernandez, F., Mangas, J., Both, R.A., and Arribas, A., 1993b, Metallogeny of the Zn-Pb deposits of the southeastern region of the Picos de Europa (Cantabria, Spain), *in* Fenoll Hach-Ali, P., Torres-Ruiz, J., and Gervilla, F., eds., Current research in geology applied to ore deposits: Granada, Spain, Universidad de Granada, p. 113–116.

Hall, W.E., and Friedman, I., 1969, Oxygen and carbon isotopic composition of ore and host rock of selected Mississippi Valley deposits: U.S. Geological Survey Professional Paper, v. 650–C, p. C140–C148.

Helgeson, H.C., 1969, Thermodynamics of hydrothermal systems at elevated temperatures and pressures: American Journal of Science, v. 267, p. 729–804.

Heredia, N., Rodríguez-Fernández, L.R., and Wagner, R.H., 1990, Carboniferous of the Palentine zone, *in* Dallmeyer, R.D., and Martínez-García, E., eds., Pre-Mesozoic geology of Iberia: Berlin, Springer-Verlag, p. 33–38.

Heredia, N., and Rodríguez-Fernandez, L.R., 1994, Tectónica: Memoria de la hoja n° 81 (Potes): Mapa Geológico Nacional a escala 1:50,000 (Mapa

Geológico Nacional, 2nd ed.), Madrid, Instituto Tecnológico Geominero de España (ITGE), p. 87–89.

Hines, F.M., 1985, Sedimentation and tectonics in north-west Santander: Institut d'Estudis Ilerdencs, European Regional Meeting, 6th, Excursion Guidebook 9, p. 371–392.

Jacobson, R.L., and Usdowsky, H.E., 1976, Partitioning of strontium between calcite, dolomite and liquids: Contributions to Mineralogy and Petrology, v. 59, p. 171–185.

Julivert, M., 1971, Decollement tectonics in the Hercynian Cordillera of northwest Spain: American Journal of Science, v. 270, p. 1–29.

Leach, D.L., and Sangster, D.F., 1993, Mississippi Valley-type lead zinc deposits: Geological Association of Canada Special Paper 40, p. 289–314.

Loredo, J., and García Iglesias, J., 1984, Estudio de inclusiones fluidas en paragénesis de minerales tipo 'Picos de Europa': Congreso Internacional de Minería y Metalurgia, 7th, Barcelona, Tome 1, p. 89–100.

Lüders, V., Gerler, J., Hein, U.F., and Reutel, C., 1993, Chemical and thermal development of ore-forming solutions in the Harz Mountains. A summary of fluid inclusions studies: Monograph Series on Mineral Deposits, v. 30, p. 117–132.

Lotze, F., 1945, Zur Gliederung der Varisziden der Iberischen Meseta: Geotektonische Forschungen, v. 6, p. 78–92.

Marquínez, J., 1978, Estudio geológico del sector SE de los Picos de Europa (Cordillera Cantábrica, NW de España): Trabajos de Geología de la Universidad de Oviedo, v. 10, p. 295–315.

Martínez-García, E., 1981, El Paleozoico de la Zona Cantábrica Oriental (Noroeste de España): Trabajos de Geología de la Universidad de Oviedo, v. 11, p. 95–127.

——1983, Permian mineralizations in the Cantabrian Mountains (north-west Spain), *in* Schneider, H.J. ed., Mineral deposits of the Alps and of the Alpine Epoch in Europe: Berlin, Springer-Verlag, p. 259–274.

Martínez-García, E., and Tejerina, L., 1979, Fluorspar deposits associated with Carboniferous and Permian rocks in Asturias and León (northwest Spain) [abs.]: International de Stratigraphie et de Géologie du Carbonifère Congrès, 9th, Urbana, IL, Abstracts, p. 130.

Martínez-García, E., Luque, C., Burkhardt, R., and Gutierrez-Claverol, M., 1991, Hozarco: Un ejemplo de mineralización de Pb-Zn-Hg de edad Pérmica (Cordillera Cantábrica, NW de España): Sociedad Española de Mineralogía Boletín, v. 14, p. 107–116.

McCrea, J.M., 1950, The isotope chemistry of carbonates and a paleotemperature scale: Journal of Chemical Physics, v. 18, p. 849–859.

Möller, P., 1983, Lanthanoids as a geochemical probe and problems in lanthanoid geochemistry. Distribution and behaviour of lanthanoids in non magmatic phases, *in* Sinha, S.P., ed., Systematics and the properties of the lanthanides: Dordrecht, D. Riedel, p. 561–616.

Möller, P., and Morteani, G., 1983, On the geochemical fractionation of rare earth elements during the formation of Ca minerals and its application to problems of the genesis of ore deposits, *in* Augustithis, S.S., ed., The significance of trace elements in solving petrogenetic problems: Athens, Theophrastus, p. 747–791.

Northrop, D.A., and Clayton, R.N., 1966, Oxygen isotope fractionation in systems containig dolomite: Journal of Geology, v. 74, p. 174–196.

Ohmoto, H., 1972, Systematics on sulfur and carbon isotopes in hydrotermal ore deposits: Economic Geology, v. 67, p. 551–578.

——1986, Stable isotope geochemistry of ore deposits: Reviews in Mineralogy, v. 16, p. 491–559.

Ohmoto, H., and Rye, R.O., 1979, Isotopes of sulfur and carbon, *in* Barnes, H.L., ed., Geochemistry of hydrothermal ore deposits: New York, Wiley Interscience, p. 509–567.

O'Neil, J.R., Clayton, R.N., and Mayeda, T.K., 1969, Oxygen isotope fractionation in divalent metal carbonates: Journal of Chemical Physics, v. 51, p. 5547–5558.

Parekh, P.P., and Möller, P., 1977, Revelation on the genesis of minerals in paragenesis with fluorites, calcites and phosphates via rare earth fractionation, *in* Nuclear techniques and mineral resources: Vienna, International Atomic Energy Agency, p. 353–369.

Potter, R.W., 1977, Pressure corrections for fluid-inclusion homogenization temperatures based on the volumetric properties of the system $NaCl-H_2O$: U.S. Geological Survey Journal of Research, v. 5, p. 603–607.

Potter, R.W., Clinne, M.A., and Brown, D.L., 1978, Freezing point depression of aqueous sodium chloride solutions: Economic Geology, v. 73, p. 284–285.

Robinson, B.W., and Kusakabe, M., 1975, Quantitative preparation of sulfur dioxide for $^{34}S/^{32}S$ analyses, from sulfides by combustion with cuprous oxide: Analytical Chemistry, v. 47, p. 1179–1181.

Rodríguez-Fernández, L.R., and Heredia, N., 1990, Palentine zone structure, *in* Dallmeyer, R.D., and Martínez-García, E., eds., Pre-Mesozoic geology of Iberia: Berlin, Springer-Verlag, p. 69–71.

Roedder, E., 1984, Fluid inclusions: Reviews in Mineralogy, v. 12, 644 p.

Sangster, D.F., 1990, Mississippi Valley type and sedex lead-zinc deposits: A comparative examination: Institution of Mining and Metallurgy Transactions, Section B, v. 99, p. B21–B42.

——1993, Evidence for, and implications of, a genetic relationship between MVT and SEDEX zinc-lead deposits: World Zinc '93 International Symposium, Hobart, Tasmania, Proceedings, p. 85–94.

Saulas, D., 1985, Etude mineralogique et geologique des gîtes Cantabriques a Ba-Zn-Pb (Cu-Hg) en limite du socle-couverture: Unpublished Thèse pour Docterur d'Etat, Orléans, France, Université d'Orléans, 292 p.

Seebold, I., Fernández, G., Reinoso, J., Alonso, J.A., Escayo, M., and Cómez, F., 1989, Yacimientos estratoligados de blenda, galena y marcasita en dolomías. Mina de Reocín (Cantabria): Recursos Minerales Españoles, Editoral Nuevas Tendencias, Consejo Superior de Investigaciones Científicas, p. 947–967.

Sheppard, S.M.H., 1986, Characterization and isotopic variations in natural waters: Reviews in Mineralogy, v. 16, p. 165–183.

Sibley, D.F., and Gregg, J.M., 1987, Classification of dolomite rock textures: Journal of Sedimentary Petrology, v. 57, p. 967–975.

Sverjensky, D.A., 1986, Genesis of Mississippi Valley-type lead–zinc deposits: Annual Review of Earth and Planetary Science, v. 14, p. 177–199.

Taylor, B.E., 1987, Stable isotope geochemistry of ore-forming fluids: Mineralogical Association of Canada Short Course Handbook, v. 13, p. 337–445.

Veizer, J., and Demovic, R., 1974, Strontium as a tool in facies analysis: Journal of Sedimentary Petrology, v. 44, p. 93–115.

Velasco, F., and Pesquera, A., 1979, Estudio óptico de la esfalerita (blenda acaramelada) de Picos de Europa, Santander (España): Estudios Geológicos, v. 35, p. 371–377.

Velasco, F., Pesquera, A., and Herrero, J.M., 1996, Lead isotope study of Zn-Pb ore deposits associated with the Basque-Cantabrian basin and Paleozoic basement, northern Spain: Mineralium Deposita, v. 31, p. 84–92.

Yusta, I., and Velasco, F., 1996, Lithogeochemistry of sedimentary sequences related to Zn-Pb ore mineralization: A case study in the Basque-Cantabrian basin (northern Spain): Society of Economic Geologists Special Publication 4, p. 654–664.

ELSEVIER

Marine Chemistry 70 (2000) 161–170

MARINE CHEMISTRY

www.elsevier.nl/locate/marchem

Copper adsorption in diatom cultures

Melchor González-Dávila*, J. Magdalena Santana-Casiano, Luis M. Laglera

Facultad de Ciencias del Mar, Departamento de Química, Universidad de Las Palmas de Gran Canaria, Las Palmas de Gran Canaria 35017, Spain

Received 15 May 1999; received in revised form 14 December 1999; accepted 15 December 1999

Abstract

The organic ligands naturally present in seawater, on the cell surface groups, and those released by the marine phytoplankton species, *Thalassiosira weissflogii* and *Phaeodactylum tricornutum*, and their physico-chemical interaction with copper ions were studied using differential pulse anodic stripping voltammetry (DPASV) as a function of pH, temperature, salinity and biomass. The acid–base properties were characterized from titration curves of diatom suspensions with proton. Three pK_a values were determined for each diatom, all of which were similar. Titration curves with copper allowed us to determine the specific adsorption of copper in a heterogeneous adsorption model. An iterative method that combines both Scatchard and Van den Berg–Ruzic approaches was used in order to determine the complexing capacity and the binding constants. High-affinity surface groups of both algae have similar affinity for copper but the concentration of these groups is 45% per cell higher for *P. tricornutum as* compared to *T. weissflogii*. The low-affinity groups in *T. weissflogii* (9.37) have higher stability constants than those in the *P. tricornutum* (9.0). After 36 h equilibrium, a ligand concentration of 18.6×10^{-16} M cell^{-1} *P. tricornutum* and 25.0×10^{-16} M cell^{-1} *T. weissflogii* with a conditional stability constant of log $K' = 9.8$ and log $K' = 10.0$, respectively, was exuded into the original seawater. In the presence of lead, high specificity was observed for the lowest stability constant ligands for copper, while the highest stability constant ligands were affected more by the presence of lead in solution. The ligands of *T. weissflogii* were less affected.

Keywords: adsorption; complexation; copper; diatoms; seawater

1. Introduction

Biological surfaces contain various functional groups, e.g., amino acid, carboxylic, hydroxy carboxylic and hydroxy groups, which may interact with H^+ ions and metal ions. The distribution of chemical species between the solid and liquid phases is of particular interest to aquatic and environmental chemists because, to a large extent, particulate and colloidal matter regulate metal ion concentrations in natural media. Biological surfaces, especially biogenic organic particles (phytoplankton and biological debris) in transporting and settling material, play a major role in the ocean by binding heavy metals and transferring them through the water column and to the sediments, thereby regulating the concentration of dissolved metal ions (Sunda, 1990; Bruland et al., 1991; González-Dávila, 1995; Volesky and Holan,

* Corresponding author. Tel.: +34-928-452-914; fax: +34-928-452-922

E-mail address: mglez@cicei.ulpgc.es (M. González-Dávila)

0304-4203/00/$ - see front matter
PII S0304-4203(00)00020-7

1995). As a whole, the chemical properties of heavy metals with respect to their interaction with suspended particles, sediments and aquatic organisms are strongly affected by the chemical forms in which dissolved metals exist in seawater (Brand et al., 1983; Sunda, 1990; Knauer et al., 1997). Although we are beginning to understand more about the organic complexation of some metals, especially copper (Van den Berg, 1984; Kramer, 1986; Coale and Bruland, 1988), more studies are needed to understand the toxicity, bioavailability, geochemical reactivity and the organic interactions in natural media.

In this work, we have examined the binding of copper to the surface and to the ligands produced by living algae, specifically to understand the significance of both processes in seawater. Two diatoms were used in our studies: *Thalassiosira weissflogii* that appears in estuarine areas, and *Phaeodactylum tricornutum* that appears in intertidal areas. Anodic stripping voltammetry (ASV) with blank subtraction was used to measure equilibrium partitioning between surfaces and solutions to determine surface complex formation equilibrium constants (Gonçalves et al., 1987; González-Dávila et al., 1995). In order to get a better understanding of the adsorption process and the effect of dissolved extracellular ligands, the effect of pH, temperature, salinity, algal biomass and the presence of lead (a highly toxic element that has been found to be complexed with organic ligands; Capodaglio et al., 1990) have been studied.

2. Experimental

Cultures of the diatoms *P. tricornutum* ccmp 631 and *T. weissflogii* ccmp 1051 were obtained from the Provasoli-Guillard National Center for Culture of Marine Phytoplankton, Bigelow laboratory for Oceanic Sciences, ME. They were cultured in continuous culture using a standard nutrient medium f/2 (Guillard and Ryther, 1962). Natural seawater (S = 36.78) used for the preparation of the medium and for most of the studies was collected northwest of Gran Canaria island (The Canary Islands) at the European Station for Time Series in the Ocean, Canary Islands (ESTOC) and also 1 mile off the coast from ~10 m depth. Axenic cultures were maintained at 292 ± 1 K, under 12-h light and 27 μmol of photon m^{-2} s^{-1} (photon flux density) in a growth chamber. All chemicals were of reagent-grade or the highest obtainable grade.

The culture medium of algae in stationary phase was harvested and centrifuged at 4000 rpm for 15 min, then washed four times with 0.45 μm filtered natural seawater and resuspended in fresh seawater. The sample was then stored in the refrigerator until used, always within 24 h. The concentration was determined previous to the study by optical counting with a hemacytometer and, where necessary, algae dry weights were determined by filtering the algal suspension through 0.45 μm cellulose nitrate membrane filters (Millipore acid-washed filters) and drying at 110°C. The final cell concentration in our studies was kept at about 1 to 3×10^7 cells l^{-1}.

2.1. Acid–base titrations

The algae from the culture media were centrifuged at 4000 rpm for 15 min in 100 ml polypropylene beakers. Dead cells (formaldehyde-treated) were washed four times with a sterile 0.7 M NaCl solution to remove exudates and debris. Finally, the algae were resuspended in 25 ml of deaerated 0.7 m NaCl. The pH was measured in a titration system similar to that used in our earlier studies (González-Dávila et al., 1995). Algae concentrations were 4 g dry weight l^{-1}. The total proton exchange capacity was determined by titrating the alga with an excess of 0.1 M HCl.

2.2. Complexation of copper

The cultured algae were harvested by centrifugation, washed, and resuspended in a 0.45 μm filtered seawater. For each sample, a short reaction time (15 min) determined by kinetic measurements was used for the adsorption studies. All the samples were equilibrated at a given pH, temperature and salinity being studied. The cell solution was then filtered through 3 μm (HA Millipore acid-washed) filters, and split into two fractions. The first fraction was acidified with concentrated HCl to pH 2 and microwave-treated (CEM-MDS-81D; 630 W, 30 min) to determine the total dissolved copper. The second fraction was used directly in order to determine the

labile copper (Gonçalves et al., 1987). Copper bound to the surfaces of algae was calculated from the difference between total added copper (including that initially present in the seawater) and total dissolved copper. Organically complexed dissolved copper in the adsorption studies was calculated by the difference between the total dissolved and the labile copper. The concentration of copper in the samples was determined by using differential pulse anodic stripping voltammetry (DPASV). In voltammetric analysis, it must be assumed that organic ligands with a weak affinity for the metal are included in the labile fraction (Coale and Bruland, 1988; González-Dávila et al., 1995). Those ligands of very strong metal affinity that are fully titrated initially do not equilibrate with the added metal and have no contribution to the estimation of the metal affinity of the organic complexes in solution. This concept is known as the analytical window and refers to the metal affinity range of the measurement (Van den Berg and Donat, 1992; Van den Berg et al., 1990).

Measurements were performed using PAR 303 static drop mercury electrode with the PAR model 348B polarographic analyzer system connected to a computer. The reduction potential was −0.6 V, the rate was 2 mV s^{-1}, the pulse height was 50 mV, and the deposition time was 10 min. The sensitivity of the method determined in acidic media was 0.8 nA nM^{-1} min^{-1} (Gonçalves et al., 1987).

For the seawater complexation studies in the presence of algae, a cell solution was left in equilibrium for 36 h, then filtered using 3 μm filters, and finally, trace metals were added to the solution, whereafter, it was left to equilibrate overnight.

3. Results and discussion

Fig. 1 shows the acid–base titration curves for the diatoms, *P. tricornutum* and *T. weissflogii*, in 0.7 m NaCl solution. The shape of the titration curves indicates that the surfaces contain a large variety of weaker acid–base groups. The model used for the description of oxide surfaces (Stumm and Morgan, 1981; Keifer et al., 1997), was applied between pH = 3 and pH = 10 to evaluate the data. The intrinsic acidity constants pK^s_{a1}, pK^s_{a2} and pK^s_{a3} were obtained from the plot of pK vs. surface charge Q.

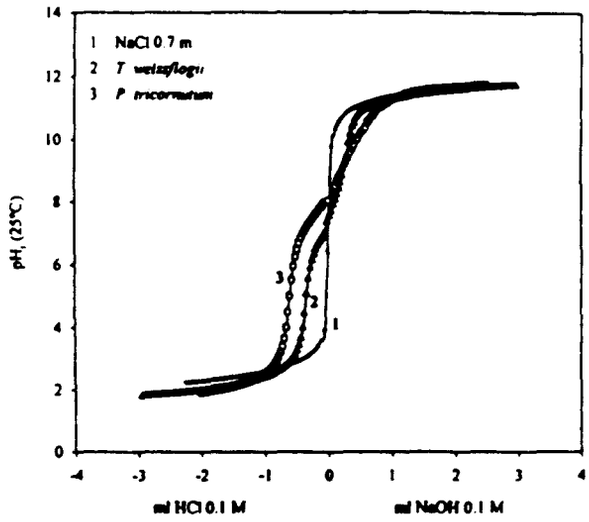

Fig. 1. Acid–base titration curves of dead *P. tricornutum* and *T. weissflogii* cells in 0.7 m NaCl suspension (4 g dry weight l^{-1}).

Values of $pK^s_{a1} = 9.12 \pm 0.02$, $pK^s_{a2} = 6.68 \pm 0.03$ and $pK^s_{a3} = 3.77 \pm 0.02$ were obtained as the result of different titrations of *P. tricornutum*. Values of $pK^s_{a1} = 9.14 \pm 0.02$, $pK^s_{a2} = 6.72 \pm 0.03$ and $pK^s_{a3} = 3.96 \pm 0.02$ were determined for *T. weissflogii*. The pK_a values under 4 are related to terminal carboxyl groups in proteins, while the pK_a values around 9 are related to α-amino groups of asparagine, glycine, alanine, leucine (pK between 8 and 9.5). The pK_{a2} values around 6.7 can be related to the presence of primary amino groups, probably due to the presence of chitin ($pK^s_{a2} = 6.8$; Gonzalez-Dávila and Millero, 1990).

The binding of trace metals on the cell surface groups is the first step necessary for the uptake of metals into the cell. Fig. 2 shows the uptake kinetics of 7.02×10^{-8} M Cu(II) on 2.03×10^7 cells l^{-1} *P. tricornutum*, including the study of the behavior of labile and complexed Cu(II) in solution. For *P. tricornutum* and *T. weissflogii* (data not shown), the inorganic dissolved copper sharply decreases during the first 15 min until its concentration reaches less than 2.5 and 5 nM, respectively, for both algae. After this first step, both the uptake and labile Cu(II) concentrations decrease linearly with the square root of time (inset in Fig 1), a characteristic result of a diffusion-controlled process (Crank, 1976). The uptake of Cu(II) for both algae is quite similar (50% of the initial value). Organically complexed dissolved

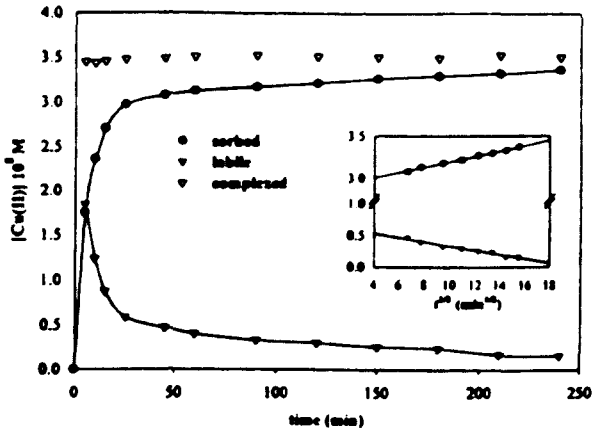

Fig. 2. Uptake kinetics of Cu(II) (7.02×10^{-8} M) on 2.03×10^{7} cells l^{-1} *P. tricornutum*. Inset: labile and uptake copper during the second step as a function of the square root of reaction time.

copper is around 45–50% of the initial value. Only 1% of the initial Cu(II) for *P. tricornutum* and 5% for *T. weissflogii* is present as inorganic dissolved copper, which corresponds to a pCu of 10.2 and 9.84, respectively. We can observe from Fig. 2 that inorganically complexed copper is taken up by algae, while the organically complexed dissolved copper did not change.

When phytoplankton cells are in equilibrium with seawater, copper binding on the cell surface groups takes place. The copper also binds with organic ligands present not only in the solution but also excreted or exuded by the cells. Metal complexing ligand concentrations and conditional stability constants were calculated by titration using the methods of Van den Berg and Kramer (1979) and Ruzic (1982). If the transformation results are linear, it is assumed that the natural chelators are within a single class of ligands, with one representative conditional stability constant. When the analytical technique is used over a wide spectral window, a linearizing plot as proposed by Scatchard or Van den Berg–Ruzic yields separate linear regions. This indicates that more than one type of ligands can be estimated. The most usual model is to consider two kinds of binding sites. This model provides a good fit of the result data in spite of the simplistic assumption on which it is based. It is characterized by a low concentration of ligands with a high conditional stability constant ($[L_1]$ and K_1^{cond}) and a higher concentration of ligands with a lower binding strength ($[L_2]$ and K_2^{cond}). Due to the well-known heterogeneity of the complexing material, the estimation of log K' is an averaged value of the stability constant of natural ligands inside the analytical window. The modeled values of K_i' and total ligand concentration obtained are not independent of each other for the same type of ligand and dependent on the detection window associated with the method used. Another aspect to be considered is the different metal ion loading conditions present in the different studies that can produce a gradual change of log K' (Buffle et al., 1990). In our work, we will present and compare complexing data obtained under different metal ion loadings. These differences were always lower than one order of magnitude, and, consequently, the error associated to the estimation of log K' is lower than the analytical error.

Values for the complexing parameters in a single ligand model are estimated through the use of a nonlinear fit of the Langmuir isotherm, similar to the one proposed by Gerringa et al. (1995). In order to determine the concentrations of the separate ligand classes and their respective conditional stability constants, a new iterative method has been developed. It allows one to determine independently the complexing capacity of both class of ligands when the two-site model is employed (Laglera et al., submitted). This method is characterized by using the Scatchard plot for the determination of L_1 and the Van den Berg and Ruzic plot for L_2. In our case, the total ligand

Table 1
Complexation parameters for natural seawater (columns 1–3) and after 36 h equilibrium period with diatoms (columns 4–6)
Experimental conditions: $pH_t = 8.02$ $\alpha_{Cu} = 25.7$, 2.06×10^7 cell l^{-1} *P. tricornutum* and 2.2×10^7 cell l^{-1} *T. weissflogii*

C_L (nM)	log K_{Cu}	log K_{Cu}^{2+}	Alga	C_L (nM)	log K_{Cu}	log K_{Cu}^{2+}
107 ± 2	7.48 ± 0.02	8.89 ± 0.02	*P. tricornutum*	146 ± 6	7.97 ± 0.04	9.38 ± 0.04
			T. weissflogii	162 ± 2	8.16 ± 0.01	9.57 ± 0.01

concentration C_L (nM) and conditional stability constant $K_{Cu^{2+}}^{cond}$ are shown in Table 1 for the original seawater and after both algae were left during 36 h in equilibrium. An inorganic side reaction coefficient (α) for Cu(II) of 25.7 at pH = 8.02 (Millero and Hawke, 1992; Santana-Casiano et al., 1995) was used. It can be clearly observed that the addition of cells increases both the total ligand concentration and the conditional stability constants of seawater, revealing that these algae excrete ligands with higher stability constant than those initially present in the seawater. If the addition of algae increases the ligand concentration by 40 nM for *P. tricornutum* and the constant rises by approximately 0.5 units, the excreted ligands should have a conditional stability constant of 9.8. For the *T. weissflogii*, the constant of the new ligands should be around 10. This organically complexed dissolved copper will compete with the copper adsorbed to the surface groups. In order to characterize the speciation of copper in natural seawater, adsorption on the cell surface groups should be considered.

Fig. 3 shows the adsorption isotherms of two *T. weissflogii* cell concentrations in seawater at pH_t = 8.02. The complexation of copper with the algal surfaces was interpreted using the Langmuir equation at constant pH, assuming that the adsorption of Cu occurs in two types of surface groups, within the range of Cu concentration used, considering that charge effects are negligible at constant pH. Fig. 4 presents the Scatchard linearization of the adsorption

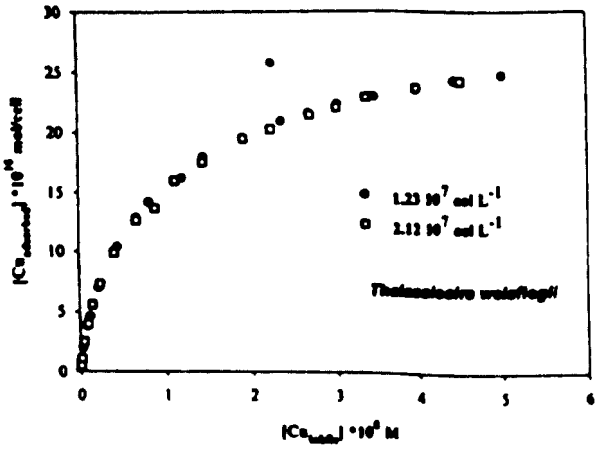

Fig. 3. Adsorption isotherms of Cu(II) on two *T. weissflogii* cell concentrations in seawater at pH_t = 8.02.

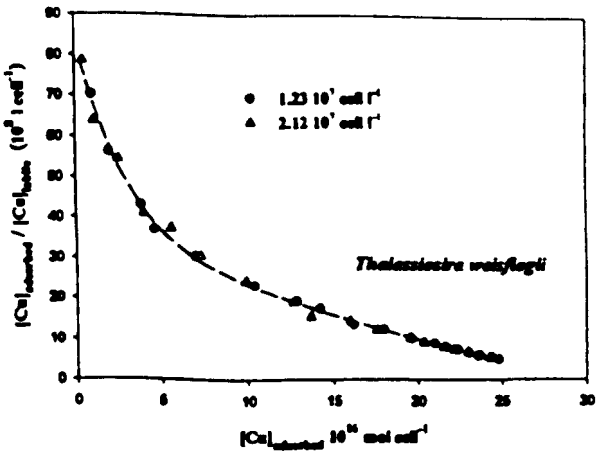

Fig. 4. Scatchard linearisation of the adsorption isotherm for two *T. weissflogii* cell concentrations. The curves correspond with model output.

isotherm for two *P. tricornutum* concentrations, where the presence of at least two types of ligands is observed. The four parameters defining the system have been evaluated by using our iterative method that independently determines the complexing capacity of both types of ligand. The data are presented in Table 2 and the fitting lines in Fig. 4 correspond to the model output. This model removes the problems associated with both the linearization of the Van den Berg–Ruzic plot at low concentrations (negative values may appear at very low concentrations and low statistic weighting for the initial data) and with the linearization of Scatchard plot at high concentrations (concentration of points due to the experimental errors at high copper concentrations) (Apte et al., 1988; Van den Berg and Donat, 1992; Ruzic, 1996; Miller and Bruland, 1997). The data in Table 2 show that the high-affinity surface groups of both algae present similar affinity for copper, but the concentration of these groups is 45% per cell higher for *P. tricornutum* than for *T. weissflogii*.

The constants we have determined from the titration data are conditional to the pH and seawater composition considered. By using the acid–base titration curves for both diatoms discussed previously and considering the competition between proton and copper for the same binding sites, intrinsic adsorption constants, K_β^i have been computed. They allow us to determine the conditional adsorption constant at other values of pH and are shown in

Table 2
Adsorption characteristics in a heterogeneous model for the surface groups of *P. tricornutum* and *T. weissflogii* at $pH_t = 8.02$
It also includes the intrinsic adsorption constants, $K^S_{\beta,i}$, valid for any pH value. $pK_{P.\ tricornutum}$ (pH = 8.02) = 9.11. $pK_{T.\ weissflogii}$ (pH = 8.02) = 9.30.

Alga	Cell l^{-1} (10^7)	$\Gamma_{max,1} \times 10^{16}$	log $K^S_{H,1}$	log $K^S_{\beta,1}$	$\Gamma_{max,2} \times 10^{16}$	log $K^S_{H,2}$	log $K^S_{\beta,2}$
P. tricornutum	1.42	1.2 ± 0.1	10.82 ± 0.05	11.94 ± 0.15	21.4 ± 0.5	8.98 ± 0.02	10.10 ± 0.12
	2.53	1.2 ± 0.2	10.67 ± 0.08	11.79 ± 0.16	22.2 ± 0.3	9.01 ± 0.02	10.13 ± 0.12
T. weissflogii	1.23	2.7 ± 0.1	10.74 ± 0.04	12.04 ± 0.16	26.8 ± 0.2	9.37 ± 0.01	10.67 ± 0.11
	2.12	2.7 ± 0.3	10.75 ± 0.06	12.05 ± 0.13	26.7 ± 0.3	9.37 ± 0.01	10.67 ± 0.12

Table 2 (González-Dávila et al., 1995). The values for the apparent acidity constants at pH = 8.02 and NaCl 0.7 M, are log $K^a_a = 9.11$ and log $K^a_a = 9.30$ for *P. tricornutum* and *T. weissflogii*, respectively.

Table 3 presents the conditional stability constants determined considering only one kind of site on the cell surface via a nonlinear fit of the titration data. These constants can be used to compare adsorption of copper on cell surface groups and complexation by diatom exudates (see Table 1). As shown above, the complexing capacities of the exudates from both diatoms have higher affinity for copper than the surface groups (four times higher for *P. tricornutum* and three times for *T. weissflogii* surface groups). For a relatively constant algal concentration, the greater the concentration of the exudation, the lesser the amount of copper that will be sorbed on the cell surface groups.

In a complex medium such as seawater, numerous trace metals will be present, interacting with the dissolved and surface organic ligands in the presence of algae. In order to study the specificity of these ligands for copper, some studies were carried out in the presence of 100 nM Pb(II). Capodaglio et al. (1990) found that lead is organically complexed in natural waters, and this complexation can affect its behavior in marine systems. The 2.06×10^7 cells l^{-1} *P. tricornutum* and 2.21×10^7 cells l^{-1} *T. weissflogii* were kept in equilibrium for 36 h, removed and the complexing capacity of the solution determined. The results are shown in Table 4. The high specificity of the ligands present in the original seawater and those exudated by algae for copper can be clearly observed. A slight increase in the complexing capacity is observed in both algae. This can be considered to be within the experimental error, but can also be considered a synergistic effect of lead for copper (Ting et al., 1991). In order to study the effect of Pb(II) on the adsorption of copper by the two diatoms studied, 100 nM of lead was also added together with an increasing Cu(II) concentration over a period of 15 min. This 100 nM of lead added to *P. tricornutum* and *T. weissflogii* with concentrations of 1.42×10^7 cells l^{-1} and 2.12×10^7 cells l^{-1} respectively, is two to three times the adsorptive capacity of the algae (33 and 60 nM, respectively). The results presented in Fig. 5 for *P. tricornutum* and in Table 5, considering both homo-

Table 3
Adsorption parameters considering a homogeneous surface, conditional to a $pH_t = 8.02$
The last two columns show the complexing capacity of the seawater medium after 36 h equilibrium with 2.06×10^7 cell l^{-1} *P. tricornutum* and 2.21×10^7 cell l^{-1} *T. weissflogii* and the estimated complexing capacity for the exudates produced by these algae.

Alga	Cell l^{-1} (10^7)	$\Gamma_{max} \times 10^{16}$ (mol cell^{-1})	log K^S_H	log K^S_β	log K'_{CuL} (medium)	log K'_{CuL} (exudates)
P. tricornutum	1.42	20.5 ± 0.5	9.13 ± 0.02	10.25 ± 0.11	9.38 ± 0.04	~ 9.8
	2.53	22.2 ± 0.8	9.11 ± 0.03	10.25 ± 0.12		
T. weissflogii	1.23	28.1 ± 0.4	9.52 ± 0.03	10.82 ± 0.12	9.57 ± 0.01	~ 10.0
	2.12	27.8 ± 0.7	9.52 ± 0.02	10.83 ± 0.11		

Table 4
Comparison of Cu(II) complexation parameters in seawater after 36 h equilibrium with 2.06×10^7 cell l^{-1} *P. tricornutum* and 2.21×10^7 cell l^{-1} *T. weissflogii* in the absence (columns 1 and 2) and in the presence (columns 4 and 5) of 100 nM Pb(II)

C_L (nM)	log K'^{2+}_{Cu}	Alga	C_L (nM)	log $K'_{Cu^{2+}}$
146±6	9.38±0.04	*P. tricornutum*	152±6	9.35±0.06
162±2	9.57±0.01	*T. weissflogii*	172±6	9.50±0.06

geneous and heterogeneous models, show that *P. tricornutum* decreases its adsorptive capacity in the presence of lead. Using the heterogeneous model, the highest affinity ligands reduce their complexing capacity by 35% and the lowest conditional stability constant ligands reduce their concentration by 15%. The lowest stability constant ligands are more selective for copper than the highest ones in the presence of lead. For *T. weissflogii*, the reduction of the adsorptive capacity in the homogeneous approach is only 10%, whereas in the heterogeneous system, the decrease observed in the adsorptive capacity agrees better with the highest error in the experimental data. Table 5 depicts the high specificity of the lowest stability constant ligands for copper in the presence of lead. The highest stability constant ligands are more affected by the presence of lead in solution. *P. tricornutum* cells have less numbers of groups capable of adsorbing copper, these groups being less specific for copper in the presence of lead that in the case of the *T. weissflogii*.

The complexation of trace metals with both ligands in solution and on the cell surface is affected by the physicochemical variables of the solution, the pH, ionic strength or the salinity of the seawater solution and temperature. The pH effect on adsorption is shown in Fig. 6, where 62 nM Cu(II) was added to 1.2×10^7 cell l^{-1} *T. weissflogii* in the pH range 3–8.4. There are 1–2 units of pH range where the adsorption increases from approximately 0% to around 100%. The pH affects all the processes which take place, i.e. chemical speciation, due to the protonation and deprotonation of both the dissolved species and the surface sites. The complexation of trace metals is an interchange reaction where both the outgoing and incoming groups are affected by the pH. In Fig. 6, we have included the effect of pH on Cu(II) speciation in the absence of algae. The labile concentration decreases at a pH higher than 5 due to the formation of organic complexes with the natural ligands in solution. In the presence of algae, no adsorption of Cu(II) is observed at low pH values. At pH higher than 4 for *P. tricornutum* (data not shown) and 4.5 for *T. weissflogii*, adsorption on surface groups and complexation with ligands are observed. After pH = 7, these processes are not affected by the pH. *T. weissflogii* has a different composition of surface groups relative to the dissolved ligands, and the maximum adsorption reached is at a higher pH than for complexation with dissolved ligands.

In a seawater medium, major cations (Na^+, Ca^{2+}, Mg^{2+}, etc.) will compete for the same binding sites as trace metals (Crist et al., 1990; Tipping, 1993; Schiewer and Volesky, 1997). Under the same experimental conditions as for the pH studies, we studied the effect of salinity in the range 12–37. The copper complexed fraction was not affected by dilution of natural seawater with deionized Q-water. However, two aspects must be considered in our experimental design. First, when the original seawater is diluted, the amount of natural organic ligands in seawater is also diluted. Second, dilution may increase the amount of organic ligands capable of complexing copper by diluting the complexing major ions. These opposing factors may explain the observed behavior. For the adsorption, an increase is found in the amount

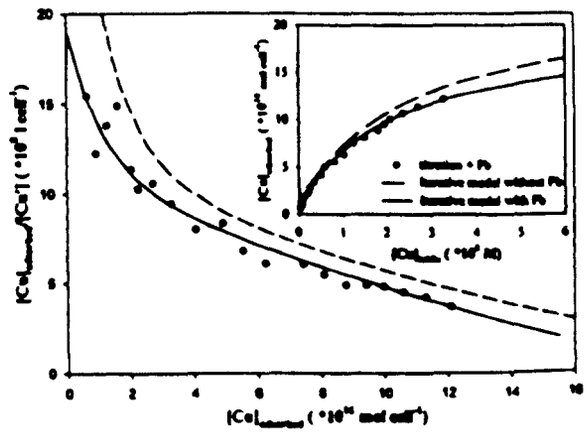

Fig. 5. Scatchard plot for the Cu(II) titration of 1.42×10^7 cell l^{-1} *P. tricornutum* in the presence of 100 nM Pb(II). The curves correspond with model output (dotted curves represent the model output in the absence of lead) Inset: Langmuir isotherms for the adsorption of Cu(II).

Table 5
Comparison of Cu(II) adsorption parameters both in a heterogeneous and homogeneous model in the presence of 1.42×10^7 cell l^{-1} *P. tricornutum* and 2.12×10^7 cell l^{-1} *T. weissflogii* in the absence and in the presence of 100 nM of Pb(II)

Alga		Heterogeneous model				Homogeneous model	
		$\Gamma_{max,1} \times 10^{16}$	$\log K_{H,1}$	$\Gamma_{max,2} \times 10^{16}$	$\log K_{H,2}$	$\Gamma_{max} \times 10^{16}$	$\log K_H$
P. tricornutum	−Pb	1.2 ± 0.6	10.75 ± 0.24	21.8 ± 0.5	9.00 ± 0.02	21.4 ± 0.7	9.12 ± 0.05
	+Pb	0.8 ± 0.2	10.52 ± 0.2	18.7 ± 0.6	9.08 ± 0.03	18.1 ± 0.6	9.18 ± 0.03
T. weissflogii	−Pb	2.7 ± 0.3	10.75 ± 0.06	26.8 ± 0.3	9.37 ± 0.01	27.9 ± 0.14	9.52 ± 0.01
	+Pb	1.6 ± 2.0	10.89 ± 0.6	26.3 ± 0.6	9.43 ± 0.03	25.3 ± 0.8	9.59 ± 0.03

of copper bound to cell surface groups as salinity decreases. The stability constants determined for the different salinity studies allow us to determine the linear regressions between both parameters for the two algae:

$$\log K_H^{cond} = 10.164 - 0.165\sqrt{S};$$

$r^2 = 0.993$; *P. tricornutum*,

$$\log K_H^{cond} = 10.607 - 0.175\sqrt{S};$$

$r^2 = 0.999$; *T. weissflogii*.

When the experiments are carried out at different temperatures from 6°C to 45°C in seawater for *P. tricornutum* (Fig. 7), we found increased adsorption and a decrease in inorganic complexed copper at higher temperatures. The organically complexed copper is not affected. This finding, together with the kinetic studies (Fig. 1), suggests that inorganic copper alone is adsorbed to the surface cell. It is possible that complexed copper increases with temperature. However, we do not observe this behavior in our experiments probably due to the greater amount of ligands being excreted by algae, due to the temperature stress. For *T. weissflogii*, an increase in temperature produces a decrease in both the labile and adsorbed concentration, whereas the complexed and total dissolved copper concentration increases. In this case, complexation is promoted by increasing temperature, which reduces the inorganic copper together with the copper previously adsorbed. The specific adsorption energy, E, determined according to González-Dávila et al. (1995), gives 6.69 ± 0.28 kJ mol^{-1} for *P. tricornutum* and -4.25 ± 0.17 kJ mol^{-1} for *T. weissflogii*. The positive specific adsorption energy of Cu^{2+} may be interpreted as the heat of hydration of Cu(II), which is higher than its heat of adsorption.

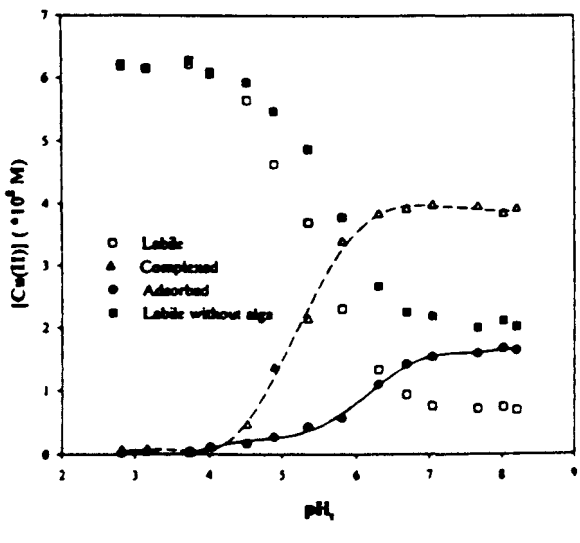

Fig. 6. Effect of pH on the Cu(II) speciation in the presence of 1.19×10^7 cell l^{-1} *T. weissflogii* (total Cu(II) concentration, 6.27×10^{-8} M).

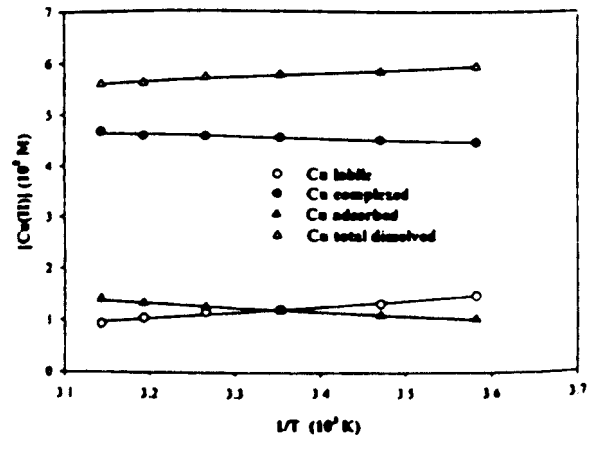

Fig. 7. Effect of temperature on the Cu(II) speciation in the presence of 1.4×10^7 cell l^{-1} *P. tricornutum* in seawater (total Cu(II) concentration, 6.98×10^{-8} M).

4. Conclusions

ASV has been shown to be a useful method when determining adsorption properties on biological surfaces. Heterogeneous surfaces with ligand concentrations of 2–8 nM for the highest stability constants ligands (log $K' = 10.7 \pm 0.1$) and 20–30 nM for the lowest stability constant ligands (log $K' = 9.1 \pm 0.2$) have been established for Cu on both diatoms. The values of the adsorptive capacities for *T. weissflogii* are the highest. However, the determination of the seawater complexing capacity by ASV only allows us to use a homogeneous model, even if more than one type of ligand is present. Accordingly, after 36 h equilibrium, a ligand concentration of 18.6×10^{-16} M cell^{-1} *P. tricornutum* and 25.0×10^{-16} M cell^{-1} *T. weissflogii* (conditional stability constant of log $K' = 9.8$ and log $K' = 10.0$, respectively) is exuded into the original seawater. The exudated compounds have more affinity for copper than the cell surface groups, when the inorganic concentrations are kept at levels below toxic values (Brand et al., 1983). The excretion of organic ligands with different properties from the surface groups can also be affected by the pH. The maximum complexation is reached around 1 pH unit lower than in adsorption.

When the lead concentration of twice the maximum adsorptive capacity of the surface groups is added, high-affinity ligands on cell surface groups for copper in both algae are found to be less specific than low-affinity ligands. The specificity of the *T. weissflogii* surface ligands that reveal affinity for copper is higher than that shown for *P. tricornutum*. We are unable to define the exact nature of this type of complexing ligands. However, the results underline the importance of complexation with organic ligands for elements such as copper, which are involved in naturally occurring biological processes.

Acknowledgements

We gratefully acknowledge the critical and constructive criticisms offered to us by the anonymous reviewers. We would like to thank Prof. Frank J. Millero for the review of the manuscript and valuable suggestions.

References

Apte, S.C., Garner, M.J., Ravenscroft, J.E., 1988. An evaluation of voltammetric titration procedures for the determination of trace metal complexation in natural waters by use of computer simulation. Anal. Chim. Acta 212, 1–21.

Brand, L.E., Sunda, W.G., Guillard, R.R.L., 1983. Limitation of marine phytoplankton reproductive rates by zinc, manganese and iron. Limnol. Oceanogr. 28, 1182–1198.

Bruland, K.W., Donat, J.R., Hutchins, D.A., 1991. Interactive influences of bioactive trace metals on biological production in oceanic waters. Limnol. Oceanogr. 36, 1555–1577.

Buffle, J., Altman, R.S., Filella, M., Tessier, A., 1990. Complexation by natural heterogeneous compounds: site occupation distribution functions, a normalised description of metal complexation. Geochim. Cosmochim. Acta 54, 1535–1553.

Capodaglio, G., Coale, K.H., Bruland, K.W., 1990. Lead speciation in surface waters of the Eastern North Pacific. Mar. Chem. 29, 221–233.

Coale, K.H., Bruland, K.W., 1988. Copper complexation in the Northeast Pacific. Limnol. Oceanogr. 33, 1084–1101.

Crank, J., 1976. The Mathematics of Diffusion. Oxford Univ. Press, New York.

Crist, R.H., Martin, J.R., Guptill, P.W., Eslinger, J.M., Crist, D.R., 1990. Interaction of metal and protons with algae. Environ. Sci. Technol. 24, 337–342.

Gerringa, L.J.A., Herman, P.M.J., Poortvliet, T.C.W., 1995. Comparison of the linear Vanden Berg/Ruzic transformation and a non-linear fit of the Langmuir isotherm applied to Cu speciation data in the estuarine environment. Mar. Chem. 48, 131–142.

Gonçalves, M.L.S., Sigg, L., Reutlinger, M., Stumm, W., 1987. Metal ion binding by biological surfaces: voltammetric assessment in the presence of bacteria. Sci. Total Environ. 60, 105–119.

González-Dávila, M., 1995. The role of phytoplankton cells on the control of heavy metal concentration in seawater. Mar. Chem. 48, 215–236.

Gonzalez-Dávila, M., Millero, F.J., 1990. The adsorption of copper to chitin in seawater. Geochim. Cosmochim. Acta 54, 761–768.

González-Dávila, M., Santana-Casiano, J.M., Pérez-Peña, J., Millero, F.J., 1995. Binding of Cu(II) to the surface and exudates of the alga *Dunaliella tertiolecta* in seawater. Environ. Sci. Technol. 29, 289–301.

Guillard, R.R.L., Ryther, J.H., 1962. Studies of marine planktonic diatoms. I. *Cyclotella nana* Hustedt and *Detonula confervacea* (Cleve) gran. Can. J. Microbiol. 8, 229–239.

Keifer, E., Sigg, L., Schosseler, P., 1997. Chemical and spectroscopic characterization of algae surfaces. Environ. Sci. Technol. 22, 759–764.

Knauer, K., Behra, R., Sigg, L., 1997. Effects of free Cu^{2+} and Zn^{2+} ions on growth and metal accumulation in freshwater algae. Environ. Toxicol. Chem. 16, 220–229.

Kramer, K.J.M., 1986. Apparent copper complexation capacity and conditional stability constants in North Atlantic waters. Mar. Chem. 18, 335–349.

Laglera, L.M., Gonzalez-Davila, M., Santana-Casiano, J.M. Determination of metallic complexing capacities of the dissolved organic matter in seawater. Scientia Marina, submitted.

Miller, L.A., Bruland, K.W., 1997. Competitive equilibration techniques for determining transition metal speciation in natural waters. Evaluation using model data. Anal. Chim. Acta 343, 161–181.

Millero, F.J., Hawke, D.J., 1992. Ionic interactions of divalents metals in natural waters. Mar. Chem. 40, 19–48.

Ruzic, I., 1982. Theoretical aspects of the direct titration of natural waters and its information yield for trace metal speciation. Anal. Chim. Acta 140, 99–113.

Ruzic, I., 1996. Trace metal complexation at heterogeneous binding sites in aquatic systems. Mar. Chem. 53, 1–15.

Santana-Casiano, J.M., González-Dávila, M., Pérez-Peña, J., Millero, F.J., 1995. Pb^{2+} interactions with the marine phytoplankton *Dunaliella tertiolecta*. Mar. Chem. 48, 115–129.

Schiewer, S., Volesky, B., 1997. Ionic strength and electrostatic effects in biosorption of protons. Environ. Sci. Technol. 31, 1863–1871.

Stumm, W., Morgan, J.J., 1981. Aquatic Chemistry. 2nd edn. Wiley, New York.

Sunda, W.G., 1990. Trace metal interactions with marine phytoplankton. Biol. Oceanogr. 6, 411–442.

Ting, Y.P., Lawson, F., Prince, I.G., 1991. Uptake of cadmium and zinc by the alga *Chlorella vulgaris*. Biotechnol. Bioeng. 37, 445–455.

Tipping, E., 1993. Modeling the competition between alkaline earth cations and trace metal species for binding by humic substances. Environ. Sci. Technol. 27, 520–529.

Van den Berg, C.M.G., 1984. Determination of the complexing capacity and conditional stability constants of complexes of copper(II) with natural organic ligands in seawater by cathodic stripping voltammetry of copper–cathecol complex ions. Mar. Chem. 15, 1–18.

Van den Berg, C.M.G., Donat, J.R., 1992. Determination and data evaluation of copper complexation in seawater using cathodic stripping voltammetry at varying detection windows. Anal. Chim. Acta 257, 281–291.

Van den Berg, C.M.G., Kramer, J.K., 1979. Determination of complexing capacities of ligands in natural waters and conditional stability constants of copper complexes by means of manganese dioxide. Anal. Chim. Acta 106, 103–120.

Van den Berg, C.M.G., Nimmo, M., Daly, P., Turner, D.R., 1990. Effects of the detection window on the determination of organic copper speciation in estuarine waters. Anal. Chim. Acta 232, 149–159.

Volesky, B., Holan, Z.R., 1995. Biosorption of heavy metals. Biotechnol. Prog. 11, 235–250.

J. Mar. Biol. Ass. U.K. (2000), 80, 559–560
Printed in the United Kingdom

Evidence of external digestion of crustaceans in *Octopus vulgaris* paralarvae

Vicente Hernández-García, Ana Y. Martín & José J. Castro

Departamento de Biología, Universidad de Las Palmas de Gran Canaria, Apartado 550, Las Palmas de Gran Canaria, Canary Islands, Spain. E-mail: ana.martin@biologia.ulpgc.es

This paper reports, for the first time, the existence of external digestion of decapod larvae by the common octopus, *Octopus vulgaris* (Mollusca: Cephalopoda), paralarvae. Zoeae of three crab species were externally digested, leaving a whole and empty exoskeleton. The attack sequence on these prey is also described, and divided into the same three phases (attention, positioning and seizure) already known for *Sepia* hatchlings.

The common octopus, *Octopus vulgaris* (Cuvier, 1797), is probably the best known cephalopod, but knowledge of this species is still very limited (Mangold, 1983; Vecchione, 1994). Sampling of planktonic individuals in the sea is infrequent, and their trophic relationships have not been described, merely hypothesized (Mangold & Boletzky, 1973; Nixon, 1985; Boucher-Rodoni et al., 1987). Currently, only two successful rearing experiments have been reported up to the benthic phase (Itami et al., 1963; Villanueva, 1995) so information on the type of prey which supports survival is particularly limited.

Juveniles and adults demonstrate external digestion when feeding on crabs (Nixon, 1984; Nixon & Mangold, 1996). Feeding starts with the administration of a paralysing agent, cephalotoxin (Nixon, 1987). Immediately after capture of the prey, the octopus squirts enzyme(s) onto it in order to break the muscle–skeletal attachments, thus allowing for easy extraction of the edible contents from the crustacean exoskeleton. This process is well documented in adult *O. vulgaris*, but has not been described in the paralarvae, although it has been reported in Vecchione (1991) for *Loligo vulgaris* hatchlings preying on small shrimps. The aim of this paper is to describe the first evidence of external digestion of crab larvae by octopus paralarvae reared in the laboratory.

Male and female *Octopus vulgaris* were captured along the east coast of Gran Canaria Island (28°57′N 15°22′W) during autumn of 1996 and spring of 1997. Animals were housed in a 12,000 l tank with open seawater flow. Spawning females deposited and incubated the egg clusters in plastic burrows located inside the tank. The embryonic development took between 25 and 30 d at 19–22°C temperature range. Once hatched, the paralarvae were transferred to 12 l transparent containers with open seawater flow. Paralarvae density was variable between 8 and 100 paralarvae l^{-1}. The bottom was siphoned daily in order to clean, remove and count the dead individuals. The illumination was a natural photoperiod throughout the whole experiment.

Octopus paralarvae were fed with recently hatched zoeae obtained from ovigerous females of several crab species collected in rocky shores. The species utilized were *Pachygrapsus marmoratus* (Fabricius, 1787), *P. transversus* (Gibbes, 1850) and *Eriphia verrucosa* (Forsskal, 1775). The maximal length of the zoeae was 2 mm, approximately the mantle length of a recently hatched paralarva.

The paralarvae frequently swam near the surface next to the best illuminated walls of the tank, where the zoeae were also concentrated. In general, paralarvae did not usually attack the first zoea they found, but persisted swimming around several before attacking one. The imminence of an attack can be predicted, because the paralarva modifies its swimming behaviour. When a prey is selected, the hatchling swims with shorter movements than usual, and keeps near to the target prey. Then, the whole body is directed straight towards the zoea, in an arrow-like position, with arms joined and pointing at the prey. All this time, the paralarva is almost immobile, sometimes rotating around the prey, probably looking for a better position from which to attack. The attack occurs at distances of from 1–2 cm, and is very fast. The zoea is handled with all the arms, and the paralarva continues swimming while feeding. Sometimes, the first attack fails, and then the paralarva moves away from its prey and repeats the attack 0.5–2 s later. We have observed up to three successive attacks on a single zoea without any signs of escape behaviour on the part of the prey.

A change in the chromatophore pattern usually happens between the second and third phase of the attack sequence. During the attention phase the paralarvae maintains the chromatophores contracted, so that a nearly transparent appearance is achieved. However, during the positioning phase and/or in the attack movement towards the prey, the dorsal chromatophores covering the central zone of the mantle, the arms chromatophores and those situated between and above the eyes are expanded, leading to an arrow like appearance on the paralarva body. After seizure of the zoea, the chromatophores are contracted again, and the transparent appearance is recovered.

The zoeae of the crab species used were dark coloured, so a recently captured zoea could easily be seen as a dark spot among the arms of the paralarva. However, the prey becomes less visible with time, until it is totally invisible. When the paralarvae finish feeding, the hardly visible remains fall towards the bottom of the tanks. Observation of these remains under the stereomicroscope indicates that they are completely empty transparent exoeskeletons. The extraction of the zoea edible content leaves a molt like carapace, with attached appendages, as the only remains. This is the reason for the progressive invisibility of the zoea among the arms. Unlike the adult octopus, the paralarvae did not dismember the zoeae, but even so, all the appendages were empty of flesh.

The attack on a prey can be separated into the same three phases already reported for *Sepia officinalis* hatchlings (Boucher-Rodoni et al., 1987; Nixon & Mangold, 1996). In the attention phase, the paralarva selects the prey. This phase can be recognized because the hatchling reduces its speed, as reported by Villanueva et al. (1996). In the next phase (positioning), the

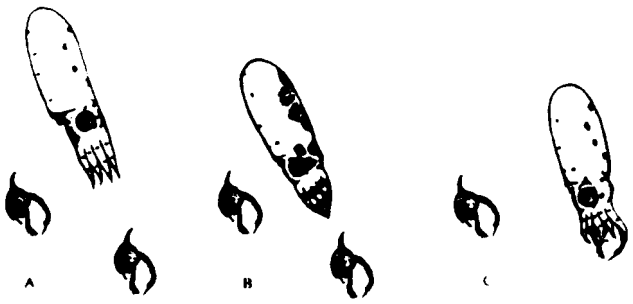

Figure 1. (A) In the attention phase, the paralarva selects its prey. (B) Positioning phase: an arrow like position and a change in chromatophore pattern indicate the imminence of the attack. (C) after seizure of the prey, the paralarva returns to its usual transparent coloration.

body is directed at the zoea, with the arm tips pointing towards the prey. In this position, the stretched body of the hatchling and the zoea form a straight line. So, the observation of the prey by the paralarva during the positioning phase probably implies a binocular fixation in this early stage, as suggested previously (see Nixon & Mangold, 1996). Seizure of the prey always takes place via a forward reaching movement (Villanueva et al., 1996), and the attack is directed towards the zoeae cephalothorax. The failure of an attack may be due to various reasons: the crab zoeae have long dorsal spines, that may damage the paralarva on contact, and also the adherence of the suckers on the prey may not be sufficiently efficient in a first attack, leading the hatchling to repeat the seizure.

At hatching, the paralarvae arms bear three large suckers, and their beaks have tooth like serration (Nixon & Mangold, 1996). Both facts may help them to keep the prey firmly attached to the oral zone, allowing the administration of the digestive enzyme(s), and, possibly, the paralysing toxin. Boucaud-Camou & Roper (1995) found a medium activity of N-acetylglycosaminidase in the posterior salivary glands of *Octopus* paralarvae. They suggested a crinophagic role for this enzyme in these glands. However, another possible function for the N-acetylglycosaminidase could be related to the external digestion of crab zoeae, since this enzyme can act consecutively to chitinase, hydrolysing the dimers and trimers of N-acetylglycosamine left by the action of this late enzyme on chitin (Grisley & Boyle, 1990). In adult octopuses *O. vulgaris* and *Eledone cirrhosa*, hole-boring of exoskeletons has been reported by various authors (see for example Nixon, 1985 and Boyle, 1990) when feeding on crabs. The mechanisms of hole-boring are still unknown, but Grisley & Boyle (1990) found a high chitinase activity in *Eledone* saliva, although no N-acetylglycosaminidase activity was detected.

Moreover, at this stage, the beaks have not reached the necessary degree of development to break fairly hard structures (e.g. crustacean exoskeletons). The beak lacks a pointed tip and the degree of darkening of the chitin implies that there is no great hardening. All of these factors have an important impact on the choice of the diet and on the related feeding behaviour (Hernandez-Garcia & Piatkowski, in press).

The external digestion of prey will make the study of trophic relationships of *O. vulgaris* paralarvae even more difficult in the sea. Visual identification of the prey which constitute the natural diet may be impossible. Thus, crustaceans would be underestimated in the diet. Therefore, it is necessary to determine how other prey are ingested via laboratory experiments, in order to get information on the state of potential prey in the digestive tracts of sampled paralarvae.

This research was supported by the Vice-Consejeria de Pesca of the Canary Islands Government, to whom we would like to express our gratitude. Also, we would like to thank Miss Catalina Caballero-Méndez and to the personnel of the Instituto de Algologia Aplicada for all their help, and specially to Professor Guillermo Garcia Reina.

REFERENCES

Boucaud-Camou, E. & Roper, C.F.E., 1995. Digestive enzymes in paralarval cephalopods. *Bulletin of Marine Science*, **57**, 313–327.

Boucher-Rodoni, R., Boucaud-Camou, E. & Mangold, K., 1987. Feeding and digestion. In *Cephalopod life cycles*. Vol. II. *Comparative reviews* (ed. P.R. Boyle), pp. 85–108. London: Academic Press.

Boyle, P.R., 1990. Prey handling and salivary secretions in octopuses. In *Trophic Relationships in the marine environment. Proceedings of the Twenty-fourth European Marine Biology Symposium* (ed. M. Barnes and R. N. Gibson), pp. 541–552. Aberdeen: Aberdeen University Press.

Grisley, M.S. & Boyle, P.R., 1990. Chitinase, a new enzyme in octopus saliva. *Comparative Biochemistry Physiology*, **95B**, 311–316.

Hernandez-Garcia, V. & Piatkowski, U., in press. Development of the darkening of the *Todarodes sagittatus* beaks and its relation to growth and reproduction. *South African Journal of Marine Science*.

Itami, K., Izawa, Y., Maeda, S. & Nakai, K., 1963. Notes on the laboratory culture of the octopus larvae. *Bulletin of the Japanese Society of Scientific Fisheries*, **29**, 514–520.

Mangold, K., 1983. *Octopus vulgaris*. In *Cephalopod life cycles*. Vol. I. *Species accounts* (ed. P.R. Boyle), pp. 335–364. London: Academic Press.

Mangold, K. & Boletzky, S. von, 1973. New data on the reproductive biology and growth of *Octopus vulgaris*. *Marine Biology*, **19**, 7–12.

Nixon, M., 1984. Is there external digestion by *Octopus*? *Journal of Zoology*, **202**, 441–447.

Nixon, M., 1985. Capture of prey, diet and feeding of *Sepia officinalis* and *Octopus vulgaris* (Mollusca: Cephalopoda) from hatchling to adult. *Vie et Milieu*, **35**, 255–261.

Nixon, M., 1987. Cephalopod diets. In *Cephalopod life cycles*. Vol. I. *Species Accounts* (ed. P.R. Boyle), pp. 201–219. London: Academic Press.

Nixon, M. & Mangold, K., 1996. The early life of *Octopus vulgaris* (Cephalopoda: Octopodidae) in the plankton and at settlement: a change in lifestyle. *Journal of Zoology*, **239**, 301–327.

Vecchione, M., 1991. Observations on the paralarval ecology of a euryhaline squid, *Loliguncula brevis* (Cephalopoda: Loliginidae). *Fishery Bulletin, National Oceanic and Atmospheric Administration, Washington, DC*, **89**, 515–521.

Vecchione, M., 1994. Systematics and the lifestyle and performance of Cephalopods. In *Physiology of cephalopod molluscs* (ed. H.O. Portner et al.), pp. 179–192. Amsterdam, BV: OPA.

Villanueva, R., 1995. Experimental rearing and growth of planktonic *Octopus vulgaris* from hatching to settlement. *Canadian Journal of Fisheries and Aquatic Science*, **52**, 2639–2650.

Villanueva, R., Nozais, C. & Boletzky, S. von, 1996. Swimming behaviour and food searching in planktonic *Octopus vulgaris* Cuvier from hatching to settlement. *Journal of Experimental Marine Biology and Ecology*, **208**, 169–184.

Submitted: June 1996; *accepted*: 15 March 1997.

GEOPHYSICAL RESEARCH LETTERS, VOL. 27, NO. 21, PAGES 3497-3500, NOVEMBER 1, 2000

Water Masses and Circulation in the Surface Layers of the Caribbean at 66°W

Alonso Hernández-Guerra

Universidad de Las Palmas de Gran Canaria, Canary Islands, Spain

Terrence M. Joyce

Woods Hole Oceanographic Institution, Woods Hole, Massachusetts

Abstract.
A meridional hydrographic section was made in August-September 1997 at 66°W from the coast of Venezuela to Woods Hole aboard the R/V Knorr. In this report, we concentrate on near surface measurements in the Caribbean. The data show two distinct water masses with different origins. From approximately 14°N to Puerto Rico, Caribbean Surface Water and Subtropical UnderWater with their source in the North Atlantic are found, as previously observed. From Venezuela to approximately 13°N, a less saline water mass with its source in the Tropics and South Atlantic is found. Within the southern portion of the section, two different velocity patterns are observed, namely, an eastward flow with a subsurface maximum near the coast of Venezuela, and a surface intensified westward jet with velocities of 130 cm s^{-1} in midbasin.

1. Introduction

The westward flowing North Equatorial Current (NEC) is the southernmost current of the North Atlantic Subtropical Gyre. It is fed by the Canary Current, which separates from the African coast at approximately 20°N, and the recirculation of the western branches of the Azores Current. The NEC spans the entire North Atlantic. Part of its flow enters the Caribbean through narrow passages [*Wilson and Johns*, 1997] and continues westward as the Caribbean Current. The Subtropical-Tropical Gyre boundary has a seasonal shift at its northernmost position in summer [*Mayer and Weisber*, 1993] and allows water from the South Atlantic to enter the Caribbean.

One important water mass in the Caribbean is the North Atlantic Subtropical UnderWater (SUW) which originates in the central tropical Atlantic. It is found beneath the surface water of the Caribbean at the salinity maximum [*Wüst*, 1964; *Kinard et al.*, 1974; *Metcalf*, 1976]. The formation of fresh surface water above the SUW is a complex process affected by rainfall, runoff and upwelling. An intermediate water mass existing in the Caribbean is the Antarctic Intermediate Water (AAIW) as seen in *Morrison and Nowlin* [1982] and *Joyce et al.* [1999]. Thus, the Caribbean contains water of both North and South Atlantic origin.

In this study we analyze near surface hydrographic, Vessel-Mounted Acoustic Doppler Current Profiles (VMADCP), thermosalinograph, and remote sensing data in the Caribbean for the purpose of describing the water masses and circulation in surface layers of the Caribbean.

2. Data

In August-September 1997, a meridional section at 66°W from Venezuela to Cape Cod (MA, USA) was carried out as part of the World Ocean Circulation

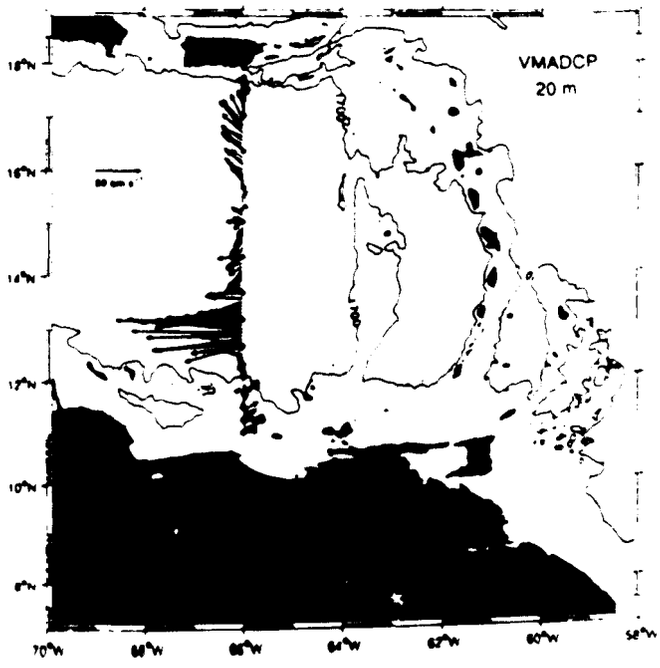

Figure 1. Locations of the CTD stations in this study shown as solid dots. We have also plotted the VMADCP velocity at 20 m depth. Notice the narrow and strong jet with velocities of 130 cm s^{-1} at approximately 13°N. For reference, the 1700 m isobath is shown.

Paper number 1999GL011230
0094-8276/00/1999GL011230$05.00

Experiment (WOCE) Program. The measurements we will show consist of underway thermosalinograph and Vessel-Mounted Acoustic Doppler Current Profiles (VMADCP) data, hydrographic station data collected in the Caribbean, from Venezuela to Puerto Rico (Figure 1), and remote sensing data.

The station data consist of 22 CTD casts following the methodology described in the WHP technical operations manual [*Joyce*, 1994] . The horizontal resolution of the casts is 3-75 km depending on the bottom topography. Salinity data from the thermosalinograph were compared to salt samples. An offset value of 0.31 was found and added to the data. Temperature values from the thermosalinograph proved to be within acceptable ranges when compared to surface CTD measurements given the spatial variability. The VMADCP data were collected using a 150 KHz narrow band sensor. Navigation was provided by a P-code GPS and gyro heading was adjusted using a four antenna, Ashtech GPS unit.

3. Results and Conclusions

To identify water masses, associated depths and circulation patterns, we will show vertical sections of VMADCP, salinity, potential density, and potential temperature (Figure 2), and potential temperature/salinity diagrams (Figure 3).

In the upper layer (<50 m, Figure 2b), the northern half of the section has fresh water with salinity values less than 35.5. *Wüst* [1964] called this water Caribbean Surface Water and it is thought that it is a mixture of North Atlantic surface waters, Amazon river water, and local freshwater runoff from South America. In the middle of the section, we observe a region of minimum salinity (<34.5) also shown in Figure 3 near the 22 kg m^{-3} potential density isopycnal. The origin of this low salinity water is the Orinoco river, as discussed later.

The next deeper water mass is the Subtropical Under-Water (SUW) [*Wüst*, 1964; *Morrison and Nowlin*, 1982] characterized by the salinity maximum (≥37). This water mass, formed in the central tropical Atlantic where evaporation exceeds precipitation, sinks along σ_θ=25.4 kg m^{-3}, at an approximate depth of 150 m (Figure 2c). This water mass is found in the northern half of the section, from approximately 14°N to Puerto Rico (Figure 2b), forming patches as previously observed by *Morrison and Nowlin* [1982]. The θ/S diagram (Figure 3) shows three different salinity values for this isopycnal: 37.2 corresponding to an area close to Puerto Rico, 37 corresponding to the rest of the northern half of the section and 36.8 near the Venezuelan coast. Although the velocity structure (Figure 2a) shows a strong mesoscale variability along the whole section, we notice that these three different locations correspond to three different velocity patterns. The northern portion of the entire section close to Puerto Rico has a strong westward velocity (≥20 cm s^{-1}), the

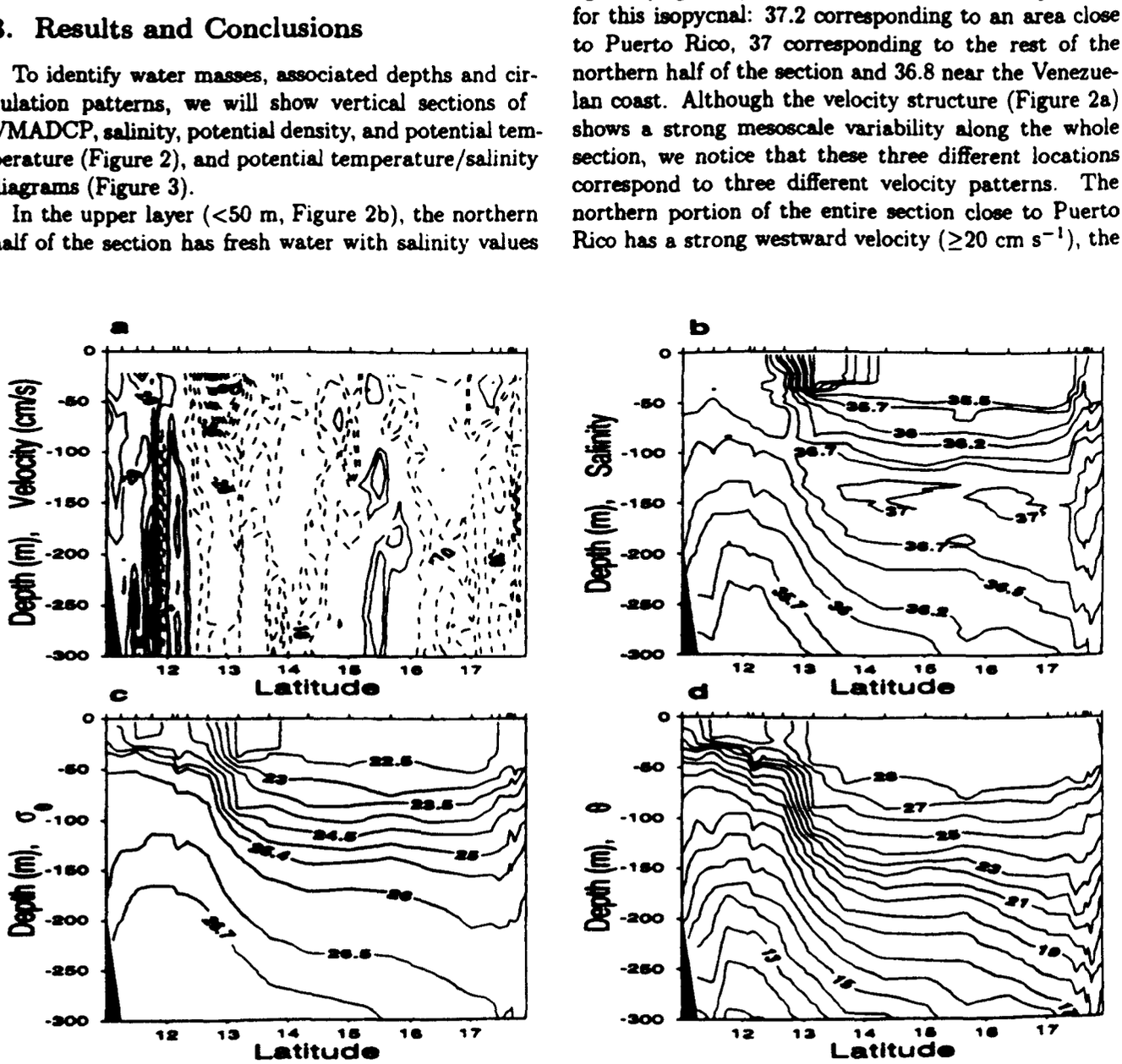

Figure 2. Section of a) VMADCP velocity (cm s^{-1}) (positive eastward), b) salinity, c) potential density, and d) potential temperature for the surface waters (<300 m) for the Caribbean. Station positions are at the top.

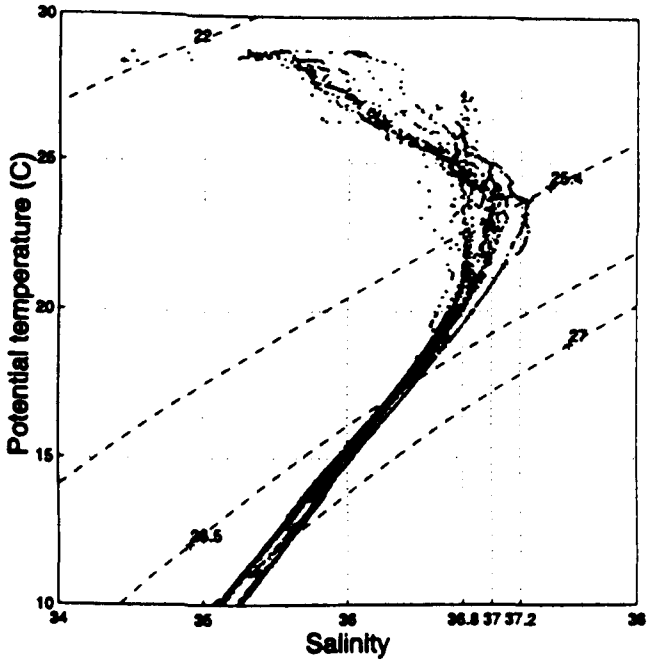

Figure 3. Potential temperature/salinity diagrams for the surface waters (<300 m) of the Caribbean.

central portion has a low and almost uniform westward velocity ($\leq$10 cm s^{-1}) and the flow is eastward near Venezuela. The flow close to Puerto Rico is probably from the Anegada-Jungfern passage because data to the immediate north of Puerto Rico (data not shown here) have similarly high salinity values of SUW.

At 150 m depth, a denser water mass is found from Venezuela to approximately 13°N where the isotherms and the isohalines depict a strong slope (Figure 2b, 2c, 2d). This water mass apparently has its origin in the South Atlantic and is part of the freshest branch of the θ/S diagram for $\theta < 20$°C. With respect to the winds, the COADS data from *da Silva and Levitus* [1994] indicate that the zero wind stress curl position has a seasonal meridional shift with its northernmost position in summer, at about 14 °N. This seasonal shift is about 1° of latitude in the Caribbean and about 10° in the open Atlantic ocean (see also *Mayer and Weisber* [1993]). This results in a seasonal variability in the Subtropical-Tropical Gyre boundary, which demarks a wind-driven connection between the Tropics and the Caribbean. What is surprising is that within this tropical gyre and the zone of upwelled dense water having a South Atlantic character, an eastward current flowing against the mean wind is observed with a subsurface velocity maximum (Figure 2a). This has not been documented in the Caribbean before although a similar flow was previously found by *Wilson and Johns* [1997] at the Grenada Passage where a strong, possible seasonal, time-dependence is suggested. Based on only our data, this eastward flow does not have an obvious explanation. It could be a localized mesoscale event or evidence of a Caribbean coastal undercurrent which is part of a return flow of tropical/South Atlantic waters entering the Caribbean.

Another significant velocity feature observed in this section is a strong westward jet with velocities of 130 cm s^{-1} at approximately 13°N (Figure 1). To further examine this structure, we show the East-West and North-South VMADCP velocity at three different depths (20, 80, and 140 m), the sea surface salinity, and sea surface temperature, these two last measurements from an underway thermosalinograph (Figure 4). Here, the East-West VMADCP velocity (Figure 4a) shows the strongest velocity at 13°N, and also a strong shear from 20 to 140 m depth. The sea surface salinity (Figure 4c) shows a minimum value between 13°N and 14°N. Therefore, the velocity jet is found at the southern boundary of the low salinity feature. Figure 4b shows that there is not any indication of a flow transporting this feature to the north and also that a $v_y < 0$ until 15°N producing a confluence or convergence of water which explains the sharp salinity gradient at the northern boundary of the low salinity structure.

In an attempt to understand the origin of this structure, we have used remote sensing satellite images. Sea Surface Temperature images from the Advanced Very High Resolution Radiometer (AVHRR) were not very useful because they only showed the southern boundary of the structure, which was also seen in the sea surface temperature data from the thermosalinograph (Figure 4d). Another type of satellite data available

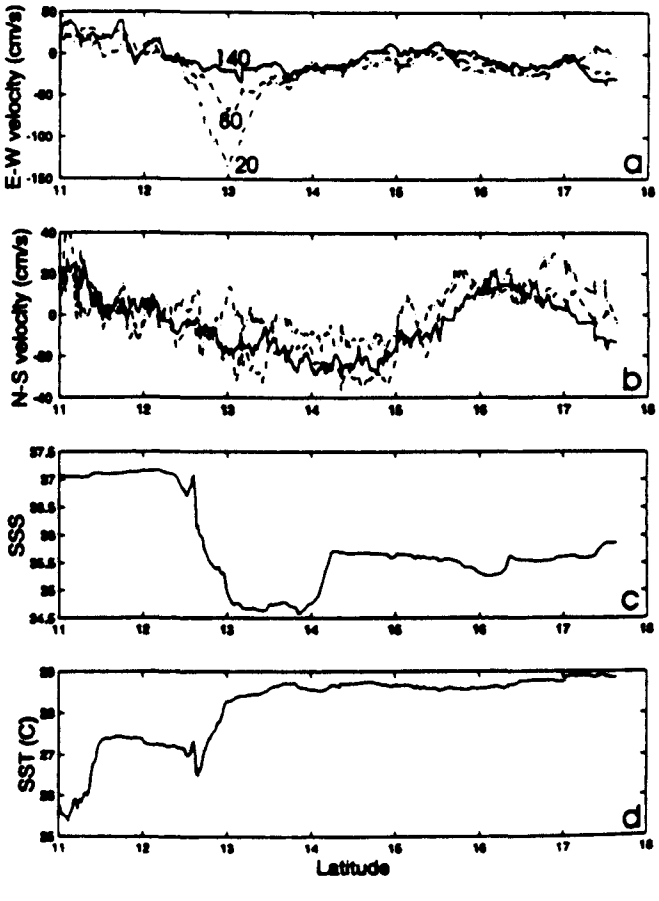

Figure 4. a) East-West VMADCP velocity for three different depths (20, 80, and 140 m), b) North-South VMADCP velocity for the same three different depths (20, 80, and 140 m), c) the sea surface salinity, and d) the sea surface temperature, these two last measurements taken from an underway thermosalinograph with a sampling depth of approximately 5 m.

to us were the ocean color images from the SeaWifs satellite. SeaWifs measures the visible radiation coming from the ocean in several spectral bands from which the chlorophyll concentration may be estimated.

Although this satellite was launched one month later than our cruise, it has been useful for our purposes. Figure 5 shows the binned chlorophyll *a* image from September 22 to 29, 1997. Here, a chlorophyll plume starting at the Orinoco river outflow is clearly seen. According to *Muller-Karger et al.* [1989], who has processed and analysed the whole archive of Coastal Zone Color Scanner (CZCS) data in the Caribbean, the plume formed at the Orinoco River is present during August through November every year. It is over 100 km wide and flows into the Caribbean Sea drifting northwest across the Caribbean, reaching Puerto Rico around October. On this occasion, the Orinoco plume passes through our section represented by the white crosses in the image. Although the hydrographic data and SeaWifs image are one month apart, it seems that the inflow transporting the Orinoco Plume from its source converges at 64°W with the eastward outflow of the Caribbean. This carries the Orinoco plume to the north until the region where the prevailing westward flow is found. Thus this westward jet may be a wind-driven phenomenon which is time dependent and tied to the Orinoco plume. There is no evidence in the available surface drifter (D. Fratantoni, personal communication, 2000) data that this jet is a permanent feature of the Caribbean circulation.

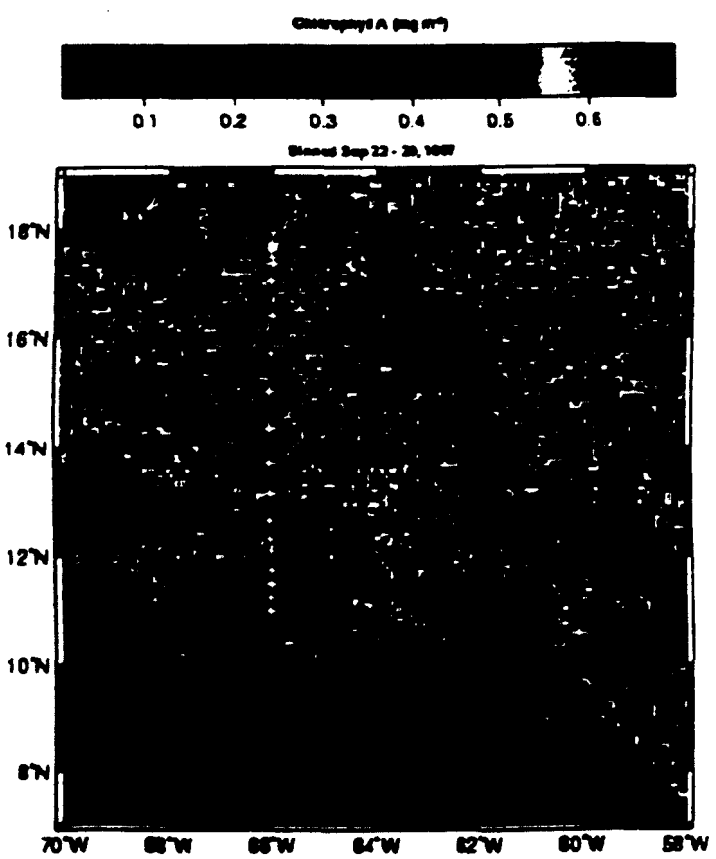

Figure 5. Weekly binned phytoplankton pigment image for the Caribbean region from September 22 to 29, 1997. The white crosses are the station positions for the cruise.

Acknowledgments.

We wish to acknowledge the support of NSF grant (OCE95-29607), the assistance of J. Dunworth-Baker in helping with some of the calculations, and to M. Caruso in providing the SeaWifs image. The first author acknowledges the grant received from the Secretaría de Estado de Universidades, Investigación y Desarrollo (Spain) for his stay at Woods Hole Oceanographic Institution. This is contribution number 10169 of the Woods Hole Oceanographic Institution.

References

da Silva, A. M., and S. Levitus, Atlas of marine data 1994, volume 1: algorithms and procedures, 83 pp., US Dept. of Commerce, December 1994.

Joyce, T. M., WOCE Operations Manual, WHP Office report WHPO 91-1, WOCE Report 68/91, revision 1, Woods Hole, Mass, USA, November 1994.

Joyce, T. M., R. S. Pickart, and R. C. Millard, Long-term hydrographic changes at 52 & 66°W in the North Atlantic Subtropical Gyre and Caribbean, *Deep Sea Res. Part II, 46*, 245-278, 1999.

Kinard, W. F., D. K. Atwood, and G. C. Giese, Dissolved oxygen as evidence for 18°C Sargasso Sea water in the eastern Caribbean Sea, *Deep Sea Res. Part I, 21*, 79-82, 1974.

Mayer, D. A., and R. H. Weisberg, A description of COADS surface meteorological fields and the implied Sverdrup transports for the Atlantic Ocean from 30°S to 60°N, *J. Phys. Oceanogr., 23*, 2201-2221, 1993.

Metcalf, W. G., Caribbean-Atlantic exchange through the Anegada-Jungfern Passage, *J. Geophys. Res., 81*, 6401-6409, 1976.

Morrison, J. M., and W. D. Nowlin, Jr., General distribution of water masses within the Eastern Caribbean Sea during the winter of 1972 and fall of 1973, *J. Geophys. Res., 87*, 4207-4229, 1982.

Muller-Karger, F.E., C.R. McClain, T.R. Fisher, W.E. Esaias, and R. Varela, Pigment distribution in the Caribbean Sea: Observations from Space, *Prog. Oceanogr., 23*, 23-69, 1989.

Wilson, W. D., and W. E. Johns, Velocity structure and transport in the Windward Islands Passages, *Deep Sea Res. Part I, 44*, 487-520, 1997.

Wüst, G., *Stratification and Circulation in the Antillean-Caribbean Basins*, Columbia University Press, New York, 1964.

A. Hernández-Guerra, Facultad de Ciencias del Mar, Universidad de Las Palmas de Gran Canaria, Canary Islands, Spain. (e-mail: alonso.hernandez@fisica.ulpgc.es)

T. M. Joyce, Department of Physical Oceanography, Woods Hole Oceanographic Institution, Woods Hole, MA 02543. (e-mail: tjoyce@whoi.edu)

(Received November 15, 1999; revised May 9, 2000; accepted August 17, 2000.)

Polar Biol (2000) 23: 679–690

ORIGINAL PAPER

S. Hernández-León · C. Almeida · A. Portillo-Hahnefeld
M. Gómez · I. Montero

Biomass and potential feeding, respiration and growth of zooplankton in the Bransfield Strait (Antarctic Peninsula) during austral summer

Accepted: 26 March 2000

Abstract Biomass (as dry weight and protein content), gut fluorescence, electron transfer system (ETS) and aspartate transcarbamylase (ATC) activities were studied in different size fractions (200–500, 500–1000 μm and 1–14 mm) in the Bransfield Strait (Antarctic Peninsula) during January 1993. Very low values of zooplankton biomass were observed in all the size classes studied. About 56% of total biomass was due to the large size fraction (1–14 mm) while the smallest one (200–500 μm) accounted for about 26%. Gut fluorescence values increased in relation to the size class considered, as expected, being the differences from the smaller to the highest size fractions of orders of magnitude. Calculated ingestion rates showed that about 60–80% of total zooplankton ingestion (< 14 mm) was due to the smaller organisms. Higher average values and higher variability of specific ETS activity was observed in the smaller size fraction while no differences between size classes were observed for the specific ATC activity. Biomass, gut fluorescence, ETS and ATC activities were not significantly different between the Bellingshausen and Weddell waters, although higher standard deviation was normally found at the former area. With the restrictions of using the above indices to estimate physiological rates, potential grazing of mesozooplankton (< 14 mm) accounted for a rather low portion (< 10%) of the primary production. The index of growth showed high values, suggesting no food limitation of mesozooplankton. Therefore, other processes such as predation should account for the very low biomass found and for the fate of a large portion of primary production.

S. Hernández-León (✉) C. Almeida A. Portillo-Hahnefeld
M. Gómez · I. Montero
Facultad de Ciencias del Mar,
Universidad de Las Palmas de G.C., P.O. Box 550,
Las Palmas de G.C., Canary Islands, Spain
e-mail: santiago.hernandez-leon@biologia.ulpgc.es
Fax: + 34-28-454490

Introduction

Studies on zooplankton communities seek to find the influence of the physical environment on the presence/absence of organisms, as well as their role in the energy flow through their biomass. Most of the feeding, metabolic and growth estimations in Antarctic waters have been done at random stations representing polar conditions but not the particular characteristics of the different water masses. Average values obtained have been used to estimate the role of zooplanktonic organisms in the general food web of the Southern Ocean ecosystem. However, high variability in biomass and physiological parameters in relation to the physical environment is probably one of the most prominent features of Antarctic waters.

A first aim of this work was to access values of biomass and feeding, respiration and growth in size-fractionated zooplankton in a region of high biological variability. In order to map areas of important spatial variability as those of Antarctic waters, it is of importance to obtain a sufficient number of data which will allow the assessment of mesoscale patterns. Typical physiological measurements seem to be of low resolution in those oceanographic surveys. In this sense, the gut fluorescence and the enzymatic approach could offer an important number of data about potential feeding, respiration and growth. Previous measurements of enzymatic indices in Antarctic waters (Bergeron et al. 1985; Schalk 1990; Drits et al. 1993) provided an important source of information about the functioning of these cold environments. However, its potential utility in mapping mesoscale features has not been of widespread use, probably because of the lack of confidence between such measurements and the true metabolic rates. However, there is some agreement in the fact that the enzymatic methodology produces good estimations of metabolism when the enzyme is not limited by intracellular substrates (Hernández-León and Gómez 1996; Packard et al. 1996; Hernández-León and Torres 1997).

When the organisms are substrate limited in nature, the application of the enzymatic methodology gives rise to an underestimation of the physiological rate under consideration. Hence, for our purposes of assessing zooplankton metabolism, this methodology will give a base line of carbon used by the organisms.

Using gut fluorescence (Mackas and Bohrer 1976), electron transfer system (ETS) (Packard 1971) and aspartate transcarbamylase (ATC) activities (Bergeron and Buestel 1979), we were able to study potential feeding, metabolic activity and growth in different size fractions of zooplankton in a region of high variability in physical structure and primary production, as well as in the distribution of phytoplankton and zooplankton biomass. However, not all the variability in zooplankton biomass is explained as an effect of the physical environment. In a previous work, Hernández-León et al. (1999) observed very low values of mesozooplankton biomass in the Bransfield Strait during late spring. Because of the very low control of zooplankton on primary production (< 3%) and because of the impossibility of assessing the growth of organisms during sampling, it was postulated that food quality and/or predation by krill are factors that can explain the low biomass found. Krill are able to predate on copepods (Price et al. 1988; Atkinson and Snÿder 1997) and they positively select mesozooplankton (Granéli et al. 1993). Recently, Atkinson et al. (1999) also showed that areas of persistently high krill abundance were characterized by exceptionally few copepods. Moreover, an inverse relationship between krill and non-krill zooplankton has been observed in Antarctic waters (Hosie 1994; Voronina et al. 1994), suggesting a top-down effect of krill on copepods. However, the question of whether this could be the effect of competition or predation, or both, remains. The indices used in this study allow the estimation of the degree of zooplankton feeding and their grazing impact, as well as whether their specific activities are typical of actively growing populations. Whether or not the organisms were potentially growing in this environment provides an insight into the importance of growth or predation in explaining the biomass values observed.

Materials and methods

The Bransfield Strait was sampled on board R.V. "Hespérides" between 19 January and 8 February 1993. Zooplankton hauls were done using a WP-2 double net equipped with a 200-µm mesh (UNESCO 1968) from 200 m (or 5–10 m from the bottom at the shallower stations) to the surface (Fig. 1). In a previous cruise in 1991, we tried to use a WP-2 net equipped with a 100-µm mesh but it was impossible to wash out the large phytoplankton in the 100- to 200-µm size fraction. As these large cells interferred in the biomass, ETS and ATC activity determinations, we opted to use the coarse net (200 µm). Samples were then size-fractionated into the 200–500, 500–1000 µm and 1–14 mm size classes, the 200- to 500-µm fraction being washed out of phytoplankton by allowing the sample to be in a water stream over the 200-µm mesh until large greenish material was not visually observed. During the cruise, high densities of salps were found at the different stations all around the Bransfield Strait. Because of advection, stolons of salps (salp chains asexually produced from buds) were collected by winch cable during descent and ascent of the vertically towed net, as observed in the upper layer from the ship deck. Therefore, while the WP-2 net was ascending, it collected all the stolons trapped in the cable, giving rise to an overestimation of salp biomass. This problem was sometimes so important that samples from some few stations needed to be rejected for biomass and physiological measurements because of the impossibility of collecting the smaller organisms. As an example, in one station (st. 61) the WP-2 sampler reached the sea surface with the net filled with salps from the cod-end to near the mouth ring. Therefore, biomass of salps could not be assessed in these vertical hauls.

Biomass was measured as protein content using the method proposed by Lowry et al. (1951) and bovine serum albumine (BSA) as the standard. The method of Peterson (1983) was used when very small samples were obtained. In some stations additional samples were obtained in order to compare biomass in terms of dry weight and protein content. Dry weight was measured at the laboratory using the procedure described by Lovegrove (1966). Samples were dried for 24 h and later weighted in a microbalance. Some samples were counted and dried in order to determine average values of weight per individual in the different size fractions.

Gut fluorescence was measured in organisms picked off the mesh and placed in a test tube with 10 ml of 90% acetone. Each sample was immediately stored at −20 °C for 24 h. After this, fluorescence of the samples was measured before and after acidification with two drops of 10% HCl with a fluorometer (Turner Design model 10), previously calibrated with pure chlorophyll (Yentsch and Menzel 1963). Chlorophyll and phaeopigments of each sample were calculated using equations for in vitro fluorimetry (Strickland and Parsons 1972) slightly modified to:

$$\text{Chlorophyll} = K \cdot (F_o - F_a)/n$$

$$\text{Pheopigments} = K \cdot (R \cdot F_a - F_o)/n$$

where K is the machine calibration constant, F_o and F_a are the fluorescence readings before and after acidification, R is the acidification coefficient and n is the number of organisms.

The electron transfer system was measured using the method of Kenner and Ahmed (1975). Details of the specific procedure are given in Hernández-León and Gómez (1996) and Gomez et al. (1996). The assay of aspartate transcarbamylase activity was done in accordance with the method of Bresnick and Mossé (1966), but assayed using the procedure given by Bergeron and Alayse-Danet (1981). In assaying the activity of this enzyme, a subsample of the first homogenate was incubated, taking into account the considerations proposed by Alayse-Danet (1980) for the determination of the initial velocity of the reaction. The homogenized samples were incubated for a minimum of three time periods and always for 15, 30 and 60 min to obtain linear relationships. ATC is expressed in nanomoles of carbamylaspartate (CA) synthesized per minute.

Results

Hydrography

The mesoscale variability during January 1993 has been described by Garcia et al. (1994) and Basterretxea and Aristegui (1999). They found the front between the Bellingshausen and Weddell waters to be characterized by the isohalyne of 34.1 psu at 5 m depth (stippled line in the figures). This front has been described using hydrographic data by several authors (Grelowski et al. 1986, Niiler et al. 1991, Rojas et al. 1996), as well as from satellite infrared imagery (Figa et al. 1998). Garcia et al. (1994) also found evidence of meandering and intense mesoscale variability at the frontal area (dipole

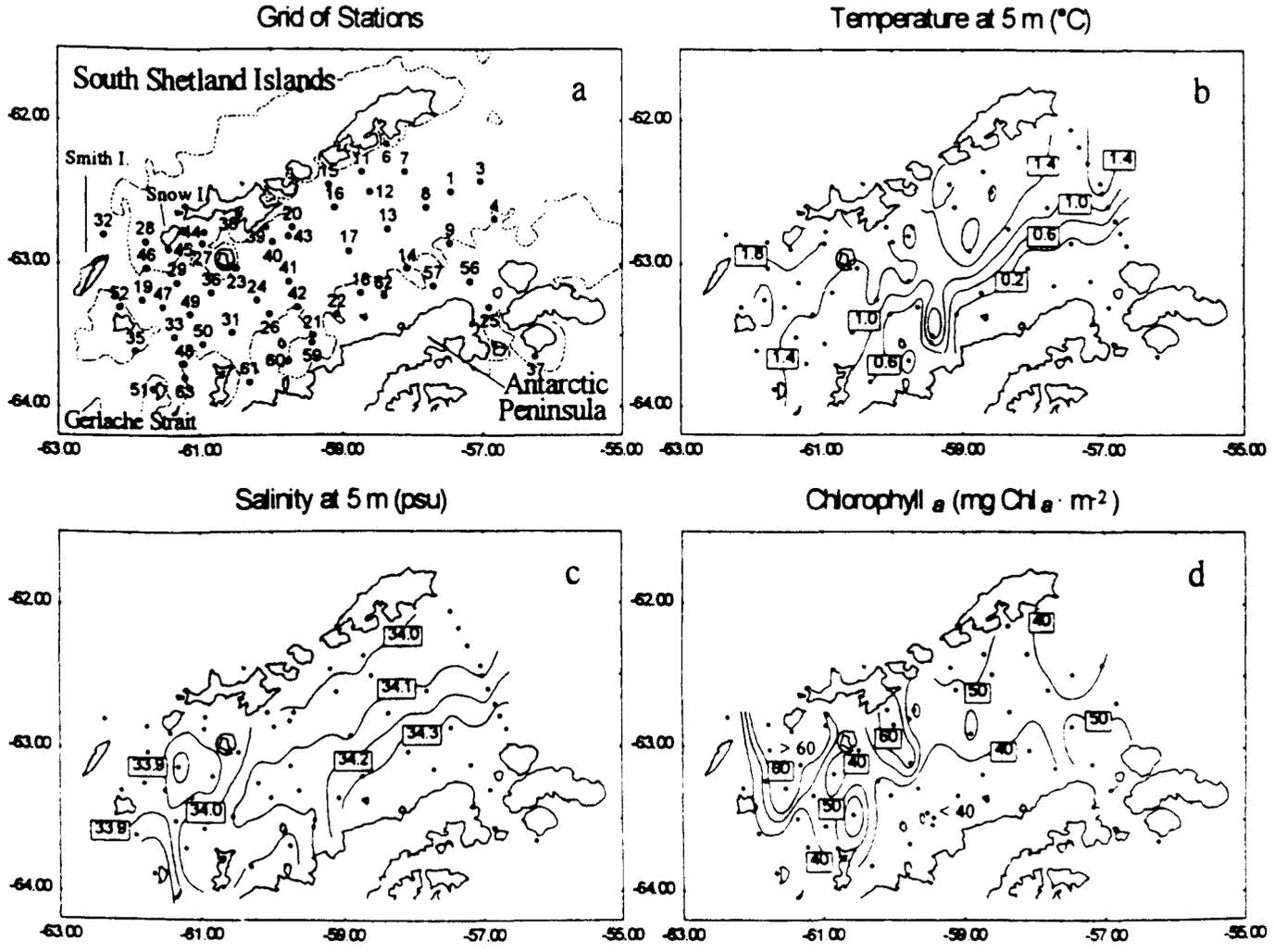

Fig. 1 a Location of stations in the Bransfield Strait (Antarctic Peninsula) during January and February 1993, b temperature (in °C), c salinity (psu) and d integrated chlorophyll (mg · m^{-2}). *Dashed line* in a is the 200-m isobath

mushroom-like eddies) using remote sensing. Basterretxea and Aristegui (1999) distinguished the strait into four characteristic zones: (1) Weddell water zone, cold (< 0.6 °C) and salty (> 34.1 psu, see Fig. 1b, c), (2) Gerlache, and (3) Bellingshausen water zones including modified Bellingshausen water from the Gerlache Strait and from the Bellingshausen Sea entering into the strait between Smith and Snow Islands, (4) Bransfield water zone with characteristics of Weddell water at depth and a mixture of waters of different origin near the surface. In order to compare with previous studies in the area (Hernández-León et al. 1999), we divided the area into two well-defined zones: (1) the Bellingshausen water, which includes water from the Gerlache Strait and the proper Bellingshausen water entering from the west into the Bransfield Strait, and (2) the Weddell water which is observed in the southeast area of the strait. The boundary between both water masses is given by the 34.1 isohalyne (see above). Chlorophyll *a* (Fig. 1d) and primary production values were always higher in the Bellingshausen water (Basterretxea and Aristegui 1999). These biological characteristics were different to the one described in the same area by Aristegui and Montero (1995) and Hernández-León et al. (1999) for December 1991, who found higher phytoplankton and zooplankton biomass related to the Weddell water. Basterretxea and Aristegui (1999) concluded, however, that phytoplankton blooms in the Bransfield Strait are advected from the nearby Gerlache or Bellingshausen Sea, following the main eastward surface currents.

Zooplankton biomass

Very low values were found in the Bransfield Strait during January (Table 1). Size-fractionated biomass presented the lower values in the 500- to 1000-µm size class while the large fraction showed the highest proportion of total biomass, being 53% in terms of dry weight and 56% as proteins. The smaller organisms were also important components of the community, representing 26% in terms of protein and 30% as dry weight.

The largest values of biomass in the small and large size fractions of zooplankton were observed in the so-called Bransfield current, which flows from the Gerlache Strait and Bellingshausen Sea through the south of the South Shetland Islands (Fig. 2). However, due to the

Table 1 Average values of biomass (mg m^{-2}), specific electron transfer system ($\mu lO_2 \cdot mg^{-1}$ protein h^{-1}, ETS) and specific aspartate transcarbamylase (nmol carbamyl aspartate mg^{-1} protein $\cdot$ min^{-1}, ATC). Biomass values in *fourth column* are given as the sum of the three fractions while specific activities are given as the average activity. Numbers of samples are given *in parentheses*. Total biomass as dry weight is not given because of the coincidence of few samples of the same size fraction (see text)

	200–500 µm	500–1000 µm	1–14 mm	Total or average
Dry weight	32.25 ± 30.63 (23)	8.61 ± 5.90 (17)	74.22 ± 131.7 (26)	-
Protein	16.12 ± 11.40 (48)	10.93 ± 6.23 (52)	34.47 ± 57.74 (48)	64.31 ± 59.56 (44)
ETS	5.38 ± 4.88 (51)	2.21 ± 1.76 (50)	2.81 ± 1.58 (47)	3.52 ± 2.37 (52)
ATC	4.76 ± 4.78 (25)	6.22 ± 5.14 (26)	4.63 ± 4.38 (32)	4.90 ± 3.53 (42)

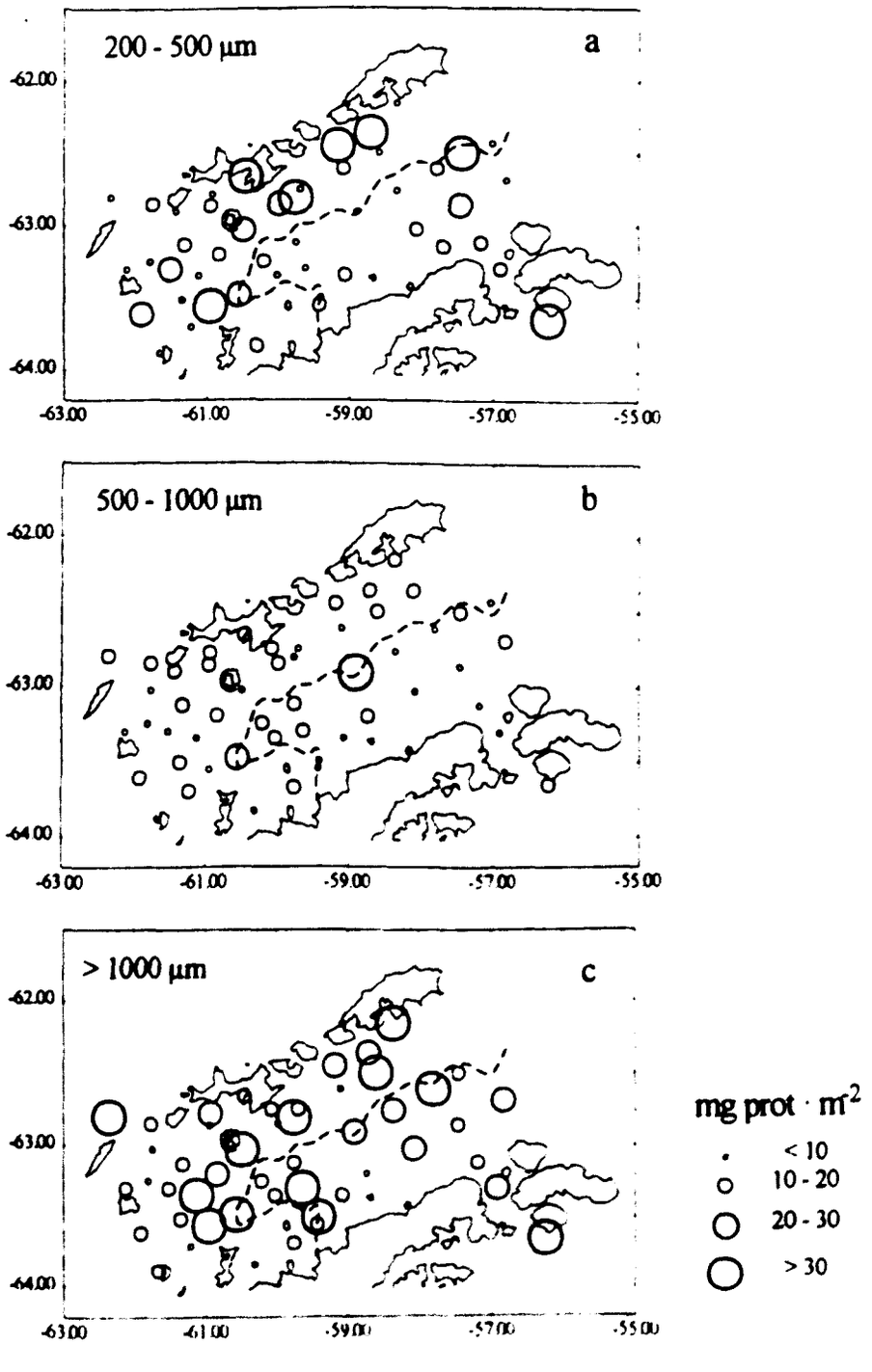

Fig. 2 Zooplankton biomass (mg protein $\cdot$ m^{-2}) in the **a** 200- to 500-µm, **b** 500- to 1000-µm, and **c** 1- to 14-mm size fractions in the Bransfield Strait (Antarctic Peninsula). The frontal zone between the Bellingshausen and Weddell waters is defined by the isohalynes of 34.1 psu (see text)

very high variability in the biomass values found, there were no significant differences in biomass (ANOVA, $P > 0.05$) between the Bellingshausen and Weddell water masses. Zooplankton distribution in the 500- to 1000-µm size fraction showed lower values but also with a high variability. Total biomass displayed the pattern observed in the small and large size fractions with a high biomass variability (Fig. 3).

Gut fluorescence and enzymatic activities

As expected, average values of gut fluorescence per individual showed increased values in relation to animal size (Table 2). Differences among species were of orders of magnitude, salps being the organisms with the largest amounts of pigments. Differences between the Bellingshausen and Weddell waters were not significant for the different size fractions and species, except salps (ANOVA, $P < 0.05$). The 500- to 1000-µm size class, as well as *Euphausia superba*, displayed a large number of higher values in the western area of the Strait (Fig. 4), coinciding with the high levels of chlorophyll entering the Bransfield Strait from the Bellingshausen Sea (Fig. 1a). However, differences in gut fluorescence in both water masses remained insignificant.

The electron transfer system showed higher and significant (ANOVA, $P < 0.05$) average values in the smaller size fraction (Table 1). In contrast, aspartate transcarbamylase activity showed no significant differences between the size classes studied. No significant differences were observed in the ETS activity between the Bellingshausen and Weddell waters, although higher variability and values were found in the Bellingshausen water (Fig. 5). This was also true for the ATC activity. Despite the high variability in ATC values, the average values of specific activity given in Table 1 are rather high, with numerous stations showing values above 6 ATC units (Fig. 6).

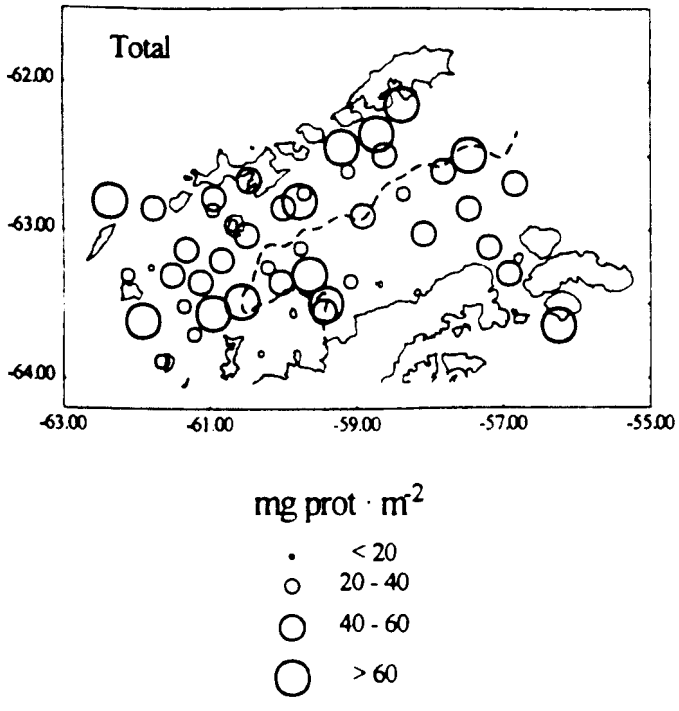

Fig. 3 Total biomass (mg protein m^{-2}) of < 14-mm mesozooplankton in the Bransfield Strait. The frontal zone between the Bellingshausen and Weddell waters is defined by the isohalynes of 34.1 psu (*dashed line*)

Discussion

The biomass obtained was at the lower end of values cited in the literature of polar areas (Conover and Huntley 1991). This could result from the sort out of all of the very large plankton (large euphausiids and large salps) due to the 14-mm mesh used as the upper limit in our biomass measurements. However, Boysen-Ennen et al. (1991) found values of 0.8–3.6 g dry weight · m^{-2} for organisms < 14.5 mm in the Weddell Sea. Atkinson et al. (1996) found values of 8.4 g dry weight m^{-2} and Ward et al. (1995) values of 13 g dry weight · m^{-2} in South Georgia. In contrast, the very low biomass values

Table 2 Specific and community ingestion rates obtained from gut fluorescence per individual (ng pigments ind^{-1}), published gut clearance rates and individual weight of Antarctic organisms. Zooplankton body carbon was assumed to be 45% of dry weight (Atkinson 1996). Numbers of samples are given *in parentheses*

	Gut fluorescence (ng pigm ind^{-1})	Gut clear (h^{-1})	Ingestion rate[a] (ng pigm ind^{-1} h^{-1})	Weight (µgC ind^{-1})	Ingestion (day^{-1})	Community ingestion (mgC m^{-2} day^{-1})
200–500 µm	1.34 ± 0.83 (40)	0.72[b]	0.97	1.35	0.86	11.61
500–1000 µm	4.01 ± 3.15 (38)	0.72[b]	2.89	7.5	0.46	2.13
Metridia gerlachei	19.97 ± 14.11 (13)	0.49[c]	9.79	81–99[c]	0.12–0.15	0.45–6.55
Rhincalanus gigas	15.72 ± 13.36 (25)	0.23–0.95[d,e]	3.62–14.93	504[d]	0.01–0.04	
Euphausia superba	91.44 ± 146.3 (30)	0.13–0.42[f,g,h]	11.89–38.41	4351[i]	0.003–0.01	
Salpa thompsoni	5617 ± 2946 (23)	0.25[i]	1404.25	1480–2250[e]	0.75–1.14	
						Total 14.19–20.29

[a] C/Chl = 50
[b] Irigoien (1998)
[c] Lopez and Huntley (1995)
[d] Atkinson et al. (1992b)
[e] Dubischar and Bathmann (1997)
[f] Pakhomov et al. (1997)
[g] Perissinotto et al. (1997)
[h] Atkinson and Snyder (1997)
[i] dw = 1.208 exp(0.104L). Kato et al. (1982)
[j] Perissinotto and Pakhomov (1998)

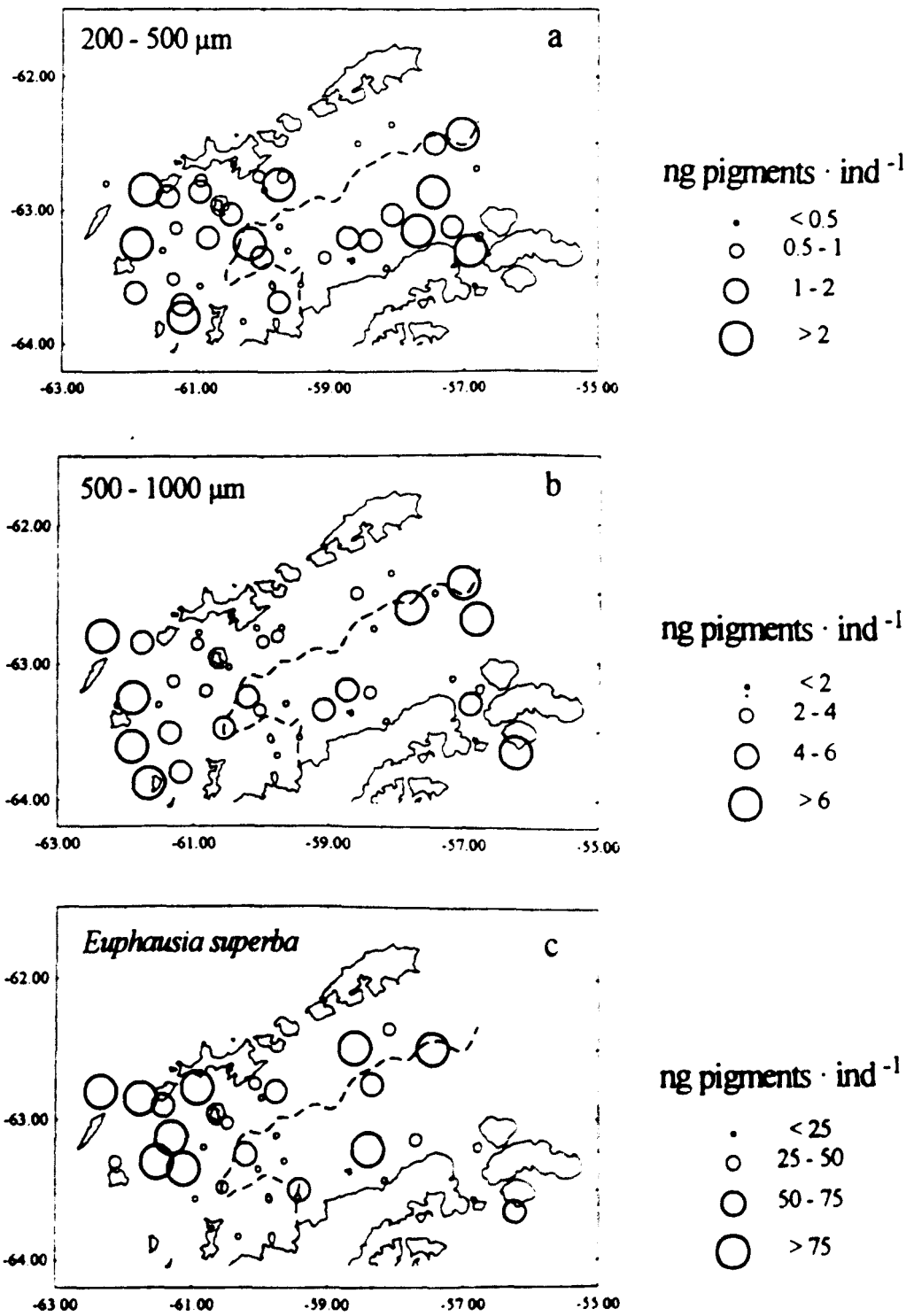

Fig. 4 Mesoscale variability of gut fluorescence in **a** small and **b** medium size fractions. **c** Gut fluorescence of *Euphausia superba*. The *dashed line* represents the frontal zone as in Fig. 3

found during January 1993 were of the same magnitude as the one found by Hernández-León et al. (1999) during December 1991 (0.087 g dry weight · m^{-2}), and comparable to the values obtained by Robins et al. (1995) in the Bellingshausen Sea (0.05–0.53 g dry weight · m^{-2}, assuming that carbon is 40% of dry weight). However, although biomass values were low during December 1991 and January 1993 (present study), its distribution in the Bransfield Strait differed in both months as shown by slightly higher biomass in the Weddell water in December, and large values and a high variability in the Bellingshausen water in January. These differences in the distribution were in agreement with the values of chlorophyll, primary production and microplankton (< 200 µm) ETS activity in both samplings (Aristegui and Montero 1995, Basterretxea and Aristegui 1999). The higher variability of biomass in the Bellingshausen water (small and large fractions) also corresponded to a higher variability of specific ETS, giving some consistency to the observed differences in

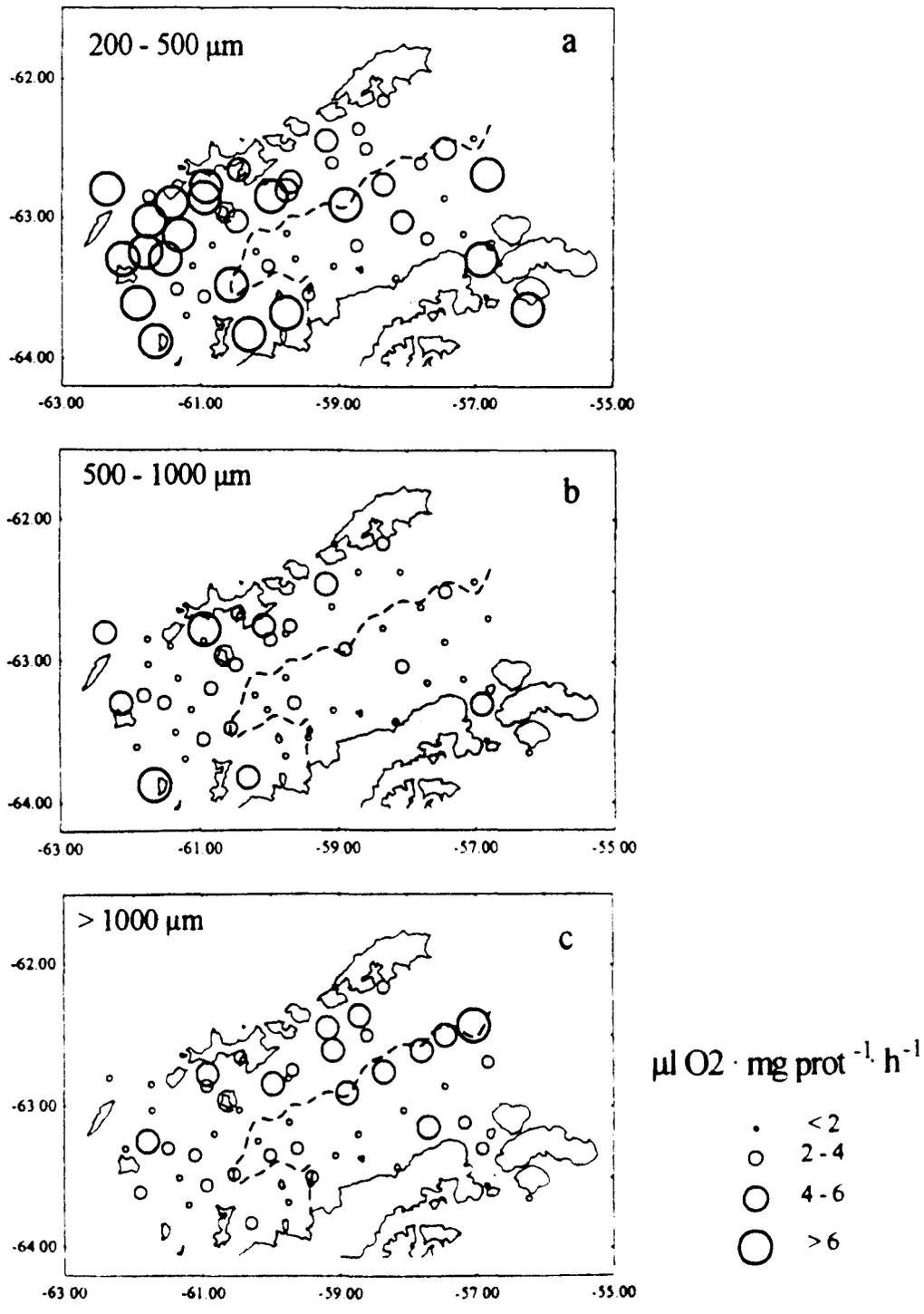

Fig. 5 Mesoscale variability of electron transfer activity (ETS) in the **a** small, **b** medium, and **c** large size fractions. The *dashed line* represents the frontal zone as in Fig. 3

phytoplankton biomass and productivity between the two water masses. The presence of such differences could be related to local physical features such as melting in shelf waters of the Antarctic Peninsula, or the different timing in the development of the bloom. This fact could give rise to biological differences in waters advected from southern areas of the Bransfield Strait, as is the case in the Bellingshausen and modified Bellingshausen waters of the Gerlache Strait. Moreover, the meandering of the front between the Bransfield current and the Weddell water (Garcia et al. 1994), as well as the higher variability in biomass or specific activities, could be examples of the complex hydrology and biological processes in the Bransfield waters. Differences in activity due to diel differences in feeding and metabolic activity could also explain the high variability in gut fluorescence (Atkinson et al. 1992a, 1996) and enzymatic activities in the more productive waters of the Bransfield current. Another source of variability in gut fluorescence could be related to feeding on non-pigmented food. There is a growing body of literature suggesting that microzooplankton is a major component in the diet of copepods

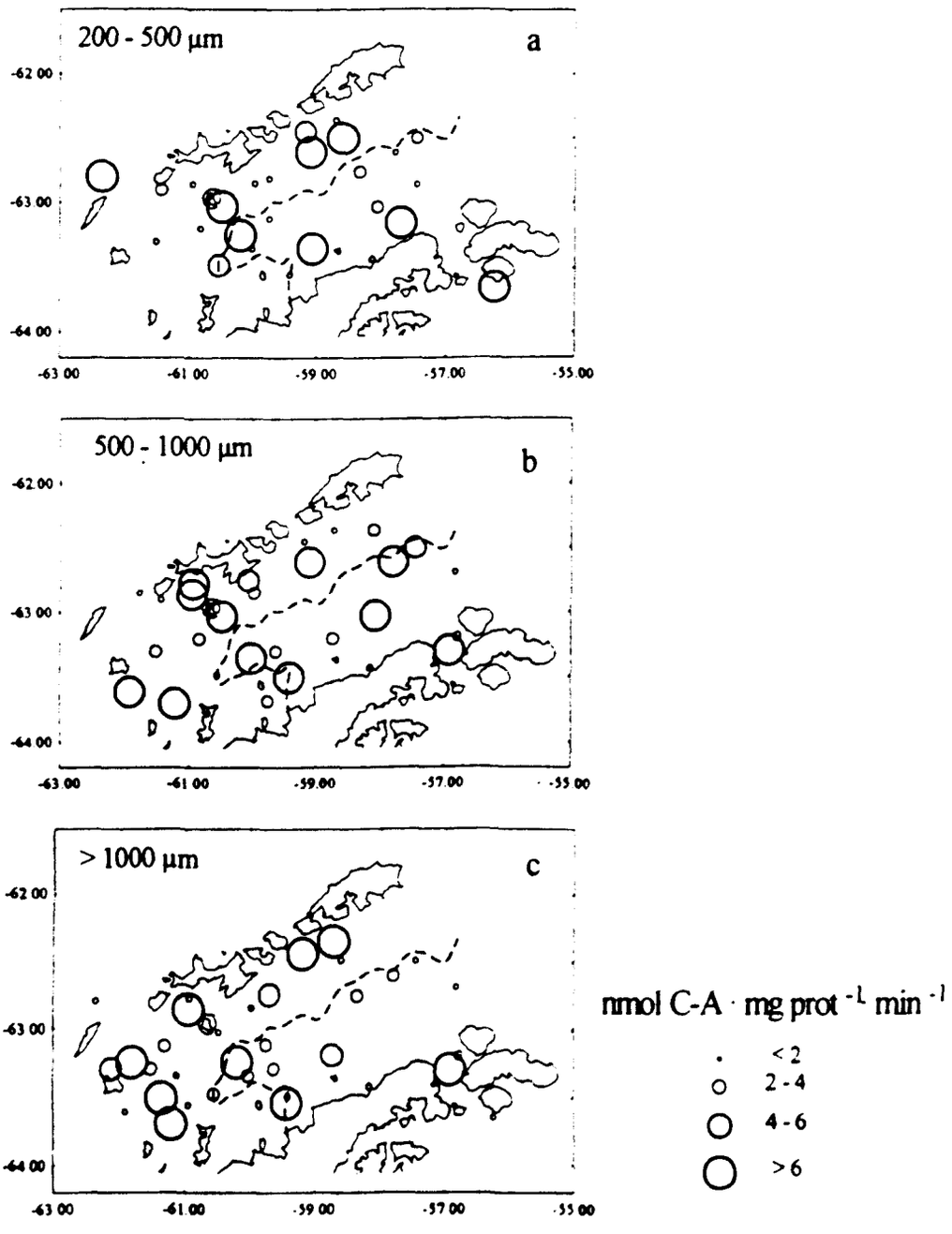

Fig. 6 Mesoscale variability of aspartate transcarbamylase activity (ATC) in the **a** small, **b** medium, and **c** large size fractions. The *dashed line* represents the frontal zone as in Fig. 3

(Dam et al. 1993; Roman and Gauzens 1997). Because of the fact that there were no significant differences in biomass and indices of physiological rates between both water masses, we will assess the grazing impact of zooplankton in all the areas studied.

Differences were also observed in the importance of biomass in the different size classes studied between December (Hernández-León et al. 1999) and January. While in December about 50% of biomass was observed to be in the smaller size fraction studied (200–500 µm), in January this fraction was less important (26%), with the large size fraction the better represented (56%). This result could reflect the interannual variability but also the progression of the different populations from spring to summer. This would imply that organisms have growth rates which might reach high values during the productive season. Average values of specific ATC activity did not show any statistical difference between the size classes studied but, in general, they were rather high. In this sense, Antarctic zooplankton during the cruise displayed values from the very low to the highest specific ATC activities that zooplankton can reach in nature (Hernández-León et al. 1995). Although there is evidence of good relationships between ATC activity and growth rates in different organisms (Bergeron and Alayse-Danet 1981; Bergeron 1982), the same relationship in crustaceans is not clear (Alayse-Danet 1980; Hernández-León et al. 1995). This is because ATC activity reflects the period of intensive cell multiplication (Koueta and Boucaud-Camou 1992) which, in those

organisms, is related to the moulting process and not to structural growth. However, because both processes are in fact coupled in nature, this enzyme can be used to distinguish organisms that are actively growing. Hernández-León et al. (1995) found that the ratio between growth and ATC suffers the same variability as the other physiological rates/enzyme activity ratios observed in the literature (e.g. respiration/ETS or glutamate dehydrogenase/ammonia excretion). Thus, with the restrictions of using those indices and using the growth/ATC obtained by Hernández-León et al. (1995) of 0.033 and a Q_{10} of 2, we found a general growth rate of 0.04 day^{-1}. Few estimates of growth rates for the Southern Ocean can be found in the literature. Schnack (1985) and Schnack et al. (1985) gave values from less than 0.01 to 0.09 day^{-1}. Lopez et al. (1993), using the egg production method, observed values of growth rates in the range 0.01–0.07 day^{-1} for *Calanoides acutus*. Values of <0.1 day^{-1} estimated for Antarctic waters seem to be normal for polar organisms, as stated by Conover and Huntley (1991), with a general value of 0.045 day^{-1} at 0 °C (Huntley and Lopez 1992). However, the range of growth rates values given above is in fact a wide range, as it represents differences in moulting rates of about 6 to more than 40 days. It is known from recent models (Huntley et al. 1994) that Antarctic copepods can have quite different stage durations related to the specificities of their life-cycles (e.g. the so-called pulse moulting). Atkinson and Shreeve (1995) found late naupliar stages of calanoid species at the beginning of December. Atkinson (1991), analysing historical data of Antarctic zooplankton, argued that the growth of early copepodites of *C. acutus* during November/December must be very rapid due to the appearance of stages CIII and CIV in about 1 month. Recently, Shreeve and Ward (1998) reported mean values of growth of 0.14 day^{-1} for *C. acutus* and of 0.05 day^{-1} for *Rhincalanus gigas* around South Georgia in summer (~3 °C), supporting the idea of a rapid growth related to food quality. The wide range of developmental rates also suggests the dependence of polar organisms on the environmental conditions (mainly on temperature and food), which could produce quite large differences in growth rates and survival. In this sense, our values of ATC activity reflected this variability with rather high values of specific activity. This fact suggests that organisms were actively growing during January 1993, having calculated a general stage duration of about 10 days (Huntley and Lopez 1992), allowing copepodites to reach stage CV during summer.

Feeding rates calculated from gut fluorescence and published gut clearance rates (Table 2) showed the higher values in the small size fraction and very variable results in the large size class. The latter fraction is composed of organisms as different in length as copepods and euphausiids with a different consumption in terms of body carbon per day (from 0.003 to 0.15 day^{-1}). Therefore, depending on the dominance of different groups, the community feeding rates are going to vary at least by 1 order of magnitude. Taking into account the community ingestion rates (Table 2) of the three size classes (<14 mm), the impact of grazing on primary production (423–3913 $mgC \cdot m^{-2} \cdot day^{-1}$, Basterretxea and Aristegui 1999) during the cruise varied between 0.4 and 4.8% based on 24-h grazing (e.g. no diel pattern). It is worth noting that 57–82% of ingestion was due to the small size fraction. However, assuming a conservative respiration/ETS ratio of 0.5 (Hernández-León and Gómez 1996), a growth/ATC ratio of 0.033 (Hernández-León et al. 1995) and an assimilation efficiency of 70%, we found that community ingestion accounted for 7.66 $mgC \cdot m^{-2} \cdot day^{-1}$ (see Table 3), which produces a grazing impact from 0.2 to 1.8% of primary production. The higher impact obtained using the gut fluorescence values and published gut evacuation rates is probably due to the fact that we assumed that, for the higher value (4.8%), all the biomass found in the large size fraction was the copepod *Metridia gerlachei*. However, if biomass in the large size fraction is dominated by small euphausiids, then the grazing impact (0.4%) is in the range of the percentage calculated from the indices of metabolism and growth. In any case, despite the uncertainties of using indices to assess feeding, metabolism and growth, the grazing impact of mesozooplankton in the Bransfield Strait estimated in both ways seems to be low ($<5\%$). Moreover, an upward calculation of ingestion assuming a 99% of pigment destruction in the gut (Conover et al. 1986) would produce a grazing impact lower than 10% for the <14-mm organisms. This is in agreement with previous works in Antarctic waters (see Atkinson and Shreeve 1995; Lopez and Huntley 1995; Dubischar and Bathmann 1997; Swadling et al. 1997) and considerably lower than values observed by Ward et al. (1995) for copepods and small euphausiids in a high-biomass scenario near South Georgia (25–56% of primary production).

Gut fluorescence was also measured in salps (Table 1). However, we were unable to calculate the biomass of these large organisms with the WP-2 net in vertical hauls (see Materials and methods). This and the

Table 3 Respiration and growth rates obtained from electron transfer system and aspartate transcarbamylase activities using the physiological/enzymatic activity ratios of the literature (see text)

	Respiration		Growth
	($\mu lO_2 \cdot m^{-2} \cdot h^{-1}$)	($mgC \cdot m^{-2} \cdot day^{-1}$)	($mgC \cdot m^{-2} \cdot day^{-1}$)
200–500 µm	43.37	0.56	0.53
500–1000 µm	12.06	0.16	0.24
1–14 mm	48.43	0.62	1.72
All size classes	113.31	1.46	3.90

escapement of large krill from our net are important shortcomings in our estimations of grazing in the Bransfield Strait. However, using maximum average biomass of salps of 183.5 and 56.3 mgC · m^{-2} around the Bransfield Strait (Huntley et al. 1989; Nishikawa et al. 1995, respectively) and our calculated ingestion rates (Table 2), we obtained a grazing impact on primary production in the range of 1.1–49.5% with an average value of 22%, assuming the highest average value of salp biomass (183.5 mgC · m^{-2}). Although maximum biomass of salps (556 and 671 mgC · m^{-2}) cited in Nishikawa et al. (1995), Huntley et al. (1989) and Schnack-Schiel and Mujica (1994) could account for a large portion (> 100%) of primary production (see Dubischar and Bathmann 1997; Perissinotto and Pakhomov 1998), the highly patchy distribution of these organisms seems to produce lower average values. Salps in the austral polar province are reported to consume only < 1% of primary production in poor salp years and about 19% in years of high abundance (Longhurst 1998). Similar calculations were made with the maximum average biomass of euphausiids (1381.1 mgC · m^{-2}) given by Nishikawa et al. (1995). The results showed a grazing impact by these organisms in the range of 0.4–3.3% (average 1.5%) of primary production, which is in agreement with the work of Pakhomov and Perissinotto (1996), who found that *E. crystallorophias* ingested a small fraction of primary production (0.02–1.12%). In *E. superba*, Pakhomov et al. (1997) found a range of 9.6–59.2% (average 30.5%), Perissinotto et al. (1997) 0.5–50.8% (average 12.4%) and Hernández-León et al. (1999) calculated 8.1%. In this sense, it is generally considered that a small portion (< 10%) of the primary production is consumed by krill (Holm-Hansen and Huntley 1984). However, dense swarms of *E. crystallorophias* can remove 13.6–96.5% of daily primary production (Pakhomov and Perissinotto 1996). Therefore, excepting the high biomass scenarios of swarms, the average values in the waters around the Bransfield Strait showed a characteristic low control of zooplankton grazing on the primary production. This fact suggests that zooplankton is not food limited in these waters. However, ingestion rates are not only driven by food quantity but also by food quality (e.g. Jónasdóttir et al. 1995; McKinnon 1996). With the limitations of the use of enzymatic indices, we estimated that zooplankton was actively growing as observed from the rather high ATC activity values (see above), indicating that food quality should not be a limiting factor as expected from the abundance of diatoms and protozoa in Antarctic waters. Moreover, the small size fraction also showed high ingestion rates accounting for about 60–80% of total ingestion.

However, the relatively low biomass of mesozooplankton in the Bransfield Strait has been justified in the literature because of the abundance of krill in such waters (Marr 1962, Smith and Schnack-Schiel 1990). The large differences in biomass found in relation to the values reviewed by Boysen-Ennen et al. (1991) could support the importance of krill in the presence of such a low biomass. Zooplankton biomass increases toward the open sea and, in general, toward the polar front (Foxton 1956; Jazdzewski et al. 1982; Boysen-Ennen et al. 1991; Robins et al. 1995) and it has also been observed that high standing stocks of phytoplankton did not coincide with high zooplankton biomass (El-Sayed 1984). Moreover, an inverse relationship between krill and non-krill zooplankton has been observed near the continent (Hosie 1994; Voronina et al. 1994). Krill are able to predate on copepods, as observed from gut contents (Hopkins et al. 1993; Nishino and Kawamura 1994) and feeding rate experiments (Price et al. 1988; Atkinson and Snÿder 1997). It is also known that euphausiids select mesozooplankton in the presence of both zooplankton and phytoplankton (Granéli et al. 1993). Atkinson et al. (1999) also observed reduced copepod abundance coinciding with high krill biomass and also suggested that copepod numbers in Antarctic waters can be controlled by a combination of competition and predation by krill. Competitive exclusion was proposed on the basis that krill can remove phytoplankton, affecting therefore copepod recruitment. However, our results as well as those of other authors cited above stress the low impact of zooplankton (< 14 mm) on primary production, including high zooplankton biomass scenarios (Ward et al. 1995). Therefore, if zooplankton is not food limited, because on average about 50% of primary production is not consumed and organisms are actively growing, the explanation for the low biomass of mesozooplankton (especially large copepods) around the Antarctic Peninsula (Robins et al. 1995; Hernández-León et al. 1999; present work) should be related to predation by krill or perhaps salps. The effect of swarms and, especially, superswarms should give some insight into the low abundances and biomass of mesozooplankton found in Antarctic waters near the continent. Superswarms of 150 km^2 (Macaulay et al. 1984), extending over 2.8–11 km (Higginbottom and Hosie 1989; Murray et al. 1995) or even 21.6 km (see Siegel and Kalinowski 1994) have been observed around the Antarctic Peninsula. The top-down effect potentially exerted due to selective feeding by krill on mesozooplankton might be studied because it would explain how phytoplankton sinking (Bodungen et al. 1986) and mainly microplankton respiration (Aristegui et al. 1996) may account for a large portion of the fate of primary production.

Acknowledgements We thank M. Garcia, J. Aristegui and G. Basterretxea for the CTD, chlorophyll and primary production data. The authors would also like to thank R. Perissinotto and S. Schnack-Schiel for their comments on the manuscript and constructive criticism. This work was supported by project "Oceanografía dinamica y productividad en el Estrecho de Bransfield durante el verano austral. 1993" (CICYT). We are also indebted to the crew and technical assistance of the RV "Hesperides".

References

Alayse-Danet AM (1980) Aspatate transcarbamylase in *Artemia* during early stages of development. In: Persoone G, Soorgeloos P, Roels O, Jaspers E (eds) The brine shrimp *Artemia*. vol 2. Universal Press, Wetteren, pp 259–275

Aristegui J, Montero MF (1995) Plankton community respiration in Bransfield Strait (Antarctic Ocean) during austral spring. J Plankton Res 17: 27–39

Aristegui J, Montero MF, Ballesteros S, Basterretxea G, Lenning K van (1996) Planktonic primary production and microbial respiration measured by ^{14}C assimilation and dissolved oxygen changes in coastal waters of the Antarctic Peninsula during austral summer: implications for carbon flux studies. Mar Ecol Prog Ser 132: 191–201

Atkinson A (1991) Life cycles of *Calanoides acutus*, *Calanus simillimus* and *Rhincalanus gigas* (Copepoda: Calanoida) within the Scotia Sea. Mar Biol 109: 79–91

Atkinson A (1996) Subantarctic copepods in an oceanic, low chlorophyll environment: ciliate predation, food selectivity and impact on prey populations. Mar Ecol Prog Ser 130: 85–96

Atkinson A, Shreeve RS (1995) Response of the copepod community to a spring bloom in the Bellingshausen Sea. Deep Sea Res 42: 1291–1311

Atkinson A, Snyder R (1997) Krill-copepod interactions at South Georgia, Antarctica. I. Omnivory by *Euphausia superba*. Mar Ecol Prog Ser 160: 63–76

Atkinson A, Ward P, Williams R, Poulet SA (1992a) Diel vertical migration and feeding of copepods at an oceanic site near South Georgia. Mar Biol 113: 583–593

Atkinson A, Ward P, Williams R, Poulet SA (1992b) Feeding rates and diel vertical migration of copepods near South Georgia: comparison of shelf and oceanic sites. Mar Biol 114: 49–56

Atkinson A, Ward P, Murphy EJ (1996) Diel periodicity of subantarctic copepods: relationships between vertical migration, gut fullness and gut evacuation rates. J Plankton Res 18: 1387–1405

Atkinson A, Ward P, Hill A, Brierley AS, Cripps GC (1999) Krill-copepod interactions at South Georgia, Antarctica. II. *Euphausia superba* as a major control on copepod abundance. Mar Ecol Prog Ser 176: 63–79

Basterretxea G, Aristegui J (1999) Phytoplankton biomass and production during late austral spring (1991) and summer (1993) in the Bransfield Strait. Polar Biol 21: 11–22

Bergeron JP (1982) L'aspartate transcarbamylase, indice de croissance des organismes marins: perspectives et limites. Actualités de Biochimie marine: indices biochimiques et milieux marins. Publication CNEXO, Actes Colloq, Brest

Bergeron JP, Buestel D (1979) L'Aspartate transcarbamylase, indice de l'activité sexuelle de la coquille Saint-Jaques (*Pecten maximus* L.) Premier resultats. In: Naylor E, Hartnoll RG (eds) Cyclic phenomena in marine plants and animals. Pergamon Press, New York, pp 301–308

Bergeron JP, Alayse-Danet AM (1981) Aspartate transcarbamylase de la coquille Saint-Jaques, *Pecten maximus* L. (mollusque lamellibranche): méthode de dosage et variations de l'activité dans le manteau et la gonade. J Exp Mar Biol Ecol 50: 99–117

Bergeron JP, Alayse-Danet AM, Razouls C (1985) Metabolic adaptations of Antarctic mesozooplanktonic systems to the phytoplankton standing crop in late austral summer. In: Gray JS, Christiansen ME (eds) Marine biology of polar regions and the effects of stress on marine organisms. Wiley, Chichester, pp 157–166

Bodungen B, Smetacek VS, Tilzer MM, Zeitzschel B (1986) Primary production and sedimentation during spring in the Antarctic Peninsula region. Deep Sea Res 33: 177–194

Boyssen-Ennen E, Hagen W, Hubold G, Piatkowski U (1991) Zooplankton biomass in the ice-covered Weddell Sea, Antarctica. Mar Biol 111: 227–235

Bresnick E, Mosse H (1966) Aspartate carbamoyltransferase from rat liver. Biochemistry J 101: 63–69

Conover RJ, Huntley M (1991) Copepods in ice-covered seas. Distribution, adaptations to seasonally limited food, metabolism, growth pattern and life cycle strategies in polar seas. J Mar Syst 2: 1–41

Conover RJ, Durvasula R, Roy S, Wang R (1986) Probable loss of chlorophyll-derived pigments during passage through the gut of zooplankton, and some of the consequences. Limnol Oceanogr 31: 878–887

Dam HG, Miller CA, Jonasdottir SH (1993) The trophic role of mesozooplankton at 47°N, 20°W during the North Atlantic Bloom Experiment. Deep Sea Res II 40: 197–212

Drits AV, Pasternak AF, Kosobokova KN (1993) Feeding, metabolism and body composition of the Antarctic copepod *Calanus propinquus* Brady with special reference to its life cycle. Polar Biol 13: 13–21

Dubischar C, Bathmann UV (1997) Grazing impact of copepods and salps on phytoplankton in the Atlantic sector of the Southern Ocean. Deep Sea Res 44: 415–433

El Sayed SZ (1984) Productivity of the Antarctic waters – a reappraisal. In: Holm-Hansen O, Bolis L, Giles R (eds) Marine phytoplankton and productivity. Springer, Berlin Heidelberg New York, pp 19–34

Figa J, Garcia MA, Puigdefàbregas J, Sánchez-Arcilla A (1998) Rasgos de mesoescala de la circulación marina superficial en el estrecho de Bransfield durante el verano austral, a partir de imágenes NOAA/AVHRR y LANDSAT/TM. In: Cantón M (ed) Ordenación del territorio y medio marino. Universidad de Las Palmas de Gran Canaria, Canary Islands, pp 495–513

Foxton P (1956) The distribution of the standing crop of zooplankton in the southern Ocean. Discovery Rep 28: 191–236

Garcia MA, Lopez O, Sospedra J, Espino M, Gracia V, Morrison G, Rojas P, Figa J, Puigdefabregas J, Arcilla AS (1994) Mesoscale variability in the Bransfield Strait region (Antarctica) during Austral summer. Ann Geoph 12: 887–902

Gómez M, Torres S, Hernández-León S (1996) Modification of the electron transport system (ETS) method for routine measurements of respiratory rates of zooplankton. S Afr J Mar Sci 17: 15–20

Granéli E, Granéli W, Mozzan Rabbani M, Daugbjerg N, Fransz G, Cuzin-Roudy J, Alder VA (1993) The influence of copepod and krill grazing on the species composition of phytoplankton communities from the Scotia-Weddell Sea. Polar Biol 13: 201–213

Grelowski A, Majewicz A, Pastuszak M (1986) Mesoscale hydrodynamic processes in the region of Bransfield Strait and southern part of Drake passage during BIOMASS-SIBEX 1983/84. Pol Polar Res 7: 353–369

Hernández-León S, Gomez M (1996) Factors affecting the respiration/ETS ratio in marine zooplankton. J Plankton Res 18: 239–255

Hernández-León S, Torres S (1997) The relationship between ammonia excretion and GDH activity in marine zooplankton. J Plankton Res 19: 587–601

Hernández-León S, Almeida C, Montero I (1995) The use of aspartate transcarbamylase activity to estimate growth rates in zooplankton. ICES J Mar Sci 52: 377–383

Hernández-León S, Torres S, Gomez M, Montero I, Almeida C (1999) Biomass and metabolism of zooplankton in the Bransfield Strait (Antarctic Peninsula) during austral spring. Polar Biol 21: 214–219

Higginbottom JR, Hosie GW (1989) Biomass and population structure of a large aggregation of krill near Prydz Bay, Antarctica. Mar Ecol Prog Ser 58: 197–203

Holm-Hansen O, Huntley ME (1984) Feeding requirements of krill in relation to food sources. J Crust Biol 4: 156–178

Hopkins TL, Lancraft TM, Torres JJ, Donnelly J (1993) Community structure and trophic ecology of zooplankton in the Scotia Sea marginal ice zone in winter (1988). Deep Sea Res 40: 81–105

Hosie GW (1994) The macrozooplankton communities in the Prydz Bay region, Antarctica. In: El-Sayed SZ (ed) Southern Ocean ecology: The biomass perspective. Cambridge University Press, London, pp 98–123

Huntley ME, Lopez MDG (1992) Temperature-dependent production of marine copepods: a global synthesis. Am Nat 140: 201–242

Huntley ME, Sykes PF, Marin V (1989) Biometry and trophodynamics of *Salpa thompsoni* Foxton (Tunicata: Thaliacea) near the Antarctic Peninsula in austral summer, 1983–1984. Polar Biol 10: 59–70

Huntley ME, Zhou M, Lopez MDG (1994) *Calanoides acutus* in Gerlache Strait, Antarctica. II. Solving an inverse problem in populations dynamics. Deep Sea Res II 41: 209–227

Irigoien X (1998) Gut clearance rate constant, temperature and initial gut contents: a review. J Plankton Res 20: 997–1003

Jazdzewski K, Kittel W, Lotocki K (1982) Zooplankton studies in the southern Drake Passage and in the Bransfield Strait during the austral summer (BIOMASS-FIBEX, February–March 1981). Pol Polar Res 3: 203–242

Jónasdóttir SH, Fields D, Pantoja S (1995) Copepod egg production in Long Island Sound, USA, as a function of chemical composition of seston. Mar Ecol Prog Ser 119: 87–98

Kato M, Segawa S, Tanoue E, Murano M (1982) Filtering and ingestion rates of the Antarctic krill, *Euphausia superba* Dana. Trans Tokio Univ Fish 5: 167–175

Kenner RA, Ahmed SI (1975) Measurements of electron transport activities in marine phytoplankton. Mar Biol 33: 119–127

Koueta N, Boucaud-Camou E (1992) Changes of aspartate transcarbamylase activity in the gonad of *Sepia officinalis* L. during the sexual cycle. Comp Biochem Physiol 102B: 413–418

Longhurst A (1998) Ecological geography of the sea. Academic Press, San Diego

Lopez MDG, Huntley ME (1995) Feeding and diel vertical migration cycles of *Metridia gerlachei* (Giesbrecht) in coastal waters of the Antarctic Peninsula. Polar Biol 15: 21–30

Lopez MDG, Huntley ME, Lovette JT (1993) *Calanoides acutus* (Giesbrecht) in Gerlache Strait, Antarctica. I. Distribution and reproduction during spring. Mar Ecol Prog Ser 100: 153–165

Lovegrove T (1966) The determination of the dry weight of plankton and the effect of various factors on the values obtained. In: Barnes H (ed) Some contemporary studies in marine science. Allen & Unwin, London, pp 429–467

Lowry PH, Rosenbrough NJ, Farr AL, Randall RJ (1951) Protein measurement with a Folin phenol reagent. J Biol Chem 193: 265–275

Macaulay MC, English TS, Mathisen OA (1984) Acoustic characterization of swarms of Antarctic krill (*Euphausia superba*) from Elephant Island and Bransfield Strait. J Crust Biol 4: 16–44

Mackas DL, Bohrer R (1976) Fluorescence analysis of zooplankton gut contents and an investigation of diel feeding patterns. J Exp Mar Biol Ecol 25: 77–85

Marr J (1962) The natural history and geography of the Antarctic krill (*Euphausia superba* Dana). Discovery Rep 32: 33–464

McKinnon AD (1996) Growth and development in the subtropical copepod *Acrocalanus gibber*. Limnol Oceanogr 41: 1438–1447

Murray AWA, Watkins JL, Bone DG (1995) A biological acoustic survey in the marginal ice-edge zone of the Bellingshausen Sea. Deep Sea Res 42: 1159–1175

Niiler PP, Amos A, Hu JH (1991) Water masses and 200 m. relative geostrophic circulation in the western Bransfield Strait region. Deep Sea Res 38: 943–959

Nishikawa J, Naganobu M, Ichii T, Ishii H, Terazaki M, Kawaguchi K (1995) Distribution of salps near the South Shetland Islands during austral summer, 1990–1991 with special reference to krill distribution. Polar Biol 15: 31–39

Nishino Y, Kawamura A (1994) Winter gut contents of Antarctic krill (*Euphausia superba* Dana) collected in the South Georgia area. Proc NIPR Symp Polar Biol 7: 82–90

Packard TT (1971) The measurement of respiratory electron transport activity in marine phytoplankton. J Mar Res 29: 235–244

Packard TT, Berdalet E, Blasco D, Roy SO, St-Amand L, Lagcé B, Lee K, Gagné J-P (1996) Oxygen consumption in the marine bacterium *Pseudomonas nautica* predicted from ETS activity and bisubstrate enzyme kinetics. J Plankton Res 18: 1819–1835

Pakhomov EA, Perissinotto R (1996) Antarctic neritic krill *Euphausia crystallorophias*: spatio-temporal distribution, growth and grazing rates. Deep Sea Res 43: 59–87

Pakhomov EA, Perissinotto R, Froneman PW, Miller DGM (1997) Energetics and feeding of *Euphausia superba* in the South Georgia region during the summer of 1994. J Plankton Res 19: 399–423

Perissinotto R, Pakhomov EA (1998) Contribution of salps to carbon flux of marginal ice zone of the Lazarev Sea, Southern Ocean. Mar Biol 131: 25–32

Perissinotto R, Pakhomov EA, McQuaid CD, Froneman PW (1997) In situ grazing rates and daily ration of Antarctic krill *Euphausia superba* feeding on phytoplankton at the Antarctic polar front and the marginal ice zone. Mar Ecol Prog Ser 160: 77–91

Peterson GL (1983) Determination of total protein. Methods of Enzymology, vol 91. Academic Press, New York

Price HJ, Boyd KR, Boyd CM (1988) Omnivorous feeding behavior of the Antarctic krill *Euphausia superba*. Mar Biol 97: 67–77

Robins DB, Harris RP, Bedo AW, Fernandez E, Fileman TW, Harbour DS, Head RN (1995) The relationship between suspended particulate material, phytoplankton and zooplankton during the retreat of the marginal ice zone in the Bellingshausen Sea. Deep Sea Res 42: 1137–1158

Rojas P, Lopez O, Garcia M, Aristegui J, Torres S, Hernández-León S, Bastarrechea G, Amengual B, Escamez J, Morales B (1996) Hidrografía del Estrecho de Bransfield durante el verano Austral 91/92. Proc V Simposio Español de Estudios Antarticos, Barcelona. Comision Interministerial de Ciencia y Tecnologia, Madrid, pp 403–411

Roman MR, Gauzens AL (1997) Copepod grazing in the equatorial Pacific. Limnol Oceanogr 42: 623–634

Schalk PH (1990) Biological activity in the Antarctic zooplankton community. Polar Biol 10: 405–411

Schnack SB (1985) Feeding by *Euphausia superba* and copepod species in response to varying concentrations of phytoplankton. In: Siegfried WR, Condy PR, Laws RM (eds) Antarctic nutrient cycles and food webs. Springer, Berlin Heidelberg New York, pp 311–323

Schnack SB, Smetacek V, Bodungen B von, Stegmann P (1985) Utilization of phytoplankton by copepods in Antarctic waters during spring. In: Gray JS, Christiansen ME (eds) Marine biology of polar regions and the effects of stress on marine organisms. Wiley, Chichester, pp 65–81

Schnack-Schiel SB, Mujica A (1994) The zooplankton of the Antarctic Peninsula region. In: El-Sayed SZ (ed) Southern Ocean ecology. The biomass perspective. Cambridge University Press, London, pp 79–92

Shreeve R, Ward P (1998) Moulting and growth of the early stages of two species of Antarctic calanoid copepod in relation to differences in food supply. Mar Ecol Prog Ser 175: 109–119

Siegel V, Kalinowski J (1994) Krill demography and small-scale processes: a review. In: El-Sayed SZ (ed) Southern Ocean ecology. The biomass perspective. Cambridge University Press, London, pp 145–163

Smith SL, Schnack-Schiel SB (1990) Polar zooplankton, part B Chemistry, biology and geology. In: Smith WO Jr (ed) Polar oceanography. Academic Press, New York, pp 527–598

Strickland JDH, Parsons TR (1972) A practical handbook of seawater analysis. Fish Res Board Can Bull 167, 281 pp

Swadling KM, Gibson JAE, Ritz DA, Nichols PD, Hughes DE (1997) Grazing of phytoplankton by copepods in eastern Antarctic coastal waters. Mar Biol 128: 39–48

UNESCO (1968) Zooplankton sampling. Monogr Oceanogr Methodol 2: 174

Voronina NM, Kosobokova KN, Pakhomov EA (1994) Composition and biomass of summer metazoan plankton in the 0–200 m layer of the Atlantic sector of the Antarctic. Polar Biol 14: 91–95

Ward P, Atkinson A, Murray AWA, Wood AG, Williams R, Poulet SA (1995) The summer zooplankton community at South Georgia: biomass, vertical migration and grazing. Polar Biol 15: 195–208

Yentsch CS, Menzel DW (1963) A method for the determination of phytoplankton chlorophyll and phaeophytin by fluorescence. Deep Sea Res 10: 221–231

ELSEVIER

Journal of Volcanology and Geothermal Research 104 (2000) 21–31

Journal of volcanology and geothermal research

www.elsevier.nl/locate/volgeores

Paleomagnetic study of the ages of lavas on the island of Lanai'i, Hawai'i

E. Herrero-Bervera[a,*], J. Margas-Viñuela[a,1], J.-P. Valet[b]

[a]*Paleomagnetic Laboratory, Hawai'i Institute of Geophysics and Planetology, School of Ocean and Earth Science and Technology, 2525 Correa Road, Honolulu, HI 96822, USA*

[b]*Institut de Physique du Globe de Paris, 4, Place Jussieu, 75252 Paris cedex 05, France*

Received 20 March 2000; revised 30 March 2000; accepted 30 March 2000

Abstract

A detailed paleomagnetic study of tholeiitic basaltic of eight sites drilled from Kaumalapau Harbor, Manele Bay and Maunalei Gulch areas was conducted to investigate the volcanic evolution of the island of Lana'i. Stepwise alternating field (AF) demagnetizations accompanied by investigations of rock magnetic properties such as low-field susceptibility versus temperature ($k-T$) and saturation isothermal remanent magnetization (SIRM) indicate that the characteristic remanent magnetization (ChRM) is primarily carried by Ti-poor magnetite. Demagnetization experiments have identified eight mean flow directions characterized by negative polarities. Our paleomagnetic results, along with the radiometric age determinations of the lavas in question indicate that the tholeiitic flows that formed the Lanai volcano were erupted very rapidly and only during the Matuyama Polarity Chron (0.780–2.58 Ma) and not during the Brunhes Chron (0–0.78 Ma), as reported previously for the K–Ar dated lavas in the Maunalei Gulch.

Keywords: Island of Lana'i; alternating field demagnetization; magnetic susceptibility measurements

1. Introduction

Lana'i is one of the islands of the Hawaiian archipelago that has been poorly studied from a geological viewpoint. Salient studies in terms of classic general geology were produced by Wentworth (1925) and Sterns (1940) and the relevant review papers about the geology of the Hawaiian Islands are by Macdonald et al. (1983), Walker (1990) and Hazlett and Hyndman (1996). The geochronology of the island of Lana'i was studied by Bonhommet et al. (1977) and Naughton et al. (1980).

Geologic and geomorphologic observations by Wentworth (1925) and Sterns (1940) show that the volcanic rocks of the island of Lana'i have a probable age between the Pliocene and early Pleistocene, and that Lana'i should be younger than the island of Moloka'i, similar in age to the west part of Maui, and older than the east part of Maui and Kaho'olawe. In addition, these sets of islands form a large single shield volcano called Maui Nui. Jackson et al. (1972) predicted an age of 1.25 Ma for Lana'i taking into account the hypothesis that the volcanoes of the Hawaiian islands become progressively older from Hawai'i to Kaua'i. Potassium–argon determinations of rocks from Lana'i were carried out by Bonhommet

* Corresponding author. Fax: +1-808-956-3188.
E-mail address: herrero@soest.hawaii.edu (E. Herrero-Bervera).
[1] Permanent address: Departemento de Física-Geología, Universidad de Las Palmas, Gran Canaria, Spain.

0377-0273/00/$ - see front matter
PII: S0377-0273(00)00197-9

et al. (1977) and Naughton et al. (1980). However, their published radiometric ages were different. The first authors obtained ages ranging from 1.20 (±0.17) to 1.46 (±0.25) Ma, whereas the second author's ages were between 0.70 (±0.03) and 0.91 (±0.07) Ma.

In the recent past, some authors have studied major submarine landslides produced by collapses of parts of the Hawaiian volcanoes. The island of Lana'i produced the Clark landslide that shows a direction of motion towards the southwest and two toes of debris accumulations (hummocky areas) that extend over distances of about 80 km from their sources (Moore et al., 1989). Considering the importance of these destructive processes that have affected the oceanic volcanic islands it is important to know the age of the materials that make up the islands and the timing of the catastrophic events that triggered the giant landslides that ended up at the bottom of the ocean. Another important aspect of this study is to know the volcanic evolution of the island of Lana'i to further understand its volcanic growth.

Taking into account the controversy derived from the radiometric ages for the lavas of Lana'i we have conducted a paleomagnetic study with the main objective of clarifying the geochronology. We have sampled the same lava flows that were previously radiometrically dated by K–Ar methods, along with other lavas that were not dated by the original authors.

2. Brief geology of Lana'i

The island of Lana'i is situated at the center of the eight major islands of the Hawaiian archipelago. It is the sixth largest in size with a length of approximately 27 km and a width of 20 km. It covers an area of 363 square kilometers with a maximum altitude of 1207 m at Lana'i Hale when taking into account the topography and bathymetry of the islands of Lana'i, Maui, Kaho'olawe, Moloka'i, and three submarine volcanoes, all of which make up a single volcanic edifice called the Maui Volcanic Complex.

The geology of Lana'i was studied by Wentworth (1925); but it was Sterns (1940) who made the most detailed mapping and a comprehensive geologic study of this island. He stated that Lana'i was an extinct shield volcano modified later by erosion and defined five geomorphic areas: (1) the central basin (Palawai and Miki basins in the south-center of the island); (2) the canyon country (east side of the island between Maunalei and Kawaiu); (3) the northwest rift zone (about 6 miles northwest of Palawai Basin); (4) the southwest rift zone (3 miles long extending southwestward from the Palawai Basin); and (5) the faulted south rift zone (southeast from Palawai Basin). The central basin is characterized by subsided structures partially filled with volcanic and sedimentary materials. Sterns (1940) and later Macdonald et al. (1983) interpreted the Palawai Basin as an old summit caldera of the Lana'i volcano 4 km in diameter, and the Miki Basin as a pit crater 1.5 km in diameter. Thus, the island of Lana'i is a shield volcano built by eruptions at the summit and along three island rift zones. The principal rift zone trends northwestward as a broad ridge, and is responsible for the conspicuous elongation of the island in that direction (NW–SE and SW). A less conspicuous bulge on the southern side of the island is the result of lava building on the southwest rift zone. The summit of the shield collapsed to form a caldera from which a shallow graben, bordered by en echelon step faults, extends south to southwest toward Manele Bay. Numerous dikes exposed in the sea cliff indicate that this Manele graben lies along another rift zone. Recently, some geologists (Moore et al., 1989) believed that these structures were associated with normal faults present in the south-central part of the island that are closely linked to the Clark landslide, and that the present shape of the island corresponds to the northeast flank of an ancient bigger volcano (Paleo Lana'i). This is one of the many reasons why it is important to study the growth of these volcanic edifices, since other landslides that had originated on the neighbor islands might have had similar triggering mechanisms to that of the island of Lana'i.

The associated eruptions of the Lana'i rifts produced lavas and spatter cones and piles of pahoehoe and 'a'a flows with gentle dips (between 2 and 18°). There is evidence that in between lava flows there was no visual proof of any development of boles, indicating that the magmatic eruptions were relatively continuous. Some of the ancient cones can be seen from the cliffs (Kahunolu, Manele, etc.) and from the gulches such as Maunalei, whereas the more recent ones are located on the southeast and southwest flanks of the island.

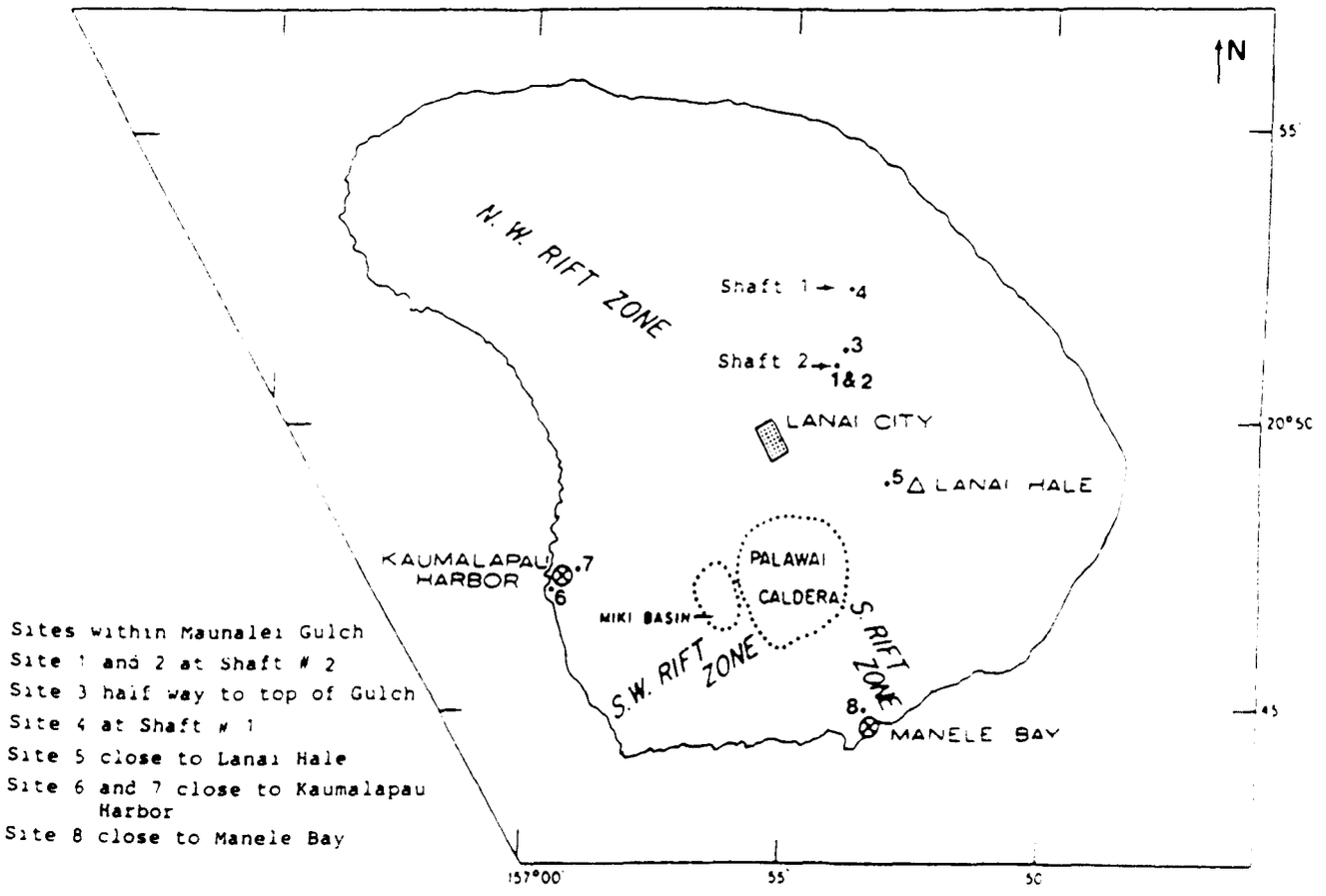

Fig. 1. Map of Lana'i, showing locations of eight paleomagnetically analyzed lava flows for the present study.

There are few petrographic and geochemical studies of Lana'i. Macdonald (1940) made a microscopic study of six specimens from Lana'i and cites pioneering petrologic studies performed by Powers (1920), Washington (1923) and Wentworth (1925). Bonhommet et al. (1977) described the petrographic analysis of the six samples used for the geochronologic determinations. In general terms these authors have pointed out that the subaerial rocks of Lana'i are mainly tholeiitic basalts ranging from olivine tholeiites to olivine-rich oceanites. The lava flows show mainly phenochrysts and microphenocrysts of olivine, hypersthene, augite, pyroxene and plagioclase. The groundmass contains plagioclase, pyroxene (augite, hypersthene and pigeonite), equant Fe–Ti oxides (ilmenite–magnetite) and apatite. According to Bonhommet et al. (1977) from the geochemical view point, the samples studied are tholeiites. All contain normative quartz and hypersthene and resemble, compositionally, tholeiites from the Mauna Loa volcano. Thus, in summary, one can say that these tholeiites from the Lana'i volcano represent the shield-building stage and that this volcano did not develop the declining stage with the formation of the alkalic cap as is the case with other Hawaiian volcanoes.

3. Paleomagnetism of the Island of Lana'i

Paleomagnetic studies of the island of Lana'i are almost nonexistent. One of the goals of this work is to report on the results obtained from a series of paleomagnetic samplings performed on tholeiitic basalts of the island. We collected oriented paleomagnetic samples from eight sites. Five of these sites were drilled in the Maunalei gulch; two sites were sampled in the Kaumalapau Harbor area and one site was sampled in the Manele Bay area.

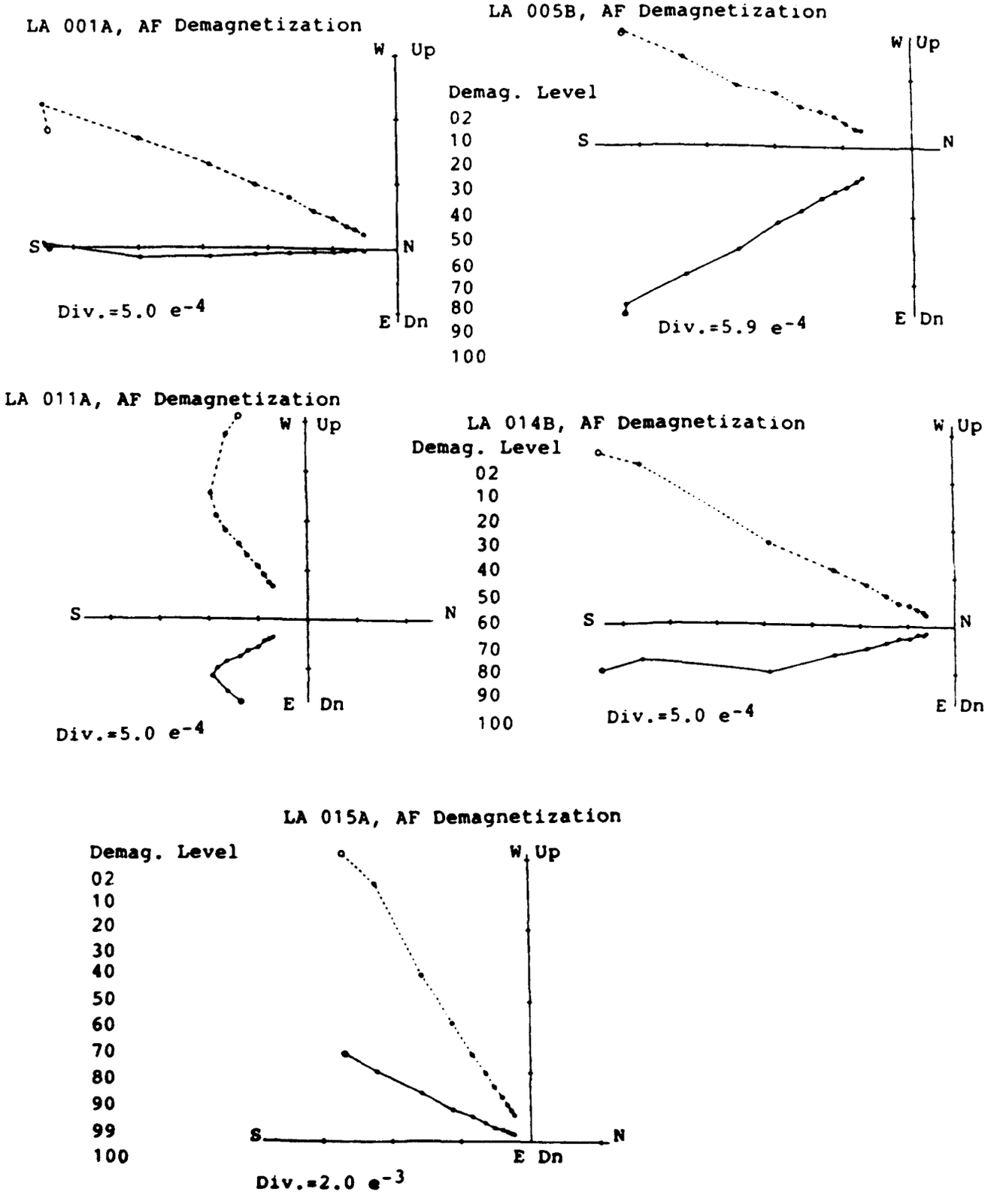

Fig. 2. Typical diagrams of progressive demagnetization (expressed in mT) of specimens from the tholeiitic lava flows sampled. Plotted points represent successive positions—in orthogonal projection—at the end point vector. Solid symbols represent projections on the vertical plane and open symbols those on the horizontal plane. Units are in A/m.

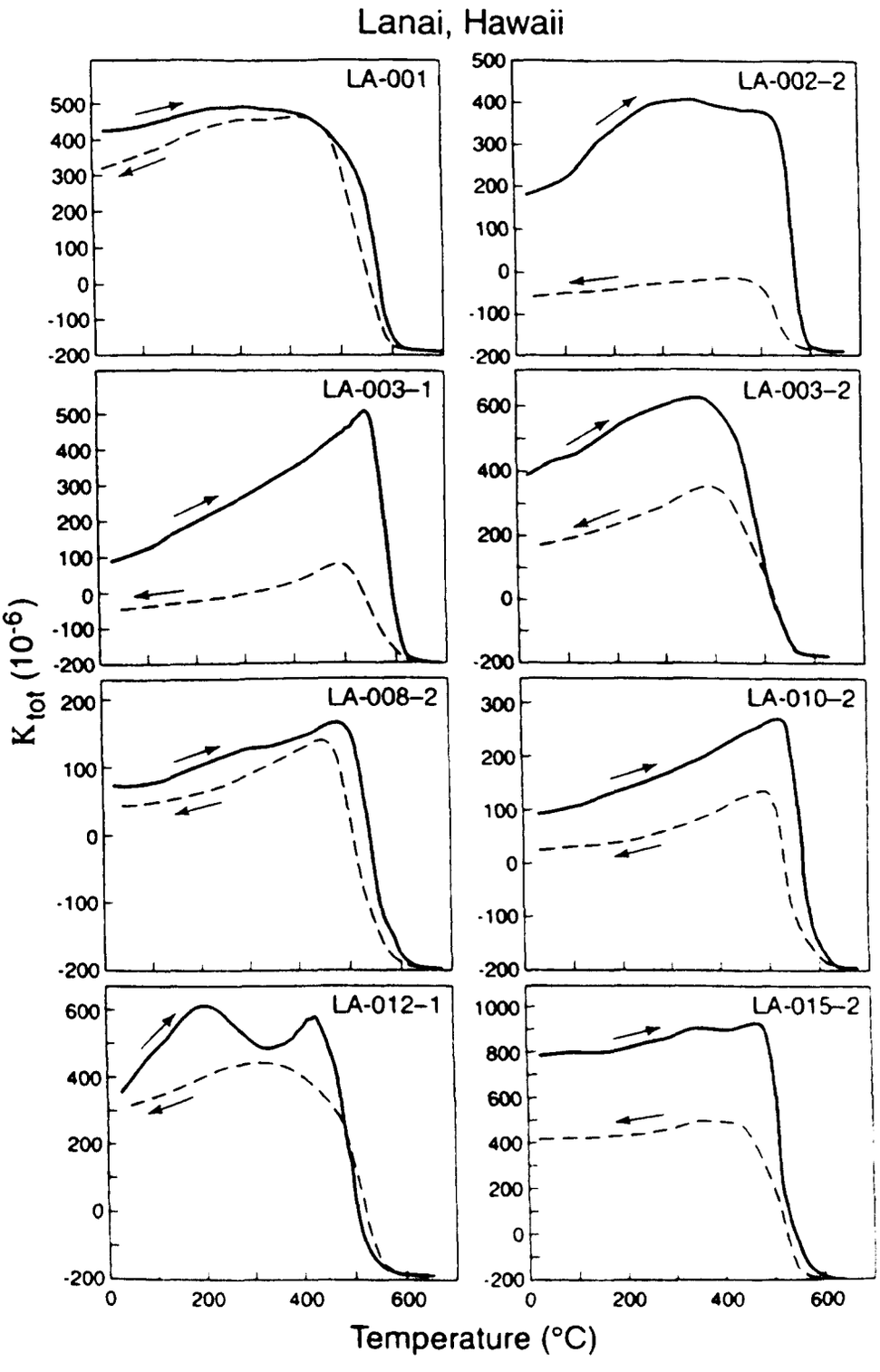

Fig. 3. Representative susceptibility versus temperature (K–T) analysis plots for the lavas of the island of Lanai'i

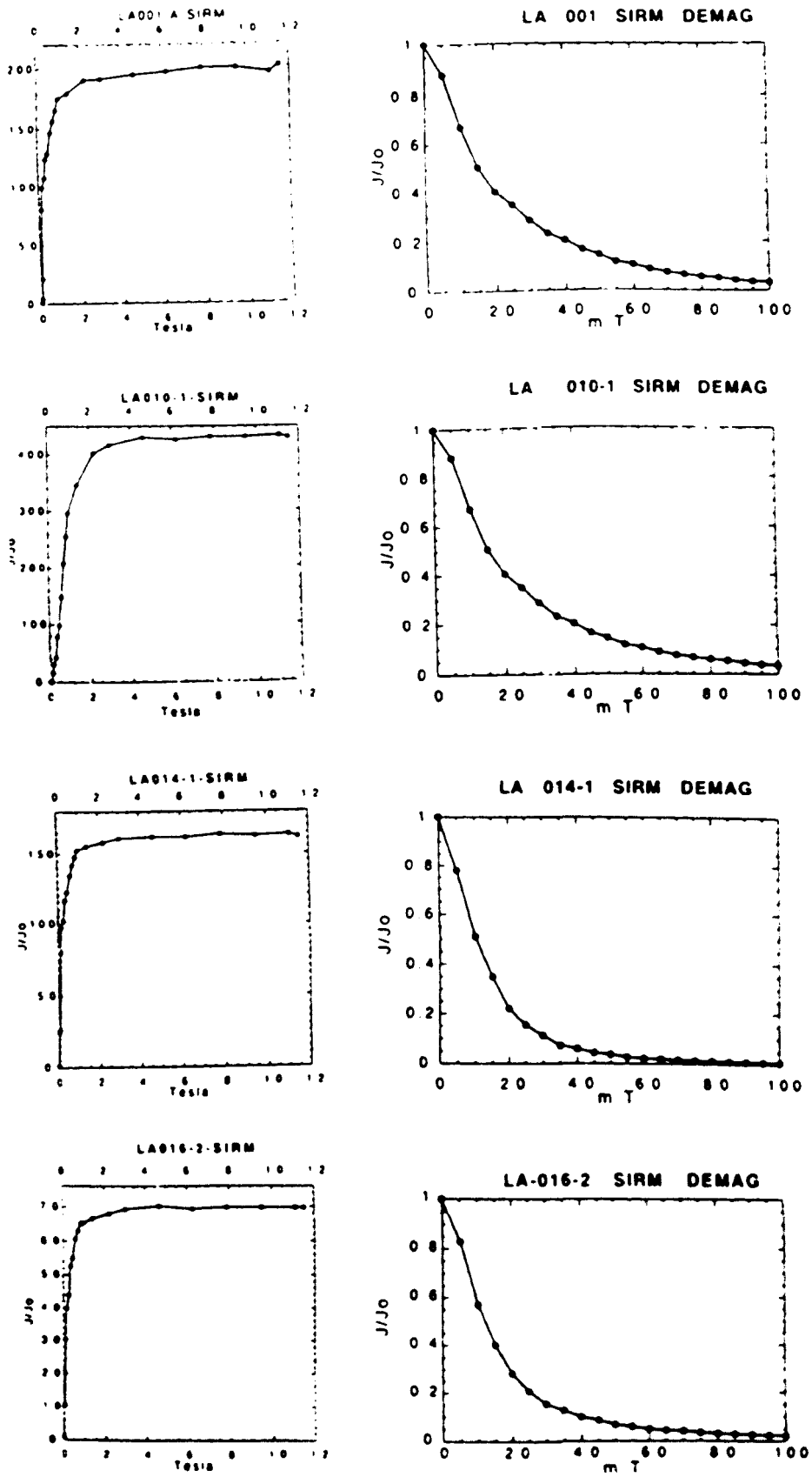

Fig. 4. Typical acquisition SIRM of representative samples and their respective demagnetization curves for lavas from the island of Lana'i

4. Field and laboratory methods

The Maunalei gulch where the sampling of the five sites took place (see Fig. 1) provides an excellent exposure for our paleomagnetic sampling, allowing near continuous sampling of eruptive sequences on a flow by flow basis from the bottom of the valley up to the top. Samples for paleomagnetic and rock magnetic experiments were taken from within massive flow interiors to avoid the effects of reheating by subsequent flows which would reset the paleomagnetic directions.

Between 5 and 10 25-mm diameter cores were collected from each lava flow for paleomagnetic analyses. All cores were drilled in the field with a portable gasoline-powered drill and were oriented in situ using an integrated sun compass and an inclinometer. Natural remanent magnetization (NRM) was measured using a 2G Superconducting Rock Magnetometer and a JR5A Spinner Magnetometer. All the specimens were progressively stepwise demagnetized using a three-axis tumbling alternating field (AF) demagnetizer. AF experiments were performed in a series of steps from 2.5 to 100 mT. Overall, AF demagnetization was very efficient in removing secondary viscous overprints that were acquired during the past ~800,000 years (see for example LA 011A) and during storage of the samples. The characteristic components were isolated between 20 and 100 mT, which indicates that the primary component is carried by magnetite. The characteristic direction of each sample was obtained by least-square analyses of at least 10 successive directions (Fig. 2). The mean flow directions were calculated by averaging at least five directions per lava flow. The within-flow dispersions did not exceed 10° in most of the cases.

Two additional rock magnetic experiments were performed on the samples. Magnetic properties were analyzed to identify the magnetic carriers of the NRM and to determine their magnetic characteristic properties as a check on the reliability of the paleomagnetic record. The first of these additional rock magnetic experiments we performed was a magnetic mineralogy study on samples taken from each one of the sites drilled for our magnetostratigraphic study. The experiment was carried out to determine Curie points. The temperature dependence of initial magnetic susceptibility was measured using low-field susceptibility measurements ($k-T$) on at least one sample per site. About eight samples were progressively heated up to generally 650°C and subsequently cooled down using a KLY2-CS3 apparatus (e.g. Hrouda, 1994 and Hrouda et al., 1977) located at the SOEST-HIGP Paleomagnetic laboratory. Several typical samples

Table 1
Flow mean directions and poles for lavas of the island of Lana'i. Declination and Inclination in degrees. K, precision parameter. α95 circle of 95% confidence. R, length of vector. Paleo Latitude and Paleo Longitude of Virtual Paleomagnetic Poles (VGPs) in degrees determined by Fisher statistics (Fisher, 1953)

		Decl	Incl	K	α95	R	PLat	PLong
Site #1	Maunalei Gulch Well Shaft #2 Drilled at Portal	179.1	−24.8	374	4.8	3.992	−82.08	209.48
Site #2	Maunalei Gulch bottom of Well Shaft #2	151.7	−19.0	131	8.1	3.970	−60.60	275.22
Site #3	Drilled on the Northwest slope of Maunalei Gulch half way to top	145.7	−42.0	8330	2.7	1.999	−58.23	305.72
Site #4	Drilled at the entrance of Well Shaft #1 on the Northwest side	169.9	−32.2	71	14.8	2.971	−50.38	218.31
Site #5	Lana'i Hale above Well Shaft #2, head of Valley	174.7	−62.8	12866	1.1	2.999	−66.16	13.64
Site #6	Kaumalapau Harbor	149.4	−59.6	22	13.4	6.7162	−57.49	336.98
Site #7	Kaumalapau Harbor Road cut (0.5 miles from Harbor)	228.9	−21.9	161	9.7	2.988	−42.25	116.63
Site #8	Manele Bay, Road cut (1.0 miles from seashore)	179.9	−20.7	574	2.8	5.991	−79.40	219.88

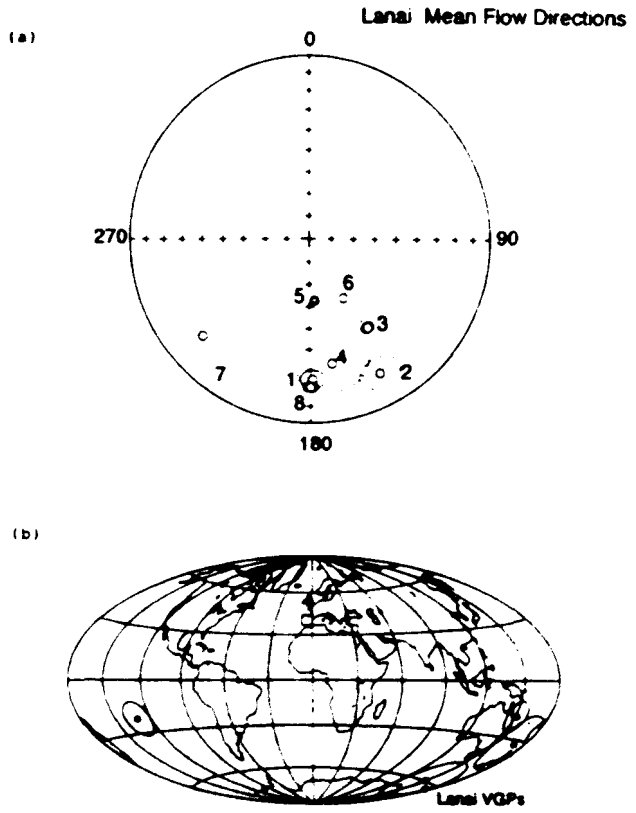

Fig. 5. (a) Mean Flow directions, with their respective circles of confidence, of eight lavas from Lana'i; (b) Virtual Geomagnetic Poles (VGPs) of eight lavas from the island of Lana'i.

of susceptibility versus (k–T) are given in Fig. 3. Most of the samples exhibit in some cases irreversible thermomagnetic behavior such as LA 003-1 and LA 008-2 where there is production of magnetite during heating. In most cases there is no reversibility and likely oxidation of magnetite into hematite during heating. In other cases there is a simple thermomagnetic behavior characterized by nearly reversible k–T curves with a single Hopkinson peak and a sharp decrease in susceptibility indicating the reaching of Curie point in the range of 560–580°C, which is characteristic of nearly pure magnetite (Fig. 3).

The second additional rock magnetic experiment performed on the samples was saturation isothermal remanent magnetization (SIRM) in a strong field followed by AF demagnetization of the same specimens. These demagnetization experiments show that this is a soft magnetization removed by about 15 mT in all cases. This result is expected with IRM that involves multidomain grains.

Fig. 4 shows three typical samples from three different sites (one in the Maunalei Gulch, the second one from Kaumalapau Harbor and the third from a Kaumalapau roadcut) that acquire an SIRM, with most of the remanence being gained between 0.5 and 1.0 Tesla after which the curves start to level off. These results also indicate that the dominant magnetic carrier in the samples is magnetite.

5. Results and discussion

The results of the paleomagnetic analyses for all eight sites involved in the study are listed in Table 1. The mean flow directions of each site have been plotted in Fig. 5. These results include the mean declination and inclination with their respective statistical parameters as well as the calculation of the Virtual Geomagnetic Poles (VGPs) for the individual lavas. As mentioned earlier, these paleomagnetic results were obtained with the main purpose of determining the magnetic polarities of the lavas and comparing the polarity results with the radiometrically dated samples obtained by the only two studies that have determined ages of the lavas in Lana'i (Bonhommet et al., 1977; Naughton et al., 1980).

The first set of radiometric ages of six samples was obtained by Bonhommet et al. (1977) by means of K–Ar analysis. The samples were collected from three general areas. The first site was located on West Lana'i and corresponds to sample 0X68 that yielded an age of 1.46 ± 0.25 Ma. The second sample 0X71, came from the Manele Bay area (part of the South Rift Zone); the age obtained was 1.35 ± 0.05 Ma. From the same area but on the road to Lana'i City sample 0X073 was dated at 1.20 ± 0.17 Ma. Three additional samples were from the area known as Kaumalapau Harbor. They are: 0X075, age 1.42 ± 0.13 Ma, 0X078, age 1.28 ± 0.08 Ma and 0X079, age 1.21 ± 0.06 Ma. The overall weighted mean age obtained by the authors was 1.30 ± 0.06 Ma.

The K–Ar ages determined by Naughton et al. (1980) for rocks from the Maunalei Gulch were obtained in an effort to fill the gaps left by previous dating work. Our sites 1–4 were drilled in the same locations where Naughton et al. (1980) determined the ages of the lavas in the Maunalei Gulch. The authors of that radiometric work sampled three different localities. One in Well Shaft 2 (Site L1) yielded an age of

0.86 ± 0.55 Ma. A site near Well Shaft 2 (Site L2) gave an age of 0.71 ± 1.27 Ma. The third site, located at the bottom of Well Shaft 1 (L3) gave an age of 0.76 ± 0.66 Ma. The overall mean for the three sites was 0.81 ± 0.66 Ma.

Our paleomagnetic determinations presented in Table 1 correspond in some cases to the sites where Bonhommet et al. (1977) and Naughton et al. (1980) collected their samples for the radiometric age determinations. For instance, our Site 2 corresponds to site L1 of Naughton et al. (1980) drilled at the pump room in Maunalei Well Shaft 2, located at 225 m above sea level in Maunalei Gulch. Our Site 3 is stratigraphically equivalent to Site L2 of Naughton et al. (1980) collected from a prominent ledge on the southwest wall of Maunalei Gulch directly upslope from the portal of Maunalei Well Shaft 2, approximately 300 m above sea level. The Naughton et al. (1980) Site L3 corresponds to our Site 4 drilled at Maunalei Shaft 1, and is located approximately 2 m above sea level in Maunalei Gulch. This sample was approximately 30 m higher stratigraphically than L2. Our paleomagnetic Site 5 is at a location known as Lana'i Hale with an approximate elevation of 1,143 m which corresponds to the highest elevation of the paleomagnetic sites (see Table 1).

With respect to the sites studied by Bonhommet et al. (1977), our paleomagnetic Site 6 drilled slightly above the shore line (about 2 m in elevation) at Kaumalapau Harbor corresponds to the samples collected at the same harbor, i.e. 0X75, 78 and 79 by Bonhommet et al. (1977). Our paleomagnetic Site 8 located on the roadcut of highway 440 approximately 0.5 miles from the shoreline and with an elevation of 68 m is equivalent to Bonhommet et al. sites 0X69 and 71 (see Table 1).

The first paper on the K–Ar dating (Bonhommet et al. 1977) of six samples from the lavas of Lana'i yielded a weighted mean of 1.30 ± 0.06 Ma and the authors of that study argue that the calculated ages of the six samples are not significantly different from one another at the 95% level of confidence. The reason why the authors of the study interpreted their results in that way was because of the rapidity with which the tholeiitic part of the Hawaiian shield volcanoes was constructed as is the case of other Hawaiian volcanoes such as the Wai'anae volcano in O'ahu (e.g. Jackson et al., 1972; Doell and Dalrymple, 1973; Herrero-Bervera and Valet, 1999; Herrero-Bervera and Coe, 1999).

The second and most recent K–Ar study of the island of Lana'i was done in an effort to sample from within the volcanic pile from sections representing the active phase of mountain building (Naughton et al., 1980). This was done in the Maunalei Gulch in the northeastern canyon district of the island, and within well shafts inside the gulch. The samples collected in the gulch were also tholeiitic basalts but the argon measurements gave relatively small amounts of the radiogenic component with consequently large uncertainties in the calculated ages. The authors of this latest radiometric age determinations pointed out that it was disturbing that there was such a significant difference between the dates found in their study (0.71–0.86 Ma, mean 0.81 Ma) and those reported by Bonhommet et al. (1977) (1.20–1.46 Ma, mean 1.30 Ma).

As a conclusion of the second radiometric effort it has been reported that the possibility exists that the area sampled in the Maunalei Gulch is, in fact, younger than that sampled by the first K–Ar dating. Naughton et al. (1980) argue that its youth is suggested by the anomaly of a low coastline on the northeast, windward side of Lana'i that, contrary to expectations, has been little affected by wave erosion, whereas the southwest side is eaten away by such erosion to form spectacular cliffs, indicative of longer exposure to this action. The same authors indicated that the well shafts in Maunalei Gulch were tunneled into regions of high dike density in order to tap the aquifer. These dikes presumably were feeders for later eruptions in the area, and might have fed flows from which the specimens for the second K–Ar study were obtained. A different interpretation could be inferred because it is the general opinion that the Maunalei dikes represent an earlier rift zone from which later shifted to the southwest (Macdonald and Abbot, 1970, p. 341).

6. Conclusions

The main characteristics that emerge from the paleomagnetic study of the eight lava flows located in different places within the island of Lana'i and the comparison with the potassium–argon determinations

of their corresponding flows can be summarized as follows:

(1) Alternating field (AF) demagnetization experiments of each one of the lava flows successfully removed the secondary magnetizations of low coercivity, isolating a stable univectorial component of magnetization interpretable as reliable recorders of the Earth's magnetic field at the time of the emplacement of the lavas under study.

(2) The AF experiments along with the low-field susceptibility versus temperature (k–T) and the saturation Isothermal Remanent Magnetization (SIRM) tests indicate that Ti-poor magnetite determines the magnetization.

(3) The characteristic component of all samples from all sites reveals a negative polarity (see Fig. 5 and Table 1).

(4) The ages obtained from the coastal areas, namely, Kaumalapau and Manele Bay (Bonhommet et al., 1977) are consistent with the reversed polarity of the studied samples.

(5) The negative magnetic polarities of the samples from the Maunalei Gulch are inconsistent with the ages obtained by Naughton et al. (1980) and by Cande and Kent (1995), which would place them within the Brunhes Chron.

(6) Site L1 should correspond with a negative polarity (within the Matuyama Chron) since the reported age (0.86 ± 0.55 Ma) is older than the last reversal. Therefore this is the only lava flow from Naughton et al. (1980) that agrees with the paleomagnetic results.

(7) The present results indicate that the lavas in the tholeiitic shield phase of the volcanic edifice were erupted very rapidly.

(8) Despite uncertainty in the ages, the uniform presence of reversed polarities suggest that the shield-building stage of the Lana'i volcano would have not exceeded 680,000 years (from 1.46 to 0.78 Ma).

Acknowledgements

We would like to express special thanks to the Lana'i Water Company for their generosity and help provided during our field trip to the Maunalei Gulch, particularly to the president of the company Mr. Vince Bagoyo and Fred "Bubba" Sandi. Also we would like to acknowledge the field assistance of Professor M.D. Fuller during one field trip to the Kaumalapau Harbor on the island of Lana'i. Our special thanks to Mr James Lau for field and laboratory assistance during the entire length of this project. This paper has been greatly improved with the constructive comments and help of Professor L. Wilson. This is SOEST contribution #5213 and HIGP contribution #1105.

References

Bonhommet, N., Beeson, M.H., Dalrymple, G.B., 1977. A contribution to the geochronology and petrology of the island of Lanai, Hawaii. Geol. Soc. Amer. Bull. 88, 1282–1286.

Cande, S.C., Kent, D.V., 1995. Revised calibration of the geomagnetic polarity timescale for the Late Cretaceous and Cenozoic. J. Geophys. Res. 100, 6093–6095.

Doell, R.R., Dalrymple, G.B., 1973. Potassium–argon ages and paleomagnetism of the Wai'anae and Ko'olau volcanic series, Oahu, Hawaii. Geol. Soc. Amer. Bull. 84, 1217–1242.

Fisher, R.A., 1953. Dispersion on a sphere. Proc. R. Soc. A 217, 295–305.

Herrero-Bervera, E., Valet, J.-P., 1999. Paleosecular variation during sequential geomagnetic reversals from Hawaii. Earth Planet. Sci. Lett. 171, 139–148.

Herrero-Bervera, E., Coe, R.S., 1999. Transitional field behavior during the Gilbert-Gauss and Lower Mammoth reversals recorded in lavas from the Wai'anae volcano, O'ahu, Hawaii. J. Geophys. Res. 104, 29 157–29 173.

Hrouda, F., 1994. A technique for the measurement of thermal changes of magnetic susceptibility of weakly magnetic rocks by the CS-2 apparatus and KLY-2 Kappabridge. Geophys. J. Int. 118, 604–612.

Hrouda, F., Jelinek, V., Zapletal, K., 1977. Refined technique for susceptibility resolution into ferromagnetic and paramagnetic components based on susceptibility temperature-variation measurement. Geophys. J. Int. 129, 715–719.

Hazlett, R.W., Hyndman, D.W., 1996. Roadside Geology of Hawaii. Mountain Press, Missoula, MT, 307 pp.

Jackson, E.D., Silver, E.A., Dalrymple, G.B., 1972. Hawaiian-Emperor chain and its relation to Cenozoic circumpacific tectonics. Geol. Soc. Am. Bull. 83, 601–618.

Macdonald, G.A., 1940. The petrography of Lanai and Kahoolawe. In: Geology and groundwater resources of Lanai and Kahoolawe, Sterns, Hawaii Division of Hydrography, Bulletin, 6, 3-95, pp. 119–147, colored geologic map.

Macdonald, G.A., Abbot, A.T., 1970. Volcanoes in the Sea: the Geology of Hawaii. University of Hawaii Press, Honolulu, HI, 441 pp.

Macdonald, G.A., Abbot, A.T., Peterson, F.L., 1983. Volcanoes in the Sea: The Geology of Hawaii, 2nd Edn. University of Hawaii Press, Honolulu, HI, 517 pp.

Moore, J.G., Clague, D.A., Holcomb, R.T., Lipman, P.W., Normark, W.R., Torresan, M.E., 1989. Prodigious submarine

landslides on the Hawaiian Ridge. J. Geophys. Res. 94, 17 465–17 484.

Naughton, J.J., Macdonald, G.A., Greenberg, V.A., 1980. Some additional Potassium-Argon ages of Hawaiian rocks: The Maui volcanic complex of Molokai, Maui, Lanai and Kahoolawe. J. Volcanol. Geotherm. Res. 7, 339–355.

Powers, S., 1920. Notes on Hawaiian Petrology. Am. J. Sci., 4th Series 50, 256–280.

Sterns, H.T., 1940. Geology and ground-water resources of the islands of Lanai and Kahoolawe, Hawaii. Hawaii Division of Hydrography, Bulleting 6, pp. 3–95, 119–147, colored geologic map.

Washington, H.S., 1923. Petrology of the Hawaiian Islands. I. Kohala and Mauna Kea, Hawaii. US Geol. Survey, Prof. pap. 735, 40 pp.

Walker, G.P.L., 1990. Geology and volcanology of the Hawaiian Islands. Pacific Sci. 44, 315–347.

Wentworth, C.K., 1925. The geology of Lanai. Bishop Museum, Bulletin 24, Honolulu, Hawaii, 72 pp.

ANALYTICAL LETTERS, 33(8), 1691–1709 (2000)

SIMULTANEOUS OPTIMIZATION OF SURFACTANT CONCENTRATION AND ORGANIC MODIFIER IN MICELLAR LIQUID CHROMATOGRAPHY. APPLICATION TO THE SEPARATION OF PHENOLIC COMPOUNDS

Keywords: liquid chromatography; micelles; CTAB; phenols; environment.

C. Mahugo Santana, Z. Sosa Ferrera and J.J. Santana Rodríguez*

Department of Chemistry, Faculty of Marine Sciencies, University of Las Palmas de Gran Canaria, 35017 Las Palmas de Gran Canaria, Spain.

ABSTRACT

The separation selectivity of eighteen phenolic derivatives in micellar high-performance liquid chromatography was studied as a function of parameters on which it depends: surfactant and organic modifier concentration. The surfactant used in this study was cetyltrimethylammonium bromide, and as organic modifier methanol. An iterative regression optimization strategy for these two parameters has been used. The equation that best explains the experimental

*To whom correspondence should be addressed.

results is $1/k' = A + B\mu + C\phi + D\mu\phi$ .We propose the use of this model in conjunction with the appropriate factorial design to predict the solute retention behaviour in micellar liquid chromatography with hibrid eluents.

INTRODUCTION

Micellar liquid chromatography (MLC) has been regarded as a powerful alternative to the conventional reverse-phase chromatography with hydro-organic eluent (RPLC), since its first reported by Armstrong and Henry[1].

The popularity of this mode of separation has increased because of several unique advantages such as the simultaneous separation of ionic and non-ionic compounds, rapid gradient capability, possibility of direct injection of physiological fluids, gradient compatibility with electrochemical detectors, enhanced luminescence detection, etc.[2-6].

Perhaps the main drawback of this separation technique is its reduced efficiency compared to conventional reversed-phase systems. Several workers have examined the reason behind the poor efficiency and the methods for improving it, especially the influence of additions of small amounts of short-chain alcohols[7-11]. The most common reasoning is that the addition of alcohols reduces the loading of the surfactant in the stationary phase and this leads to improvements in the mass transfer and wetting of the stationary phase[8].

Khaledi and co-workers[12-14] studied the effects of organic solvent on retention and selectivity of polar and ionic solutes in MLC. More recently, they studied the role of organic modifiers and micelles controlling solvent strength and selectivity in MLC[15-17].

In MLC the retention of solutes usually decreases with increasing micelle concentration and amount of organic modifier in the mobile phase. With traditional RPLC, the concentration of organic modifier is mainly used to adjust the solvent strength; its effect on selectivity is not pronounced. A sequential optimization strategy is used in RPLC as solvent strength is adjusted first, then

selectivity is optimized. In MLC the nature and concentration of the surfactant and the type and concentration of organic modifier have a pronounced effect on selectivity as well as on the mobile phase strength[12,15,17]. Due to the interactive nature of these factors a simultaneous variation of the concentration of surfactant and modifier is required to optimize the chromatographic separation. In others words, they can not be optimized independent of one another.

Some authors have explored the possibilities of predicting the solute retention in MLC with hybrid eluents with varying concentrations of surfactant and organic modifier. The studies are based in the construction of empiric models that describe the retention of solutes as function of these parameters using a minimum number of initial experiments[18-23].

The objective of this report is to provide more data for a better understanding of solute retention mechanism in MLC with hybrid eluents. And to find, if it is possible, an equation to describe it which should allow an easy way to predict the retention of a solute with a minimum effort. In this study we have used the retention data of eighteen phenolic compounds of environmental interest[24-25], in the micellar mobile phase with different concentrations of cetyltrimethylammonium bromide (CTAB) modified with different percentages of methanol.

EXPERIMENTAL

Apparatus

The chromatograph consisted of a Waters pump 510 fitted with a Waters injector model Rheodyne 7725 i with a 20 ml sample loop and a Waters 996 Photodiode Array Detector. The system and the data management were controlled by Millenium software from Waters (Waters Cromatografia S.A. Barcelona, Spain).

The stationary-phase column was a Water Nova-Pack C_{18}, 3.9 x 150 mm i.d. 4 μm particle diameter.

The analytical column and the mobile phase reservoir were water-jacketed and thermostated at 50 ± 1°C with a circulating bath.

Reagents

The surfactant cetyltrimethylammonium bromide (CTAB) for electrophoresis was obtained from Aldrich Chemical Co. (St. Louis, MO, USA) and used as received. Methanol (MeOH) was Merck (Darmstadt, Germany) grade HPLC.

The eighteen phenolic compounds used are listed in Table 1. They were obtained from Fluka Chemika (Buchs, Switzerland) and were used as received. Numbers identify the compounds in tables and figures.

Procedure

The surfactant solution was prepared by dissolving the required amount of doubly distilled, deionized water containing the desired methanol content, and the solution was filtered through a 0.45 μm nylon membrane filter (Whatman). The mobile phase was degassed in an ultrasonic bath prior to use. Stock solutions of phenolic compounds were prepared in methanol and diluted with the same solvent when necessary.

The void volume of the system was measured by multiple injections of water or methanol; it was found to be 1.1 ml and was used for all k' calculations. The k' values were measured at 50 ± 1°C; injections of 20 μ l were made with a mobile phase flow of 1 ml/min.

Data manipulation

Multiple linear regression analysis was carried out with SSPS and surface and contour map plots with Golden Surfer v.6 in a Pentium MMX (133 Mhz).

RESULTS AND DISCUSSION

The retention factor of eighteen phenolic derivatives in MLC system was

TABLE 1

List of Phenolic Derivatives used

N°	COMPOUNDS	ABREVIATION
1	PHENOL	PH
2	4-NITROPHENOL	4 NP
3	PARACRESOL	PC
4	ORTHOCRESOL	OC
5	2-CHLOROPHENOL	2-CP
6	4-CHLOROPHENOL	4-CP
7	2,4-DIMETHYLPHENOL	2,4-DMP
8	2,4,6-TRIMETHILPHENOL	2,4,6-TMP
9	2,4-DINITROPHENOL	2,4-DNP
10	4-CHLOROMETACRESOL	4-CMC
11	2-NITROPHENOL	2-NP
12	4,6-DINITRO ORTHOCRESOL	4,6-DNOC
13	2,6-DICLORO-4-NITROPHENOL	2,6-DC-4-NP
14	4-CHLORO-3,5-DIMETHYLPHENOL	4-C-3,5-DMP
15	2,4-DICHLOROPHENOL	2,4-DCP
16	THYMOL	TH
17	2,4,6-TRICHLOROPHENOL	2,4,6-TCP
18	PENTACHLOROPHENOL	PCP

determined by using CTAB as surfactant in the presence of different methanol percentages. These data allowed conclusions to be drawn regarding the models that best fit the experimental retention data.

The addition of alcohol to a micellar mobile phase would cause changes in micellar properties, such as the aggregation number and the critical micelle concentration (c.m.c.) of the surfactant. For this reason, the c.m.c values for

CTAB in the presence of different percentages of MeOH were determined by conductimetric titration[26] at 25±1° C (Table 2).

Variation of the retention factor

Eluent strength in MLC is inversely related to surfactant concentration. A linear relationship exists between the inverse of retention factor, 1/k', and surfactant concentration[2,27]. The retention decreases when the eluent strength increases as expected.

Figure 1 shows the variation of the inverse of retention factor as a function of the concentration of CTAB, keeping constant the percentage of methanol (6%) for a group of chlorinated phenols, obtaining the same behaviour for all studied compounds. Regression analysis shows good linearity obtained in every plot (Table 3).

The rate of change in the retention of the different solutes varies from one solute to another depending on its hydrophobicity and its molecular weight as well as steric impediments. Thus, it can be observed how first the higher compound, phenol elutes, then the monosubstituted derivatives and those which have two or more substitutes, and finally the heaviest compounds such as 2,4,6-TCP and PCP. This last group, since as it is bigger, shows a higher steric impediment to interact with micelles.

On the other hand, it can be observed that an increase in the percentage of methanol, keeping constant surfactant concentration, produces a smaller variation in the retention factor of the studied compounds. Figure 2 shows this behaviour for chlorinated phenols. The results of regression analysis of the data of this figure are shown in Table 4.

Regarding selectivity, α, defined as the ratio of the retention factors of two components, it seems that the separation increases with increasing eluent strength for the majority of compounds studied.

This is illustrated by examining the changes in selectivity of two pairs of compounds. Figure 3a shows the effect of varying the surfactant and the organic

TABLE 2
Critical Micellar Concentrations of Micellar Systems used as Mobile Phases

Micellar system	c.m.c. (M)	Ref.
CTAB - 2 % MeOH	$9.486\ 10^{-4}$	This work
CTAB - 5 % MeOH	$9.479\ 10^{-4}$	28
CTAB - 6 % MeOH	$9.470\ 10^{-4}$	This work
CTAB - 10 % MeOH	$9.392\ 10^{-4}$	28
CTAB - 15 % MeOH	$9.257\ 10^{-4}$	28

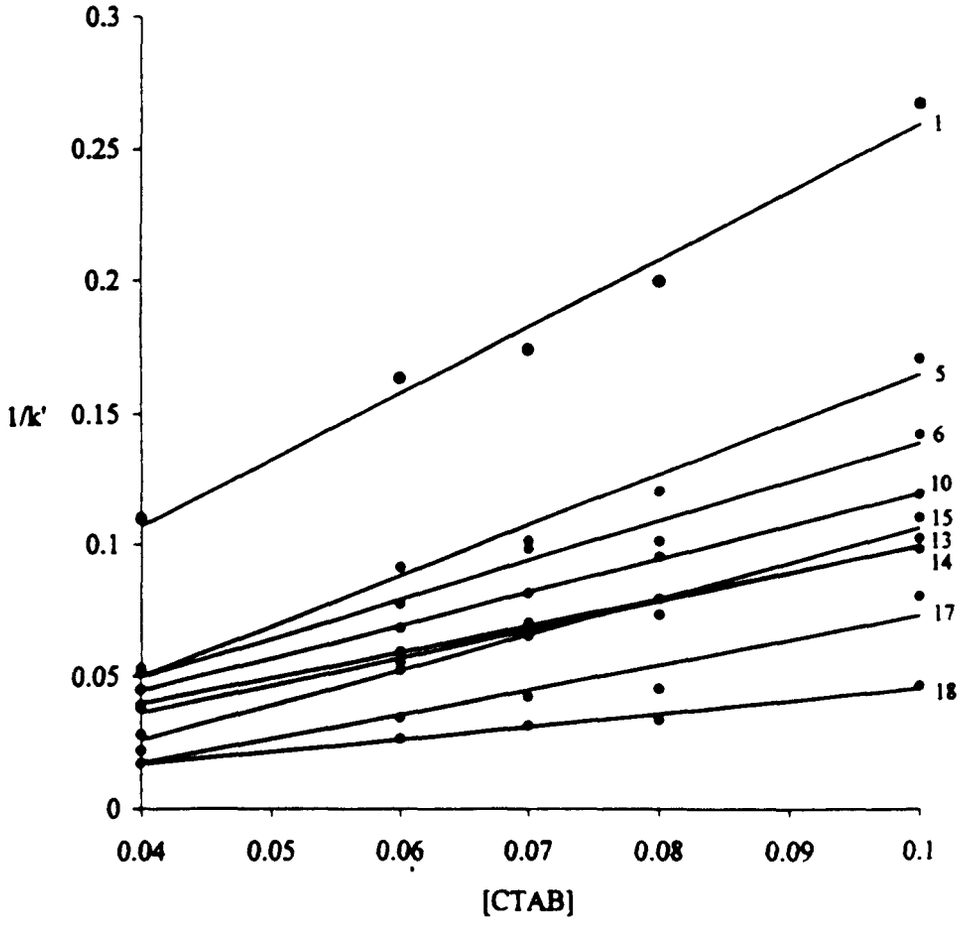

Fig. 1: Effect of surfactant concentration on the retention behaviour of phenolic compounds keeping constant the percentage of methanol (6%). The numbering refers to Table 1.

TABLE 3
Regression Analysis for Data of Figure 1

Compound	c.c.*	equation
1	0.982	$y= 2.55\ x + 4.8\ 10^{-3}$
5	0.983	$y= 1.93\ x - 27.1\ 10^{-3}$
6	0.980	$y= 1.50x - 10.4\ 10^{-3}$
10	0.999	$y= 1.26\ x - 5.8\ 10^{-3}$
15	0.985	$y= 1.35\ x - 28.1\ 10^{-3}$
13	0.983	$y= 1.06\ x - 6.3\ 10^{-3}$
14	0.999	$y= 1.00\ x - 0.2\ 10^{-3}$
17	0.916	$y= 0.94\ x - 20.4\ 10^{-3}$
18	0.986	$y= 0.48\ x - 2.6\ 10^{-3}$

* correlation coefficient

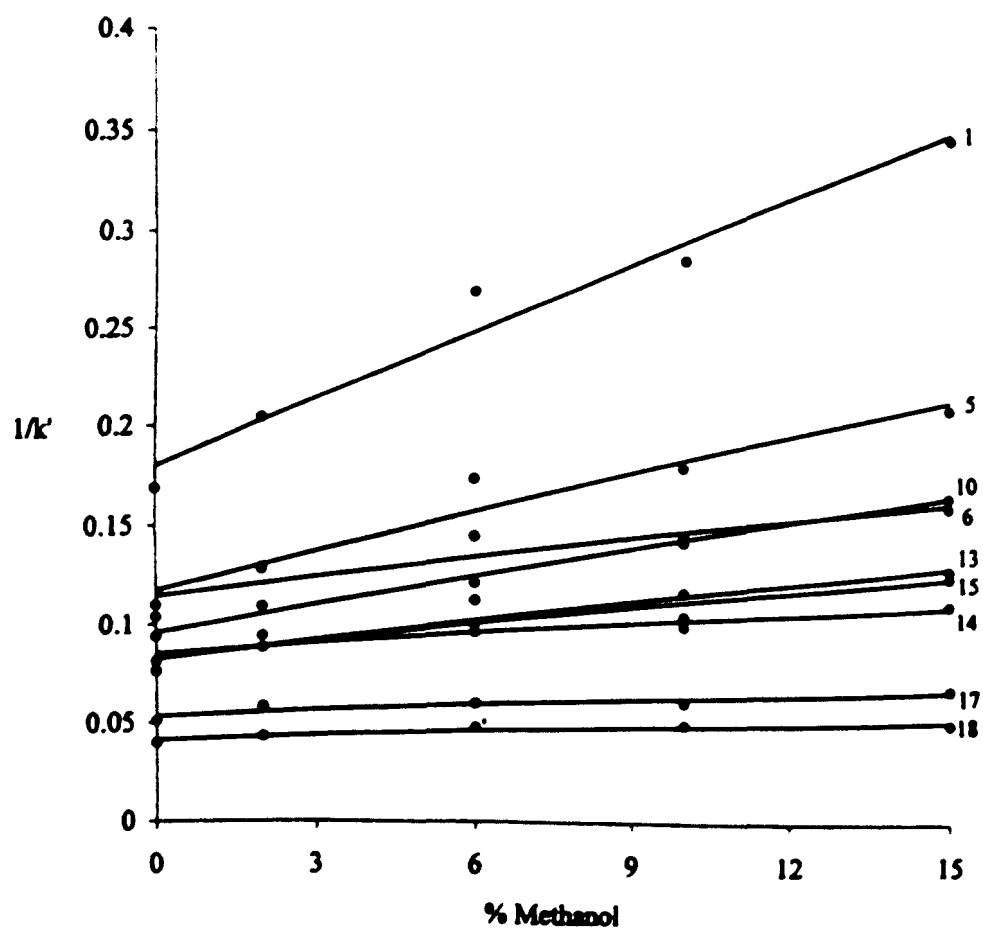

Fig. 2: Effect of percentage of methanol on the retention behaviour of phenolic compounds keeping constant surfactant concentration (0.1 M). The numbering refers to Table 1.

TABLE 4
Regression Analysis for Data of Figure 2

Compound	c.c.*	equation
1	0.965	$Y= 11.1\ 10^{-3}\ x + 0.18$
5	0.941	$Y= 6.3\ 10^{-3}\ x + 0.12$
10	0.989	$Y= 4.6\ 10^{-3}\ x + 0.10$
6	0.824	$Y= 3.1\ 10^{-3}\ x + 0.12$
13	0.912	$Y= 2.7\ 10^{-3}\ x + 0.08$
15	0.895	$Y= 3.1\ 10^{-3}\ x + 0.08$
14	0.861	$Y= 1.6\ 10^{-3}\ x + 0.08$
17	0.856	$Y= 0.9\ 10^{-3}\ x + 0.05$
18	0.895	$Y= 0.7\ 10^{-3}\ x + 0.04$

* correlation coefficient

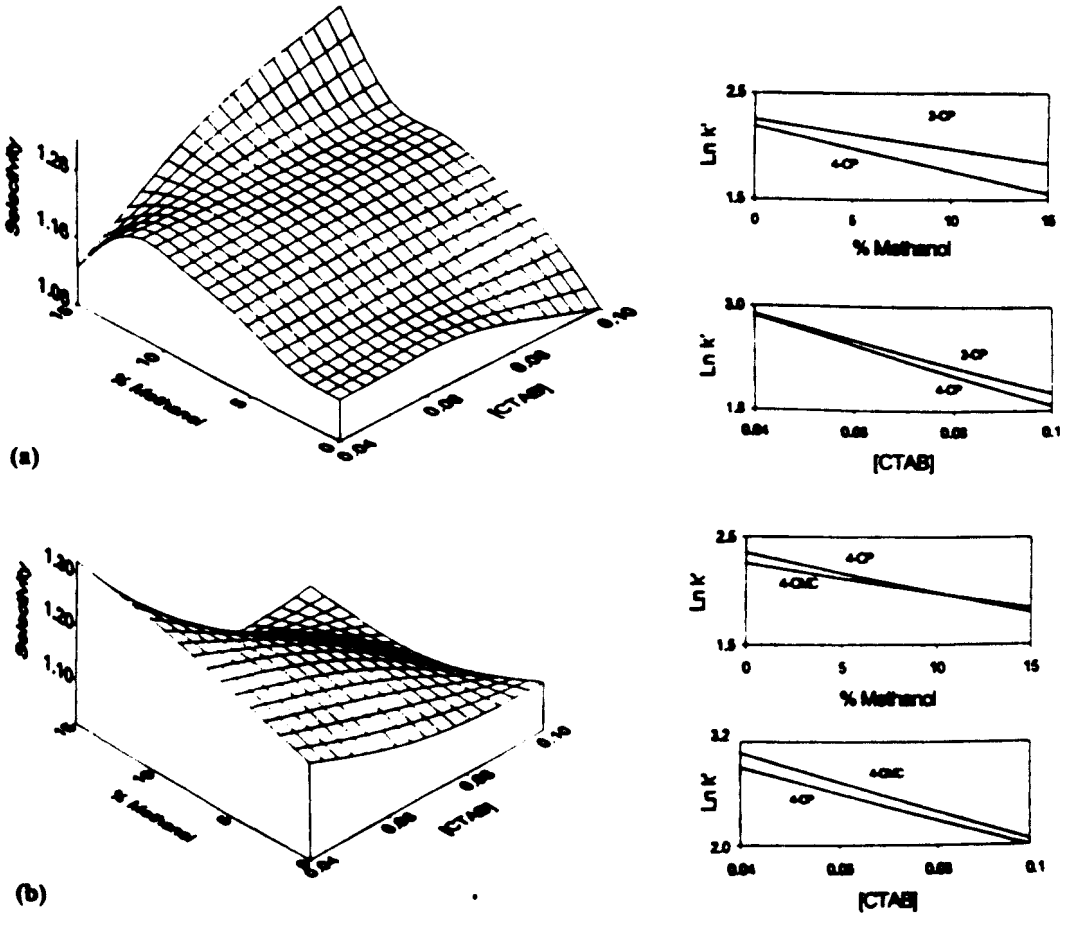

Fig. 3: Retention, ln k', as a function of the percentage of methanol at 0.1 M CTAB (upper right) and as a function of the surfactant concentration at 6% methanol (lower right); and the selectivity, α, of two compounds as a function of both surfactant and methanol concentration (left). (a) 2-CP and 4-CP. (b) 4-CMC and 4-CP.

modifier concentration on the selectivity of 2-CP and 4-CP: it is observed that when the methanol and surfactant concentrations are increased the selectivity increases. When methanol concentration is increased, 4-CP shows a stronger drop in retention than 2-CP (upper right frame). Similar changes in retention of both compounds occur varying surfactant concentration (lower right frame). The reverse is observed when the selectivity of 4-CP and 4-CMC is studied (Figure 3b); by increasing the methanol and surfactant concentrations a decrease in selectivity occurs. In this case, the variation in retention is even bigger at increasing the surfactant concentration than at increasing the methanol concentration (lower and upper right frame).

It is obvious that when both surfactant and organic modifier concentration change, their effects are combined and the reduction in retention is not the same for all compounds, and, as a result, we get the desired changes in selectivity.

Optimization of separation and selectivity

In MLC the different components of the sample react in different ways to the changes in the surfactant and organic modifier concentration. Because of that, to optimize the separation of the studied compounds, as we explained in the introduction, cannot be done the sequential way, but the simultaneous way. An iterative regression optimization strategy for two parameters has been used in MLC[13,14,20,21]. The method assumes that the retention of solutes is linearly related to the mobile phase parameters within a selected portion of the parameter space. The optimization strategy begins with a design of five points, one at each corner of the parameters space and the fifth in the center. From the preliminary experiments the following upper and lower limits were selected: the CTAB concentration ranged from 0.04 to 0.1 M and the methanol concentration from 0.0 to 15 %. Retention factor data of different compounds, obtained from five selected mobile phases, were analysed through a multiple lineal regression program in order to find the equation that can describe the behaviour of retention of solutes in different mobile phases.

The selected equations of trial, and their global mean relative fitting errors, are shown in Table 5 where μ is the total surfactant concentration, ϕ is the volume fraction of alcohol and A, B, C, D and E fitting parameters. The inclusion of an interaction term ($\mu\phi$) in the equation was needed to obtain an adequate description of the retention behaviour of the solutes in MLC with a hybrid mobile phase. The addition of new terms (μ^2 or ϕ^2) improved the accuracy of the prediction for the same compound studied. However, the coefficients (A-E) calculated for these systems are equivalent to those obtained with Eq. 2, and terms μ^2 or ϕ^2 are negligible compared to the $\mu\,\phi$ term.

In Figure 4 the calculated k' values according to eq.2 were plotted against the experimental values for all compounds in a mobile phase containing CTAB as surfactant and methanol as organic modifier. The straight lines obtained have slope values very near to unity and intercepts near zero.

The study of the accuracy in the prediction of the retention could be done showing the curves of variation of the retention factor for each solute at different mobile phase compositions. However, a plot of global resolution is more informative, since a group of solutes is simultaneously examined, and this function is of greater significance for the experimental development.

The following discussion is based on the comparison of the surface and contour maps of resolution for the separation of a mixture of phenols. Only resolution coefficients that vary with experimental conditions were chosen. This implies the exclusion of resolution coefficients of pairs of compounds that are either never separated or that can always be separated regardless of the experimental conditions and leads, in both cases, to low values in the resolution.

The normalized product of the resolution (r) was taken as the optimization criterium[13], to describe the overall separation of the peaks in the chromatogram:

$$r = \prod_{i=1}^{n-1} R_{s_{i+1,i}} \Big/ \left[\sum_{i=1}^{n-1} R_{s_{i+1,i}} /(n-1)\right]^{n-1}$$

where $R_{s_{i+1,i}}$ represents the resolution between peaks $i+1$ and i out a total of n

TABLE 5

Mean Global Relative Errors Obtained with the Eighteen Phenolic Compounds and Diverse Concentration of CTAB and Percentage Of Methanol

Equation		Relative error (%) (n = 178)
(1)	$1/k' = A + B\mu + C\phi$	11.40
(2)	$1/k' = A + B\mu + C\phi + D\mu\phi$	4.28
(3)	$1/k' = A + B\mu + C\phi + D\mu\phi + E\mu^2$	5.12
(4)	$1/k' = A + B\mu + C\phi + D\mu\phi + E\phi^2$	5.07

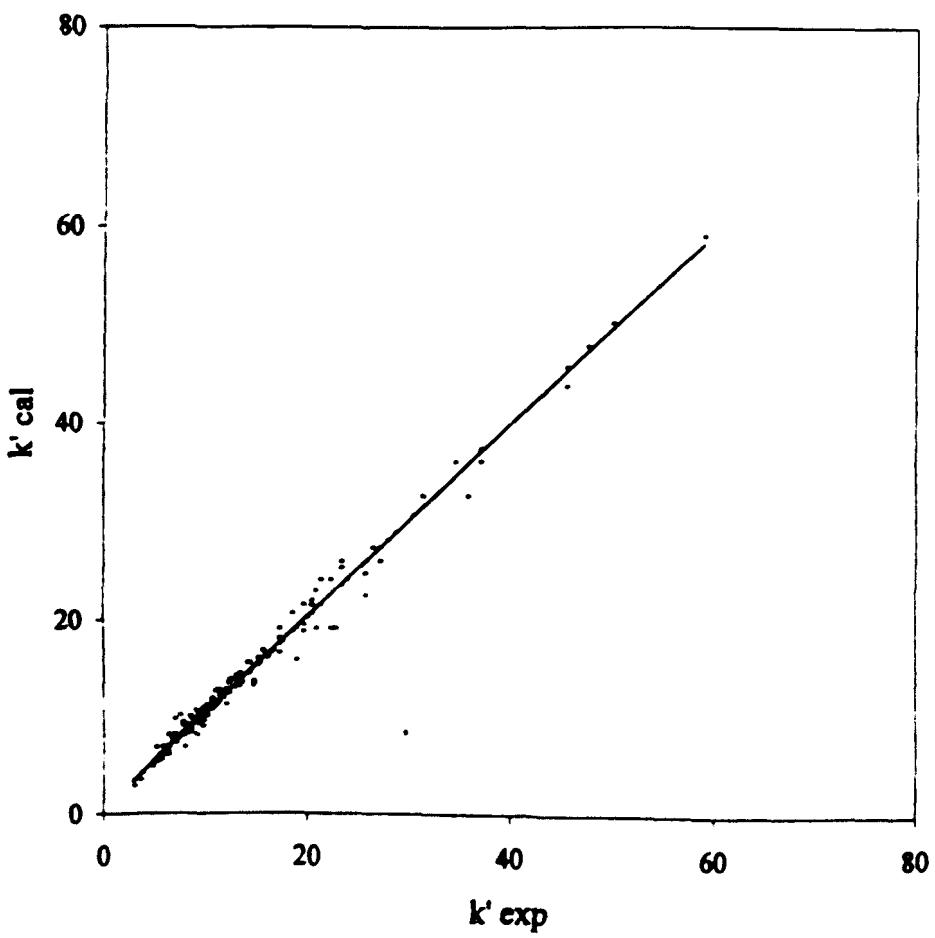

Fig. 4: Variation of calculated k' (k' cal) with Eq. 2 as a fuction of experimental k' (k' exp). $y = 0.977x + 0.520$, c.c.= 0.989, n = 178.

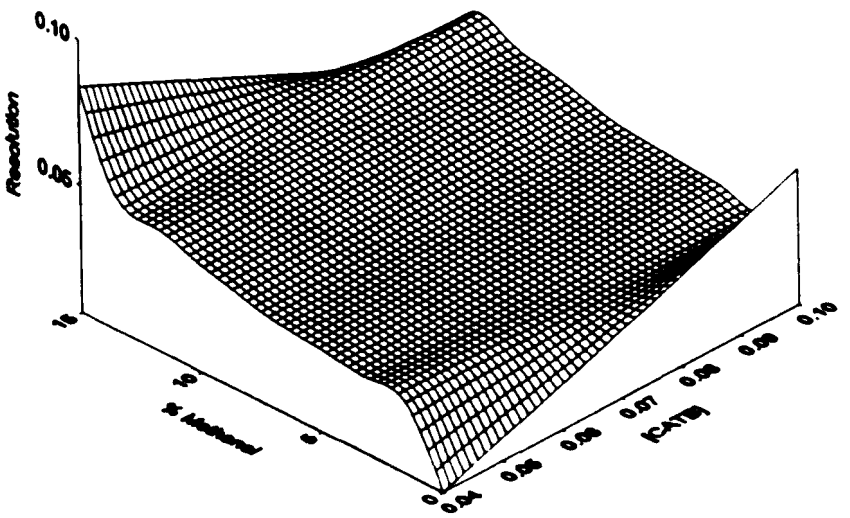

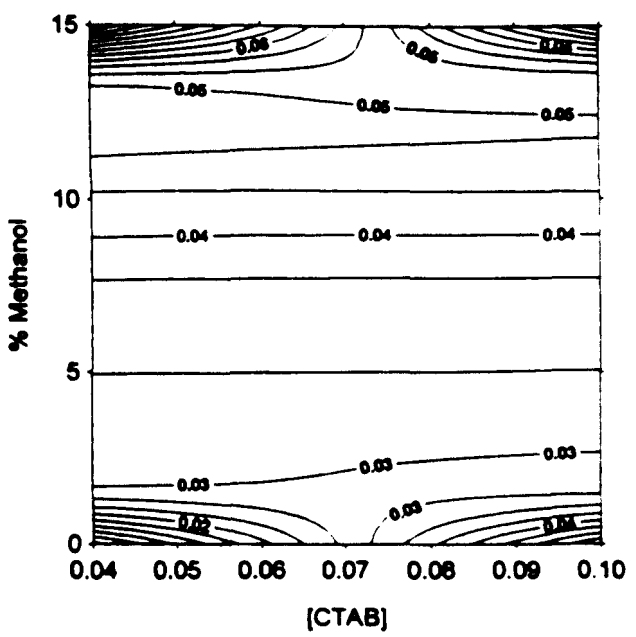

(a)

Fig.5: Resolution surface and contour map for thirteen phenolic derivatives as a function of the surfactant and organic modified concentration. The response surface on the basis of the five measurements (a). The response surface on the basis of the twelve measurements (b).

(continued)

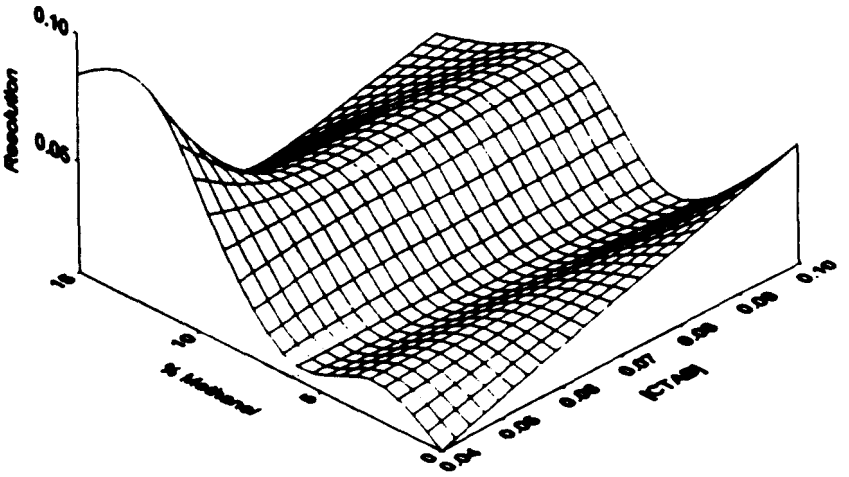

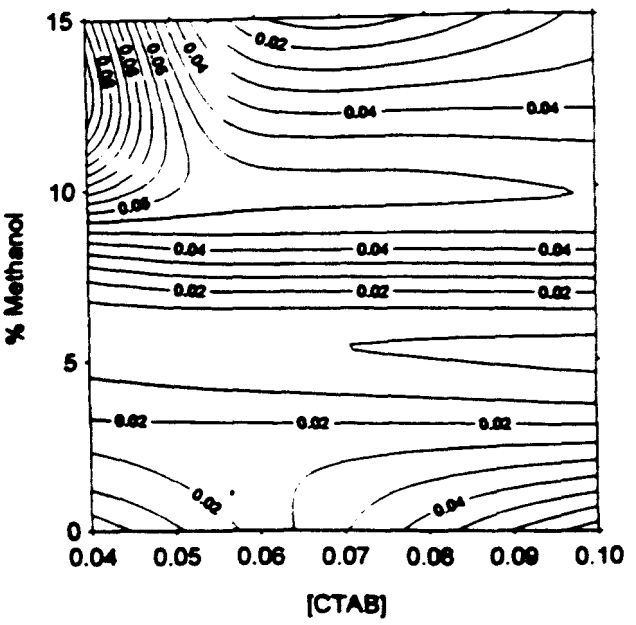

(b)

Figure 5. Continued

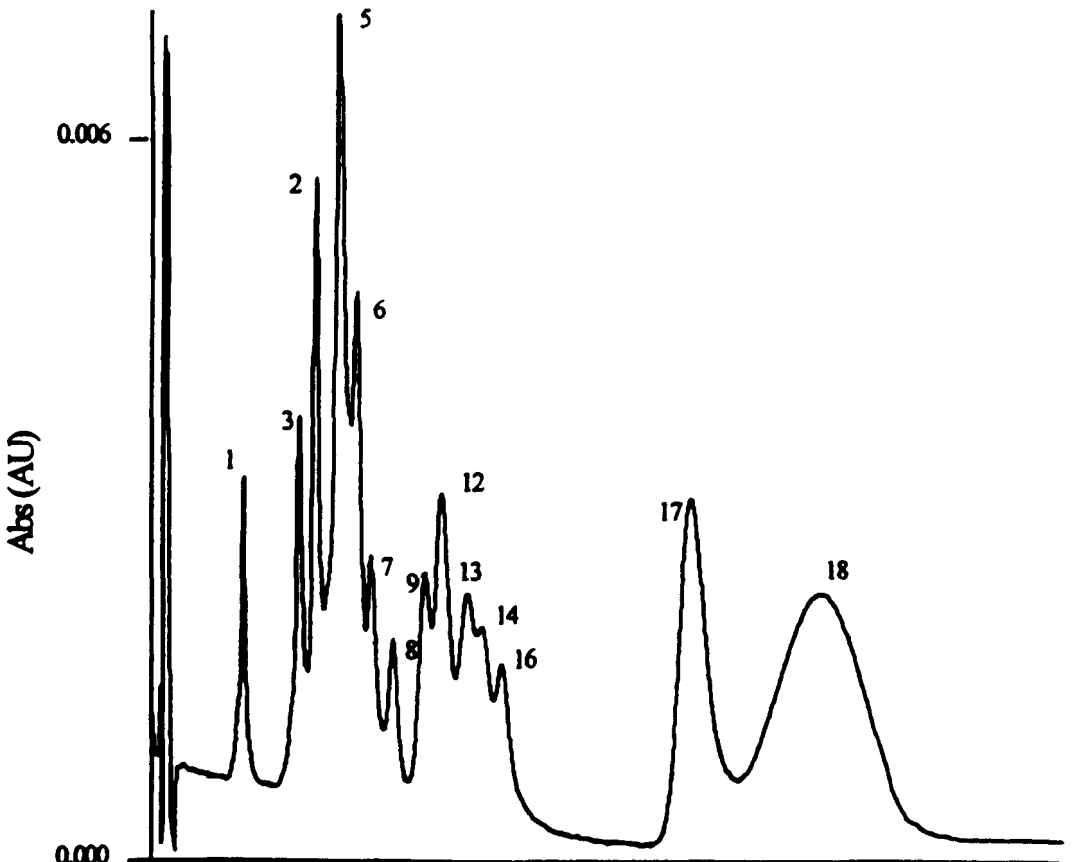

Fig. 6: Chromatograms of the fourteen phenolic derivatives at 0.04 M CTAB and 12 % Methanol. The numbering refers to Table 1.

components. The function of resolution, *r*, is maximized to obtain the optimum mobile phase. Contour maps were used to find the position of the maximum and the shape of the response surface.

Figure 5a shows the surface and contour map of resolution for the separation of a mixture of phenols using five mobile phases. It may be observed that the optimum was found for a mobile phase of 0.04 M CTAB and close to 15 % methanol. Figure 5b displays the response surface observed when a larger number of data is included in the retention modelling. The additional data-points

TABLE 6

Experimental and Calculated Retention Time of Fourteen Compounds Mixture at 0.04 M CTAB and 12 % Methanol.

	Compounds	t_r exp	t_r cal
1	PH	8.17	8.29
3	PC	13.10	13.62
2	4 NP	14.46	13.76
5	2-CP	12.52	16.15
6	4-CP	18.12	18.06
7	2,4-DMP	19.39	19.90
8	2,4,6-TMP	21.31	21.25
9	2,4-DNP	24.09	20.81
12	4,6-DNOC	25.56	24.09
13	2,6-DC-4-NP	27.79	25.57
14	4-C-3,5-DMP	29.22	27.82
16	TH	30.97	34.43
17	2,4,6-TCP	47.37	43.41
18	PCP	58.50	56.10

are used to define a finer grid over the parameter space, resulting in a more accurate response surface. In this case, the predicted optimum value is located at an intermediate elution strength at 0.04 M CTAB and 12% methanol.

Figure 6 shows the chromatogram at these conditions. As we can observe, a satisfactory separation of fourteen of the eighteen compounds studied is obtained.

Table 6 shows the experimental and predicted retention times of the fourteen separated phenolic compounds at optimum mobile phase. There is good agreement between both.

CONCLUSIONS

Due to the complex retention mechanisms involved, a separation optimization of elution strength first and then selectivity in MLC is inefficient. In fact, it is observed that an increase in elution strength can coincide with an

enhancement of selectivity. Since the surfactant and organic modifier concentration both influence the above factors, it is essential that a variation of these two parameters is examined simultaneously.

The equation $1/k' = A + B\mu + C\phi + D\mu\phi$ gives an adequate description of the retention behaviour of solutes in MLC with mobile phase of CTAB and methanol. As a consequence, it is possible to predict the retention behaviour of the solutes on the basis of a limited number of experiments. In this way it is easy to estimate the likelihood of finding the desire separation, defined by the applied criterion, within the selected parameter space.

ACKNOWLEDGEMENTS

This work was supported by funds provided by D.G.I.C.Y.T. (Spain). Research Project N° PB94-0431. Also, we thank Miguel Díaz Mederos for his collaboration in the management data with different computer programs.

REFERENCES

1. D.W. Armstrong and S. Henry, *J. Liq. Chromatogr.*, **3**, 657,(1980).
2. D.W. Armstrong, *Sep. Purif. Methods*, **14**, 213,(1985).
3. W.L. Hinze and D.W. Armstrong (Eds) *Ordered Media in Chemical Separation; ACS Symposium Serie* 342, American Chemical Society, Washington, DC 1987.
4. M.G.Khaledi, *Biochromatography*, **3**, 20, (1988).
5. M.G.Khaledi, *Trends Anal. Chem.*, 7, 293,(1988).
6. J.G. Dorsey, *Adv. Chromatogr.*, **27**, 167, (1987).
7. J.G. Dorsey, M.T. De Echegaray and J.S. Landy, *Anal. Chem.*, **55**, 924 (1983).
8. P. Yarmchuk, R. Weinberger, R.F. Hirsch and L.J. Cline Love, *J. Chromatogr.*, **47**, 283, (1984).

9. J.S. Landy and J.G. Dorsey *Anal.Chim. Acta*, **178**, 179, (1985).
10. M.F. Borgerding, R.L. Willians, W.L. Hinze and F.H. Ouina, *J.Liq.Chromatogr.*, **12**, 1367, (1989).
11. M.F. Borgerding , W.L. Hinze, L.D. Stafford, G.W. Fulp and W.C. Hamlin, *Anal. Chem.*, **61**, 1353, (1989).
12. M.G. Khaledi, J.K. Straters, A.H. Rogers and E.D. Breyer, *Anal. Chem.*, **2**, 130, (1990).
13. J.K. Straters, E.D. Breyer A.H. Rogers, and M.G. Khaledi, *J. Chromatogr.*, **511**, 17, (1990).
14. J.K. Straters, S.T. Kim and M.G. Khaledi, *J. Chromatogr.*, **586**, 221, (1991).
15. A.S. Kord and M.G. Khaledi, *Anal.Chem.*, **64**, 1894, (1992).
16. A.S. Kord and M.G. Khaledi, *Anal.Chem.*, **64**, 1901, (1992).
17. A.S. Kord and M.G. Khaledi, *J. Chromatogr.*, **631**, 125, (1993).
18. O.Jiménez, M.A. García and M.L. Marina, *J. Chromatogr.*, **A 719**, 15, (1996).
19. M.A. García, O.Jiménez and M.L. Marina, *J. Chromatogr.*, **A 675**, 1, (1994).
20. R.M. Villanueva-Camanas, J.R. Torres-Lapasio and M.J. Medina Hernández, *Chromatographia*, **40**, 279, (1995).
21. J.R. Torres-Lapasio, R.M. Villanueva-Camanas and M.C. García Álvarez-Coque, *J. Chromatogr.*, **A 677**, 239, (1994).
22. J.R. Torres-Lapasio, R.M. Villanueva-Camanas and J.M. Sanchís-Mallols, *J. Chromatogr.*, **639**, 87, (1993).
23. M.A. Rodríguez Delgado, M.J. Sánchez and F. García Montelongo, *J. Chromatogr. A* **697**, 71, (1995).
24. K.K. Chee, W.G. Lau, M.K. Wong and H.K. Lee, *Anal.Chim.Acta*, **312**, 271, (1995).
25. D. Puig and D. Barceló, *Chromatographia*, **40**, 435, (1995).

26. M.J. Rosen, *Surfactants and Interfacial Phenomena*, Wiley, New York, 2nd Ed. (1988).

27. M. Arunyanart and L.J. Cline Love, *Anal. Chem.*, **56**, 1557, (1984).

28. M.A. Rodríguez Delgado, M.J. Sánchez,V. González and F. García Montelongo, *Chromatographia*, **38**, 342, (1994).

Received: December 3, 1999
Accepted: February 2, 2000

PHYSIOLOGIA PLANTARUM 110: 530–534. 2000
Printed in Ireland—all rights reserved

ISSN 0031-9317

Polyamines in marine macroalgae: Levels of putrescine, spermidine and spermine in the thalli and changes in their concentration during glycerol-induced cell growth in vitro

Fernando D. Marián, Pilar García-Jiménez and Rafael R. Robaina*

Departamento de Biología, Facultad de Ciencias del Mar, Universidad de Las Palmas de Gran Canaria, ES-35017 Las Palmas de Gran Canaria, Canary Islands, Spain
**Corresponding author, e-mail: rafael.robaina@biologia.ulpgc.es*

Received 28 January 2000; revised 29 May 2000

The levels of putrescine (Put), spermidine (Spd) and spermine (Spm) were analyzed in naturally collected samples of the marine macroalgae *Dyctiota dichotoma*, *Gelidium canariensis* and *Grateloupia doryphora*. Polyamines (PAs) appeared in free (35–134 μg g^{-1} fresh weight) and bound TCA-insoluble form (1667–2624 μg g^{-1} fresh weight). Axenic in vitro cultures of sporelings from *G. doryphora* were established in the medium containing glycerol. This medium promoted growth and morphogenesis and also increased the free and bound PA levels in the sporelings. Tracer experiments using 70 kBq [U-^{14}C]-glycerol showed significant quantities of radioactivity in Put, Spd and Spm after 20 h of incubation. The effects of glycerol on growth were inhibited by the ornithine decarboxylase (EC 4.1.1.17) inhibitor α-difluoromethylornithine (DFMO). The presence of DFMO in the incubation medium with [U-^{14}C]-glycerol also reduced the radioactivity in PAs.

Introduction

Polyamines (PAs) are organic molecules with two or more amino groups that can be bound to cell membranes and a variety of macromolecules or can be found in a free state inside the cell. The diamine putrescine (Put) and the PAs spermidine (Spd) and spermine (Spm) are common amines found in animals and plants. In the latter, they are involved in the regulation of growth and stress responses, and are also related to plant flowering and other reproductive activities as demonstrated by changes in their concentration with the occurrence of these physiological events (Smith 1985, Evans and Malmberg 1989, Tiburcio et al. 1993, Galston et al. 1997).

Information on the presence and effects of PAs on marine macrophytes (i.e. macroalgae and seagrasses) is rather scarce. Villanueva et al. (1980) found the widely distributed common PAs Put, Spd and Spm together with their isomers Nor-spermidine and Nor-spermine in *Euglena gracilis*. Hamana et al. (1990) found that differences in the composition of PAs were related to the taxonomic position within different algal groups. Regarding potential physiological activities of PAs in macroalgae, Cohen et al. (1984) found that the PAs promoted cell division in *Chlorella*. The unicellular *Porphyridium* adsorbed PAs on the polysaccharides of the wall (Scoccianti et al. 1989, Scoccianti and Bagni 1992). Information on endogenous levels, uptake and transport within the thallus has been given for *Ulva* (Badini et al. 1994). Recently, Lee (1998) reported accumulation of Put and Spd related to lethal hyposaline stress in several species of intertidal marine macroalgae.

Cell masses with actively growing cells can be obtained by cultivating the red alga *Grateloupia doryphora* in glycerol, which is an effective carbon source that promotes growth and morphogenesis (shoot emission) of macroalga cultivated in vitro (Robaina et al. 1990a,b, Garcia-Jiménez et al. 1996). PAs induced growth and morphogenesis of sporelings of *G. doryphora* in the same way as glycerol (Garcia-Jiménez et al. 1998). Glycerol and PAs together enhanced growth and morphogenesis more than glycerol or PAs alone (Garcia-Jiménez et al. 1998). This suggests that the alteration of PA levels by glycerol results from their interaction due to their similar effects.

Abbreviations – DFMO, α-difluoromethylornithine; ODC, ornithine decarboxylase; PAs, polyamines; PES, Provasoli enriched seawater; Put, putrescine; Spd, spermidine; Spm, spermine; SW, sea water; TCA, trichloroacetic acid.

In the present work, we have studied naturally occurring levels of PAs in marine macrophytes. To address a possible physiological role in growth and development, we analyzed the changes in the endogenous levels of PAs in cell mass culture in medium containing glycerol. We have also checked the effects of α-difluoromethylornithine (DFMO), an inhibitor of PA synthesis, on glycerol-induced growth.

Materials and methods

Plant material

To check for naturally occurring PAs, unfertile samples of 3 different marine macroalgae were collected along the coast of Gran Canaria, Canary Islands, Spain: *Gelidium canariensis*, *Grateloupia doryphora* (Rhodophyta) and *Dyctiota dichotoma* (Phaeophyta).

Cultures of sporelings were established as follows: female thalli of *Grateloupia doryphora* bearing carposporophytes were collected together with the unfertile material. Disc fragments, 3 mm in diameter, containing cystocarps were excised. Aseptic culture methods were used to obtain carpospore germlings since contaminated cultures (i.e. from contaminated explants) were overgrown by contaminants. Disc fragments were disinfected and tested for sterility as previously described (Robaina et al. 1990a,b). Explants were then cultured in agarized (0.8% agar) Provasoli-enriched seawater medium (PES, Provasoli 1968) until carpospores were liberated and germinated. The carpospores were subjected to a 16-h light:8-h dark photoperiod for 30 days at 19 ± 2°C and an irradiance of 30 μmol m^{-2} s^{-1} (cool white fluorescent tubes: Sylvania Grolux, Osram Sylvania, München, Germany) measured at the level of the petri dishes. After 30 days, aseptic carpospore germlings were visible on the surface of the explant and in the culture medium. The carpospore germlings were transferred to petri dishes with liquid PES medium until they were used for the experiments.

Natural levels of PAs in *G. doryphora* were compared to those in sporelings cultured for a week in medium with or without glycerol. The germlings cultivated in PES without glycerol became sporelings with 1–4 shoots and produced biomass (2–10 mg fresh weight) which was not enough to quantify the different PA fractions. Therefore, total PAs were quantified and compared to total PAs in the naturally collected samples.

To cultivate in glycerol, the 30-day-old carpospore germlings (10 mg per replicate) were cultivated in medium containing glycerol based on PES, which was supplemented with 0.1 *M* of glycerol and 0.8% (w/v) agar in water made by dilution of the seawater (SW) with double distilled water (90:10 [v/v] SW:DDW, PES90-glycerol, Robaina et al. 1990b). The carpospores were kept in this medium for 1 week during which the sporelings became cell masses that allowed us to fractionate PAs into free and bound form (40–60 mg fresh weight).

The effect of DFMO

DFMO, an inhibitor of Put biosynthesis, was added (0.01 and 1 m*M* final concentration in the medium) to 3 replicates of sporelings cultured in medium containing glycerol. The specific growth rates (GRs) of the samples were determined after 7 days as GR (% day^{-1}) = $100 \times (W_7 - W_0)/W_0/7$, where W_7 and W_0 were the fresh weight on the 7th day and at the beginning of the experiments. The cells masses formed by these sporelings were then used in the tracer experiments described below.

Polyamine extraction and analysis

Algal samples were ground in a mortar in cold 5% trichloroacetic acid (TCA) in a 1:10 ratio of material (g fresh weight):5% TCA (ml). The supernatant containing the free TCA-soluble and the pellet with the bound TCA-insoluble PAs were separated. The pellet was hydrolyzed in sealed vials with 300 μl of 12 *M* HCl in each for 20 h at 100°C to release the bound PAs. After hydrolysis the samples were filtered and dried, and the residuals were redissolved in 300 μl of 5% TCA for dansylation. To analyze total PAs, the sporelings cultivated in the medium with or without glycerol or thallus fragments were hydrolyzed in HCl.

In the dansylation process, 45 μl of the sample were mixed with 45 μl of a saturated solution of Na_2CO_3 and 90 μl dansyl chloride (5 mg ml^{-1} acetone). The dansylation time was 10 min at 70°C. Then 25 μl of an aqueous proline solution (100 mg ml^{-1}) were added to react for 30 min in darkness with the excess dansyl chloride. Toluene (500 μl) was then added to extract the dansyl-PAs. The organic phase containing the dansyl-PAs was dried in a heat-speed vacuum and the residual was dissolved in 600 μl of acetone.

The dansyl-PAs were separated with TLC on 7.5 × 7.5 cm plates (Schleicher & Schuell, F1500 LS, 254) with chloroform/triethylamine 5:1 mixture (v/v) as a mobile phase. The plates were revealed under UV light (254 nm), and the bands refer to the dansylated standards of Put, Spd and Spm (Sigma, St Louis, MO, USA). The bands were scraped off the plate and redissolved in 800 μl acetone. The samples were shaken and centrifuged at 6000 *g* for 3 min, and 500 μl of this solution were quantified at 365 nm (excitation) and 510 (emission) with a high resolution spectrofluorimeter (SFM 25, Kontron Instruments, Zurich, Switzerland).

Tracer experiments

Cell masses obtained from germlings grown in the medium containing glycerol, glycerol + 1 m*M* DFMO and glycerol + 0.01 m*M* DFMO, were transferred for 20 h to PES medium (300 μl) with 70 kBq [U-^{14}C]-glycerol (0.75 m*M* final concentration of glycerol in the medium) ± DFMO in the same concentration as in the culture medium where they came from. After 20 h of incubation, the plant material was separated from the culture medium, washed with autoclaved SW and frozen at −20°C until PA analysis. It was necessary to pool the extract from the 3 replicates to obtain significant radioactivity in the PA bands over the background signal after dansylation and TLC procedures. Ra-

Table 1. PAs in 3 species of marine macrophytes as amounts (μg g^{-1} FW) from the whole thallus in samples of algae collected in nature (data are from 16 to 20 replicates, means ± SE. Put = putrescine, Spd = spermidine, Spm = spermine).

PAs		*Dictyota dichotoma* (brown alga)	*Gelidium canariensis* (red alga)	*Grateloupia doryphora* (red alga)
Free	Put	81 ± 2	134 ± 2	62 ± 2
	Spd	0.33 ± 0.01	0.43 ± 0.02	0.75 ± 0.02
	Spm	0.23 ± 0.01	1.81 ± 0.04	0.62 ± 0.03
Bound TCA-insoluble	Put	1667 ± 226	1998 ± 39	2624 ± 33
	Spd	7.2 ± 0.7	4.0 ± 0.2	4.3 ± 0.1
	Spm	4.1 ± 0.5	6.0 ± 0.3	5.8 ± 0.2

dioactivity in the Put, Spd and Spm bands was determined by liquid scintillation counting using Formula-989 (NEN, Boston, MA, USA) as scintillant. The experiment was repeated twice with essentially the same results.

Histology

Specimens of cell masses obtained from germlings grown in the medium containing glycerol were fixed with 2.5% glutaraldehyde in 0.1 *M* sodium cacodylate buffer containing 0.3 *M* NaCl (pH 7.4) for 4 h at room temperature. The specimens were then washed in the same buffer containing 0.3 *M* NaCl (2 × 30 min) and embedded in glycol methacrylate (GMA, Historesin TM). Serial sections, 5 μm thick, were cut on a Reichert–Jung 2050 microtome and stained with toluidine blue for observation of cell division.

Statistics

Mann-Whitney U-Wilcoxon Rank Sum test provided with the SPSS 5.1 (SPSS Inc. Chicago, IL, USA) statistic analysis software was performed to detect mean differences among treatments.

Results

The levels of PAs in the algal samples are shown in Table 1. Significant amounts of PAs were found in the free and bound TCA-insoluble fractions. There was always more of Put in both the free and the bound fractions, followed by almost the same amounts of Spd and Spm. The highest concentration of the 3 PAs was found in the TCA-insoluble fraction, which may have 50 times the amount in the free fraction.

No significant differences were obtained between collected thalli samples of *G. doryphora* and axenic sporelings cultivated for a week in PES medium without glycerol. In contrast, significant differences ($0.01 < P < 0.05$) in PAs were observed when the sporelings were cultivated in glycerol as a carbon source, as compared to the collected samples (Table 2). This accumulation of PAs matched the expected intense cell division and accumulation of substances within the cells of the sporelings growing in glycerol during the formation of the cell mass (Fig. 1A,B).

The results for sporelings cultivated in medium containing glycerol and glycerol + DFMO are shown in Table 3 and Fig. 1C,D. In 20 h of incubation in the presence of 70 kBq of radioactive glycerol, up to 0.022% of the radioactivity was encountered in the Put, Spd and Spm TLC bands of the extract from the sporelings cultivated in medium containing glycerol without DFMO. The addition of DFMO caused a decrease in the GR of the sporelings that could be seen under the stereomicroscope (Fig. 1B–D) and by the diminution of the radioactivity accumulated in PAs.

Discussion

The present results (Table 1) show the presence of Put, Spd and Spm in the marine algae studied. These results add to previous reports on the presence of PAs in other macroalgal species (Badini et al. 1994, Lee 1998) and our recent results for the marine seagrass *Cymodocea nodosa* (Marián et al. 2000). In all cases, the concentrations were within the range commonly found for PAs in higher plants (Harkess et al. 1992, Biondi et al. 1993).

In vitro, cell division transformed the sporelings of *G. doryphora* cultivated in medium containing glycerol into morphogenetic cell masses in 7 days (Garcia-Jiménez et al. 1996 and Fig. 1A,B in the present paper). The results in Table 2 suggest that the events leading to growth and morphogenesis in the sporelings might be related to a significant accumulation of PAs. The cells of *G. doryphora* metabolize glycerol which increased the respiration rate and biosynthetic activity (Robaina et al. 1995, Garcia-Jiménez et al. 1996). Therefore, PA accumulation could be simply due to the extra carbon and energy provided under heterotrophic conditions. Our results agree with those of Hamana

Table 2. PAs (μg g^{-1} FW) in sporelings of *G. doryphora* grown in culture medium with or without glycerol as a carbon source (data are from 10 to 20 replicates), compared with the results for the whole thallus as a reference (also given in Table 1). Mean ± SE; NS = not significant ($P > 0.05$); * = $0.05 \geq P > 0.01$.

PAs		Thallus	Sporelings – glycerol
Total	Put	2247 ± 149	2359 ± 712 NS
	Spd	12.2 ± 2.6	25.9 ± 2.4 NS
	Spm	3.5 ± 1.6	6.6 ± 2.4 NS
		Thallus	Sporelings + glycerol
Free	Put	62 ± 2	172 ± 6*
	Spd	0.75 ± 0.02	1.87 ± 0.1*
	Spm	0.62 ± 0.03	1.32 ± 0.03*
Bound TCA-insoluble	Put	2624 ± 33	5063 ± 81*
	Spd	4.3 ± 0.1	5.7 ± 0.2 NS
	Spm	5.8 ± 0.2	9.2 ± 0.2*

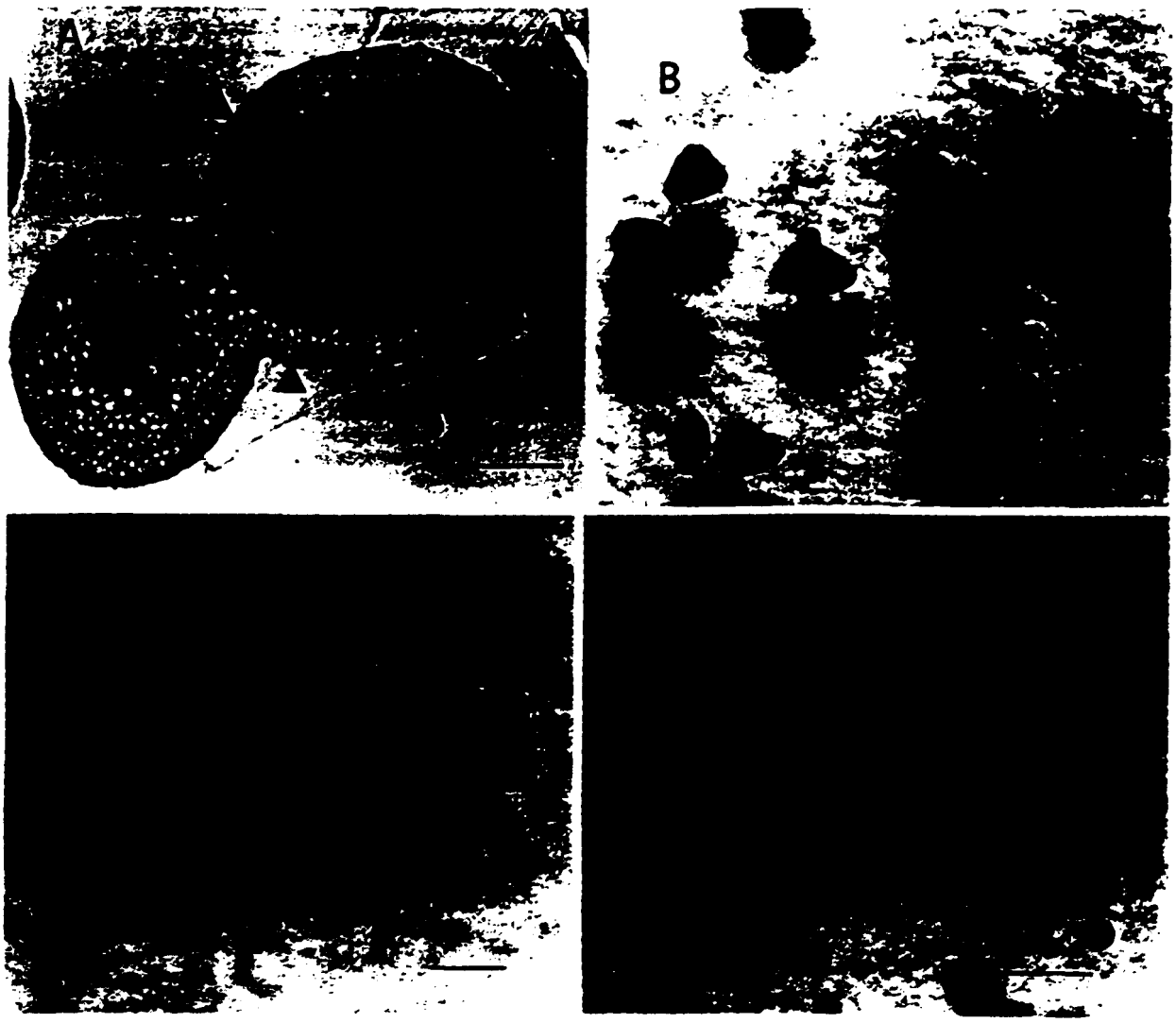

Fig. 1. (A) Cell mass derived from sporelings cultivated for 7 days in medium containing glycerol. Note cellular division (arrowheads) and the biosynthetic activity (arrows on floridean starch grains. (B–D) Sporelings cultivated in medium containing glycerol (B), glycerol + 0.01 m*M* DFMO (C) and glycerol + 0.1 *M* DFMO (D). Scale bar is 0.1 cm.

et al. (1990), for *Cyanidium caldarium* grown with or without glucose.

According to Galston et al. (1997), PAs are synthesized Put, which is formed from decarboxylation of arginine or ornithine. As shown in Table 3 and Fig. 1C,D, the addition of DFMO, an inhibitor of ornithine decarboxylase, inhibits the growth and morphogenesis promoted by glycerol. In contrast, DFMO apparently had no effect on growth of sporelings cultivated in medium without glycerol (results not shown).

Villanueva et al. (1980) reported for *Euglena gracilis* that the highest accumulation of radioactivity in Put was obtained when the cells were fed radioactive ornithine (48% of total radioactivity), followed by arginine (2.4%). The results in Table 3 show that glycerol does not seem to be a direct precursor of PA synthesis (only 0.02% of the radioactivity), at least when compared with ornithine or arginine.

In conclusion, Put, Spd and Spm have been found in several marine red and brown algae in concentrations similar to those

Table 3. Specific GR and radioactivity in Put, Spd and Spm after incubation of sporelings of *G. dorypbora* for 20 h in 70 kBq [U-^{14}C]-glycerol (0.75 m*M*) ± DFMO. Culture media were 0.1 *M* glycerol + DFMO (0.01 and 1 m*M*) and 0.1 *M* glycerol without inhibitor (+ glycerol – DFMO). Growth data are from 3 to 5 replicates. Radioactivity data are (cpm in parentheses) from the pooled extract of 3 replicates. All comparisons are as percentage of result in medium without inhibitor.

	+ Glycerol – DFMO	+ Glycerol + DFMO 0.01 m*M*	+ Glycerol + DFMO 1 m*M*
Specific GR (% day^{-1})	100 (9.2 ± 2.8)	74	2
Radioactivity in tissue as PAs (%)	100 (0.022)	86	72
Put	100 (244)	89	67
Spd	100 (150)	80	80
Spm	100 (229)	125	75

reported for terrestrial plants. In vitro, the culture of sporelings of *G. doryphora* in medium containing glycerol promoted an increase in endogenous PA levels. The effects of glycerol on growth were inhibited by the addition of DFMO which also inhibited the transformation of glycerol into PAs.

Acknowledgements – Thanks are due to Prof. A. Tiburcio for his help and technical advice that allowed us to carry out these experiments. DFMO was kindly provided by Dr Marton (University of Wisconsin, USA). This work was supported by the government of the Canary Islands (PI1998/079). The fellowship of the Spanish Plan de Formación de Personal Investigador to F. D. Marián is also acknowledged.

References

Badini L, Pitocchi R, Bagni N (1994) Polyamine transport in the seaweed *Ulva rigida* (Chlorophyta). J Phycol 30: 599–605

Biondi S, Hagège D, Rosini P, Bagni N (1993) Polyamine metabolism and ethylene synthesis in normal and habituated sugar beet callus. Physiol Plant 89: 699–706

Cohen E, Shoshana A, Heimer YH, Mizrahi Y (1984) Polyamine biosynthetic enzymes in the cell cycle of *Chlorella*. Plant Physiol 74: 385–388

Evans LV, Malmberg RL (1989) Do polyamines have a role in plant development? Annu Rev Plant Physiol Plant Mol Biol 40: 235–269

Galston AW, Kaur-Sawhney R, Altabella T, Tiburcio AT (1997) Plant polyamines in reproductive activities and response to abiotic stress. Bot Acta 110: 197–207

Garcia-Jiménez P, Robaina RR, Luque A, Tsekos I (1996) Glycerol activated cellular division and biosynthetic activity during growth and morphogenesis of carpospore seedlings of *Grateloupia doryphora* (Cryptonemiales, Rhodophyta). Phycologia 35: 261–269

Garcia-Jiménez P, Rodrigo M, Robaina RR (1998) Influence of plant growth regulators, polyamines and glycerol interaction on growth and morphogenesis of carposporelings of *Grateloupia doryphora* cultured in vitro. J Appl Phycol 10: 95–100

Hamana K, Matsuzaki S, Niitsu M, Samejima K, Nagashima H (1990) Polyamines of unicellular thermoacidophilic red alga *Cyanidium caldarium*. Phytochemistry 29: 377–380

Harkess R, Lyons RE, Kushad M (1992) Floral morphogenesis in *Rudbeckia hirta* in relation to polyamine concentration. Physiol Plant 86: 575–582

Lee TM (1998) Investigations of some intertidal green macroalgae to hyposaline stress: Detrimental role of putrescine under extreme hyposaline conditions. Plant Sci 138: 1–8

Marián FD, Garcia-Jiménez P, Robaina RR (2000) Polyamine levels in the marine seagrass *Cymodocea nodosa*. Aquat Bot (in press)

Provasoli L (1968) Media and prospects for the cultivation of marine algae. In: Watanabe A, Hattori A (eds) Cultures and Collection of Algae. Japanese Society of Plant Physiologists, Tokyo, pp 63–67

Robaina RR, Garcia-Reina G, Luque A (1990a) The effects of the physical characteristics of the culture medium on the development of red seaweeds in tissue culture. Hydrobiologia 204/205: 137–142

Robaina RR, Garcia-Jiménez P, Brito I, Luque A (1990b) Morphogenetic effect of glycerol on tissue culture of the red seaweed *Grateloupia doryphora*. J Appl Phycol 2: 137–143

Robaina RR, Garcia-Jiménez P, Brito I, Luque A (1995) Light control of the respiration of exogenous glycerol by the red macroalga *Grateloupia doryphora*. Eur J Phycol 30: 81–86

Scoccianti V, Bagni N (1992) In vitro interactions between polyamines and isolated *Porphyridium* sp. polysaccharides. Plant Physiol Biochem 30: 135–138

Scoccianti V, Bagni N, Dubinsky O, Arad S (1989) Interaction between polyamines and cells of the marine unicellular red algae *Porphyridium* sp. Plant Physiol Biochem 27: 899–904

Smith TA (1985) Polyamines. Annu Rev Plant Physiol 36: 117–143

Tiburcio AF, Campos JL, Figueras X, Besford RT (1993) Recent advances in the understanding of polyamine functions during plant development. Plant Growth Regul 12: 331–340

Villanueva VR, Adlakha R, Calvayrac R (1980) Biosynthesis of polyamines in *Euglena gracilis*. Phytochemistry 19: 787–790

Edited by P. Nissen

ELSEVIER

Aquatic Botany 68 (2000) 179–184

Aquatic botany

www.elsevier.com/locate/aquabot

Short communication

Polyamine levels in the seagrass *Cymodocea nodosa*

Fernando D. Marián*, Pilar Garcia-Jimenez, Rafael R. Robaina

Biology Department, University of Las Palmas Gran Canaria, 35017, Las Palmas G.C., Gran Canaria (Canary Islands), Spain

Received 30 July 1999; received in revised form 18 January 2000; accepted 16 May 2000

Abstract

The levels of the polyamines putrescine, spermidine and spermine were analysed in different tissues of nature-collected samples of the seagrass *Cymodocea nodosa*. The highest accumulation of polyamines was found in the apical section of the rhizome. The putrescine/spermine ratio was highest in the senescent tissue of the leaf.

Keywords: *Cymodocea nodosa*; Polyamine levels; Putrescine; Spermidine; Spermine

1. Introduction

Polyamines (PAs) are organic molecules with two or more aminic groups that act as polycations inside the cell (Evans and Malmberg, 1989; Flores, 1990). Polyamines can be bound to a variety of molecules and/or to cellular membranes; they are also found in the free state inside the cell (Torrigiani and Scoccianti, 1995). The diamine putrescine (put), and the PAs spermidine (spd) and spermine (spm) are common amines found in animals or plants. Their ubiquitous nature has been well reported before (Tabor and Tabor, 1984; Lee and Chu, 1992; Altman and Levin, 1993).

These molecules play an active metabolic role that has already been studied in terrestrial plants; they are involved in the regulation of plant growth and stress, they affect the pollen grain maturation and germination, and are also related to plant flowering (Smith, 1985; Evans and Malmberg, 1989; Harkess et al., 1992; Chibi et al., 1994; Rey et al., 1994; Das et al., 1995). Nevertheless, considering that PAs have effects similar to those of plant growth regulators (PGRs, Tiburcio et al., 1993), little is known about the incidence of PAs

* Corresponding author. Tel.: +34-28-452904; fax: +34-28-452922.
E-mail address: fmarian@biologia.ulpgc.es (F.D. Marián).

0304-3770/00/$ – see front matter
PII: S0304-3770(00)00111-X

in seagrass. Indeed, only a few studies on the effect of PGRs over their development and growth have been published in recent years (Loquès et al., 1990; Bird and Jewett-Smith, 1994; Terrados, 1995; Balestri et al., 1998). In the present work, we analyse the distribution of endogenous PAs levels over different tissues of the seagrass *Cymodocea nodosa*.

2. Materials and methods

2.1. Plant material

Several plagiotropic sprigs of *Cymodocea nodosa* (Ucria) Arscherson were collected by SCUBA at a depth of 15 m from the same meadow at Gando Bay (Gran Canaria, Canary Islands) between the end of July and August 1998, and transported to the laboratory for an assessment of endogenous PA levels. Four types of plant parts were cleaned and tested: rhizomes, roots, blades and apical sections.

2.2. Extraction and dansylation of polyamines

The method followed was a modification of those of Biondi et al. (1993), and Gallardo et al. (1994).

C. nodosa tissue was ground in a small mortar with cold 5% trichloro-acetic acid (TCA) and centrifuged at $1500 \times g$ for 15 min. The supernatant containing free acid-soluble and bound acid-soluble PAs and the pellet with the bound acid-insoluble were separated. Half of the supernatant volume was kept frozen for the subsequent dansylation of the free PA fraction. The whole pellet, and 50 μl of the supernatant, were hydrolysed in separated sealed vials with 300 μl of 12 M HCl each for 20 h at 100°C to analyse the bound fraction. After hydrolization was completed, the samples were filtered, dried and redissolved in 300 μl of 5% TCA to be dansylated. In the dansylation process, 45 μl of the sample were mixed with 45 μl of a saturated solution of Na_2CO_3 and 90 μl of dansyl chloride (5 mg/ml acetone). The dansylation reaction lasted for 10 min at 70°C. Afterwards, 25 μl of an aqueous proline solution (100 mg/ml) was added to react for 30 min at darkness with the excess of dansyl chloride. When the reaction was completed 500 μl of toluene were mixed with the samples, well shaken and then left till the two phases (organic and aqueous) separated. The organic phase, containing the PAs, was then transferred to another vial, dried in a heat-speed vacuum and the residual dissolved in 600 μl of acetone.

2.3. Separation and quantification of the PAs

The dansyl-PAs were separated with TLC on 7.5 cm × 2.5 cm plates (Schleicher&Schuell, F1500/LS, 254). The mobile phase used was a chloroform/triethylamine 5:1 mixture (v/v). The chromatography lasted for about 10 min on closed recipients. The plates were revealed under UV light (254 nm), so the put (Rf 2.5 cm), spd (Rf 1 cm) and spm (Rf under the front) bands were visible by identification of bands with those of pure standards treated in the same way. Sigma provided all the standards. These bands were scraped off from the plate and redissolved with 800 μl of acetone. The samples were shaken and centrifuged

at 6000×*g* for 3 min, and quantified at 365 nm (excitation) and 510 nm (emission) with a high-resolution spectrofluorimeter (SFM 25, Kontron Instruments).

2.4. Statistics

The Mann–Whitney test provided with SPSS 6.1.3 (SPSS, Chicago, IL) was performed to detect differences in PA levels between the apical zone of the rhizome and the rest of the plant (leaves, roots and rhizome PA levels were set together). The Bonferroni's correction to the experimentwise error rate (5%) was applied to reduce the error rate in such a set of multiple comparisons.

3. Results

3.1. Endogenous PAs levels

The most remarkable result is the high levels of PAs in the bound acid-soluble fraction (Table 1). The levels of bound acid-insoluble put are greater than those of the free fraction, but this changes, except for the spm of the leaves, with the other two diamines where the free spd and free spm amounts are greater. But these differences are smaller than when comparing the bound acid-soluble fraction with the other two fractions. Among tissues, the distribution of PAs was quite similar.

The highest amounts of free PAs were found in the apical zone of the rhizome whilst the root tissue had the lowest amounts of PAs. The apical section had four times the amount of put and spd of leaves and rhizome, and eight times the amount of roots. This pattern changed for the spm levels, 10 times the amount measured for leaf and root was found in the apical section, and only three times as much as in the rhizome.

For the bound acid-soluble and acid-insoluble PAs, again the apical meristem had, on average, for the three PAs, approximately a factor 10 as much as roots and rhizomes, but only three times the amount of leaves.

The apical section of the rhizome always had a significantly higher amount of PAs when compared with the rest of the plant. This result was the same for every PA on each PA fraction (Table 1).

4. Discussion

PAs are related to a number of development events that take place in higher plants, and a high cell-division activity is well correlated with the presence of significant amounts of endogenous PAs (Smith, 1985). Although there are no references about PAs in other seagrasses, the values reported for *C. nodosa* in this work fall within the range of those cited for terrestrial plants (Egea-Cortines et al., 1993; Gallardo et al., 1994; Rey et al., 1994; Pedroso et al., 1997). The highest amounts of PAs (free and bound fraction) are found in the apical section of the rhizome, where the highest growing activity for *C. nodosa*

Table 1
Free and bound polyamine levels (nm g^{-1} FW) in samples from different plant parts of *Cymodocea nodosa*[a]

	Free[b,e]			Bound-soluble[c,e]			Bound-insoluble[d,e]		
	put	spd	spm	put	spd	spm	put	spd	spm
Leaf	403±11	5.7±0.2	0.8±0.1	9250±784	17±0.07	24±2.45	2541±215	1.44±0.07	3.24±0.29
Root	199±8	2.5±0.1	1.03±0.15	2184±113	5.82±0.07	5.29±0.05	622±33	0.48±0.07	0.78±0.05
Rhizome	402±20	4.9±0.2	3.33±0.54	3522±136	6.1±0.68	5.64±0.05	1014±41	0.48±0.68	0.83±0.05
Apical zone	1583±147[f]	19±1.4[f]	9.17±0.49[f]	25886±488[f]	35±2.05[f]	63±2.99[f]	7530±136[f]	3.29±0.14[f]	8.43±0.39[f]

[a] Experimentwise error rate is 0.05. Comparison error rate is experimentwise error rate/number of comparisons (Bonferroni's correction). Data are mean±s.e. from 4–10 replicates.

[b] Free acid-soluble PAs.

[c] Free acid-soluble plus bound acid-soluble PAs.

[d] Bound acid-insoluble PAs.

[e] Put, putrescine; spd, spermidine; spm, spermine.

[f] Significant differences between apical zone and the rest of the plant ($p<0.0056$).

is expected. Cells in constant division and differentiation were found within the apical meristem (results not shown). Our low levels in roots are in accordance with Larkum et al. (1989).

The absolute endogenous values of PAs given for a particular plant show little information about their physiological role since there is a wide range of PAs levels found in current literature. Other authors have already used the ratios between PAs to understand their role in the development of plant tissues (Rey et al., 1994). If we consider the put/spd and put/spm ratios among tissues, they remain steady in both the free and bounded fractions, except for the free put/spm ratio on the leaf tissue, which was three times higher than in other tissues. This is a relative decrease of free spm in *C. nodosa* leaves, shown in the increase of the put/spm and spd/spm ratios. The diamine spm has been identified as an anti-senescence-inducing factor (Galston et al., 1997), thus, this accumulation of put relative to spm could be the factor promoting the senescence of the leaf. At the time of the year when the samples were collected (August), the meadow generally starts to lose leaves after reaching its biggest area. Previously, Rey et al. (1994) reported this accumulation of put in plant tissue as an indicator of senescence. The endogenous bound-PAs ratios give little information as the physiological function of this fraction is unknown (Slocum and Galston, 1985).

In conclusion, we report the presence of PAs in *C. nodosa*, a common Mediterranean seagrass, to be within the range for terrestrial plants, and their differential distribution among tissues. We found the highest levels in the meristematic tissue of the rhizome, where the greatest growing activity occurs. A possible senescence process identified in the leaf tissue is correlated with a relative accumulation of free put.

This work was partially financed by a grant from the Canarian Government, PI1998/079. We also thank the Spanish Ministry of Education and Culture for fellowship to Fernando D. Marian.

References

Altman, A., Levin, N., 1993. Interactions of polyamines and nitrogen nutrition in plants. Physiol. Plant. 89, 653–658.

Balestri, E., Piazzi, L., Cinelli, F., 1998. In vitro germination and seedling development of *Posidonia oceanica*. Aquat. Bot. 60, 89–93.

Biondi, S., Hagège, D., Rossini, P., Bagni, N., 1993. Polyamine metabolism and ethylene biosynthesis in normal and habituated sugar beet callus. Physiol. Plant. 89, 699–706.

Bird, K.T., Jewett-Smith, J., 1994. Development of a medium and culture system for in vitro propagation of the seagrass *Halophila engelmannii*. Can. J. Bot. 72, 1503–1510.

Chibi, F., Mantilla, A.J., Angosto, T., Garrido, D., 1994. Changes in polyamine synthesis during anther development and pollen germination in tobacco (*Nicotiana tabacum*). Physiol. Plant 92, 61–68.

Das, S., Bose, A., Ghosh, B., 1995. Effect of salt stress on polyamines metabolism in *Brassica campestris*. Phytochemistry 39, 283–285.

Egea-Cortines, M., Cohen, E., Arad, S., Bagni, N., Mizrahi, Y., 1993. Polyamine levels in pollinated and auxin-induced fruit tomato (*Lycopersicon esculentum*) during development. Physiol. Plant. 87, 14–20.

Evans, P.T., Malmberg, R.L., 1989. Do polyamines have roles in plant development? Ann. Rev. Plant Physiol. Plant Mol. Biol. 40, 235–269.

Flores, H.E., 1990. Polyamines and plant stress. In: Alscher, R.G., Cumming, J.R. (Eds.), Stress Responses in Plants: Adaptation and Acclimation Mechanisms. Wiley–Liss, New York, pp. 217–239.

Gallardo, M., Gallardo, M.E., Mantilla, A.J., Muñoz de Rueda, P., Sánchez-Calle, I.M., 1994. Inhibition of polyamine synthesis by cyclohexylamine stimulates the ethylene pathway and accelerates the germination of *Cicer arietinum* seeds. Physiol. Plant. 91, 9–16.

Galston, A.W., Kaur-Sawhney, R., Altabella, T., Tiburcio, A.T., 1997. Plant polyamines in reproductive activity and response to abiotic stress. Bot. Acta 110, 197–207.

Harkess, R.L., Lyons, R.E., Kushad, M.M., 1992. Floral morphogenesis in *Rudbeckia hirta* in relation to polyamine concentration. Physiol. Plant. 86, 575–582.

Larkum, A.W.D., McComb, A.J., Shepherd, S.A., 1989. Biology of Seagrasses: A Treatise on the Biology of Seagrasses with Special Reference to the Australian Region. Elsevier, Amsterdam.

Lee, T-M., Chu, C., 1992. Ethylene-induced polyamine accumulation in rice (*Oryza sativa L.*) coleoptiles. Physiol. Plant. 100, 238–245.

Loquès, F., Caye, G., Meinesz, A., 1990. Axenic culture of selected tissue of *Posidonia oceanica*. Aquat. Bot. 37, 171–188.

Pedroso, M.C., Primikirios, N., Roubelakis-Angelakis, K.A., Pais, M.S., 1997. Free and conjugated polyamines in embriogenic and non-embriogenic leaf regions of camellia leaves before and during direct somatic embriogenesis. Physiol. Plant. 101, 213–219.

Rey, M., Díaz-Sala, C., Rodríguez, R., 1994. Comparison of endogenous polyamine content in hazel leaves and buds between the annual dormancy and flowering phases of growth. Physiol. Plant 91, 45–50.

Slocum, R., Galston, A.W., 1985. In vivo inhibition of polyamine biosynthesis and growth in tobacco ovary tissues. Plant Cell Physiol. 26, 1519–1526.

Smith, T.A., 1985. Polyamines. Ann. Rev. Physiol. 36, 117–143.

Tabor, C.W., Tabor, H., 1984. Polyamines. Ann. Rev. Biochem. 53, 749–790.

Terrados, J., 1995. Effects of some plant growth regulators on the growth of the seagrass *Cymodocea nodosa* (Ucria) Ascherson. Aquat. Bot. 51, 311–318.

Tiburcio, A.F., Campos, J.L., Figueras, X., Besford, R.T., 1993. Recent advances in the understanding of polyamine functions during plant development. Plant Growth Regulation 12, 331–340.

Torrigiani, P., Scoccianti, V., 1995. Regulation of cadaverine and putrescine levels in different organs of chick-pea seed and seedlings during germination. Physiol. Plant 93, 512–518.

ELSEVIER

Aquaculture 179 (1999) 523–534

Aquaculture

Dietary and culture influences on macrophage aggregate parameters in gilthead seabream (*Sparus aurata*) juveniles

D. Montero [a,*], V.S. Blazer [b], J. Socorro [c], M.S. Izquierdo [c], L. Tort [d]

[a] *Instituto Canario de Ciencias Marinas, Gobierno de Canarias, P.O. Box 56, 35200, Telde, Las Palmas, Canary Islands, Spain*

[b] *U.S. Department of the Interior, National Biological Service, National Fish Health Laboratory, 1700 Leetown Road, Kearneysville, WV 25430, USA*

[c] *Departamento de Biología, Universidad de Las Palmas de Gran Canaria, Campus Universitario de Tafira, 35017, Las Palmas de Gran Canaria, Canary Islands, Spain*

[d] *Departamento de Biología Celular y Fisiología, Facultad de Ciencias, Universidad Autónoma de Barcelona, 08193, Cerdanyola, Barcelona, Spain*

Abstract

Macrophage aggregates (MAs) are structures in the spleen, kidney and sometimes liver of fishes which have various functions such as recycling/storing/detoxification of cellular wastes and exogenous substances. They have been also reported to be important in the specific immune response and are used as health indicators. Changes in MA density, size and pigment content have been used in national and local monitoring programs in the U.S. as indicators of contaminant exposure. However, MA number and structure can also be affected by other factors, including general stress or nutritional status of fish. An experiment was conducted to study the effects of vitamin E and $n-3$ highly unsaturated fatty acid (HUFA) deficiencies and stocking density on spleen and kidney MAs of gilthead seabream, one of the most important species for Mediterranean aquaculture. Fish were held at two stocking densities, high and low, and fed experimental diets. Diet NE had no supplemental vitamin E, Diet NFA was deficient in $n-3$ HUFA and Diet C was a control diet. Number, size and shape factor of MAs were measured using image analysis. The percentage of tissue occupied by MAs was calculated from these measurements. The results showed that high stocking density alone increased the number of splenic but not kidney MAs of fish fed the control diet. A deficiency of $n-3$ HUFA alone also increased the number of splenic

* Corresponding author. Tel.: +34-928-132-900; Fax: +34-928-132-908; E-mail: dmontero@iccm.rcanaria.es

0044-8486/99/$ - see front matter
PII S0044-8486(99)00185-4

but not kidney MAs at both stocking densities. Vitamin E deficiency alone had no significant effect on MAs in either organ. However, the combined effect of vitamin E deficiency and high stocking density increased the number and size of kidney but not splenic MAs. This study indicates that specific dietary deficiencies can influence MA accumulation and that splenic MAs may be more responsive to general stress than kidney MAs.

Keywords: Macrophage aggregates; $n-3$ HUFA; Vitamin E; Stress; *Sparus aurata*

1. Introduction

Macrophage aggregates (MAs) (also named melano-macrophage centres) are focal accumulations of pigment-containing macrophages found in the spleen, hemopoietic tissues of kidney and sometimes liver of fishes. These structures have been shown to play a role in the immune response, including humoral and inflammatory responses; storage, destruction or detoxification of exogenous and endogenous substances; and iron recycling (Wolke, 1992). Pigments related with these functions are found within MAs. Hemosiderin, related with iron storage and recycling; lipofucsin and ceroid, derived from peroxidation of cells and organelles; and melanin which may function in the hosts' defense mechanisms (Roberts, 1975; Agius and Agbede, 1984; Brown and George, 1985) can all be visualized within MAs.

MAs have been suggested as histologic (Hinton et al., 1992) and immunologic (Weeks et al., 1992) piscine biomakers of contaminant exposure or environmental stress. There are many observations suggesting a correlation between toxic substances and MAs alterations, such as size, number or pigment content (Herraez and Zapata, 1986; Kranz and Gerken, 1987; Macchi et al., 1992; Blazer et al., 1997). MA number and structure may also be affected by infectious disease states (Herraez and Zapata, 1987; Vogelbein et al., 1987; Kranz, 1989) and starvation (Agius and Roberts, 1981; Micale and Perdichizzi, 1990). We are not aware of any studies which have specifically examined nutritional effects on MA parameters. There is, however, much evidence that piscine macrophage function is influenced by certain nutrients (review by Blazer, 1991). Also, increases in macrophages containing various pigments have been observed throughout certain tissues as a consequence of nutritional problems such as oxidized/rancid fat and vitamin E deficiencies (Smith, 1979; Blazer and Wolke, 1983; Moccia et al., 1984; Wada et al., 1989, 1991).

There is also evidence that aquaculture-related stressful situations affect macrophage functions (Scott and Klesius, 1981; Angelidis et al., 1987; Pegg and Iwama, 1996). However, again there are few studies concerning potential culture stressors on MAs. Blazer et al. (1987) found an increase on liver MAs number in black bass (*Micropterus salmoides*) under heat stress conditions and Patti and Micale (1993) found an effect of photoperiod in the density of splenic MAs of *Pagellus bogaraveo*. Hence, the aim of this study was to investigate the effects of vitamin E and $n-3$ highly unsaturated fatty acid ($n-3$ HUFA) nutritional deficiencies, with and without crowding stress, on MAs of gilthead seabream, one of the most important marine fish species for Mediterranean aquaculture.

2. Materials and methods

The experiment was carried out at the Instituto Canario de Ciencias Marinas of the Government of Canary Islands, with gilthead seabream (*Sparus aurata*) juveniles. MA analyses were conducted at National Fish Health Research Laboratory, Leetown, WV.

2.1. Experimental procedures

One thousand, two hundred and sixty gilthead seabream (22 g mean body weight) supplied by a local farm (ADSA, San Bartolome de Tirajana, Canary Islands, Spain), were randomly distributed among 18 circular fiberglass tanks. Each tank was filled with 250 l of seawater and was provided with water supply at a rate of 4.0 l/min. Dissolved oxygen ranged between 6.2 and 10.5 mg/l during the experimental period. Water temperature ranged between 19.02 and 22.45°C, and natural light illuminated the tanks with a light cycle close to 12 h light/12 h dark. One hundred and ten fish per tank were randomly stocked in nine of these tanks for the high stocking density (initial density 10.56 kg/m^3), and 30 fish per tank were randomly distributed in the remaining nine tanks for the low stocking density (initial density 2.64 kg/m^3).

2.2. Experimental diets

The composition of the experimental diets is shown in Table 1. Pelleted diets were prepared with the same proximal composition and supplemented respectively with 150

Table 1
Composition of the experimental diets

Ingredients (% dry weight)	Diet		
	C	NE	NFA
Sardine meal	67.91	67.91	19.53
Oil extracted sardine meal	–	–	43.36
Sardine oil	0.96	0.96	–
Beef tallow	3.96	3.96	9.98
Starch	12	12	12
Dextrin	4	4	4
α-Cellulose	6.5	6.5	6.5
CMC[a]	0.5	0.5	0.5
Vitamin mix[b]	2	2	2
Mineral mix[c]	1.3	1.3	1.3
Choline chloride	0.9	0.9	0.9
α-tocopherol (mg/kg diet)	150	0	150

[a]Carboxymethylcellulose.
[b](mg/kg diet): retinol acetate: 25; vitamin D_3: 5; vitamin K: 20; vitamin B_{12}: 0.5; vitamin H: 1; Folic acid: 10; vitamin B_6: 40; vitamin B_1: 40; vitamin B_2: 50; pantothenic acid: 117; nicotinic acid: 200; *myo*-inositol: 2000; ascorbic acid: 5000; ethoxiquin: 100.
[c](g/kg diet): $(H_2PO_4)Ca$: 1.605; $CaCO_3$: 4.0; $FeSO_4 \cdot 7H_2O$: 1.5; $MgSO_4 \cdot 7H_2O$: 1.605; K_2HPO_4: 2.8; $Na_2PO_4 \cdot H_2O$: 1; $Al(SO_4)_3 \cdot 6H_2O$: 0.02; $ZnSO_4 \cdot 7H_2O$: 0.24; $CuSO_4 \cdot 5H_2O$: 0.12; KI: 0.02; $CoSO_4 \cdot 7H_2O$: 0.08; $MnSO_4 \cdot H_2O$: 0.08.

mg α-tocopherol/kg diet (control diet; C) and 0 mg α-tocopherol/kg diet (vitamin E deficient; NE). A third diet contained 150 mg α-tocopherol/kg diet but it was deficient in $n-3$ HUFA (NFA) (Ibeas et al., 1994) (Table 2). Each diet was fed to triplicate tanks of each stocking density.

Fish were fed twice per day at a feeding rate of 2.5% fish body weight per day, six days per week for 15 weeks. Body weight was measured at the beginning and end of the experimental period.

2.3. Blood collection and sample preparation

Fish were individually captured from each tank, ten per tank in less than eight min. Hence, fish handling time was less than 1 min per fish, to avoid capture stress effects on analyzed parameters (Pickering et al., 1982). No anaesthetic was used. Blood was obtained by caudal sinus puncture with 1 ml plastic syringe, and transferred to an Eppendorf tube coated with lithium heparin as an anticoagulant. One aliquot of blood was used for erythrocyte fragility determination and a second for plasma cortisol determination. The plasma was obtained by centrifugation at 3000 rpm for 10 min, separated and stored at −80°C. Sampled fish were not reused.

Erythrocyte fragility was determined as described by Draper and Csallany (1969) and modified by Wilson et al. (1984). This method measures the spontaneous hemolysis of erythrocytes in distilled water as compared to those incubated in phosphate buffered saline. Plasma cortisol concentrations were determined by radioimmunoassay using the trypsin–antitrypsin method described for gilthead seabream (Molinero and González, 1995). Ten fish per tank or 30 fish per treatment were used for erythrocyte fragility and cortisol assays.

2.4. Histological samples

At the end of the experiment liver, spleen and kidney of six fish from each tank (18 fish per treatment) were fixed in 10% neutral-buffered formalin. Samples were stained with hematoxylin–eosin (H&E) for histological examination (Martoja and Martoja-Pierson, 1970).

Number of MAs per square millimeter of tissue, size (μm^2), shape factor were analyzed using image analysis (MOCHA™, Jandel Scientific, San Rafael, CA, USA). The shape factor compares a given image to a perfect circle and ranges from 1 (perfect

Table 2
Proximal composition and levels of $n-3$ HUFA and vitamin E of the experimental diets

Composition (% dry weight)	Diet		
	C	NE	NFA
Crude protein	48.08	49.93	49.56
Crude lipid	12.23	12.78	12.74
Moisture	11.16	11.01	10.97
Ash	12.07	11.58	11.55
$n-3$ HUFA	1.50	1.44	0.42
α-tocopherol (mg/kg diet)	167.5	18.5	160.5

Table 3
Some biological parameters studied along the experimental period

	Initial weight (g)	Final weight (g)	Initial density (kg/m^3)	Final density (kg/m^3)	Survival (%)	Erythrocyte fragility (%)	Plasma cortisol (ng/ml)
Diet C + LD[a]	21.90 ± 2.81	82.64 ± 12.06	3.28 ± 0.03	10.04 ± 0.57	100	3.07 ± 3.01	3.91 ± 3.52
Diet C + HD	21.81 ± 2.78	85.00 ± 11.62	12.00 ± 0.12	34.01 ± 0.37	99.70	5.47 ± 17.60	16.25 ± 23.62
Diet NE + LD	21.78 ± 2.58	80.02 ± 11.67	3.27 ± 0.05	9.60 ± 0.30	100	21.26 ± 29.38	21.70 ± 26.04
Diet NE + HD	21.81 ± 2.81	81.02 ± 12.60	12.00 ± 0.12	32.40 ± 0.90	95.45	14.77 ± 23.64	16.56 ± 26.70
Diet NFA + LD	21.68 ± 2.61	73.06 ± 7.93	3.25 ± 0.04	8.77 ± 0.17	100	12.00 ± 20.58	13.86 ± 20.43
Diet NFA + HD	21.98 ± 2.75	74.34 ± 10.58	12.09 ± 0.15	28.73 ± 1.88	94.24	10.57 ± 23.88	16.36 ± 19.73
Analysis of variance							
Stocking density	n.s.	n.s.	*	*	n.s.	n.s.	*
Vitamin E in diet	n.s.	n.s.	n.s.	n.s.	n.s.	*	*
$n-3$ HUFA in diet	n.s.	*	n.s.	*	n.s.	n.s.	*
Vitamin E + density	n.s.	n.s.	n.s.	n.s.	*	n.s.	n.s.
$n-3$ HUFA + density	n.s.	n.s.	n.s.	n.s.	*	n.s.	n.s.

* Indicates significant effect at $P < 0.05$.
[a] LD: Low density; HD: High density.

circle) to 0 (Blazer et al., 1994). The percent of tissue occupied by MAs is calculated using number, size and total area of tissue examined.

A second set of slides were stained by Perl's method for iron (Luna, 1992) to qualitatively evaluate pigment distribution. With this stain, melanin appears black, hemosiderin is blue and ceroid/lipofucsin is yellow-tan.

2.5. Statistical analysis

Means and standard deviations (S.D.) were calculated for each parameter measured. All data were statistically treated using one-way ANOVA. Tukey's test for comparison of means of triplicates was applied. Student's *t*-test was used to test differences between fish held at high stocking density and low stocking density (Sokal and Rolf, 1979).

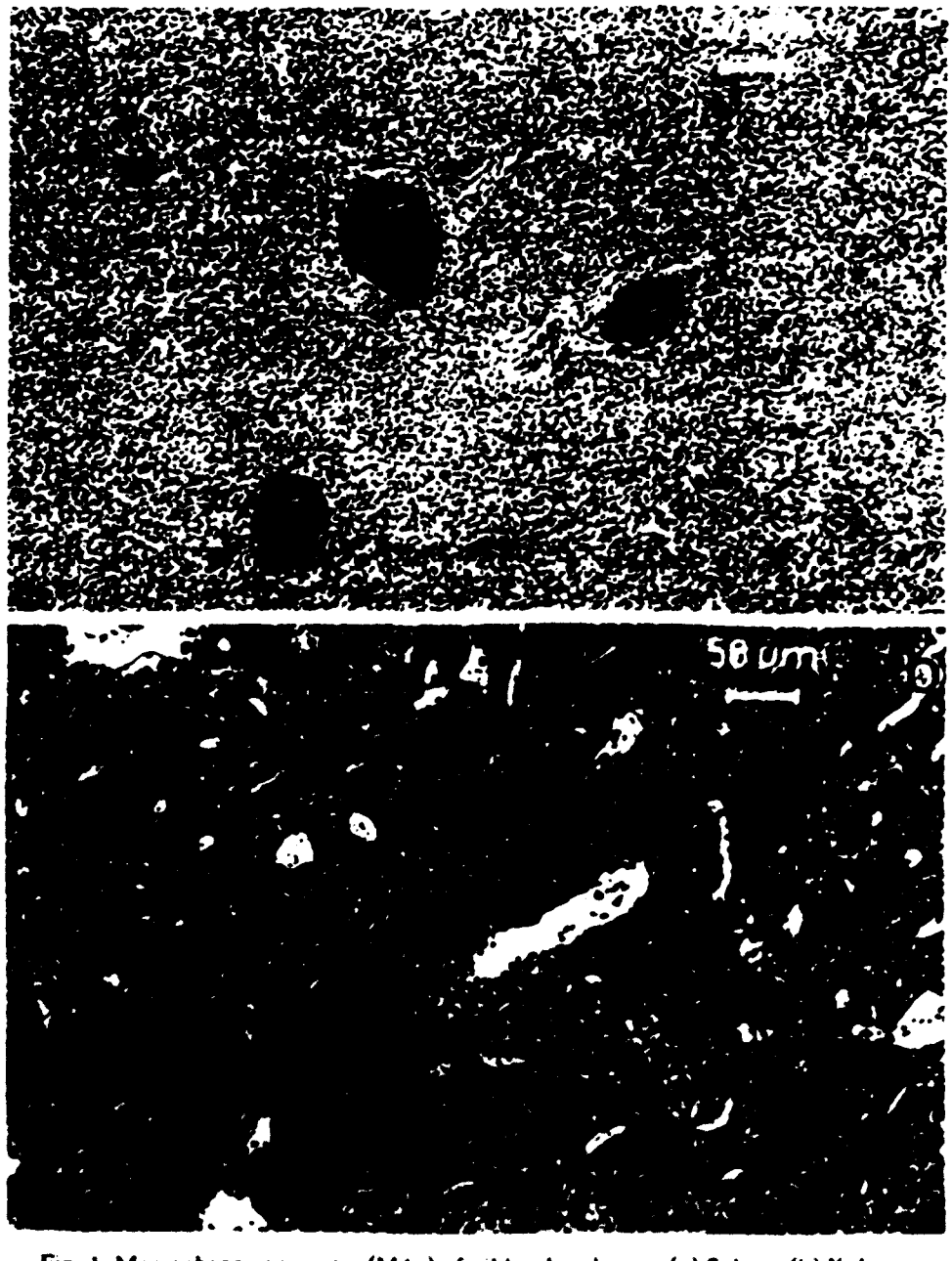

Fig. 1. Macrophage aggregates (MAs) of gilthead seabream (a) Spleen. (b) Kidney

Two-way ANOVA was applied to study combined effects of nutritional deficiencies and stocking density. In addition, correlations among erythrocyte fragility, plasma cortisol and MAs parameters were analyzed.

3. Results

All experimental diets were accepted and therefore no significant differences were found in food intake among experimental groups. A comparison of replicates indicated no significant tank effect for any parameter and so data were pooled for comparisons among treatment groups. Stocking density alone did not cause a reduction in final weight. No significant effect of vitamin E deficiency on final weight was found at either stocking density. Final fish weights and hence final stocking density were significantly reduced ($P < 0.05$) when fish were fed NFA diet at either stocking density. Neither stocking density nor nutritional deficiencies alone affected fish survival, whereas the combined effect of both factors resulted in lower percent survival (Table 3).

No statistical effect of stocking density or $n-3$ HUFA deficiency was observed on erythrocyte fragility. However, values for fish fed the $n-3$ HUFA deficient diet were intermediate between the control and vitamin E deficient fish. Vitamin E deficiency resulted in significantly higher erythrocyte fragility at both stocking densities (Table 3).

High stocking density significantly increased plasma cortisol levels in the control fish. Both nutritional deficiencies also significantly increased plasma cortisol levels at the low stocking density. No additional effect on plasma cortisol was found when nutritional deficiencies and stocking density were combined (Table 3).

MAs were found in spleen and kidney (Fig. 1). No MAs were found in liver. Stocking density produced a significant increase in number of MAs in spleen and percent of spleen occupied by MAs. Shape factor was significantly decreased and size

Table 4
MAs parameters studied in the spleen along the experimental period

	Tissue occuped (%)	MAs number ($\times mm^2$ of tissue)	MAs size (μm^2)	Shape factor
Diet C + LD[a]	0.48 ± 0.27	8.78 ± 5.15	1292.60 ± 678	0.11 ± 0.01
Diet C + HD	0.95 ± 0.57	14.39 ± 7.07	1654.19 ± 918	0.19 ± 0.08
Diet NE + LD	0.65 ± 0.38	13.44 ± 7.61	1037.58 ± 542	0.16 ± 0.06
Diet NE + HD	0.92 ± 0.56	11.88 ± 6.97	1510.92 ± 524	0.18 ± 0.07
Diet NFA + LD	1.12 ± 0.64	15.11 ± 8.33	1392.47 ± 8.33	0.18 ± 0.10
Diet NFA + HD	1.51 ± 0.66	20.75 ± 8.47	1438.37 ± 564	0.15 ± 0.07
Analysis of variance				
Stocking density	*	*	n.s.	*
Vitamin E in diet	n.s.	n.s.	n.s.	n.s.
$n-3$ HUFA in diet	*	*	n.s.	n.s.
Vitamin E + density	n.s.	n.s.	*	n.s.
$n-3$ HUFA + density	n.s.	n.s.	n.s.	n.s.

* Indicates significant effect at $P < 0.05$.
[a] LD: Low density, HD: High density.

Table 5
MAs parameters studied in the kidney along the experimental period

	Tissue occuped (%)	MAs number ($\times mm^2$ of tissue)	MAs size (μm^2)	Shape factor
Diet C + LD[a]	2.86 ± 0.80	22.66 ± 5.65	2624.88 ± 1430	0.19 ± 0.11
Diet C + HD	3.34 ± 0.82	18.17 ± 3.40	3371.29 ± 1453	0.26 ± 0.12
Diet NE + LD	3.64 ± 1.05	22.26 ± 5.44	2961.11 ± 1674	0.20 ± 0.11
Diet NE + HD	5.96 ± 0.88	24.78 ± 2.87	4438.29 ± 1678	0.22 ± 0.08
Diet NFA + LD	3.94 ± 1.02	22.26 ± 5.86	3149.21 ± 1536	0.21 ± 0.11
Diet NFA + HD	4.14 ± 0.96	21.40 ± 3.63	3323.96 ± 1271	0.25 ± 0.13
Analysis of variance				
Stocking density	n.s.	n.s.	n.s.	n.s.
Vitamin E in diet	n.s.	n.s.	n.s.	n.s.
$n-3$ HUFA in diet	n.s.	n.s.	n.s.	n.s.
Vitamin E + density	*	*	*	n.s.
$n-3$ HUFA + density	n.s.	n.s.	n.s.	n.s.

* Indicates significant effect at $P < 0.05$.
[a] LD: Low density; HD: High density.

was increased although not statistically. Vitamin E deficiency alone had no effect on splenic MAs but the combined effects of stocking density and low vitamin E levels resulted in a significantly larger splenic MAs. A deficiency of $n-3$ HUFA produced a significant increase in number and percent of spleen occupied by MAs at both stocking densities. The combination of high stocking density and $n-3$ HUFA dietary deficiency had no additional effect on splenic MAs (Table 4).

Different results were found in kidney MAs. Neither stocking density nor dietary deficiencies alone affected kidney MAs parameters. However, the combined effect of vitamin E deficiency and high stocking density significantly increased number, size and percent of kidney occupied by MAs (Table 5).

No differences were found in pigment content of MAs from fish fed different experimental diets. Seabream MAs in both tissues had large amounts of melanin which may have obscured other pigments.

4. Discussion

Most recent studies concerning MAs address their suitability as biomakers of contaminant stress (Macchi et al., 1992; Blazer et al., 1994, 1997). However, MAs are nonspecific and there are many variables potentially involved in formation and distribution of these structures (reviewed by Wolke, 1992). MAs serve as storage centers of material not only of exogenous (metals, biological agents) but also endogenous (hemosiderin, melanin, lipofucsin/ceroids) sources. Hence, it is important to understand how MA parameters may be affected by factors which alter fish metabolism indirectly (metabolic effects of stress) or directly (effects of nutritional imbalances).

High stocking density is considered an aquaculture-related chronic stressor (Vijayan and Leatherland, 1988; Barton and Iwama, 1991; Wedemeyer, 1997) leading to an elevation of plasma cortisol (Barton, 1988; Pickering and Pottinger, 1989), the main

corticosteroid in fish (Idler and Truscott, 1972). Although we did not find a strong correlation between plasma cortisol and spleen MA number ($y = 13.4 + 0.076X$; $r = 0.2324$; $P = 0.041$) when all fish were analyzed together, there was an increase in number and size of splenic MA and mean cortisol concentrations in control fish held at the high density when compared to those held at low density. On the contrary, no effects were found on kidney MAs. This suggests different roles for MAs in different tissues, which has been previously hypothesized. Kranz and Peters (1984) suggested the main function of splenic MAs of ruffe *Gymnocephalus cernua* was decomposition of effete blood cells and storage of iron. Immunological and bactericidal processes were not considered main functions of splenic MA in ruffe. However, Blazer et al. (1997) described an increase in splenic MAs in immunized striped bass when compared to nonimmunized. Hence, it may be that even among species the roles of MAs in various organs varies. Unfortunately, most studies have compared liver and spleen MAs, so little is known about kidney MA function.

The number of splenic MAs increased (although not significantly) in fish fed the vitamin E deficient diet. These fish also had increased fragility of red blood cells and hence, perhaps increased amounts of degenerating erythrocytes. Vitamin E deficiency has been reported to increase erythrocyte fragility in many species, including channel catfish (Wilson et al., 1984; Wise et al., 1993), European sea bass (Obach et al., 1993), Atlantic salmon (Hamre et al., 1994) and rainbow trout (Cowey et al., 1983; Furones et al., 1992). Vitamin E deficiency and/or rancid fats in the diet are also associated with increases in peroxidized lipids secondary to a lack of antioxidant activity (Smith, 1979; Blazer and Wolke, 1983; Moccia et al., 1984; Wada et al., 1989, 1991). Ceroid/lipofucsin, a major component of MAs, is formed from the peroxidation of cell membranes. Combined effects of dietary vitamin E deficiency and high stocking density (stress) produced an increase in MA number, size and percent tissue occupied in kidney, but not spleen. This suggests the MA of kidney may be more responsive to oxidative stress problems.

Conversely, $n-3$ HUFA deficiency statistically increased the number of MA and percentage of tissue occupied by MAs in the spleen at both stocking densities. Although fish fed NFA diet showed significantly lower growth, which is reported to be one of the most important effects of essential fatty acid deficiencies (Watanabe, 1982), we do not believe increases in MAs were due to starvation. Nutritional deficiencies of essential fatty acids and vitamin E may impair macrophage function (reviewed by Blazer, 1991) and hence increased MAs may occur due to adverse effects on the macrophages themselves. More research is required which examines immune functions, enzymes activities and other functional assays concurrently with MA development in different tissues.

In conclusion, the results of this work showed that stocking density, vitamin E and $n-3$ HUFA nutritional deficiencies produced alterations in gilthead seabream MAs, but the mechanisms are not clear. Splenic MAs appear more responsive to general stress and deficiencies of essential fatty acids than do kidney MAs. On the other hand, kidney MA were more responsive to vitamin E deficiencies. Further experiments are required to clarify the effects of stress and nutritional imbalances on MAs and to clarify their suitability as indicators of nutritional deficiencies and stress in fish.

Acknowledgements

The authors want to thank Darlene Bowling for technical assistance with the Perl's stain and Kim Jefferson for assistance with image analyses.

References

Agius, C., Roberts, R.J., 1981. Effects of starvation on the melano-macrophage centres of fish. J. Fish Biol. 19, 161–169.

Agius, C., Agbede, S.A., 1984. An electron microscopical study on the genesis of lipofucsin, melanin and haemosiderin in the hameopoietic tissues of fish. J. Fish Biol. 24, 471–488.

Angelidis, P., Baudin-Laurencin, F., Youinou, P., 1987. Stress in rainbow trout, *Salmo gairdneri*: effects upon phagocyte chemiluminescence, circulating leucocytes and susceptibility to *Aeromonas salmonicida*. J. Fish Biol. 31, 113–122, Suppl. A.

Barton, B.A., 1988. Endocrine and metabolic responses of fish to stress. Int. Assoc. Aquat. Anim. Med. Proc. 19, 41–55.

Barton, B.A., Iwama, G.K., 1991. Physiological changes in fish from stress in aquaculture with emphasis on the response and effects of corticosteroids. Annu. Rev. Fish Dis. 1, 3–26.

Blazer, V.S., 1991. Piscine macrophage function and nutritional influences. A review. J. Aquat. Anim. Health 3, 77–86.

Blazer, V.S., Wolke, R.E., 1983. Ceroid deposition, retinal degeneration and renal calcium oxalate crystals in culture clownfish. J. Fish Dis. 6, 365–376.

Blazer, V.S., Wolke, R.E., Brown, J., Powell, C.A., 1987. Piscine macrophage aggregate parameters as health monitors: effect of age, sex, relative weight, season and site quality in largemouth bass (*Micropterus salmoides*). Aquat. Toxicol. 10, 199–215.

Blazer, V.S., Facey, D.E., Fournier, J.W., Courtney, L.A, Summers, J.K., 1994. Macrophage aggregates as indicators of environmental stress. In: Stolen, J.S., Fletcher, T.C. (Eds.), Modulators of Fish Immune Responses, Vol. 1. SOS Publications, Fair Haven, pp. 169–185.

Blazer, V.S., Fournier, J.W., Weeks-Perkins, B.A., 1997. Macrophage aggregates: biomarkers for immune function in fishes? In: Dwyer, J.D., Doane, T.R., Hinman, M.L. (Eds.), Environmental Toxicology and Risk Assessment: Modeling and Risk Assessment (Sixth Volume), ASTM STP 1317. American Society for Testing and Materials, pp. 360–375.

Brown, C.L., George, C.T., 1985. Age-dependent accumulation of macrophage aggregates in the yellow perch *Perca flavescens* (Mitchill). J. Fish Dis. 8, 135–138.

Cowey, C.B., Adron, J.W., Youngson, A., 1983. The vitamin E requirement of rainbow trout (*Salmo gairdneri*) given diets containing polyunsaturated fatty acids derived from fish oil. Aquaculture 30, 85–93.

Draper, H.H., Csallany, A.S., 1969. A simplified hemolysis test for vitamin E deficiency. J. Nutr. 98, 390–394.

Furones, M.D., Alderman, D.J., Bucke, D., Fletcher, T.C., Knox, D., White, A., 1992. Dietary vitamin E and the response of rainbow trout, *Oncorhynchus mykiss* (Walbaum), to infection with *Yersinia ruckeri*. J. Fish Biol. 41, 1037–1041.

Hamre, K., Hjeltnes, B., Kryvi, H., Sandberg, S., Lorentzen, M., Lie, O., 1994. Decreased concentration of hemoglobin, accumulation of lipid oxidation products and unchanged skeletal muscle in Atlantic salmon (*Salmo salar*) fed low dietary vitamin E. Fish Physiol. Biochem. 12, 421–429.

Herraez, M.P., Zapata, A., 1986. Structure and function of the melano-macrophage centres of the goldfish *Carassius auratus*. Vet. Immunol. Immunopathol. 12, 117–126.

Herraez, M.P., Zapata, A., 1987. Trapping of intraperitoneal-injected *Yersinia ruckeri* in the lymphoid organs of *Carassius auratus*: the role of melano-macrophage centres. J. Fish Biol. 31, 235–237, Suppl. A.

Hinton, D.E., Baumann, P.C., Gardner, G.R., Hawkins, W.E., Hendricks, J.D., Muchelano, R.A., Okihiro, M.S., 1992. Histopathologic biomarkers. In: Huggett, R.J., Kimerle, R.A., Mehrle, P.M., Jr., Bergman, H.L. (Eds.), Biomarkers, Biochemical, Physiological, and Histological Markers of Anthropogenic Stress. Lewis Publisher, Boca Raton, FL, pp. 155–209.

Ibeas, C., Izquierdo, M.S., Lorenzo, A., 1994. Effect of different levels of $n-3$ highly unsaturated fatty acids

on growth and fatty acid composition of juvenile gilthead seabream (*Sparus aurata*). Aquaculture 127, 177–188.

Idler, D.R., Truscott, B., 1972. Corticosteroids in fish. In: Idler, D.R. (Ed.), Steroids in Non-Mammalian Vertebrates. Academic Press, London, pp. 127–252.

Kranz, H., 1989. Changes in splenic melano-macrophage centres of dab *Limanda limanda* during and after infection with ulcer disease. Dis. Aquat. Org. 6, 167–173.

Kranz, H., Peters, N., 1984. Melano-macrophages centres in liver and spleen of ruffe (*Gymnocephalus cernua*) from the Elbe Estuary. Helgol. Meeresunters. 37, 415–424.

Kranz, H., Gerken, J., 1987. Effects of sublethal concentrations of potassium dichromate on the occurrence of splenic melano-macrophage centres in juvenile plaice, *Pleuronectes platesa* L. J. Fish Biol. 31, 75–80, Suppl. A.

Luna, L.G., 1992. Histopathological Methods and Color Atlas of Special Stains and Tissue Artifacts. American Histolabs, Gaithersburg, MD.

Macchi, G.J., Romano, L.A., Christiansen, H.E., 1992. Melano-macrophage centres in whitemouth croaker, *Micropogonias furnieri*, as biological indicators of environmental changes. J. Fish Biol. 40, 971–973.

Martoja, R., Martoja-Pierson, 1970. Técnicas de Histología Animal. Toray-Masson, Barcelona.

Micale, V., Perdichizzi, F., 1990. A quantitative and histochemical study on melano-macrophage centres in the spleen of the teleost fish *Diplodus annularis* L. J. Fish Biol. 37, 191–197.

Moccia, R.D., Hung, S.S.O., Slinger, S.J., Ferguson, H.W., 1984. Effect of oxidized fish oil, vitamin E and ethoxyquin on the histopathology and hematology of rainbow trout, *Salmo gairdneri* Richardson. J. Fish Dis. 7, 269–282.

Molinero, A., González, J., 1995. Comparative effects of MS-222 and 2-phenoxyethanol on gilthead sea bream (*Sparus aurata* L.) during confinement. Comp. Biochem. Physiol. 111, 405–414.

Obach, A., Quentel, C., Baudin Laurencin, F., 1993. Effects of α-tocopherol and dietary oxidized fish oil on the immune response of sea bass *Dicentrarchus labrax*. Dis. Aquat. Org. 15, 175–185.

Patti, F., Micale, V., 1993. Effects of different photoperiods on melano-macrophage centres of *Pagellus bogaraveo* (Brunnich, 1768). In: Carrillo, M., Dahle, L., Morales, J., Sorgeloos, P., Svennevig, N., Wyban, J. (Eds.), From Discovery to Commercialization. Oostende-Belgium European Aquaculture Soc. 19, p. 429.

Pegg, J.R., Iwama, G.K., 1996. The effects of stress and cortisol on phagocyte function in juvenile salmonid In: Stolen, J.S., Fletcher, T.C., Bayne, C.J., Secombes, C.J., Zelikoff, J.T., Twerdok, L.E., Anderson, D.P. (Eds.), Modulators of Immune Responses. The Evolutionary Trail. SOS Publications, Fair Haven, pp. 233–239.

Pickering, A.D., Pottinger, T.G., 1989. Stress responses and disease resistance in salmonid fish: effects of chronic elevation of plasma cortisol. Fish Physiol. Biochem. 7, 253–258.

Pickering, A.D., Pottinger, T.G., Christie, P., 1982. Recovery of the brown trout, *Salmo trutta* L., from acute handling stress: a time-course study. J. Fish Biol. 20, 229–244.

Roberts, R.J., 1975. Melanin-containing cells of the teleost fish and their relation to disease. In: Ribelin, W.E., Migaki, G. (Eds.), The Pathology of Fish. University of Wisconsin Press, Madison, pp. 399–428.

Scott, A.L., Klesius, P.H., 1981. Chemiluminescence: a novel analysis of phagocytosis in fish. In: Anderson, D.P., Hennesen, W. (Eds.), Developments in Biological Standardization, Vol. 49. S. Karger, Basel, pp. 243–256.

Smith, C.E., 1979. The prevention of liver lipoid degeneration (ceroidosis) and microcytic anemia in rainbow trout (*Salmo gairdneri*) Richarson fed rancid diets: a preliminary report. J. Fish Dis. 2, 429–437.

Sokal, R.R., Rolf, J., 1979. Biometría. Blume, Madrid.

Vijayan, M.M., Leatherland, J.F., 1988. Effect of stocking density on the growth and stress-response in brook charr, *Salvelinus fontinalis*. Aquaculture 75, 159–170.

Vogelbein, W.K., Fournie, J.W., Overstreet, R.M., 1987. Sequential development and morphology of experimentally induced hepatic melano-macrophage centres in *Rivulus marmoratus*. J. Fish Biol. 31, 145–153.

Wada, S., Hatai, K., Kubota, S., 1989. Light microscopical observations of culture yellowtail *Seriola quinqueradiata*, characterized by yellow discoloration of body surface. Fish Pathol. 24, 211–218.

Wada, S., Hatai, K., Kubota, S., 1991. Histopathological study of culture striped jack with yellow fat disease. Fish Pathol. 26, 61–67.

Watanabe, T., 1982. Lipid nutrition in fish. Comp. Biochem. Physiol. B 73, 3–15.

Wedemeyer, G.A., 1997. Effects of rearing conditions on the health and physiological quality of fish in intensive culture. In: Iwama, G.K., Pickering, A.D., Sumpter, J.P., Schreck, C.B. (Eds.), Fish Stress and Health in Aquaculture. Cambridge Univ. Press, Cambridge, pp. 35–71.

Weeks, B.A., Anderson, D.P., DuFour, A.P., Fairbrother, A., Govern, A.J., Lahvins, G.P., Peters, G., 1992. Immunological biomarkers to assess environmental stress. In: Huggett, R.J., Kimerle, R.A., Mehrle, P.M., Jr., Bergman, H.L. (Eds.), Biomarkers, Biochemical, Physiological, and Histological Markers of Anthropogenic Stress. Lewis Publisher, Boca Raton, FL, pp. 211–234.

Wilson, R.P., Bowser, P.R., Poe, W.E., 1984. Dietary vitamin E requirement of fingerling channel catfish. J. Nutr. 114, 2053–2058.

Wise, D.J., Tomasso, J.R., Gatlin, D.M. III, Bai, S.C., Blazer, V.S., 1993. Effects of dietary selenium and vitamin E on red blood cell peroxidation, glutathione peroxidase activity, and macrophage superoxide anion production in channel catfish. J. Aquat. Anim. Health 5, 177–182.

Wolke, R.E., 1992. Piscine macrophage aggregates: a review. Annu. Rev. Fish Dis. 2, 91–108.

Environmental Biology of Fishes 59: 91–97, 2000.

Biology of the sand smelt, *Atherina presbyter* (Teleostei: Atherinidae), off the Canary Islands (central-east Atlantic)

José G. Pajuelo & José M. Lorenzo
Departamento de Biología, Universidad de Las Palmas de Gran Canaria, Campus Universitario de Tafira, 35017 Las Palmas de Gran Canaria, Spain (e-mail: josemaria.lorenzo@biologia.ulpgc.es)

Received 7 August 1998 Accepted 25 January 2000

Key words: age, growth, reproduction, mortality, fish

Synopsis

Atherina presbyter is a common fish off the Canary Islands. Age, growth, reproduction, and mortality of the species are studied based on sampling carried out from July 1995 to June 1996. The parameters of the total length–total weight relationship are: a = 0.004521, and b = 3.0771. Otoliths age readings indicate that the sampled population consists of four age groups (0–III years). The von Bertalanffy growth parameters for all individuals are: L_∞ = 122 mm total length, k = 0.79 year^{-1}, and t_0 = −0.21 years. Individuals grow quickly in their immature first year, attaining approximately 60% of their maximum length. After the first year, the annual growth rate drops rapidly, because the energy is probably diverted to reproduction. It is a gonochoristic species with no evidence of sexual dimorphism. The gonad is present as a single diffuse testis in males and as a single discrete ovary in females. The overall ratio of males to females is not significantly different from 1 : 1. The reproductive period of the species is protacted (February to June). The peak of the reproductive effort occurs in April–May. The size at first maturity is 68 mm. The population is being heavily exploited.

Introduction

The family Atherinidae is represented by a single genus *Atherina* in the eastern Atlantic (Quignard & Pras 1986, Creech 1992a). Members of this genus are commonly referred to as sand smelt. Historically, there has been considerable confusion as to the number and delineation of species in the genus (Creech 1992b). Kiener & Spillman (1969) and Maugé (1990) defined four species: *A. hepsetus* Linnaeus, 1758, *A. boyeri* Risso, 1810, *A. lopeziana* Rossignol & Blache, 1961, and *A. presbyter* Cuvier, 1829. Bamber & Henderson (1985) proposed the synonymy of *A. presbyter* with *A. boyeri*. However, recent studies have demonstrated that differences are present between populations of *A. presbyter* and *A. boyeri*, consistent with the existence of two species (Creech 1990, 1991, 1992b).

The population biology of *A. boyeri* has been extensively investigated at a large number of locations in the eastern Atlantic and in the Mediterranean (Kiener & Spillman 1969, Boscolo 1970, Kohler 1976, Gon & Ben-Tuvia 1983, Palmer & Cully 1983, Bamber & Henderson 1985, Fernández-Delgado et al. 1988, Henderson & Bamber 1987, Henderson et al. 1988, Creech 1990, 1991, 1992a, Fouda 1995, Tomasini et al. 1996). In contrast, published information on *A. presbyter* is very scarce. It only consists in feeding aspects (Anadon 1963, Kislalioglu & Gibson 1977, Turnpenny et al. 1981, Lens 1986, Moreno & Castro 1995), morphometry, genetic and systematic aspects (Schultz 1948, Bamber & Henderson 1985, Quignard & Pras 1986, Creech 1991, 1992b, Vasil'eva 1996), and geographical distribution (Quignard & Pras 1986, Maugé 1990).

The present paper contains the results of an investigation of *A. presbyter* in the Canary Islands (central-east Atlantic). Age, growth, spawning cycle, maturity and mortality are examined in order to understand the

life of the species and to contribute to the management of the fishery exploiting the stock. The importance of this work is enhanced by the fact that catches of *A. presbyter* have been declining and the fishing effort on it has been increasing in the area.

A. presbyter is a small pelagic fish species inhabiting inshore waters. This species occurs along the east Atlantic ocean coasts, from Kattegat and Scotland to Mauritania and penetrates into Mediterranean near the Strait of Gibraltar (Quignard & Pras 1986, Maugé 1990). In the central-east Atlantic, it is apparently confined to Canaries, Mauritania and Cape Verde islands (Maugé 1990).

In the Canary Islands, *A. presbyter* is of a great interest both as commercial target and as bait in the seasonal live-bait tuna fishery. This species is captured near surface in the littoral zone, mainly with beach seines and liftnets. It is caught consistently year-round without significant seasonal differences in landings.

Materials and methods

A. presbyter samples were collected at fortnightly intervals from commercial catches taken between July 1995 and June 1996 off Gran Canaria (Canary Islands). A total of 3101 individuals was obtained by random sampling. A subsample of 1028 specimens was taken by a random length stratified method for biological analysis.

Each fish was measured to the nearest mm for total length (TL), and weighed to the nearest 0.001 g for total body weight (TW). The weight of the gonads (GW) was measured to the nearest 0.001 g, and the sex and the stage of maturation were ascertained macroscopically. Stages of maturation were classified as follows (Holden & Raitt 1975): I = immature, II = resting, III = ripe, IV = ripe and running, V = spent. Sagittal otoliths of the fish were removed, cleaned, and stored dry.

The total length–total weight relationship was calculated over the whole period, both for males and females separately and for the population as a whole, applying a linear regression (Ricker 1973). The age was determined by interpreting growth rings on the otoliths. Counts for each specimen were performed twice, on two separate occasions, and only coincident readings were accepted. An index of average percent error (APE) developed by Beamish & Fournier (1981) was used to compare the precision of age determinations. The evolution of the mean monthlymarginal increments was analysed to validate the ageing method. The distance between the outer edge of the outermost translucent zone and the periphery of each otolith was measured in mm. Measurements were always made along the longest axis of the otolith. The 1st April was considered as 'birthdate' to assign the individual ages to age groups. The von Bertalanffy growth curve was fitted to data of the resulting age–length relationship by mean of the Marquardt's algorithm for non-linear least squares parameter estimation (Saila et al. 1988).

The sex-ratio (males : females) for the whole sample and different size classes was calculated. The reproductive season was determined according to Anderson & Gutreuter (1983) based on the monthly development of the gonadosomatic index (GSI). The length-at-sexual maturity (length at which fifty percent of the specimens had become mature) was estimated by means of a logistic function which was fitted to the proportion of mature individuals (stages III, IV, and V) by size class using a non-linear regression (Saila et al. 1988).

Length-frequency data of the catches were converted to age-frequency using the von Bertalanffy growth parameters (Pauly 1983). The total mortality rate (Z) was calculated from the length-converted catch curve using the program ELEFAN (Gayanilo et al.[1]). The rate of natural mortality (M) was determined using the method of Tanaka (1960). Following the estimation of Z and M, the fishing mortality rate (F) was estimated by subtraction. The exploitation ratio (E) was estimated dividing F by Z (Gulland 1971). The length-at-first capture (LC_{50}) was determined from the selection ogive generated from the length-converted catch curve (Pauly 1983).

Results

Males ranged in size between 52 and 113 mm total length and females between 49 and 115 mm. The range of immature individuals was 14 to 73 mm. The parameters of the total length–total weight relationship for males and females separately and for the population as a whole are given in Table 1. No significant difference in the allometric coefficient of the regression was found between males and females (t-test, $t = 0.27 < t_{0.05,550} = 1.65$). Isometric growth was observed in both sexes and for the whole sample.

[1] Gayanilo, F.C., Jr., M. Soriano & D. Pauly. 1988. A draft guide to the compleat ELEFAN. ICLARM Software 2. Contribution No. 435. 1–65.

Table 1. Parameters of the total length–total weight relationship for males, females and all fish of *A. presbyter* collected off the Canary Islands, and the possibility of isometry tested by Student t-test. *($t < t_{0.05,n>250} = 1.65$).

	a	b	se (b)	r^2	n	t-test
Males	0.006536	3.04102	0.06137	0.959	269	0.66*
Females	0.006542	3.04922	0.05920	0.962	283	0.83*
All fish	0.006118	3.07712	0.05638	0.982	1028	1.36*

Of the total otoliths examined, 912 (88.7%) were readable and used for the study of age and growth. APE value was only 2.4%. The mean monthly marginal increments in the whole otoliths with one translucent zone ranged from 0.25 to 0.36 mm between May and August. They subsequently declined to 0.05 mm in December, before gradually increasing to 0.15 by April. The marginal increments in otoliths with two and three translucent zones also declined markedly between November and March and followed a similar trend. Thus, irrespective of the number of translucent zones in the otoliths, the marginal increments declined markedly and then rose progressively only once during 12 months period, demonstrating that the translucent zones are formed annually.

Sampled population consisted predominantly of two age groups (I and II), except during the late spawning and post-spawning period when the presence of the age group 0 was recorded. Recruitment took place in May and June. Over 60% of the growth was achieved by the end of the first year (Table 2). By the end of the second year, fish had attained a mean length of 95 mm. After they had spawned, few individuals of the age group III were encountered. No evidence was found to indicate that fish of the age group III survived to spawn for a fourth season.

The relationship between age and length, derived from the assumed annual periodicity of the otoliths growth rings, is described by the growth parameters: $L_\infty = 122$ mm total length, $k = 0.79$ year^{-1}, and $t_0 = -0.21$ years (Table 3). No significant differences in growth parameters were found between sexes (Hotelling s T^2-test, $T^2 = 5.29 < {T_0}^2_{0.05.3.456} = 7.89$).

The gonad was present as a single diffuse testis in the male and as a single discrete ovary in the female. Of the 1028 fish examined, 269 (26.2%) were males and 283 (27.5%) females. The sex of the remaining 476 (46.3%) individuals could not be identified macroscopically and were immature as they had very thin and traslucent gonads. The overall ratio of males to females was 1 : 1.05 and χ^2 analysis revealed this not to be significantly different from a 1 : 1 ratio (Table 4). Sex-ratios for males and females grouped into 5-mm length classes had not significant departures from the 1 : 1 ratio.

When all the males and females were considered, irrespective of their maturity stage, the monthly mean values of GSI increased rapidly from February to April before decreasing until June (Figure 1). From July to January the values were low. The same temporal variation pattern was recorded for both sexes. The monthly mean GSI, calculated only for males

Table 2. Age–length distribution for all fish of *A. presbyter* collected off the Canary Islands.

Size (mm)	Age group (years)			
	0	I	II	III
15	11			
20	28			
25	36			
30	40			
35	56			
40	70			
45	77			
50	65			
55	47	2		
60	15	11		
65	3	28		
70		47		
75		65	4	
80		41	13	
85		33	36	
90		10	59	
95		6	45	
100		2	25	4
105			8	11
110			2	9
115			1	2
n	448	245	193	26
x	42.5	74.2	94.9	109.1
SD	6.3	5.1	4.6	2.5

Table 3. Parameters of the von Bertalanffy growth curve for males, females and all fish of *A. presbyter* collected off the Canary Islands.

	L_∞ (mm)	k (year^{-1})	t_0 (years)	r^2
Males	121.3	0.72	0.39	0.979
Females	121.5	0.69	0.47	0.981
All fish	121.8	0.79	0.21	0.989

Table 4. Number of males, females and juveniles of *A. presbyter* collected off the Canary Islands by 5-mm size class and sex-ratio tested by chi-square analysis. *($\chi^2 < \chi_{1\,0.05}^2 = 3.84$).

Size (mm)	Males	Females	Juveniles	Sex-ratio	χ^2
15			12		
20			28		
25			36		
30			41		
35			58		
40			72		
45			79		
50	1	1	66	1 : 1.00	
55	1	2	49	1 : 2.00	0.33*
60	6	8	15	1 : 1.33	0.28*
65	23	20	12	1 : 0.86	0.21*
70	20	25	7	1 : 1.25	0.55*
75	37	41	1	1 : 1.10	0.21*
80	39	43		1 : 1.08	0.19*
85	41	35		1 : 0.85	0.47*
90	38	42		1 : 1.10	0.20*
95	25	28		1 : 1.12	0.17*
100	17	18		1 : 1.05	0.03*
105	14	9		1 : 0.64	1.08*
110	5	8		1 : 1.60	0.69*
115	2	3		1 : 1.50	0.20*
Total	269	283	476	1 : 1.05	0.36*

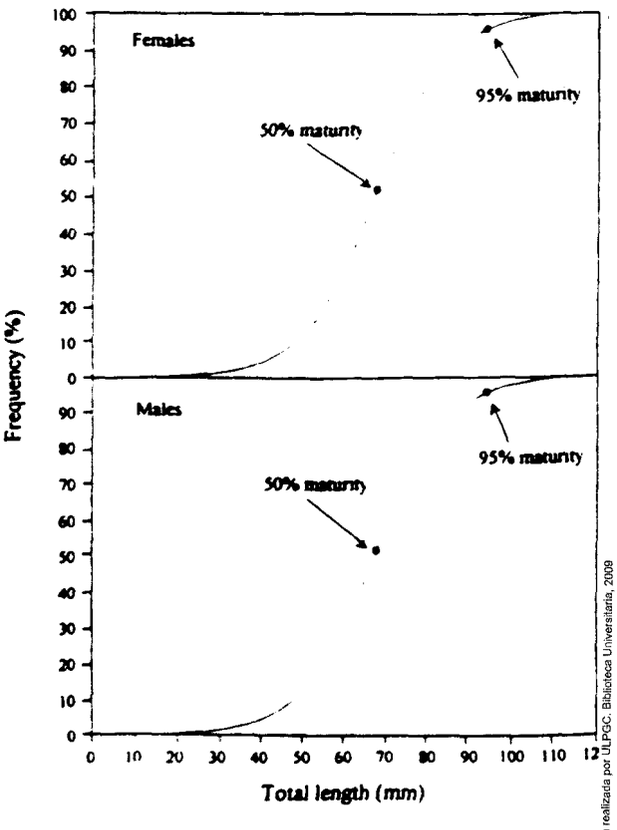

Figure 1. Sexual maturity ogive for females and males *A. presbyter* collected off the Canary Islands.

and females with ripe and running gonads, produced a similar variation pattern with higher values. GSI indicated that spawning takes place over a period of approximately 5 months. Fish of the age groups 0 and I showed lower values of GSI than those of the II and III.

No significant difference in length-at-sexual maturity was found between males and females (t-test, $t = 0.43 < t_{0.05.550} = 1.65$). The length at which fifty percent of fish had become mature was 68 mm total length (Figure 2). All males and females were mature by the end of their second year at a mean length of 93 mm.

The length-converted catch curve is shown in Figure 3. The rates of total mortality (Z), natural mortality (M) and fishing mortality (F), and the exploitation ratio (E) were calculated separately for the age groups 0 and I–III. The values for the age group 0 were: $Z = 4.66$ year^{-1}, $M = 1.01$ year^{-1}, $F = 3.65$ year^{-1} and $E = 0.78$, and for the age groups I–III were: $Z = 2.54$ year^{-1}, $M = 1.01$ year^{-1}, $F = 1.53$ year^{-1} and $E = 0.61$. The length-at-first capture was: $LC_{50} = 36$ mm.

Discussion

Otoliths of *A. presbyter* off the Canarian archipel show the ring pattern common to teleost fishes. (opaque and one translucent ring are laid down e year on the otoliths, allowing age determinat with relative ease. These rings are generally belie to be deposited during periods of fast and s growth, respectively (Williams & Bedford 1974). S sonal growth cycles might be related to physiol cal changes produced by the influence of temperat feeding regime and reproductive cycle (Morales-Ni Ralston 1990). The opaque rings are formed du spring-summer months, when the sea surface t perature reaches the highest values (24°C), and hyaline rings during winter months, when the temp ture reaches the lowest values (17°C) and the bree occurs in the species. Fernández-Delgado et al. (1 also found that annuli formation in otoliths of *A. bo* from the estuary of the Guadalquivir River takes p during spring and summer (April to July). The evid presently available suggests that a seasonal temp ture difference of 2–3°C might be sufficient to c ring formation (Morales-Nin & Ralston 1990). Du

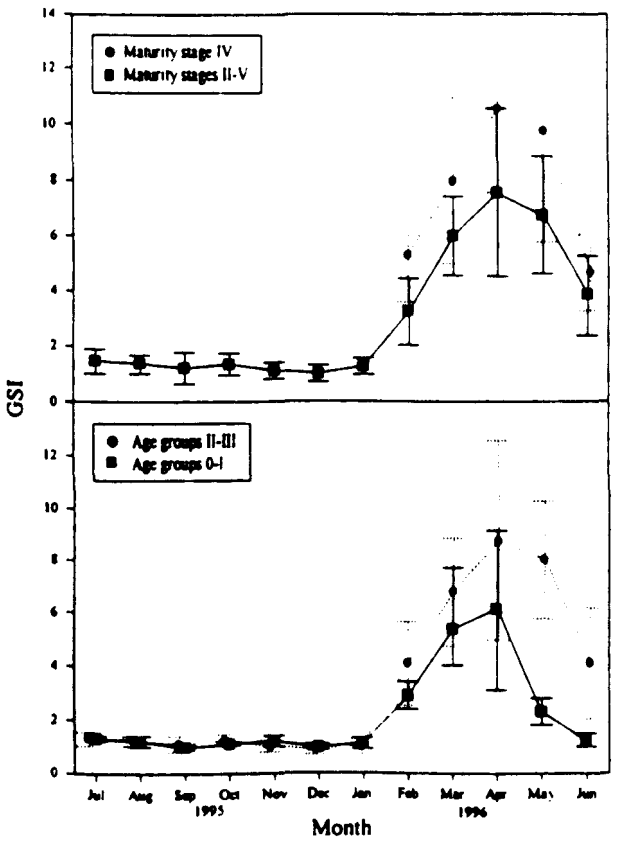

Figure 2. Mean monthly development of the gonadosomatic index (GSI) for *A. presbyter* collected off the Canary Islands at maturity stages (IV and II–V) and at age groups (0–I and II–III).

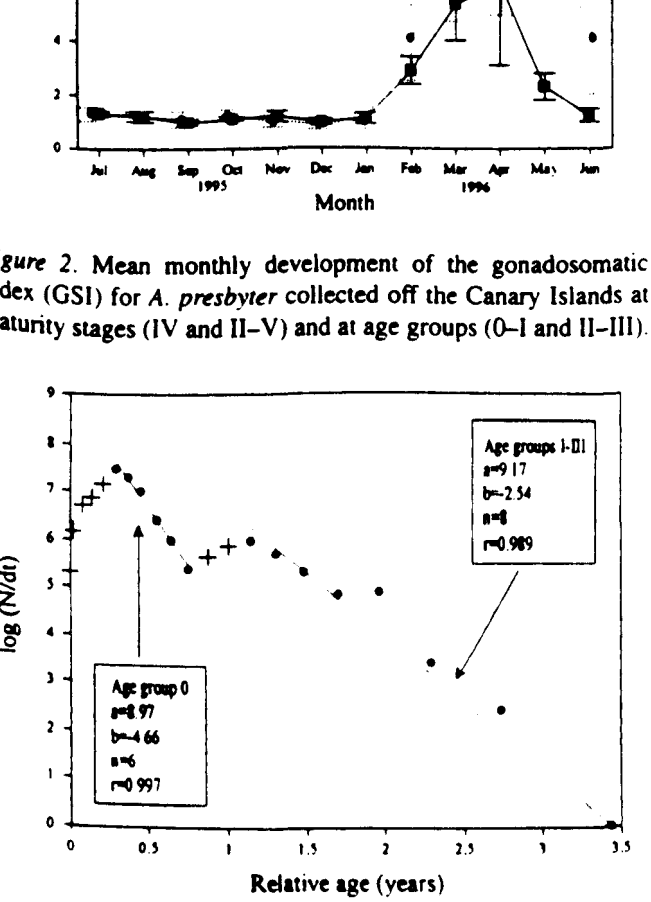

Figure 3. Length-converted catch curve for all fish of *A. presbyter* collected off the Canary Islands at age groups (0 and I–III). The initial data point (+) were not used in the regressions.

the maturity period, the metabolic energy seems to be diverted from growth, causing the formation of thin increments which are in turn reflected in hyaline seasonal growth rings.

The highest age class observed is III years. The short life cycle exhibited by *A. presbyter* concurs with the expectations of Kiener & Spillman (1969), Fernández-Delgado et al. (1988), Maugé (1990), Creech (1992a) and Rosecchi & Crivelli (1992), which proposed a 3–4 years age structure as typifying populations of Atherinidae species. As a whole, growth of *A. presbyter* is rapid, with males and females growing equally fast. The growth parameters obtained are reasonable because the theoretical maximal length value is higher than the size of the largest fish sampled and the growth coefficient value indicates rapid attainment of maximal size, characteristic of the short life species. *A. presbyter* grows quickly in its immature first year, attaining approximately 60% of the maximum length. After the first year, the annual growth rate drops rapidly. It can be related to sexual maturity, because in the studied area all individuals are mature by the second year of life. Hence, energy is probably diverted to reproduction, resulting in less energy available for somatic growth.

A. presbyter from the Canary Islands is a gonochoristic species with no evidence of sexual dimorphism. The near equal ratio of males to females is similar to ratios quoted by Boscolo (1970), Kohler (1976) and Creech (1992a) for other Atherinidae.

The spawning of *A. presbyter* occurs during five months. A prolonged breeding season is generally characteristic of repeat spawners (Nikolskii 1963) and fish living in variable and unstable and/or highly productive environments (Tomasini et al. 1996). In this area, the spawning period of several fish species is protracted (Lorenzo & Pajuelo 1996, Pajuelo & Lorenzo 1995, 1996, 1998). Tomasini et al. (1996) observed that the spawning period of *A. boyeri* in brackish lagoons of southern France spreads over 8 months (February–September). Protracted spawning appears to be a feature of the biology of Atherinidae (Boscolo 1970, Castel et al. 1977, Palmer & Cully 1983, Gon & Ben-Tuvia 1983, Henderson et al. 1988, Creech 1992a, Rosecchi & Crivelli 1992, Tomasini et al. 1996). Depending on environmental conditions and energy accumulation available, reproductive effort in atherinid species is more or less important during the spawning season (Tomasini et al. 1996).

Length-at-sexual maturity does not differ between males and females, corresponding to 67 mm total length. In the age–length relationship, this size corresponds to 0 and 1 year old specimens. In the Suez Canal, Fouda (1995) also found that males and females

of *A. boyeri* attain sexual maturity when age is approximately 1 year.

The length-converted catch curve shows a typical form of two modes and justify the estimation of two values of Z (Pauly 1983). In both cases, the exploitation ratio is higher than 0.50. Gulland (1971) suggested that, as a rule of thumb, a fish stock is optimally exploited at a level of fishing mortality which generates E = 0.50, where $F_{opt} = M$, but in the present study $F > F_{opt} = M$. More recently, Pauly (1987) proposed a lower optimum fishing mortality, $F_{opt} = 0.4\,M$ ($F > F_{opt}$). Therefore, *A. presbyter* off the Canary Islands is being heavily exploited.

In the Canarian Archipelago, where a conservation legislation on fisheries exists, a limit of catch has been implemented for *A. presbyter*. In this case, the regulation is of limited benefit. Measures such as closed seasons, closed areas or changes in fishing pattern would be desirable to safeguard the spawning stock and the recruits. If the stock decline continues, a further possible option, decommercialization, would certainly be beneficial to the stock, but the social and political arguments surrounding such a decision are beyond the scope of this paper.

Acknowledgements

The authors are very grateful to Peter B. Moyle (Department of Wildlife, Fish and Conservation Biology, University of California) and one anonymous referee for reviewing the manuscript and for valuable comments.

References cited

Anadon, E. 1963. Observaciones sobre bancos y conducta alimenticia de *Atherina presbyter* C, *Mugil provensalis* Risso, *Diplodus sargus* L. y *Diplodus vulgaris* Geofir. Bol. R. Soc. Esp. Hist. Nat. 61: 141–147.

Anderson, R.O. & S.J. Gutreuter. 1983. Length, weight, and associated structural indices. pp. 283–300. *In:* Nielsen L.A. and Johnson D.L. (eds), Fisheries Techniques, American Fisheries Society, Bethesda.

Beamish, R.J. & D.A. Fournier. 1981. A method for comparing the precision of a set of age determinations. Can. J. Fish Aquat. Sci. 38: 982–983.

Bamber, R.N. & P.A. Henderson. 1985. Morphological variation in British atherinids, and the status of *Atherina presbyter* Cuvier (Pisces: Atherinidae) Biol. J. Linn. Soc. 25: 61–76.

Boscolo, L. 1970. Observazoni sulla biologia e sulla pesca dell'*Atherina boyeri* Risso 1810 (Osteichthyes Atherinidae) vivente nelle acque dell'alto Adriatico (Observations on the biology and the fishery of *Atherina boyeri* Risso 1810 (Osteichthyes Atherinidae) off the Adriatic Sea). Boll. Pesc. Pisc. Idrob. 25: 61–76.

Castel, J., P. Cassifour & P-J. Labourg. 1977. Croissance et modifications du régime alimentaire d'un téléostéen Mugiliforme: *Atherina boyeri* Risso, 1810 dans les étangs saumâtres du basin d'Arcachon. Vie Milieu 17: 385–410.

Creech, S. 1990. The ecology and taxonomy of two European atherinids (Teleostei: Atherinidae). Ph. D. Thesis, University of Wales College of Cardiff. 143 pp.

Creech, S. 1991. An electrophoretic investigation of populations of *Atherina boyeri* Risso, 1810 and *A. presbyter* Cuvier, 1829 (Teleostei: Atherinidae): genetic evidence in support of the two species. J. Fish Biol. 39: 807–816.

Creech, S. 1992a. A study of the biology of *Atherina boyeri* Risso, 1810 in Aberthaw Lagoon on the Bristol Channel, in South Wales. J. Fish Biol. 41: 277–286.

Creech, S. 1992b. A multivariate morphometric investigation of *Atherina boyeri* Risso, 1810 and *A. presbyter* Cuvier, 1829 (Teleostei: Atherinidae): morphometric evidence in support of the two species. J. Fish Biol. 41: 341–353.

Fernández-Delgado, C., J.A. Hernando, M. Herrera & M. Bellido. 1988. Life history patterns of the sandsmelt *Atherina boyeri* Risso, 1810 in the estuary of the Guadalquivir River, Spain. Estuar. Coast. Shelf S. 27: 697–706.

Fouda, M.M. 1995. Life history strategies of four small-sized fishes in the Suez Canal, Egypt. J. Fish Biol. 46: 687–702.

Gon, O. & A. Ben-Tuvia. 1983. The biology of Boyer's sandsmelt, *Atherina boyeri* Risso, in the Bardawil Lagoon on the Mediterranean coast of Sinai. J. Fish Biol. 22: 537–547.

Gulland, J.A. 1971. The Fish Resources of the Oceans. Fishing News (Books) Ltd, West Byfleet. 255 pp.

Henderson, P.A. & R.N. Bamber. 1987. On the reproductive biology of the sand smelt *Atherina boyeri* Risso (Pisces: Atherinidae) and its evolutionary potential. Biol. J. Linn. Soc. 32: 395–415.

Henderson, P.A., R.H.A. Holmes & R.N. Bamber. 1988. Size selective overwintering mortality in the sand smelt *Atherina boyeri* Risso, and its role in population regulation. J. Fish Biol. 33: 221–233.

Holden, M.J. & D.F.S. Raitt. 1975. Manual de ciencia pesquera. Parte 2. Métodos para investigar los recursos y su aplicación. FAO Doc. Téc. Pesca 115: 1–211.

Kiener, A. & C.J. Spillman. 1969. Contribution a l'étude systématique et écologique des athérines des côtes françaises. Mem. Mus. Hist. Nat., Ser. A Zool. 40: 33–74.

Kislalioglu, M. & R.N. Gibson. 1977. The feeding relationship of shallow water fishes in a Scottish sea loch. J. Fish Biol. 11: 257–266.

Kohler, A. 1976. Observations biologique et biométriques sur *Atherina boyeri* Risso dans l'étangs du Prévost à Palavas (Hérault). Vie Milieu 26: 157–176.

Lens, S. 1986. Alimentación del pejerrey, *Atherina presbyter* Cuvier, en la Ría de Arosa. Bol. Inst. Esp. Oceanogr. 3(2): 11–36.

Lorenzo, J.M. & J.G. Pajuelo. 1996. Growth and reproductive biology of chub mackerel *Scomber japonicus* off the Canary Islands. S. Afr. J. Mar. Sci. 17: 275–280.

Maugé, L.A. 1990. Atherinidae. pp. 604–605. *In:* Quero J.C., Hureau J.C., Karrer C., Post A. and Saldanha L. (eds), Check List of the Fishes of the Eastern Tropical Atlantic, Clofeta II , UNESCO, Paris.

Morales-Nin, B. & S. Ralston. 1990. Age and growth of *Lutjanus kasmira* (Forskål) in Hawaiian waters. J. Fish Biol. 36: 191–203.

Moreno, T. & J.J. Castro. 1995. Community structure of the juvenile of coastal pelagic fish species in the Canary Islands waters. Sci. Mar. 59: 405–413.

Nikolskii, G.V. 1963. The Ecology of the Fishes. Academic Press, London. 411 pp.

Pajuelo, J.G. & J.M. Lorenzo. 1995. Biological parameters reflecting the current state of the exploited pink dentex *Dentex gibbosus* (Pisces: Sparidae) population off the Canary Islands. S. Afr. J. Mar. Sci. 16: 311–319.

Pajuelo, J.G. & J.M. Lorenzo. 1996. Life history of the red porgy *Pagrus pagrus* (Teleostei: Sparidae) off the Canary Islands, Central-east Atlantic. Fish. Res. 28: 163–177.

Pajuelo, J.G. & J.M. Lorenzo. 1998. Population biology of the common pandora *Pagellus erythrinus* (Pisces: Sparidae) off the Canary Islands. Fish. Res. 35: 1–12.

Palmer, C.J. & M.B. Cully. 1983. Aspects of the biology of the sandsmelt *Atherina boyeri* Risso, 1810 (Teleostei: Atherinidae) at Oldbury-upon-Severn, Gloucestershire, England. Estuar. Coast. Shelf S. 16: 163–172.

Pauly, D. 1983. Some simple methods for the assessment of tropical fish stock. FAO Fish. Tech. Pap. 234: 1–52.

Pauly, D. 1987. A review of the ELEFAN system for analysis of length frequency data in fish and invertebrates. pp. 7–34. *In:* Pauly D. and Morgan G.R. (eds), Length-Based Methods in Fisheries Research, ICLARM, Manila.

Quignard, J-P. & A. Pras. 1986. Atherinidae. pp. 1207–1210. *In:* Whitehead P.J.P., Bauchot M.L., Hureau J.C., Nielsen J. and Tortonese E. (eds), Fishes of the North-Eastern Atlantic and the Mediterranean, UNESCO, Paris.

Ricker, W.E. 1973. Linear regressions in fishery research. J. Fish. Res. Board Can. 30: 409–434.

Rosecchi, E. & A.J. Crivelli. 1992. Study of a sand smelt (*Atherina boyeri* Risso 1810) population reproducing in fresh water. Ecol. Fresw. Fish. 1: 77–85.

Saila, S.B., C.W. Recksiek & M.H. Prager. 1988. Basic fishery science programs. A compendium of microcomputer programs and manual of operation. Developments in Aquaculture and Fisheries Science 18: 1–230.

Schultz, L.P. 1948. A revision of six subfamilies of atherine fishes, with description of new genera and species. Proc. U.S. Nat. Mus. 98: 1–48.

Tanaka, S. 1960. Studies on the dynamics and the management of fish populations. Bull. Tokai Reg. Fish. Res. Lab. 28: 1–200.

Tomasini, J.A., D. Collart & J.P. Quignard. 1996. Female reproductive biology of the sand smelt in brackish lagoons of southern France. J. Fish Biol. 49: 594–612.

Turnpenny, A.W.H., R.N. Bamber & P.A. Henderson. 1981. Biology of the sand smelt (*Atherina presbyter* Valenciennes) around Fawley power station. J. Fish Biol. 18: 417–427.

Vasil'eva, E.D. 1996. Cranial data and some problems in the systematics of the genus *Atherina* (Atherinidae). Public. Espec. Inst. Esp. Oceanogr. 21: 199–204.

Williams, T. & B.C. Bedford. 1974. The use of otoliths for age determination. pp. 114–123. *In:* Bagenal T.B. (eds), The Ageing of Fish, Unwin Brothers, Surrey.

J. Appl. Ichthyol. 16 (2000), 41–47

ISSN 0175–8659

Received: June 10, 1998
Accepted: January 21, 1999

Reproduction, age, growth and mortality of axillary seabream, *Pagellus acarne* (Sparidae), from the Canarian archipelago

By J. G. Pajuelo and J. M. Lorenzo

Departamento de Biología, Universidad de Las Palmas de Gran Canaria, Campus Universitario de Tafira, 35017 Las Palmas de Gran Canaria, Canary Islands, Spain

Summary

Axillary seabream *Pagellus acarne* (Risso 1826) caught off the Canary Islands from January 1991 to December 1994 were studied. The length range of the catches was between 11 and 31 cm, with a modal distribution between 17 and 21 cm. The overall ratio of males to females was 1:1.74. Males were observed up to a length of 24 cm. Hermaphrodites were recorded at lengths between 15 and 23 cm. The species was characterized by protandric hermaphroditism. The reproductive season extended from October to March, with a peak in spawning activity in December–January. The size at sexual maturity was 15.8 cm total length (2 years old) for males and 19.4 cm total length (3 years old) for females. The total length–total weight relationship for the entire population is described by the parameters a = 0.0068, and b = 3.2401. Otolith age readings showed that the population exploited consisted of 10 age groups (1–10 years), including a very high proportion of individuals between 1 and 4 years old. The von Bertalanffy growth parameters for all individuals were $L_\infty = 32.98$ cm, $k = 0.22$ years^{-1}, and $t_0 = -0.87$ years. Males grew comparatively slower than females. The instantaneous rates of mortality for all fish were $Z = 0.96$ years^{-1}, $M = 0.30$ years^{-1}, and $F = 0.66$ years^{-1}. The exploitation ratio and the length at first capture were, respectively, $E = 0.69$ and $LC_{50} = 16.1$ cm. The stock is overexploited, therefore measures such as closed seasons or changes in fishing patterns would be desirable to safeguard the spawning stock and recruits.

Introduction

Axillary seabream *Pagellus acarne* (Risso 1826) is a demersal marine fish species inhabiting various types of sea bottoms, especially sand and seagrass beds. This species is a Sparid widely distributed along the European and African coasts of the Atlantic Ocean (from Denmark to Senegal, and around the Madeira, Azores, Cape Verde and Canary Islands), in the Mediterranean, and in the Black Sea (Bauchot and Hureau 1986, 1990).

In the Canary Islands, the axillary seabream is one of the main target species of the commercial small-scale fishery, contributing approximately 10% to the total catch of demersal fish (Pajuelo and Lorenzo 1995a). Catches of this species have been declining in the area for the past 15 years (Pajuelo and Lorenzo 1995a). This species is captured throughout the year with seasonal differences in landings.

Despite its economic importance in the Canary Islands and that catches in the area are declining, the axillary seabream has never been the object of intensive investigation. A thorough biological investigation was necessary to provide a basis for species management. The present work investigated aspects of the biology of *P. acarne* off the Canary Islands, including the population structure, sexuality, reproduction, age, growth and mortality. The findings of the study are discussed in relation to existing management strategies.

Materials and methods

Pagellus acarne specimens were obtained from commercial catches of the artisanal fleet fishing with traps and longlines at depths of 5–210 m off southwest Gran Canaria (27°57′24″N 15°35′23″W), Canary Islands. A total of 39 651 individuals were collected fortnightly by a random method from January 1991 to December 1994. These individuals were measured (total length, mm) and weighed (g).

A subsample of 1966 specimens was taken from the entire sampling by a random length stratified method (1-cm length class) for biological analysis. For each fish, total length (TL) was measured to the nearest mm and total body weight (TW) to the nearest 0.1 g. Sex and the stage of maturity were ascertained macroscopically and the weight of the gonads (GW) was taken to the nearest 0.01 g. Stages of maturation were classified as follows (Holden and Raitt 1975): I, immature; II, resting; III, ripe; IV, ripe and running; V, spent. Sagittal otoliths were removed and stored dry.

The mean monthly length–frequency distributions of the individuals in the catches were plotted. Data were pooled to smooth interannual variability. The mean length and the length range of the fish by depth category were also plotted.

Percentages of immatures, males, females and hermaphrodites and the overall ratio of males to females were estimated. The reproductive period was established following the monthly evolution of the gonadosomatic index (GSI), calculated as:

$$GSI = (GW/TW) \cdot 100.$$

The size at sexual maturity (total length at which 50% of the fish had become mature) was determined from the relationship between the length class (L) and the percentage of mature fish in each length class (P). This relationship is described by the logistic function (Saila et al. 1988)

$$P = \frac{a}{1 + [[(a - b)/b] \cdot (e^{-cL})]},$$

where a, b, and c are constants to estimate.

The total length–total weight relationship was calculated over the entire period applying the exponential equation (Ricker 1973):

$TW = a \cdot TL^b$.

Age was determined by counting the annual growth rings on the otoliths. The otoliths were placed in glycerin and examined under a compound microscope (15×) with reflected light against a dark background. Counts for each specimen were performed three times by the senior author. Readings for a given otolith were accepted only when two agreed. January 1 was considered as the birth date to assign individual ages to age groups. Aging was validated indirectly by examination of monthly changes in appearance of the margins of the otoliths (Morales-Nin 1987). The von Bertalanffy growth curve was fitted to the data of the resulting age–length key by means of Marquardt's algorithm for nonlinear least squares parameter estimation (Saila et al. 1988). The form of the growth curve is (Beverton and Holt 1957):

$L_t = L_\infty \cdot (1 - e^{-k(t-t_0)})$,

where L_t is the fish total length at time t, L_∞ is the asymptotic total length to which fish tend to grow, k is the growth coefficient, and t_0 is the hypothetical time when the fish total length is zero.

Length–frequency data of the catches (39 651 fish) were converted to age frequency using the von Bertalanffy growth parameters (Pauly 1983). The total instantaneous mortality rate (Z) was then calculated from the length-converted catch curve using the program ELEFAN (Gayanilo et al. 1988). The equation employed was:

$\log (N/dt) = a + b \cdot t$.

where dt is the time needed to grow from the lower to the upper limit of a given length class, t is the relative age corresponding to the midrange of the length class in question, and a and b are the parameters to estimate. The instantaneous rate of natural mortality (M) was estimated using the method of Tanaka (1960):

$M = 3/T_{max}$,

where T_{max} is the age of the oldest fish sampled. Following the estimation of Z and M, the instantaneous rate of fishing mortality (F) was estimated by substraction. The exploitation ratio (E) was estimated using the expression (Gulland 1971):

$E = F/Z$.

The length at first capture (LC_{50}) was determined from the selection ogive generated from the length-converted catch curve (Pauly 1984).

Results

The mean monthly length–frequency distributions showed a length range in the catches of 11–31 cm, with most fish distributed between 17 and 21 cm (Fig. 1). In the majority of months a bimodal distribution was observed. The first mode corresponded approximately to 19 cm and the second to 23 cm. The size ranges were wider during the autumn and winter months than during the spring and summer months. The largest individuals were more abundant in November and December. Specimens smaller than 14 cm appeared only from November to March. A decrease in the number of individuals captured was observed during the summer months.

Fish were caught at depths from 5 to 210 m, mainly between 10 and 90 m. There was a relationship between size and depth. The mean total length showed a definite increase with increasing depth. Thus, the mean total length for a depth category of less than 30 m was 12.9 cm while it was 29.3 cm in depths over 180 m (Fig. 2).

In the axillary seabream, gonads are suspended by a dorsal mesentery in the posterior region of the visceral cavity. The gonads of males and females are elongated, paired organs attached to the dorsal body wall via mesenteries. The left gonadal lobe is connected to the lateral body wall while the right lobe is attached by mesenteries to the intestine and other organs in the celomic cavity. In general, both gonadal lobes were equally well developed.

Of the total number of individuals sexed, 556 (28.2%) were males, 968 (49.2%) females, and 81 (4.1%) hermaphrodites. The sex of the remaining 361 (18.5%) fish could not be identified macroscopically; they were immature as they had very thin and translucent gonads.

The overall ratio of males to females was 1:1.74 and χ^2 analysis showed a significant difference from the ratio 1:1 ($\chi^2 = 111.38 > \chi^2_{1,0.05} = 3.84$). A high percentage of individuals smaller than 15 cm could not be sexed. Males and females had different size ranges and mean, minimum and maximum sizes (Fig. 3). Males appeared in the range 14–24 cm, and were predominant between 14 and 19 cm. Females showed a larger size distribution, from 16 to 31 cm, and were clearly predominant at sizes above 21 cm. Hermaphrodites were intermediate in size between males and females (15–23 cm).

The GSI showed higher values for females than for males (Fig. 4). For both sexes, the highest values occurred between October and March, peaking in December–January. From April to September the values were low.

Fifty per cent of males and females matured at 15.8 and 19.4 cm total length, respectively (Fig. 5). Individuals smaller than 14 cm showed little evidence of gonad maturation. A significant difference in size at sexual maturity was found between males and females (t-test, $t = 14.28 > t_{0.05,1346} = 1.65$).

The parameters of total length–total weight are given in Table 1. There was a significant difference between the sexes in the allometric coefficient of the regression (t-test, $t = 19.75 > t_{0.05,1522} = 1.65$).

Of the 1966 otoliths examined, 283 (14.4%) were rejected. Marginal zone analysis showed that the opaque zone was deposited throughout the year, but with differing frequency. The highest percentages of otoliths with opaque edges were observed between May and August (Fig. 6).

Fish aged 1–10 years were present in the samples (Table 2). The growth parameters are shown in Table 3. Significant differences in the growth parameters were found between the sexes (Hotelling's T^2-test, $T^2 = 158.31 > T^2_{0.01,3,1288} = 11.41$).

The length-converted catch curve is shown in Fig. 7. The instantaneous rates of mortality for all fish were $Z = 0.96$ years^{-1}, $M = 0.30$ years^{-1}, and $F = 0.66$ years^{-1}. The exploitation ratio and the length at first capture were, respectively, $E = 0.69$ and $LC_{50} = 16.1$ cm.

Discussion

In the Canary Islands, the highest concentration of axillary seabream occurs between 10 and 90 m depth. Below this depth, this species is replaced by other sparids present in the area such as *Pagrus pagrus* and *Dentex gibbosus*. In the depth strata where fishing fleets exploit the axillary seabream, the more frequent lengths in the catches are between 17 and 21 cm. In the age–length key, these correspond mainly to specimens between 2 and 4 years old. This study has revealed that immature individuals

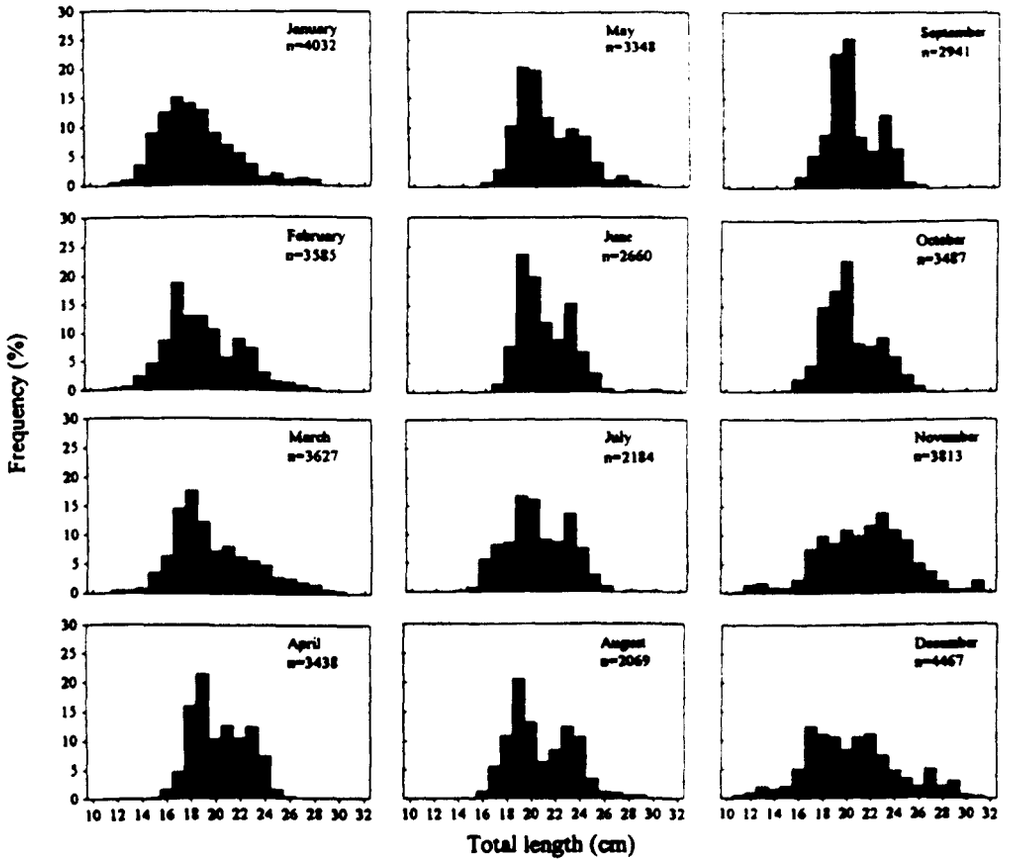

Fig. 1. Mean monthly length–frequency distributions

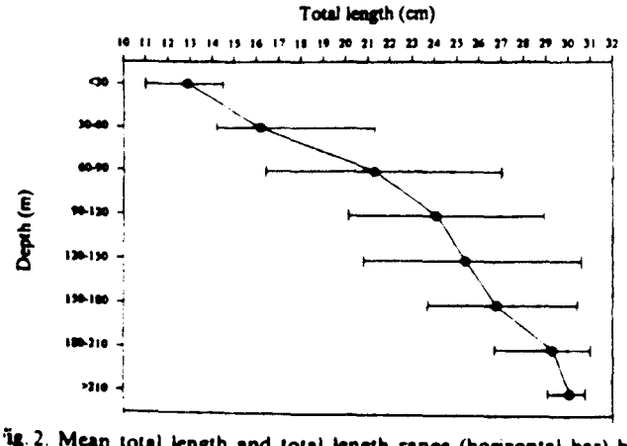

Fig. 2. Mean total length and total length range (horizontal bar) by depth category

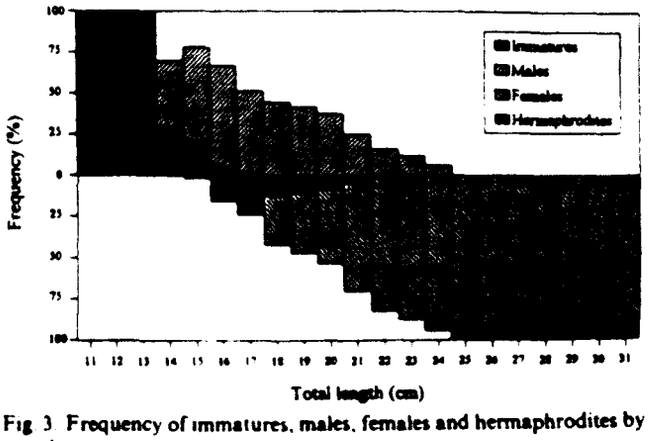

Fig 3. Frequency of immatures, males, females and hermaphrodites by size classes

inhabit the nursery areas located in shallow waters (< 30 m). The presence of specimens smaller than 14 cm during the autumn and winter months was due to recruitment. In the Alboran Sea, Caminas et al. (1990) observed the presence of small individuals corresponding to a new recruitment of axillary seabream during the autumn months.

In common with many other species of Sparidae (Buxton and Garratt 1990), the axillary seabream off the Canary Islands exhibits hermaphroditism. The presence of individuals with ovotestes, and the predominance of smaller males and larger females, suggests that this species displays protandric hermaphroditism in the area of study. Related to this, Shapiro (1984) pointed out that sex-changing fishes often have bimodal length–frequency distributions. In the case of protandric species, small individuals are usually males and large specimens are usually females. The protandry was also pointed out in studies which dealt with the sexuality of the species (Alekseev 1967; Andaloro 1982, 1983; Lamrini 1986; Caminas et al. 1990; Djabali 1991). The gradual change from all males to females, with a few hermaphrodites in the intermediate size classes, suggests that hermaphroditism marks a rather brief transitory phase between males and females (Lamrini 1986). The absence of males in the largest size classes implies that sex conversion is essential for all fish (Andaloro 1982, 1983; Lamrini 1986).

The sex structure is mainly determined by the nature of the

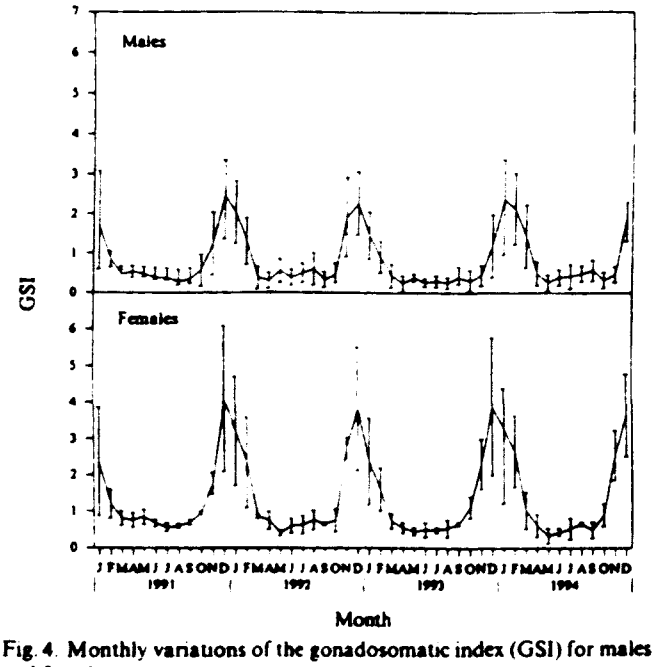

Fig. 4. Monthly variations of the gonadosomatic index (GSI) for males and females

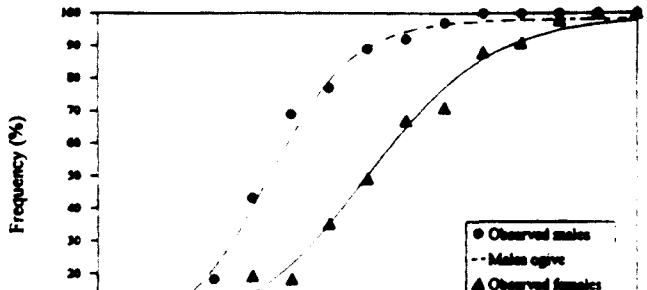

Fig. 5. Sexual maturity ogive for males and females

Table I
Parameters of the relationship between total length and total weight for males, females and all fish and the possibility of isometry tested by Student's *t*-test

	a	*b*	SE (*b*)	*n*	r^2	*t*-test
Males	0.0065	3.2416	0.0337	556	0.985	7.16*
Females	0.0062	3.2813	0.0456	968	0.991	6.16*
All fish	0.0068	3.2401	0.0275	1966	0.989	8.72*

* $t > t_{0.05,\infty} = 1.65$.

sexual change. The overall sex ratio is unbalanced in favour of females because they are fished more than males. The predominance of females has also been observed for this species in the northwest African coast (Lamrini 1986) and in the Alboran Sea (Caminas et al. 1990). Because females are caught more often than males, this species could be classed as vulnerable to unrestrained fishing. Therefore, axillary seabream fishing is an activity that can potentially threaten its target population compared with fishing for more reliable and robust stocks.

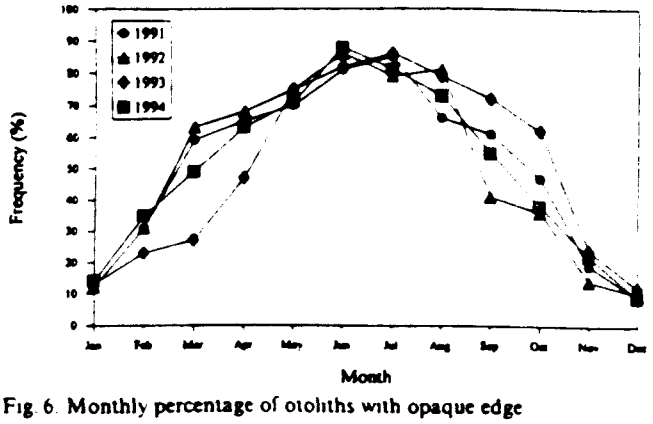

Fig. 6. Monthly percentage of otoliths with opaque edge

The axillary seabream off the Canary Islands has a defined reproductive season which extends from October to March, with a peak in spawning activity in December–January. According to Wootton (1990), the temperature appears to be the most important environmental factor influencing the reproduction of fishes, apparent for the species in this study and demonstrated in other sparids present in the Canary Islands such as *D. gibbosus* (Pajuelo and Lorenzo 1995b), *P. pagrus* (Pajuelo and Lorenzo 1996), and *Pagellus erythrinus* (Pajuelo and Lorenzo 1998). In axillary seabream, the peak spawning in the Canary Islands occurs in winter, whilst in more colder areas it takes place during spring–autumn (Andaloro 1982, 1983; Domanevskaya 1982; Bauchot and Hureau 1986; Caminas et al. 1990). There is a tendency for this species to spawn between winter and spring in low latitudes and later in the year in higher latitudes.

Related to differences in the GSI between reproductively active males and females, in reviewing the reproductive biology of the sparids it is noted that the GSI values of males are commonly lower than those of females. Buxton (1990) pointed out that the cost of producing sperm was thought to be less than that for producing eggs. Although the number of gametes produced does not necessarily need to be a function of the size of the gonad, the difference in male and female gonadosomatic indices suggests that the energy invested in gamete production by males is probably less than that invested by females.

Age at sexual maturity is 2 years for males and 3 years for females. These results are in good agreement with those reported by Andaloro (1983), Caminas et al. (1990) and Santos et al. (1995) in the Mediterranean and Lamrini (1986) in the northwest African coast, these authors pointed out that this species attained sexual maturity in the second year of life. Differences observed in sexual maturity between the sexes may be explained adequately by protandry.

The positive allometry of the total length–total weight relationship was also observed for the species in other studies (Andaloro 1982, Caminas et al. 1990, Santos et al. 1995). Differences between males and females in the length–weight relationship are explained by the different size distributions of the two sexes as a consequence of the protandric hermaphroditism.

The alternative pattern of translucent and opaque zones is easily distinguishable on the otoliths. The opaque zone is formed when the water temperature is higher (Fig. 8) and food is more abundant (Hernandez-Leon 1988), the translucent zone

Table 2
Age–length key for all fish

Size (cm)	Age group (years) I	II	III	IV	V	VI	VII	VIII	IX	X
11	2	1								
12	19	9								
13	63	14	1							
14	49	57	9							
15	23	95	17							
16	6	89	31	3						
17	3	69	47	8						
18	1	33	71	13						
19		26	85	29	1	1				
20		11	64	46	4					
21		5	35	64	10	7				
22			16	59	21	7				
23			10	25	36	14	2			
24			3	11	55	22	5	1		
25				5	20	39	13	5	2	
26				1	9	31	19	6	1	1
27					3	11	13	9	6	
28					2	4	5	11	12	1
29						1	2	8	17	3
30							1	3	2	4
31								1	2	2
n	166	409	389	264	161	137	60	44	42	11
x	12.9	15.8	19.2	21.8	23.9	25.6	27.0	28.1	28.9	29.4
SD	0.9	2.1	2.2	1.9	1.6	1.9	1.3	1.1	1.0	0.6

Table 3
Parameters of the von Bertalanffy growth curve for males, females and all fish

	L_∞ (cm)	k (years^{-1})	t_0 (years)	n	r^2
Males	27.98	0.27	−0.67	489	0.963
Females	33.90	0.21	−0.99	801	0.986
All fish	32.98	0.22	−0.87	1683	0.989

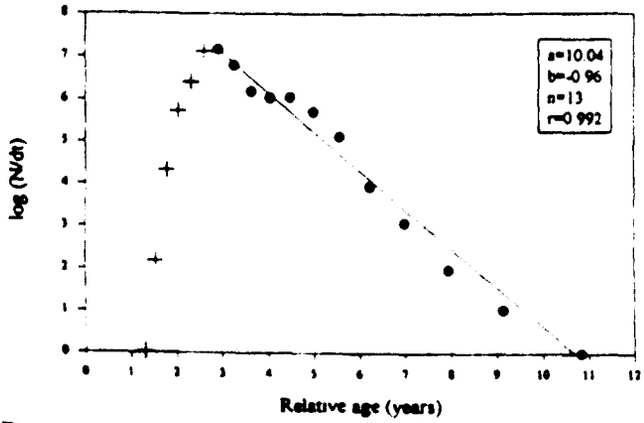

Fig. 7. Length-converted catch curve. The initial data points (+) were not used in the regression

is formed when the species spawns and the temperature is lower. The oldest age class observed was 10 years, although this age class was poorly represented in the landings. In the Mediterranean, Andaloro (1982) found that individuals of this species can reach an age of 8 years.

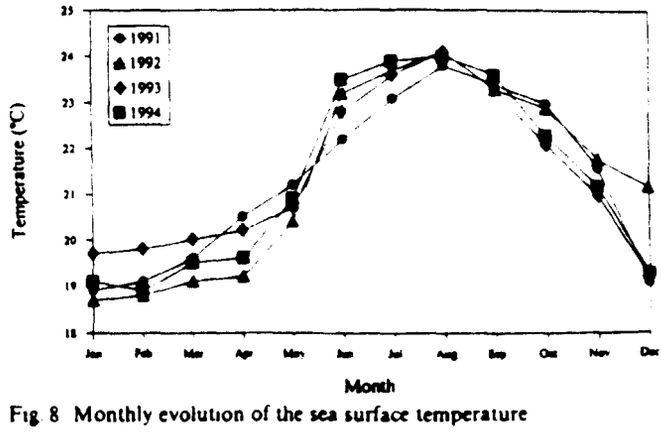

Fig. 8. Monthly evolution of the sea surface temperature

As a whole, growth of the axillary seabream off the Canary Islands is relatively slow, with males growing at a slightly faster rate than females, showing the typical pattern of the protandric sparids (Buxton 1993). Andaloro (1982, 1983) also observed that growth was different between males and females of axillary seabream. Shapiro (1984) indicated that the mean length of sex-reversed fish was slightly larger than same-age males. Therefore, differences in length between males and females of the same age cannot be considered as evidence of an intersexual difference in growth rates because females and males are the same individuals at different phases of sexual succession and, possibly, the largest males in an age group are the first to change sex (Shapiro 1984).

The growth parameters obtained for all individuals in the present study differ from those reported by Djabali (1991) for the same species off northwest Africa. Differences in growth between both regions can be attributed to differences in the size of the largest individual sampled in each area. The largest fish

found in the study conducted by Djabali (1991) was less than 23 cm total length.

The value of the instantaneous rate of natural mortality obtained in this study was lower than those given by Mennes (1984), Zoubi (1985), and Djabali (1991) off northwest Africa (0.46, 0.52, and 0.44 years^{-1}, respectively). However, the values obtained in this study for the axillary seabream were in the range of those obtained for other temperate sparid species of the Canary Islands (0.15–0.55 years^{-1}) (Pajuelo and Lorenzo 1995b, 1996, 1998; Pajuelo et al. 1997).

The length-converted catch curve showed a typical form and justified the estimation of a single value of Z (Pauly 1983). The exploitation ratio was higher than 0.50. Gulland (1971) suggested that, as a rule of thumb, a fish stock is optimally exploited at a level of fishing mortality which generates $E = 0.50$, where $F_{opt} = M$, but in the present study $F > F_{opt} = M$. More recently, Pauly (1987) proposed a lower optimum fishing mortality, $F_{opt} = 0.4 \cdot M$ ($F > F_{opt}$). Therefore, the stock of the axillary seabream of the Canary Islands is being heavily exploited. The value of the length at first capture is lower than the value of the size at sexual maturity. Over 35% of the total catch was less than this length, indicating a danger of recruitment overfishing. Therefore, a change in the fishing legislation may be necessary.

In the Canary Islands, the present legislation for axillary seabream stipulates a minimum size of 18 cm; however, this regulation is of little benefit because the minimum regulation length is smaller than the size at first maturity. The practical problem is that the axillary seabream is only one component of the exploited multispecies demersal fish community (Pajuelo and Lorenzo 1995a) and it matures at a different size than other species (Pajuelo and Lorenzo 1995b, 1996, 1998; Pajuelo et al. 1997). Therefore, this species is susceptible to exploitation at a size when many other coexisting demersal species are mature or immature. Once captured, release is of dubious benefit as they often suffer from barotrauma when brought to the surface from a depth of more than 30 m (Smale 1988). Another protection strategy was the introduction of an artificial reef, but it appears to serve only the earlier stages of the life cycle and encompasses only limited areas. When immature individuals move out of an artificial reef, they are subject to high exploitation because fishermen deploy large numbers of traps around the reef. Finally, other measures such as closed seasons or changes in fishing pattern are desirable to safeguard the spawning stock and the recruits, especially if the stock decline continues.

Acknowledgements

The authors are very grateful to Professor Dr A. G. Ramos for reading the manuscript and for valuable comments; to Ms C. Tascon for her assistance in preparing the English version of the manuscript; to Ms N. Hernandez for help in collecting the material.

References

Alekseev, F.E., 1967: Hermaphroditism and regulation of population sexual structure in *Pagellus acarne* (Risso, 1826). ICES C.M. 1967/G:7.

Andaloro, F., 1982: Resume des parametres biologiques sur *Pagellus acarne* de la mer Tyrrhenienne meridionale et de la mer Jonienne septentrionale. FAO Fish. Rep. 266, 89–92.

Andaloro, F., 1983: About the catch, the diet, the reproduction, the size frequency and distribution of *Pagellus acarne* (Risso, 1826) in the Strait of Messina area. Rapp. Comm. Int. Mer Medit. 28 (5), 33–37.

Bauchot, M.L., Hureau, J.C., 1986: Sparidae. In: Fishes of the Northeastern Atlantic and the Mediterranean, Vol. II. P.J.P. Whitehead, M.L. Bauchot, J.C. Hureau, J. Nielsen, and E. Tortonese (Eds). UNESCO, Paris, pp. 883–907.

Bauchot, M.L.; Hureau, J.C., 1990: Sparidae. In: Check-list of the fishes of the eastern tropical Atlantic. Clofeta II. J.C. Quero, J.C. Hureau, C. Karrer, A. Post, and L. Saldanha (Eds). UNESCO, Paris, pp. 790–812.

Beverton, R.J.H., Holt, S.J., 1957: On the dynamics of exploited fish populations. Fisheries Investigations Series II, XIX. HMSO, London.

Buxton, C.D., 1990: The reproductive biology of *Chrysoblephus laticeps* and *C. cristiceps* (Telesostei: Sparidae). J. Zool. (London) 220, 497–511.

Buxton, C.D., 1993: Life-history changes in exploited reef fishes on the east coast of South Africa. Env. Biol. Fishes 36, 47–63.

Buxton, C.D., Garratt, P.A., 1990: Alternative reproductive styles in seabreams (Pisces: Sparidae). Env. Biol. Fishes 28, 113–124.

Caminas, J.A.; Baro, J.; Nunez, J.C.; Ramos, F., 1990: Local fishery study of the Spanish South Mediterranean region (between Punta Europa and Cabo de Gata). III year. Report IEO/EEC Collaboration Projects XIV-B-1/1989/90.

Djabali, C., 1991: Travaux realises sur les stocks pelagiques et demersaux de la region de Beni-Saf. FAO Rapp. Peches 447, 160–170.

Domanevskaya, M.V., 1982: Specifics of the distribution of *Pagellus acarne* (Sparidae) in the southwestern Mediterranean Sea. J. Ichthyol. 22 (2), 127–130.

Gayanilo, F.C.; Soriano, M.; Pauly, D., 1988: A guide to the Compleat ELEFAN. ICLARM Software 2. Manila, ICLARM.

Gulland, J.A., 1971: The Fish Resources of the Ocean. Fishing News (Books) Ltd, West Byfleet.

Hernandez-Leon, S., 1988: Ciclo anual de la biomasa del mesozooplancton sobre un area de plataforma en aguas del Archipielago canario. Inv. Pesq. 52 (1), 3–16.

Holden, M.J.; Raitt, D.F.S., 1975: Manual de ciencia pesquera. Parte II. Metodo para investigar los recursos y su aplicacion. FAO Doc. Tec. Pesca 115.

Lamrini, A., 1986: Sexualite de *Pagellus acarne* (Risso 1826) (Teleosteen Sparidae) de la cote Atlantique Meridionale du Maroc (21°-26° N). Cybium 10 (1), 3–14.

Mennes, F., 1984: Assessments of the stocks of Sparidae and *Trachurus trachurus* off Morocco. CECAF/TECH/ 84/62, 1–170.

Morales-Nin, B., 1987: Metodos de determinacion de la edad en los osteictios en base a estructuras de crecimiento. Inf. Tec. Inst. Inv. Pesq. 143, 1–30.

Pajuelo, J.G.; Lorenzo, J.M., 1995a: Analisis y prediccion de la pesqueria demersal de las Islas Canarias mediante un modelo ARIMA. Sci. Mar. 59 (2), 155–164.

Pajuelo, J.G.; Lorenzo, J.M., 1995b: Biological parameters reflecting the current state of the exploited pink dentex *Dentex gibbosus* (Pisces: Sparidae) population off the Canary Islands. S. Afr. J. Mar. Sci. 16, 311–319.

Pajuelo, J.G.; Lorenzo, J.M., 1996: Life history of the red porgy *Pagrus pagrus* (Teleostei: Sparidae) off the Canary Islands, Central-East Atlantic. Fish. Res. 28, 163–177.

Pajuelo, J.G.; Lorenzo, J.M., 1998: Population biology of the common pandora *Pagellus erythrinus* (Pisces: Sparidae) off the Canary Islands. Fish. Res. 36, 1–12.

Pajuelo, J.G.; Lorenzo, J.M.; Ramos, A.G.; Villamil-Mata, M., 1997: Biology of the red mullet *Mullus surmuletus* (Mullidae) off the Canary Islands, Central-East Atlantic. S. Afr. J. Mar. Sci. 18, 265–272.

Pauly, D., 1983: Length-converted catch curves: a powerful tool for fisheries research in the tropics (Part I). Fishbyte 1, 9–13.

Pauly, D., 1984: Length-converted catch curves: a powerful tool for fisheries research in the tropics (Part II). Fishbyte 2 (1), 17–19.

Pauly, D., 1987: A review of the ELEFAN system for analysis of length-frequency data in fish and aquatic invertebrates. In: Length-Based Methods in Fisheries Research. D. Pauly and G. R. Morgan (Eds). ICLARM, Manila, pp. 7–34.

Ricker, W.E., 1973: Linear regressions in fishery research. J. Fish. Res. Board Can. 30, 409–434.

Saila, S.B.; Recksek, C.W.; Prager, H., 1988: Basic Fishery Science Programs: A compendium of Microcomputer Programs and Manual of Operation. Dev. Aquacult. Fish Sci. 18, 1–230.

Santos, M.M.; Montero, C.C.; Erzini, K., 1995: Aspects of the biology and gillnet selectivity of the axillary seabream (*Pagellus acarne*, Risso) and common pandora (*Pagellus erythrinus*, Linnaeus) from the Algarve (south Portugal). Fish. Res. **23** (3–4), 223–236.

Shapiro, D.Y., 1984: Sex reversal and sociodemographic process in coral reef fishes. In: Fish reproduction, strategies and tactics. G.W. Potts and R.J. Wootton (Eds). Academic Press, London, pp. 103–117.

Smale, M.J., 1988: Distribution and reproduction of the reef fish *Petrus rupestris* (Pisces: Sparidae) off the coast of South Africa. S. Afr. J. Zool. **23**, 272–287.

Tanaka, S., 1960: Studies on the dynamics and management of fish populations. Bull. Tokai Reg. Fish. Res. Lab. **28**, 1–200.

Wootton, R.J., 1990: Ecology of Teleost Fishes. Chapman & Hall, London.

Zoubi, J., 1985: Les ressources halieutiques. Etud. Rev. Cons. Peches **223**, 1–23.

Author's address: J. G. Pajuelo, Departamento de Biologia, Universidad de Las Palmas de Gran Canaria, Edificio de Ciencias Basicas, Campus Universitario de Tafira, E-35017 Las Palmas de Gran Canaria, Spain.
E-mail: josemaria.lorenzo@biologia.ulpgc.es

Mecanismos de transporte y emplazamiento de depósitos volcanoclásticos en el litoral NE de Gran Canaria (Islas Canarias)

F.J. Pérez Torrado[1], J.L. Schneider[2], D. Gimeno[3], P. Wassmer[4] y M.C. Cabrera[1]

1 Dpto. Física-Geología. Facultad de Ciencias del Mar. Universidad de Las Palmas de Gran Canaria. Campus Universitario de Tafira. 35017-Las Palmas de Gran Canaria.

2 Département des Sciences de la Terre. Université de Lille. Bât. SN5. 59655 Villeneuve d'Ascq Cedex (Francia).

3 Dpto. de Petrología, Geoquímica y Prospección Geológica. Facultad de Ciencias Geológicas. Universidad de Barcelona. Zona Universitaria de Pedralbes. 08071-Barcelona.

4 Cereg (CNRS-UP 2037). Université Louis-Pasteur. Rue de l'Argonne. 67083 Strasbourg Cedex (Francia).

ABSTRACT

A volcano-sedimentary sequence of Pliocene age is described in the Cuevas del Guincho and Trapiche areas (NE shore of Gran Canaria). Three differents kinds of volcaniclastic deposits are recognized interbedded within littoral and marine sedimentary sequence. The lower one was emplaced as a pyroclastic flow of phonolitic composition and probably belongs to Fataga volcanic group. The middle and upper ones correspond to volcaniclastic breccias of the Roque Nublo volcanic group. Whereas the lower breccia unit was emplaced as a debris flow into a shore face marine environment and derived from subaerial pyroclastic flow or lahar, the upper one corresponds to a debris avalanche deposit emplaced in a littoral environment.

The presence of these volcaniclastic deposits attests the existence of discrete volcanic activity during the volcanic hiatus recognized on Gran Canaria between the end of the Fataga volcanic group (Miocene) and the beginning of the Roque Nublo volcanic group (Pliocene).

Key words: *volcaniclastic deposits, shore face-littoral setting, volcanic hiatus, Gran Canaria.*

INTRODUCCIÓN

El crecimiento subaéreo de Gran Canaria se caracteriza por la existencia de un intervalo de inactividad volcánica hacia finales del Mioceno (entre 8,5 a 5,3 m.a., aproximadamente) y que separa los depósitos volcánicos del Grupo Fataga (en la terminología de Schmincke, 1994) de los del grupo Roque Nublo (Pérez Torrado *et al.*, 1995). Es en este intervalo cuando tiene lugar el inicio de una importante acumulación de depósitos sedimentarios en los sectores costeros del NE, E y, en menor medida, S, N y O de la isla, dando lugar a la denominada Formación Detrítica de Las Palmas —FDLP— (Gabaldón *et al.*, 1989; ITGE, 1992) (Fig. 1). Esta formación se divide en tres miembros, correspondiendo el Miembro Inferior a depósitos aluviales (arenas y conglomerados de cantos fonolíticos del Grupo Fataga) originados exclusivamente durante el hiato volcánico, mientras que el Miembro Medio comprende depósitos marinos de características litorales formados al final del hiato volcánico (entre los 5 a 4 m.a., aproximadamente), fruto de un periodo transgresivo en el que se encontraba inmersa Gran Canaria. Finalmente, el Miembro Superior incluye una sucesión de depósitos aluviales, laháricos y piroclásticos, con ocasionales lavas intercaladas, formados contemporáneamente al crecimiento del estratovolcán Roque Nublo en el centro de la isla (Pérez Torrado *et al.*, 1995).

Intercalados con los depósitos marinos del Miembro Medio de la FDLP, a cotas que oscilan entre los 50 a 110 m, se localizan en los sectores costeros del NE de Gran Canaria, una amplia gama de materiales y estructuras producto de la transformación de flujos volcánicos subaéreos (ya fueran lávicos o piroclásticos) al penetrar en el mar. El objeto de este estudio es determinar las características de estas transformaciones en los depósitos volcanoclásticos aflorantes en las áreas de Cuevas del Guincho y Trapiche (Fig. 1).

DESCRIPCIÓN DE LOS MATERIALES

La columna litoestratigráfica más completa se localiza en las Cuevas del Guincho (Fig. 2), donde se encuentra irregularmente recubierta por lavas del Volcán de Arucas (datado en unos 300.000 años). Los depósitos marinos están representados por una serie de niveles arenosos con abundantes estructuras internas e intensa bioturbación, característicos de un ambiente de shoreface, que hacia techo de la columna pasan a un nivel conglomerático muy fosilífero, característico de un ambiente de foreshore (playa de cantos). Una descripción detallada de estos depósitos marinos se encuentra en Cabrera y Pérez Torrado (1988).

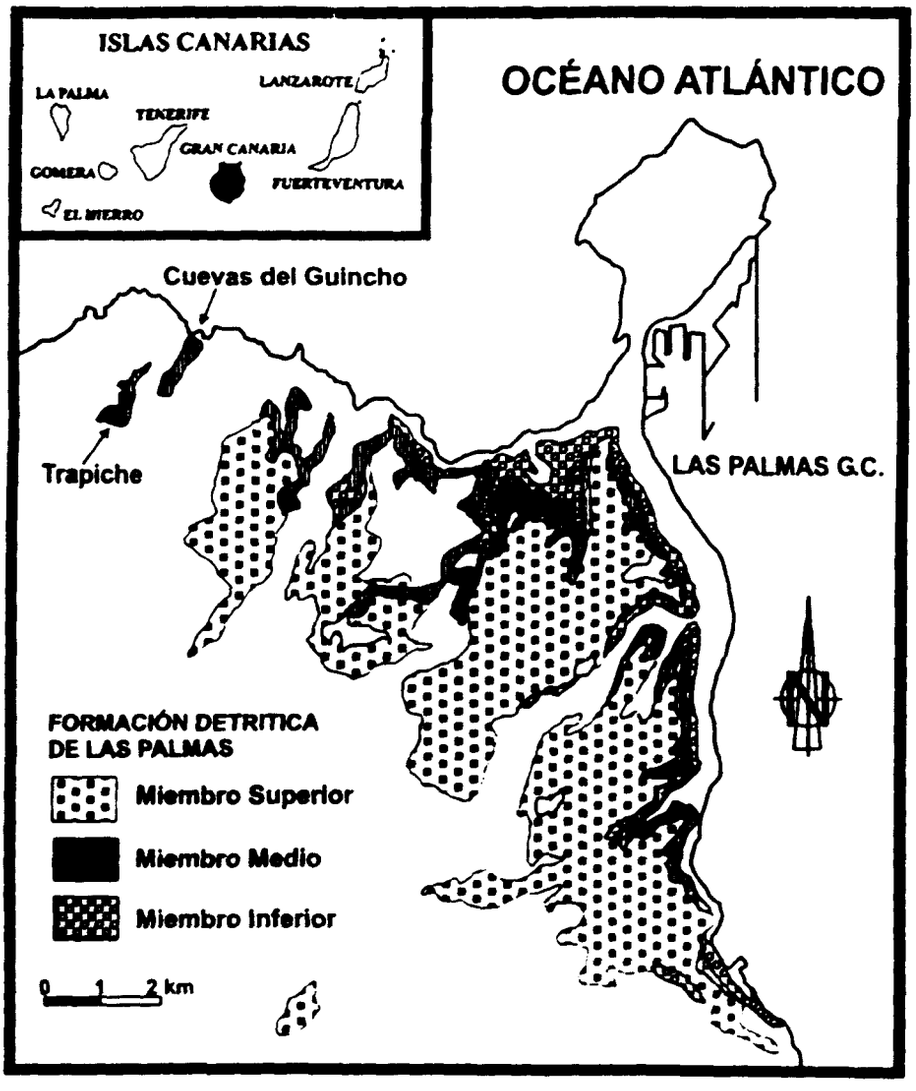

FIGURA 1: *Mapa geológico simplificado de la Formación Detrítica de Las Palmas (modificado de ITGE, 1992). En el Miembro Medio se incluyen tanto los depósitos marinos propios, como los depósitos volcánicos relacionados.*

En cuanto a los depósitos volcanoclásticos, se distinguen tres unidades con características litológicas y estructurales muy diferentes.

Unidad 1 – Tobas fonolíticas

Localizadas en la parte baja de la columna, se observan dos capas de 1 m aproximado de espesor cada una. La apariencia es muy similar a la de los depósitos de "flujo de bloques y cenizas", con un alto porcentaje de material juvenil (muy vesiculado), de color blanco, anguloso a subanguloso, con tamaños medios de unos 5 cm y ausencia total de texturas de soldadura térmica. Los líticos son también de naturaleza fonolítica, subangulosos y con tamaños algo menores que los juveniles. Tanto las bases como los techos de estas capas son en general planos. El aspecto más destacado es la existencia de restos fósiles marinos (moldes y fragmentos de bivalvos y gasterópodos) incorporados en la capa inferior y asociados a la existencia de desdoblamiento de la unidad piroclástica en 3 o 4 de orden menor y espesores del orden de 35 cm, con niveles basales mejor clasificados (arena fina), empobrecidos en pumitas. Los fósiles aparecen inmediatamente por encima de estos niveles basales.

Estos depósitos se interpretan como el resultado de la llegada de flujos piroclásticos subaéreos a un ambiente marino poco profundo, sin apenas modificación de sus estructuras internas. Sus características litológicas permiten englobarlas dentro del Grupo Fataga, lo que implicaría la existencia de discretos periodos explosivos de los volcanes de este grupo de forma casi contemporánea al inicio de la actividad volcánica del Grupo Roque Nublo.

Unidad 2 – Depósito de debris flow

Intercalado hacia la mitad de la secuencia sedimentaria forma un cuerpo de espesor variable (3 a 4 m), cuyas principales características se indican en la figura 3. Destaca el alto contenido en clastos, pudiendo superar el 50% hacia el NE del área. Estos clastos presentan tamaños muy variables, desde submilimétricos hasta unos 70 cm, subredondeados, y de naturaleza muy variada, si bien dominan los

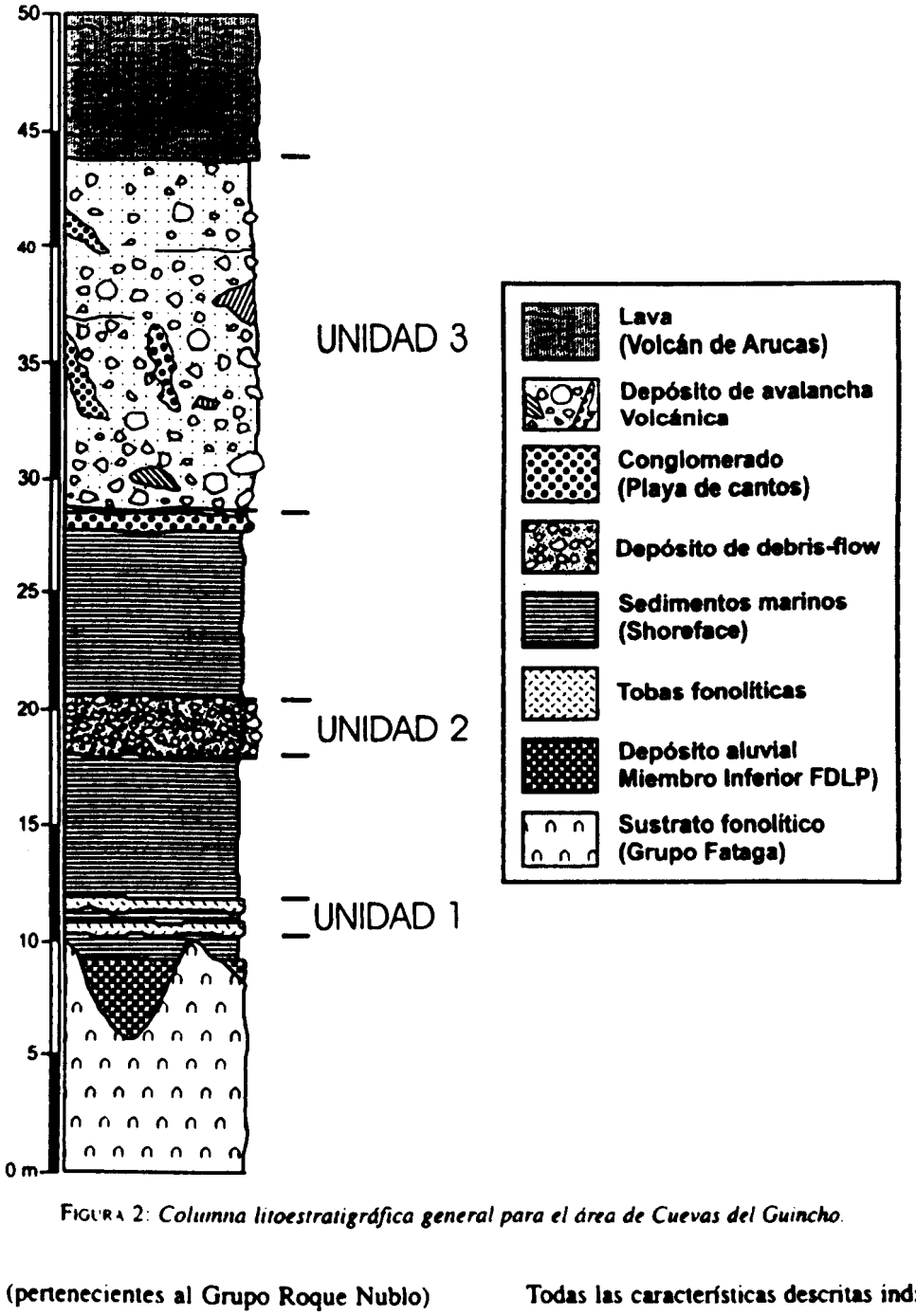

FIGURA 2: *Columna litoestratigráfica general para el área de Cuevas del Guincho.*

de carácter básico (pertenecientes al Grupo Roque Nublo) sobre otros fonolíticos (del Grupo Fataga). Incorpora también numerosos "cantos blandos" de los sedimentos marinos infrayacentes, con formas y tamaños muy variables. La matriz es de aspecto arenoso, si bien se encuentran numerosos fragmentos pumíticos dispersos en la misma. En la base del depósito se observa el desarrollo de un nivel de espesor centimétrico (5 a 10 cm), de granulometría fina y gradación inversa. A techo se localizan algunos moldes de restos vegetales.

Internamente se observa una granoselección positiva de los clastos, tanto de sus tamaños como de sus proporciones, la cual va siendo progresivamente más marcada hacia el SO. En contacto con los sedimentos marinos infrayacentes desarrolla toda una gama de estructuras, siendo diferentes las existentes en las zonas donde este depósito de debris desarrolla nivel basal de las otras zonas sin la presencia del mismo (Fig. 3).

Todas las características descritas indican que este material ha sido transportado y emplazado mediante un mecanismo de "debris flow" en un ambiente marino somero. Durante su transporte subaéreo, el flujo debió incorporar los clastos fonolíticos del lecho del barranco por donde venía encauzado, así como los fragmentos vegetales. Una vez penetra en el mar, incorpora cantidades importantes de agua, lo que provoca procesos de liquefacción en la matriz y elutriación de sus componentes más finos. Consecuentemente, el nivel basal de gradación inversa desaparece y la relación clastos/matriz se incrementa, pudiendo adquirir el flujo un comportamiento "granular" en sus zonas más distales.

La existencia de abundantes clastos de carácter básico permiten englobarlo dentro del Grupo Roque Nublo, pudiendo ser el resultado de la transformación submarina de un lahar o de un flujo piroclástico denso, equivalente a los formadores de las denominadas "ignimbritas Roque Nu-

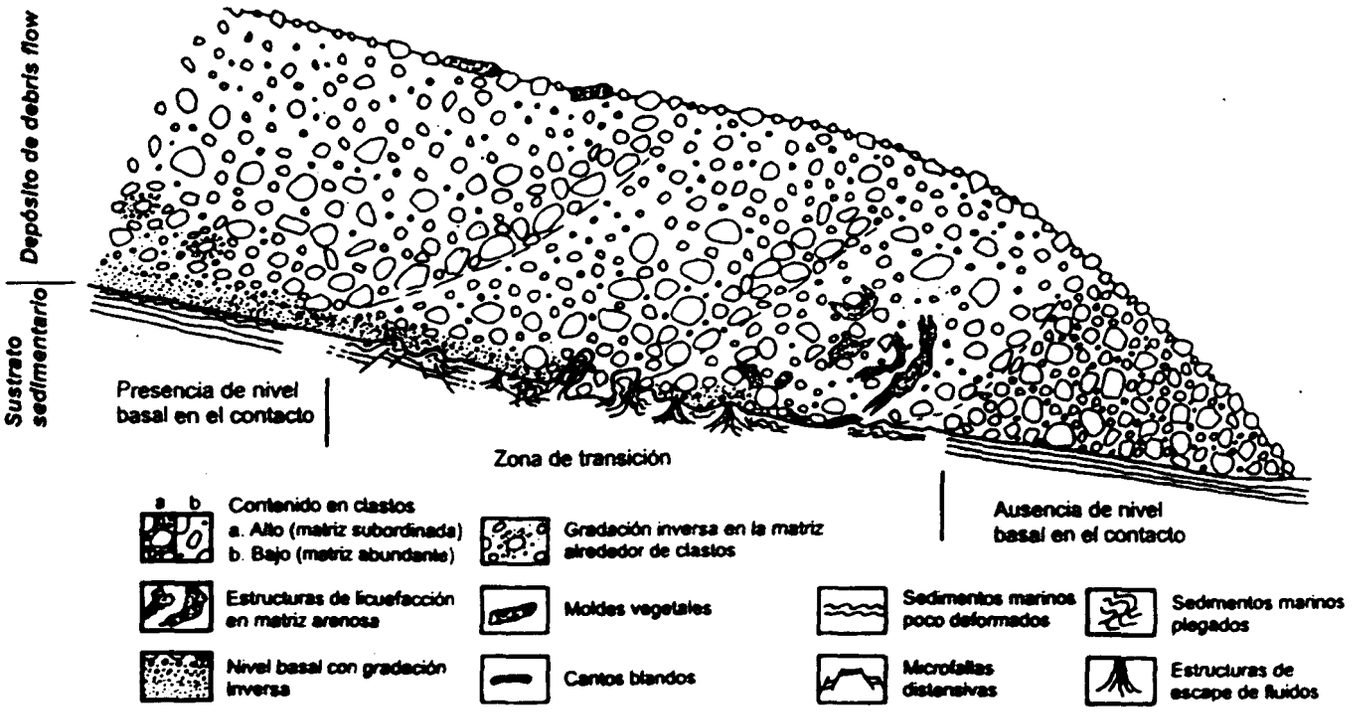

FIGURA 3: *Esquema idealizado con las principales estructuras presentes en los depósitos de debris flow estudiados.*

blo" (Pérez Torrado *et al.*, 1997). En la actualidad se está realizando un detallado estudio paleomagnético para determinar la posible temperatura de emplazamiento de este depósito y de esta forma discriminar con precisión su origen.

Unidad 3 – Depósito de avalancha de debris

A techo de la secuencia volcano-sedimentaria, se presenta como un cuerpo irregular con un espesor promedio de unos 15 m y una amplia gama de estructuras internas (Fig. 4). Está compuesto de bloques angulosos, muy heterométricos (incluso de varios metros de diámetro) y de naturaleza lávica básica o brecha volcánica, en ambos casos atribuibles a depósitos originales del Grupo Roque Nublo. Una gran parte de los bloques presenta fracturación de tipo "jig-saw". En cuanto a la matriz que los rodea, es de naturaleza similar a ellos, muy mal clasificada y con grandes variaciones en su contenido a lo largo del depósito. En ocasiones se encuentran inmersos en la matriz clastos básicos en forma de "bombas", con diámetros del orden de 10 a 20 cm, presencia de grietas radiales de contracción por enfriamiento y márgenes vítreos. Cerca de la base, se observa ocasionales "cantos blandos" derivados de los sedimentos marinos infrayacentes.

Los aspectos más destacados de este depósito, visibles fundamentalmente en el área de Trapiche y en el corte de la carretera GC-810 al paso por las Cuevas del Guincho, son: a) la intensa deformación que provoca en ciertos puntos del mismo a los sedimentos marinos infrayacentes; b) la inyección de "diques neptunianos" de varios metros de longitud (Fig. 4), por succión ascendente desde la base del depósito. El material de estos "diques" es similar a la capa de conglomerados (playa de cantos) situada justo debajo de este depósito, se sitúan de forma oblicua a la base del mismo y al final de ellos conectan con estructuras de escape de fluidos ("pipes").

Las características aquí apuntadas son típicas de los depósitos de avalanchas volcánicas (Ui y Glicken, 1986). En este caso, debe tratarse de una avalancha originada por el colapso lateral de parte del flanco N del estratovolcán Roque Nublo en el centro de la isla, de igual modo que ha sido ampliamente reconocido para sus flancos meridionales (García Cacho *et al.*, 1994). La presencia de "bombas" podría indicar un desencadenamiento del colapso por actividad volcánica y, por tanto, la avalancha pudo ser emplazada a altas temperaturas. En el momento en que penetra en el mar, ingiere agua y sufre procesos de dilatación, lo que permite la inyección de "diques neptunianos" y la presencia de "pipes".

CONCLUSIONES

Los sectores estudiados de Cuevas del Guincho y Trapiche (NE de Gran Canaria) resultan excepcionales por el hecho de que permiten observar las diferentes transformaciones sufridas por depósitos volcanoclásticos subaéreos, con génesis muy diferente, al penetrar en el mar en un ambiente litoral. Tanto el depósito de debris flow como el de avalancha volcánica, muestran numerosas estructuras que indican una importante incorporación de agua a sus flujos cuando estos entraron en el mar. Esta ingestión de agua conduce en ambos flujos a una selectiva elutriación de sus partículas más finas de la matriz y al desarrollo de

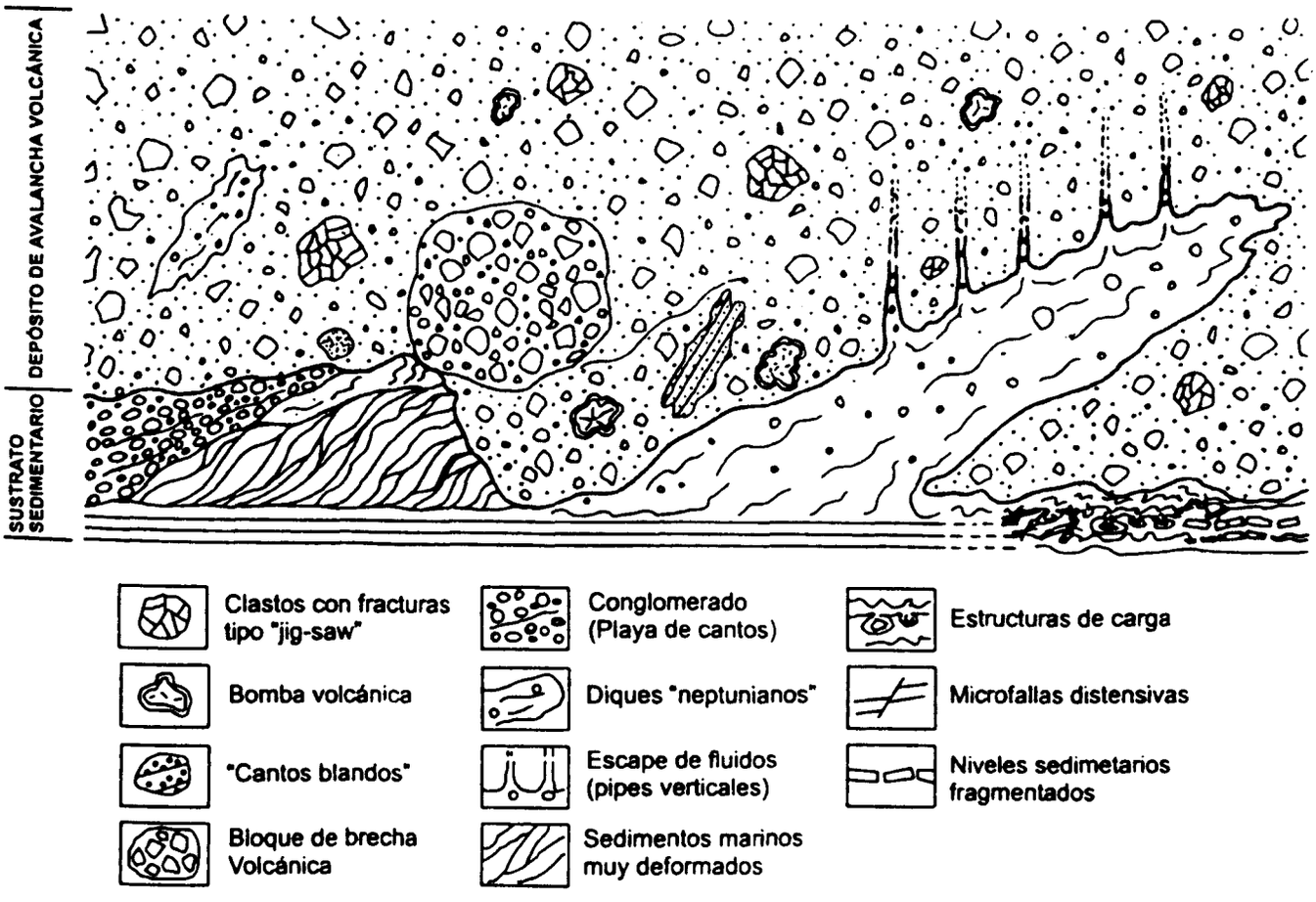

FIGURA 4: *Esquema idealizado con las principales estructuras existentes en los depósitos de avalanchas volcánicas estudiados.*

numerosas estructuras de licuefacción. Por su lado, en las capas de tobas fonolíticas, la ingestión de agua, si se produjo, debió ser poco importante, puesto que estos depósitos muestran características idénticas a sus homólogos subaéreos.

Las características litológicas de estos depósitos volcanoclásticos permiten asignarlos al Grupo Fataga (las tobas fonolíticas) y al Grupo Roque Nublo (los depósitos de debris flow y avalancha volcánica). El que todos ellos se localicen intercalados dentro de la misma secuencia sedimentaria del Miembro Medio de la FDLP, pone de manifiesto que la actividad volcánica del Grupo Fataga, aunque muy atenuada, pudo prolongarse hasta casi el inicio de la actividad del Grupo Roque Nublo. En otras palabras, el hiato volcánico ampliamente aceptado para Gran Canaria, estrictamente no existe.

REFERENCIAS

Cabrera, M.C. y Pérez Torrado, F.J. (1988): Estudio de los materiales sedimentarios y piroclásticos de "las Cuevas del Guincho" (Gran Canaria, Islas Canarias). II Congr. Geol. España, vol. 1: 55-58.

Gabaldón, V., Cabrera, M.C. y Cueto, L.A. (1989): Formación detrítica de Las Palmas. Sus facies y evolución sedimentológica. ESF Meeting on Canarian Volcanism, Lanzarote: 210-215.

García Cacho, L., Díez-Gil, J.L. y Araña, V. (1994): A large volcanic debris avalanche in the Pliocene Roque Nublo stratovolcano, Gran Canaria, Canary Islands. J. Volcanol. Geotherm. Res., 63: 217-229.

ITGE. (1992): Memoria y mapa geológico a escala 1:100.000: Gran Canaria (21-21/21-22).

Pérez Torrado, F.J., Carracedo, J.C. y Mangas, J. (1995): Geochronology and stratigraphy of the Roque Nublo Cycle, Gran Canaria, Canary Islands. J. Geol. Soc. London, 152: 807-818.

Pérez Torrado, F.J., Martí, J., Mangas, J. y Day, S.J. (1997): Ignimbrites of the Roque Nublo group, Gran Canaria, Canary Islands. Bull. Volcanol., 58: 647-654.

Schmincke, H.U. (1994): Geological field guide. 6th edition, Pluto Press, Kiel, 149 p.

Ui, T. y Glicken, H.X. (1986): Internal structural variations in a debris avalanche deposit from ancestral Mount Shasta, California, USA. Bull. Volcanol., 48: 189-194.

Journal of Coastal Research	16	2	329–335	Royal Palm Beach, Florida	Spring 2000

Distributional Pattern of Seagrasses in The Canary Islands (Central–East Atlantic Ocean)

N. Pavón-Salas†, R. Herrera†, A. Hernández-Guerra‡ and R. Haroun†

† Departamento de Biología, ‡ Departamento de Física,
Facultad de Ciencias del Mar
Universidad de Las Palmas de Gran Canaria
35017 Las Palmas, Spain

ABSTRACT

PAVÓN-SALAS, N., HERRERA R., HERNÁNDEZ-GUERRA, A. and HAROUN R., 2000. Distributional pattern of seagrasses in the Canary islands (Central–East Atlantic Ocean). *Journal of Coastal Research*, 16(2), 329–335. Royal Palm Beach (Florida), ISSN 0749-0208.

The present knowledge of the marine phanerogams of the Canary Islands is poorly documented. Earlier studies of the marine phytobenthos along the Canarian coasts provides little information on seagrass ecosystems and their distributional patterns. This contribution summarizes the available information about the three species reported for the islands: *Cymodocea nodosa* (Ucria) Ascherson, *Halophila decipiens* Ostenfeld and *Zostera noltii* Hornemann; and their distributional records is analized in relation with the main oceanographic and geomorphological conditions.

Cymodocea nodosa and *Halophila decipiens* are present in shallow subtidal areas on diverse mobile substrata, whereas *Zostera noltii* has been reported for intertidal communities in one eastern locality of Lanzarote Island, with historical records in Fuerteventura and Gran Canaria Islands. At present, the latter species is not found in any of the mentioned localities and probably its has disappeared due to anthropogenic activities (urban pollution, sediments disturbances).

Most of the localities with seagrass communities are located in the eastern and southern coasts of the islands, always in sheltered areas, protected against Trade Winds. The vertical distribution of *Cymodocea nodosa* meadows ranges from (0.3) 2 to 35 m depth, whereas *Halophila decipiens* meadows are present between 6 to 40 m depth.

ADDITIONAL INDEX WORDS: *Cymodocea nodosa*, *Halophila decipiens*, *Zostera noltii*, *Canary Current*, *trade wind*.

INTRODUCTION

Seagrass meadows are characteristically found growing on unconsolidated substrata of marine environments in tropical and temperate regions. Their pivotal role in many processes of the coastal ecosystems is well established (LARKUM *et al.*, 1989). These flowering plants are considered among the most productive in the biosphere, their meadows serve as nursery and breeding grounds for marine organisms (MCROY and MCMILLAN, 1977; YOUNG, 1978; BELL and WESTOBY, 1986), provide a suitable substratum for epiphytes and are a good source of food for marine herbivores. Seagrasses also act as sediment stabilizers: anchor and filter sediments, breaking tidal and wave energy and contributing to sediment deposition and maintenance of the shoreline (ORTH, 1977).

Earlier studies of the marine vegetation along the Canarian coasts provide little information on seagrasses ecosystems and their distributional patterns. Most publications deal with epiphytes and new records for a certain area (GONZÁLEZ, 1976; 1977; 1980; 1986; AFONSO-CARRILLO and GIL-RODRÍGUEZ, 1980; GIL-RODRÍGUEZ and CRUZ-SIMÓ, 1981; GIL-RODRÍGUEZ *et al.*, 1982; GIL-RODRÍGUEZ *et al.*, 1987; REYES, 1993).

The objectives of this study were to investigate the spatial distribution pattern of seagrasses in relation with major oceanographic and geomorphological conditions, as well as their bathymetric range along the coastlines of the Canarian Archipelago.

96079 received 13 June 1996; accepted in revision 28 February 1997

STUDY AREA

The Canarian Archipelago is located near the Northwest African Coast (Figure 1); the minimum distance between both areas is about 110 km. This volcanic archipelago is composed of seven main islands and several islets. Except in the case of Lanzarote and Fuerteventura, which share the same subtidal platform, the ocean botton may reach more than 2,000 m depth among the islands. Only in the most aged islands are there wider insular platforms, mainly located at the Southern and South-western coasts. Sandy bottoms appear in such areas.

The Northeast Trade Wind dominates the Canarian coastal climate. The wind waves related to the Trades strongly influence the morphology of the Northern coast. This factor is responsible for the strong coastal erosion in these upwind areas. The Southern coasts, which are downwind and therefore sheltered from the Trades, are characterized by a low relief with gentle sloping coastlines and sandy beaches. The main oceanographic features of this region are the Canary Current and the North-West-African coastal upwelling. The Canary Current, the easternmost branch of the North Atlantic Subtropical gyre, transports cold water from high latitudes

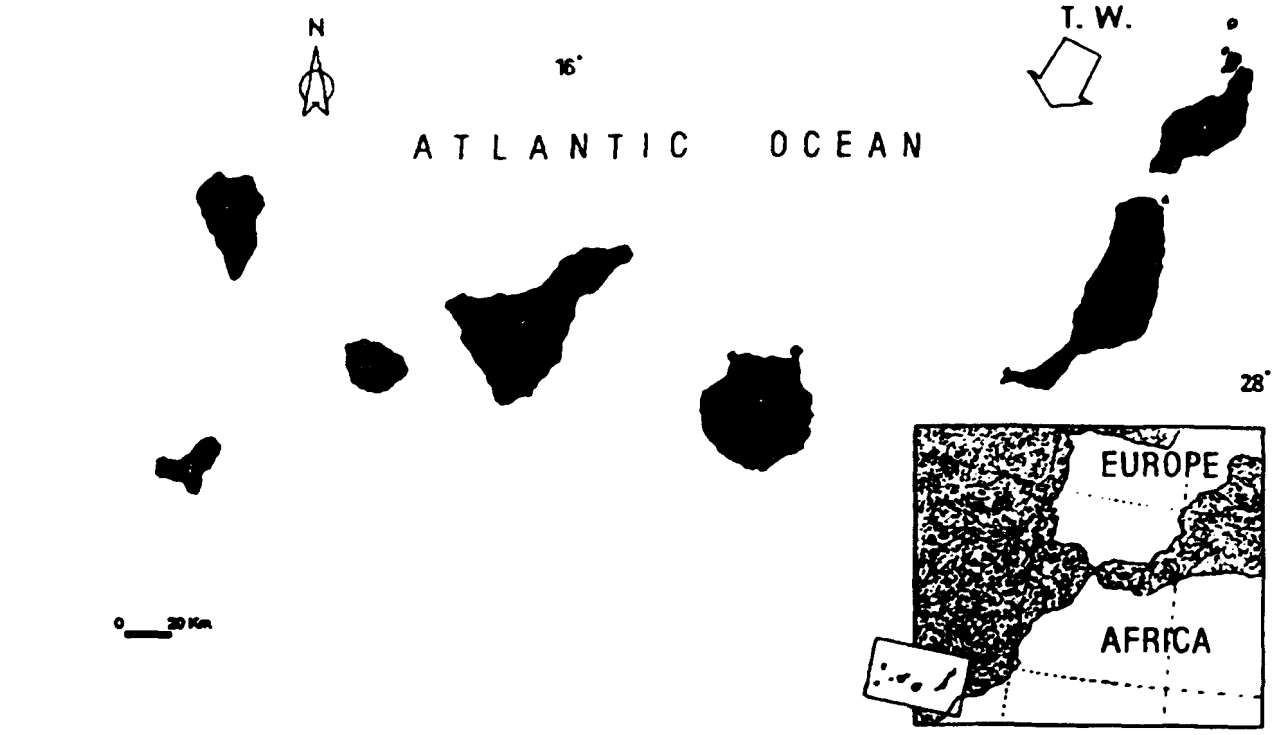

Figure 1. Location of the Canarian Archipelago in the Central-East Atlantic Ocean. L: Lanzarote; F: Fuerteventura; GC: Gran Canaria; T: Tenerife; G: Gomera; P: La Palma and H: El Hierro; T.W.: Trade Winds.

(STRAMMA, 1984). The influence of the cold upwelled water in the African coast can extend away from the coast, reaching the eastern islands of the Archipelago; this may lead a longitudinal gradient in temperature, salinity and nutrients (LLINÁS *et al.*, 1994; MITTELSTAEDT, 1991; VAN CAMP *et al.*, 1991).

MATERIALS AND METHODS

Seagrass species and their distributional patterns were recorded by SCUBA diving at several localities in the Canarian Archipelago, from 1991 to 1995. These field observations were complemented with historical records from a thorough review of the related literature. In localities where misidentifications had occurred, samples were collected and examined in the laboratory.

Two Sea Surface Temperature (SST) images from the Advanced Very High Resolution Radiometer (AVHRR) onboard US National Oceanic and Atmospheric Administration (NOAA) satellites have been processed to describe the SST pattern in the Canary Islands region. The AVHRR is a multichannel radiometer with two channels situated in the thermal infrared region of the electromagnetic spectrum where the atmosphere is almost transparent. The method used to atmospherically correct the AVHRR data and to estimate the SST is described in CASTAGNÉ *et al.* (1986). A geometrical correction of the images was carried out using ground control points. The images are presented with a pixel resolution of approximately 1 km.

Plant Description

At the present time, three seagrass species are reported for the marine flora of the Canary Islands: *C. nodosa*, *Z. noltii* and *H. decipiens*.

Cymodocea nodosa is a seagrass that contains rhizomes bearing adventitious roots and leaf bundles at their extremities. There are two types of rhizomes, orthotropic and plagiotropic, based upon its growth pattern (CAYE and MEINESZ, 1985). The leaves are alternates and opposite, and completely envelop the rhizomes. The differential characteristic of this species is the presence of leaf scars along the rhizomes and numbers of veins in the leaf (DEN HARTOG, 1970). This subtidal species, mainly occurring in the Mediterranean and on the northern parts of the Atlantic coast of Africa and the Canary Islands (DEN HARTOG, 1970; AFONSO-CARRILLO and GIL-RODRIGUEZ, 1980), is the most abundant in Canarian archipelago.

Halophila decipiens is a small plant, monoecious, with a slender rhizome not exceeding 1 mm in diameter and internodes 0.5–4.5 cm long. Roots of 2–5 cm long, 0.2–0.5 mm thick. Both, solitary roots and leaves paired born on a petiole, sprout at each node. Leaves are elliptic-oblong, with a rounded apex, a base sometimes cuneate, 5–10 mm length and not more than 5 mm width (DEN HARTOG, 1970). *H. decipiens*, the second species most abundant in the Canarian Archipelago, has a pantropical distribution in the Indian and the Pacific Oceans as well as the Caribbean Sea and the Canaries

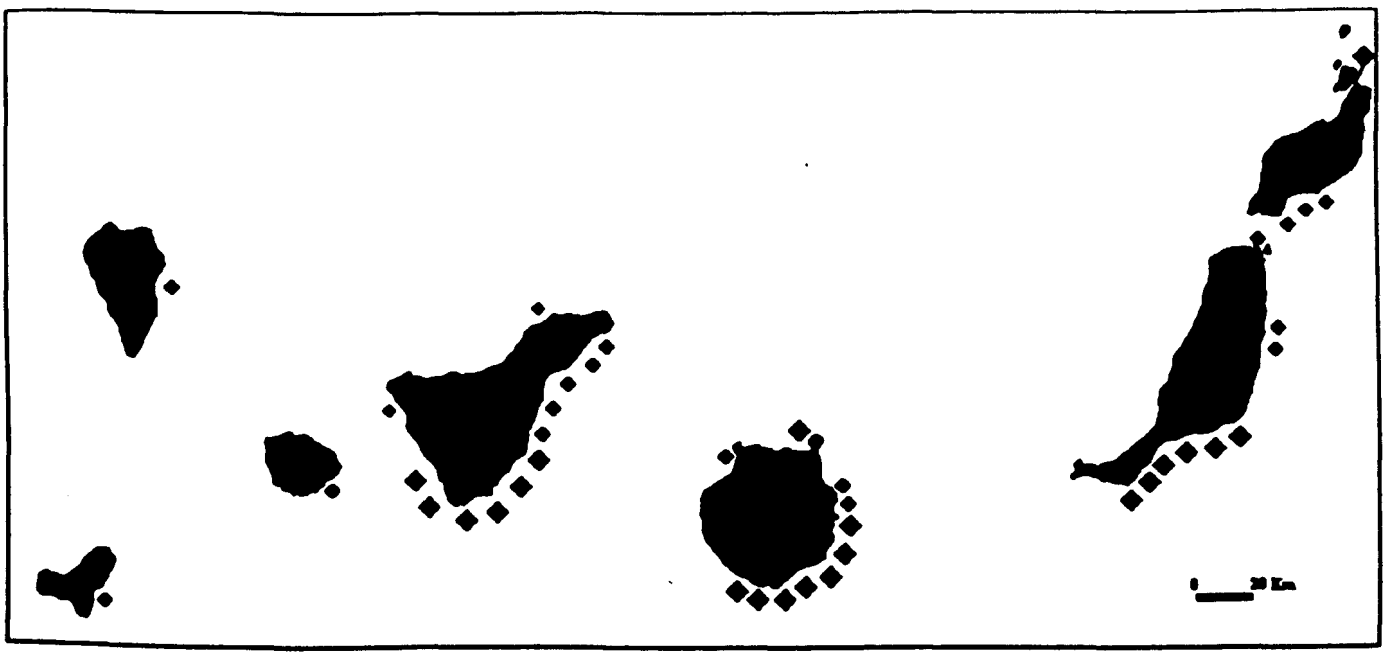

Figure 2. Distributional range of *Cymodocea nodosa* along the Canarian coasts. The different sizes of the ♦ represent a qualitative degree of the meadows extension.

(DEN HARTOG, 1970; GIL-RODRIGUEZ and CRUZ SIMÓ, 1981; GIL-RODRIGUEZ *et al.*, 1982).

Zostera noltii contains slender rhizomes of two types, plagiotropic and orthotropic, of 1 mm width, with a high number of roots. *Z. noltii*, which usually grows intertidally and has a wide distribution along the coast of western Europe and northern Africa (DEN HARTOG, 1970), is the third seagrass reported in the Canarian coasts.

RESULTS

Cymodocea nodosa

In the Canary Islands, *C. nodosa* can be found developing unispecific meadows as well as mixed with *H. decipiens* in muddy bottoms or with the green macroalga *Caulerpa prolifera* in sandy bottoms.

In relation to the structure of the meadows, it is possible to distinguish different types: from continuous meadows to patchy stands and sporadic bundles. The meadows of *C. nodosa* along the coasts of the central islands, such as Fuerteventura, Gran Canaria and Tenerife, form continuous and extensive meadows, compared with those of the marginal islands, such as Lanzarote, La Gomera, La Palma and El Hierro, where there are isolated meadows with a patchy structure.

The vertical distribution of *C. nodosa* in Canary Island ranges from 2 to 35 m depth; but there is one exception, Isla de Lobos, where it can be found in shallow tidepools (0.3 m depth).

The substrata are variable from coarse sand to muddy bottoms. In some localities, such as Las Canteras Beach, *C. nodosa* grows in mixed substratum with small rocks and coarse sand.

Distributional Pattern

Figure 2 represents the distributional range of *C. nodosa* along the Canarian coasts. The distribution area of this species begins at Alegranza, the northernmost islet which presents a mixed meadows that were sighted recently in the protected Southern coast. Between La Graciosa islet and Lanzarote island, in El Rio Strait, occurs a meadow of *C. nodosa* (WILDPRET *et al.*, 1987). In others stations along the Eastern coast of Lanzarote Island, *C. nodosa* can be found (WEBB AND BERTHELOT, 1836–1850; WILDPRET *et al.*, 1987).

The next place where this species appears is Isla de Lobos, an islet adjacent to the North-eastern coast of Fuerteventura Island. As it occurs in the others islets, the meadows grow in the protected Southern coast, but in this locality some very shallow populations were found inside shallow tidepools (0.3 m depth).

Along the coasts of Fuerteventura Island there are the highest number of meadows, all of them located in the Eastern and Southern coasts (WILDPRET *et al.*, 1987).

In Gran Canaria Island, this species is also present to a large extent on the Eastern, South-eastern and South-western coasts (Wildpret *et al.*, 1987; GONZALEZ, 1977). Besides, here there are seagrass communities in one northern locality, the Confital Bay, where a natural reef shelters a sandy beach (Las Canteras Beach). In this locality, *C. nodosa* meadows appear both in the protected inner side of the reef (GONZALEZ, 1976) as well as in the exposed outer side.

Tenerife Island contains the most continuous and extensive

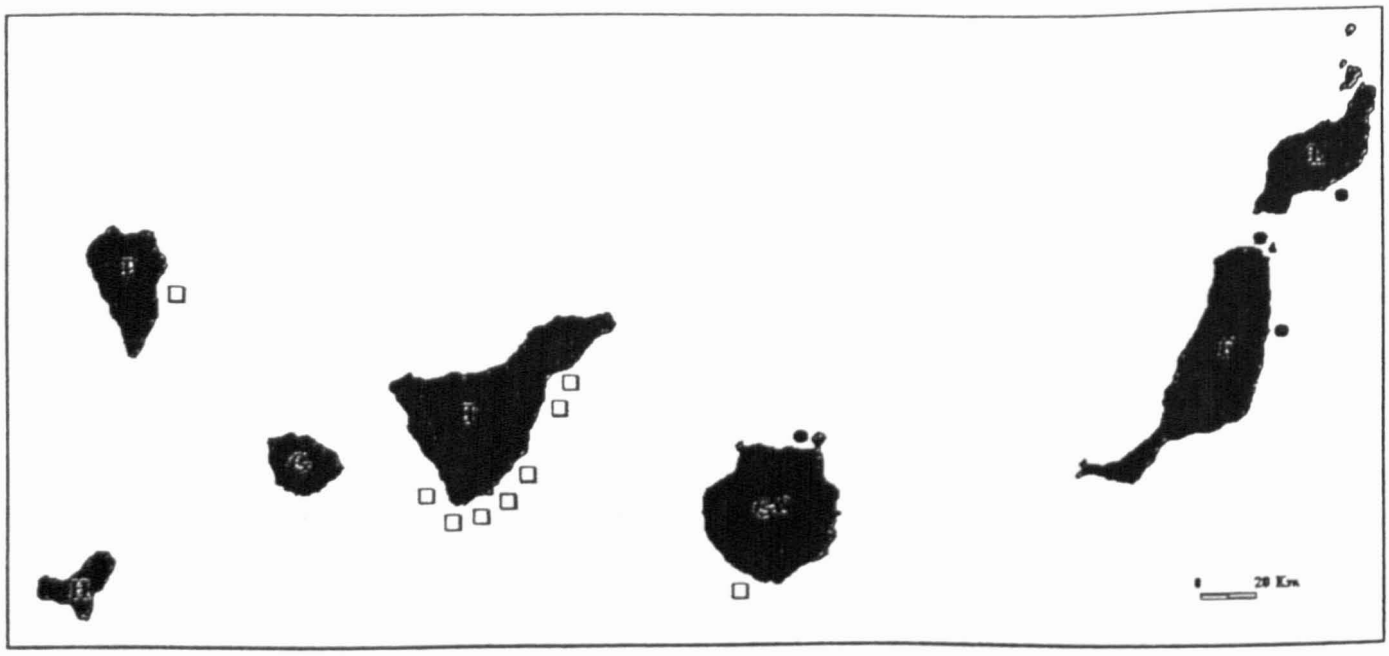

Figure 3. Distributional range of *Halophila decipiens* (□) and *Zostera noltii* (●) along the Canarian coasts.

C. nodosa meadows along the Eastern, Southeastern and Southwest coasts (WILDPRET *et al.*, 1987). Moreover, discrete meadows are recorded in the Northeastern coast. Elsewhere, there is a discrete *C. nodosa* community in one northern locality, Bajamar, (WILDPRET *et al.*, 1987): this latter station needs further confirmation.

La Gomera, La Palma and El Hierro are islands with only a single locality for this species and, in the three cases, these are located in the Eastern coasts, inside the main harbours of each island: Port of San Sebastián de La Gomera (as *Zostera marina*, SANTOS GUERRA, 1972), Port of Santa Cruz de La Palma and Port of La Estaca (WILDPRET *et al.*, 1987).

Halophila decipiens

H. decipiens can be found as unispecific meadows, in deeper water, as well as in mixed meadows with *C. nodosa* in shallower environments.

The structure of the meadows is in homogeneus patches, which are evenly distributed. The vertical distributional range of this species is between 6 and 40 m depth. The most common range is between 13 to 30 m depth.

With respect to the substrate type, *H. decipiens* has been found growing on muddy bottoms.

Distribution Pattern

In Figure 3 is represented the distributional range of *H. decipiens* along the Canarian coasts. In Gran Canaria Island, *H. decipiens* was recently found in the Southwestern coast at 17 m at Puerto Rico station (BETANCORT *et al.*, 1995). It grows predominantly in monoespecific patches but when the depth decreases, it is found mixed with another seagrass, *C. nodosa*.

In Tenerife, this species was previously found at two localities: Costa Caricia and El Confital, in the Eastern and South-eastern coast of the island (GIL-RODRÍGUEZ *et al.*, 1982). Recent studies carried out around this island resulted in a great increase of its known distributional range along the South and South-western coasts. In these localities it grows near or associated with *C. nodsa* meadows.

Elsewhere, this species was recently reported for La Palma Island, in the Port of Santa Cruz de La Palma, at 6–9m depth (HERNÁNDEZ-GONZALEZ and GIL-RODRÍGUEZ, 1993).

Zostera noltii

At present time, *Z. noltii* is not found on Canary Islands.

The last reference about this species was done by GUADALUPE *et al.* (1995), after their studies carried out in Arrecife (Lanzarote), between 1991 and 1992, who referred to it as a poorly distributed community in little patches, in a intertidal community inside the reef area. Recent surveys of this area did not confirm this record and presumably this phanerogam is not present.

Distributional Pattern

In the Figure 3 is represented the historical record for the distributional range of *Zostera noltii*; the distribution of this species was very restricted in the Canarian Archipelago. In the last century, BOLLE (1892) mentioned the presence of this species, as *Z. nana*, in Puerto Cabras (Fuerteventura Island). GONZÁLEZ (1980) reported this species in Las Canteras Beach, Confital Bay (Gran Canaria Island) with samples collected between 1976–1980. The same author, in 1983 recorded this species forming meadows with *C. nodosa* in Corralejo Beach. Later, WILDPRET and DEL ARCO (1987) reported it in

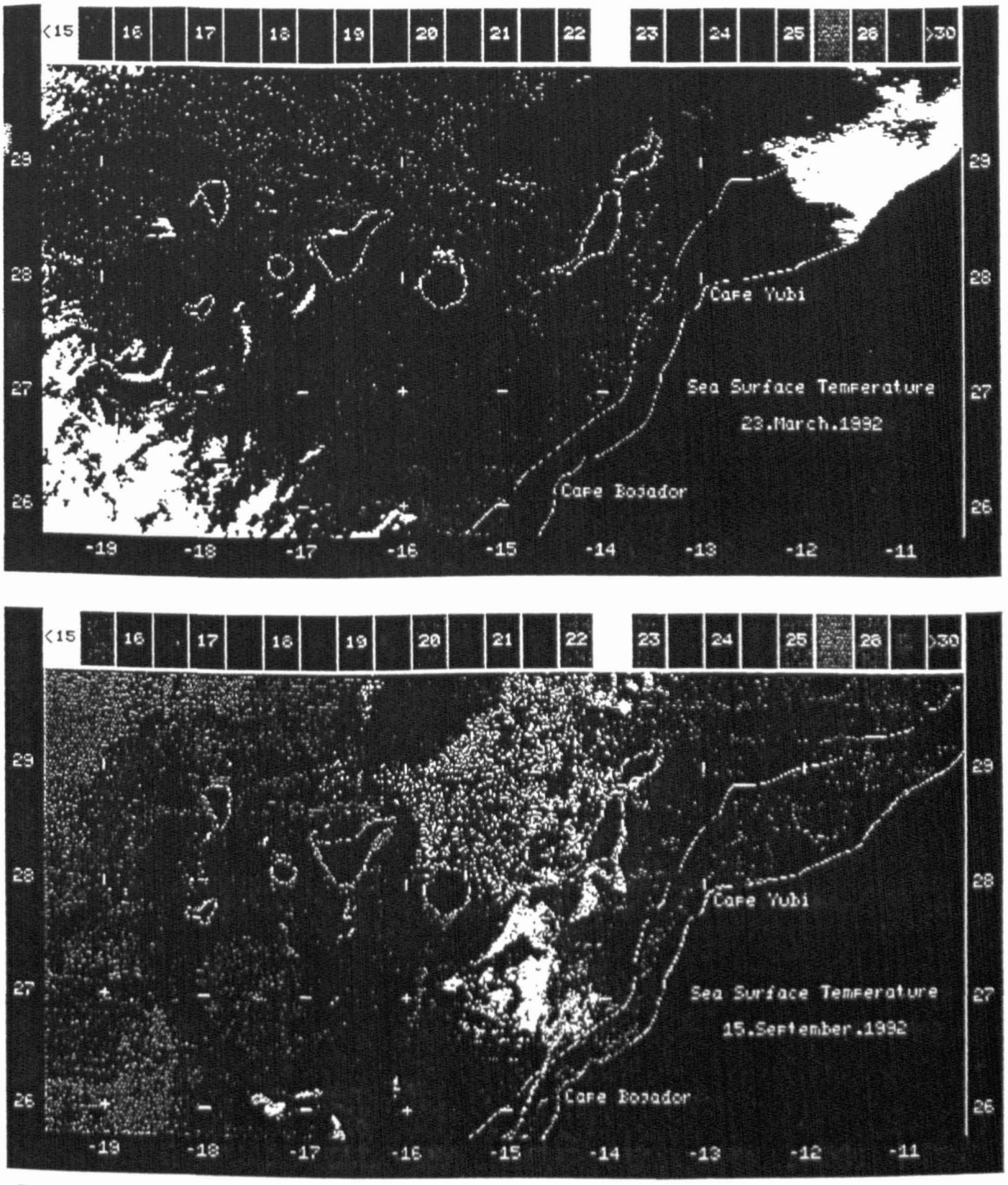

Figure 4. Images corresponding to the coldest and warmest period of the seasonal cycle. These images are colour coded, with each colour covering a Sea Surface Temperature (SST). The temperature is given in Celsius degrees. The white crosses in the images are one degree apart, both in latitude and in longitude. The two white lines along the African coast are the 0 and the 200 m isobath, the latter approximately coinciding with the edge of the shelf.

the Northern coast of Fuerteventura, but without mentioning any specific locality. The last record was on the Eastern coast of Lanzarote Island, Arrecife, where it was reported as an intertidal community inside the harbour (GIL-RODRÍGUEZ *et al.*, 1987; GUADALUPE *et al.*, 1995). At present time, *Z. noltii* is not found in any of the above-mentioned localities.

DISCUSSION AND CONCLUSIONS

The oceanographic and geomorphological features of the Canary Islands may explain the distributional pattern of seagrasses found around the islands. The north parts of the islands are exposed to the prevailing direction of Trade Winds and the Canary Current. These physical process mostly affect the northern coasts of the islands, limiting the development of seagrass meadows. Furthermore, the north area of the islands is colder than the south, as observed in Figure 4. This figure corresponds to approximately the coldest and warmest periods of the seasonal cycle in the Canarian Archipelago, and shows a large warm water wake in the leeward side of the islands, with a temperature of about 2°C higher than the north. Water temperature also increases from the Africa coast towards the more oceanic water to the west, due to the influence of the North-West-African coastal upwelling. The seasonal annual variation of temperature is 16–18 °C in winter time (March) to 23–25 °C in summer time (September).

The islands of Fuerteventura, Gran Canaria and Tenerife, in the central part of the Archipelago, possess wider subtidal platforms, with sandy substrata and gentle sloping coastlines at the eastern, southern and western littoral zones. Also, these areas are sheltered against Trade Winds. In the case of Lanzarote, La Gomera, La Palma and El Hierro, there are not extensive subtidal platforms and, as result of the shape of these islands, few littoral areas are protected against the Trade Winds.

In consequence, it seems that extensive seagrass meadows of *C. nodosa* can develop in the protected southeast and southwest coasts of Fuerteventura, Gran Canaria and Tenerife; whereas in Lanzarote, La Gomera, La Palma and El Hierro only small seagrass patches have been found, sometimes only inside harbours. The exceptional case of Las Canteras, in the north coast of Gran Canaria Island, is due to the peculiar morphology of the place, with a natural reef that shelters a sandy beach. The occurrence of *H. decipiens* in Gran Canaria, Tenerife and La Palma islands seems to be related to the combined effect of some factors, as well as seawater temperatures and substrate characteristics. The recent increase of the records of seagrass distribution in Tenerife Island may suggest that this plant is more common along the subtidal areas of the island. In the case of *Z. noltii*, its disappearance from historical localities in Gran Canaria, Fuerteventura and, more recently from Lanzarote, seems to be related to the high anthropogenic pressure on these coasts (urban pollution, sediments disturbances), which actually are part of urban areas. Nevertheless, the distributional range of this species extent to the south along the African coast, Banc d'Arguin (DEN HARTOG, 1970).

LITERATURE CITED

ALFONSO-CARRILLO J. and GIL-RODRÍGUEZ, M.C., 1980. *Cymodocea nodosa* (Ucria) Ascherson (Zannichelliaceae) y las praderas submarinas o "sebadales" en el Archipiélago Canario. *Vieraea*, 8 (2), 365–376.

BELL, J.D. and WESTOBY, M., 1989. Abundance of macrofauna in dense seagrass is due to habitat preference, not predation. *Oecologia*, 68, 205–209.

BETANCORT VILLALVA, M.J.; GONZÁLEZ HENRÍQUEZ, M.N.; HAROUN TABRAUE, R.; HERRERA PÉREZ, R.; SOLER ONÍS, E., and VIERA RODRÍGUEZ, M.A., 1995. Adiciones corológicas a la flora marina de Canarias. *Botanica Macaronesica*, 22, 75–89.

BOLLE, C., 1892. Florula insularum olium Purpurariarum, nume Lanzarote et Fuerteventura cum minoribus Isleta de Lobos et La Graciosa in Archipelago canariensi. *Bot. Jahr.*, 14, 230–257.

CASTAGNÉ, N.; LE BORGNE, P.; LE VOURCH, J., and OELY, J.P., 1986. Operational measurements of Sea Surface Temperature at CMS Lannion from NOAA-7 AVHRR data. *International Journal of Remote Sensing*, 7, 953–964.

CAYE, G. and MEINESZ, A., 1985. Observations on the vegetative development, flowering and seeding of *Cymodocea nodosa* (Ucria) Ascherson on the Mediterranean coasts of France. *Aquatic Botany*, 22, 277–289.

DEN HARTOG, C. 1970. *The Seagrasses of the World*. Amsterdam: Verh. Kon. Ned. Akad. Wet., Apd. Naturwrk. 275p.

GIL-RODRÍGUEZ, M.C. and CRUZ SIMÓ, T., 1981. *Halophila decipiens* Ostenfeld (Hidrocharitaceae), una fanerógama marina nueva para el Atlántico oriental. *Vieraea*, 11 (1-2), 207-216.

GIL-RODRÍGUEZ, M.C.; AFONSO-CARRILLO, J., and WILDPRET DE LA TORRE, W., 1982. Ocurrence of *Halophila decipiens* Ostendfeld on Tenerife, Canary Islands. *Aquatic Botany*, 12, 205–207.

GIL-RODRÍGUEZ, M.C.; AFONSO-CARRILLO, J., and WILDPRET DE LA TORRE, W., 1987. Praderas marinas de *Zostera noltii* (Zosteraceae) en las Islas Canarias. *Vieraea*, 17, 143–146.

GONZÁLEZ, M.N., 1976. Contribución al estudio del epifitismo en *Zostera marina* L. (Zosteraceae) en la Playa de Las Canteras (Gran Canaria). *Botánica Macaronésica*, 2, 59–67.

GONZÁLEZ, M.N., 1977. Estudio de la vegetación litoral de la zona de Maspalomas. *Botánica Macaronésica*, 4, 23–30.

GONZÁLEZ, M.N., 1980. Estudio biosistemático de las fanerógamas marinas de Canarias- I. *Botánica Macaronésica*, 7, 9–38.

GONZÁLEZ, M.N., 1986. Flórula y vegetación bentónica de la Playa de Las Canteras. Tesis Doctoral. Dpto. Biología. Univ. de La Laguna (unpubl.) 267 pp.

GUADALUPE, M.E.; GIL-RODRÍGUEZ, M.C., and HERNÁNDEZ-GONZÁLEZ, M.C., 1995. Fitobentos de Arrecife de Lanzarote, Reserva de la Biosfera (Islas Canarias). *Cryptogamie Algol.*, 16(1), 33–46.

HERNÁNDEZ-GONZÁLEZ, C.L. and GIL-RODRÍGUEZ, M.C., 1993. Nuevas citas para la flora marina de la isla de La Palma (Islas Canarias). *X Simposio Nacional de Botánica Criptogámica*. La Laguna, Islas Canarias: Universidad de La Laguna, pp. 44.

LARKUM, A.W.D.; MCCOMB, A.J., and SHEPHERD, S.A., 1989. *Biology of Seagrasses. A treatise on the biology of seagrasses with special references to the Australian region*. Amsterdam: Elsevier 841p.

LLINÁS, O.; RUEDA, M.J., and PÉREZ-MARTELL, E., 1994. Características termohalinas y nutrientes en aguas de las plataformas insulares canarias a finales de primavera. *Bol. Inst. Esp. Oceanogr.*, 10(2), 177–189.

MC ROY C.P. and MCMILLAN, C., 1977. Production ecology and physiology of seagrasses. *Seagrass Ecosystems: A Scientific Perspective*. New York: C.P. Mc Roy and C. Helfferich, pp. 53–87.

MITTELSTAEDT, E., 1991. The ocean boundary along the northwest African coast: Circulation and oceanographic properties at the sea surface. *Progress in Oceanography*, 26(4), 307–355.

ORTH, R. J., 1977. The importance of sediment stability in seagrass communities. *Ecology of Marine Benthos*. Columbia: University of South Carolina Press, pp. 281–300.

REYES, J., 1993. Estudio de las praderas marinas de *Cymodocea nodosa* (Cymodoceae, Magnoliophyta) y su comunidad de epífitos, en

El Médano (Tenerife, Islas Canarias). Tesis Doctoral. Dpto. Biología, Univ. de La Laguna, 424 pp.

SANTOS GUERRA, A., 1972. Contribución al estudio de la flora marina de la isla de La Gomera. *Vieraea*, 2, 86–102.

STRAMMA, L., 1984. Geostrophic transport in the warm water sphere of the eastern subtropical North Atlantic. *Journal of Marine Research*, 42, 537–558.

VAN CAMP, L.; NYKJAER, L.; MITTELSTAEDT, E., and SCHLITTENHARDT, P., 1991. Upwelling and boundary circulation off Northwest Africa as depicted by infrared and visible satellite observations. *Progress in Oceanography*, 26, 357–402.

WEBB, P.B. and BERTHELOT, S., 1836–1850. *Historie naturelle des Iles Canaries. III. Botanique. 2. Phytographia canariensis*. Paris.

WILDPRET DE LA TORRE, W. and DEL ARCO AGUILAR, M., 1987. España Insular: Las Canarias. *La Vegetación de España*. Madrid: Univ. Alcalá de Henares, Secret. Public., PEINADO, M. and RIVAS-MARTINEZ, S. (eds.), 517–544 pp.

WILDPRET, W.; GIL-RODRÍGUEZ, M.C., and APONSO-CARRILLO, J., 1987. *Cartografía de los campos de algas y praderas de fanerógamas marinas del piso infralitoral del Archipiélago Canario*. Consejería de Agricultura y Pesca, Gobierno de Canarias (unpubl.), 315 pp.

YOUNG, P.C., 1978. Moreton Bay, Queensland: A nursery area for juvenile penaeid prawns. *Aust. J. Mar. Freshw. Res.* 29, 55–75.

☐ RESUMEN ☐

El estudio de la vegetación marina en las Islas Canarias se ha ocupado vagamente de las fanerógamas marinas. Excepto recientes estudios, la mayor parte de los trabajos realizados en la zona, se limitan a señalar nuevas localidades para su distribución. El presente trabajo se basa en una exhaustiva búsqueda bibliográfica, posterior confirmación y trabajo *in situ*, y la relación de los resultados obtenidos con las características oceanográficas y geomorfológicas del Archipiélago. La distribución que presentan dichas plantas en el Archipiélago Canario sigue un modelo muy marcado: las praderas de fanerógamas se localizan en la costa este, sureste y suroeste. Es en estas zonas donde se desarrollan las más extensas comunidades, relacionadas con el carácter protegido (sotavento) de esta parte de las islas.

Bol. Inst. Esp. Oceanogr. 15 (1-4). 1999. 21-29 BOLETÍN INSTITUTO ESPAÑOL DE OCEANOGRAFÍA
ISSN: 0074-0195

Joint occurrence of high tide, surge and storm-waves on the northwest Spanish coast

G. Rodríguez[1], *A. Nistal*[2] *and B. Pérez*[2]

[1] Departamento de Física, Universidad de Las Palmas. 35017 Las Palmas de Gran Canaria, Spain
[2] Clima Marítimo. Puertos del Estado. Antonio López, 81. 28026 Madrid, Spain

Received October 1997. Accepted April 1998.

ABSTRACT

The probability of joint occurrences of astronomical tides, meteorological residues and wind-generated waves is examined by analysing simultaneous sea-level and wave-height data recorded at A Coruña from 1992 to 1996. Attention is focused on the existence of a possible statistical dependence among these parameters. Furthermore, marginal distributions for each of these parameters are examined.

Key words: High sea-level events, storm surges, astronomical tides, wind-generated waves, swell, northwest Spanish coast.

RESUMEN

Ocurrencia conjunta de mareas astronómicas, residuos meteorológicos y oleajes extremos en la costa noroeste de España

Se examina la probabilidad de ocurrencia conjunta de mareas astronómicas, residuos meteorológicos y oleaje, poniendo énfasis en la posible existencia de algún tipo de dependencia estadística entre estas variables. Para ello se analizan registros simultáneos de niveles del mar y altura de ola medidos en A Coruña desde 1992 hasta 1996. Además, se examinan las distribuciones de probabilidad marginal correspondientes a cada uno de dichos parámetros.

***Palabras clave**: Mareas astronómicas, residuos meteorológicos, oleajes extremos, marejada, costa noroeste de España.*

INTRODUCTION

The coastal environment is multivariate, with astronomical tides, wind, waves and currents all contributing to the forces experienced by coastal structures. An important problem in applied coastal oceanography is the joint occurrence of high astronomical tides, storm surges and wind-waves. The combination of these phenomena leads to extremely high water levels, increasing the risk of coastal flooding, shoreline erosion and the misfire of urban drainage systems. Furthermore, an increase in the mean water level together with large wind-waves may produce severe damages to coastal structures, which are usually designed without considering the possibility of an abnormal rise in sea level.

An example of this is the event that occurred in A Coruña on 21 January 1996. Figures 1, 2 and 3 show the measured and predicted astronomical

tides, the meteorological residues and the significant and maximum wave-height histories, respectively, for this month. It can be observed that, while wave heights were not excessive for the zone, high astronomical tides and storm surges were superposed during this period. Thus, though wave heights were not extreme, the sea surface rise made possible the elevation of the level of wave action. Consequently, the wave load smashed through the Riazor beach promenade. Furthermore, waves overtopped the wall, producing widespread flooding in the zone. This example clearly illustrates why the joint occurrences of abnormal water levels and wave heights must be considered in the design of coastal structures and the determination of the level of protection.

Many studies concerning the joint occurrence of extreme astronomical tides and storm surges can be found in the literature (e.g. Suthons, 1963; Pugh and Vassie, 1980; Twan and Vassie, 1991). However, the joint occurrence of high astronomical tides, storm surges and wind-generated waves has not been fully investigated.

The present paper addresses this important problem in applied coastal oceanography: the joint occurrence of high astronomical tides, storm

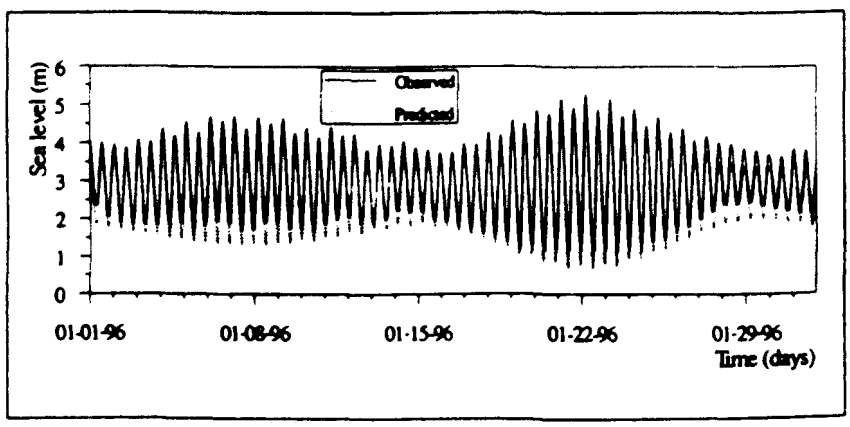

Figure 1. Observed and predicted sea levels during January 1996 at A Coruña

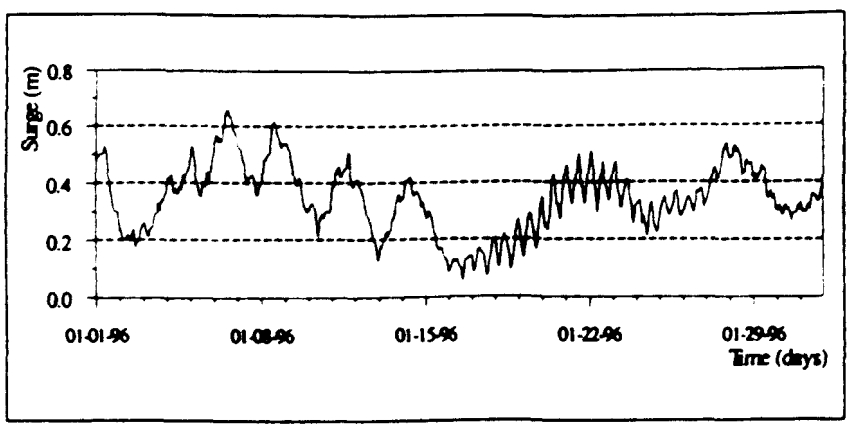

Figure 2. Observed residual surges during January 1996 at A Coruña

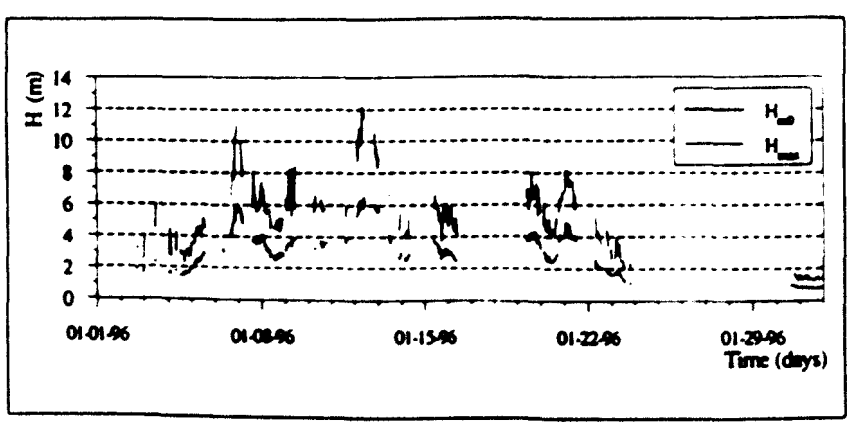

Figure 3. Observed significant and maximum wave heights during January 1996 at A Coruña

surges and high wind waves, which lead to extremely high water levels. However, it is not the objective of this study to design an adequate model to characterise the joint occurrence of extreme values of these three phenomena, but rather, to gain additional insight into the dependence among these marginal variables. This is because, although the probabilistic structure of each one of these phenomena is important, their joint probabilistic structure provides important information that is not often considered. Furthermore, it should be possible to obtain a probabilistic model of the multivariate extremes by combining the marginal models and the information on the mutual dependence among these variables.

We used experimental data to examine the possible dependence between the stochastic (storm surge) and deterministic (astronomical tide) components of the sea surface level. In addition, the correlation structures between the wave-height time histories and the storm-surge component, as well as with the astronomical tide, are examined.

DATA AND ANALYSIS

Hourly time series of seawater level and significant and maximum wave heights recorded at A Coruña by means of a tide gauge and a Waverider buoy, respectively, from 1 July 1992 to 31 December 1996, were analysed. Significant wave height, H_{m_0}, was estimated from individual wave records as

$$H_{m_0} = 4\sqrt{m_0} \qquad [1]$$

where m_0 is the zero order spectral moment, given by

$$m_0 = \int_{-\infty}^{\infty} S(f)df \qquad [2]$$

with S(f) being the estimated spectral density function. On the other hand, the maximum wave-height values are the largest wave heights observed in each hourly wave record.

It is well-known that astronomical tide can be considered a deterministic process. However, extremely high sea levels have a stochastic nature, resulting from the random occurrence of storm surges relative to the phase of the astronomical tide. Furthermore, wind-waves are also random in nature. Therefore, the prediction of the joint occurrence of these three phenomena results in a very complex problem.

Generally, a time series of observed hourly sea-surface fluctuations, Z_t, can be expressed as the sum of three components: the mean sea level, C_t, the astronomical tidal level, T_t, and the surge level, S_t, where the surface gravity waves effect has been eliminated by hydraulic filtering in the measurement device, so that

$$Z_t = C_t + T_t + S_t \qquad [3]$$

Here, the mean sea level is considered a static component. However, it is well known that it varies over long periods, due to changes in land and global water levels. Thus, it can be considered a trend component, which can often be characterised by means of a polynomial equation of order n

$$C_t = pt^n + qt^{n-1} + \Lambda + bt + a \qquad [4]$$

The astronomical tide, or periodic, component can be expressed by

$$T_t = \sum_{n=1}^{K} A_n \cos(\omega_n t + \phi_n) \qquad [5]$$

where the frequencies, n, are global constants and the amplitudes, An and phases, n, of the astronomical tidal components are properties of the location. Note that the mean seawater level, A_0, has been included in the trend term. Then, by detrending the observed time series, the stochastic surge component can be estimated as the following residual series

$$S_t = Z_t - \left[\sum_{n=1}^{K} A_n \cos(\omega_n t + \phi_n)\right] \qquad [6]$$

This definition of the surge component assumes that tide and surge are independent of one another. However, in many cases a simple subtraction of the predicted astronomical tide from the recorded sea-level heights does not work. Actually, the procedure of separating the surge from the astronomical tide in a sea-level record is a difficult task, because these phenomena are dynamically non-linear (Rossiter, 1961). Various practical methods for extracting the atmospheric effect from a sea level record have been described (e.g. Corkan, 1950, Miller, 1958). The present study used the most common procedure applied in practice, which is the simple subtraction of the predicted astronomical tide from the sea-level records.

On the another hand, as noted above, the prediction of extreme sea levels should consider the total sea level as a time-varying function, Z(t), comprising these three components and the wind-gen-

erated waves. Hence, the global sea level should be represented by

$$Z_t = T_t + S_t + W_t \qquad [7]$$

where the first of these parts is a deterministic term, T_t, which can be predicted with acceptable accuracy, whereas the other two parts are non-deterministic, but can be predicted in a statistical sense. These two stochastic terms correspond to the meteorological storm surge, S_t, and the wind-generated waves, W_t, respectively. Naturally, while the trend component has been subtracted for simplicity, it must be considered when predicting the sea-surface elevation at a given location. With this in mind, we may use a predictor, S_t^*, for the storm surge and another, W_t^*, for the wind-generated waves. Consequently, the Z_t^* predictor will be

$$Z_t^* = \left[\sum_{n=1}^{K} A_n \cos(\omega_n t + \phi_n)\right] + S_t^* + W_t^* \qquad [8]$$

This model assumes that astronomical tide, storm-surge and wind-generated waves are mutually independent. However, the principal mode of generation of surges is by tangential wind stress and by changing atmospheric pressure disturbances. That is, surge properties are mainly governed by the local atmospheric conditions, which also control the characteristics of the locally wind-generated wave fields. Therefore, it is natural to expect a certain relationship between the surge and wind-waves observed at a given location. Two simultaneous surge and wave-height time series recorded at A Coruña during 1993 and 1995, respectively, are shown in figure 4. It can be observed that during these periods, a large correlation exists between the significant wave height (solid line) and the sea-surface elevation due to atmospheric effects, or surge, with the large surges occurring almost simultaneously with the larger wind-generated waves. Nevertheless, there is a small delay between both time series, which can be justified by considering the body of water's inertia in responding to wind stress and to atmospheric pressure fluctuations. Note that surge values have been multiplied by a constant factor [4] for easier comparison.

On the other hand, although tides and surges have a different physical genesis, both can be coupled. Thus, for example, when the tide propagates in shallow coastal waters, the water depth can be increased by surge action. In this case, the predicted tide will arrive at the coast earlier than expected and will be lower in amplitude, whereas the resultant sea level will be higher. Inversely, a lowering of the mean sea level retards the propagation of the tide (Rossetier and Lennon, 1968). Two time series of sea-surface level (solid line) recorded at A Coruña during 1995 and 1996, respectively, are shown in figure 5 together with the meteorological surge (dashed line) obtained by subtracting the predicted astronomical tide. Note that surge values have been multiplied by a constant factor for comparison.

It can be observed that surge values approximately follow the same pattern that the lower envelope of the sea-level observations. It is also im-

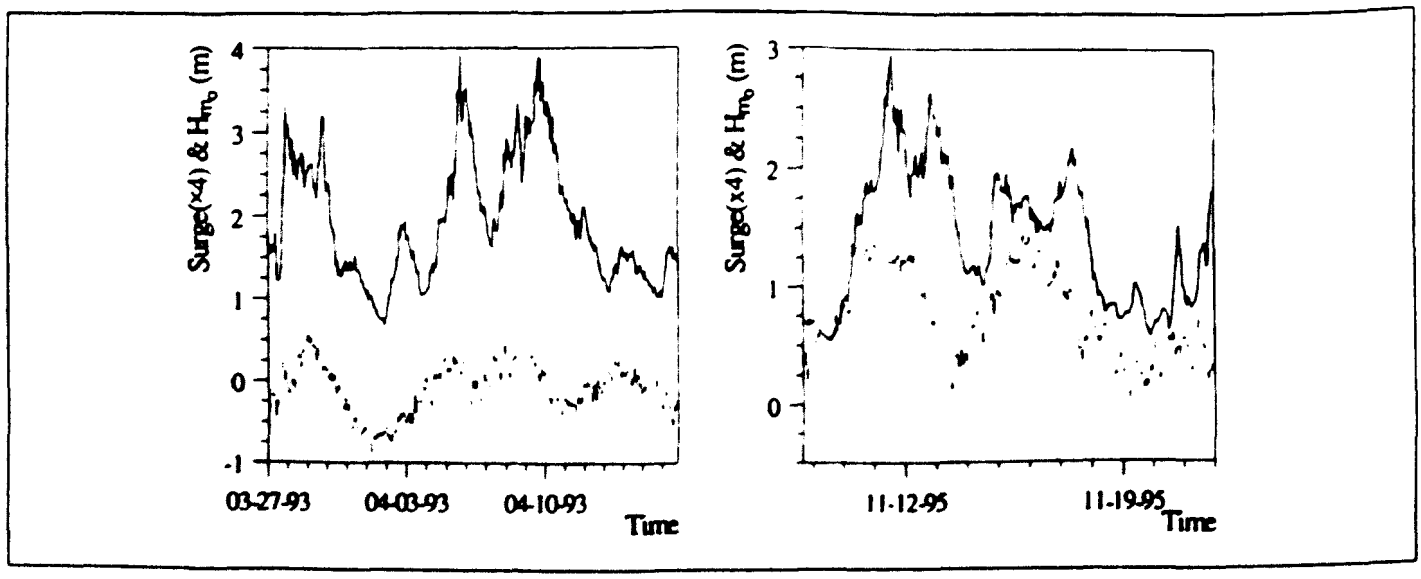

Figure 4. Significant wave height (solid line) and surge elevation (x4) (dashed line) observed at A Coruña

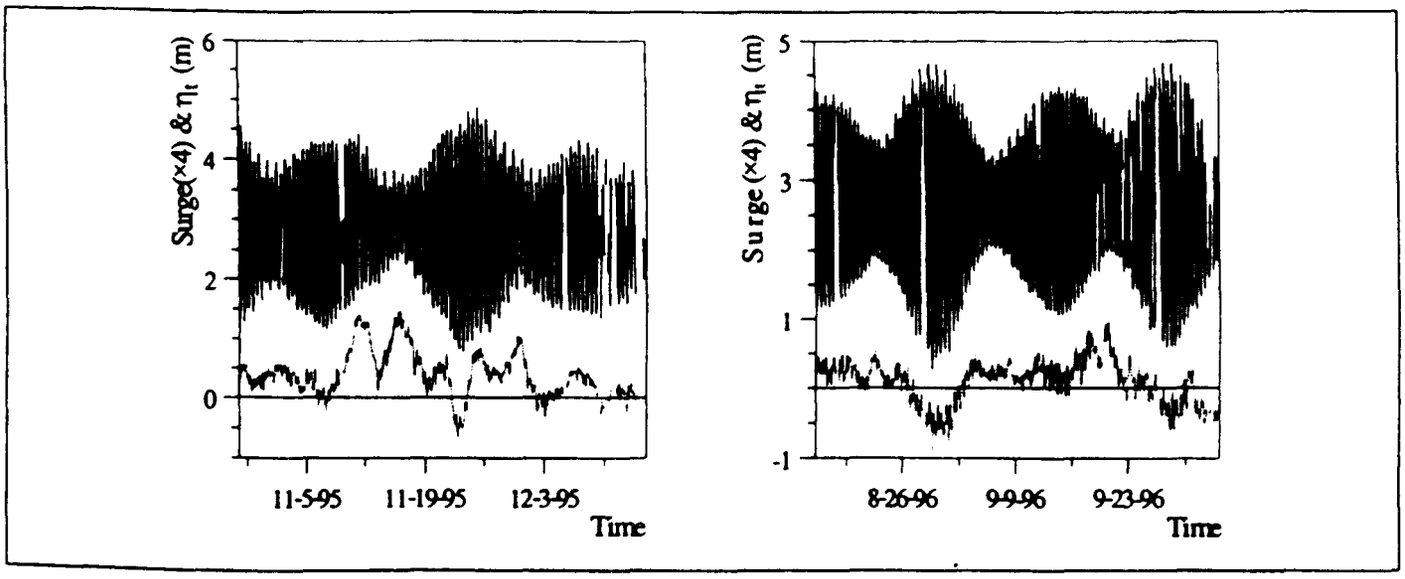

Figure 5. Sea surface level (solid line) observed at A Coruña and estimated surge (dashed line) (×4)

portant to note that the larger positive surges often occur during the low tidal-range periods, whereas the larger negative surges are more frequent at the rising tide.

In light of this experimental evidence, some degree of dependence among these physical processes should be suspected, at least in coastal waters. Thus, it becomes clear that an adequate analysis of extreme sea levels must take into account the individual probabilistic distribution of each one of the aforesaid phenomena, as well as the possible existence of some kind of dependence among the different terms giving rise to the actual sea-surface elevation. Results of such an analysis are presented in the next section.

RESULTS AND DISCUSSION

Marginal distributions

The histograms of the hourly measured significant and maximum wave heights are shown in figure 6. It can be observed that these distributions are skewed towards smaller wave heights, and that large storm-waves have a small relative frequency of

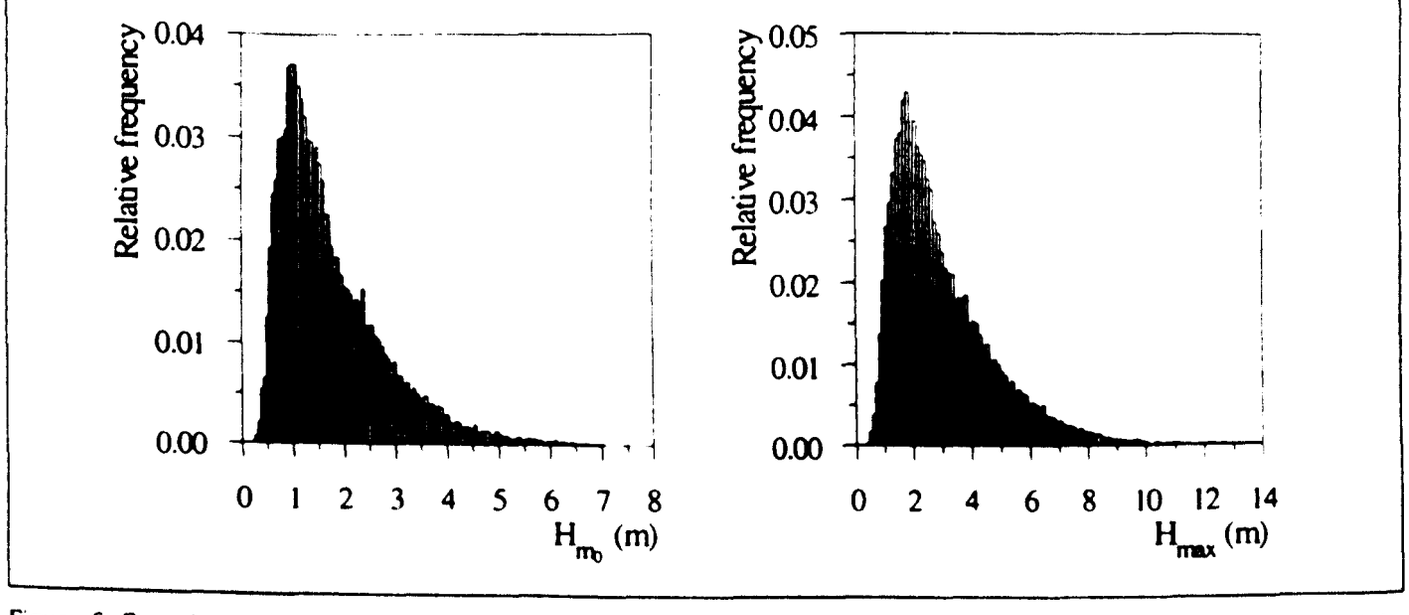

Figure 6. Experimental marginal probabilistic distributions for significant wave height (left) and maximum wave height (right)

occurrence. Both distributions are shifted to the right of zero, since the significant and maximum wave heights are not likely to attain values close to zero.

There is no accepted theoretical basis for choosing a specific distribution function to describe the hourly significant and maximum wave heights. Therefore, the experimental values have been fitted to the Rayleigh, log-normal, Gumbel and Weibull distributions, which are the most common distributions used to obtain a mathematical expression adequately describing the observations. The results suggest that the log-normal distribution provides the best description of the hourly significant and maximum wave heights. These results agree with those reported by Guedes Soares, Lopes and Costa (1988), who analysed wave data recorded at Figueira da Foz (Portugal) from 1984 to 1988.

The marginal statistical distribution of the astronomical tide was analysed by Tayfun (1979), who described the predicted component of the tide as a Gaussian process. This is a simple and natural way of representing the process, because on first consideration the model given by equation [5] represents the tidal heights as the sum of a large number of cosines. Then, by applying the central limit theorem, the process would follows a Gaussian distribution. However, the marginal distribution obtained for the predicted sea-surface level, shown in figure 7, shows a bimodal shape. This bimodal form has also been reported by Pugh and Vassie (1980) for the distribution of tidal heights at some British coastal sites, and by Walden, Prescott and Webbe (1982) for some ports on the southern coast o England. Walden and Prescott (1983) noted tha the sum of cosines denoted by equation. [5] will b distributed normally only if no constituent has dominant effect on determining the tide.

The spectral density function estimated from th predicted tidal heights is shown in figure 7 (right) It is clear that the semidiurnal constituent is th dominant term of the tide at A Coruña. Walde and Prescott (1983) found similar conditions fo some locations in British coastal waters. These au thors proposed a relatively simple stochastic mode to characterise the predicted tidal heights in thi situation. The model suggested by these author considers the superposition of a cosine wave plus random noise to explicitly reflects the dominanc of the semidiurnal constituent.

It noteworthy that the probabilistic distributio displayed by the measured sea-surface elevations shown in figure 8 (left), is practically the same a that for the predicted tidal heights. The model pro posed by Walden and Prescott (1983) is also usefu to characterise the observed elevations. On the oth er hand, the marginal distribution obtained for th meteorological residues closely fits a normal distri bution, as can be observed from figure 8 (right), al though due to the existence of some anomalou bins the Gaussian distribution did not verify th chi-square goodness-of-fit test.

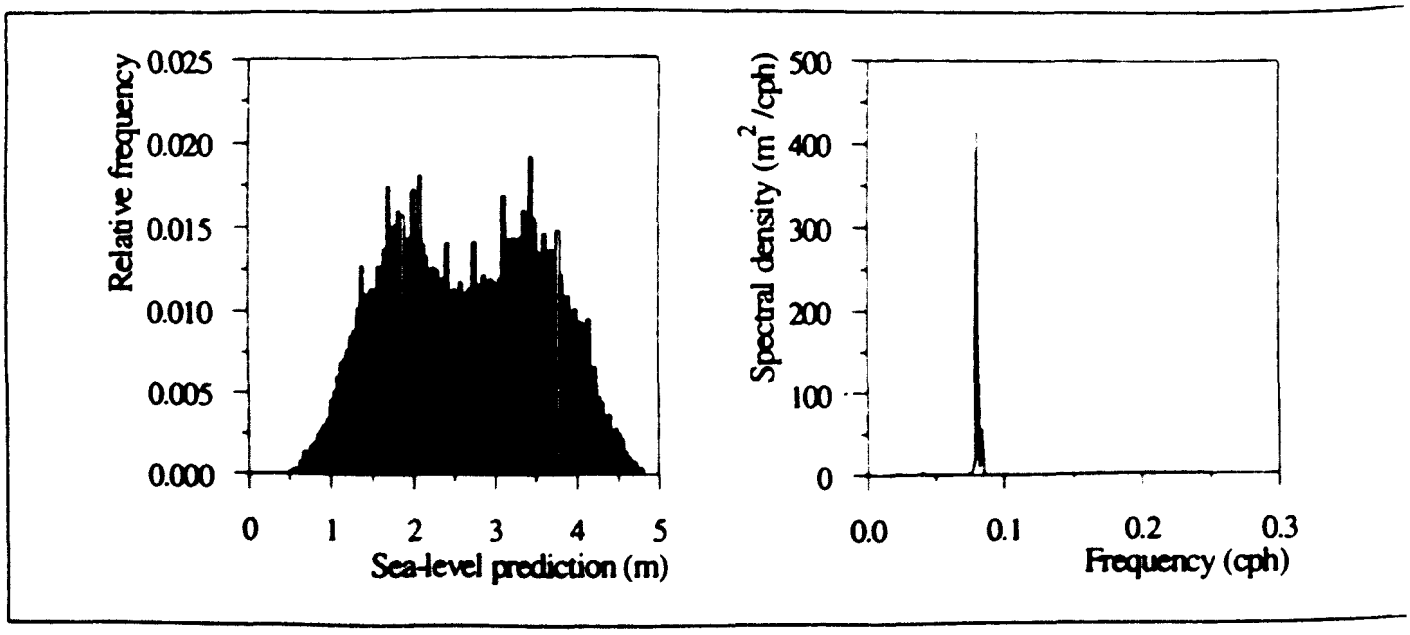

Figure 7. Experimental marginal probabilistic distributions for tidal prediction heights (left) and the corresponding spectra density function (right)

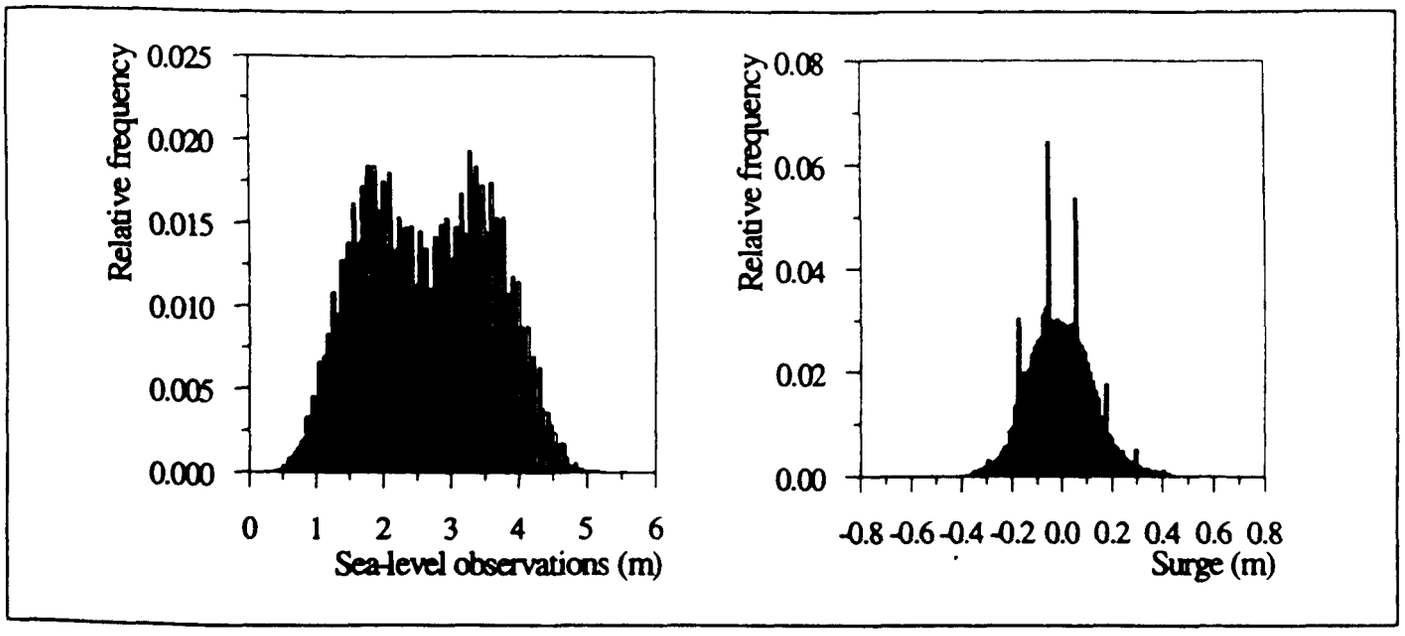

Figure 8. Experimental marginal probabilistic distributions for sea-surface level (left) and meteorological surges (right)

Joint distributions

The bivariate distributions observed for the simultaneous pairs of surge and sea-level measurements reflect a slight tendency of the surge to increase with the astronomical tidal height (figure 9, left). On the other hand, there is no evident relationship between the measured sea level and the significant wave height (figure 9, right). However, a hidden relationship between the surge level and the significant wave height can be guessed from this figure. It can be observed that the measured sea-level range decreases as the significant wave height increases, indicating that the probability of negative surges during low tides and negative surges during high tides increases with the significant wave height.

The bivariate distribution of meteorological surges and significant wave heights is represented in figure 10 for data from A Coruña. The expected trend of the surge to increase with the significant wave height, since both processes have the same

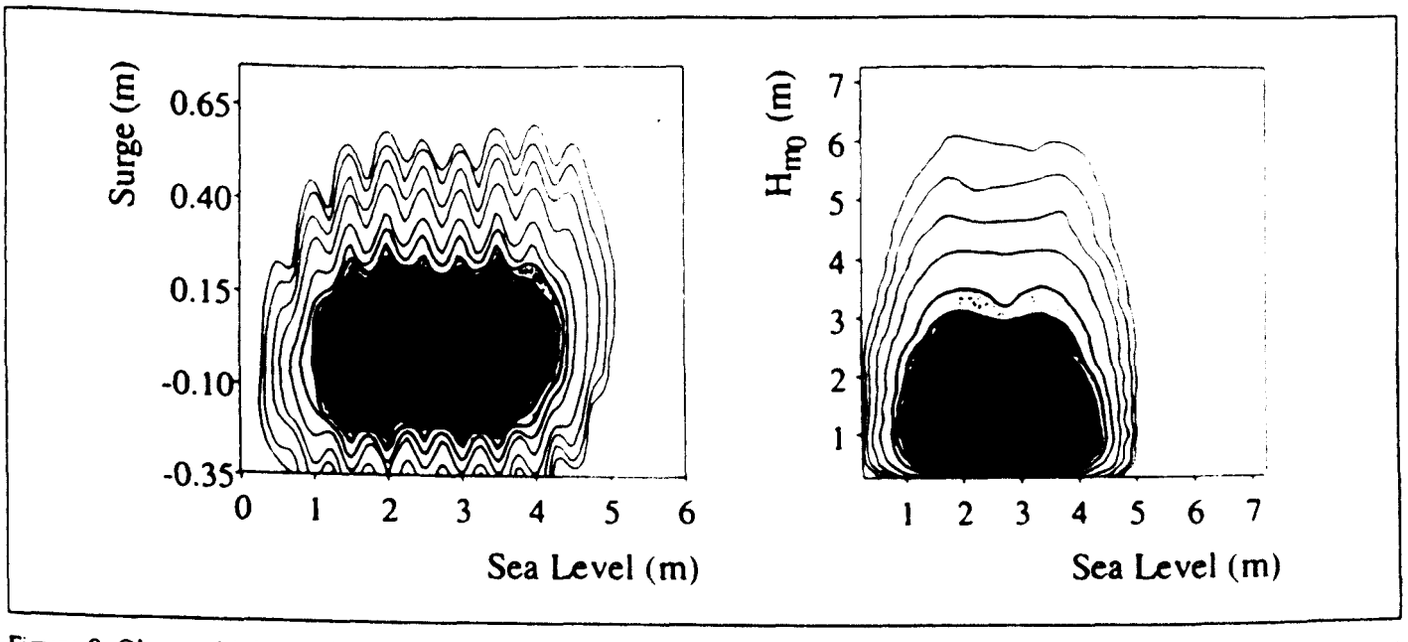

Figure 9. Observed joint probability distribution of measured sea level and meteorological surge (left) and of sea level and significant wave height (right)

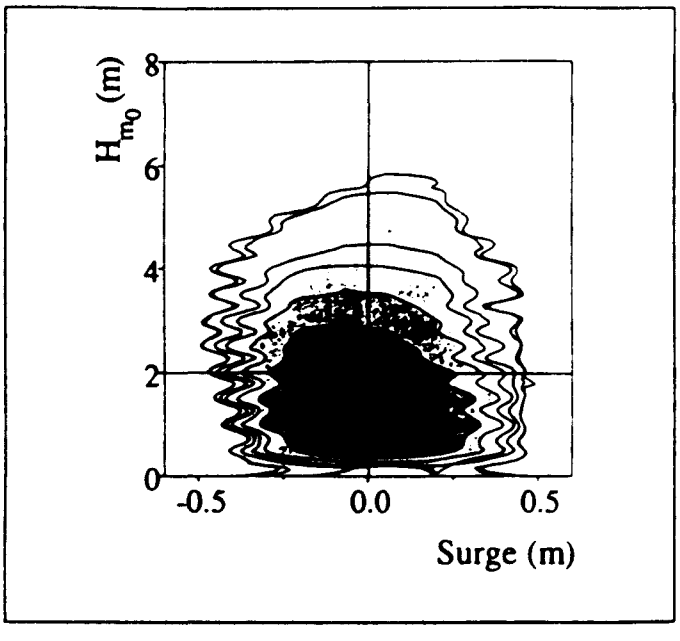

Figure 10. Observed joint probability distribution of surge and significant wave heights

physical origin, can be observed, although this becomes clear only for significant wave heights of more than 2 or 3 m.

Gaffney and Williams (1993) analysed hourly values of surge and significant wave height recorded in North Carolina coastal waters during one month. By applying a linear regression procedure, they reported the following empirical relationship between both parameters

$$S = -0.028 + 0.255H_{m_0}$$

Figure 11 shows the scatter diagrams obtained by representing all the hourly couples measured during the entire period of measurements (left) and those with surge values higher than 0.4 m (right). It can be observed that an inverse relationship is obtained by means of linear regression when using all of the data; i.e. it seems that the surge decreases as the wave height increases. This paradoxical result is due to the large percentage of mixed sea states found on the west coast of the North Atlantic, as reported by Guedes Soares and Nolasco (1992) for a site off Portugal. These authors observed a range of between 23-26 % of double- peaked sea states, corresponding to the combination of a wind sea and a swell coming from distant storms. Furthermore, during periods of low local wind velocities, the background swell becomes dominant along the North Atlantic west coasts, as reported by Rodríguez (1992). The swell-dominated sea states are characterised by long wave periods and small wave heights, and are unrelated to local wind action. Thus, the expected relationship between surges and significant wave heights would be different for the eastern North Atlantic, which is not significantly affected by the presence of swell waves, and the swell-dominated west coasts. Therefore, if only the surge values associated with meteorological residues higher than 0.4 m are considered (figure 11, right) the linear relationship between both parameters becomes positive. Note that although in this case the data

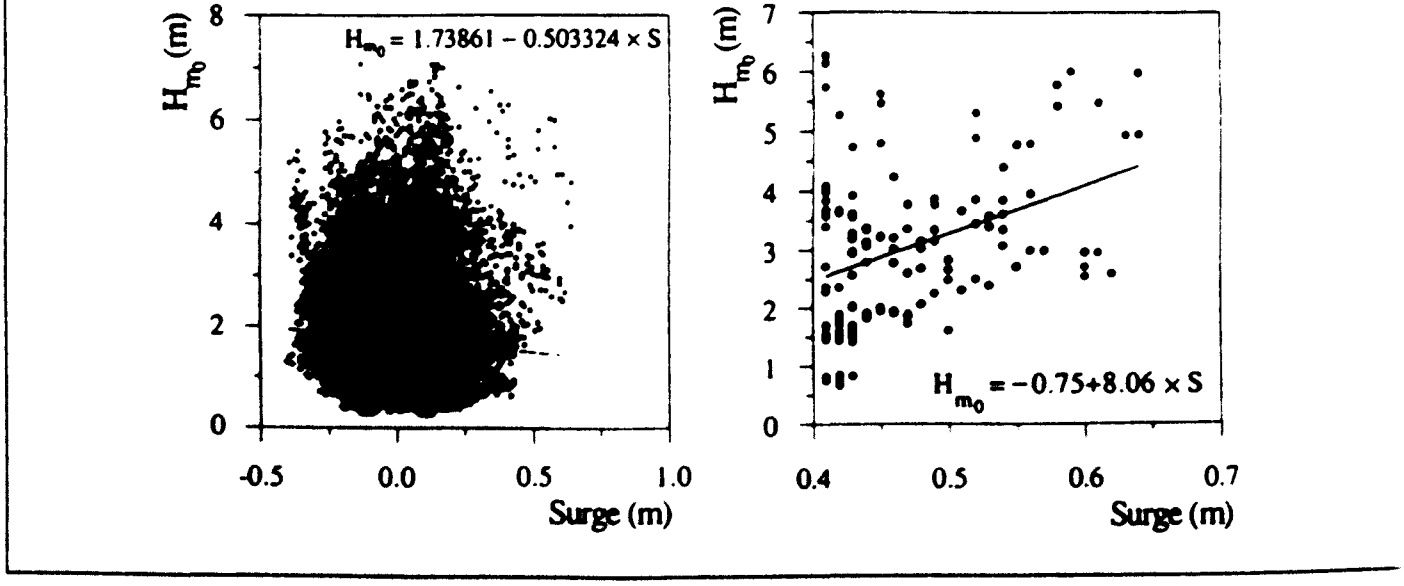

Figure 11. Scatter diagram of simultaneous observations of surge and significant wave heights, for all the observations (left) and for observations with surge higher than 0.4 m (right)

are better fitted by a linear function, the scatter remains large with a a very low correlation coefficient (close to 0.2).

CONCLUSIONS

It has been shown that the astronomical tides, meteorological residues or surges and wind-generated waves should be jointly considered, in practice. The marginal probabilistic distribution of significant and maximum wave heights are adequately described by means of the log-normal distribution, and the meteorological surges with the Gaussian probability law. However, the measured and predicted sea level required can be characterised by using a cosine plus random noise model to include the dominant effect of the semidiurnal constituent, giving rise to a bimodal probability distribution.

There is a certain degree of correlation among these processes. The relationship between surge and wind-wave heights is because both phenomena are governed by the meteorological conditions at the study locations. Surges and tides are generated by different physical processes; however, they can be related due to a coupling effect. Thus, larger positive surges often occur during low tides and the larger negative surges are more frequent at the rising tide. On the other hand, significant wave height seems to increase with surge level. However, the relationship between these two parameters is masked by the presence of a large quantity of low wave heights associated with swell-wave fields, which are not related to the local wind field.

REFERENCES

Corkan, R. H. 1950. The levels in the North Sea associated with the storm disturbance of 8 January 1949. *Phil. Trans. Roy. Soc. Lond.* A242: 493-525.

Gaffney, D. and G. Williams. 1993. Joint probability of superelevated water levels and wave heights at Duck, North Carolina. In: *Proceedings of the Waves-93 Symposium*: 905-917. New Orleans, USA.

Guedes Soares, C., L. C. Lopes and M. D. S. Costa. 1988. Wave climate modelling for engineering purposes. In: *Computer Modelling in Ocean Engineering*. B. A. Schrefler and O. C. Zienkiewicz (eds.). Balkema, Rotterdam: 169-175.

Guedes Soares, C. and M. C. Nolasco. 1992. Spectral modelling of sea states with multiple wave systems. *Journal of Offshore Mechanics and Arctic Engineering* 114: 278-284.

Miller, A. R. 1958. The effects of winds on water levels on the New England coast. *Limnol. Oceanogr.* 3: 1-14.

Pugh, D. T. and J. M. Vassie. 1980. Applications of the joint probability method for extreme sea level computations. *Proceedings of the Institution of Civil Engineers* 69: 959-975.

Rodríguez, G. R. 1992. Spectral and statistical characteristics of wind waves off Canary Islands. *Proceedings of the Institution of Civil Engineers* 695: 622-636.

Rossetier, J. R. and G. W. Lennon. 1968. An intensive analysis of shallow water tides, *Geophysical Journal of the Royal Astronomical Society*, 16: 275-293.

Rossiter, J. R. 1961. Interaction between tide and surge in the Thames. *Geophysical Journal of the Royal Astronomical Society* 6: 29-53.

Suthons, C. T. 1963. Frequency of occurrence of abnormally high sea levels on the East and South coasts of England. *Proceedings of the Institution of Civil Engineers* 25: 433-450.

Tayfun, M. A. 1979. Joint occurrences in coastal flooding. *Journal of Waterways, Port, Coastal Ocean Division* 105: 107-123.

Twan, J. A. and J. M. Vassie. 1991. Recent improvements in the joint probability method for estimating extreme sea levels. Tidal Hydrodynamics. B. B. Parker (ed.): 813-828. Wiley. New York.

Walden, A. T. and P. Prescott. 1983. Statistical distribution for tidal elevations. *Geophysical Journal of the Royal Astronomical Society* 72: 223-236.

Walden, A. T., P. Prescott and N. B. Webber. 1982. An alternative approach to the joint probability method for extreme high sea level computations. *Coastal Engineering* 6: 71-82.

Fluorescence techniques for the determination of polycyclic aromatic hydrocarbons in marine environment: an overview

J.J. Santana Rodríguez* and C. Padrón Sanz

Department of Chemistry, Faculty of Marine Sciences, University of Las Palmas de G.C., 35017 Las Palmas de G.C., Spain

Polycyclic Aromatic Hydrocarbons (PAHs) are compounds of great environmental interest because of their potential carcinogenic and mutagenic activity and their frequent occurrence in the environment, above all in the marine environment. Therefore it is an important to establish simple, sensitive and reliable methods for the determination of these compounds. In this work we report an overview on the application of fluorescence techniques to the study and determination of PAHs in marine samples: water, sediments and organisms. Conventional fluorescence spectroscopy, synchronous fluorescence spectroscopy, Shpol'skii fluorescence spectroscopy and high performance liquid chromatography (HPLC) with fluorescence detection constitute the most interesting analytical techniques for the determination of these pollutants.

In the last few years, there has been an increasing interest in the types and concentrations of organic compounds present in marine environment. Among them, notable interest has been shown in PAHs pollutants, as demonstrated by the high number of recent papers in this field.

PAHs are a class of organic compounds, which are included in the wider family of polycyclic aromatic compounds (PACs). These compounds have shown carcinogenic and/or mutagenic activity in laboratory experiments with animals. PACs are generally formed during incomplete combustion or pyrolysis of organic matter occurring in a variety of natural processes or human activities. Consequently, PAHs are ubiquitous pollutants, which are present in all environmental components. Specifically, the presence of PAHs has been reported in marine environment: sea water [5-9, 29-33], sediments [2,3,35-51], and plankton, seaweed and filter feeding organisms [52-71].

These pollutants can enter in the oceans by many routes, including petroleum spills, runoff from roads, sewage, effluents from industrial processes, and fallout from the atmosphere. Sixteen of them are included in the list of priority pollutants by US Environmental Protection Agency (Tab. I) [1]. That is why monitoring their presence and persistence is the main environmental problem, and it is essential to find analytical methods capable to identify and quantify these pollutants in the environment.

In the last few years, important advances have been made in improving existing analytical methods and developing new techniques for analysis of PAHs in marine environment, many of them appearing in scientific and technical journals and symposium proceedings.

From the various molecular spectrometric techniques compared, one singularly important trend can be seen: the absorbency and fluorescence spectra of the PACs contain far more information than those for the other classes of compounds. This is especially true for the PAHs, where many

Table I. List of priority pollutants PAHs considered by EPA (Environmental Protection Agency), their carcinogenity and ocurrence.[a]

Hydrocarbon	*Molecular formula*	*Carcinogenicity[b]*	*Occurrence[c]*
Naphthalene	$C_{10}H_8$	–	E
Acenaphtene	$C_{12}H_{10}$	–	E
Acenaphtylene	$C_{12}H_8$	–	F
Fluorene	$C_{13}H_{10}$	–	E,F,S
Phenantrene	$C_{14}H_{10}$	–	E,F,S
Anthracene	$C_{14}H_{10}$	–	E,F,S
Fluoranthene	$C_{16}H_{10}$	–	E,F,S
Pyrene	$C_{16}H_{10}$	–	E,F,S
Benzo(a)anthracene	$C_{18}H_{12}$	+	E,F,S
Chrysene	$C_{18}H_{12}$	– +	E,F,S
Benzo(b)fluoranthene	$C_{20}H_{12}$	++	E,F
Benzo(k)fluoranthene	$C_{20}H_{12}$	–	E,F
Benzo(a)pyrene	$C_{20}H_{12}$	+++	E,F,S
Dibenzo(a,h)anthracene	$C_{22}H_{14}$	+++	E,S
Benzo(g,h,i)perylene	$C_{22}H_{12}$	–	E,F,S
Indeno(1,2,3-cd)pyrene	$C_{22}H_{12}$	+	E,F

a) Reference [1]
b) +++ or ++ = strongly carcinogen; + = carcinogen; – = not carcinogen
c) E = Environment (water, air, tobacco smoke, gasoline and diesel exhaust); F = Foods; S = Curing smoke

structures have spectra with a dozen or so maxima. These maxima as well as the intervening minima, form a unique characteristic pattern of wavelengths and intensities. The pi electron system also causes the PAHs to have a different fluorescence and phosphorescence behaviour. Especially for the PAHs, the electronic transitions are determined by the size and shape of the compounds. Electronically, the PAHs are simple molecules whose spectra are only determined by the molecular resonance structures. Isomeric PAHs differ in the locations of electronic density, because the shape of the PAHs are different, and in some cases they can even differ in their numbers of aromatic rings.

Because of this fundamental reason and of the high sensitivity and selectivity of the chromatographic techniques, HPLC has been used predominantly. Single-wavelength UV absorbency or fluorescence detectors have been applied for PAHs analysis. These are used to detect PAHs because the pi electron systems of PACs determine the energies of the transition in the electronic spectra.

Between both spectroscopic techniques above mentioned, the most sensitive is fluorescence spectroscopy because of the direct measurement of the emitted light intensity with little background or interference. The present overview is centred on the methodologies which apply and/or include fluorescence in the analysis of PAHs in marine environment.

Fluorescence techniques

Conventional fluorescence spectroscopy

Conventional fluorescence spectroscopy involves generating an emission spectrum by scanning the emission wavelength, λ_{em} while the sample is irradiated at a single excitation wavelength, λ_{ex}. Similarly, an excitation spectrum is obtained by scanning the excitation wavelength while recording the emission signal at a single wavelength. Furthermore, spectrofluorimetry is a very simple method, which offers generally very low detection limits and can be used with conventional instrumentation.

This technique is very useful in quantitative analysis of PAHs because of its high sensitivity, selectivity, swiftness and relatively low cost. Moreover, it can be applied to determine PAHs in many environmental marine samples.

The use of fluorescence spectroscopy as a detection technique to determine PAHs in marine sediments was applied by Vandermeulen *et al.* [2]. After *Amoco Cadiz* accident the immediate behaviour and toxicity of freshly spilled crude oil under prevailing spill conditions in an inshore marine environment was examined. Authors simulated weathering studies because weathering states of oil ranging from sheen oil to mousse have significant effects during oil-water and oil-sediment interaction.

Observation of oiled sandy beaches suggest two mechanisms of beach contamination: general penetration and contamination of beach substrate by films of sheen oil (probably partially emulsified), and secondly the burial of discrete layers of mousse. Depending on the timing of oiling with respect to beach dynamics, large amounts of stranded oil can be accommodated within beach sediments. The results of this investigation suggested that there may be some increase in toxicity with weathering, because PAHs become available for later long-term release.

In the case of another kind of marine samples, Picer and Hocenski [3] described a relatively simple, rapid and quite reliable procedure, based on the fluorescence of PAHs, for the estimation of petroleum hydrocarbons in organisms and marine sediments. In this study lipophilic material was extracted from the samples with n-hexane or n-pentane, concentrated to approximately 1 ml, and benzene mixtures. The fluorescent material was cleaned by using a deactivated alumina column, and for the evaluation of the quenching material, the standard addition method was applied. The aim of the work was to improve the possibilities of estimating crude oil pollution of sediment and biota samples by using the standard addition method.

Applying fluorescence on solid organic substrate Vo-Dinh and White [4], investigated a simple technique based on sensitized luminescence for detecting trace amounts of polynuclear aromatic compounds. They used anthracene as the sensitizer designed to absorb excitation energy and funnel it to guest analyte compounds spotted on anthracene treated filter paper. Perylene, benzo(a)pyrene and fluoranthene mixtures were analyzed. Results indicated that anthracene can improve the fluorescence signal of perylene and benzo(a)pyrene. No fluorescence sensitization was observed for other compounds, such as fluoranthene.

As showed above, fluorescence spectroscopy is a technique applicable to the determination of PAHs in solid phases as sediments or marine organism tissues. It exists also a large number of works and publications in which this technique is applied to determine PAHs in marine water samples.

Vapu Tervo [5] determined the total amount of petroleum hydrocarbons (oil) from 52 seawater samples collected at 19 stations in the Gulf of Finland. The samples were analysed ashore by fluorescence spectroscopy. The mean concentrations obtained for "light oil" were 1.6-7.3 µg/l and for "heavy oil" 0.5-1.6 µg/l in the whole investigation area.

Law [6] also applied this technique to samples of water, sediment and oil following the wreck of the *Amoco Cadiz* in 1978. Samples were collected between April and June from the Brittany coast and western English Channel and were analysed for petroleum hydrocarbons by means of fluorescence spectroscopy, gas-liquid chromatography and gas chromatography-mass spectrometry. The concentrations of hydrocarbons found in these samples, 2-200 µg/l, were similar to those found in previous oil-spill studies.

As well, after the oil spill accident at *Mitsubishi Oil Refinery* in Kurashiki city, Ochi and Okaichi [7] measured oil residues by fluorescence spectroscopy in sea water of

Bisan Seto. In another study, achieved by Østgaard and Jensen [8], the fluorescence of carefully prepared solutions of Ekofisk crude oil in sea water was investigated, directly in the water phase, it was concluded that direct fluorescence spectroscopy constitutes a very simple and rapid method for monitoring aqueous petroleum solutions. In this work, significant fluorescence in the 290-460 nm range for oil solutions well below the concentration level of 10 ppb was observed. It was also established that, on the basis of spectra of the single components, the influence of pH on these, and data from gas chromatography/mass spectrometry, the fluorescence at 335 nm (excitation wavelength 230 nm) was dominated by petroleum naphthalenes, while the fluorescence at 300 nm (excitation wavelength 265 nm) could be ascribed to the phenols of the crude oil.

In analytical methods currently used for assaying PAHs in aqeuous media preliminary extraction of the water with organic solvents is required to remove interfering substances. With the use of micellar media, a system which enables the extraction and preconcentration of analytes, these organic solvents can be replaced, allowing a faster and reduced cost analysis. Moreover, micellar media can be used to enhance sensitivity and selectivity of many fluorimetric determinations. Thus, Santana *et al.* [9] studied the use of different micellar media, as a way to improve the spectrofluorimetric determination of benzo(a)pyrene (BaP), compound of great toxicological interest and for its significance in pollution studies. They found that BaP fluorescence intensity suffers important changes in cationic and neutral micellar media and showed the greatest increase in the presence of Triton X-100. The method was applied to determination of BaP in seawater samples enriched with this hydrocarbon.

Another variant, also applied to determination of PAHs in marine environmental samples consists in laser induced fluorescence spectroscopy. Uebel *et al.* [10] applied this methodology to the analysis of PAHs and other pollutants in marine environmental samples. They used a frequency doubled dye laser as an excitation light-source, recording the fluorescence signal and measuring each contaminant spectra in distilled water, artificial and natural seawater. Firstly the intermediate stages of phytoplankton and their breakdown-products were spectroscopically recognizable using fluorescence. Modifications of the fluorescence spectra during the ageing and dying of phytoplankton were found. Phytoplankton which is subjet to sudden death display spectra differing from those of slowly dying organisms, *e.g.* the shift of the chlorophyll maximum to shorter wavelegths was measured.

Synchronous fluorescence spectroscopy

Even though conventional fluorescence spectroscopy has an excellent sensitiviy in determining trace organic compounds, its aplication to the simultaneous determination of several fluorescent compounds in mixtures, is more limited, moreover when these compounds have a high structural similarity. This is due to the fact that the individual spectra of the compounds in the mixture can overlap. This problem can be resolved using synchronous fluorescence spectroscopy, which was firstly introduced by Lloyd [11]. Conventional fluorescence involves generating an emission/excitation spectrum by scanning the emission/excitation wavelength, while the sample is irradiated at a constant excitation/emission wavelength. Another possibility is to vary simultaneously λ_{ex} and λ_{em}. This technique has several variants, depending on the scan-rates of the two monochromators. When the scan-rate is constant for both monochromators, and therefore a constant wavelength interval, $\Delta\lambda$, is kept between λ_{em} and λ_{ex}, the technique is known as synchronous excitation fluorescence spectroscopy.

Since conventional emission and excitation fluorescence spectroscopy from mixed PAHs-solutions show great interference, the synchronous fluorescence technique can simplify the spectra and therefore some mixtures of PAHs can be quantified. In this way, Santana *et al.* [12] studied the interactions between benzo(a)pyrene and perylene with different kinds of surfactants. They developed a synchronous spectrofluorimetric method to determine simultaneously BaP and perylene using Triton X-100 as micellar medium. The limits of detection obtained were 0.27 and 0.3 ng/ml, respectively. The method was applied to the analysis of these compounds in seawater samples.

Other investigations in this field has been developed studying other PAHs such as benzo(g,h,i)perylene, chrysene, dibenzo(a,c)anthracene and coronene [13] as well as mixtures of them, in presence of anionic, cationic and non ionic surfactants. Bermejo *et al.* [14] established a method for the simultaneous determination of perylene and benzo (g,h,i)perylene using hexadecyltrimethylammonium bromide (HDTAB) micellar medium and synchronous fluorescence, obtaining limits of detection of 0.12 and 0.21 ng/ml for both compounds respectively. The method was also applied to the determination of such PAHs added to sea water samples with acceptable results, which demonstrates that synchronous fluorescence spectroscopy can be used as a rapid, simple and sensitive method for the determination of perylene and benzo(g,h,i)perilene in marine water samples.

Santana *et al.* [15] studied the spectrofluorimetric characteristics of chrysene, perylene, dibenzo(a,c)anthracene and coronene in aqueous medium and in the presence of anionic, cationic and non ionic surfactants, employed specifically to enhance the selectivity and sensitivity of the fluorescence determinations of these compounds. Using hexadecyltrimethylammonium bromide as surfactant and synchronous fluorescence, these authors established two methods for the analysis of binary and ternary mixtures of these PAHs. In the first one dibenzo(a,c)anthracene and coronene were determined simultaneously employing $\Delta\lambda$ = 89 nm, with limits of detection of 0.20 and 0.22 ng/ml, respectively. In the second method, three different values of $\Delta\lambda$ were utilized for the simultaneous determination of chrysene, perylene and coronene (41, 3 and 140 nm respectively). Limits of detection were 0.17 ng/ml for chrysene, 0.13 ng/ml for perylene and 0.14 ng/ml for coronene. Satisfactory recovery percentages were found when both methods were applied to

the analysis of binary and ternary mixtures of these PAHs added to seawater.

As well, Böckelen and Niessner [16] probed the application of several non-ionic surfactants for the extraction and enrichment of PAHs from aqueous media. Developing a spectroscopic method for the simultaneous detection of PAH-mixtures by synchronous fluorescence in micellar medium, they obtained recoveries up to 100 % with limits of detection of 6.8 and 2.6 ng/l for benzo(k)fluoranthene and benzo(a)pyrene, respectively.

Synchronous fluorescence spectroscopy has also been applied to determine PAHs in other environmental samples such as marine organisms. For example, Ariese *et al.* [17] determined the uptake of PAHs by fish, screening the gall bladder bile for PAHs metabolites. They proposed synchronous fluorescence spectroscopy as a rapid screening technique for the determination of conjugated 1-hydroxy pyrene, wich is a major metabolite in bile of fish exposed to PAHs polluted sediment. The technique was applied to a mesocosm study in which the uptake of PAHs by flounder (*Platichthys flesus*) from polluted sediment was investigated. In a subsequent study, the method was applied to the southern North Sea and in Dutch coastal and inshore water [18].

Conventional and synchronous fluorescence spectroscopy, together with solid phase spectrofluorimetry, are adequate techniques for determination of PAHs. The advantages of the latter one are that only a little amount of a convenient solid support is needed for the preconcentration of the analytes presenting inherent fluorescence, and that fluorescence measurements can be carried out directly in the solid phase. Applying these techniques to waters from different sources (tap, natural, waste and sea water), Vilchez *et al.* [19] determined by solid-phase spectrofluorimetry the content in benzo(a)pyrene, benzo(a)anthracene and pyrene, wich exhibit native fluorescence in solution at trace levels. The relative fluorescence intensity was measured with these PAHs fixed on Sephadex G-25 gel after packing the gel beads in a 1 mm silica cell. By recording the synchronous spectra at different values of $\Delta\lambda$, benzo(a)pyrene, benzo(a)anthracene and pyrene can be simultaneously determined in the presence of other PAHs.

Shpol'skii fluorescence spectroscopy

Shpol'skii spectroscopy is especially suited for the qualitative analysis of PAHs at trace levels as it combines the sensitivity inherent to fluorescence methods with the specific information that can be obtained in infrared spectroscopy. It makes use of frozen n-alkane matrices at cryogenic temperatures to considerably reduce band broadening which is the cause of the limited identification power of room temperature fluorescence. The PAHs occupy substitutional sites in the n-alkane crystal resulting in largely identical surroundings. The appearance of the Shpol'skii spectrum may vary if different n-alkanes are employed, because the fit of the PAH within the crystal is critical. A Shpol'skii spectrum consists of a number of narrow lines with a full width at half maximum of 0.1-0.01 nm. These lines are suitable for identification purposes because they form a fingerprint of the individual PAHs.

Ewald *et al.* [20] applied the technique to the study of marine sediments and demonstrated that high resolution spectrofluorimetry at 4.2 K in n-alkane matrices can be used to identify polycyclic aromatic hydrocarbons derived from triterpene, which occur in the organic matter of marine and terrestrial sediments.

Garrigues *et al.* [21-23] used this technique for the analysis of several methylated-PAHs series in marine samples: organic material, sediments and crude oils. The analytical results were compared with those reported by other methodologies and were found to be in quite good agreement, thus demonstrating the reliability of high resolution Shpol'skii spectrofluorimetry. Also, Hofstraat *et al.* [24] determined PAHs in harbour sediments by means of Shpol'skii fluorimetry and showed it was an appropriate analytical method for the quantitative and qualitative determination of PAHs in such samples. Moreover, they concluded that this technique yields low limits of detection comparable to those obtained by a standard procedure based on HPLC with fluorimetric detection.

Applied to other marine samples, Ariese *et al.* [25] investigated the applicability of high-resolution Shpol'skii spectrofluorimetry to the direct analysis of polycyclic aromatic hydrocarbons in tern and mussel samples. The sensitivity of the measurements suffered considerably from the large amounts of interfering substances (e.g. fatty components) in the crude extracts, resulting in a poor-quality Shpol'skii matrix and a high sample absorbency. Nevertheless, after a thorough study of these limiting factors, optimum conditions could be defined and a number of PAHs were detected directly without any sample clean-up.

Shpol'skii spectroscopy cannot be used for on-line detection in HPLC, since the solid matrix precludes compatibility with flow systems. Therefore Shpol'skii fluorimetry was applied by Mastenbroek *et al.* [26] as an independent identification method to the upgrade routine HPLC analysis of Polycyclic Aromatic Hydrocarbons. HPLC combined with fluorescence detection is routinely used in the Dutch Water Quality Survey to determine the PAHs content of marine sediment samples. In this study, this methodology is utilized to ascertain the identity and the purity of the peaks in the chromatograms by collecting several eluting fractions and using subsequent spectroscopic analysis. They found that low temperature Shpol'skii technique provides high-resolution fluorescence spectra of PAHs that can serve as fingerprints. Thus, important information concerning peak purity was obtained and the number of components identified was roughly doubled.

Kozin *et al.* [27] also applied high-resolution low temperature molecular luminescence technique, to the analysis of various complex environmental matrices to get isomer specific information for a wide range of PAHs and their derivatives. Using conventional lamp excitation and fluorescence and phosphorescence detection, they determined

parent priority PAHs, six-membered ring compounds, and methyl-substituted PAHs in extracts of sediment, muscles from finfish and other samples.

Hofstraat *et al* [28] employed laser induced Shpol'skii fluorimetry as a variant of the previous technique. This methodology is also applicable to the analysis of PAHs in marine environmental samples, especially the PAHs content in biotic samples. The authors showed that Shpol'skii technique can be used successfully as an independent reference method for both qualitative and quantitative confirmation of conventionally used determination methods.

Fluorescence detection in liquid chromatography

Usually, liquid chromatography using fluorescence detection (LC/fluorescence) and gas chromatography coupled to mass spectrometry (GC/MS) are the most powerful techniques for monitoring PAHs. Nevertheless, an advantage of LC/fluorescence is its ability to measure some PAHs isomers that cannot be easily quantified by GC/MS. The large and/or nonvolatile polycyclic aromatic compounds (PACs) cannot be analyzed by GC because either they will not elute or, if they do, the peaks will be unacceptably broad. In addition, some PACs are thermally unstable and decompose or rearrange pyrolytically to other structures. Because of its excellent separation and detection performance, LC has been specified as the method of choice by the U.S. EPA for the analyses of aqueous effluents for the determination of PAHs.

Water

The determination of PAHs in water and wastewater is an area which has attracted the interest of a large number of researchers for many years. It was observed a significant evolution in the techniques applied to PAHs determination in water. Prior to 1964, researchers tend to employ the separation techniques of solvent extraction, classical column liquid chromatography, and thin layer chromatography with UV absorption or fluorescence detection. Since 1980 the predominant analysis method for water samples was reverse phase high performance liquid chromatography (HPLC) with fluorescence detection. Several papers addressed proper column selection, analysis conditions, and detection. The most commonly used and most rigorous approach for trace concentration of PAHs was the methodology proposed by EPA for PAHs extraction. Currently, the use of micellar media as an extraction and preconcentration system is applied as an alternative. This methodology allows an important improvement with a reduced cost and time of analysis.

Lee *et al.* [29] determined hydrocarbons content and its evolution in several different kind of environmental samples. *Prudhoe* crude oil enriched with a number of polycyclic aromatic hydrocarbons was added as a dispersion to a controlled ecosystem enclosure suspended in *Saanich Inlet*, Canada. Concentrations of various aromatic compounds were measured by passing 5 µl of a methanol solution through an assembled liquid chromatograph equipped with a fluorescence detector. PAHs were determined in water, zooplankton, oysters, and bottom sediments. Initial water concentrations of the lower weight aromatics, naphthalenes and anthracene, were 10-20 µg/l, whereas the initial concentrations of benzo(a)pyrene, benz(a)anthracene, and fluoranthene ranged from 1 to 6 µg/l. These concentrations decrease at an exponential rate because of evaporation, photochemical oxidation, microbial degradation, and sedimentation. Only naphthalenes were significantly degraded by microbes with removal by this process of up to 5 % per day from the water. Sedimentation and photochemical oxidation were responsible for the decrease in concentrations of the higher molecular weight aromatic compounds.

The determination of PAHs in aqueous samples is rather difficult, as their concentration in water is extremely low due to their poor solubility. In order to detect the PAHs at low levels in water, a concentration step is generally required. Use of surfactants allows the extraction and preconcentration in only one step. Micelles formed by surfactants have the capability of solubilizing organic compounds in water. Using this procedure, substrates can be extracted from aqueous media in a much smaller volume nearly formed by the surfactant. In addition, aqueous solutions of surfactants have been used as mobile phases in liquid chromatography, and although this kind of mobile phase was primarily used in column chromatography and thin layer chromatography, they are now widely utilized in HPLC. One of these surfactants is Brij-35 [31,32].

In the same way, Brouwer *et al.* [32] used liquid chromatography method with fluorescence and diode-array UV detection for the trace-level determination of the sixteen EPA-priority PAHs. The system was used for the analysis of surface water samples. The procedure involved on-line micelle-mediated preconcentration on selective sorbents. In this study, the authors used the solubilizing properties of several ionic and non-ionic surfactants, to solve the problems arising from the low solubility of PAHs in water and their sorption to surfaces, and set up an on-line trace enrichment LC system with fluorescence detection. Using Brij-35 as surfactant, unwanted adsorption of the analytes on inner walls or surfaces was prevented. The limits of detection obtained were at the low to sub-ng/l level.

In a study performed by Sicilia *et al.* [33], a new approximation in the *cloud-point extraction* methodology was applied to PAHs determination in environmental samples. It was based on the use of anionic surfactants in acidic media, combined with LC/fluorescence detection. For this study, the authors considered previous works in which it was shown that anionic surfactants were separated in two isotrophic phases in acid medium at room temperature. Among others, sodium dodecane sulfonic acid (SDSA) was employed as the surfactant. It has two important advantages over non ionic surfactants, which are generally used in the cloud-point methodology for the extraction of PAHs mixtures [34]. First, it exhibits low fluorescence intensity and absorbance at the

detection wavelength of PAHs (due to absence of aromatic groups in the surfactant molecule) and second, it is characterized by a short retention time (due to its polar character).

Sediments

Dunn [35] performed a very complete investigation concerning PAHs concentration in several marine samples, by trying to determine the relationships existing between the levels of a range of PAH isomers in three different kinds of marine samples: sediments, bivalve molluscs and algae. For this reason, he applied a method based on reversed phase liquid chromatography and fluorescence detection.

Also, Obana *et al.* [36] studied some PAHs (benzo(a)pyrene, dibenzo(a,h)anthracene, and 3-metylcholanthrene), which are carcinogens for mammals after in vivo hydroxylation by mixed function oxidases. Compared to other separation techniques, the development of HPLC has permitted to analyze PAHs with good separation and high sensitivity, and to simplify the pre-treatment processes. In the study, ten PAHs were determined in sediments, oysters, and wakame seaweeds by HPLC with a fluorescence detector.

This methodology was also applied by Smith *et al.* [37] to the determination of PAHs in sediments, seawater and clams from Green Island, the most visited coral island of the Great Barrier Reef in Australia. Results showed that only sediments near powerboat moorings were found to contain low, but measurable amounts of several different PAHs, in contrast to the baseline amounts found at other locations. The presence of several PAHs at measurable levels strongly suggests that their origin was due to fuel spillage and/or exhaust emissions.

In an investigation of marine sediments from the Adriatic Sea, Guzzella and Paolis [38] evaluated PAHs contamination. During a naval cruise from Trieste to Bari they collected thirty two samples and determined PAHs in the fine sediment fraction. The quantification of PAHs content in the samples was performed also with HPLC and fluorescence spectroscopy.

Beltrán *et al.* [39] applied also a HPLC method with fluorescence detection to the determination of the sixteen PAHs considered as the most pollutants by EPA in reference to marine sediments (HS-3, NRCC). The method consisted on HPLC determination of PAHs using isocratic conditions, with spectrofluorimetric detection and programmation of wavelengths.

The organic contaminant analyses in the environment require complex procedures with several steps, such as extraction, purification and quantification. In the case of solid samples, the extraction is often performed by reflux of organic solvent. This method is long (several hours) and solvent-consuming (several hundreds of mL). Microwave-assisted solvent extraction (MASE), represents an interesting alternative method for organic contaminants extraction.

As an example of application, Kay *et al.* [45] developed a MASE technique for the extraction of PAHs in marine sediments. Optimum conditions for this technique were obtained by using the mixed-level orthogonal array design procedure. A comparison between the Soxhlet extraction and MASE methods showed that although both techniques gave comparable results on certified reference materials (HS-2 and HS-6), the MASE technique allows one to use less solvent and it is also time-saving and cost-effective, without affecting the extraction efficiency. The optimum MASE technique was coupled to two analytical techniques: HPLC with both UV and fluorescent detectors as in other previous studies [46-50], and GC-MS for the qualitative and quantitative determination of PAHs in the certified reference materials and real samples (marine sediments).

Another methodology focussed on microwave assisted extraction was applied by Letellier *et al.* [51] and used to extract PAHs from environmental matrices. The procedure was validated on marine sediment, the standard reference material (SRM 1941a). The concentrations obtained by this method were in agreement with the certified values and the concentrations measured using Soxhlet extraction.

Organisms

A large number of papers related with the application of HPLC with fluorescence detection to the PAHs analysis in marine organisms has been published [52-61]. Among them, crustaceans [56] are the most widely investigated. Indeed, they can concentrate a high level of PAHs probably because of the absence of aryl hydrocarbon hydroxylase in these species. In fact, scientists of several specialties have proposed the use of indigeneous bivalve molluscs in order to serve as biocontrollers of the detection and quantification of environmental pollutants, including carcinogens. Due to the fact that they are permanent inhabitants in specific locations and have a tendency to concentrate environmental contaminants, bivalves have been widely investigated for such studies.

In this line of investigation, Hanus *et al.* [62] described an HPLC procedure for the determination of thirteen PAH compounds in oysters at the ppb level. Recoveries obtained from spiked samples were generally close to 80 %. In a particular investigation, Mix and Schaffer [63] focussed on the determination of PAHs present in clams of the Coos Bay in Oregon (USA). In such a study, the concentrations of benzo(a)pyrene were measured in clam populations from four different intermareal Coos Bay regions. It was shown that the PAM concentrations in those clams living close to industrialized areas were higher than the others living far away from these areas and that, in general, the PAM concentration was higher in spring-summer time than during autumn and winter. The same investigators also discovered [64] that the most hydrosoluble PAHs are those which are concentrated in major proportion in such organisms.

Musial and Uthe [65] described a simple, rapid and easily automatizable method for the determination of PAHs in crustaceans. The method was based on the combination of

chromatographic techniques such as GC and LC for the identification and separation of these compounds and fluorescence spectrometry for quantification. The proposed method was valuable for individual measurements of PAHs in a range of concentration of 0.25-10 ng PAHs/g tissue.

A technique, originally developed to investigate the pollution of Dutch coastal water with metals and PCBs, was modified by Boom [66] for determining the pollution of marine organisms with PAHs. The method was based on the hydrolysis of tissue with 4 M sodium hydroxide, extraction with hexane, clean-up with 10 % deactivated aluminium oxide and quantitative determination with reversed phase HPLC and fluorescence detection. It gave satisfactory results for the analysis of PAHs in mussels.

Trying to determine the bioconcentration factors for petroleum hydrocarbons, PAHs and biogenic hydrocarbons in *Mytilus edulis*, Murray *et al.* [67] applied also this technique. PAHs were quantified by reverse phase HPLC with programmed-wavelength fluorescence detection. The results showed that the bioconcentration factors for PAHs were similar to those found for total hydrocarbons where the major hydrocarbons source was oil, whereas, at other sites, the bioconcentration factors for PAHs were an order of magnitude lower than those determined for petroleum and for hydrocarbons originating from algae.

Perfetti *et al.* [68] proposed modifying the method for determining of PAHs and producing very clean seafood extracts in less than half the time requested previously. After alkaline digestion of seafood, PAHs were partitioned into 1,1,2-trichlorotrifluoroethane. The resulting extract was cleaned up by solid-phase extraction on alumina, silica and C_{18} adsorbents, and then analyzed by gradient reversed phase liquid chromatography with programmable fluorescence detection. Average recoveries of twelve PAHs from five different matrices (mussels, oysters, clams, crabmeat, and salmon) spiked at low ppb levels ranged from 76 to 94 %. The authors obtained results which were in good agreement with the analyses of a mussel standard reference material obtained from the National Institute of Standards and Technology (NIST).

A variant of this methodology (LC/fluorescence) was presented recently by Bouzige *et al.*, [70]. The authors evaluated a new immunoaffinity solid phase extraction (SPE) methodology based on antigen-antibody interactions which was optimized for the selective extraction of PAHs in various complex environmental matrices. This immunosorbent (IS) consists of anti-pyrene antibodies immobilized on a silica support and is used as a classical SPE sorbent. The cross-reactivity of antibodies for analytes structurally related with pyrene allows the simultaneous extraction of the priority PAHs included in the US EPA priority lists. Losses due to the volatility of the two- or three-ring PAHs were avoided by coupling the extraction on-line and using the antipyrene IS with LC. The sensitivity of fluorescence associated with the selectivity of IS allowed the quantification of individual PAHs in contaminated or surface water below the 0.02 µg/l level. Off-line extraction procedures were also set up for the extraction of PAHs from complex solid environmental matrices, such as sludge or mussel extracts. The high selectivity provided by the antibodies permitted the extraction of PAHs and elimination of a great number of interferents in only one step.

Investigating the PAHs pollution in deep-sea environment (1500-1800 m depth), Escartin and Porte [71] developed also a methodology based on the measurement of bile PAHs metabolites in deep-sea fish. The authors selected five species from the NW Mediterranean for the study. Bile crude samples were directly analyzed by HPLC-fluorescence at the excitation/emission wavelengths of benzo(a)pyrene (380/430 nm). The results obtained confirm the long-range transport of PAHs to the deep-sea environment, subsequent exposure of fish inhabiting those remote areas, and fish ability to metabolize and excrete them through the bile.

References

1. Fazio, T.; Howard, W., In *Polycyclic Aromatic Hydrocarbons;* Bjorseth, A., Ed.; Marcel Dekker. New York, 1983; pp 464-468.
2. Vandermeulen, J.H.; Buckley, D.E.; Levy, E.M.; Long, B.F.N.; McLaren, P.; Wells, P.G. *Mar. Poll. Bull.* **1979**, *10(8)*, 222.
3. Piecer, .M; Hocenski, V. *VI^e Journées Étud. Pollutions, Cannes, C.I.E.S.M.* 1982, pp 177-182.
4. Vo-Dinh, T.; White, D.A. *J. Am. Chem. Soc.* **1986**, *58(6)*, 1128.
5. Tervo, V. *Fin. Mar. Res.* **1978**, *244*, 215.
6. Law, R.J. *Mar. Poll. Bull.* **1978**, *9(11)*, 293.
7. Ochi, T.; Okaichi, T. *Tech. Bull. Fac. Agr. Kagawa Univ.* **1979**, *30(2)*, 157.
8. Østgaard, K.; Jensen, A. *Intern. J. Environ. Anal. Chem.* **1983**, *14*, 55.
9. Santana, J.J.; Sosa, Z.; Afonso, A.; González, V. *Fresenius J. Anal. Chem.* **1990**, *337*, 96.
10. Uebel, U., Kubitz, J., Anders, A.J. *J. Plant. Physiol.* **1996**, *148*, 586.
11. Lloyd, J.B.F. *Analyst.* **1980**, *105*, 97.
12. Santana, J.J.; Sosa, Z.; Afonso, A.; González, V. *Anal.Chim. Acta.* **1991**, *255*, 107.
13. Santana, J.J.; Sosa, Z.; Afonso, A.; González, V. *Talanta.* **1992**, *39(12)*, 1611.
14. Bermejo A.; Hernández, J.; Santana, J.J. *Fresenius J. Anal. Chem.* **1992**, *343*, 509.
15. Santana, J.J.; Hernández, J.; Bernal, M.M.; Bermejo, A. *Analyst.* **1993**, *118*, 917.
16. Böckelen, A.; Niessner, R. *Fresenius J. Anal. Chem.* **1993**, *346*, 435.
17. Ariese F., Kok, S.J., Verkaik, M., Gooijer C., Velthorst N.H., Hofstraat J.W. In *Shpol'skii spectroscopy and synchronous fluorescence spectroscopy: (Bio) monitoring of PAHs and their metabolites;* Ariese, F., Ed.; Academish Proefschrift, Vrije Universiteit, Febodruck Enschede, Amsterdam; 1993; pp. 129-142.
18. Ariese F., Dick A., Hofstraat J.W., Gooijer C., Velthorst N.H. In *Shpol'skii spectroscopy and synchronous fluorescence spectroscopy: (Bio) monitoring of PAHs and their metabolites;* Ariese, F., Ed.; Academish Proefschrift, Vrije Universiteit, Febodruck Enschede, Amsterdam; 1993; pp. 143-163.

19. Vilchez, J.L.; del Olmo, M.; Avidad, R.; Capitán-Vallvey, L.F. *Analyst.* **1994**, *119*, 1211.
20. Ewald, M.; Moinet, A.; Saliot, A.; Albrecht, P. *Am. Chem. Soc.* **1983**, *55*, 958.
21. Garrigues, P.; Ewald, M. *Org. Geochem.* **1983**, *5(2)*, 53.
22. Garrigues, P.; de Sury, R.; Bellocq, J.; Ewald, M. *Analusis.* **1985**, *13(2)*, 81.
23. Garrigues, P.; Ewald, M. *Intern. J. Environ. Anal. Chem.* **1985**, *21*, 185.
24. Hofstraat, J.W.; van Zeijl, W.J.M.; Ariese, F.; Mastenbroek, J.W.G., Gooijer, C.; Velthorst, N.H. *Mar. Chem.* **1991**, *33*, 301.
25. Ariese, F.; Gooijer, C.; Velthorst, N.H.; Hofstraat, J.W. *Anal. Chim. Acta.* **1990**, *232*, 245.
26. Mastenbroek, J.W.G.; Ariese, F.; Gooijer, C.; Velthorst, N.H.; Hofstraat, J.W.; van Zeijl, W.J.M. *Chemosphere* **1990**, *21(3)*, 377.
27. Kozin, I.; Gooijer, C.; Velthorst, N.H.; Hellou, J.; Zitko, V. *Chemosphere.* **1996**, *33(8)*, 1435.
28. Hofstraat, J.W.; Jansen, H.J.M.; Hoornweg, G. PH.; Gooijer, C.; Velthorst, N.H.; Cofino, W.P. *Intern. J. Environ. Anal. Chem.* **1985**, *21*, 299.
29. Lee, R.F.; Gardner, W.S.; Anderson, J.W.; Blaylock, J.W.; Barwell-Clarke, J. *Environ. Sci. Technol.* **1978**, 12(7),832.
30. McKay, J.F.; Latham, D.R. *Anal. Chem.* **1980**, *52(11)*, 1618.
31. El Harrak, R.; Calull, M.; Marcé, M.; Borrull, F. *Int. J. Environ. Anal. Chem.* **1996**, *64*, 47.
32. Brouwer, E.R.; Hermans, A.N.; Lingeman, H.; Brinkman, U.A. Th. *J. Chromatogr. A* **1994**, *669*, 45-57.
33. Sicilia, D.; Rubio, S.; Pérez-Bendito, D.; Maniasso, N.; Zagatto, E.A.G. *Anal. Chim. Acta.* **1999**, *392*, 29.
34. García Pinto, C.; Pérez Pavón, J.L.; Moreno Cordero, B. *Anal. Chem.* **1994**, *66*, 874.
35. Dunn, B.P. In *Polynuclear Aromatic Hydrocarbons: Fourth International Symposium on Analysis, Chemistry, and Biology.* Battelle Press: Columbus, Ohio, 1980; pp 367-377.
36. Obana, H.; Hori, S.; Kashimoto, T. *Bull. Environm. Contam. Toxicol.* **1981**, *26*, 613.
37. Smith, J.D.; Bagg, J.; Sin, Y.O. *Aust. J. Mar. Freshw. Res.* **1987**, *38*, 501.
38. Guzzella, L.; de Paolis, A. *Mar. Poll. Bull.* 1994, *28(3)*,159.
39. Beltrán, J.L.; Ferrer, R.; Guiteras, J. *J. Liq. Chrom. & Rel. Technol.* **1996**, *19(3)*, 477.
40. García, A.I.; González, E.B.; Alonso, J.I.G.; Medel, A.S. *Chromatographia* **1992**, *33*, 225.
41. Codina, G.; Vaquero, M.T.; Comellas, L.; Puig, F.B. *Chromatographia* **1994**, *673*, 21.
42. Núñez, M.D.; Centrich, F. *Anal. Chim. Acta* **1990**, *234*, 269.
43. Van de Nesse, R.J.; Hoogland, G.J.M.; de Moel, J.J.M.; Gooijer, C.; Brinkman, U.A.Th.; Velthorst, N.H. *J. Chrom. A* **1991**, *552*, 613.
44. Brown, D.W.; McCain, B.B.; Horness, B.H.; Sloan, C.A.; Tilbury, K.L.; Pierce, S.M.; Burrows, D.G.; Chan, S-L.; Landahl, J.T.; Kraihn, M.M. *Mar. Poll. Bull.* **1998**, *37(1-2)*, 67.
45. Kay, K.; Keong, M.; Kee, H. *J. Chromatogr.. A.* **1996**, *723*, 259.
46. Zobel, H.; Ruppel, F.*LaborPraxis* **1993**, *3*, 30.
47. Grosse-Rhode, C.; Kicinksi, G.C.; Kettrup, A. *J.High Resol. Chromatogr.* **1990**, *15*, 3415.
48. Smith, J.D.; Bagg, J.; Wrigely , I. *Water Res.* **1991**, *25*, 1145.
49. Marriott, P.J.; Carpenter, P.D.; Brady, P.H.; McCormick, M.J.;. Griffiths, A.J; Hatvani, T.S.G.; Rasdell, S.G. *J. Liq. Chromatogr.* **1993**, *15*, 3229.
50. Dong, M. W.; Duggan, J.X.; Stefanou, S. *LC-GC International* **1993**, *11*, 802.
51. Letellier, M.; Budzinski, H.; Garrigues, P. *LC-GC International.* **1999**, 12(4), 957.
52. Ten Hulscher, T.E.; Vrind, B.A.; Van den Heuvel, H.; Van der Velde, L.E.; Van Noort, P.C.M.; Beurskens, J.E.M.; Govers, H.A.J. *Environ. Sci. Technol.* **1999**, *33(1)*, 126.
53. Bravo, H.A.; Salazae, S.L.; Botello, A.V.; Mandelli, E.F. *Bull. Environ. Contam. Toxicol.* **1978**, *17*, 171.
54. Brown, R.A.; Pancinov, R. *J. Environ. Sci. Technol.* **1979**, *13*, 878.
55. Chester, S.N.; Gump, B.H.; Hert, H.S.; May, N.E.; Wise, S.A. *Anal. Chem.* **1978**, *50*, 805.
56. Dunn, B.P.; Fee, J. *J. Fish. Res. Board Can.* **1979**, *36*, 1469.
57. Eaton, P.; Zitko, V. *International Council for the Exploration of the Sea*, **1978**
58. Hert, M.; Klusek, C.S.; Miller, K.M. *Environ. Sci. Tech.* **1980**, *14*, 465.
59. Pancinov, R.J.; Brown, R.A. *Environ. Sci. Tech.* **1977**, *11*, 989.
60. Payne, J.F. *Mar. Poll. Bull.* **1977**, *8*, 112.
61. Zitko, V. *Bull. Environ. Contam. Tox.* **1978**, *14*, 624.
62. Hanus, J.P.; Guerrero, H.; Biehl, E.R.; Kenner, C.T. *J. Assoc. Off. Anal. Chem.* **1979**, *62(1)*, 29.
63. Mix, M.C.; Schaffer, R.L. *Mar. Environ. Res.* **1983**, *9*, 193.
64. Mix, M.C.; Schaffer, R.L. *Mar. Poll. Bull.* **1983**,*14(3)*, 94.
65. Musial, C.J.; Uthe, J.F. *J. Assoc. Off. Anal. Chem.* **1986**, *69(3)*, 462.
66. Boom, M.M. *Intern. J. Environ. Anal. Chem.* **1987**, *31*, 251.
67. Murray, A.P.; Richardson, B.J.; Gibbs, C.F. *Mar. Poll. Bull.* **1991**, *22(12)*, 595.
68. Perfetti, G.A.; Nyman, P.J.; Fisher, S.; Joe, F.L.; Diachenko, G.W. *J. Assoc. Off. Anal. Chem.* **1992**, *75(5)*, 872.
69. Burns, K.A. *Mar. Poll. Bull.* **1993**, *26(2)*, 77.
70. Bouzige, M.; Pichon, V.; Hennion, M.C. *Environ. Sci. Technol.* **1999**, *33(11)*, 1916.
71. Escartín, E.; Porte, C. *Environ. Sci. Technol.* **1999**, *33(16)*, 2710.

Consideraciones socio-económicas sobre el momento actual de la acuicultura marina en España

Dr. José Manuel Vergara Martín

Grupo de Investigación en Acuicultura. Facultad de Ciencias del Mar.
Universidad de Las Palmas de Gran Canaria (España)

RESUMEN

El crecimiento más rápido de la acuicultura en Europa en los últimos años lo ha experimentado la cuenca Mediterránea, concentrándose en la producción de dorada y lubina en jaulas flotantes. España, país que apostó inicialmente por los sistemas de tierra, se ha volcado en los últimos años también hacia la tecnología de jaulas, situándose en la actualidad entre los principales países productores. El rápido crecimiento de este sector está originando una serie de conflictos socioeconómicos que deben ser afrontados como retos a superar de cara a la consolidación de esta actividad.

SUMMARY

The Mediterranean region has experienced the fastest growth within the Aquaculture sector, concentrated in the production of gilthead seabream and european seabass in floating cages. Spain, a country which initially bet on land-based systems, has shifted also in recent years towards the cage technology, being at present situated among leading producing countries. The fast growth of this sector is causing a series of different socio-economical conflicts which must be approached as challenges to be overcomed in order to consolidate this activity.

INTRODUCCIÓN

Según la F.A.O., el crecimiento más rápido de la acuicultura en Europa en los últimos años lo ha experimentado la cuenca Mediterránea, pasando de 80.000 Tm a más de 260.000 Tm entre 1994 y 1977. En términos de volúmenes por especies, y para 1999, las más importantes fueron el mejillón y la ostra (500.000 Tm), y la dorada y la lubina (49.000 y 39.000 Tm, respectivamente). Sin embargo, y atendiendo a su valor, las principales especies fueron la dorada y la lubina (rondando los 300 millones de euros, cada una).

La evolución de este sector piscícola Mediterráneo ha seguido la historia del

cultivo del salmón en países del norte de Europa, pasando del empleo inicial de instalaciones en tierra, con bombeo de agua hacia estanques o piscinas, y cambiando progresivamente hacia un tipo de granja que consiste en jaulas flotantes, que se fondean en aguas litorales cada vez más alejadas de la costa. La elección de este tipo de instalaciones frente a las de tierra responde, en primer lugar, al desarrollo y disponibilidad de este tipo de tecnología en los últimos años, representando una alternativa de mayor viabilidad económica, y también a la fuerte competencia de uso que soportan estas aguas litorales (turismo, asentamientos urbanos, etc.). En España, país que junto a Francia e Italia apostó inicialmente por los sistemas de tierra, recientemente se ha apreciado un punto de inflexión significativo hacia la tecnología de jaulas flotantes. Este hecho se fundamenta muy posiblemente en la realidad de los 7.000 Kms. de costa de este país, así como en la constatación de la mayor rentabilidad de estas instalaciones de engorde frente a las basadas en tierra. La variedad de tecnologías de jaulas disponibles en la actualidad, junto al impresionante potencial del mercado nacional se han sumado con toda probabilidad a las causas de esta nueva tendencia.

La producción de peces marinos de alto valor comercial en los países Mediterráneos ha experimentado un crecimiento espectacular en los últimos años, pasando de unos pocos millares de toneladas de dorada y lubina en 1984, a unas estimaciones superiores a las 100.000 toneladas para el año 2000, cuyo destino son en su totalidad los mercados Europeos. Este crecimiento es superior al experimentado en sus inicios por el sector productivo de salmón atlántico en países del Norte de Europa, que habiendo iniciado su actividad media década antes, y con los mismos mercados, ofrece una producción actual de 540.000 toneladas anuales, y que ha superado diferentes crisis de mercado – entre ellos una constante caída de precios debido a este incremento espectacular de la oferta -, mediante la progresiva reducción de costes de producción (automatización, mejora de piensos, etc.), y una eficaz política de comercialización y marketing.

Según datos de la Federación Europea de Productores de Acuicultura (F.E.A.P.), el principal país productor de dorada y lubina en la actualidad es Grecia, con unas producciones en 1999 de 21.000 y 19.000 Tm, respectivamente, seguida por Turquía y España, con un total de 13.750 y 10.000 Tm, respectivamente.

Como en todos los países del Mediterráneo, el despegue de la producción de dorada y lubina en España también ha sido espectacular, con incrementos del 29% y 56% en los años 1997 y 1998. En 1996, Andalucía y Cataluña eran las comunidades autónomas de mayor importancia en la producción de estas especies, existiendo 41 empresas operativas en este sector, tal como resumía la siguiente tabla:

Distribución de granjas de dorada y lubina por regiones en 1996

Autonomías	Nº de Uds.	% Nº de Uds.	Producción (Tm)	% produ total
Andalucía	18	44	3608	64
Baleares	2	5	220	4
Canarias	5	12	520	9
Cataluña	12	29	678	12
Murcia	1	3	582	11
Valencia	3	7	0	0
Total	**41**	**100%**	**5608**	**100%**

Fuente: APROMAR

Actualmente, el cultivo en jaulas es el sistema escogido por la mayoría de los nuevos proyectos. Así, en tan sólo seis años, entre 1990 y 1996, la producción obtenida en este tipo de instalaciones duplicó su importancia hasta representar un 34% de la producción total. Las instalaciones en tierra, donde se utilizan grandes volúmenes de agua con los consiguientes costes de bombeo y oxigenación, han perdido importancia dentro del sector de engorde, aunque lo han ganado en la fase de preengorde hasta 8-10 gramos.

Producción de Dorada y Lubina en España 1991-1998

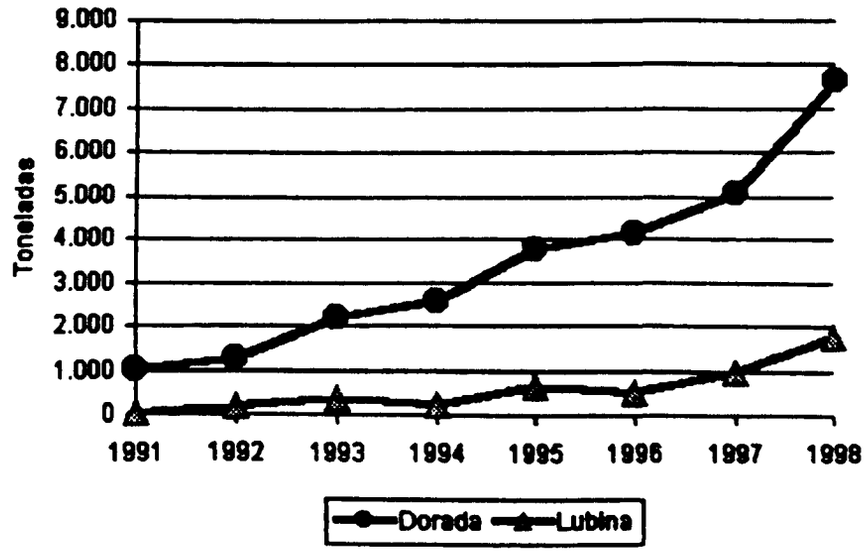

Fuente: Encuesta de Producción de Dorada y Lubina en España. 1997. ProAqua Nutrición

Las estimaciones de requerimientos de alevines de ambas especies para el año 2000 son de 66 millones para España, y de 250 millones para toda la región Mediterránea Sin embargo, este importante crecimiento en la producción, como consecuencia de la incorporación de la tecnología de jaulas flotantes para el engorde, se ha visto siempre acompañado de un crecimiento algo desfasado en instalaciones de semillero, siendo esta situación más acentuada en España, donde el crecimiento en producción en jaulas absorbe en la actualidad prácticamente toda la producción nacional de alevines, que por otra parte ronda los 50 millones anuales. Es por todo lo anterior que, pese a la tendencia constante en los últimos diez años de descenso de precios de venta de dorada y lubina adultas, los precios de venta de alevines de estas especies han experimentado unas variaciones menos drásticas, aunque también con

tendencias a la baja. Esto último, sin duda también influido por la reducción experimentada en los costes de producción. Los precios de venta de estos alevines varían significativamente dependiendo de factores como su calidad o procedencia, y de las variaciones en la demanda según las diferentes épocas del año. En la actualidad, y debido al incremento de instalaciones de jaulas, la demanda de alevines de 10 gramos ha crecido de forma importante respecto a los alevines de 2 gramos, oscilando el precio entre 50 y 60 pesetas para los primeros, y entre 40 y 50 pesetas para los segundos.

MERCADOS Y COMERCIALIZACION

En lo referente a los mercados, este es un factor de primera importancia y no siempre bien atendido o estudiado. De las casi 45.000 toneladas de dorada y lubina producidas en el Mediterráneo en 1996, Grecia ocupó la cabeza de este desarrollo, con una cuota de mercado del 42%. Estos mercados, y para estos productos, se concentran por orden de importancia en Grecia, Italia, Francia y España. El incremento progresivo de la oferta ha producido un descenso en el precio de estos productos (53% en los últimos 6 años), descendiendo consecuentemente los márgenes de beneficios empresariales. La consecuencia es un mercado global cada vez más competitivo, en países principalmente del Sur de Europa, requiriéndose cada vez niveles mayores de calidad, consistencia y fiabilidad de los proveedores, así como el empleo de métodos más sofisticados de marketing.

El mercado Español se caracteriza por un marcado déficit en la balanza comercial, importando el 66% de su consumo. Es, pues, un mercado que presenta inmensas perspectivas (pensemos además en la industria turística), aunque todavía con un muy bajo consumo de estos productos de acuicultura. Una recomendación aquí sería recuperar el retraso que nuestro país tiene en el desarrollo de su propio mercado interno, pudiéndose decir que la investigación y desarrollo de mercados es la disciplina vital de la siguiente década para este sector, muy particularmente para España.

Aproximadamente, un 70% de la producción española de mejillón va destinada al consumo interno, y el 30% restante se exporta, fundamentalmente a Italia y Francia.

Los peces marinos se destinan en un 80% al mercado nacional en la actualidad, mientras que el 45% de los alevines producidos en nuestro país se exportan hacia los mercados europeos. A nivel internacional, no cabe duda de que el mercado italiano ha sido el factor inductor del desarrollo del cultivo de dorada y lubina (unas 40.000 toneladas de pescado de acuicultura se dirigieron a este mercado en 1996). No obstante, el atractivo del mercado español ha crecido de forma espectacular, desviando una importante parte del flujo comercial internacional y reduciendo los efectos negativos de la excesiva dependencia del mercado italiano.

El crecimiento del sector ha sido motivo de presiones en los precios, sobre todo por la especial naturaleza de la acuicultura europea, con producción de especies

de alto valor económico y mercados tradicionales y muy localizados, consiguientemente, altamente sensibles a la variación de la oferta. Así, el mercado del salmón llegó a colapsarse y el peligro es mayor para las especies como la dorada, menos conocidas a nivel global.

Como se aprecia en los siguientes gráficos, los precios han disminuido sostenidamente hasta estabilizarse en torno a los 6 ecus por kilogramo. En cuanto a la producción, no ha cesado de incrementarse, observándose tasas similares de crecimiento (37% de incremento medio interanual para la dorada y 42% para la lubina).

Evolución de la producción y precios de dorada en Europa

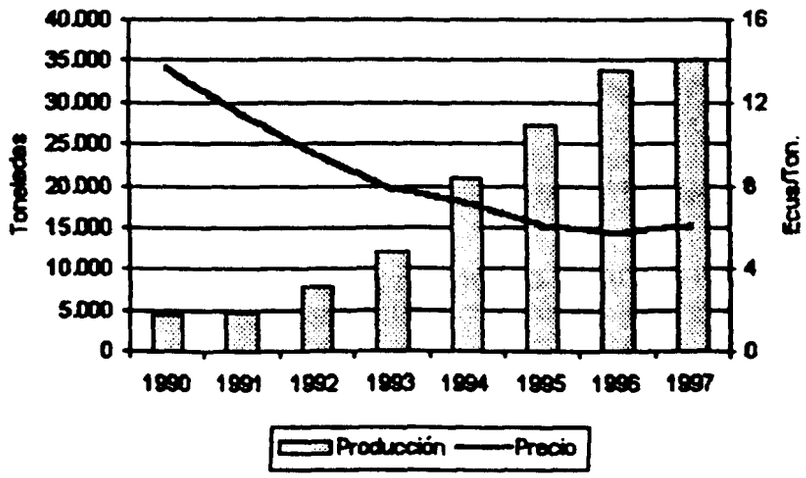

Evolución de la producción y precios de lubina en Europa

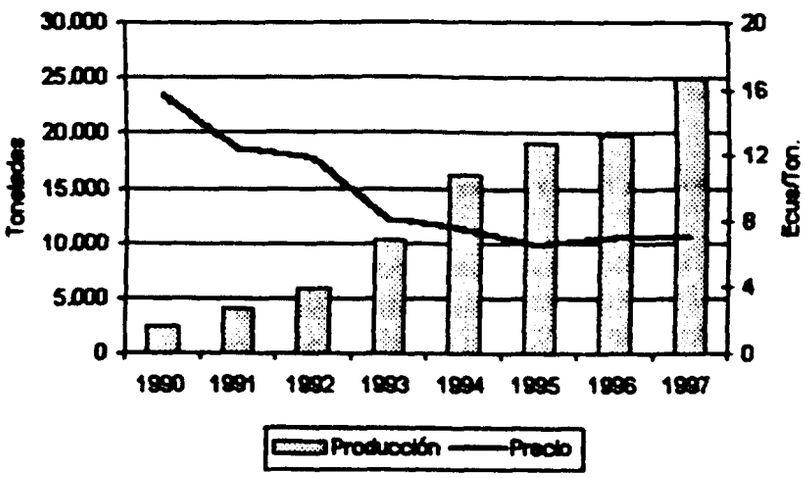

Fuente: F.E.A.P.

A nivel global, en el mercado español la dorada no es una especie muy conocida, y su presencia en la oferta de las pescaderías es escasa. La mayor parte de ella llega al consumidor a través de restaurantes, sobre todo de la costa mediterránea y en ciudades importantes como Madrid, Barcelona y Sevilla. Como consecuencia de esta escasa amplitud de la demanda, la oferta se ha centrado en

los canales tradicionales, con la consiguiente caída de precios.

La evolución mensual de los precios de la dorada y la lubina refleja claramente el impacto de estos dos factores:

Evolución mensual del precio de la dorada (Media 1996-1998)

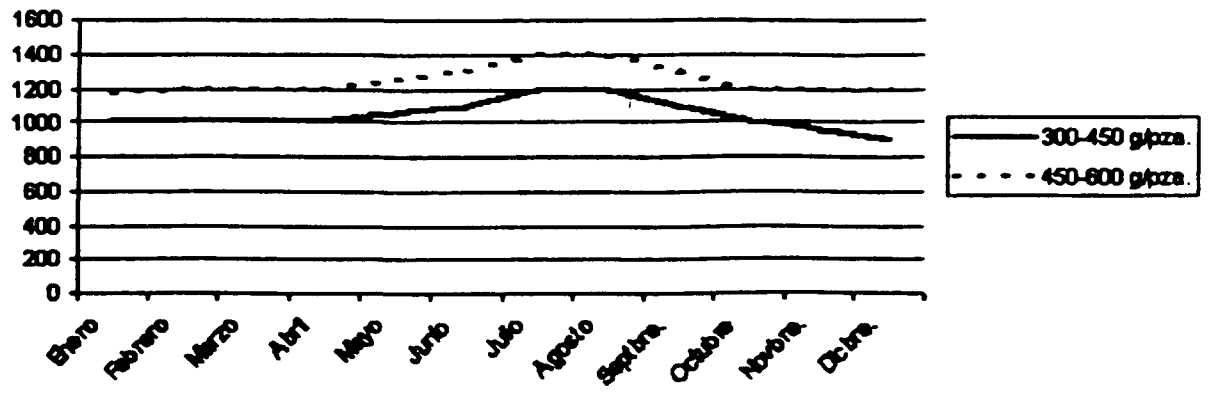

Fuente: Ministerio de Agricultura, Pesca y Alimentación

Evolución mensual del precio de la Lubina (Media 1996-1998)

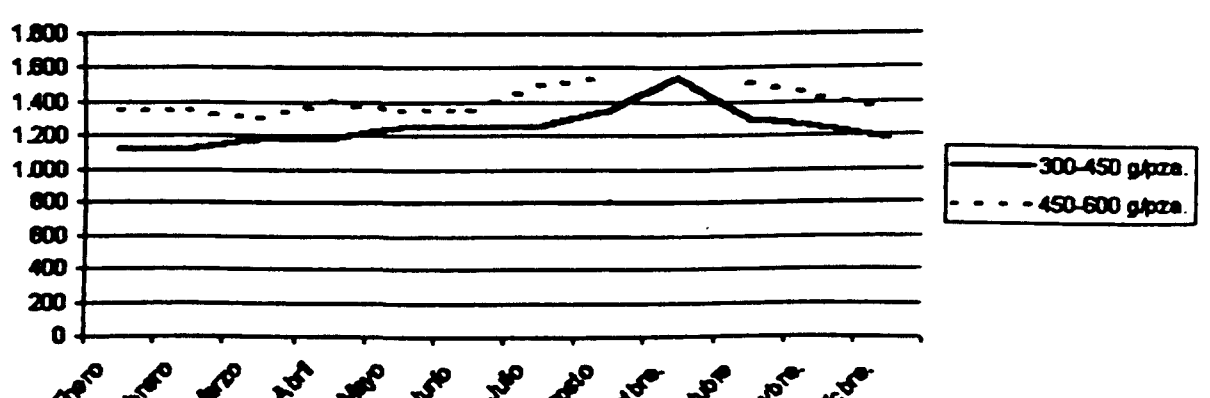

Fuente: Ministerio de Agricultura, Pesca y Alimentación

La situación global de España, según estimaciones de la F.E.A.P. y la Asociación Empresarial de Productores de Cultivos Marinos de España (A.P.R.O.M.A.R.) para el año 1999, es la de primer productor mundial de mejillones (250.000 Tm), y país situado entre los primeros productores Europeos de especies Mediterráneas (8.300 y 1.700 Tm de dorada y lubina, respectivamente), y con unas producciones significativas de rodaballo (2.000 Tm), y salmón atlántico (1.100 Tm), con un valor total aproximado de 212 millones de euros y proporcionando unos 8.000 empleos directos, de los 40.000 que este sector representa en la Unión Europea.

VENTAJAS DEL SECTOR

Entre las principales ventajas de España respecto a este sector se pueden incluir:

- **Características costeras**: La amplitud de sus costas, aún en directa competencia de usos con industrias tan potentes como el turismo, ofrece un amplio potencial de áreas litorales aptas para la instalación de cultivos piscícolas marinos. Además, el rango moderado de los valores de temperatura de sus aguas superficiales Mediterráneas y Atlánticas (archipiélago Canario), ofrece ventajas adicionales frente a otras zonas geográficamente más al Norte de la cuenca Mediterránea.

- **Mercado interior**: España posee una de las tasas más elevadas de consumo de pescado del mundo. Valores de alrededor de 42 kg/persona/año nos sitúan, junto a Países como Portugal o Noruega, como países líderes en Europa, y segundos en el mundo tras Japón.

- **Economía estable**: Los valores de los parámetros macro-económicos de nuestro país, incluyendo un sistema bancario sólido, unas buenas infraestructuras de comunicación y transporte, disponibilidad de personal cualificado, así como una infraestructura del propio sector bien estructurada (producción de alevines y piensos), favorecen el desarrollo del sector.

- Estudios recientes (Proaqua Nutrición, S.A.) sugieren que los costes de producción actuales de dorada y lubina en países como España, Grecia, Italia o Turquía (subtotal integrado por costes de personal, pienso y alevines, que representan el 70% del total), son muy similares, siendo las diferencias de eficiencia entre granjas individuales mayores que aquéllas entre los países arriba citados. Estos datos indican que **España, debido a los factores favorables arriba mencionados, se encontraría mejor situada en la batalla por la competitividad que países menos desarrollados**, toda vez que el éxito dependerá más (como así lo ha demostrado el sector del salmón Noruego) de la capacidad de aplicar técnicas específicas de reducción de costes (Incremento de la productividad, desarrollo tecnológico), que de situaciones como una mano de obra más barata.

DESVENTAJAS DEL SECTOR

Sin embargo, y entre los puntos débiles, podríamos destacar:

- **Una deficiente capacidad del sector para generar credibilidad**, debido a su rápido crecimiento, lo que está dificultando su integración en las economías locales, originando un problema de imagen que se expresa en conflictos de diversa naturaleza con la sociedad en la que se asienta.

- **Una estrategia deficiente o no siempre adecuada por parte de las diferentes Administraciones Públicas** implicadas en sus variadas actuaciones de apoyo al sector. Así, por ejemplo, el sector debe hacer frente a leyes y reglamentos complejos sobre la propiedad de la tierra,

utilización del agua, protección del medio ambiente, sanidad pública, pesca y marisqueo, etc., de los que muy pocos están redactados específicamente para promover o regular la Acuicultura, no contemplando en ningún caso el desarrollo del sector. Esta situación ha originando confusión, conflictos y un solapamiento generalizado entre competencias de diferentes Administraciones. Otra área de actuación, como la constituye las actividades de I + D, ha sido frecuentemente deficientemente gestionada, habiéndose concedido un peso inferior a la investigación aplicada que el que seguramente se requería, y no habiendo existido prácticamente transmisión del conocimiento generado al sector productivo.

- **El reducido tamaño de la mayoría de las empresas** acuícolas supone un grave freno a la competitividad del sector en los mercados internacionales.

- **La dificultad para reducir costes de producción** frente a la constante disminución de precios de mercado, en parte debido al reducido tamaño de estas empresas, pero donde también influyen factores como el porcentaje importante de instalaciones marinas que aún existen basadas en tierra (menos competitivas que las basadas en jaulas), o las reticencias a la automatización y al empleo de nuevas tecnologías que permitan esta reducción de costes.

- Además de los **impuestos** sobre el beneficio, comunes al resto de las actividades, las empresas de acuicultura marina deben afrontar el pago de un canon de ocupación de dominio público (terrestre o marítimo) y, en su caso, un canon de vertidos. En el caso de los impuestos sobre beneficios, además, las empresas se ven perjudicadas por la valoración anual de la variación de existencias en planta como parte del beneficio, a pesar de que el valor comercial del producto sea prácticamente nulo al no haber alcanzado la talla de venta. En la práctica ello supone un adelanto del impuesto, especialmente perjudicial en un sector con amplias necesidades de circulante

OPORTUNIDADES / RECOMENDACIONES

- Desarrollo del mercado nacional (marinos): Aunque hoy en día la comercialización de los productos a través de mayoristas (Mercas e hipermercados distribuidores) representa cerca del 50% de la producción, esta situación es relativamente reciente, de manera que hasta hace muy pocos años alrededor del 80% de la producción de marinos era exportado (dando lugar a la peculiaridad de haber sido un país netamente importador de productos de Acuicultura, a pesar de ser el primer consumidor Europeo de productos acuícolas frescos). El cambio de situación se debe sin duda a una creciente política comercial adecuada por parte de los productores. Por otro lado, ha de destacarse la creciente importancia de las grandes superficies, representando en la actualidad cerca del 15% de las ventas totales, y con una cuota de mercado que seguramente irá en

aumento en los próximos años. Esta oportunidad será fructífera en la medida que la producción se oriente hacia la demanda real del consumidor, y para ello el gran reto se relaciona con el tipo de producto a ofertar.

- **Debe incrementarse la producción y reducir costes** (incremento de la competitividad); incrementarse el tamaño de las empresas y mejorar la gestión en líneas generales.

- **Debe potenciarse la incorporación de nuevas especies marinas** (diversificación de la oferta), como el pulpo, la seriola, el pargo, el atún, etc., aunque sin perder posiciones de mercado con dorada y lubina.

- En el contexto de las instalaciones de jaulas flotantes marinas, el futuro se contempla en el **desarrollo de tecnologías que permitan la instalación en lugares cada vez más alejados de la costa**, para lo que habrá que dedicar un esfuerzo en investigar:
  1. Estructuras para mar abierto más baratas,
  2. Barcos de trabajo más resistentes y especializados,
  3. Sistemas de control remoto para jaulas de mar abierto,
  4. Redes más resistentes al desgaste,
  5. Sistemas de amarre y fondeo más resistentes,
  6. Productos que eviten incrustaciones y algas en las redes que respeten el medio ambiente, y
  7. Programas de control y gestión del impacto ambiental.

- Desde el punto de vista de la **comercialización de dorada y lubina**, el futuro del sector pasa por la adopción de medidas en los siguientes aspectos:

  a. *Aumentar el valor añadido del producto con nuevas presentaciones*
  Como sucede en todos los sectores productivos, la fase de introducción de la actividad se caracteriza por precios elevados que palian las ineficiencias propias de la inexperiencia y permiten rentabilidades suficientes para atraer a nuevos productores. Evidentemente, tal y como quedó demostrado con el cultivo del salmón, a medida que el sector alcanza su madurez, las rentabilidades se moderan y tienden a igualarse con las registradas en el resto de los sectores. Es entonces cuando la única posibilidad para mantenerse en la actividad es reducir costes, lo cual es cada vez más difícil, o bien aumentar el valor añadido mediante nuevas presentaciones tales como envasado al vacío, atmósfera modificada.

  b. *Mejorar la planificación del ciclo productivo* para adecuarse a la demanda

  c. *Campañas divulgativas y de imagen sectorial*
  Estas acciones deberían dirigirse a mejorar la información de los consumidores y eliminar una posible mala imagen del producto frente al capturado en su medio natural, máxime cuando más del 80% de la demanda europea de dorada y lubina es satisfecha por los

cultivos marinos. Además, también urge la realización de estudios de mercado que revelen las pautas de consumo e identifiquen el objetivo de las campañas.

d. Mejora de la calidad

Como producto alimenticio, el pescado debe adaptarse a los requerimientos de calidad de unos consumidores que son más exigentes y menos fieles a marcas determinadas. La tendencia a buscar una diferenciación regional del producto mediante denominaciones de origen o etiquetas de calidad parece poco aplicable a la producción de dorada y lubina porque son cultivadas siguiendo exactamente los mismos procedimientos: alimentación, densidad, profilaxis, etc. Pero la calidad de las aguas puede variar mucho: ausencia de industrias pesadas contaminantes, medio Atlántico o Mediterráneo, etc.

- En lo concerniente a la **superación de las barreras burocráticas** ligadas a los primeros permisos y concesiones para la instalación de nuevas granjas, A.P.R.O.M.A.R. sugiere las siguientes medidas:
  1. Homogeneización de las normativas en las diferentes comunidades autónomas;
  2. Centralización de la gestión de los permisos a través de una Ventanilla única, para reducir los procedimientos burocráticos; y
  3. Puesta al día de la normativa considerando el potencial y las limitaciones de la acuicultura en cuanto a concesiones, requisitos medio ambientales, etc.

- **La actividad de I + D** deberá ser bien planificada y orientada hacia las necesidades críticas del sector, que en estos momentos son: la mejora tecnológica de instalaciones ya existentes, la producción en mar abierto, y la transformación y elaboración de nuevos productos.

- A nivel Europeo, pocos países cuentan con políticas y marcos jurídicos favorables a la acuicultura. La reciente aparición de la acuicultura industrial, la creciente competencia por los recursos y el continuado y rápido crecimiento del sector han centrado la atención en la necesidad de adoptar nuevas políticas y marcos normativos. **Es imprescindible establecer condiciones operacionales válidas en todos los niveles** (internacional, regional, nacional, local y en las propias explotaciones) para que los acuicultores, pescadores y otros empresarios puedan ver un atractivo en explotar el potencial de la acuicultura de manera sostenible. Al mismo tiempo, al crear un entorno propicio es fundamental conseguir un equilibrio entre la necesidad de desarrollo y la de conservación de los ecosistemas marinos. Como conclusión, las actuales estructuras administrativas y jurídicas deben ser objeto de revisión y ajuste para poder dar respuesta a las características y necesidades específicas de este sector.

- **Debe fomentarse el empleo por parte del sector de herramientas que optimicen la gestión empresarial**, tales como el Análisis Estratégico (externo e interno), o Modelos Bio-Económicos.

CONCLUSIONES

El sector productivo de la acuicultura, y en particular de la acuicultura marina en España está experimentando un segundo auge, diferente por motivos que no vienen al caso al primer auge experimentado en la década de los 80. Las principales razones quizás se pudieran resumir en la fuerte presión ejercida por el desarrollo acelerado de este sector en todo el mundo en general, y en Europa en particular, además del punto de inflexión que ha supuesto la disponibilidad de la tecnología de jaulas de mar abierto para el engorde de peces.

Este hecho, constatado por las estadísticas de producción de los últimos años y el número de nuevos proyectos que ya se han incorporado a la producción o se encuentran en fase de solicitud de permisos, está originando (y evidenciando) una serie de conflictos que demandan un conjunto de medidas y estrategias que permitan superarlos. Tal como indica el Profesor Fernando González-Laxe (Revista Productos del Mar, Nº 145-146, Febrero 2000), la complejidad de la actividad de la Acuicultura marina moderna, unida al rápido crecimiento de la misma, dificultará a corto y medio plazo su integración en las economías locales donde comienza a asentarse, apareciendo una variedad de conflictos de diverso tipo:

- *Conflictos con los diferentes usuarios de los recursos costeros.*
- *Conflictos con los explotadores de los recursos vivos del mar.*
- *Conflictos como consecuencia de los posibles impactos de la acuicultura sobre el medio ambiente* (utilizado con frecuencia creciente como argumento ante conflictos del tipo anterior, pese a que repetidamente los datos científicos indican el menor impacto de este sector cuando se compara con el resto de actividades humanas).

De otro lado, la globalización de la economía mundial, incluyendo procesos más cercanos como la liberalización de los mercados europeos y su próxima unificación de moneda, plantea los consiguientes retos de competencia a este sector, que debe afrontar a la misma velocidad de su rápido crecimiento. En este contexto, el breve análisis socioeconómico presentado puede resumirse en las siguientes conclusiones:

- **Las diferentes Administraciones Públicas** (centrales y autonómicas) con competencias en la regulación, ordenación, control y apoyo a este sector, **deben realizar un significativo esfuerzo en la unificación y simplificación de criterios**, con el objetivo de ofrecer una reglamentación eficaz y específica para la acuicultura, diseñada para promover y regular esta actividad. Asimismo, el rápido crecimiento de esta industria, junto con el potencial estratégico que representa para la economía de varias Comunidades Autónomas de este País, permiten proponer la consideración de este sector como ESTRATÉGICO para la economía de estas Regiones, empleando la reglamentación específica

recomendada como su instrumento de desarrollo.

- **Las empresas del sector deben priorizar en sus estrategias la reducción de costes de producción**: A través de técnicas de mejora y selección genética de los alevines, de la mejora de piensos y estrategias alimentarias, del incremento de la productividad de la mano de obra, y de la introducción de procesos de automatización/mecanización en las granjas (La suma de costes de alimentación, alevines y personal representa más del 70% de los costes de producción).

- **Las empresas del sector deben priorizar asimismo la mejora de la comercialización**: A través del incremento del consumo en los mercados existentes, la búsqueda de nuevos mercados, la diferenciación de productos (etiquetas), y productos de valor añadido (filetes, ahumados).

- **Las empresas del sector quizás debieran considerar la mejora de su imagen corporativa**, dirigida hacia las comunidades donde pretenden asentarse, como estrategia frente a los conflictos derivados de su rápido crecimiento, incluyendo la puesta en práctica y divulgación generalizada de programas de gestión medioambiental.